13 January 2006 | $10

Science

The New World of Global Health

AAAS

There's a new kit on the block.

Introducing StrataClone™ PCR Cloning Kits: A new, more affordable choice in Topoisomerase I technology

Our StrataClone™ PCR Cloning Kit* saves you time and money with topoisomerase-based PCR cloning priced lower than the competition. The simple, three step process, >95% efficiency guarantee, and affordable pricing make StrataClone™ PCR Cloning Kits your kit of choice for topoisomerase-based PCR cloning.

- **High-performance PCR cloning at a more affordable price**
- **Clone both long and short PCR amplicons with the same kit**
- **High efficiency results in >95% clones with insert**

Need More Information? Give Us A Call:

Stratagene USA and Canada
Order: (800) 424-5444 x3
Technical Services: (800) 894-1304 x2

Stratagene Europe
Order: 00800-7000-7000
Technical Services: 00800-7400-7400

Stratagene Japan K.K.
Order: 03-5159-2060
Technical Services: 03-5159-2070

www.stratagene.com

Ask Us About These Great Products:

StrataClone™ PCR Cloning Kit	**20 reactions**	**240205**
	10 reactions	**240206**

StrataClone™ is a trademark of Stratagene in the United States.
*Patent pending.

STRATAGENE®

introducing the

Time MACHINE

the MINI PREP 96

Fully Automatic plasmid and genomic DNA purification at the push of a button.

START
ENTER

Your time is valuable.

MACCONNELL RESEARCH

800.466.7949 www.macconnell.com

GE Healthcare

Greater flexibility and binding capacity in histidine-tagged protein purification

Ni Sepharose™ products from GE Healthcare give you the greatest binding capacity available for histidine-tagged protein purification. They offer the flexibility to use a variety of formats and protocols, ensuring the highest possible purity. And with our His GraviTrap™ and HisTrap™ FF crude columns, you can now get pure histidine-tagged proteins directly from unclarified lysate in just 30 minutes.

Maximum target protein activity is assured with Ni Sepharose, thanks to its tolerance of a wide range of additives and negligible nickel ion leakage. With up to four times the capacity of competing products, dramatically increasing your yield while saving on time and resin/buffer costs is no longer pure imagination.

www.amershambiosciences.com/his

imagination at work

GE18-05

Volume 311, Issue 5758

COVER

Billions of new dollars are pouring into programs that aim to help poor countries fight such infectious diseases as AIDS, malaria, and tuberculosis. But increasing numbers of people are beginning to ask tough questions about what the money has accomplished and what can be done to more quickly translate cash into care and prevention. See page 162.

Image: Brent Stirton/Getty Images

DEPARTMENTS

139 *Science* Online
141 This Week in *Science*
147 Editors' Choice
150 Contact *Science*
153 NetWatch
155 Random Samples
173 Newsmakers
247 New Products
255 *Science* Careers

EDITORIAL

145 Good News—and Bad
by Donald Kennedy

178

NEWS OF THE WEEK

South Korean Team's Remaining Human Stem Cell Claim Demolished 156
Iran's Trouble With Molybdenum May Give Diplomacy a Second Chance 158
Plants May Be Hidden Methane Source 159
SCIENCESCOPE 159
Scripps's Offshoot Stalled in South Florida 160
More Details Sought in Assessing Health Risks 161
More Cases in Turkey, but No Mutations Found 161

NEWS FOCUS

The New World of Global Health 162
Public-Private Partnerships Proliferate
U.S. Rules on Accounting for Grants Amount to More Than a Hill of Beans 168
A Career Change Possible for North Korea's Nuclear Scientists? 170
Long Trek to Solar System's Last Frontier Begins 172

162

LETTERS

HIV Research and Access to Treatment *M. Warren* 175
Response *R. M. Grant* et al.
Continuing Progress in Neuroinformatics
M. S. Gazzaniga et al.
Loss of Grants Hurts the Vulnerable *K. Sestak*
CORRECTIONS AND CLARIFICATIONS

BOOKS *ET AL.*

Secret Weapons Defenses of Insects, Spiders, Scorpions, and Other Many-Legged Creatures 178
T. Eisner, M. Eisner, M. Siegler, reviewed by M. Berenbaum
Darwin 179
N. Eldredge, curator; reviewed by R. S. Winters

POLICY FORUM

Clinical Trials Results Databases: Unanswered Questions 180
C. B. Fisher

PERSPECTIVES

Two Geometric Solutions to a Transporting Problem 182
C. Smith
Where Have All the Transistors Gone? 183
R. P. Cowburn
>>Report p. 205
Running a Clock Requires Quality Time Together 184
J. C. Dunlap
>>Report p. 226
Titan's Zoo of Clouds 186
E. Lellouch
>>Report p. 201
When Proteomes Collide 187
J. S. Bader and J. Chant
>>Report p. 239

CONTENTS continued **>>**

HUMAN FRONTIER SCIENCE PROGRAM (HFSP)

12 quai St. Jean, 67080 STRASBOURG Cedex, FRANCE

E-mail:grant@hfsp.org
Web site: http://www.hfsp.org

OPPORTUNITIES FOR INTERDISCIPLINARY RESEARCH

The Human Frontier Science Program (HFSP) supports **international** collaborations in basic research with emphasis placed on *novel*, **innovative** and **interdisciplinary** approaches to fundamental investigations in the life sciences. Applications are invited for grants to support projects on **complex mechanisms of living organisms**.

CALL FOR LETTERS OF INTENT FOR RESEARCH GRANTS: AWARD YEAR 2007

The HFSP research grant program aims to stimulate novel, daring ideas by supporting collaborative research involving biologists together with scientists from other disciplines such as chemistry, physics, mathematics, computer science and engineering. Recent developments in the biological and physical sciences and emerging disciplines such as computational biology and nanoscience open up new approaches to understanding the complex mechanisms underlying biological functions in living organisms. Preliminary results are not required in research grant applications. Applicants are expected to develop new lines of research through the collaboration; projects must be distinct from applicants' other research funded by other sources. HFSP supports only international, collaborative teams, with an emphasis on encouraging scientists early in their careers.

International teams of scientists interested in submitting applications for support must first submit a letter of intent online via the HFSP web site. The guidelines for potential applicants and further instructions are available on the HFSP web site (www.hfsp.org).

Research grants provide 3 years support for teams with 2 – 4 members, with not more than one member from any one country, unless more members are absolutely necessary for the interdisciplinary nature of the project, which is an essential selection criterion. Applicants may also establish a local **interdisciplinary** collaboration as a component of an international team but will be considered as 1.5 team members for budgetary purposes (see below). The principal applicant must be located in one of the member countries* but co-investigators may be from any other country. Clear preference is given to **intercontinental** teams.

TWO TYPES OF GRANT ARE AVAILABLE

Young Investigators' Grants are for teams of scientists who are all within 5 years of establishing an independent laboratory and within 10 years of obtaining their PhDs.

Program Grants are for independent scientists at all stages of their careers, although the participation of younger scientists is especially encouraged.

Awards are dependent upon team size and successful teams will receive up to $450,000 per year for the whole team.

Important Deadlines:
Compulsory pre-registration for password: **20 MARCH 2006**
Submission of Letters of Intent: **30 MARCH 2006**

**Members are Australia, Canada, the European Union, France, Germany, Italy, Japan, the Republic of Korea, Switzerland, the United Kingdom and the United States.*

SCIENCE EXPRESS

www.sciencexpress.org

APPLIED PHYSICS

Optical Signatures of Coupled Quantum Dots
E. A. Stinaff et al.
A combination of electric field resonances and optical excitation can couple a pair of neutral and charged quantum dots, which can then exchange quantum-stored information.
10.1126/science.1121189

ASTRONOMY

A Radio Pulsar Spinning at 716 Hz
J. W. T. Hessels et al.
A neutron star in the Terzan 5 globular cluster is rotating 15 percent more rapidly than other known pulsars, constraining its radius to about 16 kilometers.
10.1126/science.1123430

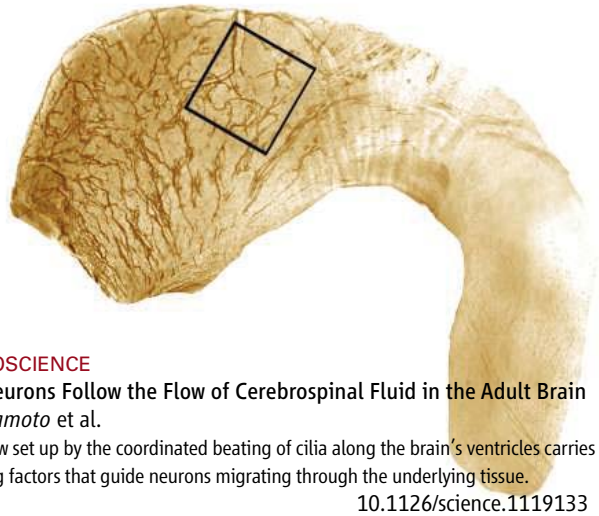

NEUROSCIENCE

New Neurons Follow the Flow of Cerebrospinal Fluid in the Adult Brain
K. Sawamoto et al.
Fluid flow set up by the coordinated beating of cilia along the brain's ventricles carries signaling factors that guide neurons migrating through the underlying tissue.
10.1126/science.1119133

TECHNICAL COMMENT ABSTRACTS

OCEAN SCIENCE

Comment on "Iron Isotope Constraints on the Archean and Paleoproterozoic Ocean Redox State" 177
K. E. Yamaguchi and H. Ohmoto
full text at www.sciencemag.org/cgi/content/full/311/5758/177a

Response to Comment on "Iron Isotope Constraints on the Archean and Paleoproterozoic Ocean Redox State"
O. J. Rouxel, A. Bekker, K. J. Edwards
full text at www.sciencemag.org/cgi/content/full/311/5758/177b

REVIEW

PHYSICS

Plasmonics: Merging Photonics and Electronics at Nanoscale Dimensions 189
E. Ozbay

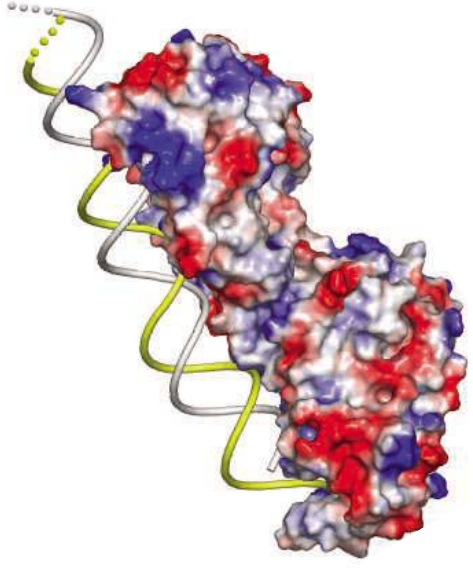

195

BREVIA

ASTRONOMY

Interferometric Coupling of the Keck Telescopes with Single-Mode Fibers 194
G. Perrin et al.
A special type of long optical fibers link between two Keck telescopes allows them to operate as a giant optical interferometer, paving the way for the next generation of optical telescopes.

RESEARCH ARTICLE

STRUCTURAL BIOLOGY

Structural Basis for Double-Stranded RNA Processing by Dicer 195
I. J. MacRae et al.
The RNA binding site of the small RNA–generating enzyme Dicer is located 65 Å from the two RNA cleavage sites, reliably producing ~25-nucleotide RNA fragments.

REPORTS

GEOPHYSICS

The Nature of the 660-Kilometer Discontinuity in Earth's Mantle from Global Seismic Observations of *PP* Precursors 198
A. Deuss, S. A. T. Redfern, K. Chambers, J. H. Woodhouse
Global detection of seismic waves reflected from a major boundary in Earth's mantle implies that the boundary is produced by multiple phase transitions.

PLANETARY SCIENCE

The Latitudinal Distribution of Clouds on Titan 201
P. Rannou, F. Montmessin, F. Hourdin, S. Lebonnois
Simulations suggest that atmospheric circulation alone, without ground sources, can explain the enigmatic distribution of methane and ethane clouds on Titan.
>>Perspective p. 186

CONTENTS continued **>>**

MEDICINAL CHEMISTRY-BASED SMALL MOLECULE DRUG DISCOVERY ENGINE

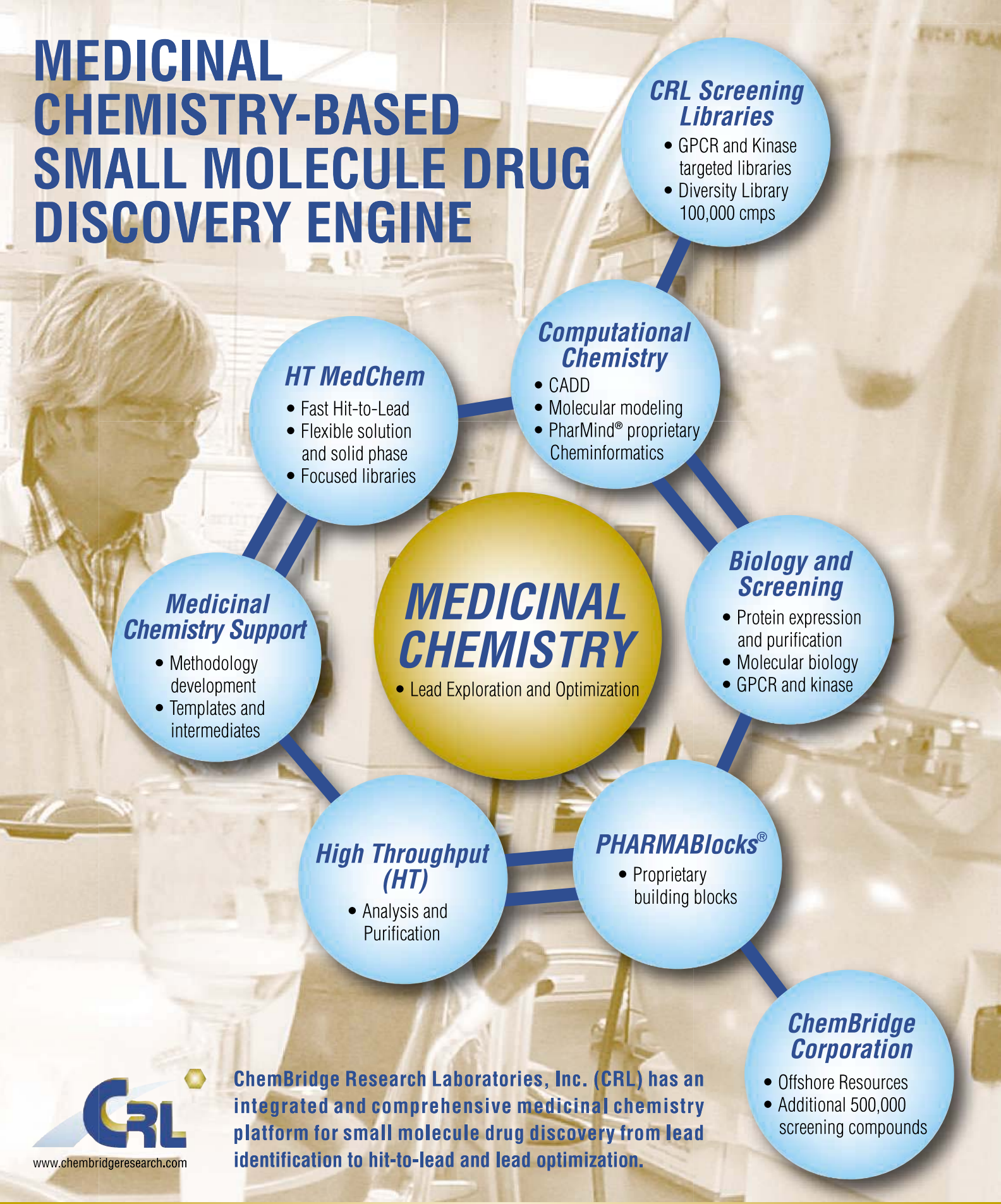

CRL

www.chembridgeresearch.com

ChemBridge Research Laboratories, Inc. (CRL) has an integrated and comprehensive medicinal chemistry platform for small molecule drug discovery from lead identification to hit-to-lead and lead optimization.

For more information: Contact CRL Business Development at business_development@chembridgeresearch.com

REPORTS *CONTINUED...*

APPLIED PHYSICS

Majority Logic Gate for Magnetic Quantum-Dot Cellular Automata 205

A. Imre, G. Csaba, L. Ji, A. Orlov, G. H. Bernstein, W. Porod

A system of coupled nanomagnets, usually used for data storage, can serve as logic gates that are stable at room temperature and therefore useful in magnet-based computer chips.

>>Perspective p. 183

MATERIALS SCIENCE

A Stretchable Form of Single-Crystal Silicon for High-Performance Electronics on Rubber Substrates 208

D.-Y. Khang, H. Jiang, Y. Huang, J. A. Rogers

Silicon is patterned onto elastomeric substrates to give flexible, wavy silicon suitable for making devices and components that can be heavily stretched or compressed.

MATERIALS SCIENCE

Grain Boundary Strengthening in Alumina by Rare Earth Impurities 212

J. P. Buban et al.

Experiments and simulations show that small amounts of yttrium strengthen alumina by forming strong bonds along alumina grain boundaries.

CHEMISTRY

Ion Distributions near a Liquid-Liquid Interface 216

G. Luo et al.

X-ray data show how the distribution of an organic ion along the interface between two liquids depends greatly on the liquids' local molecular structure.

CHEMISTRY

Femtosecond Multidimensional Imaging of a Molecular Dissociation 219

O. Geßner et al.

The precise path followed by electrons and then nuclei in the dissociation of the nitric oxide dimer is mapped out in time and space.

PLANT SCIENCE

A Bacterial Inhibitor of Host Programmed Cell Death Defenses Is an E3 Ubiquitin Ligase 222

R. Janjusevic, R. B. Abramovitch, G. B. Martin, C. E. Stebbins

During infection, pathogenic bacteria mimic and interpolate with biochemical pathways of the host plant.

CIRCADIAN RHYTHMS

PER-TIM Interactions in Living *Drosophila* Cells: An Interval Timer for the Circadian Clock 226

P. Meyer, L. Saez, M. W. Young

Two components of the circadian clock move independently into the nucleus rather than together as a complex, calling into question the current model of the clock.

>>Perspective p. 184

MOLECULAR BIOLOGY

The snoRNA HBII-52 Regulates Alternative Splicing of the Serotonin Receptor 2C 230

S. Kishore and S. Stamm

An exon is included in the mature messenger RNA of a receptor only when a small RNA inhibits a silencer sequence in the precursor RNA.

NEUROSCIENCE

Excitatory Effect of GABAergic Axo-Axonic Cells in Cortical Microcircuits 233

J. Szabadics, C. Varga, G. Molnár, S. Oláh, P. Barzó, G. Tamás

A classic inhibitory neurotransmitter unexpectedly excites axons of cortical neurons, activating local networks.

VIROLOGY

Long-Term Transmission of Defective RNA Viruses in Humans and *Aedes* Mosquitoes 236

J. Aaskov, K. Buzacott, H. M. Thu, K. Lowry, E. C. Holmes

An inactive, defective form of the dengue fever virus appropriates proteins from normal viruses to replicate and is maintained through generations of infection and transmission.

SYSTEMS BIOLOGY

Herpesviral Protein Networks and Their Interaction with the Human Proteome 239

P. Uetz et al.

Upon infection of a host cell, the protein interaction networks of herpesviruses change so that they more closely resemble those of the host cells.

>>Perspective p. 187

CELL BIOLOGY

Magnetosomes Are Cell Membrane Invaginations Organized by the Actin-Like Protein MamK 242

A. Komeili, Z. Li, D. K. Newman, G. J. Jensen

Bacteria that sense magnetic fields arrange their magnetite-containing membrane invaginations along cytoskeleton-like tracks.

AAAS
ADVANCING SCIENCE, SERVING SOCIETY

SCIENCE (ISSN 0036-8075) is published weekly on Friday, except the last week in December, by the American Association for the Advancement of Science, 1200 New York Avenue, NW, Washington, DC 20005. Periodicals Mail postage (publication No. 484460) paid at Washington, DC, and additional mailing offices.

Domestic individual membership and subscription (51 issues): $139 ($74 allocated to subscription). Domestic institutional subscription (51 issues): $650; Foreign postage extra: Mexico, Caribbean (surface mail) $55; other countries (air assist delivery) $85. First class, airmail, student, and emeritus rates on request. Canadian rates with GST available upon request, GST #1254 88122. Publications Mail Agreement Number 1069624. **Printed in the U.S.A.**

Change of address: Allow 4 weeks, giving old and new addresses and 8-digit account number. **Postmaster:** Send change of address to *Science*, P.O. Box 1811, Danbury, CT 06813–1811. **Single-copy sales:** $10.00 per issue prepaid includes surface postage; bulk rates on request.

Science is indexed in the *Reader's Guide to Periodical Literature* and in several specialized indexes.

CONTENTS continued >>

More Published

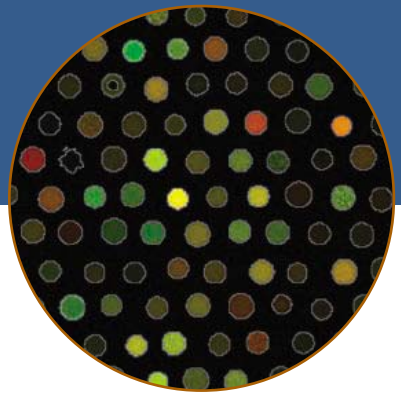

INSTRUMENTS

SOFTWARE

INFORMATICS

In a recent PubMed survey, more publications referenced GenePix® from Molecular Devices than any other slide-based microarray scanner platform. Why? Because researchers trust the results they get with GenePix scanners and Acuity® analysis software. When you trust the tools you use, you have the confidence to publish your results.

Obtaining reliable data requires high performance instruments and software that are easy to use and increase your productivity. With Molecular Devices' microarray scanning solutions, we give you that and more—so you can get more published.

Microarray Scanning

- GenePix Autoloader 4200AL: 36-slide capacity with automation
- GenePix Professional 4200A: four-laser flexibility and upgradeability
- GenePix 4000B: fastest two-laser scanner in existence
- GenePix Personal 4100A: affordable, quality two-laser scanning

Microarray Analysis Software

- GenePix Pro 6 microarray image analysis software
- Acuity 4 microarray informatics software

Expect more. We'll do our very best to exceed your expectations. For more information, visit our web site or see us at LabAutomation 2006, Booth #541.

Molecular Devices

tel. 800-635-5577 | www.moleculardevices.com

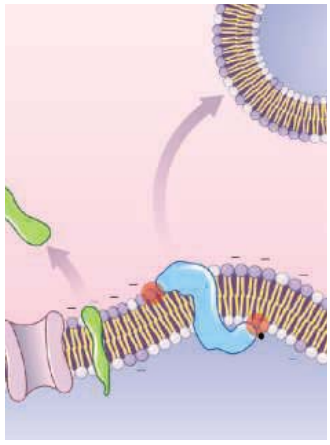

Loss of phospholipid asymmetry.

SCIENCE'S **STKE**

www.stke.org SIGNAL TRANSDUCTION KNOWLEDGE ENVIRONMENT

PERSPECTIVE: Phosphatidylserine and Signal Transduction—Who Needs Whom?
M. C. Martínez, C. Kunzelmann, J.-M. Freyssinet
The externalization of phosphatidylserine may constitute a novel signaling process in nonapoptotic lymphocytes.

GLOSSARY
Now even more terms link to detailed information in the Connections Map database of cell signaling.

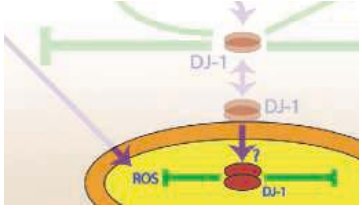

Understanding DJ-1.

SCIENCE'S **SAGE KE**

www.sageke.org SCIENCE OF AGING KNOWLEDGE ENVIRONMENT

PERSPECTIVE: Lessons from *Drosophila* Models of DJ-1 Deficiency
D. J. Moore, V. L. Dawson, T. M. Dawson
Fly models generally fail to exhibit key features of Parkinson's disease.

NEWS FOCUS: Chain of Command
M. Leslie
Study fingers abettors of life-stretching protein.

SCIENCE**NOW**

www.sciencenow.org DAILY NEWS COVERAGE

Ancient Harbors Rise Again
Archaeologists unearth history of Phoenician sea ports.

Are We Descended from Cannibals?
New study questions claim that early humans were people eaters.

Strange Quarks Make for Chunky Stars
Unstable elements texture the surface of neutron stars.

At odds with your mentor?

SCIENCE **CAREERS**

www.sciencecareers.org CAREER RESOURCES FOR SCIENTISTS

US: Bad Mentors
L. Puljak
Job postings never warn "Postdoctoral position with bad mentor available."

ITALY: The Need for Mobility
C. Berrie
Italian scientist Maria Pia Cosma felt she needed to spend time abroad in a high-profile lab.

MISCINET: Ph.D. Life—Surviving the Early Years
E. Francisco
A National Research Council research associate talks about the challenges of transitioning to a doctoral candidate.

US: A Brit in Yankeeland
GrantDoctor
The GrantDoctor discusses funding for a UK graduate student who wants to postdoc in the U.S.

GERMANY: Scientists in the Public Service
H. J. Neubert
The German civil service offers a range of careers for scientists interested in public service.

MISCINET: Ancestors of Science—Meredith Gourdine
C. Parks
An African-American physicist and engineer developed commercial uses for electrogasdynamics.

www.roche-applied-science.com

FuGENE® HD Transfection Reagent

Powerful Protein Expression

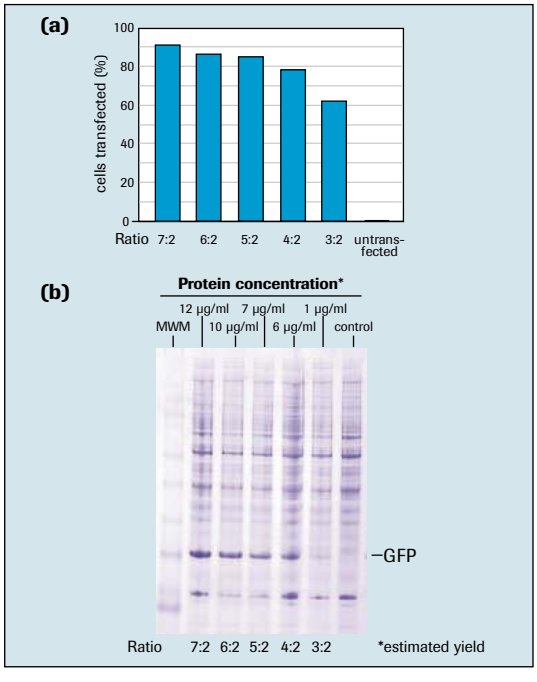

Figure 1: GFP expression in HEK-293 EBNA cells. HEK-293 EBNA suspension-adapted cells were transfected with plasmid DNA for GFP following the recommended protocol, using ratios of 7:2, 6:2, 5:2, 4:2, and 3:2 (µl FuGENE® HD Transfection Reagent:µg plasmid DNA). The percentage of cells transfected (a) was determined 28 hours post transfection and quantity of GFP protein (b) was estimated from the Coomassie Blue-stained gel at 72 hours post transfection.

FuGENE® HD Transfection Reagent is a non-liposomal, multicomponent reagent suitable for transfection of animal and insect cells for protein expression. The combination of a rapid protocol, activity in up to 100% serum, and effectiveness with many cell lines commonly used for protein expression makes it the product of choice for this application.

Achieve excellent transfection efficiency in some cell lines that are not transfected well by other reagents.

Obtain high levels of protein expression in many common adherent and suspension-adapted animal cell lines, including HeLa, NIH/3T3, COS-1, COS-7, CHO-K1, CHO-S, Hep G2, MCF-7, HEK-293 (Figure 1), and insect cell lines such as High Five and Sf9.

Minimize cytotoxicity or changes in morphology by transfecting cells at high densities.

Save time by eliminating the need to change media; the reagent functions exceptionally well in up to 100% serum.

Employ a reagent that is free of animal- or human-derived components.

For more information, visit ***www.roche-applied-science.com/transfection*** or contact your local sales representative.

Roche Diagnostics

Roche Diagnostics GmbH
Roche Applied Science
68298 Mannheim
Germany

EDITED BY STELLA HURTLEY AND PHIL SZUROMI

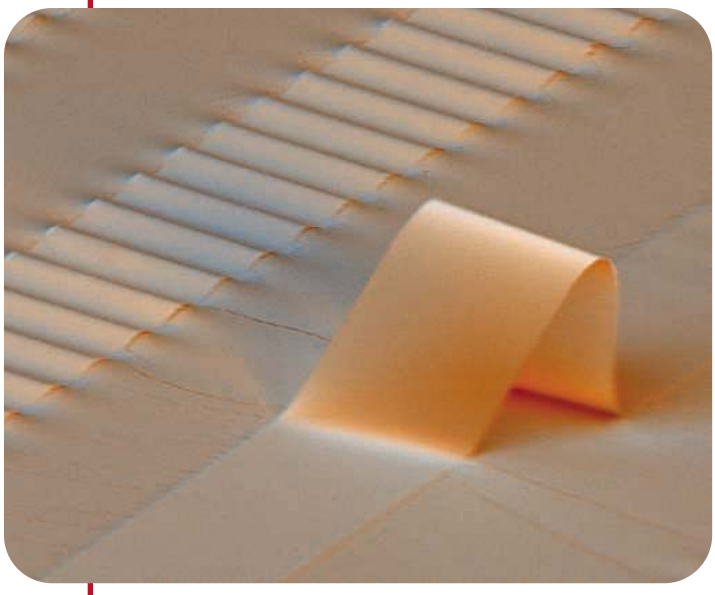

Silicon Does the Wave

Flexible materials with good electronics properties are of interest for a number of applications, including sensors and paperlike displays. Typically, the materials used are organic, because conventional semiconductor substrates, such as silicon wafers, are too thick and brittle to bend readily. **Khang *et al.*** (p. 208, published online 15 December 2005) have deposited single-crystal ribbons of silicon onto prestretched rubber made of poly(dimethyl siloxane). When the stress is released, the silicon takes on a wavy form, which is then amenable to either stretching or compression. This material was used to build a number of basic electronic components such as transistors and diodes.

Plasmons in Optoelectronics

Future electronic technology is expected to combine the size and speed of nanoscale electronic and optical circuitry. However, the length scale of electronic devices responsible for switching and amplifying signals is now below that of the wavelength of light, and the even larger waveguides, for carrying and transferring that signal. **Ozbay** (p. 189) discusses the possibilities and challenges of using surface plasmons, which are collective excitations of electrons caused by light absorption on the surface, to integrate electronics and photonics on chips.

Titan's Clouds

By modeling the circulation patterns of the thick hazy atmosphere of Titan, Saturn's largest moon, **Rannou *et al.*** (p. 201; see the Perspective by **Lellouch**) explain the formation of different types of clouds that have been observed by telescopes and spacecraft. The general circulation model, which includes cloud microphysics, mimics the distribution of methane and ethane clouds seen in Titan's nitrogen-rich atmosphere and produces both a permanent south polar cloud and sporadic clouds at more temperate latitudes.

Magnetic Logic Gates

A computer architecture based on quantum cellular automata (QCA) can be built from a series of identical, simple, and bistable units that are coupled together either electrostatically (EQCA) or magnetically (MQCA). Whereas EQCA operates only at cryogenic temperatures, the higher coupling energies in MQCA should allow operation at higher temperatures. **Imre *et al.*** (p. 205; see the Perspective by **Cowburn**) fabricated and demonstrate room-temperature operation of a three-input majority logic gate (the basic building block for MQCA logic) from a system of coupled nanomagnets. They calculate that a chip with 1010 such gates operating at 100 megahertz would dissipate less than 0.1 watt of heat.

Combating Creep

Ceramics can deform at grain boundaries, and for demanding operation at high temperatures, impurities are deliberately added to prevent deformation. **Buban *et al.*** (p. 212) have used *Z*-contrast transmission electron microscopy to locate the positions of yttrium (Y) atoms in a grain boundary in a bicrystal of alumina. The Y ions form more and stronger bonds with their neighbors than occurs with aluminum in the undoped bicrystal. These stronger bonds appear to inhibit grain boundary sliding and thus account for the significant drop in the creep rate upon yttrium doping.

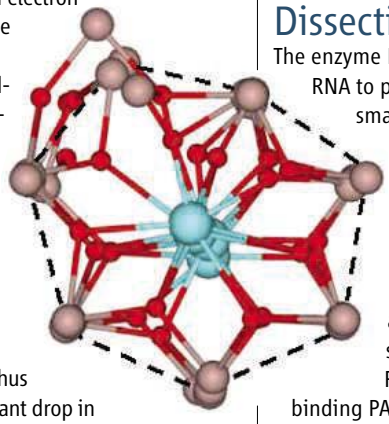

Imaging Reactions

For many rapid chemical reactions, ultrashort laser pulses have revealed precisely in what order, and at what rate, individual bonds are made and broken. However, molecules in gas or solution phase are in constant, random motion. Thus, the data often emerge averaged over every orientation, and offer little insight into the spatial characteristics of the reaction. **Geßner *et al.*** (p. 219, published online 15 December 2005) address this limitation in a study of photo-induced dissociation of the NO dimer. They simultaneously measure electron energy, through ionization as well as the angular distributions of ejected electrons and ionic products. With femtosecond time resolution, they uncovered the geometrical evolution of the dimer's electronic charge distribution, and then the reorientation of the nuclei that liberated the NO fragments.

Dissecting Dicer

The enzyme Dicer cleaves double-stranded (ds) RNA to produce ~22 nucleotide (nt) long small interfering (si) RNAs, the effector molecules that underpin RNA interference (RNAi). **MacRae *et al.*** (p. 195) have determined the structure of full-length Dicer from the eukaryote *Giardia intestinalis*. *Giardia* Dicer is a much abbreviated version of human Dicer, consisting of little more than the dual RNase III domains and an RNA-binding PAZ domain. Nonetheless, it cleaves dsRNA into the expected 25-nt siRNA fragments. The authors liken the *Giardia* Dicer structure to a hatchet; the RNaseIII domains are spaced to generate the characteristic siRNA 3′ overhang—forming the "blade"—that is connected through the long α-helical "handle" to the RNA-binding PAZ domain at the base. The distance from the active sites of the RNaseIII

Continued on page 143

CREDITS (TOP TO BOTTOM): BECKMAN INSTITUTE AND SEITZ MATERIALS RESEARCH LABORATORY, UNIVERSITY OF ILLINOIS; BUBAN *ET AL.*

The Best Laid Plans of Men with Mice…

Researchers have far too little time –

Which means they often end up with far too many mice. With Transnetyx, you can help your researchers manage their populations and advance their research at the same time.

Fast, accurate 24 and 72-hour genotyping services from Transnetyx separate the useful animals from the freeloaders, so your researcher can get that mouse off his back.

For more information and our free trial offer, visit www.transnetyx.com

Transnetyx℠
Serving Research. Saving Time.

WWW.TRANSNETYX.COM
1-888-321-2113

Continued from page 141

domains to the RNA-binding pocket of the PAZ domain, 65 angstroms, approximates to 25 base pairs of A-form dsRNA.

Keeping an Eye on the Clock

As part of the cycle of intrinsic circadian clock, two proteins, PER and TIM, are thought to slowly associate in the cytoplasm of cells. This process takes 4 to 6 hours, after which the dimers enter the nucleus of the cell and interact with other clock components and close one of the clock's feedback loops. **Meyer *et al.*** (p. 226; see the Perspective by **Dunlap**) labeled both PER and TIM in single living *Drosophila* cells with tags that emit a fluorescent signal when the proteins are in close proximity. The proteins did indeed associate with the expected time course, but, surprisingly, PER and TIM dissociated before moving to the nucleus. The extent of nuclear localization was independent of the concentrations of PER and TIM in the cytoplasm. Thus, fundamental assumptions about how the circadian clock keeps time need to be revisited.

An Exciting Inhibitory Neuron

Discovered 30 years ago, axo-axonic or Chandelier cells are the most specific inhibitory neurotransmitter γ-aminobutyric acid (GABA)ergic cell type known and are regularly used in textbooks to illustrate the strategic placement of inhibition on the axon. **Szabadics *et al.*** (p. 233) show that instead of inhibiting postsynaptic cells, axo-axonic cells can actually excite postsynaptic cells, which leads to an unprecedented phenomenon in the cortex: A single GABAergic cell that can reliably activate the cortical network.

Defective Dengue

Dengue virus infects an estimated 50 million people throughout the tropics and causes explosive outbreaks triggered by variant strains. There are several strains of virus involved and, paradoxically, a defective strain is now in circulation. **Aaskov *et al.*** (p. 236) propose that this defective form persists through complementation—defective viruses exploit the proteins from functional viruses that infect the same cell. When enough hosts have multiple infections with different strains, defective viral strains can persist and influence the epidemiology of the disease. For example, in Myanmar, the variant's spread accompanied a decline in another related strain.

Monitoring Magnetosomes

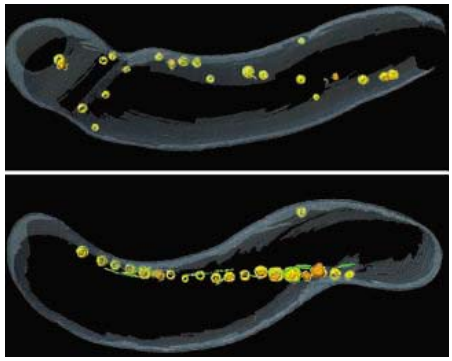

Magnetosomes are the small magnetite-containing membranes found in certain bacteria. **Komeili *et al.*** (p. 242, published online 22 December 2005) now present evidence that magnetosomes represent invaginations from the bacterial plasma membrane, rather than, as previously assumed, individual magnetite-containing vesicles. Furthermore, magnetosomes are aligned within the cell through the agency of an actin-like filamentous protein. Magnetosome assembly and intracellular organization may represent a stepping stone in intracellular complexity between organelle-less bacteria and organelle-rich eukaryotes.

Protein Network Topologies During Viral Infection

Virus infection triggers dramatic changes in the host and in the infecting virus. **Uetz *et al.*** (p. 239, published online 8 December 2005; see the Perspective by **Baker and Chant**) used yeast-two-hybrid analysis of a subset of the viral proteins and found that two herpesviruses, Kaposi sarcoma–associated herpesvirus and varicella-zoster virus, shared protein interaction network topologies. The observed topologies were distinct from the cellular networks that have been studied so far. Viral networks resemble single, highly coupled modules, whereas cellular networks are organized in separate functional submodules. The authors used simulations to show that infection may result in a change to the viral protein interaction network that renders its topology more similar to that of the host cell.

CREDIT: KOMEILI *ET AL.*

SCIENCE & ENGINEERING

VISUALIZATION CHALLENGE

CALL FOR ENTRIES

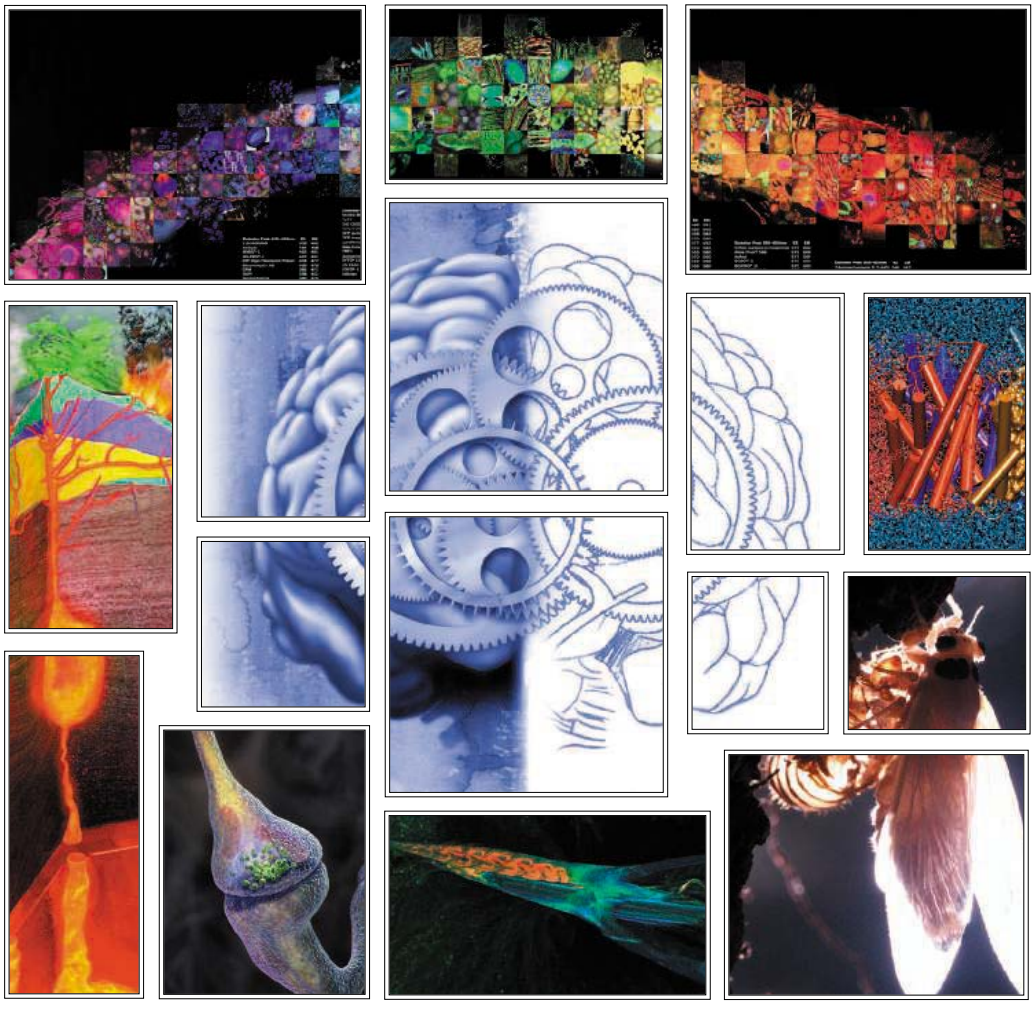

SCIENCE AND ENGINEERING'S MOST POWERFUL STATEMENTS ARE NOT MADE FROM WORDS ALONE

When the left brain collaborates with the right brain, science emerges with art to enhance communication and understanding of research results—illustrating concepts, depicting phenomena and drawing conclusions.

The National Science Foundation (NSF) and the journal *Science*, published by the American Association for the Advancement of Science, invite you to participate in the fourth annual Science and Engineering Visualization Challenge. The competition recognizes scientists, engineers, visualization specialists and artists for producing or commissioning innovative work in visual communication.

ENTRY DEADLINE: MAY 31, 2006

Award categories: Photographs, Illustrations, Interactive Media, Non-Interactive Media and Informational Graphics. Winners in each category will be published in the Sept. 22, 2006 issue of *Science* and *Science* Online, and will be displayed on the NSF Web site.

Complete Entry Information: www.nsf.gov/news/special-reports/scivis/index AND www.sciencemag.org/prizes/

Donald Kennedy is Editor-in-Chief of *Science*.

Good News—and Bad

THIS YEAR, FOR THE FIRST TIME IN HALF A CENTURY, THE FIRST DAY OF HANUKAH AND CHRISTMAS DAY converged—good news for my family mix. But just before that day, the *Science* family found itself absorbed in a different temporal convergence, one that brought both good news and bad to us and to our readers in the scientific community. The troubling story of Professor Woo Suk Hwang and his colleagues appeared everywhere, as questions about a paper they had published in this journal unfolded amid a welter of charges, countercharges, proposed retractions, and two investigations. At about the same time, on the front page above the fold in the *New York Times*, appeared Judge John Jones' opinion in the Dover, Pennsylvania, school board case.


The New York Times

Intelligent Design Derailed

By now, the Christian conservatives who once minated the school board in Dover, Pa., ought to their recklessness in forcing biology classes to about "intelligent design" as an alternative to theory of evolution. Not only were they voted off school board by an exasperated public last No

Christian values, who combined to drive the board to adopt an imprudent and unconstitutional policy. Judge Jones's decision was a striking repudiation of intelligent design, given that Dover's policy was minimally intrusive on classroom teaching. Ad

For most of the scientific community, this second story relieved a longstanding concern. Some school boards (famously in Kansas and Pennsylvania, but also in many other U.S. states) had voted either to limit the teaching of evolution in science classes or to introduce it along with alternative explanations that were essentially religious in character. The rising tide of evangelical Christianity and its alliance with a conservative political movement seemed to foreshadow a national suspicion of science or a deep confusion about what science is or isn't, or possibly both.

The Dover decision was a decisive, elegantly crafted resolution of the question before the court. Was intelligent design (ID) a new proposal, generated by the school board for consideration by students and teachers as an alternative to evolution, based on scientific grounds? Or was it instead a Trojan Horse proxy for the older notion of creationism? Judge Jones said, in no uncertain terms, that ID was not science, but rather creationism redux, and that it did not belong in a science classroom. He added that its advocates, "who so staunchly and proudly touted their religious convictions in public, would time and again lie . . . to disguise the real purpose behind the ID Policy." The decision, in which the losers were charged attorneys' fees, can be found at http://www2.ncseweb.org/wp/. It's worth reading.


The Washington Post

Stem Cell Advance Is Fully Refuted

Investigator Says Korean's Colonies Do Not Exist

By Rick Weiss
Washington Post Staff Writer

The scandal surrounding disgraced South Korean stem cell researcher Hwang Woo Suk deepened yesterday as an investigatur

The other story is a deeply disappointing one: for the scientists who did the work; for the scientific community (and especially those who have been excited by the therapeutic prospects of stem cell science); and for this journal. At this writing, we don't have a final report from an investigation now underway at Seoul National University. But preliminary findings and admissions by Hwang point to considerable fraud, leaving open only the question of whether some of the findings published in *Science* and other journals by Hwang's research group may survive.

A journal cannot go into authors' laboratories in search of fraud. But we can and do encourage appropriate authorities to conduct investigations, and we supply information freely as investigations proceed. More actively, we are committed to examining our processes and ourselves in an effort to extract lessons for the future. In examining the reports by reviewers of the Hwang papers, we saw no reason to lack confidence in the authenticity of the data. But there is more to do, and at the end of this process we will be able to report to our readers and others what we have learned about how we might modify our treatment of papers with unusual potential impact.

One question we have been asked by mainstream journalists is whether this is an indictment of the peer review system. Not at all; we believe strongly in the peer review system, but we have never thought it infallible. Carefully reviewed studies sometimes turn out to be wrong because later attempts at repetition fail. But peer review requires authors to provide more data and more confirming material, making it likelier that careful efforts at confirmation will follow.

Fraud is something quite different, and very hard to detect. Of course, reviewers or editors might be sent to the authors' labs to look at the notebooks, imposing costly and offensive oversight on the vast majority of scientists in order to catch the occasional cheater. That's a bad idea. The reporting of scientific results is based on trust. It's better to trust our colleagues, despite the fact that on rare occasions one of them might disappoint other scientists and those hoping for cures.

–Donald Kennedy

10.1126/science.1124498

How do you isolate mRNA?

Introducing the SpyLine™ Poly A+ Capture Kit!

The SpyLine Poly A+ Capture Kit offers a simple, rapid and cost-effective method for isolating poly A+ mRNA from cultured mammalian cells for direct QRT-PCR.

The SpyLine Poly A+ Capture Kit features a 96-well PCR plate coated with oligo (dT) for selective capture of poly A+ mRNA from crude mammalian cell lysates. Reagents can be added directly to the capture plate for subsequent RT-PCR or real-time quantitative RT-PCR cycling and analysis.

Superior Sensitivity for siRNA knockdown

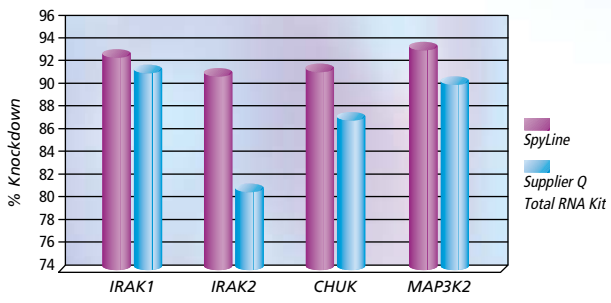

Figure 1. Percent knockdown for targets as measured by QRT-PCR. The figure above is a comparison of percent knockdown as detected for each target. One plate was purified by the SpyLine Poly A+ Capture Kit, while the other was purified using Supplier Q's 96-well Total RNA Purification Kit. Quantitative RT-PCR was run on the 2 sets of purified RNA using Applied Biosystems TaqMan® Gene Expression Assays.

Rapidly isolate poly A+ mRNA for direct RT-PCR or real-time QRT-PCR

Superior tool for gene expression analysis and knockdown measurement

Optimized for high-throughput platforms

*For more information visit us at Lab**Automation 2006, booth #456** or online at: **sigma-aldrich.com/spyline***

sigma-aldrich.com

LEADERSHIP IN LIFE SCIENCE, HIGH TECHNOLOGY AND SERVICE
SIGMA-ALDRICH CORPORATION • BOX 14508 • ST. LOUIS • MISSOURI 63178 • USA

SIGMA®

BIOCHEMISTRY

Lifting a Switch

Two-component systems enable microbes to respond to environmental conditions. Signal transduction begins when a dimeric integral membrane protein senses an external signal, and one of the monomers phosphorylates the other on a histidine residue. This phosphoryl group is then transferred to the cytosolic response regulator protein, which initiates changes in gene expression. *Salmonella typhimurium* PhoPQ promotes virulence of this pathogen in humans, and the activity of the sensor component PhoQ can be repressed by divalent cations, such as calcium and magnesium.

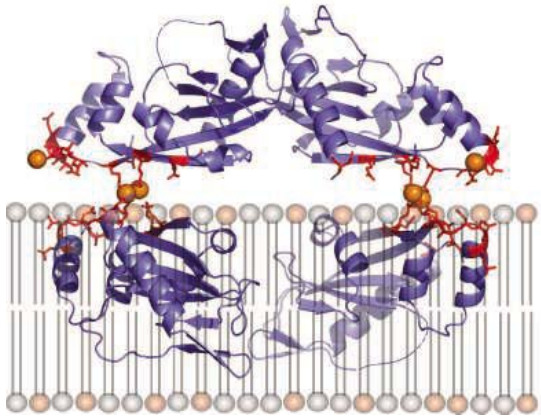

Model of the crystallographic tetramer, with the calcium ions (orange) located between the planar surface of the PhoQ dimer and a superimposed lipid bilayer.

Cho *et al.* describe the structure of the external domain of PhoQ, with four monomers in the asymmetric unit of the crystal. They find that two of the monomers associate in a fashion similar to what would be expected for the in vivo PhoQ dimer and that together they display a planar surface rich in acidic residues. Biochemical and structural experiments pinpoint at least three calcium-binding sites per monomer on this surface, which would allow the dimer to lie flat on top of the negatively charged head groups of the lipid bilayer. This positioning leads the authors to propose that displacement of the divalent ions (for instance, by cationic antibiotic peptides) would trigger a lever-like movement of the sensor domain up off of the membrane surface, thereby turning on the kinase. — GJC

J. Mol. Biol. 10.1016/j.jmb.2005.12.032 (2005).

IMMUNOLOGY

Stress and Immunity

Our psychological states influence our physical health, not least through their effects on the immune system. Nevertheless, how the nervous and immune systems interact in the context of stress or depression remains an open question. Wheway ***et al.*** have investigated the role of neuropeptide Y (NPY), a regulator produced by sympathetic nerves that innervate secondary lymphoid organs. T cells lacking the NPY receptor Y1 responded considerably more vigorously to activation in culture than did Y1-positive T cells. This hyperreactivity was evidenced as an increase in the severity of pathology caused by activating these cells in a mouse model of colitis. In contrast,

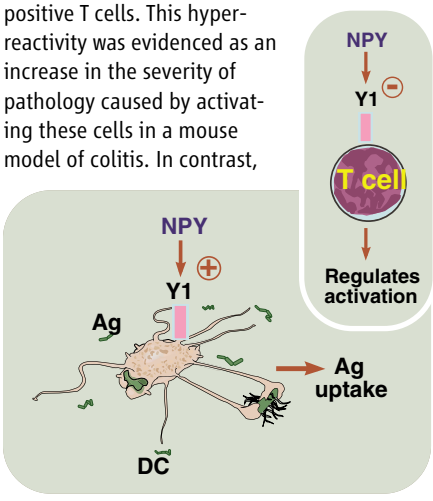

Cell-type–specific effects of NPY.

CREDITS: (TOP) CHO *ET AL.*, *J. MOL. BIOL.* 10.1016/J.JMB.2005.12.032 (2005); (BOTTOM) WHEWAY *ET AL.*, *J. EXP MED.* **202**, 1527 (2005)

Y1-deficient mice were themselves relatively resistant to inflammation induced by activated T helper-1 cells, reflecting an apparent defect in dendritic cell (DC) function. One explanation for these seemingly divergent results is that NPY mediates distinct effects on different cells of the immune system. Thus, although T cells can be impeded directly through Y1 receptor signaling, they can also be stimulated indirectly through NPY-assisted activation of the antigen (Ag)–presenting cell function. The mechanistic basis of this dichotomy may further understanding of the neuroimmune interface and yield therapeutic benefits. — SJS

J. Exp. Med. **202**, 1527 (2005).

CELL BIOLOGY

Pulling into a Rest Stop

The recent explosion of research on the interaction of small RNAs with messenger RNAs (mRNAs), which can lead either to cleavage of the double-stranded RNA complex or to translational repression, has intersected with studies of the life cycles of mRNAs, which in some cases spend part of their time in cytoplasmic processing bodies in a translationally dormant state, before degradation or reactivation. Beliakova-Bethell ***et al.*** have observed that the protein and RNA components of the yeast retrovirus-like element Ty3 congregate in cytoplasmic foci that also contain nascent virus-like particles. These sites turn out to be a way station for other proteins already shown to reside in processing bodies, among them Dhh1, a helicase that is involved in translational repression and is required for Ty3 retrotransposition. Hence it appears that the demands of assembling proteins onto an RNA genome may be facilitated by the translational stasis imposed within processing bodies. — GJC

RNA **12**, 94 (2006).

GEOLOGY

Powered by Hydrogen

The evidence for earliest life on Earth comes not from fossils but from shifts in the carbon isotopes of preserved and altered carbonate minerals or rocks. In younger rocks, possible isolated bacterial fossils have been described. The metabolism of these early fossils has been uncertain, and some have suggested that they resemble cyanobacteria, implying at least some oxygenic photosynthesis and a rapid and early evolution of this biochemical pathway. One of the earliest indicators of more widespread life is in 3.4-billion-year-old rocks in Australia that contain abundant layered carbonaceous matter interpreted to be fossil microbial photsynthetic mats.

Tice and Lowe have examined the geochemistry of these early mats in order to decipher their origin and likely metabolism. The reduced oxidation state of iron and trace elements, notably cerium, indicates that the water column was

Science's 2005 Breakthrough of the Year

Evolutionary Biology

Watch the Breakthrough of the Year video at
www.sciencemag.org/sciext/btoy2005

Get the insider's perspective on the editorial featured in this issue of *Science*...interviews with researchers on their extraordinary findings on how evolution proceeds and an insightful commentary by Donald Kennedy—*Science*'s Editor-in-Chief.

FREE ACCESS to this issue until 31 March 2006

Produced by Biocompare and *Science*

biocompare®
The Buyer's Guide for Life Scientists.™

Science
AAAS

highly anoxic. Tice and Lowe argue that uranium mobility was controlled by carbonate, not by oxygen as has been proposed. Together these data imply that the mats represent anoxygenic photosynthesis and a metabolism based on hydrogen gas as the source of electrons. — BH

Geology **34**, 37 (2006).

MATERIALS SCIENCE

Beading a Band

Plastic deformation in semicrystalline or amorphous materials is often restricted to very thin shear bands. For metallic glasses, these bands are particularly important because the associated work-softening leads to a plastic instability in tension that limits the potential of these materials as structural materials. Despite the appearance of liquid-like features at fracture surfaces, there is some controversy over the local temperature rise at the bands.

Lewandowski and Greer use a fusible coating and find that the local temperature can reach as high as a few thousand Kelvin over a few nanoseconds. Specimens were coated with a thin film of tin, which formed hemispherical beads when heated. By measuring the half-width of the beads or their volumes, the authors were able to calculate the enthalpy required to form the beads, and thus the local temperature flux during specimen deformation. The same calculations, however, predict that the shear bands should be much larger than the 10 to 20 nm typically observed. Thus, the authors conclude that although local heating is important in understanding the changes that take place at the bands, the thickness of the bands is controlled by local structural changes, such as the formation of nanocrystals and voids. — MSL

Nat. Mater. **5**, 15 (2006).

CHEMISTRY

Coated Catalysts

One cause of deactivation in heterogeneous catalysts is that the metallic nanoparticles can aggregate over time, leading not only to a loss of active surface but also to less favorable electronic or support interactions that depend on particle size. Jiang and Gao have explored the use of hyperbranched polymers for encapsulating palladium nanoparticles in the context of supported catalysts, in this case by functionalizing the channels in mesoporous silica SBA-15 with polyamidoamine dendrimers. The selectivity of hydrogen-ation of allyl alcohol to 1-propanol increased for generations three and four of the dendrimer versus generations one and two, and the formation of acetone was about a factor of 4 lower for the generation-three catalyst versus Pd supported on alumina. The catalysts retained their activity after several rounds of reuse or after storage for 1 month under ambient conditions. — PDS

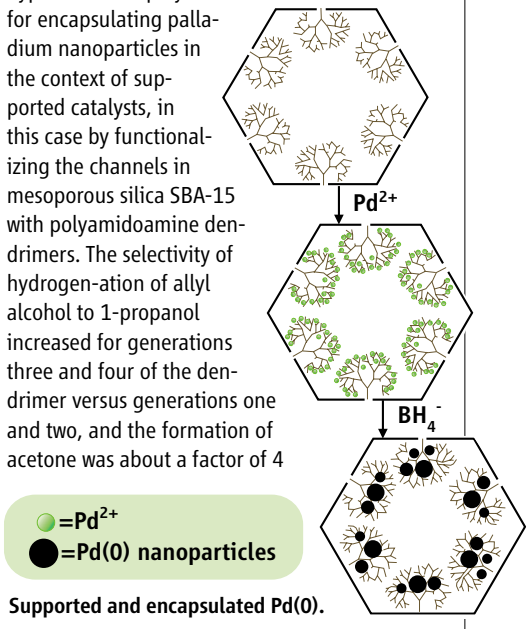

Supported and encapsulated Pd(0).

J. Am. Chem. Soc. 10.1021/ja056424g (2005).

edited by Gilbert Chin

Science stke AAAS

www.stke.org

<< Not Recognizing Ourselves

Toll-like receptors (TLRs) recognize conserved motifs in microbial molecules, enabling them to initiate immune responses against pathogens. Whereas most TLRs are found on the cell surface, those that recognize bacterial and viral nucleic acids are inside. Barton *et al.* investigated the functional importance of the endosomal localization of TLR9, a TLR that is activated by DNA containing unmethylated CpG motifs, which occur frequently in bacterial and viral DNA. Immunofluorescence analysis of chimeric receptors containing the transmembrane or cytosolic domains of TLR9 or TLR4 (which is found on the plasma membrane) revealed that localization depended on the transmembrane domain. TLR9N4C, a chimeric receptor made of the TLR9 ectodomain and the TLR4 cytosolic and transmembrane domains, localized to the cell surface. Dendritic cells expressing TLR9N4C responded to CpG DNA as effectively as cells expressing TLR9 did. However, dendritic cells expressing TLR9N4C, unlike those expressing TLR9, failed to respond to herpes simplex virus; moreover, macrophages expressing TLR9N4C, but not macrophages expressing TLR9, were stimulated by exposure to extracellular mammalian DNA. Thus, the authors propose that the intracellular localization of TLR9 may be critical to prevent it seeing self DNA. — EMA

Nat. Immunol. **7**, 49 (2006).

CREDITS: JIANG AND GAO, *J. AM. CHEM. SOC.* 10.1021/JA056424G (2005)

www.sciencemag.org

Science

1200 New York Avenue, NW
Washington, DC 20005
Editorial: 202-326-6550, FAX 202-289-7562
News: 202-326-6500, FAX 202-371-9227

Bateman House, 82-88 Hills Road
Cambridge, UK CB2 1LQ
+44 (0) 1223 326500, FAX +44 (0) 1223 326501

Subscription Services For change of address, missing issues, new orders and renewals, and payment questions: 800-731-4939 or 202-326-6417, FAX 202-842-1065. Mailing addresses: AAAS, P.O. Box 1811, Danbury, CT 06813 or AAAS Member Services, 1200 New York Avenue, NW, Washington, DC 20005

Institutional Site Licences please call 202-326-6755 for any questions or information

Reprints: Author Inquiries 800-635-7181
Commercial Inquiries 803-359-4578
Corrections 202-326-6501

Permissions 202-326-7074, FAX 202-682-0816

Member Benefits Bookstore: AAAS/BarnesandNoble.com bookstore www.aaas.org/bn; Car purchase discount: Subaru VIP Program 202-326-6417; Credit Card: MBNA 800-847-7378; Car Rentals: Hertz 800-654-2200 CDP#343457, Dollar 800-800-4000 #AA1115; AAAS Travels: Betchart Expeditions 800-252-4910; Life Insurance: Seabury & Smith 800-424-9883; Other Benefits: AAAS Member Services 202-326-6417 or www.aaasmember.org.

science_editors@aaas.org	(for general editorial queries)
science_letters@aaas.org	(for queries about letters)
science_reviews@aaas.org	(for returning manuscript reviews)
science_bookrevs@aaas.org	(for book review queries)

Published by the American Association for the Advancement of Science (AAAS), *Science* serves its readers as a forum for the presentation and discussion of important issues related to the advancement of science, including the presentation of minority or conflicting points of view, rather than by publishing only material on which a consensus has been reached. Accordingly, all articles published in *Science*—including editorials, news and comment, and book reviews—are signed and reflect the individual views of the authors and not official points of view adopted by the AAAS or the institutions with which the authors are affiliated.

AAAS was founded in 1848 and incorporated in 1874. Its mission is to advance science and innovation throughout the world for the benefit of all people. The goals of the association are to: foster communication among scientists, engineers and the public; enhance international cooperation in science and its applications; promote the responsible conduct and use of science and technology; foster education in science and technology for everyone; enhance the science and technology workforce and infrastructure; increase public understanding and appreciation of science and technology; and strengthen support for the science and technology enterprise.

Information for Contributors

See pages 102 and 103 of the 6 January 2006 issue or access www.sciencemag.org/feature/contribinfo/home.shtml

EDITOR-IN-CHIEF **Donald Kennedy**
EXECUTIVE EDITOR **Monica M. Bradford**
DEPUTY EDITORS **R. Brooks Hanson, Katrina L. Kelner**
NEWS EDITOR **Colin Norman**

Editorial supervisory senior editors Barbara Jasny, Phillip D. Szuromi; **senior editor/perspectives** Lisa D. Chong; **senior editors** Gilbert J. Chin, Pamela J. Hines, Paula A. Kiberstis (Boston), Beverly A. Purnell, L. Bryan Ray, Guy Riddihough (Manila), H. Jesse Smith, Valda Vinson, David Voss; **associate editors** Marc S. Lavine (Toronto), Jake S. Yeston; **online editor** Stewart Wills; **associate online editor** Tara S. Marathe; **book review editor** Sherman J. Suter; **associate letters editor** Etta Kavanagh; **information specialist** Janet Kegg; **editorial manager** Cara Tate; **senior copy editors** Jeffrey E. Cook, Harry Jach, Barbara P. Ordway; **copy editors** Cynthia Howe, Alexis Wynne Mogul, Jennifer Sills, Trista Wagoner; **editorial coordinators** Carolyn Kyle, Beverly Shields; **publication assistants** Ramatoulaye Diop, Chris Filiatreau, Joi S. Granger, Jeffrey Hearn, Lisa Johnson, Scott Miller, Jerry Richardson, Brian White, Anita Wynn; **editorial assistants** E. Annie Hall, Lauren Kmec, Patricia M. Moore, Brendan Nardozzi, Michael Rodewald; **executive assistant** Sylvia S. Kihara; **administrative support** Patricia F. Fisher

News senior correspondent Jean Marx; **deputy news editors** Robert Coontz, Jeffrey Mervis, Leslie Roberts, John Travis; **contributing editors** Elizabeth Culotta, Polly Shulman; **news writers** Yudhijit Bhattacharjee, Adrian Cho, Jennifer Couzin, David Grimm, Constance Holden, Jocelyn Kaiser, Richard A. Kerr, Eli Kintisch, Andrew Lawler (New England), Greg Miller, Elizabeth Pennisi, Robert F. Service (Pacific NW), Erik Stokstad; Katherine Unger (intern); **contributing correspondents** Barry A. Cipra, Jon Cohen (San Diego, CA), Daniel Ferber, Ann Gibbons, Robert Irion, Mitch Leslie (NetWatch), Charles C. Mann, Evelyn Strauss, Gary Taubes, Ingrid Wickelgren; **copy editors** Linda B. Felaco, Rachel Curran, Sean Richardson; **administrative support** Scherraine Mack, Fannie Groom **bureaus:** Berkeley, CA: 510-652-0302, FAX 510-652-1867, New England: 207-549-7755, San Diego, CA: 760-942-3252, FAX 760-942-4979, Pacific Northwest: 503-963-1940

Production director James Landry; **senior manager** Wendy K. Shank; **assistant manager** Rebecca Doshi; **senior specialists** Jay Covert, Chris Redwood **Preflight director** David M. Tompkins; **manager** Marcus Spiegler; **specialist** Jessie Mudjitaba

Art director Joshua Moglia; **associate art director** Kelly Buckheit; **illustrators** Chris Bickel, Katharine Sutliff; **senior art associates** Holly Bishop, Laura Creveling, Preston Huey; **associate** Nayomi Kevitiyagala; **photo researcher** Leslie Blizard

***Science* International**

Europe (science@science-int.co.uk) **editorial: international managing editor** Andrew M. Sugden; **senior editor/perspectives** Julia Fahrenkamp-Uppenbrink; **senior editors** Caroline Ash (Geneva: +41 (0) 222 346 3106), Stella M. Hurtley, Ian S. Osborne, Stephen J. Simpson, Peter Stern; **associate editor** Joanne Baker **editorial support** Alice Whaley; Deborah Dennison **administrative support** Janet Clements, Phil Marlow, Jill White; **news: international news editor** Eliot Marshall **deputy news editor** Daniel Clery; **correspondent** Gretchen Vogel (Berlin: +49 (0) 30 2809 3902, FAX +49 (0) 30 2809 8365); **contributing correspondents** Michael Balter (Paris), Martin Enserink (Amsterdam and Paris), John Bohannon (Berlin); **intern** Michael Schirber

Asia Japan Office: Asca Corporation, Eiko Ishioka, Fusako Tamura, 1-8-13, Hirano-cho, Chuo-ku, Osaka-shi, Osaka, 541-0046 Japan; +81 (0) 6 6202 6272, FAX +81 (0) 6 6202 6271; asca@os.gulf.or.jp; **asia news editor** Richard Stone +66 2 662 5818 (rstone@aaas.org) **japan news bureau** Dennis Normile (contributing correspondent, +81 (0) 3 3391 0630, FAX 81 (0) 3 5936 3531; dnormile@gol.com); **china representative** Hao Xin, + 86 (0) 10 6307 4439 or 6307 3676, FAX +86 (0) 10 6307 4358; haoxin@earthlink.net; **south asia** Pallava Bagla (contributing correspondent +91 (0) 11 2271 2896; pbagla@vsnl.com)

EXECUTIVE PUBLISHER **Alan I. Leshner**
PUBLISHER **Beth Rosner**

Fulfillment & Membership Services (membership@aaas.org) **director** Marlene Zendell; **manager** Waylon Butler; **systems specialist** Andrew Vargo; **specialists** Pat Butler, Laurie Baker, Tamara Alfson, Karena Smith, Vicki Linton; **circulation associate** Christopher Refice

Business Operations and Administration director Deborah Rivera-Wienhold; **business manager** Randy Yi; **senior business analyst** Lisa Donovan; **business analyst** Jessica Tierney; **financial analyst** Michael LoBue, Farida Yeasmin; **rights and permissions: administrator** Emilie David; **associate** Elizabeth Sandler; **marketing: director** John Meyers; **marketing managers** Darryl Walter, Allison Pritchard; **marketing associates** Julianne Wielga, Mary Ellen Crowley, Catherine Featherston, Alison Chandler; **director of international marketing and recruitment advertising** Deborah Harris; **international marketing manager** Wendy Sturley; **marketing/member services executive:** Linda Rusk; **japan sales** Jason Hannaford; **site license sales: director** Tom Ryan; **sales and customer service** Mehan Dossani, Kiki Forsythe, Catherine Holland, Wendy Wise; **electronic media: manager** Lizabeth Harman; **production associates** Sheila Mackall, Amanda K. Skelton, Lisa Stanford, Nichele Johnston; **applications developer** Carl Saffell

Advertising director worldwide ad sales Bill Moran

Product (science_advertising@aaas.org); **midwest** Rick Bongiovanni: 330-405-7080, FAX 330-405-7081 • **west coast/w. canada** B. Neil Boylan (Associate Director): 650-964-2266, FAX 650-964-2267 • **east coast/e. canada** Christopher Breslin: 443-512-0330, FAX 443-512-0331 • **uk/europe/asia** Tracey Peers (Associate Director): +44 (0) 1782 752530, FAX +44 (0) 1782 752531 **japan** Mashy Yoshikawa: +81 (0) 33235 5961, FAX +81 (0) 33235 5852 **israel** Jessica Nachlas +9723 5449123 • **traffic manager** Carol Maddox; **sales coordinator** Deiandra Simms

Classified (advertise@sciencecareers.org); **u.s.: sales director** Gabrielle Boguslawski: 718-491-1607, FAX 202-289-6742; **inside sales manager** Daryl Anderson: 202-326-6543; **west coast/midwest** Kristine von Zedlitz: 415-956-2531; **east coast** Jill Downing: 631-580-2445; **canada, meetings and announcements** Kathleen Clark: 510-271-8349; **line ad sales** Emnet Tesfaye: 202-326-6740; **sales coordinators** Erika Bryant; Rohan Edmonson Christopher Normile, Joyce Scott, Shirley Young; **international: sales manager** Tracy Holmes: +44 (0) 1223 326525, FAX +44 (0) 1223 326532; **sales** Christina Harrison, Svitlana Barnes; **sales assistant** Helen Moroney; **japan:** Jason Hannaford: +81 (0) 52 789 1860, FAX +81 (0) 52 789 1861; **production: manager** Jennifer Rankin; **assistant manager** Deborah Tompkins; **associates** Christine Hall; Amy Hardcastle; **publications assistants** Robert Buck; Natasha Pinol

AAAS Board of Directors retiring president, chair Shirley Ann Jackson; **president** Gilbert S. Omenn; **president-elect** John P. Holdren; **treasurer** David E. Shaw; **chief executive officer** Alan I. Leshner; **board** Rosina M. Bierbaum; John E. Burris; John E. Dowling; Lynn W. Enquist; Susan M. Fitzpatrick; Richard A. Meserve; Norine E. Noonan; Peter J. Stang; Kathryn D. Sullivan

AAAS
ADVANCING SCIENCE, SERVING SOCIETY

Now you can *affordably* monitor Biomolecular Binding Reactions in real time.

SR7000 New Surface Plasmon Resonance Instrument:

- High quality, kinetic data
- Flexible: you design it to do your work
- Affordable: a fraction of other instruments
- Easy to set up and use

NOW AVAILABLE
Autosampler
ADDS TO
Flexibility & Throughput

Uses/Features:

- Response vs. time and reflectivity data
- For kinetics (on, off, equilibrium), relative affinity, sequence recognition, concentration, ligand fishing
- For epitope screening and mapping
- For method development…before running more expensive tests
- Extremely sensitive: Savitzky Golay Smoothed Data rms Noise = 0.45 µRIU = 0.33 RU = 3.3e-05 deg. (Raw Data rms Noise = 0.97 µRIU = 0.71 RU = 7.1e-05 deg)
- Excellent baseline stability: Maximum drift 3.1 µRIU/hour [1 µRIU = 0.73 RU = 7.3e-05 Deg]
- Given ready chemistry (slide with surface and analyte to test against it), the instrument can be up and producing data within an hour out of the box.
- Uses off-the-shelf HPLC fluidics

Imagine the perfect SPR instrument for you.

Reichert
Analytical Instruments

Reichert, Inc.
3374 Walden Avenue • Depew, NY 14043
Toll Free: 888-849-8955 • Tel: (716) 686-4500
Fax: (716) 686-4555 • Email: info@reichert.com
www.reichertai.com

Accelerate protein purification & analysis

Reliable sample preparation and fractionation processes are key to the success of proteomics research. Pall's extensive offering of protein sample prep and detection products provide the right solution for all your needs.

- Enchant® kits for *abundant protein removal*
- Biosepra® chromatography sorbent for *protein enrichment, fractionation and preparation*
- Minimate™ TFF systems for *large scale (up to 1L) protein purification and concentration*
- Ultrafiltration spin devices for *fast, small scale protein purification, concentration & desalting*
- Low fluorescent blotting membranes for *westerns*
- Vivid™ microarray slides for *nano immunoassays*

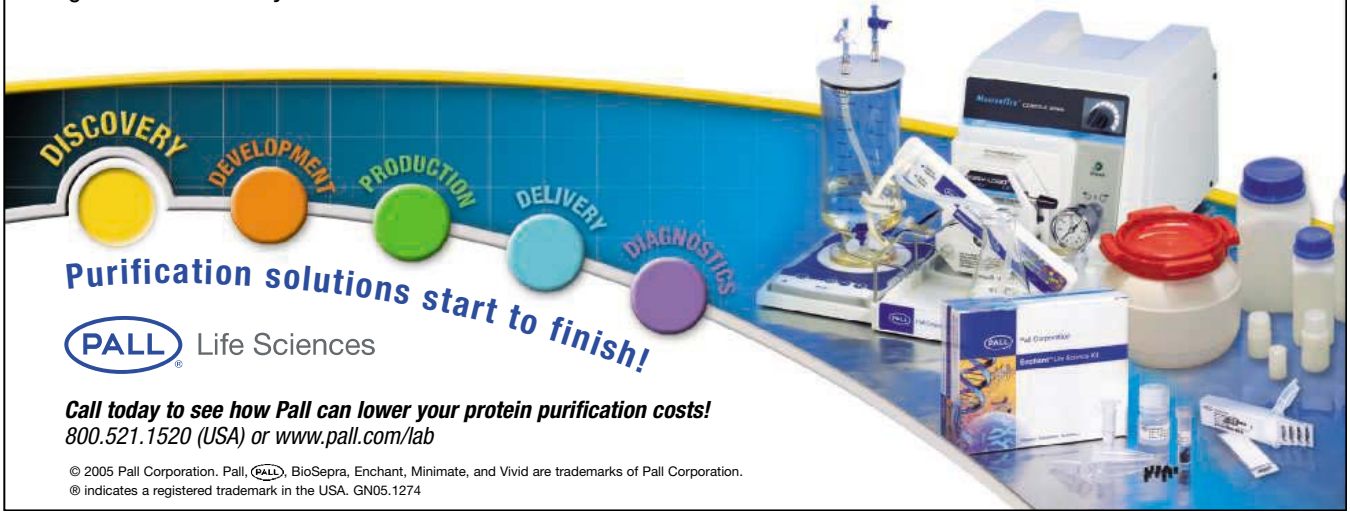

PALL® Life Sciences

Call today to see how Pall can lower your protein purification costs!
800.521.1520 (USA) or www.pall.com/lab

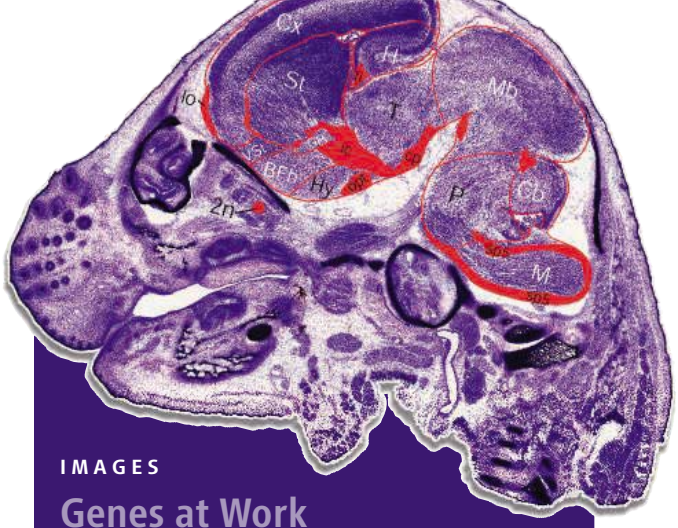

IMAGES

Genes at Work

GenePaint displays portraits of activity levels for more than 1000 mouse genes involved in development and other functions. The gene expression atlas from the Max Planck Institute of Experimental Endocrinology in Hannover, Germany, holds a complete set of slices from a 14-day-old embryo and selected images for other pre- and postnatal stages. Researchers used probes that tag messenger RNA to indicate each gene's activity level in the slices. You can find out which genes are cranking away in a specific organ system or in about 100 structures, such as the lens of the eye. You can also search the data by expression patterns, including whether a particular gene's activity is local or widespread. A virtual microscope lets users zoom in on a slice down to the cellular level. The site also offers anatomy guides that feature labeled sections such as this head of a 15-day-old embryo (above).
>> www.genepaint.org

RESOURCES

The Final Cut

Talk about a split personality. The short version of the protein BCLX prompts cells to kill themselves, whereas the long version keeps them alive. Thanks to the process called alternative splicing, most proteins in the body come in multiple versions that often perform different jobs or toil in different tissues. Researchers can track these variants with ProSplicer from the National Central University in Taiwan. The site pinpoints splicing sites in nearly 22,000 human genes by comparing genomic data with information such as messenger RNA and protein sequences. Search for your favorite gene to call up a map that shows which DNA segments code for amino acids and which get left out in the different protein versions.
>> prosplicer.mbc.nctu.edu.tw

DATABASE

Something in the Air >>

Last month, the Environmental Protection Agency (EPA) proposed new limits on $PM_{2.5}$, tiny particles spewed from power plants and vehicles that are implicated in heart attacks and other diseases (*Science*, 6 January, p. 27). A new air-quality database funded by the nonprofit Health Effects Institute in Boston can help researchers untangle how $PM_{2.5}$ causes illness. The site, run by the contractor Atmospheric and Environmental Research of Lexington, Massachusetts, houses measurements gathered between 2000 and 2004 by an EPA network that monitors fine particles at 54 sites and by more than 200 other stations around the country. Click on a U.S. map to see trends in fine particle levels and components such as ammonium and sulfate at a specific location. You can also download daily measurements of $PM_{2.5}$ and other pollutants, along with meteorological data such as temperature and wind speed. The database is free, but users have to e-mail the company to request access.
>> hei.aer.com/login.php

TOOLS

Mapping Bushmeat Threats

Commercial hunters pursuing "bushmeat" are decimating chimpanzees, gorillas, and other mammals in Central Africa. Since NetWatch's last visit (*Science*, 25 June 2004, p. 1883), the Web site of the Bushmeat Crisis Task Force has added a mapping feature that can help researchers gauge threats to these species and craft conservation strategies. The tool lets users chart the ranges of 33 animals that often end up in the cooking pot and overlay variables that affect species' vulnerability, such as human population density and the locations of major roads, reserves, and logging concessions. This example, right, for instance, shows that roads allowing hunters access to the forest crisscross the chimpanzees' range (light green).
>> www.bushmeat.org/IMAP/mapserver.htm

WEB LOGS

Weighty Matters

If somebody uses mass spectrometry to make a noteworthy discovery or releases a tool for viewing data files, you'll hear about it from chemist Kermit Murray of Louisiana State University in Baton Rouge. Murray's 4-year-old Mass Spectrometry Blog offers resources, tips, and news for scientists who rely on this method for determining a sample's chemical makeup. For example, recent posts announced a tutorial on Fourier transform mass spectrometry and linked to a commentary on distributing academic lectures via podcasts. >> msblog.kermitmurray.com

Send site suggestions to >>
netwatch@aaas.org. Archive: www.sciencemag.org/netwatch

CREDITS (TOP TO BOTTOM): MAX PLANCK INSTITUTE OF EXPERIMENTAL ENDOCRINOLOGY; GARY BRAASCH/CORBIS

Big online news from *Science*

New website – retooled and redesigned.

If you're a scientist, the online version of *Science* puts a world of essential knowledge at your fingertips. And we're now proud to announce the launch of our redesigned website, which makes it even easier to keep up with the latest breakthroughs, browse journal archives, or find career advice. New features include saved searches and content, a hotlist of the most popular article downloads, and a daily science news feed – to name just a few. Discover the new online version of *Science*. Visit **www.sciencemag.org** today.

Science
AAAS

GET THE BIG PICTURE IN *SCIENCE*

Hurricane refugees trying to sleep in Arizona.

NEW KATRINA HEALTH INITIATIVE

Researchers launched a massive telephone survey this week of Hurricane Katrina survivors, collecting data for what they hope will be an unprecedented close-up of the health and mental health of thousands of people still weathering the aftermath of the disaster.

Harvard Medical School and the National Institute of Mental Health, with $1 million from the National Institutes of Health, are working together on the project, called the Hurricane Katrina Advisory Group Initiative. At a 5 January press conference, the project's director, Harvard epidemiologist Ronald Kessler, said the survey was a "unique" initiative that will involve repeated telephone interviews with 2000 people—half from the New Orleans area and half from the hurricane's path in Louisiana, Alabama, and Mississippi. Names will be gathered from Red Cross and other aid lists as well as from random dialing of 250,000 numbers to find displaced people. "We've got to beat the bushes all around the country," said Kessler.

The baseline interview will be 2 hours long—"They want to talk to us," Kessler noted—and everyone will be contacted again for shorter follow-up interviews every 3 months over 2 years so researchers can "keep our fingers on the psychological pulse of this population."

Reports will be posted, starting in late February, on the project Web site (www.hurricanekatrina.med.harvard.edu). The survey is designed to give instant guidance to policymakers and will include answers to a question about the "three top things" that respondents think need to be done to improve matters.

Kessler said there are reports of depression, anxiety, excess drinking and smoking, and an increase in suicides among people uprooted by Hurricane Katrina. Psychologist Anthony Speier, director of disaster operations in Louisiana's Office of Mental Health, said the prolonged displacement is taking its toll: "From reports, the level of anxiety is increasing, not decreasing."

MODEST PROPOSAL

My dangerous idea is one that most people immediately reject without giving it serious thought: School is bad for kids. It makes them unhappy, and as tests show, they don't learn much. … Just call school off. Turn them all into apartment houses."

—Psychologist and computer scientist Robert Shank, one of 117 deep thinkers who have so far responded to this year's annual New Year's question by the Edge Foundation: "What's your dangerous idea?" (www.edge.org)

CREDITS (TOP TO BOTTOM): AP; JULIAN PENDERHUME; WHO

World of the Dodo

It wasn't long after Dutch colonists settled on the island of Mauritius in the 17th century that the hapless dodo was driven extinct. Since then, dodo researchers haven't had much to work with other than a handful of composite skeletons in museums and anecdotal reports from early mariners. Last month, however, a Dutch-Mauritian team of scientists reported the discovery of a rich deposit of dodo bones on the island. "It's of vital importance," says paleontologist Julian Hume of the Natural History Museum in London, who has joined the group to study the bones. "More has been written about this bird than practically any other, yet we practically know nothing about it."

Reconstruction of dodo environment.

The bones were found last October after archaeologist Pieter Floore assembled a team, including scientists from the University of Mauritius, to reconstruct the prehistoric environment of the island. The researchers came upon a mass of bones in a marshy section of a sugarcane plantation. "I had the feeling that we found one every 10 minutes. … [It] was amazing," says Kenneth Rijsdijk, a physical geographer with the Geological Survey of the Netherlands. By studying the cores drilled from the marsh, the researchers intend to reconstruct the ecology and environment in which the dodo lived at least 2000 years ago.

THE SICKNESS OF RUSSIA

The Russian economy will continue to take a terrific beating from population decline and falling life expectancies, according to two reports issued last month.

The financial losses could amount to some $400 billion over the next 2 decades, estimates a Russian business lobby group, Delovaya Rossiya. Industrial growth is already being crippled by shortages of workers, whose numbers are likely to drop by 3.6 million over the next 5 years, the group finds.

That warning echoes findings by the World Bank, whose report *Dying Too Young* relates that since 1990, Russia's population has fallen from roughly 150 million to 143 million, in large part because of deaths from premature heart disease, accidents, and alcoholism. With fertility rates constantly declining in the climate of prolonged economic uncertainty, the report predicts that the country's population could drop another 20 million by 2025. "Short, brutal lives for Russia's men" mean that their life expectancy, which at 58 is the lowest in Europe, could plummet to 53 if current trends hold.

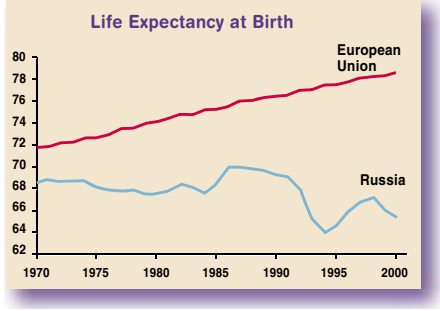

European and Russian life expectancies, 1970–2000.

Molybdenum and Iran's nuclear ambitions
158

Protests stall Scripps's Florida venture
160

CLONING

South Korean Team's Remaining Human Stem Cell Claim Demolished

In an announcement that researchers worldwide both expected and feared, Woo Suk Hwang's last remaining claim to have advanced the promising field of human embryonic stem (ES) cells has been declared fraudulent. In a report released on 10 January, a committee at Seoul National University (SNU) found that Hwang and his colleagues fabricated data in their breakthrough 2004 *Science* paper reporting the first creation of a stem cell line from a cloned human blastocyst. In an interim report in late December, the committee had already determined that a second paper by the team, published in 2005, was fraudulent (*Science*, 6 January, p. 22).

The final report concludes that Hwang and his colleagues did successfully clone a dog, which the scientists reported in *Nature* in August 2005. It also said that the Hwang team made some progress toward cloning early-stage human embryos. But the 2004 publication amounts to "none other than deceiving the scientific community and the public at large," the report says. (An English summary of the report is available on the SNU Web site at www.snu.ac.kr/engsnu.)

In the two papers published in *Science*, Hwang and his co-workers had claimed to have accomplished three firsts. The 2004 paper reported the cloning of a human blastocyst, through a process known as somatic cell nuclear transfer, and the derivation of ES cells from that cloned blastocyst; the 2005 paper reported the derivation of 11 human ES cell lines genetically matched to patients.

The verdict. Myung-Hee Chung, head of the Seoul National University panel, announces that Woo Suk Hwang's team produced no cell lines from cloned human blastocysts.

ES cells, which are derived from week-old embryos, hold great medical promise because they can in theory develop into any tissue type in the body. Researchers around the world have derived dozens of cell lines from human embryos created through in vitro fertilization. But many hope that cloned embryos could produce ES cells tailor-made to match a patient's DNA. They predict that such cells could shed light on heritable diseases and offer hope for new therapies for patients suffering from maladies including spinal cord injury and diabetes.

With both papers now thoroughly discredited, "we're back to the time prior to [Hwang's 2004] publication; there is no evidence at all that we can make [stem cells] from human embryos created through nuclear transfer," says Alan Trounson, a stem cell researcher at Monash University in Clayton, Australia. Hwang's team had also claimed phenomenal advances in efficiency in its 2005 paper, reporting that it needed fewer than 20 eggs to produce each stem cell line. Work in most other mammals suggests that it usually takes 100 to 200 eggs for one stem cell line, and many researchers say the unraveling of Hwang's work resurrects the question of whether the technique will ever be efficient enough for routine clinical application.

To check the veracity of the 2004 paper, the committee collected 23 samples of the cell line supposedly described in the work, which the team called NT-1. Twenty samples came from Hwang's lab, and one each from the Korean Cell Line Bank; MizMedi Hospital in Seoul, where several collaborators worked; and the lab of Hwang's collaborator at SNU, Shin Yong Moon. The committee said it asked three independent labs to test the DNA from all 23 samples, and all three labs reported identical results.

Those results suggest that Hwang and his colleagues falsified much of the data in the paper. Hwang's team claimed that NT-1 was an exact genetic match with cells of donor A, but the committee found that the line "is quite distinct from what was reported in the *Science* article." The committee reported that 11 of Hwang's 20 samples matched the DNA of a cell line derived at MizMedi from an embryo created through in vitro fertilization. The other nine samples from Hwang's lab, as well as the three samples from outside sources, all shared a signature that could not be traced to any other known cell line.

The signature of those samples is somewhat puzzling. It is a very close match with the DNA fingerprint of a second woman who donated oocytes for the project, called donor B in the report. But the evidence suggests that it could not have come from nuclear transfer. For 40 of 48 nuclear DNA markers tested, donor B and the NT-1 samples matched. But for eight markers, donor B was heterozygous whereas the cell line was homozygous. The mitochondrial DNA of the woman is a perfect match with that of the cell line.

That suggests that the cell line might have arisen from either accidental or deliberate parthenogenetic activation, in which an

CREDIT: CHUNG SUNG-JUN/GETTY IMAGES

Can money buy global health? 162

Punching the academic clock 168

Pluto or bust 172

unfertilized oocyte is triggered to divide. Several teams around the world have created ES cell lines from parthenogenetically activated oocytes from mice, and at least one team has derived a cell line from a monkey parthenote. Indeed, Hwang and his co-authors wrote in the 2004 paper that they could not rule out the possibility of a parthenogenetic cell line. (Because the team used somatic cells and oocytes from the same donor, it was difficult to tell the difference between a cloned cell line and one derived from a parthenote.)

The SNU committee confirmed that Hwang's team successfully cloned a dog to create Snuppy. The committee asked three independent test centers to compare tissue from four dogs: the egg donor, Snuppy, the adult Afghan from which somatic cells had been taken, and the surrogate mother. The labs sequenced mitochondrial DNA and checked 27 nuclear DNA markers to confirm that the adult Afghan was the source of Snuppy's nuclear DNA. Cloning a dog was considered particularly tricky because of the animal's complex reproductive cycle. "It's surprising," Trounson says. "I would have thought cloning a dog would be more difficult than a human [embryo]."

And the investigating committee found that Hwang's group did make some progress toward creating cloned embryos. The report notes that there are three main steps in producing ES cells through somatic cell nuclear transfer: nuclear transfer itself, blastocyst formation, and extraction of the cell line. The committee found that Hwang's team appears to have successfully produced cloned human blastocysts in about 10% of their cloning attempts—something that no other team had managed at the time of the first paper and which only one other team—led by Alison Murdoch in Newcastle, U.K.—has done since.

But the committee's investigation indicates that Hwang and his colleagues couldn't pull off the crucial next step. Although the report says Hwang's team claimed to see what they called cell colonies, which some on Hwang's team saw as success in establishing cell lines, "the scientific bases for claiming any success are wholly lacking." There is no evidence of extant cell lines, and "no record of further confirmatory experiments could be found," the report says.

The committee also made it clear that Hwang had lied about how his team obtained oocytes. For months, Hwang denied that any members of his team had donated eggs. After an investigative TV program reported that a member of Hwang's team had told them she donated eggs, Hwang admitted that members of his team had donated but that he had only learned about it after the fact and lied to protect the women's privacy. One graduate student who voluntarily donated eggs told the committee that Hwang personally accompanied her to MizMedi Hospital for the egg-retrieval process. And 2 months later, members of the Hwang team asked female technicians working in the lab to sign a form volunteering to donate eggs.

Validated. Tests confirm that Snuppy, pictured here with Hwang, is a real clone.

The committee also confirmed earlier rumors that Hwang's team had used vastly more oocytes than it claimed in the two *Science* papers. The team reported using only 427 oocytes for the experiments they described in the two papers, but investigators found that the team had received 2061 human oocytes from four hospitals between November 2002 and November 2005.

The report does not clarify how many people in the lab knew about the fraud, but it does identify certain individuals who it alleges falsified data at various steps.

At SNU, the report will now be taken up by a disciplinary committee. Korean media have also reported that public prosecutors could begin an investigation as early as this weekend into Hwang's allegation that his team's stem cells were deliberately swapped with others derived at MizMedi, allegations that members of Hwang's team were paid $50,000 to keep quiet, and possible misuse of government subsidies. Meanwhile, an investigation at the University of Pittsburgh in Pennsylvania is expected to issue its report on the role of Gerald Schatten, a senior author on the 2005 paper, in the scandal later this month.

Science has asked MizMedi's Sung Il Roh to set up an independent investigative panel to look into MizMedi's contributions to the *Science* papers as well as papers contributed to the journal *Stem Cells*, which contained images identical to those published in the 2004 *Science* paper. Roh says he will comply.

Science, too, plans to conduct an internal investigation into its handling of both the 2004 and 2005 papers, says Editor-in-Chief Donald Kennedy, and will let readers know what it finds. The journal plans to "reconstruct the history" of each paper, examining the original submissions and changes made at every stage of review. Among other issues, *Science* will examine whether it could have "pressed" Hwang's group further for more evidence that the embryos described in the 2004 paper were cloned and not parthenogenic, says Kennedy. *Science* has also contacted members of its senior editorial board, composed of outside scientists, to seek their counsel on how the journal might modify its procedures—such as whether authors should detail their contributions—which is something else *Science* will be considering.

"It's worth finding out, 'Is there someplace I got duped?' " says Mike Rossner, managing editor of the *Journal of Cell Biology*, which has declined to publish 13 papers that passed peer review but were found to have potentially manipulated images. "I really think journal editors have to be more proactive … rather than hiding behind the veil of review and saying, 'Our reviewers approved it, so it's OK.' "

Science's close competitor *Nature* commissioned its own analysis after questions arose about the validity of the paper it published by Hwang on the first cloned dog. In late December, *Nature* asked a scientist from the National Human Genome Research Institute in Bethesda, Maryland, to conduct independent tests to determine whether the dog, Snuppy, was a clone. Findings from those tests announced this week agree with the report from SNU that the team's report was legitimate.

–DENNIS NORMILE, GRETCHEN VOGEL, AND JENNIFER COUZIN

With reporting by Sei Chong in Seoul.

CREDIT: CHUNG SUNG-JUN/GETTY IMAGES

NUCLEAR WEAPONS

Iran's Trouble With Molybdenum May Give Diplomacy a Second Chance

Defying the West, Iran this week vowed to resume R&D on uranium enrichment and other sensitive elements of a nuclear program alleged to include weapons research. But U.S. officials and analysts believe it will take months for Iran to solve a key technical challenge in purifying uranium isotopes—unless it gets outside help.

Iran's decision has endangered talks with three European countries on a diplomatic solution to the crisis and has exasperated officials at the International Atomic Energy Agency (IAEA) in Vienna, Austria, which is responsible for verifying that Iran's nuclear program is peaceful. The move also jeopardizes a Russian proposal to allow Iran to carry out uranium enrichment on Russian soil. The world is "running out of patience with Iran," IAEA director Mohamed ElBaradei said to the U.K.-based Sky News on 9 January.

All that glitters … Technical troubles at the Uranium Conversion Facility near Esfahan may buy negotiators time to persuade Iran to accept constraints on its nuclear program.

CREDIT: VAHID SALEMI/AP PHOTO

Iran claims that its nuclear program is strictly for producing energy. To that end, it insists on exercising its right under the Nuclear Non-Proliferation Treaty to transform uranium ore, predominantly containing uranium-238, into fuel enriched in the rarer, fissile isotope uranium-235.

The United States and some European nations argue, however, that Iran's peaceful program is a cover for weapons development. Western officials point out that Iran kept most elements of its nuclear effort secret for more than a decade until they were exposed by an exile group in 2002. Also cited as evidence of Iran's intent are bulk purchases of materials such as zirconium, which can be used in fuel rods or warheads.

Western scrutiny of late has focused on R&D at the Esfahan Nuclear Technology Center's Uranium Conversion Facility (UCF). At this complex, Iran intends to convert milled uranium ore, or yellowcake, into uranium hexafluoride (UF_6), potentially to be separated into isotopes by centrifuges at a giant facility under construction in Natanz. Iran had suspended R&D at Natanz in 2004; Iranian officials began removing IAEA seals there on 10 January, in the presence of IAEA inspectors.

As a prelude to enrichment, Iran announced last May that it had converted 37 tons of yellowcake into uranium tetrafluoride (UF_4), a solid. This was a big step. Creating purified UF_6, which can be fed as a gas into centrifuges for isotope separation, would be a much bigger one. According to an official at the U.S. State Department, Iran has struggled to convert UF_4 into UF_6, a dangerous process involving highly toxic and corrosive fluorine gas. The official also claims that Iranian UF_4 is tainted with large amounts of molybdenum and other heavy metals. These oxyfluoride impurities in UF_6 "might condense" and thereby "risk blockages" of valves and piping, an IAEA specialist told *Science*.

Reducing impurities to allow production of uranium fuel for peaceful uses, containing a few percent U-235, should not be a huge challenge, according to experts. But more sophisticated equipment is required to reduce impurities enough to make highly enriched uranium, containing 20% or more U-235. Only a handful of countries can do it. For a weapons effort, filtering out molybdenum "is a fairly significant problem," says nuclear nonproliferation expert Rose Gottemoeller, director of the Carnegie Endowment for International Peace's Moscow office.

The key question, some Western analysts say, is whether Iran can get help to make clean UF_6. During the early 1990s, China offered to share its uranium-enriching skill with Iran by building the UCF but abandoned the project in 1998 under pressure from the U.S. government. China probably has not passed forbidden knowledge to Iran, which is believed to have constructed the UCF based on Chinese blueprints, experts judge. Supporting this assessment are comments by Mohamed Saeedi, deputy chief of Iran's Atomic Energy Organization. In the Iranian newspaper *Kayhan* last April, Saeedi described a visit to Beijing in 1998 during which Iranian officials sought to persuade China to follow through with construction of the UCF. They were rebuffed. The Chinese, Saeedi said, "told us that … we would only make some headway in the primary stages and encounter difficulties in the next high-tech stages of the project, just as they did … [before] the Russians came to their assistance."

U.S. officials are worried that China's tutor—Russia—could solve the impurities problem for Iran. "It's not in Russia's interest to fix that problem," argues Gottemoeller, noting that Russia's goal is to remain the long-term supplier of fuel to Iran's nuclear power program. But some fear that if Iran were to agree to Russia's proposal to conduct enrichment on Russian soil—negotiations on this proposal are set to resume next month—it could learn enough indirectly to overcome the UF_6 obstacle. At a minimum, some argue, Iran would need access to "imported technology" that countries have vowed to place off-limits, according to the 29 August 2005 issue of *NuclearFuel*, an industry newsletter.

If Iran solves the molybdenum problem, that would raise another concern: It could trade such knowledge to North Korea. Last month, a South Korean official told *Science* that intelligence indicates Iran may have assisted North Korea's alleged uranium-enrichment program in exchange for technical help with ballistic missiles. (Officially, South Korea maintains a studied ambivalence about whether North Korea's enrichment program exists; see p. 170.)

IAEA is unaware of such evidence: "We do not have any leads to act on, nor have our investigations turned up any such connection," says an agency spokesperson, Melissa Fleming. Even without airtight evidence, observers say, these scenarios are worrisome enough to justify a redoubled diplomatic effort to reach an agreement with Iran.

–RICHARD STONE

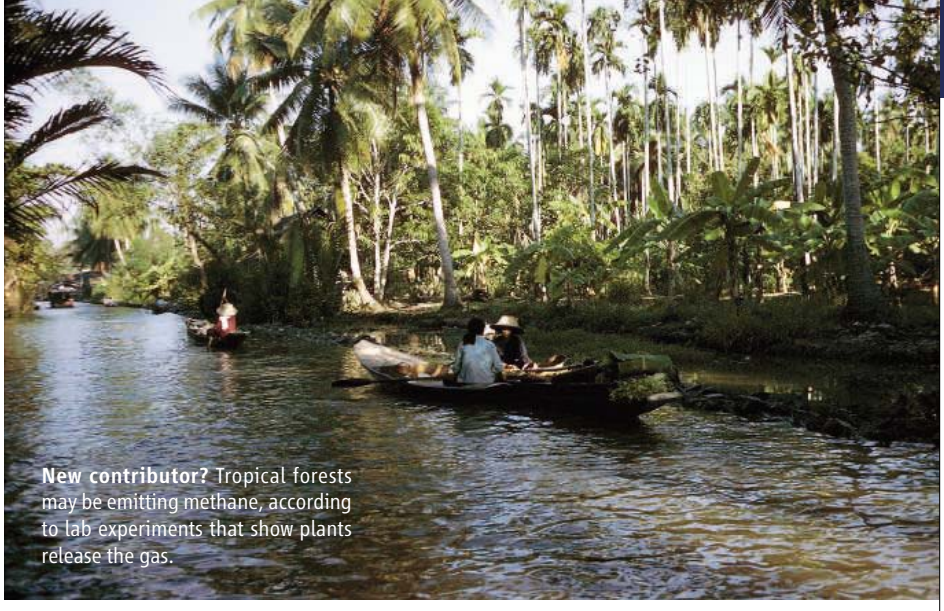

New contributor? Tropical forests may be emitting methane, according to lab experiments that show plants release the gas.

CREDIT: PHOTOS.COM

BOTANY

Plants May Be Hidden Methane Source

Thanks to microbes, methane bubbles out of rice paddies and escapes from the back ends of termites and the front end of cows. Over the years, researchers have gained a good handle on these and other sources of this potent greenhouse gas. But a report in the 12 January issue of *Nature* suggests that one source has been overlooked: plants. Although the surprising finding doesn't change the total amount of methane emitted to the atmosphere, it could force a reappraisal of how much various sources contribute, how to mitigate some of them, and how they might change. "This paper will shake the methane community," predicts Christian Frankenberg of the University of Heidelberg, Germany.

Methane is largely made by microbes. Living in oxygen-poor environments, they ferment organic matter or reduce carbon dioxide. Methane is also produced in massive quantities from wild and controlled fires and is released from natural gas leaks. But among biological processes, researchers had no idea that anything other than microbial anaerobic reduction was responsible.

The clue for the new research came from chloromethane, a halogenated organic gas that avidly destroys ozone and was thought to come mainly from burning biomass. But a few years ago, Frank Keppler, a geochemist now at the Max Planck Institute for Nuclear Physics in Heidelberg, and colleagues discovered that living plants make chloromethane (*Science*, 11 July 2003, p. 206). Because methane is also released from burning biomass, Keppler and his colleagues wondered whether plants might make it, too.

The group first tested dead plants, placing leaves from about 30 species in a chamber with typical atmospheric oxygen concentrations. They released between 0.2 and 3 nanograms of methane per gram of dry plant matter, a relatively paltry amount. When they then conducted similar experiments with living plants, however, the rates per gram of plant matter "increased dramatically," Keppler says, jumping to 10 to 100 times those of the dead leaves. As a control, they grew some plants hydroponically to exclude microbes and saw comparable results. Moreover, the methane was slightly enriched in carbon-13 compared to bacterially produced methane, further suggesting that the plants were making it. "It must be a new mechanism," says Keppler, although what that could be, no one knows. Some experts remain skeptical. "I'm kind of incredulous," says methane chemist Ronald Sass of Rice University in Houston, Texas.

How much could plants contribute to the methane budget? The authors estimate—very roughly, they admit—that it could be between 10% and 30% of the 500 million to 600 million metric tons that enter the atmosphere annually. Other experts caution that their assumptions are quite uncertain and that further lab and field experiments are necessary to determine whether these emissions account for much in the wild.

But if plants do emit sizable amounts of methane, says biogeochemist Michael Keller of the University of New Hampshire, Durham, then some of the known sources have been overestimated and/or an important sink is missing. Either way, it could necessitate rethinking of strategies for reducing methane emissions, such as from rice paddies, wetlands, or cattle. And it raises a host of questions about how plant emissions might change from global warming or deforestation. "The implications for understanding the methane cycle are immense," says wetlands biogeochemist Vincent Gauci of the Open University in Milton Keynes, U.K.

–ERIK STOKSTAD

Help for Libyan Children

ROME—With the lives of five foreign medics in the hands of a Libyan court rather than an executioner, the plight of more than 350 children infected with the HIV virus is drawing global attention. Late last month, a coalition of governments including the United States, the United Kingdom, and Bulgaria agreed to pay an undisclosed amount to improve conditions at a clinic in Benghazi, Libya, treating the children. In spite of ample funding, says a European ambassador who requested anonymity, the clinic has been plagued by "unnecessary delays, substandard laboratory supplies, and poor management." Libyan officials declined comment.

The medics, four Bulgarians and one Palestinian, won a reprieve in late December when the Libyan Supreme Court lifted their death sentences and ordered a retrial. The medics stand accused of deliberately infecting the children with HIV in a Libyan hospital where they worked. European AIDS researchers familiar with the case are expected to testify that the evidence points to poor hospital hygiene instead (*Science*, 8 April 2005, p. 182). "I am ready to testify," says Vittorio Colizzi, an Italian molecular pathologist at Tor Vergata University in Rome, who was an expert witness in the earlier trial. The medics have been in jail for 7 years and say the Libyan police tortured them into making false confessions.

–JOHN BOHANNON

Cells Sell Quelled?

In a Missouri court next week: the first hurdle to getting a pro–stem cell research amendment into the state constitution. A pro-research coalition wants to put a measure on the ballot next November that would sanction human research cloning, or somatic cell nuclear transfer (SCNT), while outlawing reproductive cloning. But a group called Missourians Against Human Cloning has asked the Cole County Circuit Court for an injunction against the ballot measure, and a judge will hear arguments on the issue on 19 January.

The measure specifies that to "clone a human being" means "to implant in a uterus" a cloned embryo to initiate a pregnancy. The anticloning group argues that that language is "unfair and deceptive"; they say a blastocyst created by SCNT is a human being. Supporters of the amendment disagree.

Coalition spokesperson Connie Farrow says if their language is rejected, they'll reword it. The deadline for signature collection is 9 May.

–CONSTANCE HOLDEN

RESEARCH FACILITIES

Scripps's Offshoot Stalled in South Florida

In the fall of 2003, representatives from Florida Governor Jeb Bush's office worked overtime in secret negotiations to persuade leaders of the Scripps Research Institute, a biotech juggernaut based in San Diego, California, to open a new campus in Palm Beach County, Florida. The state's hope was that an East Coast branch of Scripps would attract biotechnology companies that would help Florida diversify from a tourism-based economy. Their lure: sunshine, beaches, and a package of more than $500 million in land and other incentives to help the institute build new research facilities and hire a world-renowned faculty. On 9 October 2003, Bush announced the deal, and Scripps officials quickly began hiring researchers to work at an interim Florida campus. Last September, Bush and Richard Lerner, Scripps's president, broke ground on the first of a planned trio of permanent research buildings at a former orange grove called Mecca Farms, about 125 kilometers north of Miami.

Now this promising marriage is in danger of falling apart. In November, responding to a suit filed by environmental groups, a federal judge ruled that Palm Beach County officials failed to secure all the proper environmental permits for Mecca Farms, which lies adjacent to some of the county's last remaining pristine wetlands. Getting the required permits could delay the opening of research facilities by up to 2 years, and Scripps officials fret that they can't wait that long. Scripps Florida has already hired 160 top scientists, who work in temporary and cramped laboratory facilities at Florida Atlantic University (FAU), a commuter school 19 kilometers east of Mecca Farms. "These folks can go anywhere they want, and if we don't get this resolved soon, they will," says Steve Kay, who chairs the biochemistry department at Scripps in San Diego and has been closely involved with the launch of Scripps Florida.

Last month, Scripps officials suggested scrapping plans to build at Mecca Farms and proposed splitting its new campus: An initial trio of permanent facilities would be built at FAU, with future development to take place at an industrial tract called Florida Research Park (FRP) about 3 kilometers up the road from Mecca Farms. This proposed solution is gaining traction within Florida, but some state and local officials are calling for Scripps to either stick with the original plan or build the entire campus at FRP, the original backup site to Mecca Farms.

Unsettled. Amid protests, Scripps leaders Douglas Bingham (*above, left*) and Richard Lerner (*above, right*) broke ground in September with Florida Governor Jeb Bush at Scripps's proposed new home at Mecca Farms.

Mary McCarty, a Palm Beach County commissioner who is among the biggest critics of the proposed split campus, says the proposal would undermine one of the main reasons county officials initially agreed to sink as much as $200 million into the Mecca Farms campus: the development of a single center that promised to bring high-paying biotech jobs, as well as a new science-oriented high school, residential housing, and a town center. McCarty, whose district includes Mecca Farms, argues that separating Scripps from biotech development at the FRP site would hurt the chances of creating a nexus of biotech companies in south Florida: "My concern is that they are just worried about Scripps and not the long-term vision of the state."

McCarty suggests that Scripps build at FRP, where industrial use is already permitted. But Kay and other Scripps officials note that the environmental groups that fought the siting of Scripps at Mecca Farms have already suggested they may do the same if Scripps moves to FRP. Those groups are worried about the thousands of homes and other development that may spring up near either site, Kay notes: "The saddest thing of all is that Scripps has become a pawn in a long-standing debate about Florida development."

Some of Scripps's new hires on the FAU campus say the standoff has already taken a toll. "We have scaled back significantly on recruitment," says proteomics expert Pat Griffin. "To be able to recruit high-caliber people, you have to have a known timetable. That's out the window." "If they continue to play games with us, young people will become nervous. Postdocs could go elsewhere," adds Donny Strosberg, an infectious disease researcher, who left a biotech CEO job in Paris just prior to joining Scripps Florida.

Just how the face-off will be resolved remains unclear. Last week, Scripps Chief Operating Officer Douglas Bingham said in a letter to county officials that the institute was prepared to locate its initial trio of research buildings at any site in Palm Beach County that can be delivered without further delay or controversy. Already, other cities, such as Boca Raton, have proposed sites in hopes of landing Scripps amid the squabble. But last week, Scripps President Richard Lerner and FAU President Frank Brogan also reached a tentative deal to house the initial three research buildings on the FAU campus—the county would only have to pay an estimated $6 million more than the $200 million it was already planning to spend on the new buildings and surrounding infrastructure. (The county has already spent $110 million at Mecca Farms, but it is likely to recoup those costs by selling off the land to developers.) Palm Beach County commissioners met this week to consider the alternatives, but few observers expected an immediate resolution to the impasse. Notes Scripps Florida chemist Peter Hodder: "It's been going back and forth like this for 2 years."

–ROBERT F. SERVICE

CREDITS: TAYLOR JONES/*PALM BEACH POST*/ZUMA PRESS

REGULATORY SCIENCE

More Details Sought in Assessing Health Risks

The Bush Administration this week proposed new federal standards for analyzing health and environmental risks underlying regulations that ask for more details on the evidence that a pollutant causes harm. Experts agree that the changes should improve the quality of assessments, although one critic worries that the bar would be set so high that it could also slow the pace of new regulations.

The draft bulletin* "provides clear, minimum standards for the scientific quality of federal agency risk assessments," says John Graham, the outgoing director of the Office of Management and Budget's (OMB's) Office of Information and Regulatory Affairs. Graham, a former Harvard University professor who in the past 5 years has bolstered the office's influence on agency rulemaking, says the standards should help risk assessments pass scientific review more quickly.

The proposed rules include steps that aren't always routine, such as requiring that agencies weigh both positive and negative studies. The document also asks agencies preparing assessments that could have a major economic or policy impact to look more closely at the uncertainties, including variability in the population and both middle estimates and the range of risks. Some agencies tend to emphasize the high end of risk, says an OMB official. "This is a big change in practice, especially for parts of EPA [the Environmental Protection Agency]," explains the official.

Kimberly Thompson, a risk expert at the Massachusetts Institute of Technology in Cambridge and president-elect of the Society for Risk Analysis, applauds the greater emphasis on quantitative tools. "This basically outlines things agencies should have been doing all along," agrees Granger Morgan of Carnegie Mellon University in Pittsburgh, Pennsylvania, who chairs EPA's scientific advisory board. But toxicologist Jennifer Sass of the Natural Resources Defense Council in Washington, D.C., suggests that scientists won't be able to meet the standards for risks for which there are little underlying data. "I'm concerned that regulations will die at OMB" as a result, she says.

Graham leaves next month to head the Pardee RAND Graduate School in Santa Monica, California. The comment period closes on 15 June, and the proposed bulletin will also be reviewed by the National Academies.

–JOCELYN KAISER

* www.whitehouse.gov/omb/inforeg/proposed_risk_assessment_bulletin_010906.pdf

AVIAN INFLUENZA

More Cases in Turkey, but No Mutations Found

The H5N1 avian influenza strain has sprung another surprise on public health experts, infecting at least 14 people in Turkey in the past few weeks. That's a "very high and worrying" number, says virologist Albert Osterhaus of Erasmus University in Rotterdam, the Netherlands, given that fewer than 150 people (half of them fatally) are known to have been stricken during its 2-year rampage across large swaths of Asia.

The slim bit of good news this week is that the virus does not appear to have mutated and become more dangerous to humans, says epidemiologist Guénaël Rodier, who leads a 10-member World Health Organization (WHO) team of experts investigating the incidents and assisting the Turkish government. But the outbreak among birds, first reported in October, is much worse than originally believed, Rodier says, and the lack of control and protection measures has given the virus ample opportunity to cross the species barrier.

As *Science* went to press, only four of the 14 cases—including two fatalities—identified by the National Influenza Centre in Ankara had been independently confirmed by the U.K.'s National Institute for Medical Research, a WHO Collaborating Center for influenza. But because of the high quality of testing by the Ankara center, WHO expects the remaining 10 cases to be confirmed as well. The cases occurred in six provinces in central, northern, and eastern Turkey.

As in East Asia, the disease appears to have stricken people who have been in close contact with dead or ill poultry, often members of the same family, and often children. "We feel it's very similar to the situation in Asia," says Rodier. There's little to suggest that H5N1 has become more easily transmissible from poultry to people, or between humans, traits that could trigger a pandemic, he says. Preliminary genetic analyses by the U.K. laboratory confirm that the Turkey strain is very similar to one circulating last year in western China, says WHO spokesperson Maria Cheng.

Rodier believes that safer handling of dead and infected poultry, plus more aggressive monitoring and control efforts, might have prevented some of the infections. "It's too bad that it took human cases to trigger more awareness," he notes. **–MARTIN ENSERINK**

Canada Targets Chemicals

Canada has decided to examine all chemicals that could break down to perfluorocarboxylic acids (PFCAs), which cause cancer and developmental problems in lab animals. In 2004, Canada temporarily banned four polymers that contain precursors to PFCAs; those and similar polymers are widely used in products including stain repellents and paint additives.

The broader review comes as the country's regulatory body, Environment Canada, releases risk assessments that say PFCAs can bioaccumulate; previous studies have shown increasing levels of the chemicals in Arctic animals. The chemical industry argues that PFCAs are a legacy of past pollution, but University of Toronto chemist Scott Mabury says up to 4% of PFCAs come from humanmade products.

–REBECCA RENNER

Shakeup at CNRS

PARIS—Physicist Catherine Bréchignac is returning to the helm of France's largest research institute. The National Center for Scientific Research (CNRS) announced this week that Bréchignac, the institute's director-general between 1997 and 2000, will return as CNRS president. She replaces physicist Bernard Meunier (right), who stepped down last week.

It was widely known that Meunier was at odds with CNRS director-general Bernard Larrouturou over an ongoing reorganization. Both men declined comment, but in a letter to center staff, Meunier said he had hoped to cut red tape and make CNRS "strong, reactive, daring, and open to society."

A CNRS spokesperson says the agency's dual leadership structure will be replaced with a single director in the next few months, but it's too early to say who. **–MARTIN ENSERINK**

At NIH: The Inevitable

The 0.1% cut to the budget of the National Institutes of Health (NIH) will soon hit investigators' bottom lines. This week, NIH decided to trim the 2006 payout for continuing grants by 2.35%, the first cut in recent memory. New grants will be funded at equivalent 2005 levels, with student and postdoc stipends mostly level. Advocates wince, citing biomedical inflation of at least 3%. **–JOCELYN KAISER**

An array of well-heeled new players has dramatically reshaped how wealthy countries tackle infectious diseases of the poor. But increasingly, these ambitious efforts are confronting their own limitations

The New World of Global Health

A REVOLUTION IS UNDER WAY THAT IS fundamentally altering the way the haves of the world assist the have-nots. Over the past 7 years, a cadre of deep-pocketed, impassioned players has committed more than $35 billion to fight the diseases of the world's poor. At the forefront of these efforts is the Bill and Melinda Gates Foundation, which since 1999 has pledged $6 billion—roughly the budget of the World Health Organization (WHO) during the same time—to battling HIV/AIDS, malaria, tuberculosis, and other long-underfunded diseases.

Close on the foundation's heels are a half-dozen other massive new efforts, including the Global Fund to Fight AIDS, Tuberculosis, and Malaria, which has promised $4.8 billion to 128 countries, and the President's Emergency Plan for HIV/AIDS Relief (PEPFAR) from the Bush Administration that has pledged $15 billion to help selected countries. The Global Alliance for Vaccines and Immunization (GAVI), with half of the $3 billion in its coffers supplied by the Gates Foundation, is helping 72 countries fortify the immune systems of their children. And thanks in part to a star-studded cast that is championing the cause—including the rocker Bono, matinee idols Angelina Jolie and Richard Gere, former U.S. presidents Jimmy Carter and Bill Clinton, U.K. Prime Minister Tony Blair, U.N. Secretary-General Kofi Annan, and economist-cum-firebrand Jeffrey Sachs—stories on global health now routinely grace the covers of news magazines.

But amid all the heartfelt praise, the organizations at the forefront of the global health movement are now undergoing both increasing outside scrutiny and internal soul-searching about what they are actually accomplishing. Their goals are hugely, some would say impossibly, ambitious—for instance, upping childhood immunization rates to 90%, or providing "universal access" to anti-HIV drugs. And achieving these grand objectives is proving tougher than many anticipated. Many countries, for instance, face cumbersome procurement policies that make it difficult to translate dollars into drugs. Shortages of trained health-care workers mean that those drugs that are available may not be used properly. Corruption has bedeviled a few large grants, whereas many other aid recipients have found themselves drowning in the required paperwork.

The organizations leading the charge are also beset with growing pains, struggling with issues of accountability, credit, and even fundamental direction. There is also considerable confusion about how all these new entities fit together, as well as how they mesh with old-timers such as WHO, the United Nations Children's Fund (UNICEF), and the World Bank. "There've been lots of creative ideas and lots of new people," says Barry Bloom, dean of Harvard University's School of Public Health. "But there's one missing piece. There's no architecture of global health."

Seeds of change

No single event triggered the outpouring of funds for global health, says Columbia University's Sachs, who cites everything from an obscure 1978 health conference in the USSR to a 1993 report by the World Bank. Bill Gates has called the report, *Investing in Health*, a profound influence. In it the authors made the case that increasing funding for battling diseases in poor countries (then estimated at a mere $41 per person each year—1/30th what was spent in rich countries) would not only reduce the burden of disease but also dramatically improve the economies of poor nations.

CREDIT: GIDEON MENDEL/CORBIS

Critical care. A counselor in South Africa explains the HIV test to children of an infected mother.

Until then, says Seth Berkley, who helped write the report and now heads the International AIDS Vaccine Initiative, health problems were seen "as a drain on the system"—not as a fundamental cause of poverty.

The exploding AIDS epidemic helped underscore the report's dire message about the link between poor health and poverty. AIDS also spawned a powerful activist community that highlighted the slow pace of drug development—and the vast inequities between rich countries and those too poor to afford powerful anti-HIV drug cocktails.

Even before the Gateses jumped in, Cable News Network mogul Ted Turner in 1997 pledged $1 billion, much of it for fighting disease, to the United Nations to help the world's poor. Two years later, Bill and Melinda Gates began donating billions of dollars' worth of Microsoft stock to their foundation, which by 2001 had $21 billion in assets and a strong focus on global health. The size and boldness of their initial grants—including $750 million to kickstart GAVI—jolted public health veterans. "Everyone started dreaming," says Jim Yong Kim, who recently left the head job at WHO's HIV/AIDS program to return to Harvard University. "It was the first time we thought that way. Before, it was scraping for the pennies that would fall off the table."

Boosting vaccination

Because few interventions provide as much bang for the buck as vaccinating children, immunization programs have long been a cornerstone of public health efforts. Since the 1970s, WHO, UNICEF, and Rotary International together have staged massive campaigns that have substantially raised vaccination rates against many childhood diseases. In 1990, for instance, an estimated 75% of the world's children received the combined diphtheria-pertussis-tetanus (DPT) vaccine—a jump from 20% a decade earlier. But soon those efforts began to falter. DPT vaccination rates never climbed again throughout the 1990s. In addition, several years typically passed before developing countries received the benefits of new vaccines introduced into wealthy countries, and even then, vaccines often didn't reach the poorest of the poor.

Launched in 2000 as a public-private partnership outside the U.N. umbrella, GAVI set out to do things differently. Rather than stage pilot projects and then attempt to expand them from the "top down," it took a "bottom-up" approach, asking countries how they would use the money to increase coverage with existing and new vaccines. By hiring UNICEF to do bulk purchasing and distribution, GAVI hoped to drive down vaccine prices and prevent corruption simultaneously. Grants would be canceled if countries did not properly audit their own efforts. Leaders in the global health movement repeatedly refer to the "catalytic" and "galvanizing" impact that GAVI has had on how other organizations operate.

As of September 2005, GAVI had made 5-year commitments to 72 countries for $1.6 billion worth of support. This has led to the vaccination of some 100 million children, sparing more than 1 million from premature death due to *Haemophilus influenzae* B, pertussis, hepatitis B, measles, and other diseases, GAVI claims.

In many ways, GAVI's task is easier than those facing programs designed to treat HIV-infected people or to prevent the spread of malaria. Vaccines are, relatively speaking, a simple tool to use. "GAVI is pushing more money through systems that generally were working pretty well," says Roy Widdus, who led a now-defunct GAVI predecessor called the Children's Vaccine Initiative.

Hands on. Bill Gates drops the polio vaccine into the mouth of a boy in New Delhi.

New Global Health Efforts

ORGANIZATION	FOCUS	YEAR LAUNCHED	DONORS	PLEDGED, COMMITTED, OR SPENT FUNDS*
Bill and Melinda Gates Foundation	Global health	2000	Bill and Melinda Gates	$6.2B
The Global Fund to Fight AIDS, Tuberculosis and Malaria	Financing treatment and prevention	2002	Governments, foundations, corporations	$8.6B
President's Emergency Plan for AIDS Relief (PEPFAR)	Financing and delivery of HIV/AIDS prevention and treatment	2004	U.S. government	$15B
International Finance Facility for Immunization	Financing vaccine delivery/GAVI	2005	U.K., France, Italy, Spain, Sweden	$4B
Multi-Country HIV/AIDS Program	Financing scale-up of existing government and community prevention and treatment efforts	2000	World Bank	$1.1B
Global Alliance for Vaccines and Immunization (GAVI)	Financing and delivery of childhood vaccines	1999	Gates Foundation, governments	$3B
Public-Private Partnerships	Drugs, vaccines, microbicides, diagnostics	n/a	Philanthropists, governments, industry	$1.2B
Anti-Malaria Initiative in Africa	Cut malaria incidence in half by 2010 in 15 countries	2005 (proposed)	U.S. government	$1.2B
United Nations Foundation	Children's and women's Health	1998	Ted Turner	$360M

* Overlap exists between organizations (e.g., PEPFAR money supports the Global Fund).

CREDITS: JEFF CHRISTENSEN/AFP/GETTY IMAGES

Pro Bono. The Irish rock star devotes much of his free time to helping Africa battle infectious diseases.

CREDIT: ASSOCIATED PRESS

Even so, underimmunization of children remains a major concern. As UNICEF recently pointed out, more than 2 million children a year still die from vaccine-preventable diseases. GAVI has also had to reassess its own overly optimistic projections. GAVI initially envisioned that after 5 years of "bridge" funding, countries would have figured out how to finance and provide the increased immunizations themselves. But that's not happening, says Tore Godal, who headed GAVI from its inception until last January and now works as an independent health adviser in Geneva. Poor countries simply did not get the increase in health budgets that GAVI had anticipated, says Godal. As a result, GAVI recently decided to offer bridge funding for 10 years. Even so, it remains unclear whether countries can take over as initially envisioned.

William Muraskin, a history professor at The City University of New York, Queens College, criticizes GAVI for several "fundamental flaws." In an article published in the November 2004 *American Journal of Public Health*, he asserts that GAVI's bottom-up philosophy is illusory. He also contends that countries "had to be wooed" and "financially enticed" to accept GAVI's goals as their own. In particular, he questions the group's emphasis on hepatitis B vaccine. He points out that GAVI has immunized more children with it than all the other vaccines combined. "I'm not opposed to hepatitis B vaccination, but I do know that for many countries that adopted it, it was low man on the totem pole" compared to devoting resources to malaria, respiratory diseases, and malnutrition, he says.

Godal counters that no one forces countries to submit proposals. "It is up to the countries to decide what they want to apply for within the remit of GAVI," he says, adding that the hepatitis B vaccine indeed was a priority for many. GAVI Executive Secretary Julian Lob-Levyt says its most sobering challenge will be finding the money to purchase expensive new vaccines now on the horizon, such as those in the pipeline for pneumococcal disease, rotavirus, and human papillomavirus.

Gates fate?

In December 2004, officials at the Bill and Melinda Gates Foundation invited a power-packed group of outsiders to the Carter Center in Atlanta, Georgia, to discuss the direction of what had recently become the world's largest philanthropy. Former U.S. President Jimmy Carter attended the small gathering, as did a select group of leaders from academia and nonprofits, the prime minister of Mozambique, WHO's Jim Kim, the director of the Wellcome Trust, and the president of the U.S. National Academy of Sciences. The group lavished praise on the Gateses, but a few participants voiced misgivings that the young foundation's global health program was starting to head off course. Carter in particular gave a blunt speech criticizing the program for having become too enamored with basic research at the expense of delivering drugs and preventives today. Patty Stonesifer, who co-runs the foundation with Bill Gates Sr., recalls the essence of Carter's message this way: "I'm an impatient man—I want to save some people now."

By and large, the global health community has appreciation that borders on reverence for the way the Gates Foundation has reinvigorated their efforts. And from the outset of its global health program, the foundation has attempted to fund projects like GAVI that deliver existing medicines as well as riskier basic research

Pressing Needs Remain

Disease Burden and Funding Comparison

CONDITION	GLOBAL DISEASE BURDEN (million) DALYs*	R&D FUNDING ($Millions)	R&D FUNDING per DALY*
Cardiovascular	148.190	9402	$63.45
HIV/AIDS	84.458	2049	$24.26
Malaria	46.486	288	$6.20
Tuberculosis	34.736	378	$10.88
Diabetes	16.194	1653	$102.07
Dengue	0.616	58	$94.16

**Disability-Adjusted Life Year, a measure of healthy life lost.*

SOURCE: MALARIA R&D ALLIANCE

Estimated Percentage of People on Antiretroviral Therapy Among Those in Need (as of June 2005)

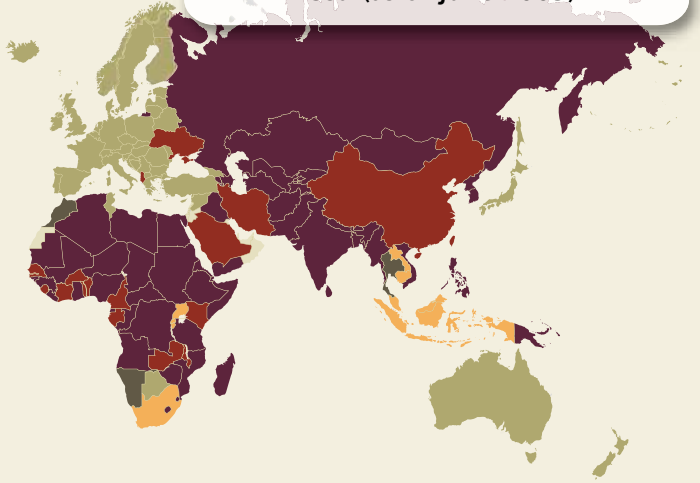

endeavors. Yet several people *Science* interviewed, who requested anonymity, complained that the foundation over the past 3 years has tilted too far toward duplicative, fundamental research that often fails and has also lost its nimble derring-do, becoming more like the U.S. National Institutes of Health (NIH). "How can Bill Gates have his name attached to an organization that's slower than the U.S. government?" asks one. "They've gone from being an easy foundation with which to deal to one that's very complicated and bureaucratic," says another.

Several critics attribute the shift to Richard Klausner, the former director of the U.S. National Cancer Institute (NCI), who ran the foundation's global health program from 2002 until announcing his resignation last September (*Science*, 16 September 2005, p. 1801). In particular, they point to two programs that started under Klausner's tenure.

One is Grand Challenges in Global Health, a bold effort to fund research that could lead to breakthroughs deemed most likely to improve health in poor countries. The foundation has won plaudits from both inside and outside the research community for aggressively seeking ideas from more than 1000 scientists around the world. But the process took too long, say critics—more than 2 years. And some are unhappy with the 43 final selections, most of which focus on fundamental, long-term, high-risk research. Critics say the Grand Challenges are diverting $436 million of foundation money to support the kinds of research that NIH should fund. Although several of the winning proposals are unusually inventive and provocative, there is also a distinctly developed-world flavor to these labs: All but three projects are headed by researchers from the United States, Europe, or Australia. "The Grand Challenges are very, very much NIH stuff," says Peter Piot, head of the United Nations Joint Programme on HIV/AIDS (UNAIDS). "I always felt the strength of the Gates Foundation was that it was very serious money backed by a big name catalyzing work in developing countries."

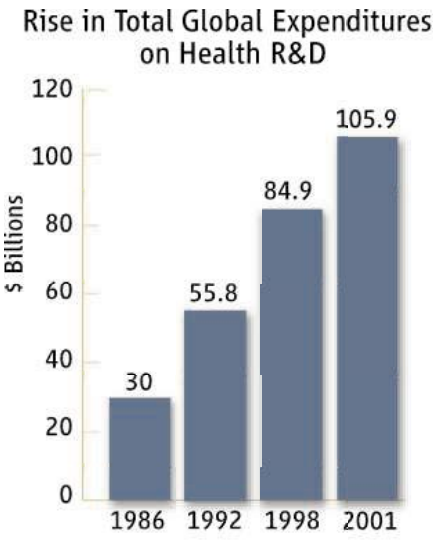

Raising the bar. The rise in funds has triggered a rise in expectations.

Klausner says the foundation can't be all things to all people, explaining that the increased emphasis on research and development reflects the wishes of Bill and Melinda Gates. "It's a complicated set of tradeoffs," says Klausner, who also had strong outside support during his tenure.

Another project that has received substantial Gates funding—and raised some eyebrows—is the Global HIV/AIDS Vaccine Enterprise, a multi-institutional effort to draw a blueprint for the field and then create consortia of researchers to address the most critical questions. NIH, a partner in the enterprise, has already committed more than $300 million to what's called the Center for HIV/AIDS Vaccine Immunology (CHAVI), and Gates has pledged another $360 million to form similar groups. Some AIDS vaccine investigators fear that a small group of elite, well-funded researchers will receive the lion's share of the money to explore questions that they would have pursued without the extra help.

Although it has yet to be announced publicly, the Gates Foundation indeed plans to award part of its $360 million Enterprise money to at least two members of the CHAVI team. And another CHAVI team member won a $16.3 million Grand Challenges award from Gates to do related work.

Foundation officials defend their choices. Helene Gayle, who heads the HIV/AIDS program for the foundation, says, "There's a logic to going with success" and that they didn't want to exclude "the usual suspects" just because they were already well funded. Gayle adds that Gates is specifically working with NIH to make sure that they do not fund researchers for the same work twice. And she says the foundation made an effort to select lesser known people, too, in an attempt to create a network of researchers who might not otherwise collaborate. "So maybe some of the same players," says Gayle, "but we hope a different game."

AIDS aid

Funding on HIV/AIDS dwarfs that of any other infectious disease. Between 1996 and 2005, annual spending on AIDS programs in developing countries shot from $300 million to more than $8 billion, according to UNAIDS estimates, with most of this astonishing jump coming from the Global Fund, the World Bank's Multi-Country AIDS Program (MAP), and PEPFAR. In contrast, WHO says the next largest killers, malaria and tuberculosis,

SOURCE: AIDSCAP

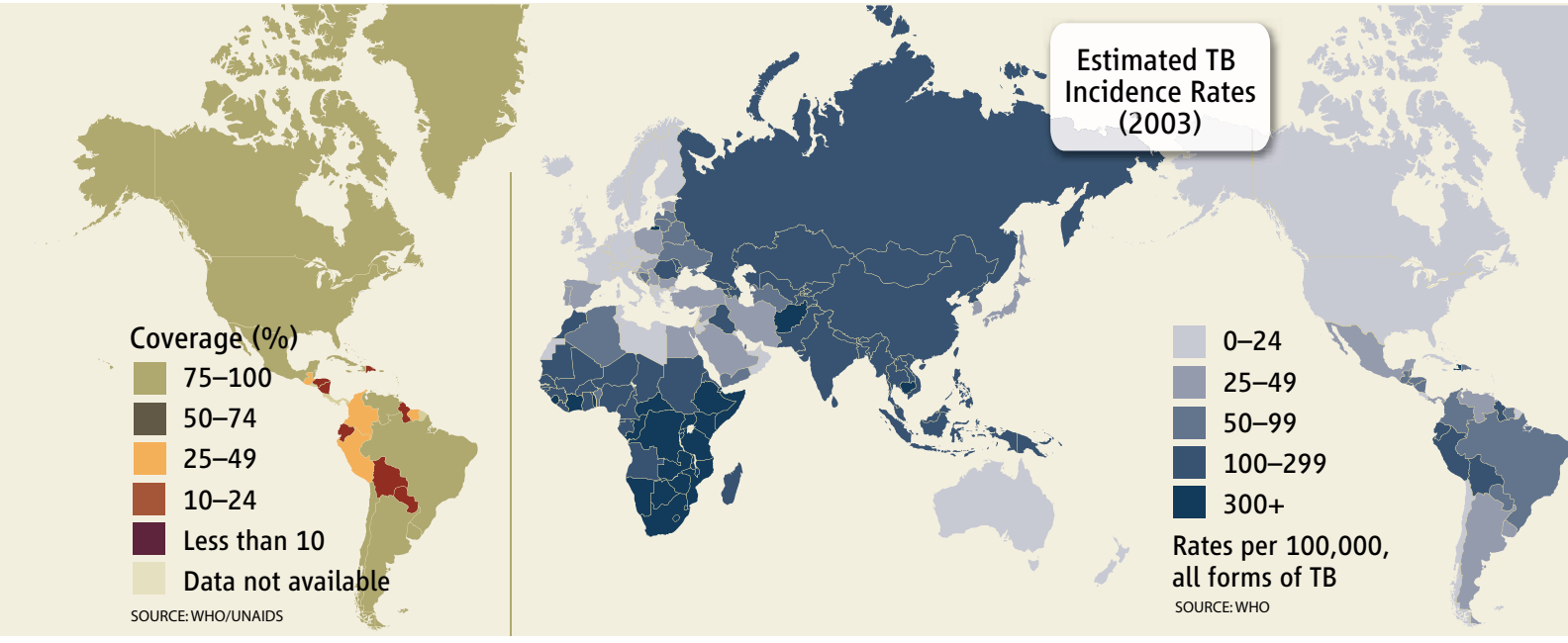

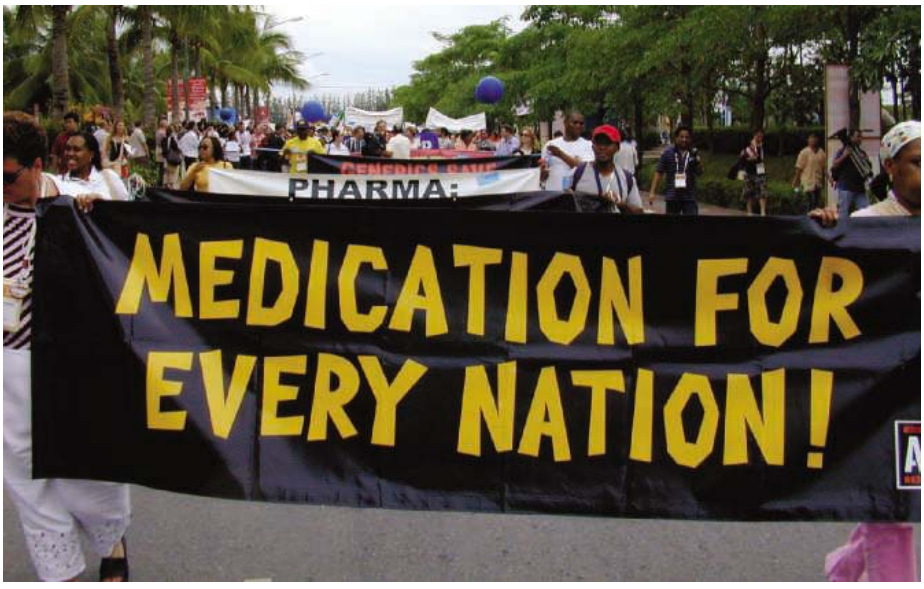

Leading the way. The global health movement received a huge boost from AIDS activists, shown here staging a protest march in Thailand.

together receive less than $2 billion each year.

But people are questioning how much improvement this investment in HIV/AIDS is buying on the ground. A related concern is the amount of time grant recipients are spending simply sorting out the massive amounts of red tape created by the various programs and their overlapping agendas.

The biggest AIDS donor is the Global Fund. Like GAVI, the fund has rigorously avoided the top-down approach; it prides itself on being "country owned" and inclusive. Transparency and accountability are the buzzwords. The fund, which supports everything from providing antimalarial bed nets to anti-HIV drugs, has no staff permanently in countries and channels money through local financial institutions, as opposed to the World Bank. Rather than offering central drug procurement, the fund encourages countries to strengthen their own supply-and-distribution systems.

But critics say the goal of giving countries complete autonomy has come at too steep a price. The fund disburses money to countries only when they hit specific milestones, and since January 2004, they have been falling behind, according to Aidspan, a New York City–based watchdog of the Global Fund. The gaps in disbursement suggest that "deliverables" such as drugs and bed nets aren't reaching populations as quickly as hoped. "The thing I really want to know about is not dollars disbursed but pills in mouths," says Bernard Rivers, who heads Aidspan.

The fund is "a very good thing, but there are huge problems in terms of operating it," agrees Winstone Zulu, an AIDS and TB activist in Zambia. Zulu says other longtime donors closed their pocketbooks when the fund arrived, but that the new money has become ensnarled in bureaucratic tangles, and some critical programs in Zambia had to shut down.

Global Fund Director Richard Feachem agrees that it's a "mixed portfolio" when it comes to countries "turning the money into products." Procurement is a "key bottleneck," he says, as some countries have "sclerotic" procedures. "They were designed to prevent corruption, and they actually prevent procurement," says Feachem. "We're doing a lot of changing in thinking."

In two countries, Ukraine and Uganda, the fund suspended grants because of serious country mismanagement and outright corruption. A handful of other countries have almost had their grants canceled for failing to reach milestones.

On top of these problems, the fund has never had as much money as its creators envisioned. "The Global Fund is chronically begging for money from the rich countries," says Sachs, one of its key proponents. "And this has meant that the Global Fund has not been as clear or inviting as it should have been to poor countries to put up very bold strategies." In the latest financing round this September, donors committed $3.7 billion for 2006–'07—far short of the projected $7 billion the fund says it needs.

The World Bank's much smaller MAP, which provides more flexible aid both to deliver medicines and to build health systems, faces similar concerns. A review of six MAP projects in 2004 found that the bank did not offer enough technical guidance, nongovernmental organizations (NGOs) were often included more in name than in practice, and none conducted adequate monitoring and evaluation.

The Bush initiative PEPFAR is the most recent entry into AIDS aid. It got off to a fast start in delivering drugs to people largely because of its top-down strategy that includes staff on the ground and central procurement. Salim Abdool Karim of the University of KwaZulu-Natal in South Africa says PEPFAR has been "amazingly successful" in his country and has had "much better politically sensitive management on the ground" than the Global Fund.

Yet Karim and many others take exception to some of PEPFAR's requirements, which are tightly tied to the Bush Administration's conservative agenda. For instance, those who receive PEPFAR grants must have a policy "explicitly opposing prostitution," which Karim and others say has threatened their research and prevention efforts with sex workers. "This is reprehensible," says Karim. PEPFAR has also been criticized for devoting one-third of its prevention budget to abstinence programs, downplaying the value of condoms in the general population, and limiting the use of generic drugs by insisting that they first be approved by the U.S. Food and Drug Administration. (A U.S. Institute of Medicine panel is reviewing PEPFAR and plans to release its findings by this spring.)

A report issued in November 2005 by 600 treatment activists, *Missing the Target*, sharply rebuked the Global Fund, PEPFAR, the World Bank, and others for failing to work together as effectively as possible in delivering anti-HIV drugs. "A much more systematic approach to setting goals, measuring progress, and assessing and addressing barriers is needed."

Thirty's a crowd. A confusing cluster of efforts aims to help Tanzania with its HIV/AIDS epidemic.

Architectural indigestion

UNAIDS issued a report in May 2005 that had telling cartoons about the tangle of various stakeholders working on HIV/AIDS in Tanzania

CREDITS (TOP TO BOTTOM): K. BUCKHEIT/*SCIENCE*; ADAPTED FROM UNAIDS/UNAIDS; J. COHEN/*SCIENCE*

Public-Private Partnerships Proliferate

The label "neglected diseases" packs a rhetorical wallop, as it conjures up needy causes that the world callously has ignored. But the phrase is losing some of its punch when it comes to malaria, tuberculosis, Chagas, dengue, visceral leishmaniasis, and African trypanosomiasis. Although profit-minded pharmaceutical companies have long shied away from research and development on drugs against maladies that mainly afflict the poor, 63 drug projects now under way are targeting these very diseases. As Mary Moran wrote in the September 2005 issue of *PLoS Medicine*, "The landscape of neglected-disease drug development has changed dramatically during the past five years."

Moran heads the Pharmaceutical R&D Project at the London School of Economics and Political Science. In its recent analysis of drug-development projects for neglected diseases (it did not analyze vaccines or diagnostics), Moran's team credited a raft of new "public-private partnerships" (PPPs)—80% of which are funded through philanthropies—for the surge in new efforts.

Pioneered by the Rockefeller Foundation and later by the Bill and Melinda Gates Foundation, PPPs link big pharmaceutical companies or smaller biotechs with academics, nongovernmental organizations, and multilateral groups such as the World Health Organization. Ten years ago, not a single PPP for global health existed. Today, there are nearly 100 of them, in the most liberal definition, with a combined war chest of more than $1 billion. "It's a seismic change," says Seth Berkley, head of the International AIDS Vaccine Initiative, which, at 10 years of age, is the granddaddy of PPPs for global health.

Moran and her co-workers predict that as many as nine products now in development will come to market in the next 5 years. In each case, the companies have agreed to sell any resultant drugs to poor governments at deep discounts or no profit. Moran's group further notes that between 1975 and 2000, the pharmaceutical industry developed a meager 13 new drugs for neglected diseases—and because of their high prices, only one was widely used.

Companies that enter into PPPs have little prospect of making money on the drugs they develop, but Moran notes that they face relatively limited financial risk because their partners typically pay for the most expensive part of the process: staging large, clinical trials. This "no profit–no loss" business model does offer big pharma benefits: a good public image and an introduction to developing-country markets and researchers who might help them elsewhere.

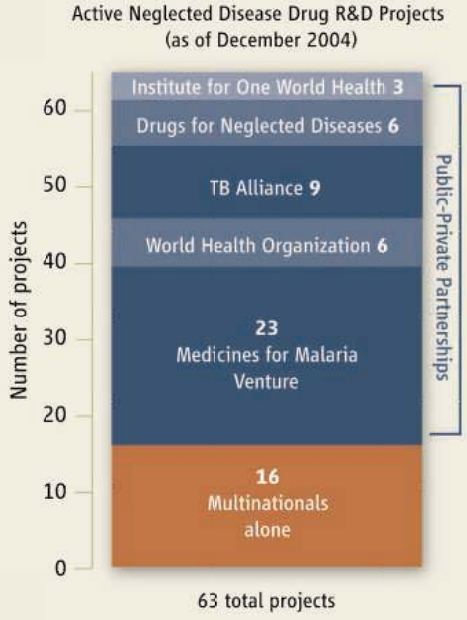

Business as unusual. PPPs account for nearly 75% of R&D projects under way to develop drugs to treat neglected diseases.

Although the entry of big pharma into this field is welcome—and, some say, long overdue—the problem is by no means solved, cautions Peter Hotez of George Washington University in Washington, D.C. In an article in the November 2005 issue of *PLoS Medicine*, he and his co-authors point out that many diseases remain neglected. "When people speak of global health, the first thing you hear about is HIV/AIDS, malaria, TB, and you're liable to think that's all there is," says Hotez, who works on hookworm vaccines. Hookworm, schistosomiasis, leprosy, and 10 other neglected tropical diseases "affect at least as many poor people as the big three," they write. And they contend that for a mere 40 cents per person a year, four existing drugs could be used to quickly reduce the harm caused by seven of these scourges. **–J.C.**

SOURCE: PHARMACEUTICAL R&D POLICY PROJECT

and Mozambique (see graphic). The illustrations could have spotlighted just as aptly the architecture of aid for tuberculosis, malaria, and other diseases that all have a plethora of eager new players trying to help.

The cartoons depict a spaghettilike squiggle of lines connecting dozens of bubbles that represent UNAIDS, WHO's 3 by 5 program (which failed to reach its goal of having 3 million people on treatment by the end of 2005), UNICEF, PEPFAR, the Global Fund, the World Bank's MAP, and a variety of other donors, local ministries, and NGOs. The overall effect is a comical mess, but the problem is anything but. "We were stepping on each other's toes, and in some countries it was destructive," says Debrework Zewdie, who heads MAP and also sits on the board of the Global Fund. "Imagine the amount of time that countries spend catering to the different donors rather than fighting epidemics."

The UNAIDS report described a potential solution. In April 2004, the various stakeholders met in Washington, D.C., for a Consultation on Harmonization of International AIDS Funding and agreed to try to quell confusion by instituting a principle called "the three ones." It calls on each country to have one HIV/AIDS budget, one national AIDS coordinating committee, and one national monitoring and evaluation system that can report the same data to each donor.

As a follow-up to the D.C. consultation, UNAIDS formed a Global Task Team to analyze the "institutional architecture" that connects the various stakeholders in HIV/AIDS. Among the team's sweeping recommendations: establish a joint U.N.–Global Fund problem-solving team to address bottlenecks and develop a scorecard to rate performances of donors and recipients alike. "We're trying to bring some order into the universe," explains UNAIDS Director Piot.

Others are beginning to ask similar "architectural" questions about the broader universe of global health. In the November issue of *Nature Reviews Microbiology*, former GAVI head Godal argues for a more "holistic" approach that embraces the differences between bilateral, multilateral, and targeted approaches such as GAVI—rather than fighting about which one works best. "We need a summit of key players and a continuous kind of work plan to address issues in a systematic way and not on an ad hoc basis," says Godal.

If there's one universal, time-tested truth in the global battle against infectious diseases, it is this: easier said than done. For decades, rich countries have attempted to help poor ones, and poor ones have struggled to help themselves. Yet preventable, treatable, and even curable illnesses have continued to gain ground and cause massive suffering. The revolution that is sweeping through the global health effort has clearly brought more money, tools, creative ideas, and momentum than ever before. But the goal—narrowing the gap between aspirations and actions—remains a staggering challenge, and what already has become evident to many of the new and old players alike is that they have to monitor progress more vigorously, make midcourse corrections more quickly, and work together more effectively. Because at the end of the day, the question is not simply whether this revolution has done some good, but whether, as Jimmy Carter asked of the Gates Foundation, it has fully exploited all the remarkable possibilities. **–JON COHEN**

RESEARCH MANAGEMENT

U.S. Rules on Accounting for Grants Amount to More Than a Hill of Beans

The latest government proposal exposes the problems facing scientists who strive to do good research without stepping over the line

Stalking a kidney gene defect could make Lisa Guay-Woodford a lawbreaker.

Like scientists everywhere, the pediatric nephrologist at the University of Alabama, Birmingham (UAB), knows that she can improve her chances of winning a grant from the National Institutes of Health (NIH) by including preliminary data in her application. But gathering those kidney data poses a dilemma for Guay-Woodford. Simply put, it's against the law to apply resources from an existing grant toward a new project. And Guay-Woodford knows that the U.S. government isn't playing games. Last spring, her university paid $3.4 million to settle allegations that it overstated how much time and effort its scientists had devoted to certain federal grants.

These and other administrative rules about how universities spend government money are intended to guard against the misuse of taxpayer dollars, and they are being enforced more firmly than ever. In the past 3 years, for example, Harvard University, the Mayo Clinic, Northwestern University, Cornell University, and Johns Hopkins University have paid the Justice Department more than $21 million to settle cases similar to UAB's. Although none of the schools has acknowledged committing a crime, scientists are increasingly concerned that the laws, for all their good intentions, don't square with how science is done. And many university administrators think that the gap is widening. In November, the Department of Health and Human Services (HHS) issued a notice urging more rigorous timekeeping and beefed up research compliance programs (www.oig.hhs.gov/fraud/complianceguidance.html#1). The comment period closes on 30 January.

"There's a dynamic tension" between accountability and intellectual freedom, says Guay-Woodford, who has $1.5 million in NIH grants this year and runs a seven-person lab. But she worries about the future of U.S. research if the bean counters prevail. "Where's the creative energy that has been the hallmark of science?" she asks. "Where's that going to go?"

"An elaborate fiction"

The federal government didn't always press scientists to follow its rules to the letter. The 1958 regulation under which time and effort reporting falls, known as circular A-21, allows for some flexibility, and "since no one was enforcing it, people shaded more on the latitude of it," says Peter Anderson, a pathologist at UAB. University administrators asked Anderson to design an education program on the regulations for faculty after UAB's settlement with the Justice Department.

"We want to be sure that we're getting what we're paying for."

—Karen Tiplady, NSF

But federal attitudes appear to have stiffened in recent years. The process began in February 2003, when Northwestern University in Evanston, Illinois, agreed to settle government claims that its scientists had spent less time than promised on federally funded research. "Federal agencies are [now] less willing to treat universities differently than they would treat a defense contractor" with regard to documenting costs and time spent on projects, says Robert Kenney, director of the grants and contracts group at the Washington, D.C., law firm Hogan & Hartson, which has defended several institutions sued by the government.

Federal agencies such as NIH and the National Science Foundation (NSF), which dispense billions of dollars each year in academic research grants, require applicants to estimate how much time they will spend on a particular project and, if successful, to notify the funder if their workload changes during the course of the project. In other words, a 25% commitment means 10 hours in a 40-hour workweek, or 20 hours in a scientist's more typical 80-hour week. Because weekly schedules fluctuate, with commitments added and dropped, schools tend to ask for records only once a quarter or even less often.

Government officials say that the accounting practices, although burdensome, are crucial. "We want to be sure that we're getting what we're paying for," says Karen Tiplady, chief of the cost-analysis and audit-resolution branch at NSF. The estimates guide funding decisions by determining whether an experiment's goals are achievable and whether a project is appealing. "If the principal investigator is going to be very strongly involved in the intellectual leadership of the project, NIH wants to be assured that that person is spending sufficient time" on it, says Donna Dean, who helped oversee extramural research funding at NIH before becoming senior science adviser at Lewis-Burke Associates, a Washington, D.C., consulting firm.

CREDITS (LEFT TO RIGHT): ANN HAMILTON/ATLANTA VA MEDICAL CENTER

All in a Day's Work >>

Atlanta cardiologist Samuel Dudley juggles caring for patients, doing basic research on heart-rhythm disorders, teaching students, and performing administrative duties during one recent 12-hour day.

A fundamental assumption of both the laws and the new HHS guidance is that it's relatively easy for scientists to allocate their time among various projects. But, researchers note, the boxes on the forms don't always mesh with the real world. Take the hectic life of cardiologist Samuel Dudley. His 14-person lab at the Atlanta VA Medical Center in Georgia runs on grants from NIH, the Veterans Administration, and the American Heart Association, each with its own set of time-reporting rules. Dudley also teaches, runs an NIH-funded clinical trial at nearby Emory University, and sees patients at the VA medical center, where he's chief of cardiology.

Adhering to the rules for his lab research is "extra-special complicated," Dudley explains, citing complementary grants from different funders involving heart rhythm problems in pigs. "One title is 'Superoxide and the Pathogenesis of Atrial Fibrillation,' and the other is 'Nitric Oxide and the Pathogenesis of Atrial Fibrillation,' " he says. Then there's the problem of accounting for what he actually does, such as a recent project on how oxidative stress influences membrane proteins that go awry in atrial fibrillation. "It wasn't in the aims of either [grant]," he says, but "it's related to both."

Dudley faces a similar problem when purchasing equipment for pig surgery. "If I buy a piece of equipment to operate on a pig and I've got two pig grants, what do I do" about assigning the equipment's cost, he asks. "The fairest way would be to split it down the middle," he admits. But that choice means extra paperwork. Dudley prefers to assign each piece of equipment to a particular grant. "Sometimes filling the commitments of these grants requires a flexibility that is not built into the system," he says.

Others are more blunt. "The so-called time spent on a grant is an elaborate fiction," says Steven Block, a biophysicist at Stanford University in California. "What's relevant is whether I do the work."

CREDITS (LEFT TO RIGHT): ANN HAMILTON/ATLANTA VA MEDICAL CENTER

Stumbling blocks

But for auditors, a scientist's productivity isn't what matters. One of the most common problems in a federal audit, say Kenney and Constance Atwell, a consultant to NIH and other government agencies, is a university's failure to properly document faculty time and effort. The forms might not be signed, or submitted, or they might be completed by an individual "who didn't know what the effort actually was," says Kenney. "Compliance officer positions are probably the biggest growth industry in terms of administrative positions at major research universities," says Tony DeCrappeo, president of the Council on Governmental Relations in Washington, D.C., which helps schools address compliance issues. Most schools, he says, "are in the process of reassessing their compliance structures."

"The so-called time spent on a grant is an elaborate fiction. What's relevant is whether I do the work."

—Steven Block, Stanford University

Two common stumbling blocks are trying to separate time spent on patient care from that spent on a clinical trial and assigning to existing federal grants effort devoted to gathering preliminary data for an unfunded project. This so-called piggybacking or bootlegging is "a time-honored practice. … Anyone who says they don't [do this], I would say, is a liar," says Block.

Although some rules are bent because researchers feel they have no choice, other violations appear to be unintentional. One frequent misstep is in the denominator used to calculate time and effort. Many scientists mistakenly believe that NIH, which funds the majority of U.S. scientific research, bases its measurements on a 40-hour workweek. That assumption "is not correct," says Kenney, and making it can get universities into trouble. Notes UAB's Anderson, "I don't know how many times I've had people say, 'I'll just go home and work on my grant, and that way it won't count.' " All effort matters, he emphasizes, and needs to be counted in the equation.

Scientists and university administrators would like the government to focus on the accomplishments of a research project rather than the percentage of a researcher's time devoted to it. "Time is sort of false," says Nancy Wray, director of the office of sponsored projects at Dartmouth College in Hanover, New Hampshire. Dartmouth is currently fighting an accusation from HHS that it overbilled NIH $36,268 on a diagnostic radiology grant.

Although Wray and others wish to de-emphasize time, the government seems to be heading in the opposite direction. The November HHS guidance appears to stress "timekeeping" more heavily than does A-21, the existing regulation. Although the guidance would be voluntary, universities are dubious that auditors will see it that way. "Either there are rules or there aren't rules," says Pierre Hohenberg, senior vice provost for research at New York University, which is reviewing its time and effort reporting procedures. "The government getting into the business of just being helpful … is easily misinterpreted."

All of this debate doesn't solve Guay-Woodford's dilemma about how to assemble her kidney grant proposal. So she's planning to do it in the evenings and on weekends. "That is, I think, in keeping with the spirit of the guidelines," she says. "I'm not spending 3 weeks doing nothing else. … But it's not absolutely [sticking] to the letter."

–JENNIFER COUZIN

A Career Change Possible for North Korea's Nuclear Scientists?

Banking on a successful resolution of the nuclear crisis, experts are drawing up plans to ensure that North Korea's weapons talent is not perilously left out in the cold

SEOUL—Tucked away in a corner of North Korea's Yongbyon nuclear complex is a Soviet reactor designed for research but allegedly used in the 1980s to make plutonium. Suppose North Korea were to fire it up again: Would the West be outraged? Not necessarily. Some experts in weapons control are proposing a deal between North Korea and the big powers that would allow North Korean scientists to keep a hand in nuclear technology. If this happens, the vintage Soviet reactor might come back on line to make radioisotopes for medicine, not plutonium for bombs.

This is one potential outcome of negotiations between six nations—China, Japan, Russia, South and North Korea, and the United States—on North Korea's nuclear future. The parties have been in a tense standoff for 3 years on how to roll back nuclear weapons development, and the talks have been in recess since autumn. But diplomats say they hope negotiations can resume as early as next month in Beijing.

Behind the scenes, meanwhile, officials and experts are wrestling with a daunting set of challenges. They need a credible plan for dismantling North Korea's weapons complex, verifying that weapons R&D has ceased, scrubbing radioactive hot spots, and finding employment for thousands of nuclear specialists and support staff. Cleaning these Augean stables could cost up to $500 million.

Proposals are being crafted mostly out of the public eye. "Nobody wants to talk about future activities. It may affect the atmosphere of the talks," says Maeng-Ho Yang, a foreign policy researcher at the Korea Atomic Energy Research Institute in Daejeon, South Korea. But in interviews with *Science*, South Korean and U.S. experts lifted the veil on emerging plans. Possibilities include collaborations between North Korean nuclear researchers and counterparts in South Korean and U.S. national labs, an international science center in Pyongyang, and flagship projects such as radioisotope production. Other suggestions came to light last month in a report from the Center for Strategic and International Studies (CSIS), a think tank in Washington, D.C. Its proposals are grounded in an effort begun 15 years ago to reduce the threat of Russia's nuclear arsenal.

North Korean officials have refused to discuss such programs. "They feel it's premature and perhaps erodes their negotiating position" to broach the subject before a comprehensive agreement is reached, says one Bush Administration official, who requested anonymity due to the sensitivity of the negotiations. At the same time, the United States and South Korea want to move quickly after a settlement. "There's an enormous incentive to get the job done," says Matthew Bunn, a nonproliferation expert at Harvard University.

A fuzzy picture

In last September's round of Six-Party Talks, North Korea agreed to give up its nuclear arms ambitions in exchange for economic and energy assistance, a pledge that the United States would not attack it, and the normalization of relations with the United States. There are two main sticking points. North Korea wants to know precisely when it will receive a light-water reactor, which the other parties promised to discuss providing "at an appropriate time." It would generate electricity for the energy-starved country with negligible risk of plutonium being diverted for weapons use. The second impasse: Diplomats want to know precisely when and how North Korea will dismantle its weapons program.

The CSIS report calls on Six-Party negotiators to push for an ambitious effort modeled after the U.S. Cooperative Threat Reduction (CTR) programs. Launched after the Soviet breakup in 1991, CTR programs have secured nuclear materials and redirected weapons expertise in the former Soviet Union, and they were recently expanded to eliminate the vestiges of weapons R&D in Iraq and Libya. Threat-reduction programs could anchor work in nonmilitary objectives and squelch North Korean attempts to export sensitive nuclear technologies. In addition, CTR "would establish beachheads of cooperation which may have a spillover effect, helping to break down the North's isolation and to integrate it into the international community," states the report, authored by CSIS analysts Joel Wit, Jon Wolfsthal, and Choong-suk Oh.

The project's first order of business would be to identify all components of North Korea's nuclear R&D complex—no simple task. Six-Party negotiators concede that their knowledge of North Korea's nuclear program is incomplete. During the Cold War, the Soviet Union "trained several thousand nuclear scientists," claims Yang. If "every facet" of North Korea's program is taken into account, the CSIS report estimates that up to 10,000 workers were involved. But those with critical expertise who could aid weapons R&D, observers believe, number in the dozens. No key player is known to have defected.

North Korea's nuclear complex is thought to involve dozens of facilities, only a few of which are known publicly. Preeminent among these is Yongbyon, particularly its 5-megawatt reactor and radiochemical laboratory for extracting plutonium from spent fuel. Dismantling Yongbyon would involve removing the nuclear materials (possibly to Russia), safely storing hot pieces of the reactor, cleaning up radioactive contamination at the site, and finding alternative careers for thousands of workers.

Hot spot. North Korea's nuclear complex at Yongbyon lies at the center of a technology-development program that may involve as many as 10,000 workers.

A thornier issue is dealing with unknown or unidentified installations. In October 2002, U.S. officials charged that North Korea is engaged in a clandestine effort to create a uranium bomb. North Korea denied the allegations, withdrew from the nuclear nonproliferation treaty, and ordered resident inspectors

CREDIT: ASSOCIATED PRESS

Getting to the bottom of it? A U.S. delegation visited Yongbyon's spent fuel storage facility in January 2004. If a deal is struck with North Korea, cleaning up radioactive contamination and redirecting scientists to civilian projects are high priorities at Yongbyon.

CREDIT: SIEGFRIED HECKER

from the International Atomic Energy Agency to leave the country at the end of 2002, precipitating the current crisis. Japanese officials have told *Science* that they are swayed by U.S. intelligence, described publicly by the CIA as indicative of North Korean attempts to acquire components for precision centrifuges to isolate weapons-grade uranium isotopes. China and Russia have expressed skepticism about the allegations; publicly, South Korean officials have been noncommittal.

It looks as though the Six-Party Talks may avoid an agreement that directly addresses the alleged program to make highly enriched uranium (HEU) for bombs. Instead, diplomats are hoping for a subtler approach that would save face for the North Korean government. It would still involve unfettered access to North Korea's nuclear scientists, who U.S. officials insist must be part of any deal. Interviews could yield clues to where to look for enrichment facilities—a centrifuge hall, or more exotic approaches such as electromagnetic isotope separation, a technique with less detectable facilities exploited by Iraq in the 1980s. "For total verification, you need a lot of North Korean scientists to talk," says Jooho Whang, a professor of nuclear engineering at Kyung Hee University in South Korea.

A red star to guide it

One long-term dilemma is how to steer North Korean weaponeers into civilian work. The fear is that specialists might beat a path to Iran or some other country aspiring to nuclear statehood.

The U.S.-led initiative to engage Russian weapons scientists offers lessons for working with the North Koreans. To build trust between the Cold War superpowers, the effort started with small-scale collaborations between researchers from the U.S. nuclear weapons design labs and peers in Russia's closed nuclear cities. This "lab-to-lab" program was augmented in the mid-1990s by the International Science and Technology Center (ISTC), a fund in Moscow and Kiev that has spent more than $600 million employing weapons scientists from Russia and other former Soviet nations on civilian projects.

Plans are afoot to develop a sister lab–style program with North Korea. "It's a very good idea," says former Los Alamos National Laboratory director Siegfried Hecker, an architect of the first lab-to-lab contacts with Russian scientists in the early 1990s. However, U.S. and Russian nuclear scientists were mutual admirers before collaborations were permitted, whereas North Korea's nuclear science community is largely a black box. "We will have to partner closely with the Russians, Chinese, and South Koreans, who know the North Korean scientists better than we do," says Rose Gottemoeller, director of the Carnegie Endowment for International Peace's center in Moscow. Another caveat, Bunn says, is that there is presumed to be a "huge difference in the technological level" between North Korean and U.S. researchers and, as a consequence, "less eagerness on both sides" to work together.

But some U.S. nuclear scientists—including Hecker, who has been to North Korea twice—are eager to get things going. Isotope production, he says, is one potential lab-to-lab project that would interest North Korea.

A first step might be to defang North Korea's IRT-2000 research reactor, where, up until 1992 Western investigators believe, uranium-238 was irradiated to produce enough plutonium for one or two warheads. One nonproliferation objective is to retool the IRT, assembled in 1965, to use low-enriched uranium fuel instead of HEU. North Korea's IRT is already being used to make iodine-131 for cancer therapy, Hecker learned during his second trip to Pyongyang last August. U.S. and North Korean researchers could expand production of isotopes for medicine, agriculture, and industry. An alternative, the CSIS report notes, is to shut down the reactor and instead produce isotopes at a cyclotron obtained from Russia in the 1990s.

Observers envision wider cooperation through a Korean ISTC in Pyongyang. But it "would have to differ drastically" from its Moscow and Kiev brethren, Hecker says. For example, it might have to offer jobs rather than individual grants because money is so tightly controlled in North Korea.

Down the road, nonproliferation experts hope that North Korea's chemical and biological weaponeers will be brought into the fold. Analysts estimate that North Korea has stockpiled as much as 5000 tons of chemical weapons, which would rival Iraq's program before the 1991 Gulf War. Efforts to eliminate Russia's chemical arsenal could offer lessons, the CSIS report notes. The report states that dual-use biological facilities could be used, at a minimum, "to monitor outbreaks of diseases within North Korea and form part of a broader disease tracking system in Northeast Asia."

How all this will play out in upcoming Six-Party Talks is anybody's guess. Following last September's agreement, U.S. negotiators suggested CTR to North Korean diplomats, according to a Bush Administration official. "They came back in a very negative way," the official says. "They don't want to talk about it now." But other envoys have found North Korean officials more receptive to the idea.

Confusion over North Korea's stance also reflects contrasting negotiating tactics: North Korea is striving to clarify a sequence of concessions and rewards, whereas the United States is aiming first to work out the scope of the dismantlement activities that North Korea would be prepared to accept. The negotiating teams have internal battles between hawks and doves, and matters have been complicated by the resignation earlier this month of the State Department's North Korea envoy Joseph DeTrani.

One thing is certain: If North Korea permits the dismantlement of weapons facilities and the redirection of nuclear scientists, tensions would be eased considerably in Northeast Asia. And the economic and security benefits could well entice the reclusive regime into speeding up its rapprochement with the rest of the world.

–RICHARD STONE

Far from home. New Horizons will take nearly 10 years to reach Pluto.

PLANETARY SCIENCE

Long Trek to Solar System's Last Frontier Begins

Next week, a NASA spacecraft sets off to find out whether Pluto and the Kuiper belt hold the key to the solar system's origins

For explorers of the solar system's planets, one destination remains unvisited. Next week, a NASA spacecraft will embark on a nearly 10-year, 6-billion-kilometer journey to cross Pluto off the list. The $650 million New Horizons mission will also fly by two smaller bodies in the Kuiper belt, a region outside the orbit of Neptune that contains icy leftovers from the formation of the solar system.

A huge Atlas V launcher with two additional rocket stages will first propel the 465-kilogram spacecraft on a fast, 1-year trip to Jupiter. The giant planet's gravity will then accelerate the craft toward the outer reaches of the solar system and an encounter with Pluto in the summer of 2015. And the clock is ticking: If the launch is delayed beyond 28 January, a Jupiter gravity assist won't be possible, and the mission will take several more years to reach Pluto.

Ever since its discovery in 1930, icy Pluto has been considered a planetary oddball. Measuring just 2274 kilometers across, it's much smaller than the other planets, and it travels around the sun in an inclined, elliptical 248-year orbit. Pluto and its large moon Charon are more akin to the other denizens of the Kuiper belt, and a special committee of the International Astronomical Union is currently discussing whether Pluto deserves its planetary status.

Principal investigator S. Alan Stern of the Southwest Research Institute in Boulder, Colorado, says a mission to Pluto was first put to NASA in May 1989. "If people had told me back then that it would take 26 years before the Pluto encounter would actually happen, I would have been incredulous," says Stern. In fact, researchers proposed five Pluto missions to NASA in the 1990s, ranging from the very small and lightweight Pluto Fast Flyby to the massive and costly Mariner Mark II.

The situation changed in 2002, when the U.S. National Research Council ranked a Pluto mission as a high priority in its influential Decadal Survey report. "NASA and Congress finally realized that this was not a pet project of a handful of Pluto aficionados but an important mission to learn more about the Kuiper belt and the origin of the solar system," Stern says. James W. Christy, formerly of the U.S. Naval Observatory and the astronomer who discovered Charon in 1978, agrees: "In 2015, the veil of mystery will suddenly be removed. Anything that we anticipate will be overwhelmed by surprises."

As New Horizons races past Pluto and Charon, its telescope, color camera, and infrared spectrometer will map the surfaces and study the composition and geology of what many space scientists consider a double planet. "These may be the most ancient surfaces that we have ever seen in the solar system," says Christy. He also believes that the surfaces may have been shaped by the strong tidal forces between Pluto and Charon that eventually led to their current synchronous rotation, with both objects always presenting the same face toward each other.

The spacecraft's ultraviolet spectrometer will study Pluto's tenuous atmosphere, which has a pressure at the surface just 1/100,000 that of Earth's. The nitrogen-rich atmosphere is the main reason for the rush to get New Horizons on its way: Sometime within the next 20 years or so, it will condense onto the surface as Pluto moves farther away from the sun in its elliptical orbit and cools. "No one can tell you when the atmosphere will collapse," says Stern. "We may well be there in time, but then again, we may be too late." Smaller instruments will study dust particles, charged particles escaping Pluto's atmosphere, and particles in the solar wind.

The mission reaped a windfall in October, when astronomers announced that the Hubble Space Telescope had discovered another two small moons orbiting Pluto. "New Horizons had already been designed for the eventuality of newly found moons," says Stern. "For instance, it is capable of tracking multiple objects during the flyby." Stern expects more discoveries to follow, and Christy agrees: "The new discovery will motivate astronomers to search for even smaller objects. We may be surprised to find debris of various sizes in the system."

Once New Horizons is past Pluto and Charon, planetary scientists will be looking forward to comparing the other icy worlds beyond Neptune's orbit with the more familiar (and smaller) comets that crisscross the solar system. Incidentally, about a year before New Horizons' Pluto flyby, the European Space Agency's (ESA's) Rosetta spacecraft will begin orbiting comet Churyumov-Gerasimenko and will deploy a small lander on its surface. According to ESA's chief scientist Bernard Foing, the future results of New Horizons and Rosetta will provide important clues on the conditions that prevailed when the solar system was born.

NASA's New Horizons "is a challenging mission to the edge of the solar system. There is still much to learn about this unexplored double planet," says Foing. As for Pluto's disputed planetary status, Foing simply describes the small, icy body as "a very interesting object." But Stern and Christy both strongly oppose Pluto's "demotion." "Pluto was defined as a planet in 1930," says Christy. "It requires an extraordinary reason to change history." **–GOVERT SCHILLING**

Govert Shilling is an astronomy writer in Amersfoort, the Netherlands.

CREDIT: NASA

EDITED BY YUDHIJIT BHATTACHARJEE

IN THE COURTS

SAVING THE EVIDENCE. A Virginia state forensic serologist who passed away in 1999 is continuing to serve the cause of justice.

Upon joining the crime lab in 1973, decades before DNA testing became available, Mary Jane Burton instituted the practice of attaching evidence, usually bits of cloth containing bodily fluids, to case files. Last month, outgoing Governor Mark Warner announced that DNA found in the samples had exonerated two men wrongly convicted of sexual assault in 1981 and 1985, bringing the total number of exonerations based on Burton's evidence to five. The most recently exonerated pair had already completed prison terms and requested privacy.

A review begun last year of some 165,000 case files is focusing on Burton's samples and could net as many as 30 exonerations, estimates Virginia Department of Forensic Science Director Paul Ferrara. He notes that Burton was not thinking about DNA analysis as she collected her samples. "She never mentioned those letters," he says.

MOVERS

COMMAND CENTER. The new leader of Berlin's Museum of Natural History has been given complete oversight of the 196-year-old institution—which has run up a tab for $160 million in needed repairs. Paleontologist Reinhold Leinfelder, 48, took up the reins this month as general director, a post that replaces a rotating triumvirate that lacked management experience and often complicated decision-making (*Science*, 2 July 2004, p. 35).

The museum has already committed $22 million to renovate part of its exhibition halls, and Leinfelder has helped find an additional $36 million for the east wing, still in ruins from World War II. But he must line up major funding to modernize the infrastructure and conserve valuable specimens.

Leinfelder, who previously headed a network of museums in Bavaria, says he loves "to show what science does." In 1999, he secured $1.3 million for the Bayerische Staatssammlung für Paläontologie und Geologie to purchase a fossil of the famous early bird *Archaeopteryx*.

Staff members seem glad to have him on board. "It's a new era," says Matthias Glaubrecht, curator of mollusks at the Berlin museum.

AWARDS

VISIONARIES. The inventors of the electronic eye and a team of educators have received the National Academy of Engineering's highest awards for technological achievement and engineering education.

Physicists George Smith, 75, and Willard Boyle, 81, share the $500,000 Charles Stark Draper Prize for their invention in 1969 of the charge-coupled device, the chip that captures images in digital cameras, video recorders, telescopes, medical equipment, and other devices. "We knew that that was the thing," says Smith about the moment of discovery at Bell Laboratories in Murray Hill, New Jersey. Willard calls the award "a great honor."

The academy's $500,000 Bernard M. Gordon Prize for engineering education is being given to Jens Jorgensen, 69, retired from the University of Washington, Seattle; John Lamancusa, 49, of Pennsylvania State University, University Park; Lueny Morell, 53, of Hewlett Packard Co. in Mayagüez, Puerto Rico; Allen Soyster, 62, of Northeastern University in Boston; and José Zayas-Castro, 50, of the University of South Florida in Tampa. Starting in 1994, the group developed the Learning Factory, a program in which students and partners from industry tackle real-world design problems. So far, more than 10,000 students and 200 companies have collaborated on more than 1200 projects.

Three Q's >>

As chancellor of two major research institutions—University of California, Berkeley, and the University of Texas, Austin—**Robert Berdahl** spent more than a decade promoting the value of academic research. So it's hardly a stretch for him to move into the presidency of the 62-member Association of American Universities, a position he accepted last week. The 68-year-old former history professor will take on the 5-year gig this spring, succeeding the retiring Nils Hasselmo.

Q: So should we say congratulations or condolences?
A: Oh, definitely congratulations. I don't have to worry about a medical school, or a football team, or raising lots of money. I'm excited.

Q: A slew of recent reports touting the importance of academic research has raised hopes that the U.S. government will put more money into science. Is this a case of excess exuberance?
A: People are always going to hope for more than is possible. But we academics aren't the only ones making the case. It's industry leaders and the pundits, too. So I think the time is right.

Q: If there really is a looming shortage of scientists, won't the free market solve the problem? What can universities do?
A: Students make their own opportunities. A lot of new industries have been created by new graduates. But they can't do it if they aren't prepared and don't see science as an attractive career. And they can get that training at a university.

Got a tip for this page? E-mail people@aaas.org

CREDITS (TOP TO BOTTOM): CARL LYNN/AP PHOTO/*RICHMOND TIMES DISPATCH*; SNSB; PEG SKORPINSKI

Need help taking your next career step?

ScienceCareers.org Workshops

Learn good interviewing skills from actual industry science recruiters. Join ScienceCareers.org and local Boston scientists as they discuss –

Interviewing Skills for Scientists and Technical Professionals Entering Industry Science

January 30, 2006
MIT Campus, Building 10-230
Cambridge, MA
2:30 p.m. check-in
3:00 p.m. seminar

For information and to register, search for MIT at:
http://sciencecareers.sciencemag.org/meetings

Sponsored by the MIT Careers Office, MIT Postdoctoral Advisory Council, MIT Graduate Student Council and brought to you by ScienceCareers.org

next wave *now part of:*

ScienceCareers.org

We know science AAAS

Chemical weapons among arthropods 178

Balancing clinical database goals 180

Nanotech magnetic logic gates 183

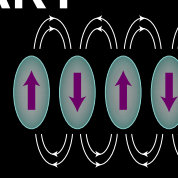

LETTERS

edited by Etta Kavanagh

HIV Research and Access to Treatment

THE POLICY FORUM "PROMOTE CHEMOPROPHYLAXIS RESEARCH, DON'T PREVENT IT" (R. M. GRANT *ET al.*, 30 Sept. 2005, p. 2170) provides a strong rationale for continuing, and even increasing, field research on the applicability of using antiviral drugs to prevent HIV infection in high-risk individuals and subpopulations, particularly in the developing world. It also cogently elaborates best practices for conducting such research ethically. The authors, however, finesse too smoothly three major issues that have been and will continue to be cause for controversy: liability, adjunct therapy, and access.

"Lack of a guarantee for ultimate access…**would undermine the very basis of doing research** in that community or population."
—Warren

Although in some cases, expectations may be unreasonable, there is growing acceptance that compensation for physical harm, antiretroviral treatment for HIV infection during the course of the trial, and a binding commitment for access to the product under investigation if proven safe and effective are legitimate and achievable in clinical research no matter where it is conducted.

Treatment or compensation for physical harm should be a universal standard for medical research. HIV treatment worldwide is coming to be seen as an accepted goal, so those relatively few participants who become infected while in studies can justifiably insist on availability from the study until national programs replace it. Lack of a guarantee for ultimate access, for whatever reason, would undermine the very basis of doing research in that community or population. Increasingly, the international debate is not about the ethics of whether these protections and benefits are appropriate and should be provided, but the logistics of how they can be delivered over many years.

Although there may be no strict international ethical consensus about how to provide for individuals or communities that participate in such research, trial volunteers clearly have the right to negotiate for whatever support they consider necessary and to refuse to participate if it is not provided by sponsors, manufacturers, research institutions, and governments that wish to conduct or support such research.

To argue that research began before such understandings and systems were in place, that "goodwill efforts" would be sufficient, or that prices have come down does not excuse anyone from doing the difficult work of resolving each situation to the satisfaction of all directly concerned. "Good faith" and "a balance" between means and ends should not let anyone conducting or supporting research off that hook.

MITCHELL WARREN

AIDS Vaccine Advocacy Coalition, 101 West 23rd Street, #2227 New York, NY 10011, USA.

Response

WARREN HIGHLIGHTS DIFFICULT AND IMPORTANT issues that apply to all medical research. We agree there are no easy solutions. Clear progress will require ongoing collaboration between communities, investigators, sponsors, and governments. As we all struggle to make best practices even better, we think that research that meets all current standards should proceed, provided that local ethical review boards and fully informed participants agree.

We are taking steps to ensure that PrEP will be accessible to vulnerable populations if it is found to be safe and effective for them. All African countries, and many in Asia and Latin America, are included in Gilead's global access program, which offers tenofovir at the cost of manufacturing, which recently decreased to U.S. $0.57 per day (*1*). A range of agreements have been made to make PrEP available to study participants after the trial, if PrEP is found to be useful. Appropriate long-term implementation of research findings is being promoted through ongoing communication between investigators, communities, research sponsors, health care sponsors, and governments. If found to be highly effective in current trials, PrEP is expected to be affordable, with cost-effectiveness that is comparable to current prevention programs (*2*).

Some people around the world are dying of AIDS because combination antiretroviral treatment is not yet available to them. As members of the global community affected by HIV/AIDS, PrEP researchers and sponsors have made donations to the Global Fund, taught medical courses, assisted with funding applications, provided equipment, helped design and construct clinics, and provided laboratory and clinical services. Antiretroviral therapy has become available through public programs in all regions where PrEP research is conducted. PrEP research protocols also provide primary care and laboratory testing for persons found to be infected during the study, because we have the resources, and we need to learn whether PrEP attenuates the course of HIV infection, if some are not completely protected (*3*, *4*).

"[A] lifelong guarantee of treatment **could exhaust limited research resources and does nothing for** those who elect not to participate in research."
—Grant *et al.*

The issue of whether trial sponsors should guarantee lifetime antiretroviral therapy led to contentious debates in vaccine research (*5*). The present outcome of this debate is that trials rely on publicly funded programs in the host countries to provide antiretroviral treatment to infected trial participants. This outcome reflects both financial and ethical considerations: a lifelong guarantee of treatment could exhaust limited research resources and does nothing for those who elect not to participate in research. PrEP trials have similar ethical, financial, and logistical con-

straints (*6*). Despite these constraints, PrEP trials in resource-poor settings have set aside funds for treatment of side effects, if they occur.

The sponsors of PrEP trials are public and nonprofit institutions that have nothing to gain from marketing of the drug and have little influence over global policies. The drug developer is donating the drug and matching placebo for the trials but is not providing any funding, partly because they have no current plans to market the drug for prevention (*7*). The sponsors and investigators offer well-designed studies, with all available safeguards, which claim to find new ways to stop the spread of HIV to trial participants and their communities. We also offer our goodwill to the struggles for social justice. While goodwill alone is never sufficient, it is a necessary foundation on which we all build.

ROBERT M. GRANT,[1] JOHN P. MOORE,[2] EDITH CLARKE,[3] JAVIER R. LAMA,[4] WILLARD CATES JR.,[5] THOMAS COATES,[6] MYRON S. COHEN,[7] MARTIN DELANEY,[8] MARK A. WAINBERG,[9] VIVIAN LEVY,[1] JEFF MCCONNELL,[1] KATHLEEN M. MACQUEEN[5]

[1]Gladstone Institute of Virology and Immunology/University of California, 1001 Potrero Street, San Francisco, CA 94110, USA. [2]Weill Medical College, Cornell University, New York, NY 10021, USA. [3]Ghana Health Service, Ministry of Health, Accra, Ghana. [4]Asociación Civil Impacta Salud y Educación, Grimaldo del Solar 805, Lima, Peru. [5]Family Health International, Research Triangle Park, P.O. Box 13950, Research Triangle Park NC 27709, USA. [6]University of California at Los Angeles, 10940 Wilshire Boulevard, Suite 1220, Los Angeles, CA, USA. [7]University of North Carolina, 130 Mason Farm Road CB# 7030, Chapel Hill, NC, 27599, USA. [8]Project Inform, 205 13th Street, #2001, San Francisco, CA 94103, USA. [9]McGill University AIDS Center, Montreal, QC H3A 2T5, Canada.

References

1. Gilead Sciences Press Release. Gilead Reduces Prices for Viread® and Truvada® in the Developing World (www.gilead.com/wt/sec/pr_750303) (2005).
2. A. Hill, paper presented at the 3rd IAS Conference and HIV pathogenesis and treatment, Rio de Janeiro, 2005.
3. J. D. Lifson *et al.*, *J. Virol.* **74**, 2584 (2000).
4. B. Rosenwirth *et al.*, *J. Virol.* **74**, 1704 (2000).
5. J. Cohen, *Science* **281**, 22 (1998).
6. "Don't shoot the messenger: an update on tenofovir research" (AIDS Vaccine Advocacy Coalition, 2005) (available at http://www.avac.org/reports.htm).
7. J. Cohen, *Science* **309**, 1002 (2005).

Continuing Progress in Neuroinformatics

MOST PEOPLE WOULD RECOGNIZE THAT THE Decade of the Brain (1990–2000, established by Presidential Proclamation 6158, 17 July 1990) successfully enriched research on neural function and provided a fruitful beginning to greater support and progress (*1*). This effort highlighted the scientific excitement surrounding research on the brain and its significance for public health. One of the most prominent programs to come from this initiative has been the National Institute of Mental Health–based Human Brain Project (HBP) (*2*), a program to promote and fund activities seeking to collect, archive, model, and openly share primary neuroscience data from the molecular to systems levels (see www.nimh.nih.gov/neuroinformatics/index.cfm).

Supporting as many as 42 individual projects and hundreds of investigators, the HBP has been the mechanism through which the field of neuroscience has enjoyed the production of valuable resources. It has made possible rich three-dimensional brain imaging atlases, cellular recording databases from implanted electrodes, the dissemination of complete functional neuroimaging data sets (*3*), and the development of sophisticated analysis and visualization tools, and it has spawned the genesis of neuroinformatics as an active area of research (*4*). As part of the Roadmap initiative, the NIH now considers it time to identify new ways in which this field can best be integrated with initiatives from other institutes and funding agencies if we are to advance research and development of informatics tools and resources for neuroscience. In light of this decision, it was announced that the program had expired (NIH NOT-NH-05-104) and the last applications for funding under the HBP were collected 22 September 2005. And yet, a new, specifically defined component for neuroinformatics and databasing appears to be missing from these recently announced federal programs.

Neuroinformatics, like bioinformatics, is now an accepted and legitimate area of research (*5*) and should not be ignored or given short shrift under new federal research directives. Several of us are current and former HBP grantees, and we are alarmed that the NIH has chosen to poorly support neuroinformatics under the NIH Roadmap and Neuroscience Blueprint initiatives. As those who have used databases for research for some time, we also realize their power for maximizing the return on investment (public funds for research). With belt tightening clearly under way, we should be redoubling our efforts to make the most of what we already have. Congress and the public should demand nothing less.

"We are alarmed that the NIH has chosen to poorly support neuroinformatics under the NIH Roadmap and Neuroscience Blueprint initiatives."

—Gazzaniga *et al.*

We hope that the spirit of the original HBP and associated efforts originating during the Decade of the Brain toward the management and mining of increasingly vast arrays of brain data being collected can be resurrected and reenergized. The Roadmap and Blueprint programs appear to be the best means for this to happen. Unless a real and decisive action plan is implemented soon, many existing efforts may shut down. It would be disappointing, indeed, to see current efforts falter and to be forced to wait another decade for federal funding agencies to appreciate the work left to be done toward building a comprehensive database of the human brain and its disorders.

MICHAEL S. GAZZANIGA,[1] JOHN D. VAN HORN,[1] FLOYD BLOOM,[2] GORDON M. SHEPHERD,[3] MARCUS RAICHLE,[4] EDWARD JONES[5]

[1]Center for Cognitive Neuroscience, 6162 Moore Hall, Dartmouth College, Hanover, NH 03755, USA. [2]Department of Neuropharmacology, The Scripps Research Institute, 10550 North Torrey Pines Road, La Jolla, CA, 92037, USA. [3]Department of Neurobiology, Yale University School of Medicine, 333 Cedar Street, SHM C303, Post Office Box 208001, New Haven, CT 06520–8001, USA. [4]Washington University School of Medicine, East Building, Room 2116, 4525 Scott Avenue, St Louis, MO 63110, USA. [5]Center for Neuroscience, Department of Psychiatry, University of California School of Medicine, 203J 1544 Newton Court, Davis, CA 95616, USA.

References

1. E. G. Jones, L. M. Mendell, *Science* **284**, 739 (1999).
2. M. F. Huerta, S. H. Koslow, A. I. Leshner, *Trends Neurosci.* **16**, 436 (1993).
3. J. D. Van Horn, S. T. Grafton, D. Rockmore, M. S. Gazzaniga, *Nat. Neurosci.* **7**, 473 (2004).
4. M. F. Huerta, S. H. Koslow, *Neuroimage* **4**, S4 (1996).
5. D. C. Van Essen, *Curr. Opin. Neurobiol.* **12**, 574 (2002).

Loss of Grants Hurts the Vulnerable

THE DECISION TO WITHDRAW THE GLOBAL FUND grants to treat AIDS, tuberculosis, and malaria from Myanmar (formerly Burma), one of the world's poorest countries ("Global Fund pulls Myanmar grants," J. Cohen, News of the Week, 26 Aug. 2005, p. 1312), has attracted attention from activists, scientists, and Burmese expatriates. It seems that the United Nations and the Global Fund have fallen into a mindset of 20th century "sanction-oriented policies," despite the hard lessons learned from previous sanctions on countries such as Cuba, Iraq, and North Korea. What should perhaps be obvious, after the years of futile pressure applied on these countries, is that sanctions ultimately punish only the most vulnerable segments of the totalitarian society instead of those who are in power and truly accountable.

Surprisingly, the UN and the Global Fund ignored the warnings of Jeffrey Sachs and others who have argued that sanctions in Myanmar are likely to be conterproductive (*1*). Epidemiologists agree that the consequences of letting these infectious diseases take their course in Burma could be dire. Responsible officials in the UN and the Global Fund should therefore understand that the decision to abandon 600,000 Burmese HIV/AIDS sufferers plus tuberculosis and malaria patients would likely unleash epidemics of unprecedented proportions. Because of the steep increase in the number of the new cases, Southeast

Asia requires outside AIDS programs more than any other region. Withdrawal of these grants under current circumstances should not be an option.

KAROL SESTAK

Tulane University School of Medicine, Tulane National Primate Research Center, Covington, LA 70433, USA. E-mail: Ksestak@tulane.edu

Reference

1. J. D. Sachs, Irrawaddy.org, "Sachs on Sanctions" (available at www.irrawaddy.org/, Oct. 2004).

CORRECTIONS AND CLARIFICATIONS

REPORTS: "Ubiquitination on nonlysine residues by a viral E3 ubiquitin ligase" by K. Cadwell and L. Coscoy (1 July 2005, p. 127). In Fig. 3B, the top left panel was inadvertently duplicated and printed a second time as the top right panel. The correct version of the top right panel of Fig. 3B appears here. The conclusions of the paper are not affected by this error.

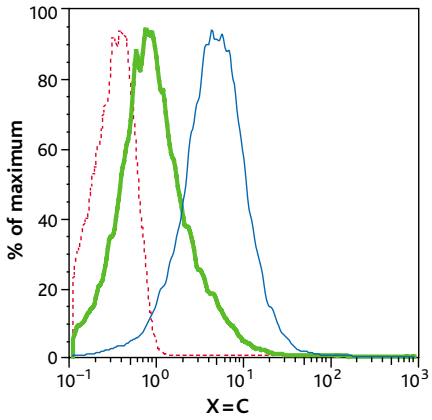

REPORTS: "Hf-W chronometry of lunar metals and the age and early differentiation of the Moon" by T. Kleine *et al.* (9 Dec. 2005, p. 1671). The URL for the Supporting Online Material was incorrect. The Supporting Online Material can be found at www.sciencemag.org/cgi/content/full/1118842/DC1. In addition, this report was published online 24 November 2005 on *Science* Express. Please include this information when citing this paper.

REPORTS: "The chemistry of deformation: how solutes soften pure metals" by D. R. Trinkle and C. Woodward (9 Dec. 2005, p. 1665). In the last sentence of the first full paragraph on p. 1667, there was an error in the equation for the solute barrier energy scale. It should be $25\sqrt{c}|E_{int}|$.

TECHNICAL COMMENT ABSTRACTS

Comment on "Iron Isotope Constraints on the Archean and Paleoproterozoic Ocean Redox State"

Kosei E. Yamaguchi and Hiroshi Ohmoto

Rouxel *et al.* (Reports, 18 February 2005, p. 1088) argued that changes in the iron isotopic composition of sedimentary sulfides reflect changes in the oxidation state of the atmosphere-ocean system between 2.3 and 1.8 million years ago. We show that misinterpretations of the origins of these minerals undermine their conclusions.

Full text at www.sciencemag.org/cgi/content/full/311/5758/177a

Response to Comment on "Iron Isotope Constraints on the Archean and Paleoproterozoic Ocean Redox State"

Olivier J. Rouxel, Andrey Bekker, Katrina J. Edwards

We reported a secular trend in iron isotope values of Precambrian sedimentary pyrite and related it to the changing redox state of Precambrian oceans. We restate that the iron cycle before 1.8 billion years ago was different from that now and reflected the rise of atmospheric oxygen and the subsequent moderate atmospheric oxygen level in the Paleoproterozoic.

Full text at www.sciencemag.org/cgi/content/full/311/5758/177b

Letters to the Editor

Letters (~300 words) discuss material published in *Science* in the previous 6 months or issues of general interest. They can be submitted through the Web (www.submit2science.org) or by regular mail (1200 New York Ave., NW, Washington, DC 20005, USA). Letters are not acknowledged upon receipt, nor are authors generally consulted before publication. Whether published in full or in part, letters are subject to editing for clarity and space.

CHEMICAL ECOLOGY

Bug Sprays or Class (Insecta) Warfare

May Berenbaum

Dodging a chemical defense. Although the glandular secretion of the desert darkling beetle *Eleodes longicollis* is highly effective against ants, the grasshopper mouse *Onychomys torridus* evades that defense by forcing the rear of the beetle into the sand. The mouse then consumes almost all of its prey, leaving as remnants only the abdominal tip (with intact glands) and low-nutrient legs and wings.

Secret Weapons
Defenses of Insects, Spiders, Scorpions, and Other Many-Legged Creatures

by Thomas Eisner, Maria Eisner, and Melody Siegler

Belknap (Harvard University Press), Cambridge, MA, 2005. 384 pp. $29.95, £18.95, €27.70. ISBN 0-674-01882-6.

It is not without good reason that chemical warfare among living organisms has long been a subject of almost limitless appeal. Small and seemingly overmatched creatures can best much bigger foes by spraying, squirting, dribbling, or oozing noxious substances in their direction. That fact has a certain satisfying David-and-Goliath element that embodies the idea of fair play—at least as long as humans aren't caught in the cross fire. Much of what the scientific community knows of this world is due to the work of Thomas Eisner, a professor of chemical ecology at Cornell University. He and his colleagues have devoted more than half a century to elucidating the chemical warfare battle plans, strategies, and weapons of arthropods that refuse to surrender without putting up a fight. These fascinating stories have been recounted in arcane technical language in hundreds of scientific papers published in refereed journals; there, they have been read with delight by researchers but for the most part have been inaccessible to the general public.

Chemical deterrent redirected. In southern Arizona, the predatory reduviid bug *Apiomerus flaviventris* uses the defensive chemical weaponry of a common roadside weed (*Heterotheca psammophila*) for its own protection. Females harvest the resin and apply it to their eggs. Emerging nymphs, which scrape the sticky resin from the egg clusters, may also use it to help hold on to prey they grasp with their forelegs.

Fortunately, in *Secret Weapons: Defenses of Insects, Spiders, Scorpions, and Other Many-Legged Creatures,* Eisner, his wife and long-time collaborator Maria Eisner, and Melody Siegler (a neurobiologist at Emory University) open this literature to a wider audience. The book—which nicely complements Eisner's earlier *For Love of Insects* (*1*)—comprises a collection of 69 short essays, each focused on a particular arthropod and its chemical defense strategy. The text is technically precise but—with the word limits and other restraints of scientific literature lifted—the prose is bright and engaging. Every essay is accompanied by a short bibliography (for those intent on learning all of the technical details), and most also provide diagrams of the chemical structures of the defensive compounds discussed.

To the benefit of both the general reading public and interested scientists, besides repackaging the half-century of work in more accessible prose, the authors illustrate it in bright colors and striking images. One of the most frustrating limitations of the scientific literature—at least until the relatively recent advent of electronic publishing—has been editors' reluctance to devote space to photographs and their aversion to the use of color images (largely due to cost considerations). The book's captivating images demonstrate the explanatory power of pictures. Eisner and his colleagues have skillfully captured the staggering diversity of exudates and delivery systems that arthropods possess—sights that have simply not been readily available even to the scientists who avidly peruse the chemical ecology literature. The book offers an invaluable source of illustrations for all audiences, but it is likely to be particularly useful to educators; I only wish that a CD-ROM of the images was made available for classroom use.

The book is not intended to be a comprehensive treatise on arthropod chemical defense. As the authors explain in the prologue, they favored those stories that could be effectively illustrated, generally with their own images. As a consequence, most of the essays focus on animals from North America (where the authors are based). This bias nonetheless serves to underline the universality of chemical defense among arthropods. There is no need to resort to exotic tropical locales for compelling examples. (In fact, some of the species described—such as *Pieris rapae*, the cabbage butterfly—are literally garden-variety pests.) That the essays are ordered taxonomically does not make the book particularly easy to use by a nonspecialist. For that matter, even entomology graduate students might stumble in a preliminary exam if asked, say, to identify the Polyxenida as an order within the class Diplopoda (only arthropod cognoscenti are likely to be familiar with the so-called bristle millipedes). But the thorough, well-organized index will allow readers access to text by either scientific or common name.

In addition to the essays, the book includes a short section on how to study insects and their kin (and even conduct a few experiments in chemical ecology). Few of us, however, are likely to develop Eisner's uncanny ability to detect the tell-tale signs of chemical defense—bright colors, aggregative behavior, odd postures, distinctive cuticular structures, and, of course, pungent odors. Regrettably, technology still imposes sensory limits on readers. I fervently hope that, at some point in the future, a scratch-and-sniff edition of *Secret Weapons* will become available. Readers might then share more of the sensory experiences that Eisner and colleagues have been privy to for all these years.

The reviewer is in the Department of Entomology, 320 Morrill Hall, University of Illinois at Urbana-Champaign, 505 South Goodwin Avenue, Urbana, IL 61801, USA. E-mail: maybe@uiuc.edu

References

1. T. Eisner, *For Love of Insects* (Harvard Univ. Press, Cambridge, MA, 2003). Reviewed by I. T. Baldwin, *Science* **303**, 958 (2004).

10.1126/science.1121896

CREDITS: TOM EISNER

EXHIBITS: EVOLUTION

The World Through Darwin's Lens

R. Scott Winters

In 1837—a year after the *HMS Beagle* returned to England—Charles Darwin began documenting his emerging ideas in a journal referred to as "Notebook B." Amidst the handwritten text is a simple figure: a spindly-line "tree" of relationships with a single ancestral root. Preceding this seminal evolutionary tree, at the top of the page, Darwin scribbled the words "I think." Notebook B is one of 400 or so artifacts on display in the American Museum of Natural History's exhaustive exhibit *Darwin*. Touted as the most in-depth exhibition on Darwin, the displays feature many items that have not been seen together since his lifetime. *Darwin*—curated by the eminent evolutionary biologist Niles Eldredge, who also wrote the accompanying book—is the latest in the New York museum's series on great thinkers and explorers that has included Leonardo da Vinci, Ernest Shackleton, and Albert Einstein. The exhibit will continue at the American Museum of Natural History until 29 May 2006, after which it will travel to Boston, Chicago, Toronto, and finally London (in time for the 2009 bicentennial of Darwin's birth).

Upon entering the exhibit, guests encounter Darwin's magnifying glass. This semaphore guides the viewer through the displays by focusing on two central themes. The first is of Darwin as a critical observer who paid careful attention to details while methodically gathering a large body of evidence to support his theory. The second is that all of biology—and perhaps the whole of science—has been transformed and understood through the lens of Darwin's contributions.

In the first section, the exhibit illustrates how observations of the world informed Darwin's nascent theory: his world before *The Origin of Species*. Darwin's family and early life are framed in the context of a developing naturalist. There is a re-creation of Huttons Unconformity (the famed outcrop at Siccar Point, Scotland), which illustrates a changing and ancient Earth, and Darwin's geologic hammer is on display. Visitors then encounter Darwin's epic, five-year voyage aboard the *HMS Beagle*. One of the treasures of the entire exhibit is the original letter from Reverend J. S. Henslow (an important mentor for Darwin while he was at Cambridge) informing Darwin of the opportunity to participate in the *Beagle*'s voyage. The exhibit immerses guests in Darwin's explorations on the voyage through fossils, a diorama of the Galapagos, live animals, and collected specimens. We also learn more about Darwin through his letters and personal effects, including the pistol and Bible that he carried throughout his journey.

Darwin

Niles Eldredge, curator

At the American Museum of Natural History, New York, through 29 May 2006; Museum of Science, Boston, 2 December 2006 to 22 April 2007; Field Museum, Chicago, 15 June 2007 to 1 January 2008; Royal Ontario Museum, Toronto, 8 March 2008 to 4 August 2008; Natural History Museum, London, October 2008 to March 2009. www.amnh.org/exhibitions/darwin

Darwin
Discovering the Tree of Life

by Niles Eldredge

Norton, New York, 2005. 272 pp. $35. ISBN: 0-393-05966-9.

The second section of the exhibit takes us from Darwin's exploration of the world to his internal exploration of ideas. Here the exhibit's layout changes from linear to circular. The nexus of the exhibit is an elaborate re-creation of Darwin's study at Down House. Visitors are exposed to the social and personal context of Darwin's life while he wrestled to bring his theory into focus: his pursuit and marriage of Emma Wedgwood (including his "pros and cons" list), the impact of his 10-year old daughter Annie's death, and his letter to Charles Lyell concerning Alfred Wallace's essay with its remarkable similarity to Darwin's developing ideas. The section's high point is an original manuscript page from *The Origin of Species*. Radiating from Darwin's study, the exhibit follows the impact of Darwin's greatest contribution, evolution by natural selection, on science and society.

Toward the end of the exhibit is a display entitled *Social Reaction of Darwin* that addresses various controversies, historical and contemporary, including creationism and intelligent design. Included are examples of the disclaimer stickers, proposed by some U.S. school districts, to be put on high school biology textbooks to proclaim that evolution by natural selection is merely a theory and only one of many possible explanations for the history of life on Earth. Today, in states such as Pennsylvania and Kansas, the debate over the teaching of evolution in public schools continues. In this context, *Darwin* becomes more than an exceptional museum experience; it helps to bridge a widening science-education gap in this country.

10.1126/science.1123277

Island clues. Darwin's consideration of the fauna of the Galapagos Islands was a key step toward his conclusions that all species are related and that species change with time.

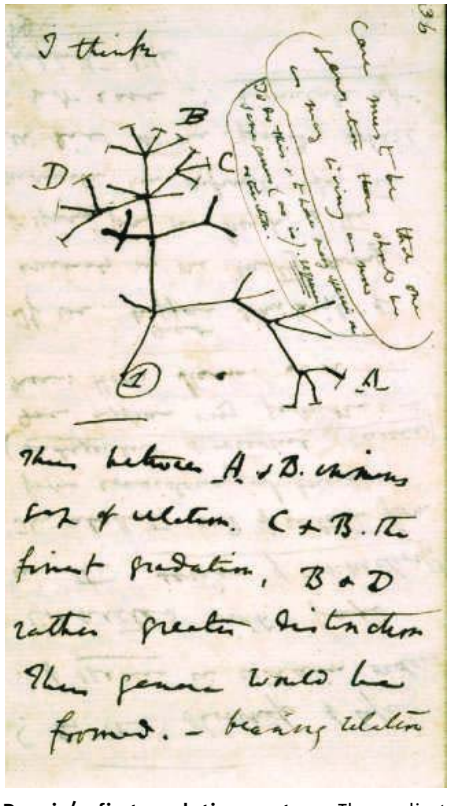

Darwin's first evolutionary tree. The earliest known sketch by Darwin, from his Notebook B, of ancestor-descendant relations.

The reviewer is in the Division of Oncology, Children's Hospital of Philadelphia, 34th Street and Civic Center Boulevard, Philadelphia, PA 19104, USA. E-mail: winters@email.chop.edu

PUBLIC HEALTH

Clinical Trials Results Databases: Unanswered Questions

Hasty legislation mandating posting will not be enough to ensure public safety.

Celia B. Fisher

Public outcry over pharmaceutical companies' failure to report safety data from research on antidepressants and COX-2 inhibitors has exerted pressure on industry, researchers, and policy-makers to ensure transparent and unbiased reports of clinical trials results (*1*–*3*). One response receiving international attention is creation of clinical trials registries and results databases (*4*). In general, clinical trials registries provide a public record of the nature and eligibility criteria of newly initiated, ongoing, and closed trials. Results databases are public postings of all clinical trials findings, including potentially adverse side effects. Although there has been widespread debate on the rationale and criteria for registries, much of the dialogue (as well as legislation introduced in the U.S. Congress and in more than 20 states) fails to address key questions about results databases (*5*).

The original intent of registries was to inform patients about clinical trials in which they might participate (*6*, *7*). However, their purpose has expanded. The International Committee of Medical Journal Editors (ICMJE) sought to guard against "positive results bias" in publication of clinical trials by limiting acceptance of manuscripts to studies that had been entered into a registry at their inception (*8*). The ICMJE announcement prompted U.S. state and federal legislation [Fair Access to Clinical Trials (FACT) Act has been introduced in the House of Representatives and Senate], proposals from international bodies such as the World Health Organization, and creation of voluntary industry registries (*9*–*14*).

Summaries of and links to publications reporting the results of completed clinical trials are also available from Web sites posted by the U.S. National Institutes of Health (*7*) and the Pharmaceutical Research and Manufacturers of America (PhRMA) (*12*), and a handful of industry registries, but they are not required. However, the FACT Act and some state legislation propose a mandatory linkage.

Implications for Clinical Trials Science

The current legislative proposals call for posting and open access to all raw or summative clinical trials data from successful studies, as well as those that have failed or produced equivocal results or data contradictory to a report submitted for review. However, there has been no discussion about whether the availability of large bodies of data from studies that may or may not have scientific merit will improve or distract from the peer-review process. Moreover, the absence of guidelines for how to include a large body of ancillary data in peer review of submitted manuscripts could compromise actual or perceived fairness of review. Results databases are not a substitute for systematic scientific peer review and scientific rigor.

The Public Library of Science (PloS) recently introduced an open-access journal called *PloS Clinical Trials* that promises to provide peer-reviewed data not affected by "the direction of results, size, or significance" of the trial (*15*). To defray the cost of peer review and open access, the journal charges a fee of $2500 upon acceptance of the article for publication with a nonspecified sliding scale for those lacking sufficient funds. It is too early to tell what effect this will have on the science establishment's ability to maintain and to monitor high standards of research design, analysis, and dissemination. However, lack of emphasis on the direction of results or size, elements critical to good scientific method, risks diluting scientific standards for peer review.

"Results databases are not a substitute for systematic scientific peer review and scientific rigor."

Participant and Patient Protections

In the United States, subject protections are currently instituted through Institutional Review Board (IRB) review of protocols before implementation and by safety and data monitoring boards during the conduct of clinical trials. Some have argued that access to safety data from previous studies will help potential research subjects evaluate the risks of enrolling in new studies. It is also hoped that public databases will improve prescribing and treatment by helping health-care providers and patients keep pace with rapid advances. However, public databases could compromise such protections.

Ethical and scientific evaluation of the potential for and significance of adverse participant reactions in a clinical trial requires: (i) an understanding of the health status of the participant population, (ii) the types of side effects that were or were not anticipated, (iii) the immediate and long-term health consequences of an adverse event, (iv) evidence of a clear causal relation between the event and the product under investigation, and (v) statistical power necessary to draw conclusions regarding causal relations. Public databases that include constantly updated tables or summaries of adverse events in the absence of such scientific understanding risk raising unmerited public or health provider confidence or concern. Health and safety protection of current and potential research participants can be strengthened through new guidelines for streamlining current safety data monitoring procedures that emphasize reporting of product-relevant anticipated adverse events and more timely review of serious unanticipated adverse events.

Results databases are also not substitutes for safety monitoring of commercially available products. Safety concerns may not be apparent until a commercially approved product is studied in a new patient population, until practitioners have prescribed it to a wider heterogeneous population, or until consequences of product misuse come to light. Although reporting of adverse events is mandatory for marketed products, currently there is no process for evaluating safety data of postmarket products across independently conducted trials or for a national communication channel to encourage and facilitate physician reporting—to companies and the FDA—of serious, unanticipated, and significant adverse events in everyday practice. An active postmarket monitoring interface is essential to long-term understanding of how medical products benefit or adversely affect the public.

Health-Care Practice and Cost

Even in large-scale clinical trials, the validity of results rests on representative sampling, dropout rates, and replication. Practitioners and their professional organizations rely on a system of peer review and FDA approval to help filter multiple sources of information about health products and to establish consensus on standards of care. These data-filtering mechanisms are used by physicians and hospitals to make decisions about health product purchases and by health management organizations to establish criteria for coverage of prescription drugs and medical procedures.

The author is the director for the Center for Ethics Education, Fordham University, and Marie Ward Doty Professor of Psychology, Bronx, NY 10458, USA. E-mail: fisher@fordham.edu

Pressures from patients for physicians to modify prescribing based on public postings of data that have not been subjected to peer review and regulatory interpretation may lead to premature withdrawal of patients from useful treatment regimens or prescriptions for off-label use of a marketed product. Legislative proposals, like the FACT Act 2005, seek to limit such negative consequences by requiring prominent display of a statement indicating when trials are assessing the safety, effectiveness, or benefit of a use not described in the approved labeling for the drug, biological product, or device. However, this problem may be compounded by proposed government actions calling for nonpromotional language in database postings that prohibit sponsors from providing conclusions about the implications of the data for product efficacy and treatment decisions. Public dissemination of decontextualized results summaries may also exert pressure on the FDA to approve or withdraw products prematurely. The establishment of professional guidelines for the application of database information for prescribing may help address these problems.

CREDIT: JOE SUTLIFF

Administrative resources required to maintain and monitor results databases may increase the costs of health-care products. Pressure to access constantly changing results databases may also create an unreasonable medical "standard of care," which, in turn, can trigger medical malpractice cases and increase professional liability insurance rates. The relation of clinical trials results databases to product use and purchase must also be considered. What if, for example, preliminary results reported in a database supporting less costly products discourage hospitals from purchasing a proven but more expensive device?

How will health insurance plans react to results databases? Will a single study indicating a negative result of a postmarket product discourage health-care plans from covering its use? Might health-care insurers pressure physicians to switch to less costly medications on the basis of preliminary trials posted on a results database? To provide adequate answers to these questions, health-product stakeholders need to push for cost-effectiveness studies and guidelines for the use of databases in health-care practice, purchase, and insurance coverage.

Industry Sustainability

Sponsors are concerned that failure to post results could be construed as sponsor fraud or negligence; product liability actions could become more frequent. At the same time, manufacturers that do publicize preliminary product findings on mandatory databases might be accused of fraudulently promoting an insufficiently tested product. Posting of results on databases may create undue investor hype. Product manufacturers may have to carry errors and omissions (E&O) insurance to cover this type of exposure, and products liability premiums could be adversely affected. Some have argued that mandatory posting of clinical trials results databases could place companies at risk of violating Securities and Exchange Commission Rules against hyping a drug under FDA review through "forward-looking statements" as defined by the Private Securities Litigation Reform Act of 1995 (*16*). If a company posts positive results from the first study completed and then completes a second one that does not support the first, the company might well be accused of misleading investors.

Premature posting of data from unapproved compounds or off-label usage studies could hamper competition. Posting results on unapproved compounds or new applications of marketed products could erode intellectual property protections. Posting of premarket product trial results could reveal competitively valuable analyses or end points derived from intensive negotiation with FDA and international regulatory authorities. For example, there are rules in the United States, Europe, and other countries that allow generic manufacturers and other applicants to obtain approval through abridged procedures by referencing safety and efficacy data in the public domain. Public posting of raw data or full study reports could be used as a basis for such applications, thereby compromising regulatory exclusivity for marketing authorization holders, hurting investor return, and discouraging research funding.

To ensure scientific integrity, advance public health, and sustain health-care innovation, some U.S.-based and international organizations have proposed creating a "blind" data repository linked to a clinical trials registry. In this model, investigators and/or sponsors would be required to submit their data on project completion, but release into a public database would coincide with article submissions and/or approval by FDA or an international body (*5*, *11*).

Clinical research on drugs, biologics, and medical devices is a multisite, multistate, global enterprise that requires a solution that is national and global. All legislated or voluntary clinical trials results databases must consider implications for harmonization across government and private sponsors, state and federal legislation, global and national studies, and products that are approved or commercially available in some but not all countries (*5*, *17*).

Conclusions

Timely and transparent reporting of clinical trials results is essential to effective health-care decision-making and public confidence. However, policies hastily crafted to assuage public concerns may produce unanticipated problems. Clinical researchers and the pharmaceutical industry must take a leadership role, showing greater willingness to engage with other players. But it is not their responsibility alone. Government policies must take into account protections for public health and industry sustainability. Doctors and hospitals must also provide timely information. Continued dialogue among stakeholders is necessary to ensure that steps taken will enhance scientific and social responsibility and will contribute to the vitality and sustainability of clinical trials research.

References and Notes

1. K. Gilpin, *New York Times*, 2 June 2004; (www.antidepressantsfacts.com/2004-06-02-NYT-NY-sues-GSK-paxil.htm).
2. Center for Drug Evaluation and Research, Food and Drug Administration, "Questions and answers: FDA regulatory actions for the COX-2 selective and non-selective non-steroidal anti-inflammatory drugs (NSAIDs)"; (www.fda.gov/cder/drug/infopage/COX2/COX2qa.htm).
3. A. Gardner, *HealthDay News*, 29 August 2005; (www.healthday.com/view.cfm?id=526217).
4. J. Couzin, *Science* **307**, 189 (2005).
5. "Clinical trials registries and results databases white paper," Proceedings from the Fordham University Summit on Bio-Pharmaceuticals in the 21st Century: Responsibility, Sustainability, and Public Trust, New York, 10 to 11 January 2005 (Fordham Univ., New York, 2005); (www.clinicaltrialsethics.org/White%20Paper.htm).
6. A.T. McCray. *Ann. Intern. Med*. **133**, 609 (2000).
7. See also (www.clinicaltrials.gov/).
8. ICMJE, "Clinical trial registration: A statement from the International Committee of Medical Journal Editors." *N. Engl. J. Med*. **351**, 1250 (2004); (www.nejm.org).
9. S. 470—The Fair Access to Clinical Trials (FACT) Act (February 2005, 109th Congress); (http://olpa.od.nih.gov/tracking/109/senate_bills/session1/s-470.asp).
10. World Health Organization International Clinical Trials Registry Platform; (www.who.int/ictrp/en/).
11. International Federation of Pharmaceutical Manufacturers and Associations, "Global industry position on disclosure of information about clinical trials" (6 January 2005); (www.ifpma.org/News/NewsReleaseDetail.aspx?nID=2205).
12. The Pharmaceutical Research and Manufacturers of America (PhRMA) Clinical Study Results Database; (www.clinicalstudyresults.org/).
13. American Medical Association offers guidelines for clinical trial registry; (www.ama-assn.org/ama/pub/category/print/13949.html).
14. GeMCRIS: Genetic modification clinical research information system; (www.gemcris.od.nih.gov/).
15. In 2006 (http://clinicaltrials.plosjournals.org); now available through (www.plos.org/journals).
16. "Posting trial data could run afoul of law against misleading investors," *FDA Week* (12 November 2004); (http://insidehealthpolicy.com) (by subscription).
17. World Health Organization, International clinical trials registry platform (ICTRP); (www.who.int/ictrp/en/).

10.1126/science.1119685

STRUCTURAL BIOLOGY

Two Geometric Solutions to a Transporting Problem

Cage-like protein assemblies envelop vesicles that carry materials from place to place in a cell. By changing the geometry of these cages, cells can transport a range of cargo sizes.

Corinne Smith

Establishing an efficient and reliable transport mechanism is a formidable challenge, as any commuter will testify. And yet, for living organisms, transport of cargo such as proteins into and throughout the cell is vital to survival and development. Intracellular transport mechanisms rely mainly on membrane-derived vesicles to shuttle cargo throughout the cell. These vesicles arise through a budding process from the plasma membrane at the cell surface or from the membranes of intracellular organelles. During budding, a number of proteins form a shell or coat around the outside of the vesicle, promoting the inclusion of specific cargo into the forming carrier. This has led to its description as a "coated vesicle" when it detaches. Now, a study by Stagg *et al.* (*1*) provides a structural view of two outer components of a vesicle coat, revealing a distinctive polyhedral lattice that may allow vesicles to accommodate a range of cargo sizes.

The importance of the role of protein coats to vesicular transport in eukaryotes has stimulated great interest, and the best studied of these has been the clathrin coat. When visualized by electron microscopy, clathrin-coated vesicles that bud from the plasma membrane reveal a striking polyhedral pattern reminiscent of a fullerene (see the figure). This pattern arises from the outermost protein in the coat, clathrin. Clathrin assembles from three-legged individual components called triskelions to form a polygonal lattice around the vesicle. The nature of the arrangement of these triskelions within the lattice was first visualized in a cryo–electron microscopy map of clathrin coats (*2*, *3*), and recently the resolution was extended to approximately 8 Å (*4*).

As well as clathrin coats, there are coat protein complexes I and II (COPI and COPII) that mediate vesicle transport steps between the endoplasmic reticulum and the Golgi apparatus organelles. Although an increasing amount of high-resolution structural information is being gathered on these coats through protein x-ray crystallography, until recently there was no information on the arrangement of COP coat components around the vesicle (*5*–*7*).

The COPII coat has five main functional components that are highly conserved in all eukaryotic cells. Sar1p, a small guanosine triphosphatase, binds first to the membrane of the vesicle and initiates membrane curvature (*8*). Sar1p then stimulates the binding of a complex of two further components, Sec23p and Sec24p. Together, these three proteins function in the selection of cargo for vesicle-mediated transport. The proteins Sec13p and Sec31p later bind to form the second layer of the COPII coat (*5, 7, 9*). This is analogous to the situation in clathrin-coated vesicles where adaptor proteins bind the vesicle membrane to form an inner layer to which an outer shell of clathrin binds (*10*, *11*). Hence, both transport processes make a vesicle coat with two layers—one involved in binding to the membrane and recruiting cargo, the other with possibly a more structural role.

When the surface of COPII vesicles was viewed by quick-freeze/deep-etch electron microscopy, it was hard to define the nature of the arrangement of the coat proteins (*12*). Now, Stagg *et al*. have discovered that mammalian Sec13p and Sec31p can assemble in the absence of Sec23p and Sec24p to form polygonal cages (*1*). The authors further used cryo–electron microscopy and single-particle reconstruction to determine a three-dimensional map of these cages. The resulting 30 Å resolution map (see the figure) shows that, remarkably, these polygonal cages use a geometry that is completely different from that of clathrin cages. Sec13p and Sec31p form a cuboctahedral cage whose faces are squares or triangles rather than the hexagons or pentagons visualized in a clathrin coat.

The intricate pattern created by assembled clathrin molecules has an enduring fascination. Now we see evidence for the adoption of a different, but equally striking, geometric pattern in a related cellular process. Geometrically definable structures feature in other areas of biology, most notably in the structure of viruses, where the requirement is for economic formation of a capsule structure from a few simple building blocks. But although the viral coat is generally of a fixed size, coated vesicles seen in vivo vary considerably in size and so their coat must be correspondingly flexible. As Stagg *et al*. discuss, this could be facilitated in both clathrin-coated and COPII vesicles through the geometry of their cage structures, where the cage size can be changed by coordinating the relative numbers of triangles and squares or pentagons and hexagons. This is of particular relevance because COPII proteins have recently been implicated in the transport of very large cargo such as procollagen-I, although their precise role remains to be clarified (*13, 14*).

The two cages (see the figure) can self-assemble to form a stable but open "meshlike" structure, and this raises important questions. Do Sec13p and Sec31p have a role in stabilizing the COPII vesicle, as Sar1p, Sec23p, and Sec24p drive its formation (*8*)? Are cage structures of particular relevance to coordinating the prompt assembly and disassembly of vesicle coats? Is the very open nature of the cage important for allowing potential binding partners unimpeded access to the inner layer of the coat? It must certainly be significant that in two distinct cases, cage structures are formed by vesicle coat proteins. It therefore seems likely that the properties of stability, permeability, and self-assembly that are intrinsic to these structures are important for cellular

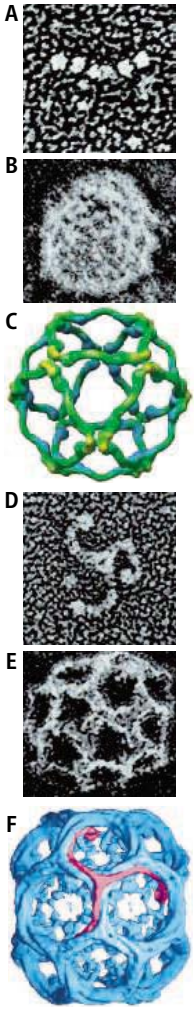

Cellular cages. (**A** and **B**) Quick-freeze/deep-etch electron micrographs showing the surface structure of the Sec13-Sec31p heterotetramer (A) and a COPII-coated vesicle (B). (**C**) Three-dimensional map of assembled mammalian Sec13-Sec31p obtained by cryo-electron microscopy and single-particle reconstruction to 30 Å resolution. (**D** and **E**) Quick-freeze/deep-etch electron micrographs showing the surface structure of an individual clathrin triskelion (D) and a clathrin-coated vesicle (E). (**F**) Three-dimensional map of assembled clathrin and the adaptor protein AP2 obtained by cryo–electron microscopy and single-particle reconstruction to 21 Å resolution (*2*). The inner coat layer is removed for clarity in this picture. A single triskelion is highlighted in pink. Images (A), (B), (D), and (E) were reprinted with permission from (*12*), copyright 2001 National Academy of Sciences, U.S.A. Image (C) was reprinted with permission from (*1*). Image F was reprinted with permission from (*15*), copyright 2000, with permission from Elsevier.

The author is in the Department of Biological Sciences, University of Warwick, Coventry CV4 7AL, UK. E-mail: corinne.smith@warwick.ac.uk

transport mechanisms. Determining precisely which characteristics of a cage structure drive this choice should prove interesting.

Whatever the answers to these questions, Stagg *et al*. provide us with an intriguing new structure that, like clathrin, helps cells solve the problem of forming capsules of varying size while precisely controlling their formation and contents. Further cryo–electron microscopy maps could tell us the position of other COPII coat components in relation to the cage and, at higher resolutions, define the location of individual Sec13p and Sec31p subunits, and the nature of the interactions that define lattice assembly.

References and Notes

1. S. M. Stagg *et al*., *Nature* **439**, 234 (2006)
2. C. J. Smith, N. Grigorieff, B. M. Pearse, *EMBO J.* **17**, 4943 (1998).
3. A. Musacchio *et al*., *Mol. Cell* **3**, 761 (1999).
4. A. Fotin *et al*., *Nature* **432**, 573 (2004).
5. L. C. Bickford, E. Mossessova, J. Goldberg, *Curr. Opin. Struct. Biol.* **14**, 147 (2004).
6. G. Z. Lederkremer *et al*., *Proc. Natl. Acad. Sci. U.S.A.* **98**, 10704 (2001).
7. X. Bi, R. A. Corpina, J. Goldberg, *Nature* **419**, 271 (2002).
8. M. C. Lee *et al*., *Cell* **122**, 605 (2005).
9. C. Barlowe *et al*., *Cell* **77**, 895 (1994).
10. F. M. Brodsky, C. Y. Chen, C. Knuehl, M. C. Towler, D. E. Wakeham, *Annu. Rev. Cell Dev. Biol.* **17**, 517 (2001).
11. M. E. Edeling, C. J. Smith, D. J. Owen, *Nat. Rev. Mol. Cell Biol.* **7**, 32 (2006).
12. K. Matsuoka, R. Schekman, L. Orci, J. E. Heuser, *Proc. Natl. Acad. Sci. U.S.A.* **98**, 13705 (2001).
13. J.C. Fromme, R. Schekman. *Curr. Opin. Cell Biol*. **17** 345 (2005).
14. P. Watson, D. J. Stephens, *Biochim. Biophys. Acta,* **1744**, 304 (2005).
15. B. M. Pearse, C. J. Smith, D. J. Owen, *Curr. Opin. Struct. Biol.* **10**, 220 (2000).

16. C.S. thanks R. B. Freedman, J. M. Lord, A. D. Smith, D. J. Owen *et al.* for helpful discussions.

10.1126/science.1123754

APPLIED PHYSICS

Where Have All the Transistors Gone?

A universal logic gate has been constructed with magnetic nanostructures. Such devices could lead to a new generation of microelectronics.

R. P. Cowburn

Today's digital microelectronic circuits are constructed from transistors that switch currents on and off to process the code and data associated with modern information technology. Transistors may not always take center stage, however, as Imre *et al*. (*1*) report on page 205 of this issue. As integrated circuits become ever more dense, the problems in building good transistors multiply. Most researchers attack this problem by advanced optimization of the materials and design of transistors, but Imre *et al.* are part of a group of researchers with a more radical solution: Get rid of the transistors. Imre *et al.* have experimentally demonstrated a universal logic gate, from which all of the logic functions needed in digital microelectronics can be constructed, that is based on magnetic nanostructures and uses no transistors.

Electrons possess the properties of both charge and spin. Charge is responsible for electricity and is the quantity sensed by the transistors in an integrated circuit. Spin, on the other hand, is responsible for magnetism and is not used in most integrated circuits. The blossoming field of spintronics seeks to make use of the spin of the electron in digital microelectronics (*2*). Such a dramatic change at the microscopic level may necessitate an equally dramatic change in the top-level architecture of devices. This will be particularly the case for devices based upon the quantum mechanical interaction of single spins, but may well also be true even for spintronic devices built on classical ferromagnets, such as that proposed by Imre *et al.*

The architecture chosen by Imre *et al.* is based on the concept of cellular automata.

The author is at the Blackett Physics Laboratory, Imperial College London, Prince Consort Road, London SW7 2BW, UK. E-mail: r.cowburn@imperial.ac.uk

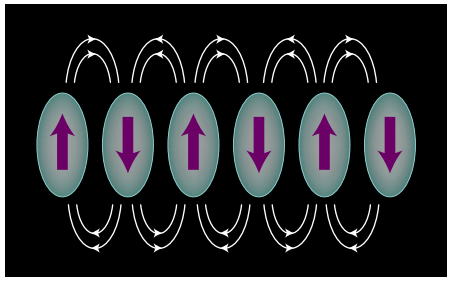

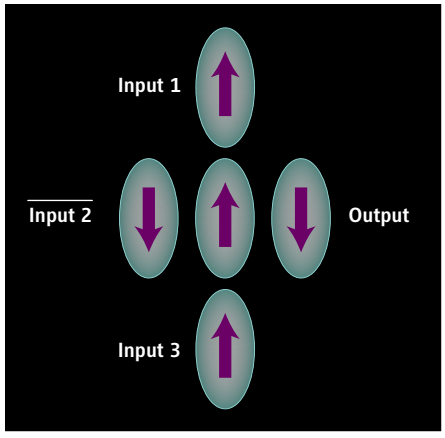

Chain of logic. (**Left**) In a simple array of magnetic nanostructures, stray fields couple the magnetization directions (arrows) in an antiparallel fashion from one nanostructure to the next, allowing information to be passed down a chain. (**Right**) Universal logic gate made from five nanostructures. The magnetization of the central nanostructure aligns itself with the net stray magnetic field from the three inputs. This majority state is then communicated to the output nanostructure.

Cellular automata are networks of cells with rules that describe how neighboring cells interact; they can, when correctly arranged, perform computations, as previously demonstrated by Amlani *et al*. using single-electron devices (*3*). Although these devices were operational only at cryogenic temperatures, the results opened the tantalizing possibility of computation without conventional transistors, and hence a new approach to the continuation of scaling of microelectronics far into the future.

Five years ago, we showed that magnetic nanostructures could allow a physical implementation of a cellular automata architecture that would work at room temperature (*4*): Quantum mechanical exchange within the nanostructure locks all of the spins together, forming a single giant macrospin of enormous moment and hence much greater thermal stability. As Imre *et al.* now show, not only can information propagate across a cellular automata device formed from magnetic nanostructures, but complete logic functions can also be implemented (see the figure).

The choice of demonstration logic gate is important here. Although any of the conventional Boolean functions such as AND or NOT could have been implemented, Imre *et al.* have chosen to implement the less known three-input inverting MAJORITY function. This function simply takes the majority state of its three inputs and then inverts it. This seemingly esoteric function is extremely useful, because with one of the three inputs tied permanently high (that is, the input always has the logic value 1), the gate simply performs the NOR operation on the remaining two inputs. Conversely, if the fixed input is tied permanently low (logic value 0), then the NAND operation is performed on the remaining inputs. Thus, with a single gate, the key functions of NAND and NOR can both be implemented.

From combinations of these, any arbitrary logic function can then be constructed.

There are a number of attractive reasons to consider using spintronics in general, and magnetic logic in particular, for digital microelectronics devices. Magnetic systems tend to be nonvolatile—they retain data when power is removed—which is an increasingly important trait in a world of mobile and wearable computing. Devices based on spintronics can be very dense and continue to operate well when scaled to small sizes; in particular, they do not exhibit leakage current when small (although there are some new challenges for very small magnetic particles, known collectively as the superparamagnetic limit).

The work of Imre *et al.* has two particularly noteworthy features. First, they used an adiabatic clocking scheme in which the energy barriers between discrete data states are gradually lowered and then raised again; this allows the system to move gradually from one computational state to another without the wasted energy that is inherent in conventional architectures (*5*). Given that one of the most pressing problems in the future scaling of microelectronics is how to manage the waste heat, it is of interest that "hot clocking" (as it is sometimes known) is intrinsic to the architecture. Second, the convenience of having a single universal gate goes deeper than simply saving the effort of designing others. It also opens the possibility of reconfigurable logic, in which the actual function of the gate can be changed after the hardware has been built. At the very least, this allows a single chip to be used for many different applications, reducing both costs and time to market. In principle, the hardware could be reconfigured within a few nanoseconds, allowing the microprocessor to adapt its very architecture to the best form for the computation in hand at that instant (*6*).

Challenges still remain before magnetic logic can be widely used. Imre *et al.* have not yet addressed any issues of speed, although their work is closely related to the emerging memory technology known as MRAM (magnetic random-access memory), where subnanosecond switching speeds are commonplace (*7*). Perhaps the greatest challenge facing magnetic logic is the identification of specific applications where its strengths will be most keenly felt. There would be little advantage in constructing an entire microprocessor from magnetic logic elements; there may be great benefit to implementing a specific functional block within a hybrid system on a chip. Many people believe that the future of microelectronics lies in a diverse hybrid of technologies on a single platform, each doing what it does best. Imre *et al.* have brought us one step closer to having a valuable new technology to add to the menu.

References

1. A. Imre *et al.*, *Science* **311**, 205 (2006).
2. S. A. Wolf *et al.*, *Science* **294**, 1488 (2001).
3. I. Amlani *et al.*, *Science* **284**, 289 (1999).
4. R. P. Cowburn, M. E. Welland, *Science* **287**, 1466 (2000).
5. R. P. Feynman, *Feynman Lectures on Computation*, A. J. G. Hey, R. W. Allen, Eds. (Addison-Wesley, Reading, MA, 1996).
6. G. A. Prinz, *Science* **282**, 1660 (1998).
7. H. W. Schumacher, C. Chappert, R. C. Sousa, P. P. Freitas, *J. Appl. Phys.* **97**, 123907 (2005).

10.1126/science.1122441

PHYSIOLOGY

Running a Clock Requires Quality Time Together

The strictly timed disassembly of a protein complex before entry of its constituents into the nucleus influences the 24-hour period of the circadian clock.

Jay C. Dunlap

A defining characteristic of circadian clocks, the biological timekeepers that control metabolic and behavioral activities through the cycle of day and night, is their ~24-hour period length, and all models for circadian clocks must explain how to construct a feedback loop that takes about a day to close. The cellular transcription regulators PERIOD (PER) and TIMELESS (TIM) are essential components of the fruit fly (*Drosophila melanogaster*) clock mechanism, and the model for the *Drosophila* clock has assumed that a major aspect of the ~24-hour time constant is the long time it takes for PER and TIM to associate in the cell cytoplasm before they enter the nucleus. On page 226 in this issue, Meyer *et al.* (*1*) report that this long-assumed lag in PER-TIM association does not exist. Rather, PER and TIM bind to each other right away, so a lag in their association cannot contribute to the 24-hour time constant (see the figure). Instead, it now appears that the entry of TIM and PER into the nucleus is delayed through the action of an interval timer whose existence comes as a complete surprise, and whose pace, moreover, is influenced by PER.

Enhanced online at www.sciencemag.org/cgi/content/full/311/5758/184

Half a century ago when scientists asserted that the molecular basis of circadian rhythms would be found in biochemical feedback loops that closed within the confines of a cell, one point of disbelief was the long time constant. Everyone accepted that feedback regulation could feature in networks, but everyone knew that these closed right away. How could a biochemical feedback loop be the basis of a biological clock characterized by a ~24-hour period length? Many early models for circadian clocks simply ignored the conundrum of the long time constant and settled for a plausible description of a feedback loop. But those models that took it seriously tried every imaginable solution (*2*), including counting functions (where a simple step happens over and over again), tape loop models (where a series of events plays out, the last of which reinitiates the series), models that relied on slow diffusion of clock proteins to take up time, and even (early on) models derived from the cellular sensing of subtle geophysical variables (the mysterious Factor X) (*2*). It led some to believe that even though clocks in unicellular organisms might be confined to cells, fundamentally different mechanisms might be at work in multicellular organisms (*3*).

Inevitably, as the problem of biological timing gradually gave way to the continued onslaught of genetics and biochemistry, it became apparent that daily expression of clock proteins, often apparently driven by negative-feedback loops involving activation and repression of gene expression, was a central feature of the circadian rhythm mechanism in eukaryotes (*2*). Stability of period length is conferred by the way these loops, of which there are usually two or more, are assembled and interlocked. In the fungus *Neurospora crassa*, for instance, a heterodimeric complex of the transcription factors WHITE COLLAR-1 and -2 (WC-1 and -2; collectively the WCC) activates expression of the transcription factor FREQUENCY (FRQ). FRQ then dimerizes and associates with a FRQ-interacting RNA helicase, the complex acting to reduce activity of the WCC (one loop). At the same time, the complex promotes the synthesis of more WC-1 (a second loop) (*4*, *5*). In *Drosophila*, a heterodimeric complex of the transcription factors CLOCK (CLK) and CYCLE (CYC) acti-

The author is in the Department of Genetics, Dartmouth Medical School, Hanover, NH 03755, USA. E-mail: jay.c.dunlap@dartmouth.edu

vates expression of PER and TIM (the protagonists of today's particular story), and then PER (perhaps helped by TIM) reduces the activity of the CLK-CYC complex (the first loop). In the second *Drosophila* loop, CLK-CYC drives expression of two other transcription factors: VRILLE, which inhibits expression of CLK, and PAR DOMAIN PROTEIN 1, which acts afterward to activate CLK expression. The two loops are interconnected by the action of CLK-CYC (*6*). In mammals, similar loops involve a complex that contains two transcription factors, CIRCADIAN LOCOMOTER OUTPUT CYCLES KAPUT (CLOCK) and BMAL1. The complex drives expression of four other transcription factors: CRYPTOCHROME 1 and 2, and PERIOD 1 and 2, all of which act in some way to block the activity of the CLOCK-BMAL1 complex (one loop). In a second loop, CLOCK-BMAL1 promotes expression of RevErbα (which acts first to repress *BMAL1*) and RETINOIC ACID RECEPTOR–RELATED ORPHAN RECEPTOR ALPHA (RORA), which acts subsequently to activate *BMAL1* (*7*). A point nicely made in reviews [e.g., (*5, 8–10*)] and textbooks (*2, 11*) is similarity in the overall layout of the loops, a feature that becomes even more apparent as one moves closer phylogenetically: For every protein activity seen in the interlocked *Drosophila* clock loops there exists a corresponding activity in a mammalian loop, even though the proteins executing these activities may be unrelated by amino acid sequence. Based on the degree to which this conceptual thread can be followed through the eukaryotes, many chronobiologists believe that what we learn about model system clocks can have immediate relevance for understanding all circadian clocks, and will eventually have clinical application, for instance, in understanding sleep disorders (*12*).

It's instructive to see how current clock models address the question of how intracellular feedback loops can achieve the long circadian time constant. In *Neurospora*, the stability of FRQ appears to be a major determinant of the long time constant (*13*), and this stability is determined by posttranslational phosphorylation of FRQ that leads to its ubiquitination and turnover (*2, 5*). Also contributing is the fact that all the steps in two interlocked loops keep either loop from running too fast. In mammals, so much effort has been spent describing the components of the varied, interconnected, and nested loops that the problem of the long time constant has received little explicit attention. The consensus, however, is that posttranslational modification and turnover of pertinent proteins, as well as the 3- to 4-hour lag between transcription and translation of clock proteins, make the major contributions (*9, 10*). In *Drosophila*, the principal model animal clock, it has been presumed that a major determinant of the long time constant is the long time it takes PER and TIM to associate in the cytoplasm and accumulate before they enter the nucleus (*8*, *14*). Based on the findings of Meyer *et al.* (*1*), aspects of this presumption can now be relegated to the dustbin of history.

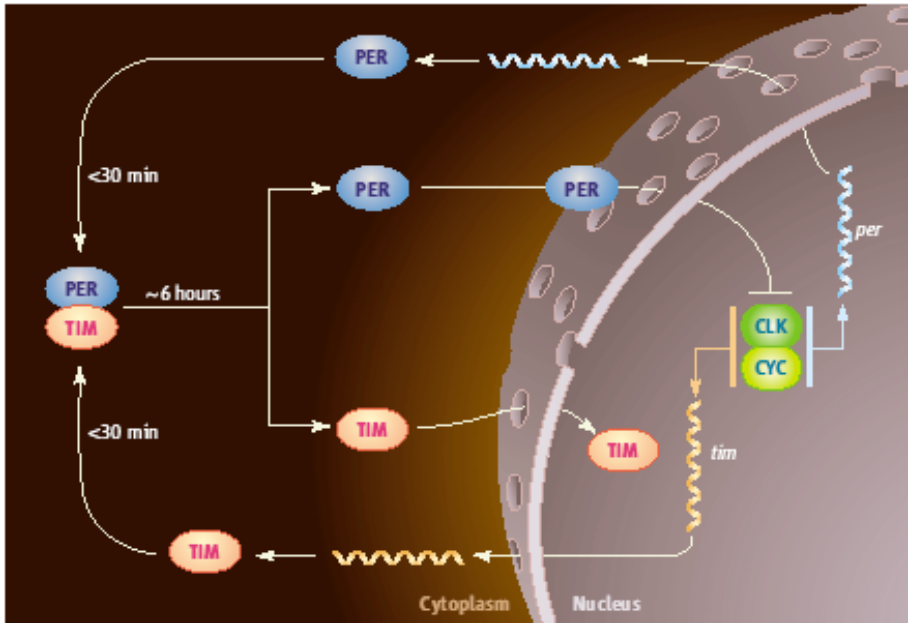

An interval timer influences the schedule of molecular events in the *Drosophila* circadian clock. Transcription of *per* and *tim* in the nucleus is driven by the combined action of transcription factors CLK and CYC. The resulting transcripts move to the cytoplasm where PER and TIM are made. These proteins rapidly associate into a heterodimer and remain as such for a long period of time. The duration of this interval, which contributes to the long time constant of the circadian clock, is set by a PER-influenced interval timer. Eventually PER and TIM enter punctate cytoplasmic foci (not shown) before their dissociation from each other and separate entry into the nucleus. PER then goes on to depress the activity of the CLK-CYC complex, thereby reducing expression of *per* and *tim*.

Meyer *et al*. (*1*) used a cultured cell line derived from late-stage *Drosophila* embryos (Schneider 2 or S2 cells). Although these cells do not have a circadian clock, they can carry out individual steps in the molecular cycle with fidelity, allowing examination of cell biological events associated with the clock. TIM and PER were tagged with fluorescent chromophores and their association was followed by fluorescence resonance energy transfer. This technique is well suited for documenting protein interactions because the strength of the fluorescent signal decreases exponentially with increased distance between tagged proteins. The authors report that TIM and PER associate in the cytoplasm within 30 min of their synthesis (no lag!), remain associated, enter discrete foci in the cytoplasm, and then after ~6 hours, abruptly dissociate and separately enter the nucleus. The separate nuclear entry is consistent with recent in vivo studies [(e.g., (*15*)]. The time interval of cytoplasmic association of TIM and PER is largely independent of intracellular expression levels of either or both of these proteins. Yet, as expected, TIM is still required to help PER into the nucleus, thereby validating a long-held tenet of *Drosophila* molecular clock models. Studies of mutant forms of *Drosophila* clock proteins also support the conclusions. The long-period mutant, tim^{UL}, has been viewed as altered in a nuclear function (TIM^{UL} holds onto PER too long and thereby lengthens the period length of the clock cycle); appropriately then, in the assay of Meyer *et al.*, the timing of delay before nuclear entry of TIM and PER is unaffected. In contrast, period lengthening due to the per^{L} mutation is characterized by delayed nuclear entry of these proteins (*16*). This is often modeled as poor association between PER^{L} and TIM; consequently, TIM cannot stabilize PER^{L} in the cytoplasm, causing PER^{L} to accumulate slowly and thereby yielding an extra long lag in the time to nuclear entry. In the study by Meyer *et al*., the delayed association is not seen (PER^{L} associates with TIM just as readily as does wild-type PER), but interestingly, the extra long lag (~9 hours) before nuclear entry of PER and TIM still occurs. This recapitulation of the basic phenotype of PER^{L} validates the use of S2 cells in this assay, and demonstrates that the interval timer regulating TIM and PER nuclear entry is influenced by PER.

Although some recent molecular analyses of the fly clock have focused on the importance of PER and the fact that it can "go it alone" in terms of repressing gene activity (*17*), the present study reminds us of the caveat of a PER-centric clock view—that TIM is still needed. The

study also provides a pleasingly different cytoplasmic activity for PER that is clearly distinct from its typecast nuclear role as a transcriptional repressor. The data necessitate a revision of the clock model through deletion of the lag associated with PER-TIM accumulation and insertion of an as-yet ill-described PER (and TIM?)-associated interval timer affecting nuclear entry. PER TIM heterodimerization can be seen perhaps as permitting subsequent posttranslational events that actually fix the schedule of nuclear translocation. But how this all happens—including the nature of the punctate concentrations of PER and TIM that appear in the cytoplasm before their separation and nuclear entry, the other proteins involved, and the nature of the interval timer and its role in setting the circadian time constant—is still a big unknown.

References

1. P. Meyer, L. Saez, M. W. Young, *Science* **311**, 226 (2006).
2. J. C. Dunlap, in *Chronobiology: Biological Timekeeping*, J. C. Dunlap, J. J. Loros, P. Decoursey, Eds. (Sinauer, Sunderland, MA, 2004), pp. 210–251.
3. M. Menaker, Ed., *Biochronometry* (National Academy of Sciences, Washington, DC, 1971).
4. K. Lee, J. J. Loros, J. C. Dunlap, *Science* **289**, 107 (2000).
5. D. Bell-Pedersen *et al.*, *Nat. Rev. Genet.* **6**, 544 (2005).
6. S. A. Cyran *et al.*, *Cell* **112**, 329 (2003).
7. T. K. Sato *et al.*, *Neuron* **43**, 527 (2004).
8. R. Allada, P. Emery, J. S. Takahashi, M. Rosbash, *Annu. Rev. Neurosci.* **24**, 1091 (2001).
9. L. Cardone, P. Sassone-Corsi, *Nat. Cell Biol.* **5**, 859 (2003).
10. S. M. Reppert, D. R. Weaver, *Annu. Rev. Physiol.* **63**, 647 (2001).
11. A. Sehgal, Ed., *Molecular Biology of Circadian Rhythms* (Wiley, New York, 2003).
12. K. L. Toh *et al.*, *Science* **291**, 1040 (2001).
13. Y. Liu, J. Loros, J. C. Dunlap, *Proc. Nat. Acad. Sci. U.S.A.* **97**, 234 (2000).
14. A. Sehgal *et al.*, *Science* **270**, 808 (1995).
15. O. T. Shafer, M. Rosbash, J. W. Truman, *J. Neurosci.* **22**, 5946 (2002).
16. K. Curtin, J. Huang, M. Rosbash, *Neuron* **14**, 365 (1995).
17. P. Nawathean, M. Rosbash, *Mol. Cell.* **13**, 213 (2004).

10.1126/science.1122839

PLANETARY SCIENCE

Titan's Zoo of Clouds

Saturn's moon Titan exhibits a variety of cloud structures, probably a result of a dynamically controlled methane cycle similar to that of water on Earth.

Emmanuel Lellouch

In planetary exploration, progress does not always come where you expect. In recent years, the predominantly nitrogen atmosphere of Saturn's moon Titan, often touted as a laboratory for understanding the early Earth, has not revealed as many clues about the complexity of its chemical evolution as was hoped. On the other hand, a wealth of new data suggest that, in terms of physical processes, Titan's surface and atmosphere may be more similar to those of Earth than any other body in the solar system. On page 201 of this issue, Rannou *et al.* (*1*) demonstrate that many observed features of Titan's clouds can be explained in terms of a dynamically controlled methane cycle sharing essential features with the water cycle on Earth, but with important differences.

Given the cold temperatures prevailing in Titan's troposphere (94 K at the surface, 71 K at 40-km altitude), methane, the second most abundant gas in Titan's atmosphere (about 5% of the atmosphere at the surface), is condensable in its liquid or solid forms, as is water on Earth. Whether methane actually condenses to form clouds, however, depends on many factors. The latest analyses of the Voyager data (*2*) left little room for clouds, finding instead an abundance of methane in the upper stratosphere well in excess of vapor-pressure equilibrium. Yet, 10 years ago, clouds were discovered in ground-based observations (*3*) from their effect on the near-infrared brightness of Titan's disk and shown to be present at 15- to 25-km altitude. This breakthrough initiated a decade of uninterrupted progress. The observations could distinguish between sparse clouds, variable over time scales of hours, which were suggestive of convective evolution, and large storm systems. Since 2000, direct imaging and spectral imaging observations (*4*–*6*) provided the ultimate proof for the existence of clouds and revealed their geographic locations. Temporal monitoring of the clouds from ground-based observations and their imaging from Cassini indicate that there are currently two classes of clouds on Titan: large storms near the south pole, variable but with relatively long lifetimes of several weeks; and short-lived (typically one terrestrial day), often elongated clouds at mid-southern latitudes (40°S) (see the figure) .

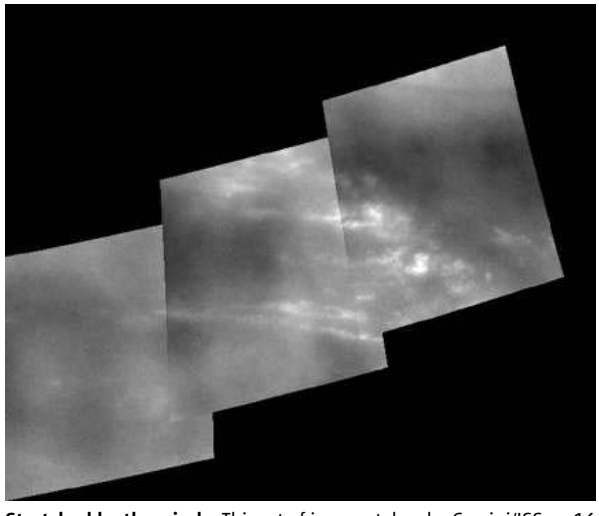

Stretched by the winds. This set of images taken by Cassini/ISS on 16 December 2004 shows Titan's temperate clouds near 38°S latitude. The clouds across the middle frame extend ~250 km and are probably elongated by zonal wind shears. The right frame is suggestive of active cumulus centers. These mid-latitude clouds are probably good analogs to the clouds in Earth's intertropical convergence zone.

CREDIT: CASSINI IMAGING TEAM AND NASA/JPL/SSI 0

Why are the Titan clouds located at these particular latitudes? On Titan, with the exception of a surface boundary layer, perhaps a few kilometers high, the troposphere is mostly controlled by radiative, rather than convective, processes. As a result, the level of free convection, where parcels of moist air become buoyant upon condensation and can ascend in the atmosphere, is normally well above the top of the boundary layer. Convective clouds can possibly form if the thickness of this convective surface layer is increased by enhanced surface temperatures, and it was initially proposed (*4*) that clouds at the south pole result from the maximum insolation currently experienced by this region.

This explanation is a little too simple. As is also true on Earth, even at southern summer solstice—which for Titan occurred in October 2002—the south pole is probably not the point where surface temperatures are highest. Radiative time scales in Titan's troposphere are so long that the surface temperatures tend to be fixed by the annually averaged insolation. In addition, the amount of solar energy that reaches the surface is limited by absorption by the stratospheric haze, which appears to be enhanced year-round in polar regions owing to the general atmospheric circulation (*7*).

Titan's smoglike haze is the ultimate product of high-altitude methane photochemistry, which is also responsible for the production of numerous gaseous species that can be transported downward and condense in the cold lower stratosphere. With no equivalent on Earth, this mechanism produces stratospheric photochemical clouds, which although difficult to visually distinguish against the haze, are identified spectroscopically in the winter polar regions (*8*). Interactions also exist between the haze, which

The author is at the Observatoire de Paris, F-92195 Meudon, France. E-mail: emmanuel.lellouch@obspm.fr

extends all the way down to the surface, and the tropospheric methane clouds. Haze particles provide condensation seeds for the clouds, whereas clouds, upon sedimentation, tend to wash out the smog particles from the lower atmosphere.

For the first time, Rannou *et al.* (*1*) propose an integrated description of this highly complex system in which atmospheric dynamics play a key role. The coupling of a Titan general circulation model—already successful in explaining Titan's now well-characterized superrotating circulation, haze distribution, and stratospheric composition (*9*)—with a cloud microphysical model allows Rannou *et al*. to predict cloud locations, altitudes, opacities, lifetimes, and morphologies. Calculations show that the dynamical forcing in Titan's troposphere results in the formation of two Hadley cells of unequal size, extending to ±60° latitudes, an analog of the intertropical convergence zone in the summer hemisphere, and smaller oblique cells in polar regions. This situation, remarkably similar to that on Earth (and Mars), preferentially produces clouds in upwelling branches of the circulation (currently at 40°S and near the south pole, as observed). Clouds are also predicted in other locations: One of the surprises is the prediction of a thick methane cloud at the north pole, virtually impossible to observe in the polar night. The bestiary of Titan clouds, still less rich than its terrestrial counterpart (for example, mountain-created or marine clouds are unlikely to occur in Titan), is clearly growing in complexity.

Yet, the model presented by Rannou and colleagues is unable to address longitudinal and small-scale phenomena. In a recent issue of *Science*, two reports shed new light on the temperate clouds. From Cassini data, Griffith *et al*. (*10*) witness the time evolution of several of these clouds. In what looks like a familiar cumulus-type development, active cloud centers rise typically 20 km up to the tropopause in half an hour before falling back or dissipating; in some cases, horizontal growth follows the updraft. Roe *et al.* (*11*) report that the temperate clouds tend to be clustered in longitude, with a primary population on the Saturn-facing hemisphere, suggestive of a geographic control that was envisaged earlier (*6*). The explanation they put forward is that of local injections of methane, raising the humidity and thereby lowering the level of free convection. This hypothesis implies enrichment of gaseous methane in a latitude band, a situation not present in the model of Rannou *et al.* and that should be verifiable by observations.

Does it rain (and if so, where?) on Titan? The methane cycle described by Rannou *et al*. leads to a net transport of methane from the tropics, where surface evaporation prevails and only the largest raindrops can reach the surface, to the polar regions where precipitation dominates. In fact, Titan's rainstorms may be much more violent and rare than those on Earth, given that the amount of condensable material on Titan is typically 50 times as large as that on Earth and the convective flux a factor of 2000 smaller (*12*). This situation, which may represent an extreme analogy to the current evolution of the terrestrial climate under increasing greenhouse conditions, is consistent with both the compelling evidence for flow-shaped landscapes and the absence of surface liquids at the Huygens site (*13*).

Although Titan's methane cycle and Earth's water cycle share the fundamental property that the sources are at the surface, the ultimate source on Titan that replenishes the methane in the atmosphere against irreversible photochemical loss has yet to be identified. With the long-standing hypothesis of vast liquid deposits being increasingly ruled out by existing data, a geologic source such as volcanic outgassing or geysering presents a seductive possibility—one that is almost irresistible for some researchers [for example, see (*14*)]—but the indisputable evidence remains to be found.

References

1. P. Rannou *et al*., *Science* **311**, 201 (2006).
2. R. E. Samuelson *et al*., *Planet. Space Sci*. **45**, 959 (1997).
3. C. A. Griffith *et al*., *Nature* **395**, 575 (1998).
4. M. E. Brown *et al*., *Nature* **420**, 795 (2002).
5. H. G. Roe *et al*., *Astrophys. J.* **618**, L49 (2005).
6. C. C Porco *et al., Nature* **434**, 159 (2005).
7. P. Rannou *et al*., *Nature* **418**, 853 (2002).
8. R. E. Samuelson *et al*., *Planet. Space Sci*. **45**, 941 (1997).
9. F. Hourdin *et al*., *J. Geophys. Res.* **109**, E12005 (2004).
10. C. A. Griffith *et al*., *Science* **310**, 474 (2005).
11. H. G. Roe *et al*., *Science* **310**, 477 (2005).
12. R. D. Lorenz *et al*., *Geophys. Res. Lett*. **32**, L01201 (2005).
13. M. Tomasko *et al*., *Nature* **438**, 765(2005).
14. C. Sotin *et al*., *Nature* **435**, 786 (2005).

10.1126/science.1122628

SYSTEMS BIOLOGY

When Proteomes Collide

Although the protein interaction network of herpesvirus does not resemble that of its human host, it merges at multiple points with the human network during infection. Such a strategy may optimize conditions for establishing a pathogenic state.

Joel S. Bader and John Chant

Mapping protein interactions and transactions (such as phosphorylation, ubiquitination, and degradation) within a cell or organism is essential to developing a molecular understanding of physiology. Over the past decade, protein interaction mapping has evolved from low-throughput manual screens to systematic interrogations of entire proteomes, from viruses to humans (see the figure). The study by Uetz *et al*. on page 239 in this issue (*1*) is an exciting entry to the field. The authors present protein interaction maps for two herpesviruses—Kaposi sarcoma–associated herpesvirus (KSHV) and varicella-zoster virus (VZV)—generated by two-hybrid screening, an experimental method that identifies protein-protein interactions. Computationally "docking" the KSHV protein interaction map onto the human map reveals the pathogen's network-level strategies for integrating with its host.

Two-hybrid screening is challenging owing to high false-positive and false-negative error rates. False-positives can be pruned by expert-generated decision trees (*2*–*4*) or statistically modeled confidence scores (*5*, *6*). Data quality can be independently assessed using moderate-throughput biochemical methods that test protein-protein physical association (*3*, *7*).

False-negatives have been more difficult to address. Estimates of false-negative rates based on comparisons to protein interaction lists culled from the literature are biased by the examples selected for analysis and by systematic differences between screens. Consequently, the numbers of protein-protein interactions in human, simple model organisms, and even viruses remain uncertain. The high false-negative rate and low coverage—that is, extreme uncertainty about how many interaction partners remain to be discovered—skew observed network properties (*8*). This situation is reminiscent of the uncertainty in predicting the number of genes encoded in the human genome.

A key advance made by Uetz *et al*. is the generation of a map that has, for perhaps the first time, crossed the halfway point toward completion. Their map for KSHV, with 89 annotated genes, reveals 123 protein-protein interactions that include 70% of those previously known. Earlier two-hybrid interaction maps have covered a far smaller fraction of known interactions, typically 5% or less (*3*, *7*). The two-hybrid method can interrogate each interaction in two distinct orientations ("bait" and "prey"), providing an internal assessment of coverage. One remaining puzzle is that only 1 of 123 KSHV interactions and 19 of 173 VZV interactions were observed in both orientations.

High coverage did not come at the expense of low specificity: 50% of selected interactions

J. S. Bader is in the Department of Biomedical Engineering and High-Throughput Biology Center, Johns Hopkins University, 3400 North Charles Street, Baltimore, MD 21215, USA. E-mail: joel.bader@jhu.edu J. Chant is at Genentech, Inc., 1 DNA Way, South San Francisco, CA 94080, USA. E-mail: jchant@gene.com

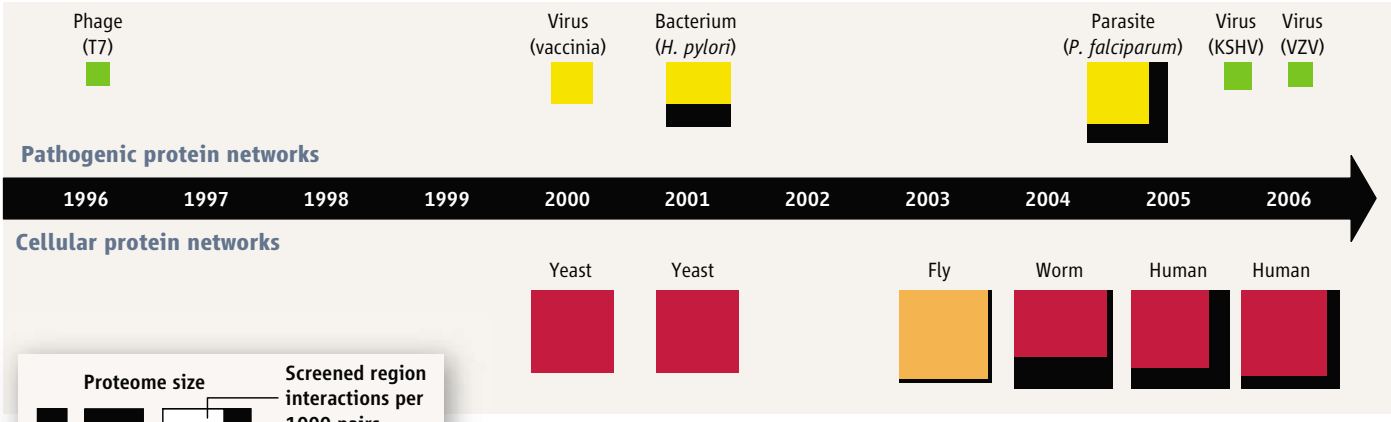

Evolution of protein interaction screens. The timeline depicts a history of genome-scale screens for protein interaction networks in pathogens (above axis) and cells (below axis). Each screen is represented by a box whose side length quantitatively represents the number of protein-coding loci in the corresponding genome on a logarithmic scale. Two-hybrid screens are based on pairwise tests, and the colored region of each box represents the protein pairs tested (height = baits and width = preys in the screen). The color represents the density of high-confidence interactions per 1000 pairs tested.

were confirmed by an independent biochemical approach. This is somewhat less than the 80% confirmation rate reported for other high-throughput efforts (*3*, *7*), but still indicates that most of the observed interactions are real.

Given these high-quality data and unrivaled coverage, what can we see that has not been evident in previous low-coverage maps? Are there fundamental differences between the wiring of viral and cellular networks?

Protein networks examined before the Uetz *et al*. study have generally been described as small-world networks, similar to human social networks. Small-world networks show clustered organization of components in local "neighborhoods" (if Alice knows Bob and Bob knows Carol, Alice and Carol are more likely to know each other). Globally, however, these networks have short paths connecting any two components. Short paths, or the colloquial "six degrees of separation" of social networks, are a hallmark of networks with random connections. Small-world networks are interesting because they share characteristics of highly organized networks locally and random networks globally. Amazingly, the viral protein interaction network lacks clustering: Local order is not enhanced over a randomized network.

Uetz *et al*. suggest that the lack of clustering reflects a single, cohesive module arising from high connectivity between all viral proteins. Highly connected modules in cellular protein networks often correspond to protein complexes or pathways. Perhaps the observations by Uetz *et al*. are not so surprising: A viral network is similar in structure to a large protein complex or the protein interaction network of an organelle, rather than that of a cellular network. Supporting this conjecture is the origin of certain organelles, notably the mitochondrion and chloroplast, from bacterial precursors. A lack of local clustering may be a general property of pathogen networks: *Helicobacter pylori* and *Plasmodium falciparum* also lack clustering beyond a random model (*9*).

How, then, does a pathogen merge its network into a host organism? Does it hijack the function of a single host protein interaction module that controls a specific biological process? Uetz *et al*. answer this question with computational modeling. They inferred viral-human protein interactions by identifying human and viral proteins that are homologs of pairs of proteins known to interact in yeast, worm, or fly. Biochemical tests confirmed 70% of the computational predictions. The inferred host-pathogen interactions were then used to dock the viral network into a human network generated by similar bioinformatic techniques.

Rather than targeting a single module in the human network, the virus melds into multiple, weakly connected human modules. The decentralized structure of cellular protein interaction networks might have evolved to prevent an attack on a single module from compromising the entire system (*10*).

Systems biology aficionados will note that the degree distribution of the viral network peaks at three interactions per protein, whereas for reported cellular networks, a single interaction per protein is most common. The viral network degree distribution also decays faster than the power-law decay of cellular networks, with proportionally fewer highly connected hub proteins. Higher coverage and fewer components relative to cellular networks contribute to these differences. Nevertheless, the differences are important because power-law decay has influenced theoretical models of network evolution. The evolutionary mechanisms most consistent with the power-law decay and local clustering of cellular networks are variants of preferential attachment (*11*, *12*), or rich-get-richer schemes, in which proteins that already have interactions are likely to accumulate more. Viral networks may require additional evolutionary mechanisms to be emphasized or introduced. Given that viruses evolved from more complex genomes, uncompensated gene loss could be an important component of evolutionary models.

The Uetz *et al*. study combines accumulated fragmentary information into a systems-level picture—a so-called percolation transition. The authors demonstrate conclusively that we have sufficient information to transfer knowledge through comparative proteomics and infer new protein interactions with high specificity. Completing these maps enhances our understanding and remains a driving goal. Understanding host and pathogen networks, how they merge during infection, and how protein modifications, gene regulation, RNA interference phenotypes, and other systems-level maps can be combined for a multilayered view will deliver on the promise of systems biology to control human diseases ranging from pathogenic infection to cancer.

References

1. P. Uetz *et al.*, *Science* **311**, 239 (2006); published online 8 December 2005 (10.1126/science.1116804).
2. T. Ito *et al.*, *Proc. Natl. Acad. Sci. U.S.A.* **98**, 4569 (2001).
3. S. Li *et al.*, *Science* **303**, 540 (2004).
4. P. Uetz *et al.*, *Nature* **403**, 623 (2000).
5. L. Giot *et al.*, *Science* **302**, 1727 (2003).
6. J. S. Bader, A. Chaudhuri, J. M. Rothberg, J. Chant, *Nat. Biotechnol.* **22**, 78 (2004).
7. J. F. Rual *et al.*, *Nature* **437**, 1173 (2005).
8. J. D. Han, D. Dupuy, N. Bertin, M. E. Cusick, M. Vidal, *Nat. Biotechnol.* **23**, 839 (2005).
9. S. Suthram, T. Sittler, T. Ideker, *Nature* **438**, 108 (2005).
10. S. Maslov, K. Sneppen, *Science* **296**, 910 (2002).
11. A. L. Barabasi, R. Albert, *Science* **286**, 509 (1999).
12. M. Middendorf, E. Ziv, C. H. Wiggins, *Proc. Natl. Acad. Sci. U.S.A.* **102**, 3192 (2005).

10.1126/science.1123221

Plasmonics: Merging Photonics and Electronics at Nanoscale Dimensions

Ekmel Ozbay*

Electronic circuits provide us with the ability to control the transport and storage of electrons. However, the performance of electronic circuits is now becoming rather limited when digital information needs to be sent from one point to another. Photonics offers an effective solution to this problem by implementing optical communication systems based on optical fibers and photonic circuits. Unfortunately, the micrometer-scale bulky components of photonics have limited the integration of these components into electronic chips, which are now measured in nanometers. Surface plasmon–based circuits, which merge electronics and photonics at the nanoscale, may offer a solution to this size-compatibility problem. Here we review the current status and future prospects of plasmonics in various applications including plasmonic chips, light generation, and nanolithography.

Today's state-of-the-art microprocessors use ultrafast transistors with dimensions on the order of 50 nm. Although it is now routine to produce fast transistors, there is a major problem in carrying digital information to the other end of a microprocessor that may be a few centimeters away. Whereas copper wire interconnects carry digital information, interconnect scaling has been insufficient to provide the necessary connections required by an exponentially growing transistor count. Unlike transistors, for which performance improves with scaling, the delay of interconnects increases and becomes a substantial limitation to the speed of digital circuits (*1*). This limitation has become more evident over the past 1 to 2 years, as the annual increase rate of the clock speed of microprocessors slowed greatly.

Optical interconnects such as fiber optic cables can carry digital data with a capacity >1000 times that of electronic interconnects. Unfortunately, fiber optic cables are ~1000 times larger compared with electronic components, and the two technologies are difficult to combine on the same circuit. External optical interconnects that can connect different parts of the electronic chips via air or fiber cables have also been proposed. However, the resulting bulky configuration has limited the implementation of this idea. The ideal solution would be to have a circuit with nanoscale features that can carry optical signals and electric currents. One such proposal is surface plasmons, which are electromagnetic waves that propagate along the surface of a conductor. The interaction of light with matter in nanostructured metallic structures has led to a new branch of photonics called plasmonics. Plasmonic circuits offer the potential to carry optical signals and electric currents through the same thin metal circuitry, thereby creating the ability to combine the superior technical advantages of photonics and electronics on the same chip.

Nanotechnology Research Center, Bilkent University, Bilkent, Ankara 06800 Turkey.

*To whom correspondence should be addressed. E-mail: ozbay@bilkent.edu.tr

Plasmonic Chips: Light on a Wire

What limits the integration of optical and electronic circuits most is their respective sizes. Electronic circuits can be fabricated at dimensions below 100 nm. On the other hand, the wavelength of light used in photonics circuits is on the order of 1000 nm. When the dimensions of an optical component become close to the wavelength of light, the propagation of light is obstructed by optical diffraction (*2*), which therefore limits the minimum size of optical structures including lenses, fibers, and optical integrated circuits. Although the introduction of photonic crystals brings a partial solution to these problems, the photonic crystal itself has to be several wavelengths long, because the typical period is on the order of half of a wavelength (*3*).

Surface plasmon–based photonics, or "plasmonics," may offer a solution to this dilemma, because plasmonics has both the capacity of photonics and the miniaturization of electronics. Surface plasmons (SPs) provide the opportunity to confine light to very small dimensions. SPs are light waves that occur at a metal/dielectric interface, where a group of electrons is collectively moving back and forth (*4*). These waves are trapped near the surface as they interact with the plasma of electrons near the surface of the metal. The resonant interaction between electron-charged oscillations near the surface of the metal and the electromagnetic field of the light creates the SP and results in rather unique properties. SPs are bound to the metallic surface with exponentially decaying fields in both neighboring media. The decay length of SPs into the metal is determined by the skin depth, which can be on the order of 10 nm—two orders of magnitude smaller than the wavelength of the light in air. This feature of SPs provides the possibility of localization and the guiding of light in subwavelength metallic structures, and it can be used to construct miniaturized optoelectronic circuits with subwavelength components (*5*). Such plasmonic optoelectronic circuits, or plasmonic chips, will consist of various components such as waveguides, switches, modulators, and couplers, which can be used to carry the optical signals to different parts of the circuit.

Plasmonic waveguides are used to guide the plasmonic signals in these circuits and can be configured by using various geometries (*6*). Thin metal films of finite width embedded in a dielectric can be used as plasmonic waveguides. This geometry offers the best propagation results for a surface plasmon–based waveguide, because the measured propagation length for operation with light at a wavelength of 1550 nm is reported to be as long as 13.6 mm. However, the localization for both directions is on the order of a few micrometers in this plasmonic waveguide geometry (*7*). To achieve subwavelength localization, one can reduce the width of the wire and subsequently use the SPs to guide the light underneath this nanowire. In nanowires, the confinement of the electrons in two dimensions leads to well-defined dipole surface plasmon resonances, if the lateral dimensions of the wire are much smaller than the wavelength of the exiting light. By using this method, a 200-nm-wide and 50-nm-high gold nanowire was fabricated. This plasmonic waveguide was then locally excited at a light wavelength of 800 nm (*8*). By direct imaging of the optical near field with subwavelength-resolution photon scanning tunneling microscopy, light transport was observed along the nanowire over a distance of a few micrometers. Although this is a clear demonstration of subwavelength guiding, the losses associated with the resistive heating within the metal limit the maximum propagation length of light within these structures. In order to avoid the ohmic losses, one can envision using an array of nanoparticle resonators. The resonant structure of the nanoparticles can be used to guide the light, whereas the reduced metallic volume means a substantial reduction in ohmic losses. Stefan Maier and co-workers (*9*) used such a structure (Fig. 1A), in which nanoscale gold dots were patterned on a silicon-on-insulator wafer to define the plasmon propagation path. Figure 1B shows scanning electron micrographs (SEMs) of the fabricated plasmonics waveguides designed for operation at a wavelength of 1500 nm. The waveguide structure is not uniform across its width where the size of the metal dots is reduced from 80 nm × 80 nm at the center to 50 nm × 50 nm at the edges. This has the effect of confining the

energy more intently to the middle of the guide (Fig. 1A). This structure has been shown to have a decay length longer than 50 μm, whereas theoretical simulations predict a decay length in the order of 500 μm. Figure 1A shows that although the localization along the *x* direction is subwavelength, the localization extends a few periods along the *y* direction, which corresponds to localization on the order of a wavelength. Therefore, the subwavelength localization of SPs is limited only to the *x* direction.

To achieve localization in both directions, a new type of highly localized plasmon has been analyzed and experimentally demonstrated in metals with V-shaped grooves (*10*). The major features of plasmons in V grooves include a combination of strong localization, single-mode operation, the possibility of nearly 100% transmission through sharp bends, and a high tolerance to structural imperfections. For the localization and guiding to occur, the wedge angle (θ) of the V groove should be smaller than a critical angle. For V grooves made from silver with a vacuum wavelength of 0.6328 μm, this critical wedge angle is found to be 102°. The measured lateral localization of a structure with a 40° wedge angle is ~300 nm, which is superior to the nanoparticle-based plasmonic waveguides. However, the reported experimental and theoretical decay lengths for the same V groove–shaped plasmonic waveguide are 1.5 μm and 2.25 μm, respectively, which are obviously too short for any application of these plasmonic structures. The propagation distance performance of the V groove–shaped SP waveguides has been recently extended to 250 μm (*11*). By using focused ion-beam milling techniques, 460-μm-long V groove–shaped plasmonic waveguides were fabricated on gold layers that were deposited on a substrate of fused silica. Scanning near-field optical microscope measurements of these structures were made at optical communication wavelengths (1425 to 1620 nm). For a structure with a 0.6-μm-wide and 1.0-μm-deep groove wedge (corresponding to a ~17° wedge angle), the SP propagation lengths were measured to be within 90 to 250 μm. The mode was well confined along the lateral direction, and the measured mode width was 1.1 μm.

Thus there is a basic trade-off in all plasmon waveguide geometries between mode size and propagation loss. One can have a low propagation loss at the expense of a large mode size, or a high propagation loss with highly confined light. A hybrid approach, where both plasmonic and dielectric waveguides are used, has been suggested as a solution to this trade-off (*12*). These waveguides are designed for 1500-nm operation and exhibit losses on the order of –1.2 dB/μm, and they can guide light around 0.5-μm bends. Light can also be efficiently coupled between more conventional silicon waveguides, where these plasmon waveguides with compact couplers and surface plasmon optical devices can be constructed by using planar circuit fabrication techniques. Introducing gain to the plasmonic waveguides can also bring a solution to the limited propagation distances. This situation is theoretically investigated by considering the propagation of SPs on metallic waveguides adjacent to a gain medium (*13*). The analytic analysis and numeric simulation results show that the gain medium assists the SP propagation by compensating for the metal losses, making it possible to propagate SPs with little or no loss on metal boundaries and guides. The calculated gain requirements suggest that lossless, gain-assisted surface plasmon propagation can be achieved in practice for infrared wavelengths.

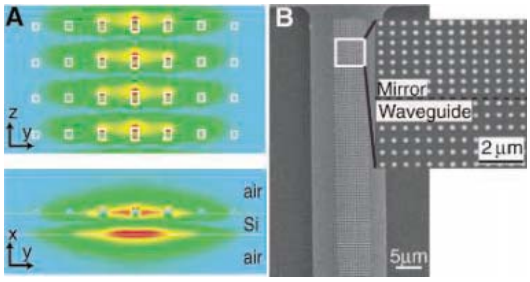

Fig. 1. (**A**) FDTD simulations show the electric field produced within the plasmon waveguide structure. (**B**) A plasmon waveguide consists of nanoscale gold dots on a silicon-on-insulator surface. [Adapted from (*9*)]

Recently, a new kind of SP geometry has been suggested to solve theoretically the issue of confinement versus propagation length (*14*). The new mechanism for confining much more field in the low-index region rather than in the adjacent high-index region is based on the relative dispersive characteristics of different surface plasmon modes that are present in these structures. The structures have a subwavelength modal size and very slow group velocity over an unusually large frequency bandwidth. Simulations show that the structures exhibit absorption losses limited only by the intrinsic loss of the metal. Currently, there is no experimental data that supports these simulations. However, the new suggested SP structure is quite promising and deserves attention from the experimental research groups that are working on plasmonic waveguides.

Plasmonic chips will have optical input and output ports, and these ports will be optically connected to conventional diffraction-limited photonic devices by plasmonic couplers (*8*). The couplers should have high conversion efficiency, along with a transmission length that is longer than the optical wavelength to avoid the direct coupling of the propagating far-field light to the nanophotonic devices inside the plasmonic chip. A promising candidate for this feature can be fabricated by combining hemispherical metallic nanoparticles that work as a plasmonic condenser and a nanodot-based plasmonic waveguide (*15*). When the focused plasmons move into the coupler, the transmission length through the coupler is 4.0 μm. Nanodots can also be used for focusing SPs into a spot of high near-field intensity having a subwavelength width (*16*). Figure 2A shows the SEM image of such a sample containing 19 200-nm through-holes arranged on a quarter circle with a 5-μm radius. The SPs originating from these nanodots are coupled to a metal nanostrip waveguide. A near-field scanning optical microscopy (NSOM) image of this structure was taken at 532-nm incident wavelength with horizontal polarization. The near-field image (Fig. 2B) shows that the focused SPs propagate along the subwavelength metal guide, where they partially penetrate into the 100-nm-wide bifurcation at the end of the guide, thus overcoming the diffraction limit of conventional optics. The measured propagation distance is limited to 2 μm, and the propagation distances are expected to be much longer with improved fabrication processes and by using properly designed metal-dielectric hybrid structures. The combination of focusing arrays and nanowaveguides may serve as a basic element in planar plasmonic circuits.

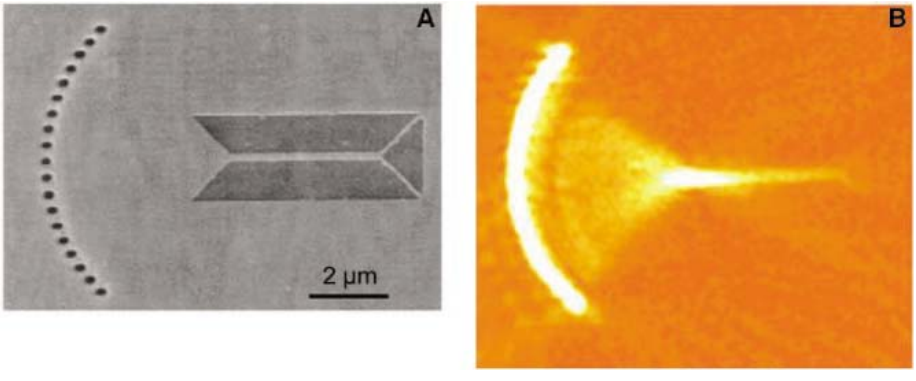

Fig. 2. (**A**) SEM image of a nanodot focusing array coupled to a 250-nm-wide Ag strip guide. (**B**) NSOM image of the SP intensity showing subwavelength focusing. [Adapted from (*15*)]

Active control of plasmons is needed to achieve plasmonic modulators and switches.

Plasmonic signals in a metal-on-dielectric waveguide containing a gallium section a few microns long can be effectively controlled by switching the structural phase of gallium (*17*). The switching can be achieved by either changing the waveguide temperature or by external optical excitation. The signal modulation depth can exceed 80%, and switching times are expected to be in the picosecond time scale. The realization of an active plasmonic device by combining thin polymer films containing molecular chromophores with thin silver film has also been reported (*18*). The molecular plasmonic device consists of two polymer layers, one containing donor chromophore molecules and the other containing acceptor fluorophore molecules. Coupled SPs are shown to provide an effective transfer of excitation energy from donor molecules to acceptor molecules on opposite sides of metal film up to 120 nanometers thick. The donors absorb incident light and transfer this excitation energy by dipole-dipole interactions to the acceptors. The acceptors then emit their characteristic fluorescence. These results are preliminary demonstrations for active control of plasmonic propagation, and future research should focus on the investigation of electro-optic, all-optical, and piezoelectric modulation of subwavelength plasmon waveguide transmission.

Extensive research efforts are being put forth in order to achieve an all-plasmonic chip. In the near term, plasmonic interconnects may be used to address the capacity problem in digital circuits including microprocessors. Conventional electronic interconnects may be used to transfer the digital data among the local arrays of electronic transistors. But, when a lot of data need to travel from one section of a chip to another remote section of the chip, electronic information could be converted to plasmonic information, sent along a plasmonic wire, and converted back to electronic information at the destination. Unfortunately, the current performance of plasmonic waveguides is insufficient for this kind of application, and there is an urgent need for more work in this area. If plasmonic components can be successfully implemented as digital highways into electronic circuits, this will be one of the "killer applications" of plasmonics.

Plasmonic Light Sources

The emerging field of plasmonics is not only limited to the propagation of light in structures with subwavelength dimensions. Plasmonics can also help to generate and manipulate electromagnetic radiation in various wavelengths from optics to microwaves. Since their introduction by Nakamura in 1995 (*19*), InGaN-based semiconductor light emitting diodes (LEDs) have become promising candidates for a variety of solid-state lightning applications (*20*). However, semiconductor-based LEDs are also notorious for their low light-emission efficiencies. Plasmonics can be used to solve this efficiency problem (*21*). When InGaN/GaN quantum wells (QWs) are coated by nanometer silver or aluminum films, the resulting SPs increase the density of states and the spontaneous emission rate in the semiconductor. This leads to the enhancement of light emission by SP-QW coupling, which results in large enhancements of internal quantum efficiencies. Time-resolved photoluminescence spectroscopy measurements were used to achieve a 32-fold increase in the spontaneous emission rate of an InGaN/GaN QW at 440 nm (*22*). This enhancement of the emission rates and intensities results from the efficient energy transfer from electron-hole pair recombination in the QW to electron vibrations of SPs at the metal-coated surface of the semiconductor heterostructure. This QW-SP coupling is expected to lead to a new class of super bright and high-speed LEDs that offer realistic alternatives to conventional fluorescent tubes.

Similar promising results were obtained for organic LEDs (OLEDs), which are now becoming popular as digital displays. In an OLED, up to 40% of the power that can be coupled into air is lost due to quenching by SP modes. A periodic microstructure can be used to recover the power that is normally lost to SPs. Using this approach, strong photoluminescence has been reported from a top-emitting organic light-emitting structure, where emission takes place through a thin silver film (*23*). The results indicate that the addition of a nanopatterned dielectric overlayer to the cathode of top-emitting OLEDs should increase light emission from these structures by two orders of magnitude over a similar planar structure. The dielectric layer acts to couple the surface plasmon-polariton modes on the two metal surfaces, whereas its corrugated morphology allows the modes to scatter to light. An OLED using a π-conjugated polymer emissive layer sandwiched between two semitransparent electrodes was also reported (*24*). One of the electrodes was an optically thin gold film anode, whereas the cathode was in the form of an optically thick aluminum (Al) film with patterned periodic subwavelength two-dimensional (2D) hole array that showed anomalous transmission in the spectral range of the polymer photoluminescence band. At similar current densities, a sevenfold electroluminescence efficiency enhancement was obtained with the patterned Al device compared with a control device based on imperforated Al electrode, demonstrating that the method of patterning the electrodes into 2D hole arrays is efficient for this structure. Plasmonics can also be used to enhance the performance of lasers (*25*). A metal nano-aperture was fabricated on top of a GaAs vertical cavity surface emitting laser (VCSEL) for subwavelength optical near-field probing. The optical near-field intensity and the signal voltage of nano-aperture VCSELs exhibit record high values because of the localized surface plasmons in metal nanostructures. The enhancement factors of the optical near-field and voltage signal are 1.8 and 2, respectively. Reducing the nano-aperture reduces the optical resolution of the VCSEL probe from 240 nm to 130 nm. These results show that plasmon enhancement will be helpful for realizing high-resolution optical near-field VCSEL probes.

SPs also play a key role in the transmission properties of single apertures and the enhanced transmission through subwavelength hole arrays (*26*, *27*). There has been intense controversy on the physical origin of the enhanced transmission in these structures (*28*). Recent theoretical and experimental analyses suggest that the enhanced transmission can be explained by diffraction assisted by the enhanced fields associated with SPs (*29*, *30*). Although SPs are mostly studied at optical frequencies, they can also be observed at the microwave, millimeter-wave, and THz frequencies (*31*). By texturing the metallic surface with a subwavelength pattern, we can create SPs that are responsible for enhanced transmission observed at microwave and millimeter wave frequencies for 1D and 2D gratings with subwavelength apertures (*32*, *33*). A subwavelength circular aperture with concentric periodic grooves can be used to obtain enhanced microwave transmission near the surface plasmon resonance frequency (*34*). These results show that enhanced transmission from a subwavelength circular annular aperture with a grating is assisted by the guided mode of the coaxial waveguide and coupling to the surface plasmons. A 145-fold enhancement factor is obtained with a subwavelength circular annular aperture surrounded by concentric periodic grooves. The same structure also exhibits beaming properties that are similar to the beaming effects observed from a subwavelength aperture at optical wavelengths (*35*). Figure 3 shows the electromagnetic waves from a subwavelength circular annular aperture surrounded by concentric periodic grooves. The radiated electromagnetic waves have a very strong angular confinement around the surface mode resonance frequency, in which the angular divergence of the beam is ±3°. Enhanced transmission at THz wavelengths is also reported for a freestanding metal foil perforated with periodic arrays of subwavelength apertures (*36*). The peak transmission at the lowest frequency resonance is ~0.6 for each aperture array, which is a factor of ~5 larger than the fractional area occupied by the apertures. Doped semiconductors exhibit a behavior at THz frequencies similar to that of metals at optical frequencies, thus they constitute an optimal material for THz plasmonics (*37*). Enhanced transmission of THz radiation is observed by using arrays of subwavelength apertures structured in n-type silicon. This enhancement can be explained by the resonant tunneling of SPs that can be excited at THz wavelengths

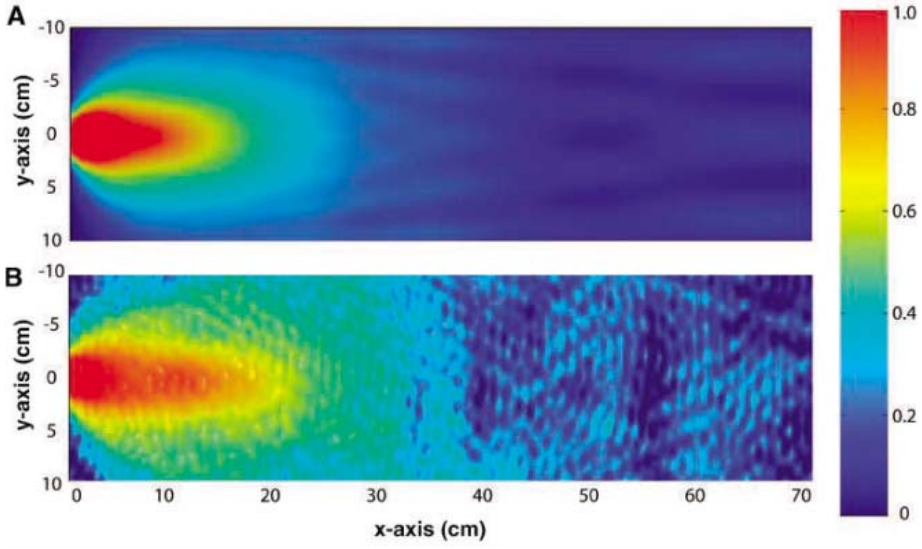

Fig. 3. Calculated (**A**) and measured (**B**) electric field distribution from a subwavelength circular annular aperture with a grating at the resonance frequency. The measured electric field intensity is confined to a narrow spatial region and propagates without diffracting into a wide angular region, which is in good agreement with the simulations.

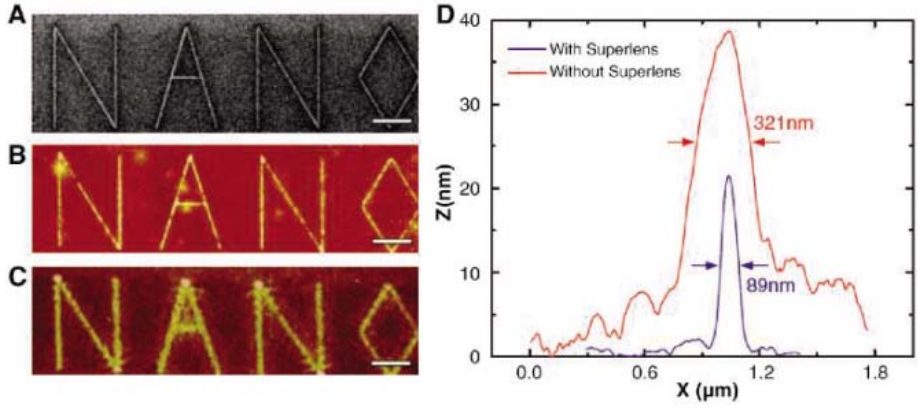

Fig. 4. The images of an arbitrary object obtained by different methods. (**A**) FIB image of the object. (**B**) The image obtained on photoresist with a silver superlens. (**C**) The image obtained on photoresist with conventional lithography. (**D**) Comparison of both methods. [Adapted from (*40*)]

in doped semiconductors. The transmission increases markedly as the aperture size is augmented and as the array thickness is reduced.

Plasmonic Nanolithography

The minimum feature size used within state-of-the-art electronic circuits is on the order of 50 nm, and new lithography techniques need to be developed to fabricate these integrated circuits with nanometer-scale dimensions. Optical projection lithography at shorter optical wavelengths can be used to reach the desired feature sizes. However, the change of the illumination wavelength to shorter wavelengths means new light sources, photoresists, and optics that are becomingly increasingly more complex as the wavelength becomes smaller. SPs result in a strongly enhanced nanoscale spatial distribution of an electrical field near the metal surface. When the resonance frequency falls within the sensitivity range of a photoresist, the resulting enhanced optical field that is close to the metal surface can locally cause increased exposure of a thin layer of resist directly below the mask. Because the technique is not diffraction limited, it can produce subwavelength structures using broad beam illumination of standard photoresist with visible light. Using this technique, sub–100-nm lines have been patterned photolithographically at a wavelength of 436 nm (*38*). Theoretical simulations of plasmonic nanolithography predict even better performance (*39*). Finite difference time domain (FDTD) simulations of isolated silver particles on a thin resist layer show that broad beam illumination with p-polarized light at a wavelength of 439 nm can produce features as small as 30 nm, or $\lambda/14$, where λ is the wavelength. Depending on the exposure time, lateral spot sizes ranging from 30 to 80 nm with exposure depths ranging from 12 to 45 nm can be achieved.

The performance of plasmonic nanolithography can be boosted by using the "superlens" concept introduced by Pendry (*40*). A superlens can be used to enhance evanescent waves via the excitation of surface plasmons. The gain obtained from plasmonic excitation inside the superlens compensates for the loss of the evanescent waves outside of the superlens. The reconstructed evanescent waves can then be used to restore an image below the diffraction limit on the other side of the lens. This unusual lens can be constructed by using a thin slab of material with negative permittivity or permeability, or both. By using silver as a natural optical superlens, sub–diffraction-limited imaging with 60 nanometer half-pitch resolution, or one-sixth of the illumination wavelength, was demonstrated (*41*). By proper design of the working wavelength and the thickness of silver, which allows access to a broad spectrum of subwavelength features, arbitrary nanostructures can also be imaged with good fidelity. Figure 4 compares the performance of this superlens-based plasmonic nanolithography to conventional nanolithography. A 365-nm exposure wavelength was used for both nanolithography experiments. The word "NANO" was printed as a mask by a focused ion beam (FIB) system (Fig. 4A). Figure 4B was obtained with the superlens, and the resulting image on the resist is almost perfect. Figure 4C shows the diffraction limited image obtained from the conventional lithography. Figure 4D numerically compares both methods. Although the resolution achieved by conventional methods is limited to ~320 nm, the plasmonic nanolithography method was able to generate an image with ~four times better resolution. Super-resolution imaging using the same method was also reported for a 50-nm-thick planar silver superlens at wavelengths around 365 nm (*42*). Gratings with periods down to 145 nm can be resolved, which agrees well with the FDTD simulations. These are the preliminary demonstrations of superlens-based plasmonic nanolithography, and additional research for further improvements in subwavelength resolution, aerial coverage, and uniformity is needed. After these improvements, plasmonic nanolithography may be a viable alternative to other nanolithography systems.

Future Directions and Challenges

The field of plasmonics offers several research opportunities. These include plasmonic chips that function as ultra–low-loss optical interconnects, plasmonic circuits and components that can guide light within ultracompact optically functional devices, nanolithography at deep subwavelength scale, superlenses that enable optical imaging with unprecedented resolution, and new light sources with unprecedented performance. To fulfill the promise offered by plasmonics, more research needs to be done in these areas. Some of the challenges that face

plasmonics research in the coming years are as follows: (i) demonstrate optical frequency subwavelength metallic wired circuits with a propagation loss that is comparable to conventional optical waveguides; (ii) develop highly efficient plasmonic organic and inorganic LEDs with tunable radiation properties; (iii) achieve active control of plasmonic signals by implementing electro-optic, all-optical, and piezoelectric modulation and gain mechanisms to plasmonic structures; (iv) demonstrate 2D plasmonic optical components, including lenses and grating couplers, that can couple single mode fiber directly to plasmonic circuits; and (v) develop deep subwavelength plasmonic nanolithography over large surfaces.

Conclusion

The research on plasmonics has made major advances in the past few years. Besides creating new photonics devices, which are considerably smaller than the propagating light's wavelength, plasmonics is expected to be the key nanotechnology that will combine electronic and photonic components on the same chip.

References and Notes

1. M. J. Kobrinsky *et al.*, *Intel Technol. J.* **8**, 129 (2004).
2. M. Born, E. Wolf, *Principles of Optics* (Cambridge Univ. Press, Cambridge, 1999).
3. J. D. Joannopoulos, R. D. Meade, J. N. Winn, *Photonic Crystals: Molding the Flow of Light* (Princeton Univ. Press, Princeton, 1995).
4. H. Raether, *Surface Plasmons* (Springer, Berlin, 1988).
5. W. L. Barnes, A. Dereux, T. W. Ebbesen, *Nature* **424**, 824 (2003).
6. S. A. Maier, H. A. Atwater, *J. Appl. Phys.* **98**, 011101 (2005).
7. P. Berini, R. Charbonneau, N. Lahoud, G. Mattiussi, *J. Appl. Phys.* **98**, 043109 (2005).
8. J. R. Krenn, J. C. Weeber, *Philos. Trans. R. Soc. London Ser. A* **362**, 739 (2004).
9. S. A. Maier, P. E. Barclay, T. J. Johnson, M. D. Friedman, O. Painter, *Appl. Phys. Lett.* **86**, 071103 (2005).
10. D. Pile *et al.*, *Appl. Phys. Lett.* **87**, 061106 (2005).
11. S. I. Bozhevolnyi, V. S. Volkov, E. Devaux, T. W. Ebbesen, *Phys. Rev. Lett.* **95**, 046802 (2005).
12. M. Hochberg, T. Baehr-Jones, C. Walker, A. Scherer, *Opt. Exp.* **12**, 5481 (2004).
13. M. P. Nezhad, K. Tetz, Y. Fainman, *Opt. Exp.* **12**, 4072 (2004).
14. A. Karalis, E. Lidorikis, M. Ibanescu, J. D. Joannopoulos, M. Soljacic, *Phys. Rev. Lett.* **95**, 063901 (2005).
15. W. Nomura, M. Ohtsu, T. Yatsui, *Appl. Phys. Lett.* **86**, 181108 (2005).
16. L. Yin *et al.*, *Nano Lett.* **5**, 1399 (2005).
17. A. V. Krasavin, A. V. Zayats, N. I. Zheludev, *J. Opt. Pure Appl. Opt.* **7**, 85 (2005).
18. P. Andrew, W. L. Barnes, *Science* **306**, 1002 (2004).
19. S. Nakamura, G. Fasol, *The Blue Laser Diode: GaN-Based Light Emitting Diode and Lasers* (Springer, Berlin, 1997).
20. E. F. Schubert, J. K. Kim, *Science* **308**, 1274 (2005).
21. J. Vuckovic, M. Loncar, A. Scherer, *IEEE J. Quant. Electr.* **36**, 1131 (2000).
22. K. Okamoto *et al.*, *Appl. Phys. Lett.* **87**, 071102 (2005).
23. S. Wedge, J. A. E. Wasey, I. Sage, W. L. Barnes, *Appl. Phys. Lett.* **85**, 182 (2004).
24. C. Liu, V. Kamaev, Z. V. Vardenya, *Appl. Phys. Lett.* **86**, 143501 (2005).
25. J. Hashizume, F. Koyama, *Opt. Exp.* **12**, 6391 (2004).
26. T. W. Ebbesen *et al.*, *Nature* **391**, 667 (1998).
27. T. Thio *et al.*, *Opt. Lett.* **26**, 1972 (2004).
28. H. J. Lezec, T. Thio, *Opt. Exp.* **12**, 3629 (2004).
29. J. Pendry, L. Martin-Moreno, F. J. Garcia-Vidal, *Science* **305**, 847 (2004).
30. W. L. Barnes *et al.*, *Phys. Rev. Lett.* **92**, 107401 (2004).
31. A. P. Hibbins, B. R. Evans, J. R. Sambles, *Science* **308**, 670 (2004).
32. S. Akarca-Biyikli, I. Bulu, E. Ozbay, *Appl. Phys. Lett.* **85**, 1098 (2004).
33. M. Beruete *et al.*, *Opt. Lett.* **12**, 3629 (2004).
34. H. Caglayan, I. Bulu, E. Ozbay, *Opt. Exp.* **13**, 1666 (2005).
35. H. J. Lezec *et al.*, *Science* **297**, 820 (2002).
36. H. Cao, A. Nahata, *Opt. Exp.* **12**, 1004 (2004).
37. J. G. Rivas, M. Kuttge, P. H. Bolivar, H. Kurz, *Phys. Rev. Lett.* **93**, 256804 (2005).
38. X. Luoa, T. Ishihara, *Appl. Phys. Lett.* **84**, 4780 (2004).
39. P. G. Kik, S. A. Maier, H. A. Atwater, *Phys. Rev. B* **69**, 045418 (2004).
40. J. B. Pendry, *Phys. Rev. Lett.* **85**, 3966 (2000).
41. N. Fang, H. Lee, C. Sun, X. Zhang, *Science* **308**, 534 (2005).
42. D. O. S. Melville, R. J. Blaikie, *Opt. Exp.* **13**, 2127 (2005).

43. This work was supported by the projects EU–DALHM, EU–NOE–METAMORPHOSE, EU–NOE–PHOREMOST, and TUBITAK-104E090. E.O. also acknowledges partial support from the Turkish Academy of Sciences.

10.1126/science.1114849

Interferometric Coupling of the Keck Telescopes with Single-Mode Fibers

G. Perrin,[1*] J. Woillez,[2] O. Lai,[3] J. Guérin,[1] T. Kotani,[1] P. L. Wizinowich,[2] D. Le Mignant,[2] M. Hrynevych,[2] J. Gathright,[2] P. Léna,[1] F. Chaffee,[2] S. Vergnole,[4] L. Delage,[4] F. Reynaud,[4] A. J. Adamson,[5] C. Berthod,[6] B. Brient,[6] C. Collin,[1] J. Crétenet,[7] F. Dauny,[1] C. Deléglise,[6] P. Fédou,[1] T. Goeltzenlichter,[1] O. Guyon,[8] R. Hulin,[1] C. Marlot,[1] M. Marteaud,[1,7] B.-T. Melse,[1] J. Nishikawa,[9] J.-M. Reess,[1] S. T. Ridgway,[10] F. Rigaut,[11] K. Roth,[11] A. T. Tokunaga,[12] D. Ziegler[1]

Increasing the resolving power of telescopes to image compact astronomical sources requires large apertures; however, 100 m is probably a technological limit for single apertures. Creating a larger aperture will require combining telescopes into interferometric arrays and using aperture synthesis techniques. The goal of 'OHANA (Optical Hawaiian Array for Nanoradian Astronomy) is to investigate the value of single-mode fibers for kilometric baselines and to combine the large optical telescopes (*1*) of the Mauna Kea Observatory (fig. S1) into an 800-m interferometer (*2*) to image faint objects at resolutions below 1 milli–arc sec and at near-infrared wavelengths.

Here we report the first results obtained using 2 × 300–m-long fluoride glass fiber cables to combine the Keck telescopes in the near infrared between 2 and 2.3 μm. Single-mode fibers were proposed to propagate coherent light for astronomical interferometry (*3*). The long distances and large numbers of mirrors required in optical interferometers are a cause of low throughput (1% for the Keck interferometer) (*4*). Fibers have attenuations of 3 to 1 dB/km in the near infrared, leading to potential transmissions superior to those of optical trains in the J, H, and K bands (near-infrared astronomical photometric bands in which the atmosphere is transparent). The large dispersion of the 300-m-long fiber pair was matched, and the contrast was optimized above 96% in a 300-nm-wide band (*5*). Twisting nonbirefringent fibers to match polarization planes solved polarization issues. The Keck bulk optics delay lines (*6*) were used, because equivalent fibered delay lines are not mature yet. This delay line problem, together with the bandwidth limitation, may be overcome with photonic crystal fibers in the future.

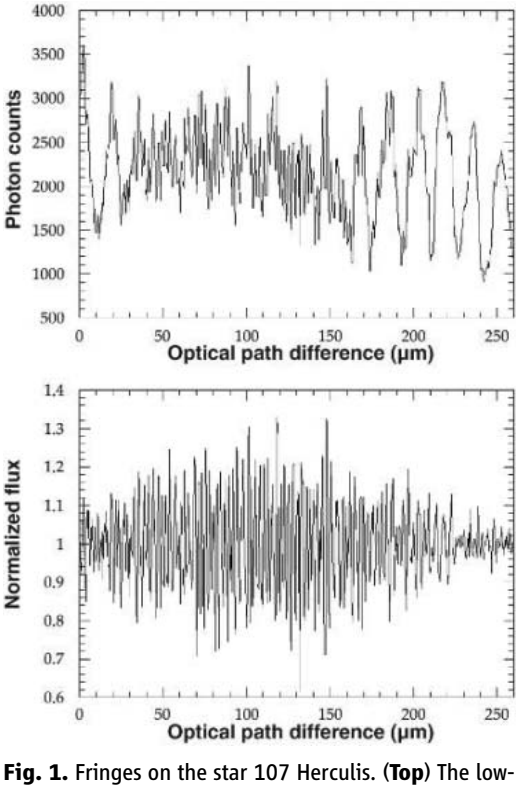

Fig. 1. Fringes on the star 107 Herculis. (**Top**) The low-frequency intensity fluctuations are due to vibrations. (**Bottom**) The signals were high-pass filtered to remove the low-frequency vibrations.

The adaptive-optics (*7*) corrected beams were injected into the fibers at the Nasmyth foci. Fibers were routed down to the interferometric laboratory (fig. S2). The fiber outputs fed the delay lines toward the beam combiner (fig. S3); most of the Keck interferometer classical optical train was bypassed with the single-mode fibers. Although the Keck baseline is 85 m, our setup is equivalent to a ~500-m interferometer with respect to coherent propagation. Before on-sky tests, fringes were acquired in auto-collimation mode, in which a white light source (bandwidth >300 nm) propagated upward from the beam combiner to the injection modules and was reflected back to the combiner. The acquired interferograms showed negligible dispersion (fig. S4) but a 75% fringe contrast, possibly because of slight dispersion and birefringence.

On-sky tests were performed on 18 June 2005. The fringe scan frequency was 200 Hz and the exposure time per sample was 1 ms. First fringes (Fig. 1) were detected on 107 Herculis (A7V star, K magnitude = 4.6, diameter 0.42 milli–arc sec) with a 99% expected visibility on the 85-m baseline. The measured fringe contrast was only 25% and dispersion was clearly high. A simulated maximum fringe contrast of 35% was expected due to different dichroic plates in the two adaptive optics systems (setup for 'OHANA only). Despite cloudy conditions, a minimum transmission was derived: 1.1×10^6 photons were expected per exposure on 107 Herculis, whereas 6×10^3 were measured, hence a coherent flux transmission of 0.5%. Given the then probable low transmission of the atmosphere in the infrared, this is at least as good as the 1% transmission of the classical system but lower than our estimated transmission of 4%. This transmission could be improved to 10% with optimized optics and 100-m-long fibers and hence may be a potential gain over classical beam trains.

References and Notes

1. Canada-France-Hawaii Telescope, Gemini North, United Kingdom Infrared Telescope, Subaru, Keck I and II, and NASA's Infrared Telescope Facility.
2. J.-M. Mariotti, V. Coudé du Foresto, G. Perrin, Z. Peiqian, P. Léna, *Astron. Astrophys. Suppl. Ser.* **116**, 381 (1996).
3. C. Froehly, in *Scientific Importance of High Angular Resolution at Optical and Infrared Wavelengths*, M. H. Ulrich, K. Kjär, Eds. (European Southern Observatory, Garching, Germany, 1981), p. 285.
4. R. Millan-Gabet, M. M. Colavita, private communication.
5. T. Kotani, G. Perrin, S. Vergnole, J. Woillez, J. Guérin, *Appl. Opt.* **44**, 5029 (2005).
6. M. M. Colavita, P. L. Wizinowich, R. L. Akeson, *Proc. SPIE* **5491**, 454 (2004).
7. P. Wizinowich *et al.*, *Publ. Astron. Soc. Pac.* **112**, 315 (2000).
8. The authors are thankful to the board of the California Association for Research in Astronomy for allocating Keck telescope time, the Keck Observatory staff, the interferometer team at Keck and at the Jet Propulsion Laboratory. We are also grateful to former Canada-France-Hawaii Telescope (CFHT) Executive Director G. G. Fahlman for his key role in the project and to the CFHT staff. The 'OHANA project is supported in France by the Ministry of Research, Paris Observatory, and CNRS. The authors dedicate these first fringes to J.-M. Mariotti, who originated the idea of the 'OHANA project.

Supporting Online Material

www.sciencemag.org/cgi/content/full/311/5758/194/DC1
Figs. S1 to S4

16 September 2005; accepted 9 November 2005
10.1126/science.1120249

[1]Laboratoire d'Etudes Spatiales et d'Instrumentation en Astrophysique (LESIA), Unite Mixte de Recherche (UMR) 8109, Observatoire de Paris, 92190 Meudon, France. [2]W. M. Keck Observatory, Kamuela, HI 96743, USA. [3]Canada France Hawaii Telescope Corporation, Kamuela, HI 96743, USA. [4]Institut de Recherche en Communications Optiques et Microondes (IRCOM), UMR 6615, 87060 Limoges, France. [5]United Kingdom Infrared Telescope, Hilo, HI 96720, USA. [6]Technical Division of Institut National des Sciences de l'Univers, 92195 Meudon, France. [7]Galaxies Etoiles Physique et Instrumentation (GEPI), UMR 8111, Observatoire de Paris, 92190 Meudon, France. [8]Subaru Telescope, Hilo, HI 96720, USA. [9]National Astronomical Observatory of Japan, Mitaka, Tokyo, 181-8588, Japan. [10]National Optical Astronomy Observatory, Tucson, AZ 85719, USA. [11]Gemini Observatory, Hilo, HI 96720, USA. [12]Institute for Astronomy, University of Hawaii, Honolulu, HI 96822, USA.

*To whom correspondence should be addressed. E-mail: guy.perrin@obspm.fr

Structural Basis for Double-Stranded RNA Processing by Dicer

Ian J. MacRae,[1,3] Kaihong Zhou,[1,3] Fei Li,[1] Adrian Repic,[1] Angela N. Brooks,[1] W. Zacheus Cande,[1] Paul D. Adams,[4] Jennifer A. Doudna[1,2,3,4]*

The specialized ribonuclease Dicer initiates RNA interference by cleaving double-stranded RNA (dsRNA) substrates into small fragments about 25 nucleotides in length. In the crystal structure of an intact Dicer enzyme, the PAZ domain, a module that binds the end of dsRNA, is separated from the two catalytic ribonuclease III (RNase III) domains by a flat, positively charged surface. The 65 angstrom distance between the PAZ and RNase III domains matches the length spanned by 25 base pairs of RNA. Thus, Dicer itself is a molecular ruler that recognizes dsRNA and cleaves a specified distance from the helical end.

RNA interference (RNAi) is an ancient gene-silencing process that plays a fundamental role in diverse eukaryotic functions including viral defense (*1*), chromatin remodeling (*2*), genome rearrangement (*3*), developmental timing (*4*), brain morphogenesis (*5*), and stem cell maintenance (*6*). All RNAi pathways require the multidomain ribonuclease Dicer (*7*). Dicer first processes input dsRNA into small fragments called short interfering RNAs (siRNAs) (*8*), or microRNAs (miRNA) (*9*), which are the hallmark of RNAi. Dicer then helps load its small RNA products into large multiprotein complexes termed RNA-induced silencing complexes (RISC) (*10*). RISC and RISC-like complexes use the small RNAs as guides for the sequence-specific silencing of cognate genes through mRNA degradation (*11*), translational inhibition (*12*), and heterochromatin formation (*13*).

Dicer products are typically 21 to 25 nucleotides long, which is the ideal size for a gene silencing guide, because it is long enough to provide the sequence complexity required to uniquely specify a single gene in a eukaryotic genome. Several models have been proposed for how Dicer generates RNA fragments of this specific size (*14*–*16*), but structural information is lacking. In an effort to deepen our understanding of the initiation step of RNAi, we determined the crystal structure of an intact and fully active Dicer enzyme.

Conservation of a highly active Dicer in *Giardia intestinalis*. We identified an open reading frame in *Giardia intestinalis* that encodes the PAZ and tandem RNase III domains characteristic of Dicer (*7*), but lacks the N-terminal DExD/H helicase, C-terminal double-stranded RNA binding domain (dsRBD), and extended interdomain regions associated with Dicer in higher eukaryotes (Fig. 1A). A recombinant form of this protein possesses robust dicing activity in vitro (Fig. 1B). The RNA fragments produced by *Giardia* Dicer are 25 to 27 nucleotides long, which is similar to a class of small RNAs associated with RNAi-mediated DNA elimination in *Tetrahymena* (*17*) and RNA-directed DNA methylation in plants (*18*). dsRNA cleavage by *Giardia* Dicer is magnesium-dependent, although several other divalent cations including Mn^{2+}, Ni^{2+}, and Co^{2+} also support catalytic activity (*19*). The presence of discrete dicing intermediates separated by intervals of ~25 nucleotides indicates that *Giardia* Dicer processes dsRNA from the helical end in a fashion similar to human Dicer (*20*). However, in contrast to human Dicer, *Giardia* Dicer has a low affinity for its small RNA product (~1 μM) (*19*) and displays multiple turnover kinetics (*20*).

Structural overview. We determined the crystal structure of the full-length *Giardia* Dicer at 3.3 Å resolution (table S1). The structure reveals an elongated molecule that, when viewed from the front, takes on a shape resembling a hatchet; the RNase III domains form the blade and the PAZ domain makes up the base of the handle (Fig. 2A). The PAZ domain is directly connected to the RNase IIIa domain by a long α helix that runs through the handle of the molecule. This "connector" helix is encircled by the N-terminal residues of the protein, which form a platform domain composed of an antiparallel β sheet and three α helices. A large helical domain bridges the two RNase III domains and forms the back end of the blade. Viewing Dicer from the side reveals a contiguous flat surface that extends along one face of the molecule.

Two–metal-ion mechanism of dsRNA cleavage. The two RNase III domains of Dicer sit adjacent to each other in the blade region and form an internal heterodimer that is similar to the homodimeric structure of bacterial RNase III (fig. S1). Although previous bacterial RNase III crystal structures revealed a single catalytic metal ion in each RNase III domain (*21*), subsequent studies implicated two metal ions in the hydrolysis of each strand of the dsRNA (*22*).

During our biochemical characterization of *Giardia* Dicer, we noticed that the enzyme is potently inhibited by trivalent lanthanide cations such as Er^{3+} (*19*). Lanthanides often bind more tightly to cation binding sites than divalent cations do, a property previously used to identify transient Mn^{2+} binding sites in proteins (*23*). Inspection of the anomalous difference electron density map from a crystal derivatized with $ErCl_3$ revealed a pair of Er^{3+} cations in the active site of each RNase III domain of *Giardia* Dicer (Fig. 2B). The prominent Er^{3+} metal (M1) in each domain resides between four strictly conserved acidic residues, which make up the previously identified Mn^{2+} binding site of bacterial RNase III (*21*). The second Er^{3+} binding site (M2) lies adjacent to the first, outside of the acidic residue cluster. The distances between the two Er^{3+} metals in the RNase IIIa and IIIb domains are ~4.2 Å and ~5.5 Å, respectively. These distances are similar to those previously observed in the active site of RNase H (4.1 Å) (*24*), avian sarcoma virus (ASV) integrase (3.6 Å) (*25*), the restriction enzyme *EcoR*V (4.2 Å) (*26*), and the group I intron (3.9 Å) (*27*), all of which are thought to use a two–metal-ion mechanism of catalysis. The 17.5 Å distance between the

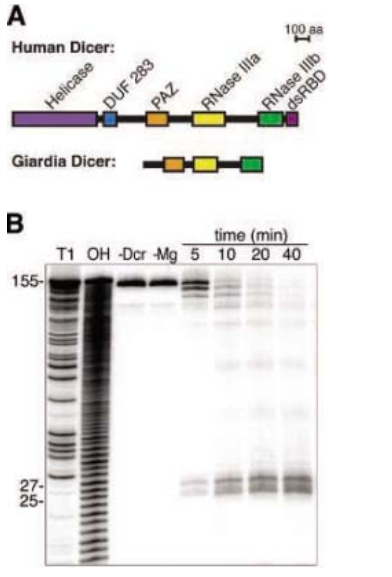

Fig. 1. *Giardia* encodes an active Dicer enzyme. (**A**) Schematic representation of the primary sequence of human and *Giardia* Dicers. (**B**) Time course of in vitro *Giardia* Dicer dsRNA cleavage assay. RNA product sizes were determined by comparison with RNase T1 and alkaline hydrolysis (OH) sequencing ladders (lanes 1 and 2). Dicing requires the protein (Dcr) and Mg^{2+} (lanes 3 and 4).

[1]Department of Molecular and Cell Biology, [2]Department of Chemistry, [3]Howard Hughes Medical Institute, University of California, Berkeley, CA 94720, USA. [4]Physical Biosciences Division, Lawrence Berkeley National Laboratory, Berkeley, CA 94720, USA.

*To whom correspondence should be addressed: E-mail: doudna@berkeley.edu

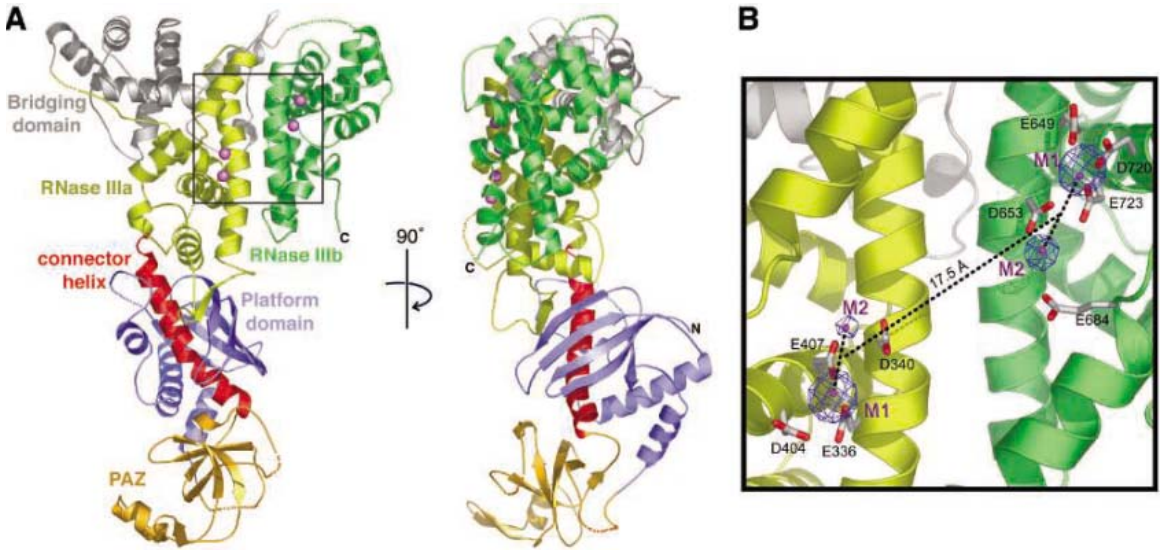

Fig. 2. Crystal structure of *Giardia* Dicer. (**A**) Front and side view ribbon representations of Dicer showing the N-terminal platform domain (blue), the PAZ domain (orange), the connector helix (red), the RNase IIIa domain (yellow), the RNase IIIb domain (green) and the RNase-bridging domain (gray). Disordered loops are drawn as dotted lines. (**B**) Close-up view of the Dicer catalytic sites; conserved acidic residues (sticks); erbium metal ions (purple); and erbium anomalous difference electron density map, contoured at 20σ (blue wire mesh). Dashed lines indicate distances described in the text.

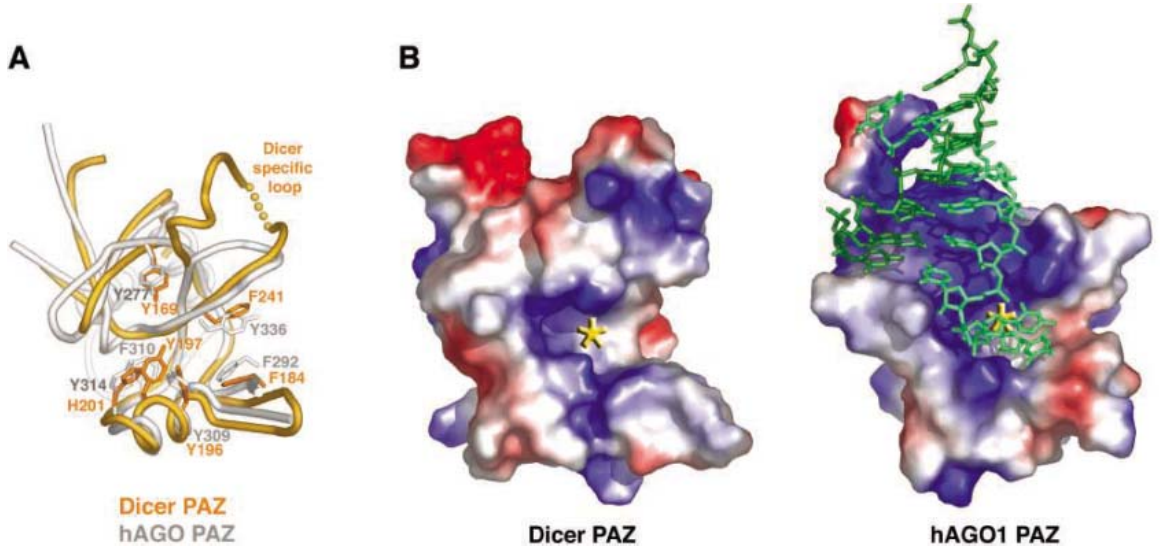

Fig. 3. Structural features of the Dicer PAZ domain. (**A**) Superposition of the C_α atoms of PAZ domains from *Giardia* Dicer (orange) and human Argonaute1 (white). Amino acids forming the 3′ overhang-binding pocket are shown as sticks. (**B**) Electrostatic surface representation of the PAZ domains of *Giardia* Dicer and Argonaute1 (hAGO1). Asterisks denote 3′ overhang-binding pockets. The RNA in Argonaute1 PAZ structure is drawn as green sticks.

metal-ion pairs closely matches the width of the dsRNA major groove. We also observed Mn^{2+} in all M1 and some M2 sites in crystals grown in high concentrations of $MnCl_2$. Therefore, we propose that the Er^{3+} metals seen in *Giardia* Dicer denote true catalytic metal-ion binding sites and that *Giardia* Dicer uses a two–metal-ion mechanism of catalysis. Given the high level of sequence conservation throughout the RNase III family, it is likely that all RNase III enzymes, including bacterial RNase III and Drosha, contain similar catalytic metal-ion binding sites.

Structural features of the Dicer PAZ domain. The PAZ domain is an RNA binding module found in Dicers and in the Argonaute family of proteins that are core components of RISC and other siRNA- and miRNA-containing complexes. Previous studies of PAZ domains from several Argonaute proteins revealed a degenerate oligonucleotide/oligosaccharide-binding (OB) fold that specifically recognizes dsRNA ends containing a 3′ two-base overhang (*28*–*31*). Superposition of the PAZ domains of *Giardia* Dicer and human Argonaute1 reveals that the two domains share the same overall fold and 3′ two-nucleotide RNA binding pocket (Fig. 3A).

The Dicer PAZ domain contains a large extended loop that is conserved among Dicer sequences and absent in Argonaute (fig. S1). The Dicer-specific loop dramatically changes the electrostatic potential and molecular surface surrounding the 3′ overhang-binding pocket relative to the Argonaute PAZ domain (Fig. 3B). The presence of many basic amino acid residues in the extra loop could substantially affect the way the RNA is recognized and perhaps handed off to other complexes by each family of proteins.

A model for siRNA formation. The structure of *Giardia* Dicer immediately suggests how Dicer enzymes specify siRNA length. Measuring from the active site of the RNase IIIa domain to the 3′ overhang-binding pocket in the PAZ domain gives a distance of ~65 Å (Fig. 4), which matches the length of 25 dsRNA base pairs. To produce a likely model of a Dicer-dsRNA complex, the positions of the metal-ion pairs bound in each RNase III domain were used to anchor the two scissile phosphates of an ideal A-form dsRNA helix into the RNase III active sites. This placement positions the twofold symmetry element of the dsRNA coincident with the pseudo twofold symmetry axis relating the two RNase III domains, which is analogous to how restriction enzymes typically bind dsDNA substrates (*32*). Bacterial RNase III has been proposed to bind dsRNA in a similar fashion (*16*, *33*). Outside of the RNase III region, the modeled dsRNA extends along a flat surface formed by the platform domain. This surface contains a large positively charged region that could interact directly with the nega-

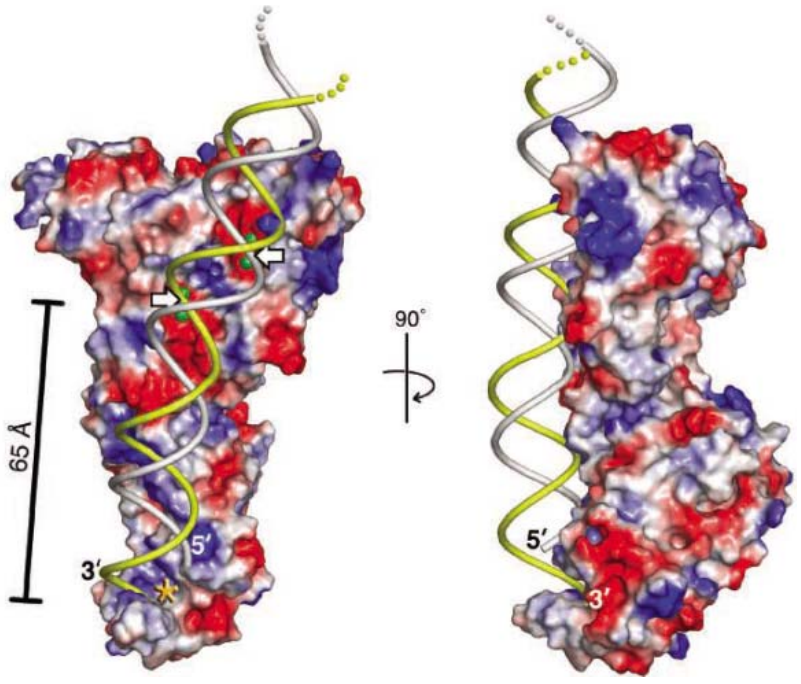

Fig. 4. A model for dsRNA processing by Dicer. Front and side views of a surface representation of *Giardia* Dicer with modeled dsRNA. Red and blue represent acidic and basic protein surface charge, respectively. Electrostatic surface potentials do not include contributions from bound metal ions. Putative catalytic metal ions are shown as green spheres. White arrows point to scissile phosphates. Asterisk denotes PAZ domain 3′ overhang-binding pocket.

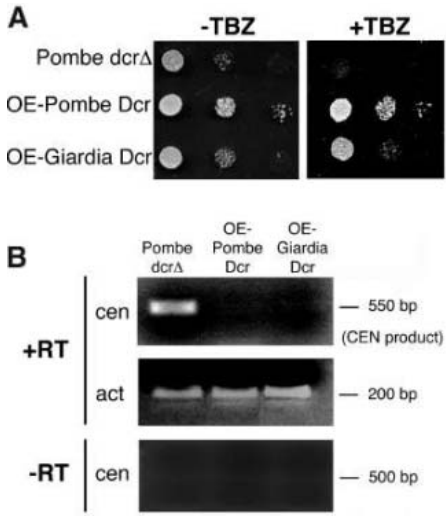

Fig. 5. *Giardia* Dicer supports RNAi in vivo. (**A**) Overexpression (OE) of *Giardia* Dicer rescues the TBZ sensitivity of the *S. pombe Dicer delete (dcr*Δ). Growth was assayed by spotting 10-fold serial dilutions of cultures indicated. (**B**) Overexpression of *Giardia* Dicer restores transcriptional silencing at centromeres (cen). Transcript levels were determined by semiquantitative reverse-transcriptase polymerase chain reaction. Actin (act) served as an internal control. bp, base pair.

tively charged phosphodiester backbone of the modeled dsRNA helix. The 3′ end of the RNA duplex falls directly into the 3′ overhang-binding pocket of the PAZ domain, and the 5′ end lies adjacent to the Dicer-specific PAZ domain loop. There are exactly 25 nucleotides between the 3′ end of the helix bound to the PAZ domain and the scissile phosphate in the RNase IIIa domain.

Thus, Dicer is a molecular ruler that measures and cleaves ~25 nucleotides from the end of a dsRNA. The length of the small RNAs produced by Dicer is set by the distance between the PAZ and RNase III domains, which is largely a function of the length of the connector helix. This model of dsRNA processing is consistent with the proposed architecture of human Dicer based on biochemical studies in which the RNase IIIa and IIIb domains were shown to produce the siRNA 5′ and 3′ ends, respectively (*16*). Furthermore, closing the ends of a dsRNA substrate by hybridization or ligation greatly diminished dicing activity (*20*, *34*), which may explain why circular viral dsRNA is resistant to RNAi (*35*).

Giardia **Dicer can support RNAi in fission yeast.** Given that *Giardia* Dicer lacks some of the domains commonly associated with Dicer enzymes, most notably the N-terminal helicase, we wondered if the structure represents an intact Dicer or merely the catalytic subunit of a larger complex required for complete Dicer function in vivo. To address this question, we introduced the *Giardia* Dicer gene into a strain of the fission yeast *Schizosaccharomyces pombe* that contains a deletion of its endogenous Dicer (*dcr*Δ).

Like most Dicer proteins, the *S. pombe* Dicer contains an N-terminal helicase domain and a C-terminal dsRBD. The *S. pombe dcr*Δ strain is defective in RNAi and is hypersensitive to the microtubule-destabilizing drug thiobendazole (TBZ) because of chromosome missegregation (*36*). Plasmid expression of *S. pombe dcr1*$^{+}$ fully rescued TBZ sensitivity of the *dcr*Δ cells. A partial functional rescue of TBZ sensitivity was also achieved by episomal expression of *Giardia* Dicer, indicating that *Giardia* Dicer can suppress the chromosome segregation defect (Fig. 5A). Furthermore, *Giardia* Dicer restores silencing of centromeric regions that are aberrantly transcribed in the *dcr*Δ mutant (Fig. 5B). These results demonstrate that *Giardia* Dicer is sufficient to function as an intact Dicer in vivo.

A conserved architecture in Dicer enzymes. Considering the structural role played by the connector helix that links the PAZ and RNase III domains (Fig. 2), we wondered whether larger Dicer proteins found in higher eukaryotes contain an analogous helix. Sequence alignment of the region directly following the PAZ domain of several evolutionarily diverse Dicer enzymes reveals a conserved pattern of hydrophobic and hydrophilic amino acids that is predicted to form a long α helix by secondary structural analysis (fig. S2). All Dicers contain a conserved proline about 11 amino acid residues from the predicted N terminus of the helix. In the crystal structure of *Giardia* Dicer, this proline induces a distinct kink that aids in directing the helix toward the RNase IIIa domain.

Most Dicer proteins contain a conserved region of ~100 amino acids termed ''domain of unknown function 283'' (DUF283), which lies between the helicase and PAZ domains in the primary sequence. Low but consistent sequence homology between the N-terminal domain of *Giardia* Dicer and DUF283 (fig. S3) suggests that in the Dicers of higher eukaryotes, DUF283 forms a platform structure similar to that of *Giardia* Dicer.

The conserved Dicer architecture, together with the demonstration that *Giardia* Dicer can substitute for *S. pombe* Dicer in vivo, argues that the mechanism of Dicer-catalyzed dsRNA processing is conserved. Moreover, these results indicate that all Dicers evolved from a common ancestral enzyme. Because *Giardia* is one of the most anciently diverged members of the eukaryotic kingdom, we may consider that the earliest eukaryotic organisms had a similar Dicer enzyme and therefore were capable of RNAi-like processes. It will be of evolutionary interest to determine the cellular function of Dicer and RNAi in *Giardia*.

The structure of *Giardia* Dicer also provides new insight into eukaryotic RNase III enzymes in general. This family of enzymes performs a range of specific cellular functions involving the cleavage of dsRNA [reviewed in (*37*)]. The structure of Dicer illustrates

how the presence of RNA binding modules, like the PAZ and platform domains, can impart a specific function to the otherwise nonspecific double-stranded RNase activity of the RNase III dimer (*38*). This is likely to be the structural paradigm for all eukaryotic RNase III enzymes that have specific activities and cellular functions.

References and Notes

1. D. Baulcombe, *Trends Microbiol.* **10**, 306 (2002).
2. T. A. Volpe *et al.*, *Science* **297**, 1833 (2002).
3. K. Mochizuki, N. A. Fine, T. Fujisawa, M. A. Gorovsky, *Cell* **110**, 689 (2002).
4. A. Grishok *et al.*, *Cell* **106**, 23 (2001).
5. A. J. Giraldez *et al.*, *Science* **308**, 833 (2005).
6. S. D. Hatfield *et al.*, *Nature* **435**, 974 (2005).
7. E. Bernstein, A. A. Caudy, S. M. Hammond, G. J. Hannon, *Nature* **409**, 363 (2001).
8. S. M. Elbashir, W. Lendeckel, T. Tuschl, *Genes Dev.* **15**, 188 (2001).
9. G. Hutvagner *et al.*, *Science* **293**, 834 (2001).
10. Q. Liu *et al.*, *Science* **301**, 1921 (2003).
11. S. M. Hammond, E. Bernstein, D. Beach, G. J. Hannon, *Nature* **404**, 293 (2000).
12. R. S. Pillai *et al.*, *Science* **309**, 1573 (2005).
13. A. Verdel *et al.*, *Science* **303**, 672 (2004).
14. M. A. Carmell, G. J. Hannon, *Nat. Struct. Mol. Biol.* **11**, 214 (2004).
15. P. D. Zamore, *Mol. Cell* **8**, 1158 (2001).
16. H. Zhang, F. A. Kolb, L. Jaskiewicz, E. Westhof, W. Filipowicz, *Cell* **118**, 57 (2004).
17. C. D. Malone, A. M. Anderson, J. A. Motl, C. H. Rexer, D. L. Chalker, *Mol. Cell. Biol.* **25**, 9151 (2005).
18. Z. Xie *et al.*, *PLoS Biol.* **2**, E104 (2004).
19. I. J. MacRae, K. Zhou, J. A. Doudna, data not shown.
20. H. Zhang, F. A. Kolb, V. Brondani, E. Billy, W. Filipowicz, *EMBO J.* **21**, 5875 (2002).
21. J. Blaszczyk *et al.*, *Structure* (*Camb*) **9**, 1225 (2001).
22. W. Sun, A. Pertzev, A. W. Nicholson, *Nucleic Acids Res.* **33**, 807 (2005).
23. M. Sundaramoorthy, H. L. Youngs, M. H. Gold, T. L. Poulos, *Biochemistry* **44**, 6463 (2005).
24. M. Nowotny, S. A. Gaidamakov, R. J. Crouch, W. Yang, *Cell* **121**, 1005 (2005).
25. G. Bujacz *et al.*, *J. Biol. Chem.* **272**, 18161 (1997).
26. I. B. Vipond, G. S. Baldwin, S. E. Halford, *Biochemistry* **34**, 697 (1995).
27. M. R. Stahley, S. A. Strobel, *Science* **309**, 1587 (2005).
28. J. B. Ma, K. Ye, D. J. Patel, *Nature* **429**, 318 (2004).
29. J. J. Song *et al.*, *Nat. Struct. Biol.* **10**, 1026 (2003).
30. A. Lingel, B. Simon, E. Izaurralde, M. Sattler, *Nature* **426**, 465 (2003).
31. K. S. Yan *et al.*, *Nature* **426**, 468 (2003).
32. A. K. Aggarwal, *Curr. Opin. Struct. Biol.* **5**, 11 (1995).
33. D. L. Akey, J. M. Berger, *Protein Sci.* **14**, 2744 (2005).
34. A. Repic, J. A. Doudna, unpublished data.
35. J. Chang, P. Provost, J. M. Taylor, *J. Virol.* **77**, 11910 (2003).
36. I. M. Hall, K. Noma, S. I. Grewal, *Proc. Natl. Acad. Sci. U.S.A.* **100**, 193 (2003).
37. D. Drider, C. Condon, *J. Mol. Microbiol. Biotechnol.* **8**, 195 (2004).
38. W. Sun, E. Jun, A. W. Nicholson, *Biochemistry* **40**, 14976 (2001).

39. We thank members of the Doudna and Berger labs for helpful discussions, A. Fischer for work with tissue culture, and D. King for mass spectrometry analysis. We are grateful to C. Ralston and J. Dickert for technical support on beam lines 8.2.1 and 8.2.2 at the Advanced Light Source at the Lawrence Berkeley National Lab. I.J.M. is a Howard Hughes Medical Institute fellow of the Life Sciences Research Foundation. This work was supported in part by a grant from NIH (to J.A.D.). Dicer coordinates and structure factors have been deposited in the Protein Data Bank with accession code 2FFL.

Supporting Online Material

www.sciencemag.org/cgi/content/full/311/5758/195/DC1
Materials and Methods
Figs. S1 to S5
Table S1
References

21 October 2005; accepted 7 December 2005
10.1126/science.1121638

REPORTS

The Nature of the 660-Kilometer Discontinuity in Earth's Mantle from Global Seismic Observations of *PP* Precursors

Arwen Deuss,[1]* Simon A. T. Redfern,[1] Kit Chambers,[2] John H. Woodhouse[2]

The 660-kilometer discontinuity, which separates Earth's upper and lower mantle, has been detected routinely on a global scale in underside reflections of precursors to *SS* shear waves. Here, we report observations of this discontinuity in many different regions, using precursors to compressional *PP* waves. The apparent absence of such precursors in previous studies had posed major problems for models of mantle composition. We find a complicated structure, showing single and double reflections ranging in depth from 640 to 720 kilometers, that requires the existence of multiple phase transitions at the base of the transition zone. The results are consistent with a pyrolite mantle composition.

The characteristics of the 660-km discontinuity determine the convective style of the mantle, distinguishing potentially between whole-mantle and layered-mantle convection (*1*, *2*). The key question is whether this discontinuity is caused by a phase transition (*3*, *4*) or by a change in chemical composition (*5*). The latter would favor two-layer mantle convection, whereas the former would allow whole-mantle convection. Answers have been sought in seismology by studying the detailed seismic characteristics of this discontinuity and comparing them with predictions from mineral physical models of the mantle. Most seismic studies (*6*–*8*) find evidence in favor of the post-spinel phase transition in olivine from ringwoodite to perovskite and magnesiowüstite (*9*).

Precursors to the *SS* and *PP* waves have been used extensively to study the global seismic characteristics of the transition-zone discontinuities, in particular the 660-km discontinuity. These precursors arrive before the major *PP* (or *SS*) wave because they are not reflected from Earth's surface but from a discontinuity below the surface bounce point of the *PP* (or *SS*) wave (fig. S1). Precursors are named *PdP* (or *SdS*), where *d* is the depth of the discontinuity, thus *P*660*P* (or *S*660*S*) are the underside reflections of the 660-km discontinuity. These data are unusual in probing the mantle discontinuities with good global coverage, beneath both continents and oceans, and they can be used to draw inferences in many different regions.

Studies of the 660-km discontinuity have been hampered because, although it is easily observed in long-period *SS* precursors on a global scale, it has not been seen before using long-period *PP* precursors (*10*). This was interpreted to mean that the bulk modulus is continuous across the boundary (*11*), placing major constraints on the mineral physics of the post-spinel phase transition and on average mantle composition. In particular, these observations cannot be reconciled with a pyrolite mantle composition and are not consistent with the widely used Preliminary Reference Earth Model (PREM) (*12*); both models predict large reflection amplitudes in both *PP* and *SS* for the 660-km discontinuity (Fig. 1). It also implied a rather small density jump at the base of the transition zone, which would favor whole-mantle convection. Matters are further complicated by short-period observations of P′P′ precursors (*13*), which show that the 660-km discontinuity is sharp and prominent in a few isolated places in the Southern Hemisphere (*14*). Although P′P′ has a different ray path, it has been difficult to reconcile sharp short-period reflections with the absence of long-period reflections for the same discontinuity.

[1]Department of Earth Sciences, University of Cambridge, Cambridge CB3 0EZ, UK. [2]Department of Earth Sciences, University of Oxford, Oxford OX1 3PR, UK.

*To whom correspondence should be addressed. E-mail: deuss@esc.cam.ac.uk.

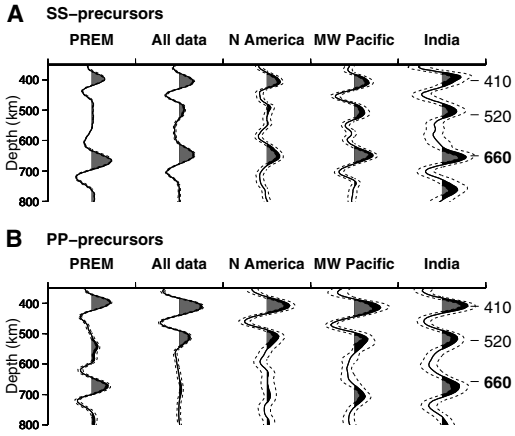

Fig. 1. Stacked traces for synthetic data computed for PREM (with discontinuities at 400- and 670-km depths), the whole data set, North America (484 traces), the mid-West Pacific (808 traces), and India (272 traces). The dashed lines represent the 95% confidence levels, and the gray areas denote robust reflections for which the lower 95% confidence level still is above zero (*15*). (**A**) The 660-km discontinuity is clearly seen in all *SS* precursor stacks. (**B**) PREM predicts a strong signal from the 660-km discontinuity in *PP* precursors, which is not seen in the stack for all data. Some signal from this discontinuity, however, can been seen in regional stacks, in particular in the Pacific and India. The depths are corrected for crustal and mantle structure using CRUST5.1 (*27*) and S20RTS (*28*).

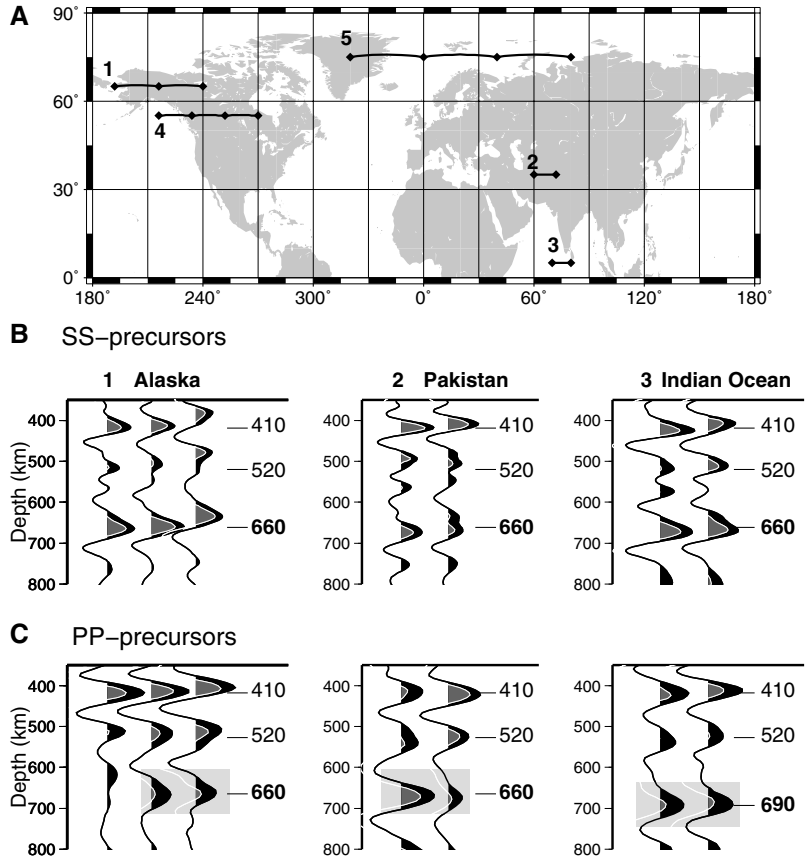

Fig. 2. Stacked traces for *PP* and *SS* precursors for spherical regions in the Northern Hemisphere. The data are filtered between 15 and 75 s. (**A**) Locations of the stacks; diamonds denote the center of each spherical region with a radius of 1000 km. Stacked results for locations 4 and 5 are shown in Fig. 3. (**B**) Stacks for *SS* precursors, for locations 1, 2, and 3. Dark gray areas denote robust reflections for which the lower 95% confidence is still above zero. The 95% confidence levels have been omitted for clarity. (**C**) Stacks for *PP* precursors. Rectangular gray boxes denote areas where robust reflections from the 660-km discontinuity are seen.

Here, we study the 660-km discontinuity on both a global and a regional scale by comparing a large data set of *PP* and *SS* seismograms (fig. S2). The *SS* and *PP* seismograms were initially filtered in the same long-period band of 15 to 75 s to remove short-period noise and make all data sensitive to the same structure. The precursors to *PP* and *SS* have small amplitude and cannot be observed in individual seismograms. Thus, we stack the traces to suppress incoherent noise and reveal the precursors (*15*).

We first made stacks of the whole data set and confirmed previous observations (*10*, *11*) that reflections of the 660-km discontinuity are below the noise level for *PP*, whereas strong reflections are seen for *SS* (Fig. 1). Both *PP* and *SS* also show reflections from the 410- and 520-km discontinuities. To determine whether the 660-km discontinuity could be seen on a regional basis, we divided the surface of Earth into several large geographical regions (fig. S3). Now, some signal from the 660-km discontinuity becomes visible in *PP*, in particular in the mid-West Pacific and India regions (Fig. 1B). North America does not show a robust signal.

Then, we divided the surface of Earth into 407 spherical regions of ~1000-km radius (see Fig. 2A for selected locations), and we stacked all seismograms with bounce points in each spherical region. Reflections from the 410-km discontinuity can be seen in *PP* and *SS* in most stacks, and the topography is similar (*16*). In certain regions, we again see clear reflections from the 660-km discontinuity in *PP*, which are comparable in amplitude to the *SS* reflections. For example, reflections with relative *P*660*P* to *PP* (*P*660*P*/*PP*) amplitudes of 1.5 to 3% are observed in Alaska, Pakistan, and the Indian Ocean (Fig. 2C, locations 1, 2, and 3). In many other regions, we do not see *P*660*P*, for example, in the most western stack of Alaska (Fig. 2C, location 1). Corresponding reflection amplitudes for *S*660*S*/*SS* (Fig. 2B) vary between 3 and 5%.

We also investigated the *PP* data at shorter periods of 8 to 75 s (Fig. 3), which result in *PP* having a wavelength and Fresnel zone similar to *SS* and thus having similar sensitivity to the sharpness of jumps in velocity and density at the discontinuity. Many of the 660-km reflections are still present, but some of the less robust long-period reflections (Fig. 3, B and D) now show two peaks at 660- and 720-km depths in the short-period data in, for example, Canada (Fig. 3C, location 4), or one single peak at 720-km depth as seen in Alaska (Fig. 3E, location 5). The global distribution of observations of *P*660*P* (Fig. 3A) correlates with regions where we have a high number of *PP* data points (fig. S2), which suggests that the discontinuity might become visible in a larger number of stacks as more data become available.

Because we see strong reflections from depths ranging from 650 to 750 km in both short-and long-period data bands in many different regions (Fig. 3A), we suggest that the null results in previous studies of *PP* precursors are probably due to the fact that the discontinuity is highly variable on a regional scale, causing reflections to cancel out when large areas are stacked together. Our observations of *P*660*P* imply nonzero changes in bulk modulus and larger changes in density, as compared with previous studies (*10*, *11*). This also makes our long-period *P*660*P* observations compatible with the short-period P′P′ observations of the 660-km discontinuity (*14*). The bulk modulus and density jumps at a 660-km depth must vary laterally with lower values in regions where the

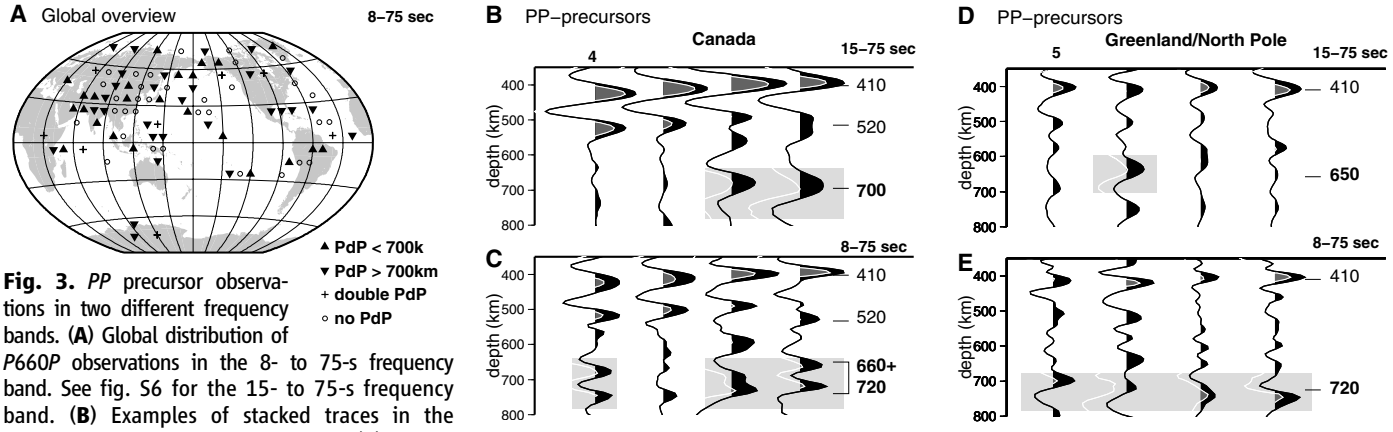

Fig. 3. *PP* precursor observations in two different frequency bands. (**A**) Global distribution of *P660P* observations in the 8- to 75-s frequency band. See fig. S6 for the 15- to 75-s frequency band. (**B**) Examples of stacked traces in the longer period band of 15 to 75 s and (**C**) shorter period band of 8 to 75 s for Canada (Fig. 2, location 4), where double reflections become visible. (**D**) Long-period stacks for the Greenland/North Pole area (Fig. 2, location 5), where (**E**) sharp reflections from 720-km depth can be seen in the short periods.

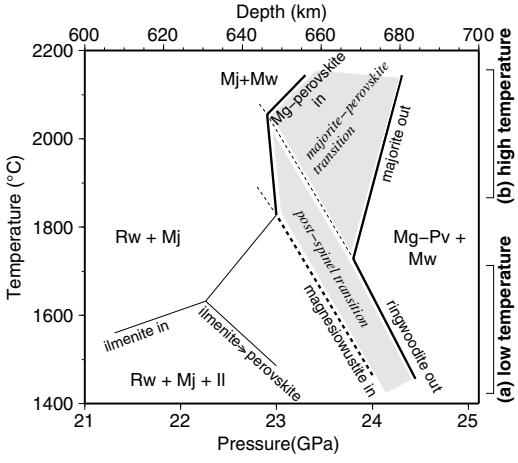

Fig. 4. Phase diagram for a pyrolitic mantle at 600- to 700-km depth, after Hirose (*22*). The shaded field indicates the perovskite-forming phase transitions that determine the characteristics of the 660-km discontinuity. (a) At low temperatures (1400°C to 1700°C), Mg-perovskite forms from the postspinel transition, with a negative Clapeyron slope over a narrow depth interval (bold dashed lines). (b) At high temperatures (1800°C to 2200°C), Mg-perovskite forms over a wider depth interval, principally from the breakdown of majorite garnet with a positive Clapeyron slope (solid bold lines). Thin lines show additional phase transitions forming ilmenite and perovskite at shallower depths of 600 to 640 km. Rw, ringwoodite; Mj, majorite garnet; Pv, perovskite; Il, ilmenite; Mw, magnesiowüstite. Ca-perovskite is also present in all phase fields.

660-km discontinuity is not seen in *PP* and with larger values in areas where observations are made.

The 660-km discontinuity has usually been interpreted in terms of the post-spinel transition in olivine from ringwoodite to perovskite and magnesiowüstite (*3*, *4*), which is a phase change with a negative Clapeyron slope (*17*). If lateral variations in temperature were the sole cause of lateral variations in the properties of the 660-km discontinuity, such variations would be completely described by the Clapeyron slope of the transformation. The discontinuity should be deeper in colder areas (i.e., subduction zones) and shallower in hotter areas (i.e., mantle plumes), and we should see the same effect in both *PP* and *SS* precursors. However, *PP* and *SS* show different behavior in the same location. Thus, the regional variation in the 660-km discontinuity cannot be explained by lateral temperature variations on the postspinel phase transition only and implies the presence of additional phase transitions and/or lateral differences in mantle composition.

The appropriate candidates for the source of multiple discontinuities are phase changes in the non-olivine mantle components. The two most commonly used mantle composition models are the piclogite model, which contains 40% olivine (*18*), and the pyrolite model with 60% olivine (*3*, *19*). The residuum, non-olivine, mineralogy (60 to 40% respectively) contains garnet in the transition zone. Near a 660-km depth, these mantle models have a transition from majorite garnet to perovskite, with a positive Clapeyron slope in addition to the post-spinel phase transition in olivine. This transition is well known in mineral physics but is often ignored in seismology (*8*, *10*, *11*). The combination of these phase changes leads to a delicate balance that can impede or enhance convection and also leads to multiple discontinuities, depending on the local temperature and mantle model (*20*).

Two scenarios are consistently found in recent mineral physical studies (*21*–*23*), depending on the temperature regime and aluminum (Al) content of the mantle (Fig. 4): (a) For low-temperature geotherms, the post-spinel transition with its negative Clapeyron slope is dominant at a 660-km depth. Additional transitions in the residuum from majorite garnet to ilmenite to perovskite at 610- to 640-km depth lead to multiple seismic discontinuities, which have indeed been seen in regional seismic studies of subduction zones (*24*); (b) At higher temperatures, the transition from majorite garnet to perovskite becomes dominant with a positive Clapeyron slope. There is no post-spinel transition, and ilmenite is no longer stable. Majorite garnet coexists with perovskite over a relatively large pressure and temperature range, and the transition is more diffuse, resulting in a smaller seismic discontinuity at a 660-km depth followed by a strong gradient in seismic properties across a 660- to 720-km depth.

To determine whether the range of mineral physical models could explain the range of the seismological observations, we computed *P660P*/*PP* and *S660S*/*SS* amplitudes (*25*) for different mineral physical models to compare with the amplitudes seen in our observations. We used recently published profiles (*21*, *20*) for the jumps in seismic velocity and density for both pyrolite and piclogite composition. These profiles have been computed from mineral physical phase diagrams for different geotherms (*26*) that are representative of average mantle temperatures.

We find that our variations in *S660S*/*SS* and *P660P*/*PP* amplitudes, and even the absence of *P660P* in certain regions, can be explained by changes in temperature or Al content for a pyrolite mantle composition (*21*). In regions where we find reflections from the 660-km discontinuity in *PP*, our amplitudes correspond very well with amplitudes predicted by a model with 5% Al and a 1700 K geotherm (dashed line in Fig. 5B), which corresponds to scenario (a) where the post-spinel transition is dominant. Increasing the temperature to a 1900 K geotherm corresponds to moving toward scenario (b) and explains regions where reflections from the 660-km discontinuity are not found in

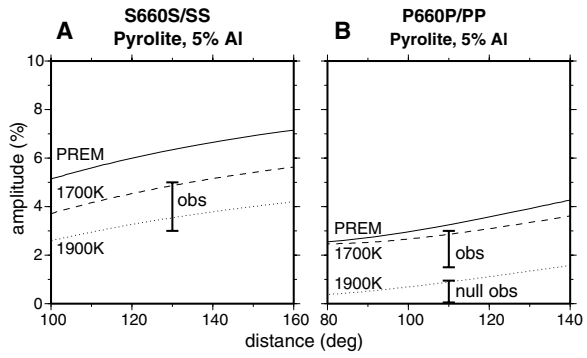

Fig. 5. Amplitudes of (**A**) *S660S*/*SS* and (**B**) *P660P*/*PP* as a function of epicentral distance range for the pyrolite model with 5% Al and mantle geotherms of 1700 K (dashed line) and 1900 K (dotted line) (*21*). The amplitudes for PREM are given for comparison (solid lines). The ranges of amplitudes found in our data are given by error bars at the average epicentral distance range, where "obs" denotes amplitudes of robust observations of *P660P* and *S660S* and "null obs" corresponds to the amplitudes when *P660P* is not observed.

PP (dotted line in Fig. 5B). Both the 1700 and 1900 geotherms also give amplitudes that fall within the range of observed amplitudes of the *SS* precursors (dashed and dotted lines in Fig. 5A). At the same time, the effect on the phase diagram of lowering Al content is identical to that of lowering the temperature. So, a lower Al content of 3% but a higher 1900 K geotherm would also lead to observable *P660P*/*PP* amplitudes (fig. S7A). We find that piclogite seismic profiles (*20*), on the other hand, cannot explain the range of amplitudes seen for *P660P*/*PP* and *S660S*/*SS* (fig. S7B).

Multiple reflectors in the depth range 660 to 720 km, or a single reflector near 720-km depth, have been explained before by multiple phase changes in garnet and ilmenite in the lower temperature regime of scenario (a) (*20*) or the end point of transformation from majorite garnet to perovskite in scenario (b). An alternative explanation for reflections from 720-km depth is possible in subduction zones. Subducted basaltic crust at the bottom of the transition zone is mainly composed of mid-oceanic ridge basalt (MORB), which has a phase transition to perovskite at 720-km depth with a positive Clapeyron slope (*23*) and could be invoked to explain some of our reflections from this depth.

Our results show a complicated seismic structure at the 660-km discontinuity, requiring lateral variations in temperature and/or minor elements such as Al in the mantle transition zone. This will influence lower mantle slab penetration and upwelling of plumes differently from region to region. Thus, the characteristics of the 660-km discontinuity and its impedance contrast can no longer be taken as a global constant when modeling mantle convection.

References and Notes

1. A. W. Hofmann, *Nature* **385**, 219 (1997).
2. G. Schubert, D. L. Turcotte, P. Olsen, *Mantle Convection in the Earth and Planets* (Cambridge University Press, Cambridge, UK, 2001).
3. A. E. Ringwood, *Composition and Petrology of the Earth's Mantle* (McGraw-Hill, New York, 1975).
4. J. Ita, L. Stixrude, *J. Geophys. Res.* **97**, 6849 (1992).
5. D. L. Anderson, *Theory of the Earth* (Blackwell Scientific, Boston, Mass., 1989).
6. P. M. Shearer, *Geophys. Monogr.* **117**, 115 (2000).
7. G. Helffrich, *Rev. Geophys.* **38**, 141 (2000).
8. S. Lebedev, S. Chevrot, R. van der Hilst, *Science* **296**, 1300 (2002).
9. E. Ito, E. Takahashi, *J. Geophys. Res.* **94**, 10637 (1989).
10. C. H. Estabrook, R. Kind, *Science* **274**, 1179 (1996).
11. P. M. Shearer, M. P. Flanagan, *Science* **285**, 1545 (1999).
12. A. Dziewonski, D. Anderson, *Phys. Earth Planet. Inter.* **25**, 297 (1981).
13. *P′P′* is shorthand for *PKPPKP*. This is an underside reflected *P* wave that travels the outer core and mantle. *PP* travels only the mantle.
14. H. M. Benz, J. E. Vidale, *Nature* **365**, 147 (1993).
15. Methods and other information available as supporting material on *Science* Online.
16. K. Chambers, J. H. Woodhouse, A. Deuss, *Earth Planet. Sci. Lett.* **235**, 610 (2005).
17. The Clapeyron slope is the slope of the transition curve in a pressure (P) versus temperature (T) phase diagram (dP/dT). These are obtained from experimental work and first-principles computer simulations. A positive (negative) Clapeyron slope corresponds in seismology with a shift to greater (lesser) depth as temperature increases.
18. J. D. Bass, D. L. Anderson, *Geophys. Res. Lett.* **11**, 237 (1984).
19. T. Irifune, A. E. Ringwood, *Earth Planet. Sci. Lett.* **86**, 365 (1987).
20. P. Vacher, A. Mocquet, C. Sotin, *Phys. Earth Planet. Inter.* **106**, 275 (1998).
21. D. J. Weidner, Y. Wang, *J. Geophys. Res.* **103**, 7431 (1998).
22. K. Hirose, *J. Geophys. Res.* **107**, 278 (2002).
23. K. Hirose, Y. Fei, Y. Ma, H.-K. Mao, *Nature* **7397**, 53 (1999).
24. N. A. Simmons, H. Gurrola, *Nature* **405**, 559 (2000).
25. K. Aki, P. Richards, *Quantitative Seismology, Vol. 1* (W. H. Freeman, San Francisco, 1980).
26. The geotherm is referenced to the temperature at a 660-km depth. For an adiabat of 1500 K (or 1600 K), which is generally assumed to be representative of average mantle temperatures, the geotherm at a 660-km depth is 1700 K (or 1850 K).
27. W. D. Mooney, G. Laske, G. Masters, *Eos* **76**, F421 (1995).
28. J. Ritsema, H. van Heijst, J. Woodhouse, *Science* **286**, 1925 (1999).

29. We thank L. Stixrude, A. de Ronde, and C. Chapman for interesting discussions. A.D. was supported by a Newly Appointed Science Lecturers Grant of the Nuffield Foundation.

9 September 2005; accepted 30 November 2005
10.1126/science.1120020

The Latitudinal Distribution of Clouds on Titan

P. Rannou,[1]* F. Montmessin,[1,2] F. Hourdin,[3] S. Lebonnois[3]

Clouds have been observed recently on Titan, through the thick haze, using near-infrared spectroscopy and images near the south pole and in temperate regions near 40°S. Recent telescope and Cassini orbiter observations are now providing an insight into cloud climatology. To study clouds, we have developed a general circulation model of Titan that includes cloud microphysics. We identify and explain the formation of several types of ethane and methane clouds, including south polar clouds and sporadic clouds in temperate regions and especially at 40° in the summer hemisphere. The locations, frequencies, and composition of these cloud types are essentially explained by the large-scale circulation.

After Voyager flybys in the early 1980s, many arguments supported the idea of condensate clouds on Titan. Because of the cold temperature at the tropopause (~70 K at altitudes of 40 to 60 km), most of the species formed in the upper atmosphere by photochemistry exceed saturation when descending. Methane, which is probably supplied at the surface, would also condense somewhere below the tropopause when transported upward. The detection of C_4N_2 ice by Voyager's IRIS (Infrared Interferometer Spectrometer and Radiometer) instrument at the north pole (*1*) constitutes the first direct evidence of condensates on Titan. Later, clouds were observed in disk-average spectra in the near-infrared (*2*, *3*) and shown lofted around 16 ± 5 km and at 27 ± 3 km. More recently, a large cloud was imaged near the south pole (*4*–*8*) at ~25 km. Cassini images (*6*, *9*) as well as recent telescope observations (*10*) also show frequent clouds scattered in the southern hemisphere at temperate mid-latitudes. These clouds are found preferentially near 40°S and are elongated in the east-west direction, forming an arc of several hundred kilometers. They are also found clustered at some preferential longitudes (*11*).

Analysis of infrared data (*12*) suggested that methane saturation ratios (the ratio between the methane partial pressure and the

[1]Service d'Aéronomie, Institut Pierre Simon Laplace, Université de Versailles-St-Quentin, BP3, 91371 Verrières le Buisson, France. [2]NASA-Ames Research Center, Moffett Field, CA 94035, USA. [3]Laboratoire de Météorologie Dynamique/IPSL, Université de Paris 6, 75252 Paris Cedex 05, France.

*To whom correspondence should be addressed. E-mail: pra@aero.jussieu.fr

methane saturation pressure) as high as 1.5 or 2 are possible. The scarcity of cloud seeds and the low wettability of aerosols by methane were invoked to justify the inhibition of the nucleation process. Several one-dimensional cloud models (*13*–*15*) predicted that the ethane and methane drops may reach diameters of several tens and hundreds of micrometers, respectively. Methane clouds could also be triggered when air parcels cool while moving from equator to pole, perhaps as a result of the quasi-barotropic motion of the atmosphere (*16*). Even with sophisticated cloud microphysics, one-dimensional models do not capture all the characteristics of the methane cycle because the vertical and sometimes the horizontal large-scale circulations are represented with simple analytical laws (*13*, *14*, *16*). The methane cycle, including condensation, has also been studied in the frame of a circulation model (*17*), but no cloud microphysics was included. Condensation was instead forced at critical saturation equal to 1 or 1.5. These models predicted that methane essentially condenses in the low troposphere, at latitudes in the ±60° range, at altitudes of 5 or 15 km, depending on the critical saturation.

To investigate the origin of clouds on Titan in a self-consistent way, we have coupled a cloud microphysical model to a general circulation model (GCM) (*18*–*21*). The results presented here follow a simulation of 25 Titan years, which is the time required to achieve a converged state. Figure 1 shows the cloud extinction along with the wind stream function at the season of Cassini arrival, two terrestrial years after the northern winter solstice. In this simulation, the haze is strongly scavenged (removed by cloud sedimentation) below 50 km at latitudes between 40°S and 40°N and around 10 km in polar regions. The scavenging produces a haze inversion layer (a zone where extinction locally increases with altitude; fig. S1) similar to that inferred from telescope data (*22*). We also identify in Figs. 1 and 2 several types of clouds: (i) widespread permanent ethane clouds, or mist, formed above the tropopause and in the troposphere everywhere in the polar regions (beyond ±60° latitude); (ii) sporadic (i.e., localized in space and time) methane clouds at altitudes between 15 and 18 km and within ±60° latitude; (iii) frequent and thick sporadic methane clouds at 15 km altitude around 40° in the summer hemisphere (south in 2005); and (iv) thick and frequent methane clouds at both poles below 30 km altitude. The physical properties that we report for these clouds match well with recent observations (Table 1).

In the stratosphere, the meridional circulation is dominated by a large pole-to-pole cell with winds ascending in the summer hemisphere and descending at the winter pole. A secondary cell, turning in the opposite direction, also exists at altitudes between 50 and 200 km in the summer hemisphere (fig. S1). The pole-to-pole cell changes direction every twelve terrestrial years (a Titan year lasts 30 terrestrial years) with a transition between two opposite cells of about three terrestrial years. The large cell downwelling branch at the winter pole is the place where chemical compounds and haze particles are brought from the stratosphere down to the troposphere (*23*, *24*). Because the tropopause is a cold point, chemical species (ethane in our model) condense on aerosols during the descent, producing a thick polar cloud everywhere below 60 km. Drops formed there are micrometer sized, smaller than but compatible with previous estimates (*14*). The related sedimentation time scale of hundreds of terrestrial days (Table 2) is long enough to maintain this cloud aloft in the polar region and to maintain a saturation ratio close to 1 (Fig. 3A). This widespread, long-lived polar cloud is rather well mixed with the winter polar haze layer (polar hood). Indirect clues for this polar cloud have been found by the Voyager IRIS, thanks to spectroscopic signatures of some condensates (*1*) or their infrared opacity (*25*). A similar process occurs at the summer pole because of the descending branch of the secondary cell, except that the aerosols and chemical species are not brought massively from the stratosphere by the descending winds, as at the winter pole. Polar haze and ethane clouds tend to increase during winter and to decrease during summer, but they persist all year round.

In the troposphere, where methane condenses, the situation is more symmetric about the equator as a result of much longer dynamical and radiative time scales. Air masses rise aslant from ~5 km near the equator to 12 km at latitude 40° in the summer hemisphere (tropics are at latitudes ±27° on Titan), then move almost vertically above 12 km and sink at high latitudes, around 60° in both hemispheres, forming two Hadley cells and an analog of the intertropical convergence zone on Earth (Fig. 1). Smaller oblique cells also appear in the polar regions, and in a stably stratified atmosphere as on Titan, these cells are triggered by strong temperature contrasts ($\Delta T \approx 5$ K) between mid-latitude regions and polar regions (fig. S2). These oblique motions occur because warm air masses move poleward into a much colder environment. They are less dense and are lifted by buoyancy along their trajectory. We find that the ascending and descending branches of these cells have a constant potential temperature below ~4 km, compatible with slantwise instabilities. In the

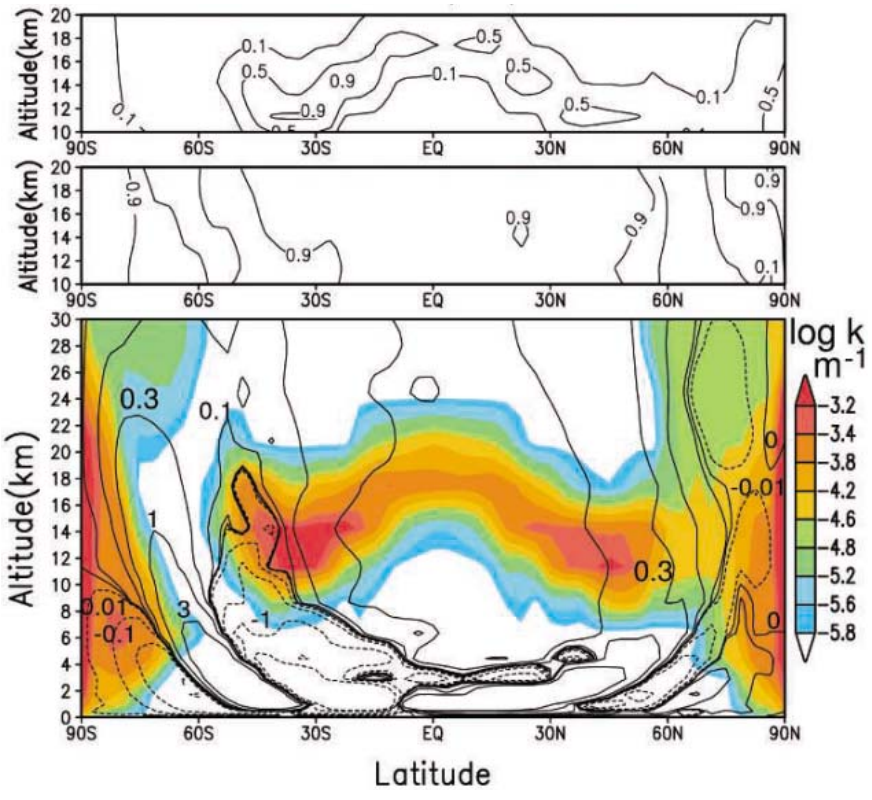

Fig. 1. (**Bottom**) Cloud extinction (m^{-1}) at 620 nm, averaged over one terrestrial year around the Cassini/Huygens arrival time, shown along with the stream function (10^9 kg s^{-1}) averaged over 7 years (one Titan season) before the arrival (continuous lines denote clockwise motion). Each result is actually the mean result of four consecutive Titan years. (**Middle**) The percentage of methane in drop composition (the remaining part is ethane). (**Top**) The fraction of time that cloud extinction exceeds a threshold of $k = 10^{-4}$ m^{-1}.

±40° latitude range, the meridional circulation has a less defined structure with uprising and downwelling motions associated with inertial instabilities. This produces vertical and horizontal mixing able to carry methane upward and to produce a broad region (between 40° in the summer hemisphere and 50° in the winter hemisphere, and below 15 km near the equator and tropics and below 12 km at the latitude edges of the region) where methane mixing ratio is almost constant (see Fig. 3B for the annual mean).

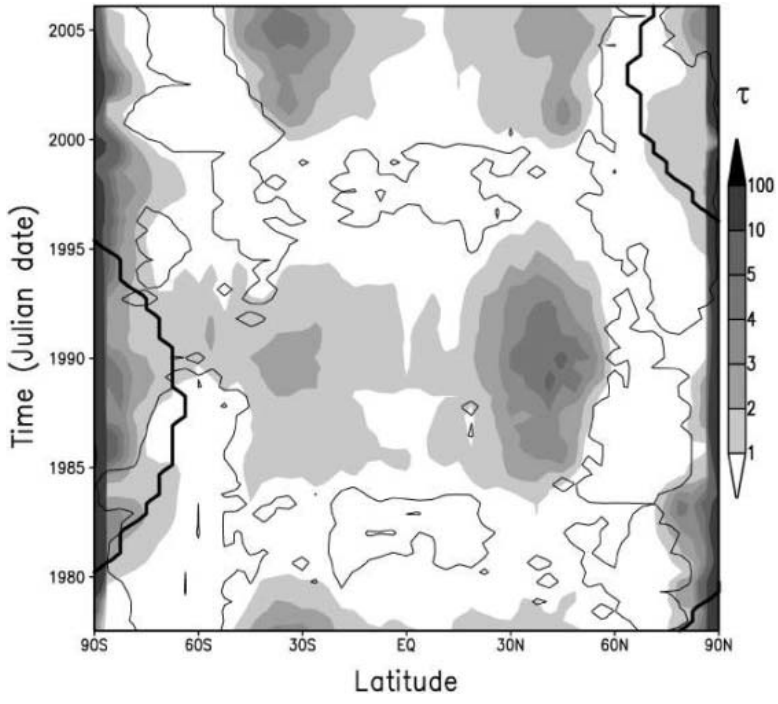

Fig. 2. Cloud column opacity (τ) at ~2 μm above 10 km altitude as a function of time and latitude. The dark thin contours show the level where 90% of the condensed material in cloud drops is methane. The thick lines show the edge of the polar night. Clouds are essentially made of methane between ±50° and near the poles, where the thick polar clouds appear. The broad cloud layer in both polar regions (poleward of latitudes ±60°) is made of ethane. Around equinoxes, during the wind cell turnover, cloud activity decreases near the equator because the aerosol concentration decreases by a factor of ~10. The summer methane polar clouds (south as observed by Cassini) tend to disappear—as observed in 2005—a few years after the summer solstice (which was in 2002) and to reappear after the following equinox (about 2010). We also expect a gradual vanishing of the summer mid-latitude clouds (at –40° in 2005) about 5 or 6 years after the summer equinox (i.e., about 2008). The mid-latitude clouds will reappear in the other hemisphere after the equinox (about 2015). These predictions should allow us to discriminate between the dynamical origin of the latitudinal cloud distribution and other possible origins, such as the location of the sources on the surface (*11*).

Methane clouds that have been observed to date appear at locations where ascending motions are predicted in our model. The observed south polar cloud (*4*–*7*, *9*) appears at the top of the oblique cells (exactly at the south pole, at altitudes of 20 to 30 km). The large recurrent zonal (longitudinal direction) clouds at 40°S (*9*–*11*), as well as the linear and discrete clouds found at several locations between 14°S and 83°S and clustered at 40°S (*6*), are correlated with the ascending branch of the tropospheric Hadley cell (at 40°S in 2005) and to the broad region where vertical mixing occurs (Fig. 1). Consistently, our model produces clouds at the places where clouds are actually observed (Table 1), but it also predicts clouds that have not (or not yet) been observed. Generally, in our model, methane condenses at ~15 km at ±60° latitude and at 18 km near the equator. Clouds are formed at these levels anywhere methane is transported upward by the circulation (Fig. 1). Methane clouds frequently appear in the ascending branch of the tropospheric Hadley cell at ~40° in the summer hemisphere (south in 2005). The mixing process due to inertial instabilities also produces thin clouds between ±30° (about 10% of the time) and more important clouds (between 10 and 50% of the time) at winter mid-latitudes (between 40° and 60°), although wind is descending there (Fig. 2). The mixing process produces a broad region (from 30° in the summer hemisphere to 60° in the winter hemisphere and below ~10 km; Fig. 3B shows the annual mean value) where the methane ratio is almost uniform and close to 5% (which is about the surface value in the ±30° range). Between tropics, the warm temperatures and the presence of clouds bound the saturation ratio close to 1, consistent with Huygens observations (*26*). Between 40° and 60° winter latitudes, temperature sharply decreases with latitude (fig.

Table 1. Cloud classification.

Cloud type	Location/origin	Optical thickness	Drop radius (μm)	Lifetime	Related observations
Ethane mist	Both polar regions below 60 km / Descending branch of stratosphere cells	~1 to 5	1 to 3	Permanent structure	C_4N_2 detected at winter pole (*1*); cloud opacity (*25*); summer pole not yet observed
Polar methane	Poleward 75° at both poles and below 30 km / Slantwise cells between mid-latitudes and poles	~10 to 100	10 to 100	Terrestrial day	5 to 25 km, scattered in south (summer) polar region (*4*, *6*–*8*); north (winter) pole not observed yet
Sporadic tropical methane	~40° in summer hemisphere at or below 20 km / Ascending branch of the troposphere Hadley cell	~1 to 100	10 to 100	Terrestrial day	5 to 7% of the disk*, time scale = 2 days (*2*, *3*); discrete and streak clouds clustered around 40°S (*6*, *9*–*11*) and between 63°S and 83°S (*6*)
Sporadic intertropical methane	Between ±30° at or below 20 km / Mixing process due to inertial instabilities	~1 to 100	10 to 100	Hour	0.5% of the disk*, time scale = hours (*3*); streak cloud at 14°S, 23°S (*6*); not observed in north (winter) hemisphere

*Data used by (*2*, *3*) are disk-integrated near-infrared spectra; determination of cloud location thus strongly depends on hypothesis, and clouds may actually be elsewhere than near the equator.

S2), producing a permanent zone of supersaturation (Fig. 3A) in the regions depleted in aerosols (fig. S1). This pocket of supersaturation is fed by mixing, and clouds that form at the lower edge of the aerosol-depleted region do not efficiently remove the excess methane. These conditions are favorable to form frequent winter mid-latitude clouds.

With radii of ~30 to 100 μm, methane drops rapidly settle and evaporate a few kilometers lower, in subsaturated layers. The sedimentation time scale is much smaller than the time scale to restore, by mixing or upward advection, the methane saturation ratio up to the critical saturation ratio (the ratio at which nucleation is triggered, predicted to be $S \approx 1.02$ in our model with our parameter set; table S1). Therefore, methane clouds essentially appear as sporadic clouds rather than as a permanent cloud deck. Their lifetime is limited by their sedimentation time scale (several terrestrial days), but small clouds have very short lifetimes due to a shorter evaporation time scale (hours) (Table 2).

Table 2. Average time scales in Titan atmosphere.

Physical process	Polar region	Tropical regions
Cloud microphysics	Hour*	Hour*
Ethane cloud sedimentation†	Terrestrial year	
Sporadic methane cloud sedimentation†	Day to week	Day to week
Aerosol sedimentation†	Decades to century	Decades to century
Horizontal meridional wind‡	Century	Decades to century
Horizontal zonal wind§	Terrestrial day	Terrestrial day
Vertical wind‖	Century	Century
Vertical mixing processes¶		Decades#

*Relaxation time from situations out of equilibrium. †Scale height H divided by sedimentation speed. ‡For latitudinal motions: Titan radius R divided by latitudinal wind speed v. §For zonal (longitudinal) motions: Titan perimeter $2\pi R$ divided by zonal wind speed u. ‖Mixing due to inertial instabilities between ±60°. ¶For vertical motions: Scale height H divided by vertical wind speed w. #Roughly estimated from situations out of equilibrium.

The zonal wind speed—several tens of meters per second—exceeds the speed of the two other wind components, and it has a vertical gradient (U'_z) of ~0.5 m s^{-1} km^{-1} between the ground and ~20 km (*27*). This may explain why tropospheric clouds at mid-latitudes, which have vertical extents of a few kilometers, appear elongated in the zonal direction. Dimensions L of several hundred kilometers ($L \approx \Delta U \times \Delta t \approx 2 \times 10^5$ m) are explained by the differential zonal speed inside the cloud ($\Delta U \approx U'_z \times \Delta z \approx 2.5$ m s^{-1}) due to their vertical extent ($\Delta z \approx 5$ km) and their formation lifetime (one terrestrial day: $\Delta t \approx 10^5$ s). At both poles, cloud structures are also produced by the oblique cells that carry methane-rich air upward from the surface at ±40° latitudes to higher altitudes in polar regions, where it condenses. Very near the poles, the cells have a strong vertical component that produces clouds at the same place as those observed (*6*). The methane polar cloud is pinned very near the poles. It is variable in time and space and also has a variable vertical extent that may occasionally reach up to 30 km. In our model, the air is very stable, the latent heat is negligible, and therefore no convection can produce the polar clouds with the mechanism proposed in (*4*).

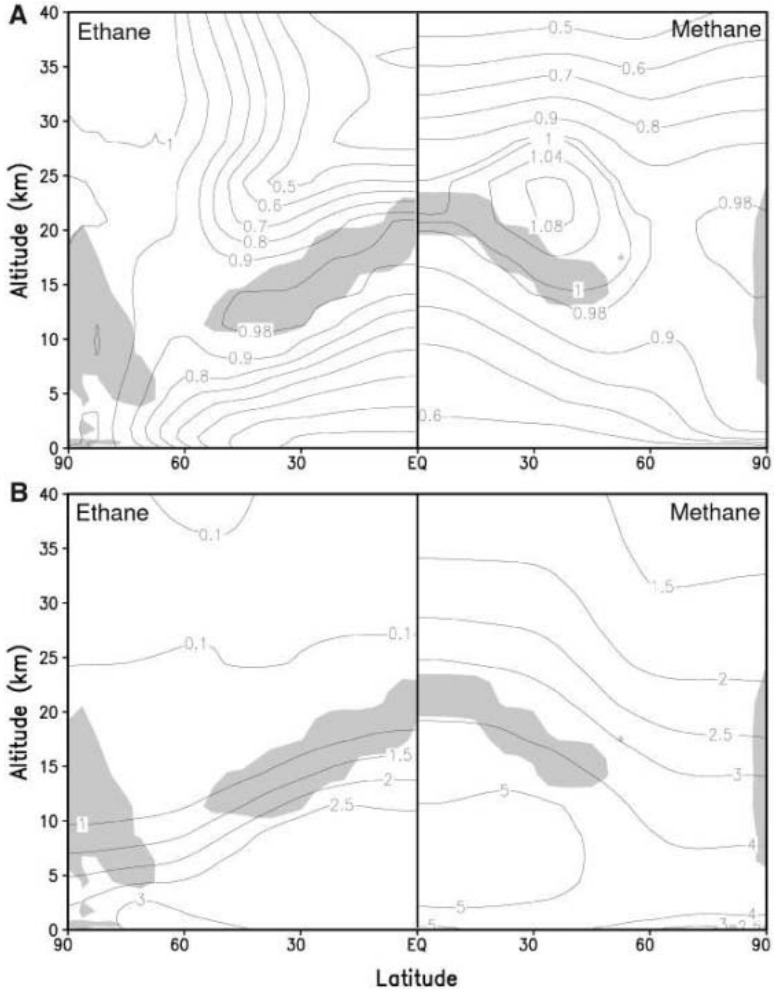

Fig. 3. (**A**) Annual mean of ethane (left) and methane (right) saturation ratios. Here we find that high saturation levels are tightly correlated to cloudy regions (Fig. 1). The shaded areas show places where ethane and methane annual condensation rates are larger than threshold values of 10^{-21} and 6×10^{-17} m^3 of ice per m^3 of atmosphere per second, respectively. On the left, ethane condenses below 60 km in the polar regions and then evaporates during the descent. This allows maintenance of the ethane concentration close to saturation down to the surface in the polar regions. Lower troposphere circulation and mixing processes transport ethane-humid air from the poles to warmer undersaturated tropical regions, where air masses rise up and cool leading ethane close to saturation again around 15 km or 18 km. On the right, a similar process is at work for methane, except that the source is at the surface. Rising motions in the tropics and in both polar regions generate a layer where methane saturation is close to 1 at ~20 km near the equator, at 15 km at mid-latitudes, and between 10 and 20 km at the poles. Methane saturation ratio sharply drops above 25 km. Methane annual mean saturation ratio close to 1 at 12° is more consistent with Huygens observations (*26*) than with previous estimations from Voyager IRIS data (*30*). (**B**) Ethane and methane mixing ratios. Both species are rather constant in the first 10 km and within ±40°. Shaded areas have the same meaning as in the upper panel.

Ethane precipitation occurs essentially in large regions poleward of ±70°, with ~0.2 mm per Titan year in polar regions and a few micrometers per year elsewhere. The methane cycle is a balance between the surface evaporation and precipitation. Methane evaporates between the tropics (in the ±30° range) and precipitates near the poles. In tropical regions, most of the methane clouds evaporate before reaching the ground, except for the largest ones. At latitudes of ±70°, methane precipitation does not exceed 1 cm per year, but poleward of ±70° it can reach 1 m per year. The global cycle then drives methane from equatorial and tropical to polar regions. Methane is probably not stable in tropical regions on geological time scales, and because the Huygens landing site was humid and marked by river channels, this indicates that a source of methane is still active on Titan (*28*). Global average values of precipitation rates found here are consistent with previous work (*14*, *17*).

The methane cycle on Titan has some similarities with water cycles on Earth and on Mars. As with water on Earth and Mars, the methane source on Titan is at the surface. The major cloud pattern on these planets essentially appears in ascending branches of the circulation: (i) The Hadley cell system produces a cloud belt in the intertropical convergence zone on Earth and on Mars and also produces the frequent clouds at 40° in the summer hemisphere on Titan. (ii) The poleward ascending motions beyond the Hadley cell, developed as baroclinic waves on Earth and on Mars and as slantwise convection in our two-dimensional model of Titan, produces clouds because water or methane-rich air is transported toward cold regions. This mechanism produces the south polar cloud. Baroclinic waves are believed not to be produced on Titan (*17*). In these three atmospheres, clouds are generally good tracers of the circulation and can reveal some of its important features.

Gravitational tides caused by Saturn are known to disturb the large-scale circulation (*29*). This effect is specific to Titan and could explain the longitudinal large-scale distribution of the clouds (*11*) by triggering nucleation at preferential longitudes. Surface heterogeneities (albedo contrasts and topography) and waves may also play a role in circulation and in cloud meteorology. These questions must be addressed further, in the frame of a three-dimensional model.

Some cloud properties may be defined, in reality, at scales smaller than the model grid [e.g., cloud overshoots, subscale inhomogeneities as observed by (*9*)]. Interaction between clouds and haze in our model may also lead to removal of aerosols more efficiently than observed in reality (*27*). Clouds in our circulation model are necessarily simplified relative to the real clouds. However, the main cloud features predicted in this work find a counterpart in reality. The correct behavior of our model allows us to analyze the formation mechanism associated with each type of observed cloud and offers a new insight into cloud physics on Titan.

References and Notes

1. R. E. Samuelson, L. A. Mayo, M. A. Knuckles, R. J. Khanna, *Planet. Space Sci.* **45**, 941 (1997).
2. C. A. Griffith, T. Owen, G. A. Miller, T. Geballe, *Nature* **395**, 575 (1998).
3. C. A. Griffith, J. L. Hall, T. R. Geballe, *Science* **290**, 509 (2000).
4. M. E. Brown, A. H. Bouchez, C. A. Griffith, *Nature* **420**, 795 (2002).
5. S. G. Gibbard *et al.*, *Icarus* **169**, 429 (2004).
6. C. C. Porco *et al.*, *Nature* **434**, 159 (2005).
7. H. G. Roe, I. De Pater, B. A. Macintosh, C. P. McKay, *Astron. J.* **591**, 1399 (2002).
8. A. H. Bouchez, M. E. Brown, *Astron. J.* **618**, L53 (2005).
9. C. A. Griffith *et al.*, *Science* **310**, 474 (2005).
10. H. G. Roe, A. H. Bouchez, C. A. Trujillo, E. L. Schaller, M. E. Brown, *Astron. J.* **618**, L49 (2005).
11. H. G. Roe, M. E. Brown, E. L. Schaller, A. H. Bouchez, C. A. Trujillo, *Science* **310**, 477 (2005).
12. R. Courtin, D. Gautier, C. P. McKay, *Icarus* **114**, 144 (1995).
13. R. E. Samuelson, L. A. Mayo, *Planet. Space Sci.* **45**, 949 (1997).
14. E. L. Barth, O. B. Toon, *Icarus* **162**, 94 (2004).
15. R. D. Lorenz, *Planet. Space Sci.* **41**, 647 (1993).
16. E. L. Barth, O. B. Toon, *Geophys. Res. Lett.* **31**, L17S07 (2005).
17. T. Tokano, F. M. Neubauer, M. Laube, C. P. McKay, *Icarus* **153**, 130 (2001).
18. F. Hourdin *et al.*, *Icarus* **117**, 358 (1995).
19. P. Rannou, F. Hourdin, C. P. McKay, *Nature* **418**, 853 (2002).
20. P. Rannou, F. Hourdin, C. P. McKay, D. Luz, *Icarus* **170**, 443 (2004).
21. See supporting material on *Science* Online.
22. E. F. Young, P. Rannou, C. P. McKay, C. A. Griffith, K. Noll, *Astron. J.* **123**, 3473 (2002).
23. S. Lebonnois, D. Toublanc, F. Hourdin, P. Rannou, *Icarus* **152**, 384 (2001).
24. F. Hourdin, S. Lebonnois, D. Luz, P. Rannou, *J. Geophys. Res.* **109**, E10005 (2004).
25. L. A. Mayo, R. E. Samuelson, *Icarus* **176**, 316 (2005).
26. H. B. Niemann *et al.*, *Nature* **438**, 779 (2005).
27. M. Tomasko *et al.*, *Nature* **438**, 765 (2005).
28. C. Sotin *et al.*, *Nature* **435**, 786 (2005).
29. T. Tokano, F. M. Neubauer, *Icarus* **158**, 499 (2002).
30. R. E. Samuelson, N. R. Nath, A. Borysow, *Planet. Space Sci.* **45**, 959 (1997).

31. Supported by the Programme National de Planétologie du CNRS. This work was performed while F.M. held a tenure from the National Research Council associateship program.

Supporting Online Material

www.sciencemag.org/cgi/content/full/311/5758/201/DC1
Materials and Methods
Figs. S1 and S2
Table S1
References

4 August 2005; accepted 9 November 2005
10.1126/science.1118424

Majority Logic Gate for Magnetic Quantum-Dot Cellular Automata

A. Imre,[1]* G. Csaba,[2] L. Ji,[1] A. Orlov,[1] G. H. Bernstein,[1] W. Porod[1]

We describe the operation of, and demonstrate logic functionality in, networks of physically coupled, nanometer-scale magnets designed for digital computation in magnetic quantum-dot cellular automata (MQCA) systems. MQCA offer low power dissipation and high integration density of functional elements and operate at room temperature. The basic MQCA logic gate, that is, the three-input majority logic gate, is demonstrated.

In magnetic devices, information is encoded in the magnetization state of ferromagnetic materials. Although commonly used for data-storage applications, there are relatively few attempts to exploit magnetic phenomena for logic functionality (*1*–*5*). One of the possible architectures suitable for logic using nanomagnets is the quantum-dot cellular atomata (QCA) signal-processing approach (*6*). QCA are built from simple, (nominally) identical, bistable units that are locally connected to each other solely by electromagnetic forces; consequently, the signal-processing function is defined by the physical placement of the building blocks that constitute the computing architecture (*7*–*9*). Recently, Cowburn and Welland (*2*) described the realization of magnetic QCA (MQCA) operation in chains of 110-nm-diameter disk-shaped magnetic particles that manifest collective behavior. In this system, the preferred magnetization direction of the disks (the representation of binary information), as well as the magnetization reversal process (the information propagation), is primarily determined by coupling-induced magnetic anisotropy in the chains. Our approach to MQCA is similar in spirit, but we use an additional shape-induced anisotropy component to separate the directions for magnetic information representation and information propagation in the array (*5*).

The QCA concept can be realized in different physical systems. It was originally proposed to use electrostatically coupled arrays of quantum dots and Coulomb-blockade phenomena to perform binary operations (*6*). The

[1]Center for Nano Science and Technology, Department of Electrical Engineering, University of Notre Dame, Notre Dame, IN 46556, USA. [2]Institute for Nanoelectronics, Technical University of Munich, Arcisstrasse 21, D-80333 Munich, Germany.

*To whom correspondence should be addressed. E-mail: aimre@nd.edu

first functional electrostatic QCA (EQCA) cell was experimentally demonstrated (*10*) in 1997, followed by the logic gate (*11*) and the shift register (*12*). Micrometer-sized metal (Al) dots separated by thin (a few nm) oxide tunnel barriers were used in these experiments, which were performed at subkelvin temperatures owing to small charging energies ($\sim k_B \times 1$ K, where k_B is the Boltzmann constant) achievable with this fabrication technique (*13*). Room-temperature EQCA can be achieved only for the size of a cell reduced to molecular scale (*14*, *15*), the technology for which has not yet been demonstrated.

As an advantage compared to the above-mentioned electrostatic devices, logic gates featuring single-domain magnets on the size scale of 10 to 100 nm (above the superparamagnetic limit, but within the single-domain limit) are expected to operate at room temperature because of their relatively large magnetic energies (*5*, *16*). Consider an elongated single-domain magnet similar in shape and magnetic state to the larger magnets in the one-domain state shown in Fig. 1. Being of submicrometer size, elongated single-domain magnets are strongly bistable, because their remanent magnetization (magnetization at zero external field) always points along their long axis owing to shape-induced magnetic anisotropy. Even though a magnetizing force can temporarily rotate the magnetization away from the long axis, the magnet relaxes to either of the two remanent states when the force is removed. The process of temporarily magnetizing perpendicular to the long axis can be pictured as the magnetizing force pulling down and then releasing the energy barrier between the remanent ground states.

For the one-domain state, unlike the two-domain or vortex configurations (also shown in Fig. 1), the magnetic flux lines close outside of the magnets, creating strong magnetic stray fields that can be used to couple elements in close proximity through dipole-dipole interactions. The resulting magnetization pattern for an array of nanomagnets depends on their physical arrangement. For example, arranging several of these magnets to be colinear along their long axes results in a line of magnets favoring their magnetization to point in the same direction, i.e., the ferromagnetically ordered state. Placing them side-by-side and in parallel results in a line that favors antiparallel alignment of the magnetic dipoles, i.e., the antiferromagnetically ordered state. In MQCA, these coupling-induced ordering phenomena are used to drive the computation.

Figure 2 shows a line of antiferromagnetically coupled (AFC) nanomagnets elongated in the "vertical" direction (the *y* direction). Also shown on the right-hand side of the line is a "horizontal" nanomagnet (the *x* direction), which can be used as an input to set the state of the linear array. In the absence of the input

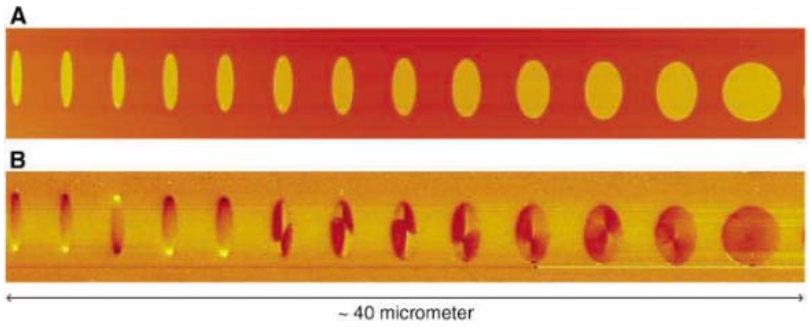

Fig. 1. Magnetic states of patterned ferromagnetic elements. (**A**) Topographic atomic force microscope (AFM) image of thin-film, polycrystalline NiFe magnetic elements in a row, made by electron-beam lithography and lift-off. While one axis of the oval elements is kept the same, the aspect ratio of the axes is varied between 7.5 (on the left side) to 1 (on the right side). (**B**) MFM image of remanent magnetization. Strong contrast in the MFM images of one-domain magnets represents the location of magnetic poles. This image reveals one-domain, two-domain, and vortex configurations, depending upon the size and shape (aspect ratio) of the elements.

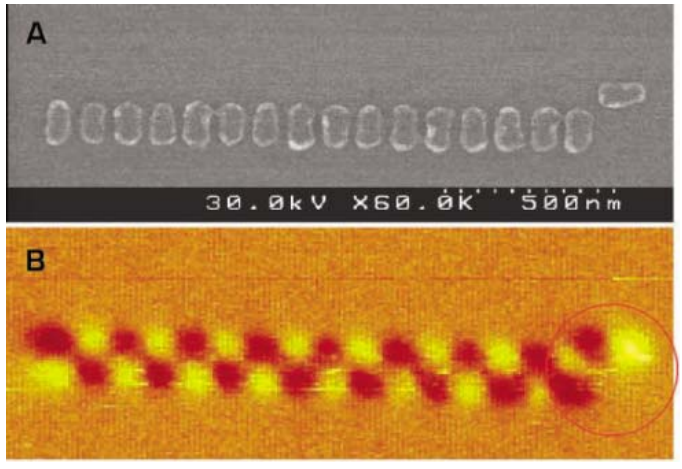

Fig. 2. Antiferromagnetic ordering in a line of nanomagnets. (**A**) Scanning electron microscope (SEM) image of a chain of 16 coupled nanomagnets of size 70 nm by 135 nm and 30-nm permalloy thickness. The separation between the vertically elongated magnets is 25 nm. The antiferromagnetic ordering along the chain is controlled by an additional, horizontally oriented elongated driver magnet. (**B**) MFM image of the same chain shows alternating magnetization of the magnets as set by the state of the horizontal driver magnet (circled).

magnet, the ground state of the AFC line could be one of two possible complementary, alternating dipole configurations (either up-down-up-down…etc. or down-up-down-up…etc.). Setting the state of the input magnet by an external field in the *x* direction breaks this symmetry and favors one of the two possible complementary states of the line. This input magnetic field, if designed properly, can also be used to act as an adiabatic clocking field (hereafter referred to as the clock-field) to facilitate the switching of the line from some arbitrary state to the AFC ground state. The effect of such a horizontal field on the vertical dots is to add an *x* component of magnetization to the preferred *y* direction. For sufficiently strong clock-fields (typically several hundred Oe), the magnetization vectors of all nanomagnets in the line can be forced to point in the *x* direction, but this state will persist only so long as the clock-field is maintained, and the nanomagnets will return to their preferred state with magnetization in the *y* direction upon removal of this field. The crucial point here is that this switching behavior from magnetization in the *x* direction to either up or down in the *y* direction is strongly influenced by any additional fields, such as coupling fields from either the neighbors or the input magnet. The effect of the clock-field in the *x* direction is to place the line of coupled magnets into an intermediate state, and the magnetic fringe fields from inputs and neighbors then determine which ground-state configuration the array assumes after removal of the clock-field. We have both studied this switching behavior through extensive micromagnetic simulations (*16*) and observed it experimentally (Fig. 2B).

We introduce in Fig. 3 a gated AFC line that performs majority logic. The nanomagnets are arranged in two intersecting lines, such that the dipole coupling of the nanomagnets produces ferromagnetic ordering along the vertical line and antiferromagnetic ordering along the horizontal line. This structure is similar to that proposed in (*17*) [and also studied in (*18*)], except that we consider the

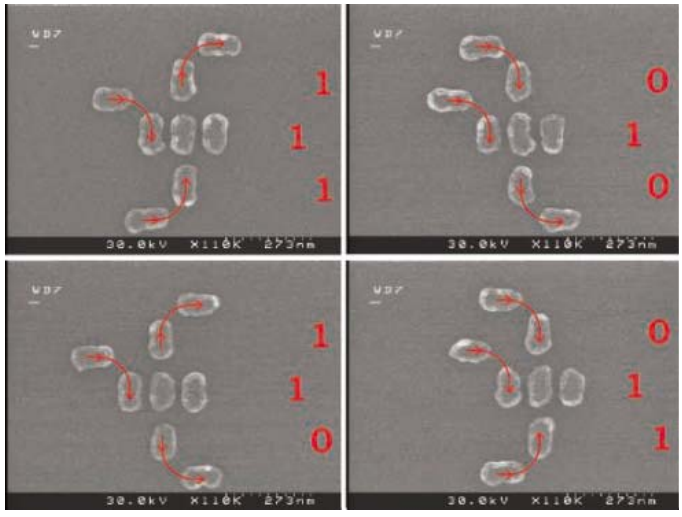

Fig. 3. Majority gates designed for testing all input combinations of the majority-logic operation. The arrows drawn superimposed on the SEM images illustrate the resulting magnetization direction due to a horizontally applied external clock-field. The magnetic state of the AFC inputs has the opposite effective votes on the central magnet as compared with the FC inputs, so AFC and FC inputs are assigned the same logical value for opposite magnetizations. The bit value "0" is assigned to magnetization direction down along the vertical axis of FC input magnets and the central magnet, and value "1" is assigned to magnetization up. The AFC input is defined oppositely.

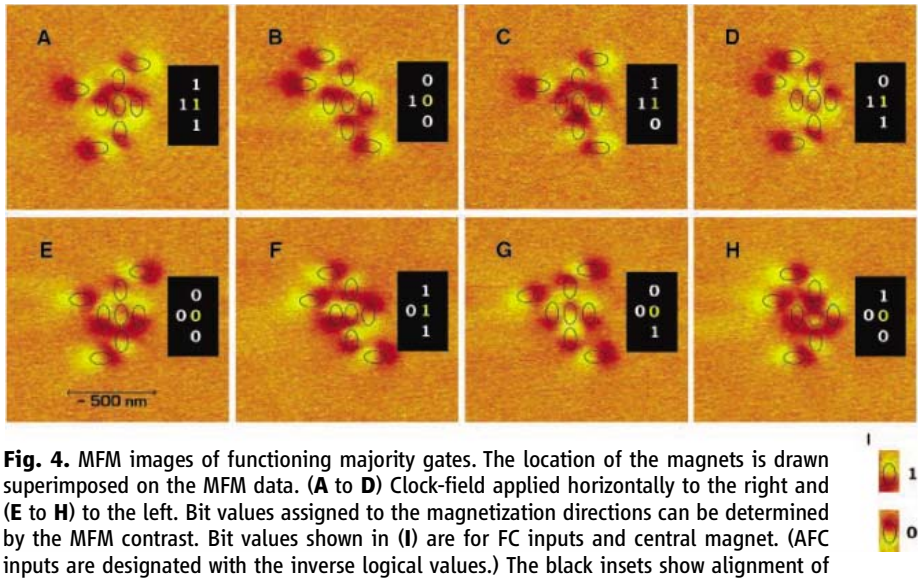

Fig. 4. MFM images of functioning majority gates. The location of the magnets is drawn superimposed on the MFM data. (**A** to **D**) Clock-field applied horizontally to the right and (**E** to **H**) to the left. Bit values assigned to the magnetization directions can be determined by the MFM contrast. Bit values shown in (**I**) are for FC inputs and central magnet. (AFC inputs are designated with the inverse logical values.) The black insets show alignment of magnetic dipoles, accounting for antiferromagnetic and ferromagnetic coupling, and demonstrate correct MQCA majority logic gate functionality.

output of the gate to be in the AFC line instead of the FC line. Consider the simplest arrangement of five nanomagnets, i.e., a central nanomagnet surrounded by four others. Three of the neighbors can be used as inputs driven by additional driver nanomagnets oriented in the *x* direction, along the clock-field. The fourth neighbor, to the right of the central magnet in Fig. 3, is the output. Our gate is constructed so that the ferromagnetic and antiferromagnetic coupling to the central dot have the same strength, and therefore it switches to the state to which the majority of inputs force it. By varying the positions of the driver nanomagnets, all eight input logic combinations can be tested, as suggested in the figure.

Simulations (*19*) of the magnetic states of the majority gates after applying a horizontal clock-field show that as the clock-field falls, switching inside the gate begins at the input magnets and ends at the output magnet. Figure 4 demonstrates final states after two experiments in which a clock-field of 500 Oe with ~30-s rise and fall times (*20*) was applied in opposite directions. Inputs (000), (001), (010), and (011) were written by the driver magnets when the clock-field was oriented to the left and (100), (101), (110), and (111) when oriented to the right. The function of the majority gate is given in the included truth table (Table 1) in terms of the central magnet. The magnetic force microscopy (MFM) data (*21*) in Fig. 4 show correct alignment of all magnetic dipoles of the gates.

Our investigations demonstrate that correct operation of the majority-gate structure (as defined by every magnet being consistent with the applied field) was found in about 25% of the set of fabricated gates when the applied clock-field was aligned to the horizontal with approximately ±1° of accuracy. It is important to note that the probability of all eight nanomagnets assuming the correct orientation is less than 0.4%. We observed a much larger fraction of fully correct logic gates, which demonstrates that our results cannot be random events. We believe that fabrication variations are responsible for yields of less than 100% (*22*). The run-to-run reliability was about 50%, indicating that between runs, about half of the working gates were in common. We believe that this was mostly due to clock-field misalignment between runs.

Table 1. Summary of logic states in the majority gate for all input combinations (truth table). The logic state of the central nanomagnet is determined by the logical majority vote of its three input neighbors, of which the ferromagnetically coupled neighbors vote directly and the antiferromagnetically coupled neighbor votes inversely to its magnetic state. The logic state of the central magnet is written inverted to the output magnet by antiferromagnetic coupling. If programmed by the first-input bit value, a majority gate can function as a two-input NAND gate (upper four rows of the table) or as a two-input NOR gate (lower four rows of the table).

Logic state of input magnets	Logic state of central magnet	Logic state of output magnet
000	0	1
001	0	1
010	0	1
011	1	0
100	0	1
101	1	0
110	1	0
111	1	0

The three-input majority gate discussed above can be viewed as a programmable two-input NAND or NOR gate, depending on the state of any one of the three input magnets and accounting for inversion at the output magnet. Therefore, any Boolean logic function can be built by a network of majority gates. The inputs used in this work are set by the external clock-field and cannot be programmed independently; different combinations of the input values are realized by different physical arrangements of driver magnets. Nevertheless, the intersection of the horizontal and vertical wires, which is common to all structures, can correctly perform majority-logic functionality. We are currently developing inputs that can be controlled independently.

The minimum time necessary for magnetic switching is limited by magnetization precession in the nanomagnets and is on the order of 100 ps (*23*). The adiabatic pumping scheme

further increases the clock-cycle time in MQCA devices by one or two orders of magnitude to eliminate precession from the switching process and to ensure predictable operation. Our simulations show that the majority gate reported here has an inherent operating speed of 100 MHz and dissipation below 1 eV per switching event. As a worst-case estimate of the power dissipation in an MQCA system, at these speeds, and assuming that all nanomagnets switch in each clock cycle, 10^{10} gates would dissipate ~0.1 W.

We performed Monte Carlo simulations in the single-domain approximation to investigate whether the realization of larger-scale systems is feasible (*24*). Variations in nanomagnet shape and edge roughness were taken into account in the distribution of the coupling fields at which switching occurs, i.e., switching fields (distribution of the demagnetization tensor elements), and thermal fluctuations were modeled by adding a stochastic field to the coupling field. We found that for our structures, the impact of switching-field variations is far more important than the effect of thermal fluctuations. Strongly coupled dots (<100-nm dot separation) fabricated by high-quality lithography (with switching-field variations less than 10%) exhibit magnetic ordering over 10 to 20 magnets. This result agrees well with our previous experiments (*25*, *26*) for samples fabricated by electron-beam lithography and lift-off (supporting online text). Even with better fabrication technology, the number of nanomagnets that can be clocked together is limited. Therefore, a larger-scale device would have to operate by means of local clocking of subarrays that realize a few gates only. The small number of magnets switching at the same time ensures that error levels can be kept acceptably small. This concept has been developed for EQCA (*27*). The most suitable architecture for adiabatically clocked MQCA devices appears to be a pipelined structure. Because of the sequential arrangement of logic gates, there will inevitably be pipeline latency; however, new data can be fed into the pipeline at each clock cycle. Clocking zones can be defined by locally applied clock-fields. Pipelined architectures are desirable in their own right owing to their highly parallelized computing environment.

Integration of MQCA elements with electronic circuitry is possible in a manner similar to that for magnetic random access memory (MRAM) elements (*28*). Furthermore, integration of MQCA arrays into MRAM cells is also feasible, thus allowing the possibility of "intelligent memory" whereby the magnetic layer of an MRAM cell could not only store a single bit of information, but could also perform basic logical processing. This may provide an opportunity to increase the functionality and integration density of an MRAM device.

In summary, MQCA information propagation and negation have been demonstrated previously (*2*, *25*, *26*), and our present work indicates that logic functions can also be realized in properly structured arrays of physically coupled nanomagnets. The technology for fabricating such nanometer-scale magnets is currently under development by the hard disk drive industry (*29*). Whereas the latter work focuses entirely on data-storage applications, and physical coupling between individual bits is undesirable, our work points out the possibility of also realizing logic functionality in such systems and indicates the potential of all-magnetic information-processing systems that incorporate both memory and logic.

References and Notes

1. A. Ney, C. Pampuch, R. Koch, K. H. Ploog, *Nature* **425**, 485 (2003).
2. R. P. Cowburn, M. E. Welland, *Science* **287**, 1466 (2000).
3. D. A. Allwood *et al.*, *Science* **296**, 2003 (2002).
4. D. A. Allwood *et al.*, *Science* **309**, 1688 (2005).
5. G. Csaba, A. Imre, G. H. Bernstein, W. Porod, V. Metlushko, *IEEE Trans. Nanotechnol.* **1**, 209 (2002).
6. C. S. Lent, P. D. Tougaw, W. Porod, G. H. Bernstein, *Nanotechnology* **4**, 49 (1993).
7. A. I. Csurgay, W. Porod, C. S. Lent, *IEEE Trans. Circ. Syst. I* **47**, 1212 (2000).
8. G. Csaba, A. I. Csurgay, W. Porod, *Int. J. Circ. Theory Appl.* **29**, 73 (2001).
9. G. Csaba, W. Porod, A. I. Csurgay, *Int. J. Circ. Theory Appl.* **31**, 67 (2003).
10. A. O. Orlov, I. Amlani, G. H. Bernstein, C. S. Lent, G. L. Snider, *Science* **277**, 928 (1997).
11. I. Amlani *et al.*, *Science* **284**, 289 (1999).
12. R. K. Kummamuru *et al.*, *IEEE Trans. Electron Devices* **50**, 1906 (2003).
13. A. O. Orlov *et al.*, *Mesoscopic Tunneling Devices*, H. Nakashima, Ed. (Research Signpost, Trivandrum, Kerala, India, 2004), p. 125.
14. G. L. Snider *et al.*, *J. Appl. Phys.* **85**, 4283 (1999).
15. C. S. Lent, *Science* **288**, 1597 (2000).
16. G. Csaba, W. Porod, *J. Comput. Electron.* **1**, 87 (2002).
17. M. C. B. Parish, M. Forshaw, *Appl. Phys. Lett.* **83**, 2046 (2003).
18. S. A. Haque, M. Yamamoto, R. Nakatani, Y. Endo, *J. Magn. Magn. Mater.* **282**, 380 (2004).
19. The micromagnetic simulations were performed using the Object Oriented Micromagnetic Framework (M. J. Donahue, D. G. Porter, OOMMF User's Guide, Version 1.0 Interagency Report NISTIR 6376, http://math.nist.gov/oommf/) of the National Institute of Standards and Technology.
20. The magnetizing process, i.e., the application of the clock-field, was performed in the homogeneous field of an electromagnet capable of a maximum 7000 Oe. Owing to limitations imposed by the ramping rate of the generated field, the frequency of the clock-field was about 0.01 Hz in our experiments.
21. Magnetic force microscopy images were taken in a Digital Instruments Nanoscope IV with standard magnetic probes.
22. Antiferromagnetic ordering was investigated in a large set of AFC lines designed to be identical. In a small percentage of results, we have found the ordering to fail even in the simplest, two-magnet systems. The identified faulty pairs performed highly repeatably, which indicates that the errors are related to fabrication variations (*30*).
23. Th. Gerrits, H. A. M. van den Berg, J. Hohlfeld, L. Bar, Th. Rasing, *Nature* **418**, 509 (2002).
24. G. Csaba, thesis, University of Notre Dame, IN (2003).
25. A. Imre, G. Csaba, G. H. Bernstein, W. Porod, V. Metlushko, *Proc. IEEE Nanotechnol.* **2**, 20 (2003).
26. A. Imre, G. Csaba, G. H. Bernstein, W. Porod, V. Metlushko, *Superlatt. Microstruct.* **34**, 513 (2003).
27. J. Timler, C. S. Lent, *J. Appl. Phys.* **91**, 823 (2002).
28. C. A. Ross, *Annu. Rev. Mater. Res.* **31**, 203 (2001).
29. J. M. Slaughter *et al.*, *J. Supercon.* **15**, 19 (2002).
30. G. H. Bernstein *et al.*, *Microelectr. J.* **36**, 619 (2005).

31. This work was supported in part by grants from the Office of Naval Research, the W. M. Keck Foundation, and the National Science Foundation.

Supporting Online Material

www.sciencemag.org/cgi/content/full/311/5758/205/DC1
SOM Text
References

23 September 2005; accepted 1 December 2005
10.1126/science.1120506

A Stretchable Form of Single-Crystal Silicon for High-Performance Electronics on Rubber Substrates

Dahl-Young Khang,[1,3,4] Hanqing Jiang,[2] Young Huang,[2]* John A. Rogers[1,2,3,4]*

We have produced a stretchable form of silicon that consists of submicrometer single-crystal elements structured into shapes with microscale, periodic, wavelike geometries. When supported by an elastomeric substrate, this "wavy" silicon can be reversibly stretched and compressed to large levels of strain without damaging the silicon. The amplitudes and periods of the waves change to accommodate these deformations, thereby avoiding substantial strains in the silicon itself. Dielectrics, patterns of dopants, electrodes, and other elements directly integrated with the silicon yield fully formed, high-performance "wavy" metal oxide semiconductor field-effect transistors, p-n diodes, and other devices for electronic circuits that can be stretched or compressed to similarly large levels of strain.

Progress in electronics is driven mainly by efforts to increase circuit operating speeds and integration densities, to reduce the power consumption of circuits, and, for display systems, to enable large area coverage. A more recent direction seeks to develop methods and materials that enable high-performance circuits to be formed on unconventional substrates with unusual form factors (*1*, *2*), such as flexible plastic substrates for

paperlike displays and optical scanners (*3*–*7*), spherically curved supports for focal plane arrays (*8*, *9*), and conformable skins for integrated robotic sensors (*10*, *11*). Many electronic materials can provide good bendability when prepared in thin-film form and placed on thin substrate sheets (*12*–*17*) or near neutral mechanical planes in substrate laminates (*18*, *19*). In these cases, the strains experienced by the active materials during bending can remain well below the typical levels required to induce fracture (~1%). Full stretchability, a much more challenging characteristic, is required for devices that can flex, stretch, or reach extreme levels of bending as they are operated or for those that can be conformally wrapped around supports with complex curvilinear shapes. In these systems, strains at the circuit level can exceed the fracture limits of nearly all known electronic materials, especially those that are well developed for established applications. This problem can be circumvented, to some extent, with circuits that use stretchable conducting wires to interconnect electronic components (such as transistors) supported by rigid isolated islands (*20*–*25*). Promising results can be obtained with this strategy, although it is best suited to applications that can be achieved with active electronics at relatively low coverages. We report a different approach, in which stretchability is achieved directly in thin films of high-quality, single-crystal Si that have micrometer-scale, periodic, "wave"-like geometries. These structures accommodate large compressive and tensile strains through changes in the wave amplitudes and wavelengths rather than through potentially destructive strains in the materials themselves. Integrating such stretchable wavy Si elements with dielectrics, patterns of dopants, and thin metal films leads to high-performance, stretchable electronic devices.

Figure 1 presents a fabrication sequence for wavy, single-crystal Si ribbons on elastomeric (rubber) substrates. The first step (top panel) involves photolithography to define a resist layer on a Si-on-insulator (SOI) wafer, followed by etching to remove the exposed parts of the top Si. Removing the resist with acetone and then etching the buried SiO_2 layer with concentrated hydrofluoric acid releases the ribbons from the underlying Si substrate. The ends of the ribbons connect to the wafer to prevent them from washing away in the etchant. The widths (5 to 50 μm) and lengths (~15 mm) of the resist lines define the dimensions of the ribbons. The thickness of the top Si (20 to 320 nm) on the SOI wafers defines the ribbon thicknesses. In the next step (middle panel), a flat elastomeric substrate [poly(dimethylsiloxane) (PDMS), 1 to 3 mm thick] is elastically stretched and then brought into conformal contact with the ribbons. Peeling the PDMS away lifts the ribbons off of the wafer and leaves them adhered to the PDMS surface. Releasing the strain in the PDMS (that is, the prestrain) leads to surface deformations that cause well-defined waves to form in the Si and the PDMS surface (Fig. 2, A and B). The relief profiles are sinusoidal (top panel, Fig. 2C), with periodicities between 5 and 50 μm and amplitudes between 100 nm and 1.5 μm, depending on the thickness of the Si and the level of prestrain in the PDMS. For a given system, the periods and amplitudes of the waves are uniform to within ~5% over large areas (several square centimeters). The flat morphology of the PDMS between the ribbons and the absence of correlated phases in waves of adjacent ribbons suggest that the ribbons are not strongly coupled mechanically. Figure 2C (bottom panel) shows micro-Raman measurements of the Si peak, measured as a function of distance along one of the wavy ribbons. The results provide insights into the stress distributions.

The behavior in this static wavy configuration is consistent with nonlinear analysis of the initial buckled geometry in a uniform, thin, high-modulus layer on a semi-infinite low-modulus support (*26*, *27*)

$$\lambda_0 = \frac{\pi h}{\sqrt{\varepsilon_c}},\ A_0 = h\sqrt{\frac{\varepsilon_{pre}}{\varepsilon_c} - 1} \qquad (1)$$

where $\varepsilon_c = 0.52\left[\frac{E_{PDMS}\left(1-\nu_{Si}^2\right)}{E_{Si}\left(1-\nu_{PDMS}^2\right)}\right]^{2/3}$ is the critical strain for buckling, ε_{pre} is the level of prestrain, λ_0 is the wavelength, and A_0 is the amplitude. The Poisson ratio is ν, the Young's modulus is E, and the subscripts refer to properties of the Si or PDMS. The thickness of the Si is h. This treatment captures many features of the as-fabricated wavy structures. Figure 2D shows, for example, that when the prestrain value is fixed (~0.9% for these data), the wavelengths and amplitudes both depend linearly on the Si thickness. The wavelengths do not depend on the level of prestrain (fig. S1). Furthermore, calculations that use literature values (*28*, *29*) for the mechanical properties of the Si and PDMS (E_{Si} = 130 GPa, E_{PDMS} = 2 MPa, ν_{Si} = 0.27, ν_{PDMS} = 0.48) yield amplitudes and wavelengths that are within ~10% (maximum deviation) of the measured values. The strains computed from the ratio of the effective lengths of the ribbons (as determined from the wavelength) to their actual lengths [as determined from surface distances measured by atomic force microscopy (AFM)], which we refer to as ribbon strains, yield values that are approximately equal to the prestrain in the PDMS, for prestrains up to ~3.5%. The peak (that is, the maximum) strains in the Si itself, which we refer to as Si strains, can be estimated from the ribbon thicknesses and radii of curvature at the extrema of the waves according to $\kappa h/2$, where κ is the curvature, in regimes of strain where the waves exist and where the critical strain (~0.03% for the cases examined here) is small as compared to the peak strains associated with bending. For the data of Fig. 2, the peak Si strains are ~0.36 (±0.08)%, which is more than a factor of 2 smaller than the ribbon strains. This Si

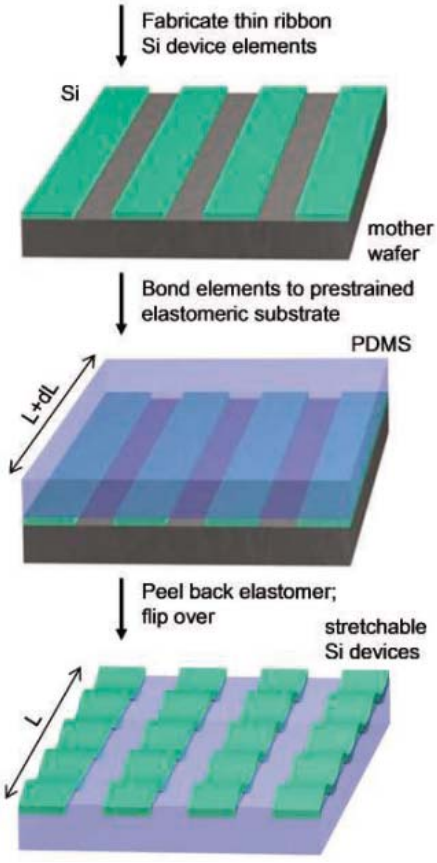

Fig. 1. Schematic illustration of the process for building stretchable single-crystal Si devices on elastomeric substrates. The first step (**top**) involves fabrication of thin (thicknesses between 20 and 320 nm) elements of single-crystal Si or complete integrated devices (transistors, diodes, etc.) by conventional lithographic processing, followed by etching of the top Si and SiO_2 layers of a SOI wafer. After these procedures, the ribbon structures are supported by, but not bonded to, the underlying wafer. Contacting a prestrained elastomeric substrate (PDMS) to the ribbons leads to bonding between these materials (**middle**). Peeling back the PDMS, with the ribbons bonded on its surface, and then releasing the prestrain, causes the PDMS to relax back to its unstrained state. This relaxation leads to the spontaneous formation of well-controlled, highly periodic, stretchable wavy structures in the ribbons (**bottom**).

[1]Department of Materials Science and Engineering, [2]Department of Mechanical and Industrial Engineering, [3]Beckman Institute for Advanced Science and Technology, [4]Seitz Materials Research Laboratory, University of Illinois, Urbana-Champaign, Urbana, IL 61801, USA.

*To whom correspondence should be addressed. E-mail: jrogers@uiuc.edu (J.A.R); huang9@uiuc.edu (Y.H.)

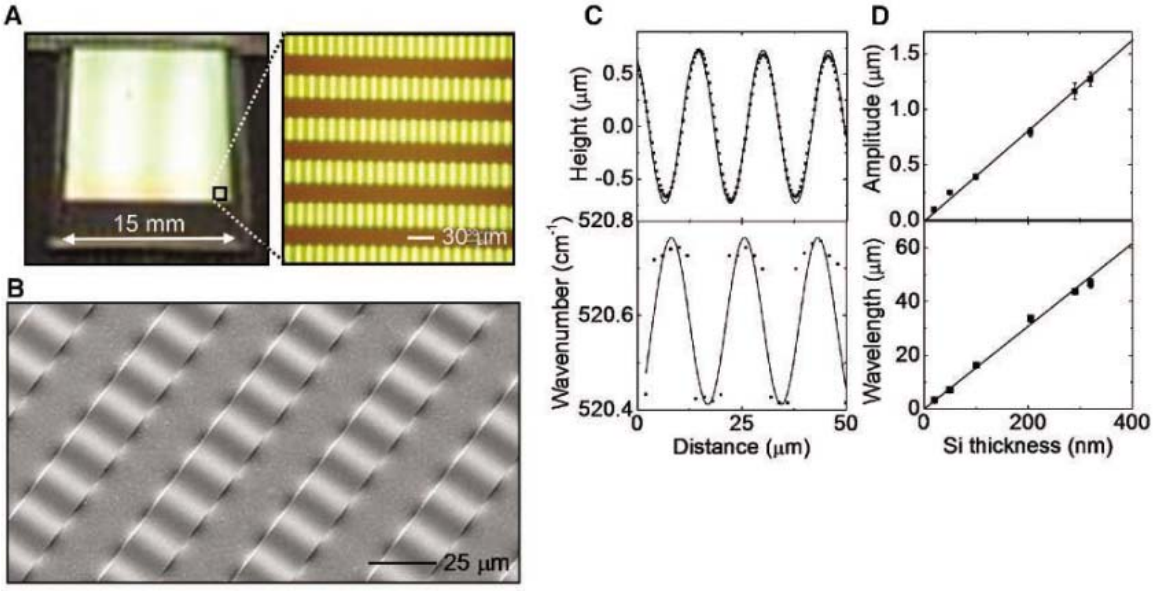

Fig. 2. (**A**) Optical images of a large-scale aligned array of wavy, single-crystal Si ribbons (widths = 20 μm, spacings = 20 μm, thicknesses = 100 nm) on PDMS. (**B**) Angled-view scanning electron micrograph of four wavy Si ribbons from the array shown in (A). The wavelengths and amplitudes of the wave structures are highly uniform across the array. (**C**) Surface height (top panel) and wavenumber of the Si Raman peak (bottom panel) as a function of position along a wavy Si ribbon on PDMS, measured by AFM and Raman microscopy, respectively. The lines represent sinusoidal fits to the data. (**D**) Amplitudes (top panel) and wavelengths (bottom panel) of wavy Si ribbons as a function of the thickness of the Si, all for a given level of prestrain in the PDMS. The lines correspond to calculations, without any fitting parameters.

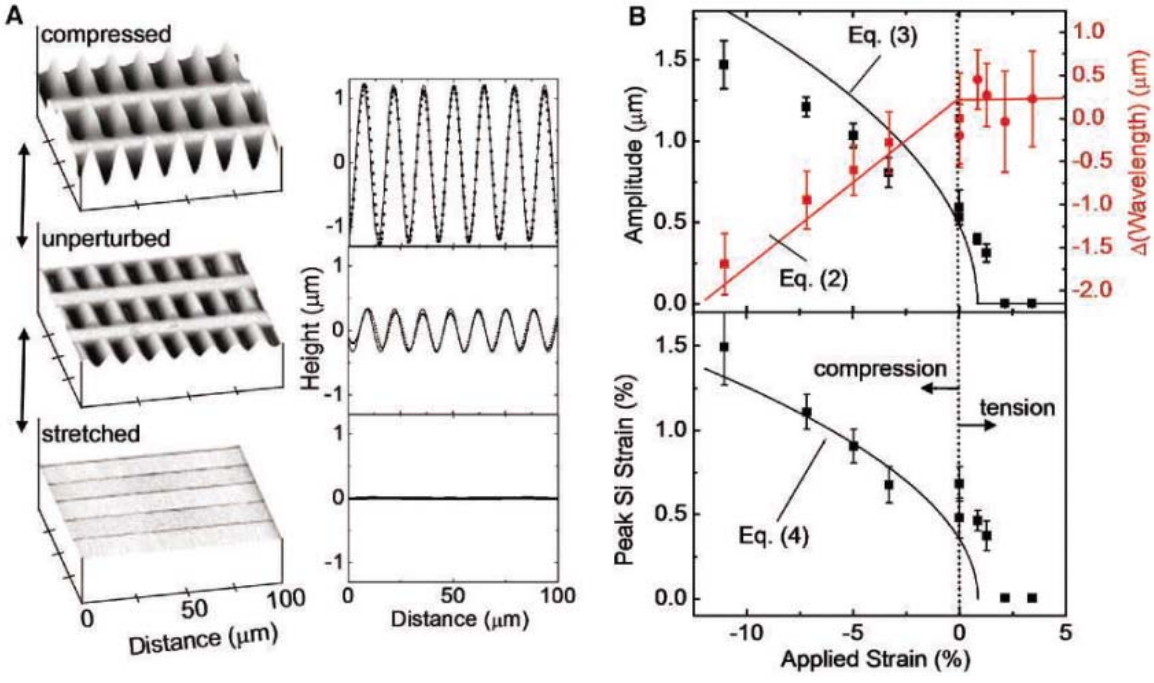

Fig. 3. (**A**) Atomic force micrographs (left panels) and relief profiles (right panels; the lines are the sinusoidal fits to experimental data) of wavy single-crystal Si ribbons (width = 20 μm, thickness = 100 nm) on PDMS substrates. The top, middle, and bottom panels correspond to configurations when the PDMS is strained along the ribbon lengths by −7% (compression), 0% (unperturbed), and 4.7% (stretching), respectively, measured at slightly different locations. (**B**) Average amplitudes (black) and changes in wavelength (red) of wavy Si ribbons as a function of strain applied to the PDMS substrate (top panel). For the wavelength measurements, different substrates were used for tension (circles) and compression (squares). Peak Si strains as a function of applied strain are shown in the bottom panel. The lines in these graphs represent calculations, without any free fitting parameters.

strain is the same for all ribbon thicknesses, for a given prestrain (fig. S2). The resulting mechanical advantage, in which the peak Si strain is substantially less than the ribbon strain, is critically important for achieving stretchability. Buckled thin films have also been observed in metals and dielectrics evaporated or spin-cast onto PDMS (in contrast to preformed, transferred, single-crystal elements and devices, as described here) (*30*–*32*).

The dynamic response of the wavy structures to compressive and tensile strains applied to the elastomeric substrate after fabrication is of primary importance for stretchable electronic devices. To reveal the mechanics of this process, we measured the geometries of wavy Si ribbons by AFM as force was applied to the PDMS to compress or stretch it parallel to the long dimension of the ribbons. This force creates strains both along the ribbons and perpendicular to them, due to the Poisson effect. The perpendicular strains lead primarily to deformations of the PDMS in the regions between the ribbons. The strains along the ribbons, on the other hand, are accommodated by changes in the structure of the waves. The three-dimensional height images and surface profiles in Fig. 3A present representative compressed, unperturbed, and stretched states (collected from slightly different locations on the sample). In these and other cases, the ribbons maintain their sinusoidal (lines in the right-hand panels of Fig.

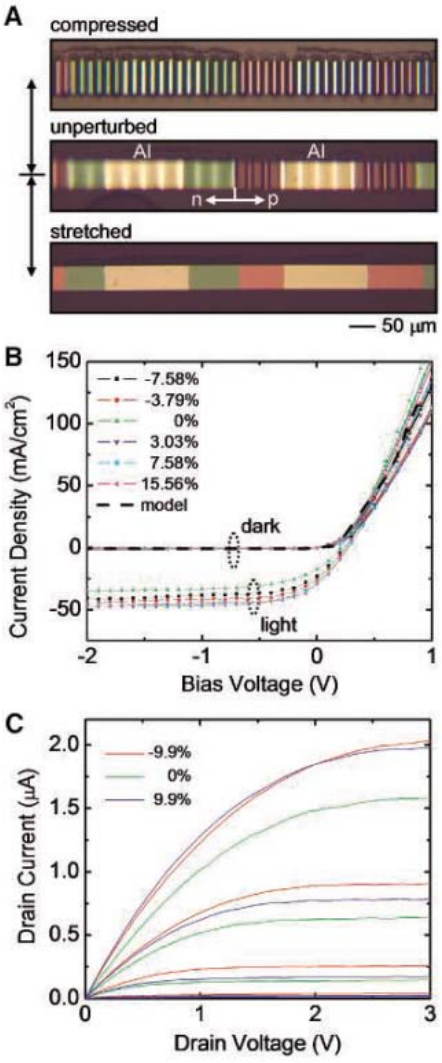

Fig. 4. (**A**) Optical images of a stretchable single-crystal Si p-n diode on a PDMS substrate at –11% (top), 0% (middle), and 11% (bottom) applied strains. The Al regions correspond to thin (20 nm) Al electrodes; the pink and green regions correspond to n (boron)– and p (phosphorous)–doped areas of the Si. (**B**) Current density as a function of bias voltage for stretchable Si p-n diodes, measured at various levels of applied strain. The curves labeled "light" and "dark" correspond to devices exposed to or shielded from ambient light, respectively. The solid curves show modeling results. (**C**) Current-voltage characteristics of a stretchable Schottky-barrier Si MOSFET, measured at –9.9%, 0%, and 9.9% applied strains (the gate voltage varied from 0 V to –5 V, with a 1-V step).

3A) shapes during deformation, in which approximately half of the wave structure lies beneath the unperturbed position of the PDMS surface, as defined by the regions between the ribbons (fig. S3). Figure 3B shows the wavelength and amplitude for compressive (negative) and tensile (positive) applied strains relative to the unperturbed state (zero). The data correspond to averaged AFM measurements collected from a large number (>50) of ribbons per point. The applied strains were determined from the measured end-to-end dimensional changes of the PDMS substrate. Direct surface measurements by AFM, as well as contour integrals evaluated from the sinusoidal wave shapes, show that the applied strains are equal to the ribbons strains (fig. S4) for the cases examined here. [The small-amplitude (<5 nm) waves that persist at tensile strains larger than the prestrain minus the critical strain might result from slight slippage of the Si during the initial buckling process. The computed peak Si strains and ribbon strains in this small- (or zero-) amplitude regime underestimate the actual values.] The results indicate two physically different responses of the wavy ribbons to applied strain. In tension, the waves evolve in a non-intuitive way: The wavelength does not change appreciably with applied strain, which is consistent with post-buckling mechanics. Instead, changes in amplitude accommodate the strain. In this regime, the Si strain decreases as the PDMS is stretched; it reaches ~0% when the applied strain equals the prestrain. By contrast, in compression, the wavelengths decrease and amplitudes increase with increasing applied strain. This mechanical response is similar to that of an accordion bellows, which is qualitatively different than the behavior in tension. During compression, the Si strain increases with the applied strain, due to the decreasing radii of curvature at the wave peaks and troughs. The rates of increase and magnitudes of the Si strains are, however, both much lower than the ribbon strains, as shown in Fig. 3B. These mechanics enable stretchability.

The full response in regimes of strain consistent with the wavy geometries can be quantitatively described by equations that give the dependence of the wavelength λ on its value in the initial buckled state, λ_0, and the applied strain $\varepsilon_{applied}$ according to

$$\lambda = \begin{cases} \lambda_0 & \text{for tension} \\ \lambda_0(1+\varepsilon_{applied}) & \text{for compression} \end{cases} \quad (2)$$

This tension/compression asymmetry can arise, for example, from slight reversible separations between the PDMS and the raised regions of Si, formed during compression. For this case, as well as for systems that do not exhibit this asymmetric behavior, the wave amplitude A, for both tension and compression, is given by a single expression, valid for modest strains (<10 to 15%) (*33*)

$$A = \sqrt{A_0^2 - h^2\frac{\varepsilon_{applied}}{\varepsilon_c}} = h\sqrt{\frac{\varepsilon_{pre}-\varepsilon_{applied}}{\varepsilon_c} - 1} \quad (3)$$

where A_0 is the value corresponding to the initial buckled state. These expressions yield quantitative agreement with the experiments without any parameter fitting, as shown in Fig. 3A. When the waviness, which accommodates the tensile/compressive strains, remains, the peak Si strain is dominated by the bending term and is given by (*33*)

$$\varepsilon_{Si}^{peak} = 2\varepsilon_c\sqrt{\frac{\varepsilon_{pre}-\varepsilon_{applied}}{\varepsilon_c} - 1} \quad (4)$$

which agrees well with the strain measured from curvature in Fig. 3B (see also fig. S5). Such an analytic expression is useful to define the range of applied strain that the system can sustain without fracturing the Si. For a prestrain of 0.9%, this range is –27% to 2.9% if we assume that the Si failure strain is ~2% (for either compression or tension). Controlling the level of prestrain allows this range of strains (that is, nearly 30%) to balance desired degrees of compressive and tensile deformability. For example, a prestrain of 3.5% (the maximum that we examined) yields a range of –24% to 5.5%. Such calculations assume that the applied strain equals the ribbon strain, even at extreme levels of deformation. Experimentally, we find that these estimates are often exceeded because of the ability of the PDMS beyond the ends of the ribbons and between the ribbons to accommodate strains, so that the applied strain is not completely transferred to the ribbons.

We have created functional, stretchable devices by including at the beginning of the fabrication sequence (Fig. 1, top panel) additional steps to define patterns of dopants in the Si, thin metal contacts, and dielectric layers using conventional processing techniques (*33*). Two- and three-terminal devices, diodes, and transistors, respectively, fabricated in this manner provide basic building blocks for circuits with advanced functionality. A dual transfer process in which the integrated ribbon devices were first lifted off of the SOI onto an undeformed PDMS slab, and then to a prestrained PDMS substrate, created wavy devices with metal contacts exposed for probing. Figure 4, A and B, show optical images and electrical responses of a stretchable p-n–junction diode for various levels of strain applied to the PDMS. We observed no systematic variation in the electrical properties of the devices when stretched or compressed, to within the scatter of the data. (The deviation in the curves is due mainly to variations in the quality of probe contacts.) As expected, these p-n–junction diodes can be used as photodetectors (at reverse-biased state) or as photovoltaic devices, in addition to their use as normal rectifying devices. The photocurrent density was ~35 mA/cm² at a reverse bias voltage of ~–1V. At forward bias, the short-circuit current density and open-circuit voltage were ~17 mA/cm² and 0.2 V, respectively, which yields a fill factor of 0.3. The shape of the response is consistent with modeling (solid curves in Fig. 4B). The device properties do not change substantially, even after

~100 cycles of compressing, stretching, and releasing (fig. S6). Figure 4C shows current-voltage characteristics of a stretchable, wavy, Si, Schottky-barrier metal oxide semiconductor field-effect transistor (MOSFET) formed with procedures similar to those used for the p-n diode, and with an integrated thin layer (40 nm) of thermal SiO_2 as a gate dielectric (*33*). The device parameters extracted from electrical measurements of this wavy transistor [linear regime mobility ~100 cm^2/Vs (likely contact-limited), threshold voltage ~–3 V] are comparable to those of devices formed on the SOI wafers under the same processing conditions (figs. S7 and S8). As with the p-n diodes, these wavy transistors can be reversibly stretched and compressed to large levels of strain without damaging the devices or substantially altering their electrical properties. In both the diodes and the transistors, deformations in the PDMS beyond the ends of the devices lead to device (ribbon) strains that are smaller than the applied strains. The overall stretchability results from the combined effects of device stretchability and these types of PDMS deformations. At compressive strains larger than those examined here, the PDMS tended to bend in ways that made probing difficult. At larger tensile strains, the ribbons either fractured, or slipped and remained intact, depending on the Si thickness, the ribbon lengths, and the strength of bonding between the Si and PDMS.

These stretchable Si MOSFETs and p-n diodes represent only two of the many classes of wavy electronic devices that can be formed. Completed circuit sheets or thin Si plates can also be structured into uniaxial or biaxial stretchable wavy geometries. Besides the unique mechanical characteristics of wavy devices, the coupling of strain to electronic properties, which occurs in many semiconductors, might provide opportunities to design device structures that exploit mechanically tunable periodic variations in strain to achieve unusual electronic responses. These and other areas appear promising for future research.

References and Notes

1. S. R. Forrest, *Nature* **428**, 911 (2004).
2. For recent progress and reviews, see *Proc. IEEE* **93**, issues 7 and 8 (2005).
3. J. A. Rogers *et al.*, *Proc. Natl. Acad. Sci. U.S.A.* **98**, 4835 (2001).
4. H. O. Jacobs, A. R. Tao, A. Schwartz, D. H. Gracias, G. M. Whitesides, *Science* **296**, 323 (2002).
5. H. E. A. Huitema *et al.*, *Nature* **414**, 599 (2001).
6. C. D. Sheraw *et al.*, *Appl. Phys. Lett.* **80**, 1088 (2002).
7. Y. Chen *et al.*, *Nature* **423**, 136 (2003).
8. H. C. Jin, J. R. Abelson, M. K. Erhardt, R. G. Nuzzo, *J. Vac. Sci. Technol. B* **22**, 2548 (2004).
9. P. H. I. Hsu *et al.*, *IEEE Trans. Electron. Devices* **51**, 371 (2004).
10. T. Someya *et al.*, *Proc. Natl. Acad. Sci. U.S.A.* **101**, 9966 (2004).
11. H. C. Lim *et al.*, *Sens. Act. A* **119**, 332 (2005).
12. J. Vandeputte *et al.*, U.S. Patent 6,580,151 (2003).
13. T. Sekitani *et al.*, *Appl. Phys. Lett.* **86**, 073511 (2005).
14. E. Menard, R. G. Nuzzo, J. A. Rogers, *Appl. Phys. Lett.* **86**, 093507 (2005).
15. H. Gleskova *et al.*, *J. Noncryst. Solids* **338**, 732 (2004).
16. S.-H. Hur, O. O. Park, J. A. Rogers, *Appl. Phys. Lett.* **86**, 243502 (2005).
17. X. F. Duan *et al.*, *Nature* **425**, 274 (2003).
18. Z. Suo, E. Y. Ma, H. Gleskova, S. Wagner, *Appl. Phys. Lett.* **74**, 1177 (1999).
19. Y.-L. Loo *et al.*, *Proc. Natl. Acad. Sci. U.S.A.* **99**, 10252 (2002).
20. T. Someya *et al.*, *Proc. Natl. Acad. Sci. U.S.A.* **102**, 12321 (2005).
21. S. P. Lacour, J. Jones, S. Wagner, Z. G. Suo, *Proc. IEEE* **93**, 1459 (2005).
22. S. P. Lacour *et al.*, *Appl. Phys. Lett.* **82**, 2404 (2003).
23. D. S. Gray, J. Tien, C. S. Chen, *Adv. Mater.* **16**, 393 (2004).
24. R. Faez, W. A. Gazotti, M. A. De Paoli, *Polymer* **40**, 5497 (1999).
25. C. A. Marquette, L. J. Blum, *Biosens. Bioelectron.* **20**, 197 (2004).
26. X. Chen, J. W. Hutchinson, *J. Appl. Mech.* **71**, 597 (2004).
27. Z. Y. Huang, W. Hong, Z. Suo, *J. Mech. Phys. Solids* **53**, 2101 (2005).
28. *Properties of Silicon* (INSPEC, Institution of Electrical Engineers, New York, 1988).
29. A. Bietsch, B. Michel, *J. Appl. Phys.* **88**, 4310 (2000).
30. N. Bowden *et al.*, *Nature* **146**, 146 (1998).
31. W. T. S. Huck *et al.*, *Langmuir* **16**, 3497 (2000).
32. C. M. Stafford *et al.*, *Nat. Mater.* **3**, 545 (2004).
33. Materials and methods are available as supporting material on *Science* Online.

34. We thank T. Banks for help with processing using the facilities at the Frederick Seitz Materials Research Laboratory. This work was supported by the Defense Advanced Research Projects Agency–funded Air Force Research Laboratory–managed Macroelectronics Program Contract FA8650-04-C-7101, by the U.S. Department of Energy under grant DEFG02-91-ER45439, and by NSF under grant DMI-0328162.

Supporting Online Material

www.sciencemag.org/cgi/content/full/1121401/DC1
Materials and Methods
Figs. S1 to S8

17 October 2005; accepted 5 December 2005
Published online 15 December 2005;
10.1126/science.1121401
Include this information when citing this paper.

Grain Boundary Strengthening in Alumina by Rare Earth Impurities

J. P. Buban,[1] K. Matsunaga,[1]* J. Chen,[2] N. Shibata,[1] W. Y. Ching,[2] T. Yamamoto,[3] Y. Ikuhara[1]†

Impurity doping often alters or improves the properties of materials. In alumina, grain boundaries play a key role in deformation mechanisms, particularly in the phenomenon of grain boundary sliding during creep at high temperatures. We elucidated the atomic-scale structure in alumina grain boundaries and its relationship to the suppression of creep upon doping with yttrium by using atomic resolution microscopy and high-precision calculations. We find that the yttrium segregates to very localized regions along the grain boundary and alters the local bonding environment, thereby strengthening the boundary against mechanical creep.

Structural ceramics have a large range of applications for engines and turbines. To avoid failure, the material needs to have a high resistance to deformations at the very high operating temperatures. Deformations almost always nucleate at atomic-scale defects, particularly grain boundaries (GBs). A commonly used and well-studied structural ceramic is alumina (Al_2O_3). However, GBs in Al_2O_3 are known for having a weak resistance to deformations via sliding because of creep (*1*–*5*) at high temperatures. One method to improve the resistance to sliding due to creep is through the addition of small amounts of rare earth elements (*4*, *5*). These additives (i.e., dopants) are known to segregate to the GBs and are expected to retard GB sliding. Systematic measurements of GB sliding by creep tests were investigated by using a pair of bicrystals (*6*). One was pristine and the other was Y-doped, with a tilt angle about the [0001] axis of ~18°, corresponding to a Σ value of 31 (*7*). Here, the Σ value represents the degree of geometrical coincidence at GB. These results showed that Y doping increased the creep resistance for even a single GB by two orders of magnitude. Several simple models to explain the increase in GB creep resistance due to rare earth impurity doping have been proposed (*4*, *5*), but the atomic-scale mechanism of how these dopants actually strengthen grain boundaries is still very unclear and controversial. This is mainly because of poor understanding of the atomic structure of alumina GBs and how it is affected by rare earth doping.

We describe the results of our investigation of the atomic mechanism of Y doping and of the increase in grain boundary mechanical strength with the use of *Z*-contrast

[1]Institute of Engineering Innovation, University of Tokyo, 2-11-16, Yayoi, Bunkyo, Tokyo 113–8656, Japan. [2]Department of Physics, University of Missouri–Kansas City, 5100 Rockhill Road, Kansas City, MO 64110–2499, USA. [3]Department of Advanced Materials Science, University of Tokyo, 5-1-5, Kashiwanoha, Kashiwa, Chiba 277–8561, Japan.

*Present address: Department of Materials Science and Engineering, Kyoto University, Yoshida-Honmachi, Sakyo, Kyoto 606–8501, Japan.

†To whom correspondence should be addressed. E-mail: ikuhara@sigma.t.u-tokyo.ac.jp

images obtained by scanning transmission electron microscopy (STEM), performed on the same bicrystal pair used in the creep tests in (*6*), to determine the GB structure. STEM used in the present study is JEM2100F (200 kV, JEOL, Limited, Tokyo, Japan. We follow with a theoretical analysis of the GB structure and bonding using a combination of first principles and static lattice calculations.

A number of previous studies have used high-resolution TEM (HRTEM) to characterize the structure of pristine and Y-doped alumina GBs (*8*–*14*). Although much information on the atomic structure can be obtained through HRTEM, finding the specific atomic-scale location of dopants remains a very difficult task. However, because the image intensity in the STEM is roughly proportional to the square of the atomic number Z (i.e., the heaviest elements appear the brightest) (*15*), the Z-contrast technique is especially well suited for understanding the role of heavy impurities in a crystal of lighter atoms (*16*, *17*). Figure 1A shows a Z-contrast image of an undoped Σ31 GB in Al_2O_3 (*18*). Bright spots in the image correspond to atomic columns of Al (columns of oxygen do not scatter strong enough to be seen in the image). The schematic overlay (Fig. 1B) illustrates the presence of periodic structural units along the boundary plane. A notable feature of the GB structure is the presence of a seven-member ring of Al ions leading to a large open structure.

For the Y-doped Σ31 GB, the Z-contrast image is shown in Fig. 1C. The most striking features are the unusually bright columns that lie periodically along the boundary plane, indicating the presence of Y. By using nanoprobe energy dispersive spectroscopy (EDS) in the STEM, we confirmed Y to be confined to the boundary plane, consistent with the direct observation. Figure 1D shows a structural schematic of the Y-doped Al_2O_3 GB superimposed on the image. Here, the structural units observed at the Y-doped boundary closely resemble the units found in the undoped case, suggesting that Y does not alter the basic GB structure on length scales greater than ~0.1 nm. Instead it appears that Y^{3+} simply replaces Al^{3+} at the specific site on the cation sublattice. The Y-containing columns are only found at the center of the seven-membered ring and periodically along the GB, suggesting that Y preferentially segregates to special cation sites.

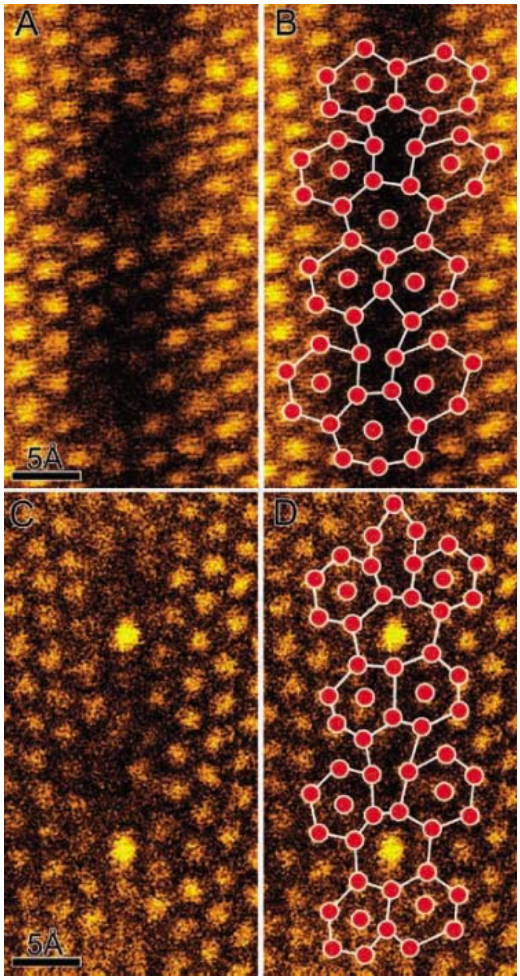

Fig. 1. *Z*-contrast images of undoped and Y-doped alumnia GBs. (**A**) *Z*-contrast STEM image of pristine Σ31 [0001] tilt GB in alumina. (**B**) Same image with overlay to illustrate the aluminum atomic column arrangement of the structural units. Note the large open structure of the seven-member ring unit, which is nearly periodic along the GB. (**C**) *Z*-contrast STEM image of Y-doped Σ31 [0001] tilt GB in alumina. (**D**) Same image with overlay to illustrate the atomic column arrangement. The two brightest columns indicate the presence of the heavy Y ions. These Y-containing columns are found right at the center of the seven-member ring unit. Images were processed by Gaussian smoothing.

Furthermore, the amount of Y present at the GB is very small and is much less than a monolayer.

Static lattice calculations (*11*, *12*, *18*, *19*) were performed to determine the lowest energy structure of the Al_2O_3 GB. A simulation cell of the Σ31 boundary (1240 atoms) was used to systematically calculate various rigid body translation states of the adjacent crystal across the boundary to find the most stable GB structure, using two-body Buckingham-type ionic potentials (*20*, *21*) for atomic relaxations. Figure 2A displays a schematic of the theoretically predicted lowest energy structure for the undoped case. This structure agrees well with the experimentally observed GB structure shown in Fig. 1, and the seven-membered ring structure with a large open space is clearly reproduced.

To locate the most energetically stable site for Y segregation, a single Y ion was substituted at various columns (marked a through p in Fig. 2A) at and near the boundary plane. The Y-containing atomic structure was allowed to relax by using the Buckingham ionic potentials. Each Al column contains four distinct Al sites, and the segregation energy for each distinct site was calculated. An additional calculation was performed to evaluate the bulk Y-segregation energy by introducing Y at the middle (far from the GB) of the Al_2O_3 crystal slab in the Σ31 simulation cell. Lastly, the Y-segregation energy for each particular ionic site along the grain boundary was obtained from the total energy difference between the energy of the supercell for Y substituted in the bulk and the energy of the supercell where the cation site in question is occupied by a single Y ion.

The segregation energy for each column was averaged over the four Al sites along the [0001] axis (Fig. 2B). The Y-segregation energies for sites more than 5 Å away from the boundary approximate the bulk value. On the other hand, Y segregation becomes energetically favorable near the grain boundary plane. In particular, the site right in the middle of the seven-membered ring shows the lowest segregation energy, which is consistent with the experimental results. Because both Y and Al ions are isovalent, the main difference between the two ions is the ionic radius. For comparison, the ionic radius for Al is 67.5 pm, whereas Y is 104 pm. Thus, the preferential segregation of Y to the center of the large seven-membered ring must be due to the facility of an expanded region to accommodate the larger ion.

Static lattice calculations are useful to qualitatively investigate candidates for stable GB structures when they can be verified experimentally. However, they have their basis in empirical interatomic potentials and thus are not suitable for a quantitative evaluation of the

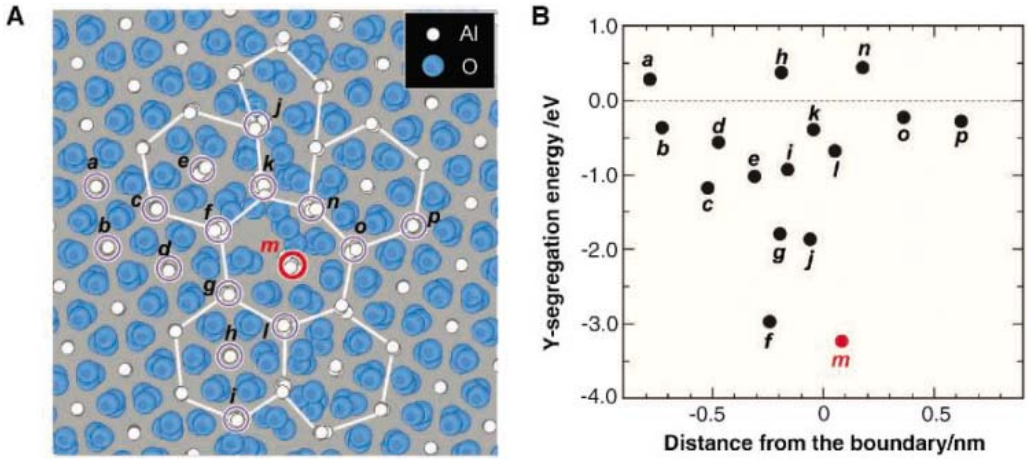

Fig. 2. Theoretical GB structure and segregation energies. (**A**) Schematic of the lowest energy GB structure obtained by static lattice calculations. Bold lines mark the GB structure that the structure observed in the *Z*-contrast image (Fig. 1). Columns labeled a through p mark the location of the Al columns where the Y-segregation energies were investigated. Column m in the middle of the seven-membered ring shows the lowest segregation energy. (**B**) Plot of the average Y-segregation energies for each column marked as a function of distance from the GB plane. Dashed line corresponds to the formation energy of Y substitution for Al in the bulk.

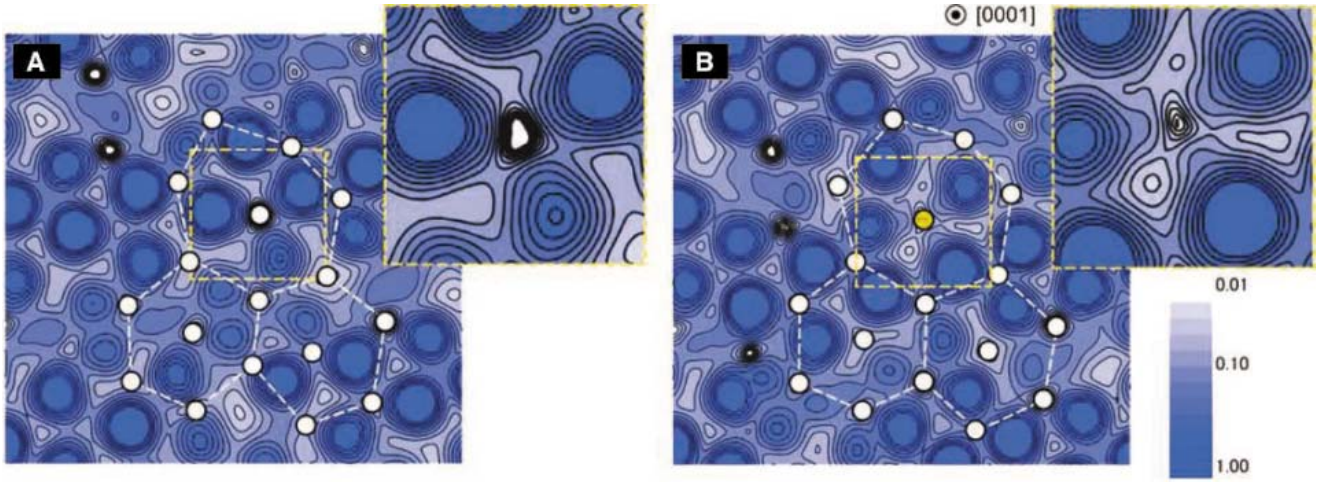

Fig. 3. Charge density map. A charge density map for the undoped GB (**A**) is shown for a (0001) plane near an Al ion in the middle of the seven-membered ring, where the charge density from the neighboring O ions (appearing as graduated blue spots) can be easily seen. (Insets) The nodes between the charge density of the O ions with the Al ion are typical of ionic bonding. A charge density map for the Y-doped GB (**B**) is displayed with a similar (0001) plane. The elongation of the O charge density toward the Y ion in the center of the seven-membered ring indicates covalent-type bonding. White circles indicate the location of Al ions, and the yellow circle indicates the location of the Y columns.

energetics, chemical, or bonding environment of the GB. Because the valence shell of Y contains a d electron, changes in the bonding environment at the GB are expected after doping with Y. Ab initio calculations can provide accurate information on the local atomic bonding and charge distributions, and we performed high precision ab initio calculations with the use of the Vienna Ab Intitio Simulation Package (VASP) (*18*). A large periodic supercell with 700 atoms containing two oppositely oriented GBs was constructed by using the structure obtained from static lattice calculations described above. First, the supercell was fully relaxed to obtain the most accurate GB structure for the undoped case. The results showed that further relaxations occurred. However, these relaxations were relatively small (less than 0.1 nm), yielding a GB structure that still matched the structure observed in the STEM image. The calculated GB energy, obtained from the difference between the total energy of the model and that of a perfect crystal model of same size, is 3.93 J/m^2. The fairly large GB energy reflects the complexity of the Σ31 GB. Next, assuming that all four distinct Al sites were substituted with Y ions in the column at the center of the seven-membered ring (the location that was observed in the STEM image), the structure was fully relaxed, and again the final structure matched well with the corresponding experimental image. The calculated GB energy for the Y-doped case is found to be 3.48 J/m^2, which is smaller than the pristine one and indicates that the GB is energetically stabilized upon Y doping [see (*18*) for more details].

Changes in the bonding character between the Y-O bonds and the Al-O bonds can be best illustrated by plotting the charge density maps. Figure 3, A and B, shows the charge density maps along the (0001) plane for the undoped and the Y-doped cases, respectively. Because of the complexity of the GB structure in Al_2O_3, cations and anions do not lie on the same (0001) plane. Therefore, we have carefully selected appropriate (0001) planes, which are close to a cation belonging to the center column of the seven-membered ring such that the charge densities of the neighboring oxygen ions can also be clearly seen. To facilitate visualization, we indicated schematically the locations of the cation columns. The charge density map for the undoped GB (Fig. 3A) shows the presence of sharp nodes between the oxygen charge densities and the charge density from the Al ion in the center of the seven-membered ring. In contrast, the Y-doped GB charge density map (Fig. 3B) shows that the oxygen electron densities are elongated toward

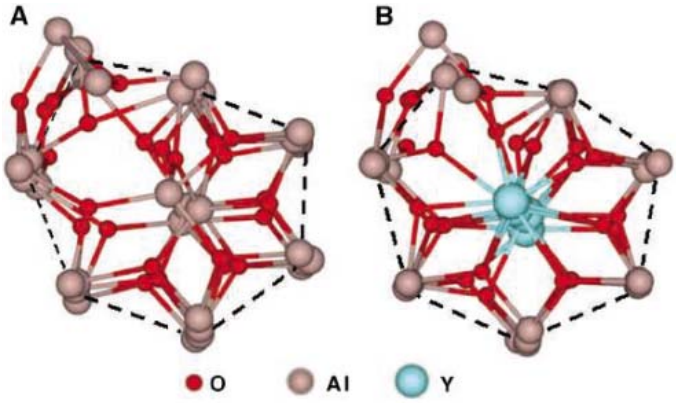

Fig. 4. Coordination changes illustrated by VASP. Here, the bonds, represented by sticks, are drawn in accordance with the bond length cutoffs mentioned in the text. (**A**) A ball-and-stick model for the seven-membered ring found along the GB in the undoped case. The column of Al ions is shifted from the center of the seven-membered ring, causing the coordination for these Al to be reduced to fivefold, whereas Al ions in the bulk are sixfold coordinated. (**B**) A similar ball-and-stick model when Y ions replace the Al ions in the middle of the seven-membered ring. The Y ions form a column near the center of the seven-membered ring, which allows bonds to be formed with a larger number of O anions, thereby increasing the coordination number up to 7. Bold dashed lines indicate the approximate perimeter of the seven-membered rings for comparison with previous figures.

the Y ion, indicating a stronger covalency for the Y-O bonds. It can be seen that Y at the center column interacts considerably with the surrounding oxygen ions. An increase in covalent character of Y-O bonds in bulk Al_2O_3 has also been theoretically suggested in previous studies (*22*, *23*).

Differences between the local atomic environments at the seven-membered ring were also found from the results of the ab initio calculations. In particular, we find that the coordination of the cation site in the middle of the seven-membered ring changes notably depending on whether the site is occupied by Al or by Y. The coordination numbers can be determined by simply counting the number of nearest neighbors of a particular ion that lie within a distance of a maximum bond-length cutoff. Here, we used a cutoff of 0.22 nm for the Al-O bonds and 0.29 nm for the Y-O bonds, which were determined in a previous study (*24*). By using the relaxed structures from the ab initio calculations, we exemplify (Fig. 4, A and B) the coordination changes through ball and stick illustrations of the seven-membered rings for the undoped and the Y-doped, respectively. Because the illustrations are two-dimensional projections of three-dimensional structures, it may be difficult to determine the coordination number from these figures alone. The reported coordination numbers were thus obtained from the numerical data. Additional illustrations (fig. S1) show the bonding from a different perspective. In the undoped case, for the four distinct Al ions that are found along the central column in the center of the seven-member ring, we find that one Al site is only fourfold coordinated and the remaining three sites are only fivefold coordinated with neighboring O ions according to the cutoff criteria, less than the sixfold coordination in the bulk. The central Al ions do not lie at the exact center of the seven-membered ring but are attracted toward the region that contains a higher concentration of oxygen ions, preventing some oxygen ions on the opposite side of the seven-membered ring from forming bonds. However, when these undercoordinated Al ions are all replaced by Y ions, the larger Y ions remain near the center of the seven-membered ring, forming more bonds and thus allowing the coordination to increase to sixfold for one of the ions and to sevenfold for the remaining three ions. Such increases in the coordination numbers of Y in the center of the seven-membered ring contribute to lowering the GB energy.

The actual mechanism for GB creep is still not well understood, although a number of models have been proposed (*25*, *26*). However, no matter which mechanism is correct, atomic bonds must continuously be broken and reformed as the two grains move with respect to each other. Therefore, GBs containing a larger number of bonds and higher bond strength should exhibit a higher creep resistance than that for a boundary with fewer and/or weaker bonds. Looking at the structure of the pristine GB, we find that the seven-membered rings have fewer bonds (lower coordination number) than the grain interior, implying that these seven-membered rings are mechanically weak points along the GB.

However, upon Y doping our results show that the large Y ions are energetically more stable at the expanded regions (in this case, the seven-membered rings). These are the same locations where, in the pristine boundary, the bonds are less in number and weaker than in the bulk. The presence of Y at these seven-membered rings increases the number of bonds, and the bond strength is increased because of the higher covalency of the Y-O bonds. This should result in a much stronger GB, which explains why the Y-doped GBs can have such a large increase to creep resistance despite the fact that only a small amount of Y is present. Similar effects are expected for other rare earth elements (e.g., La and Zr), although the degree of bond strength enhancement in the expanded regions along the GB and the increase in bonding coordination for each specific element may depend on the ion size and should play a large factor in how much the creep resistance can be increased. This mechanical strengthening of grain boundaries via rare earth doping should also be applicable to other ceramic oxides.

References and Notes

1. R. M. Cannon, W. H. Rhodes, A. H. Heuer, *J. Am. Ceram. Soc.* **63**, 46 (1980).
2. A. H. Heuer, N. J. Tighe, R. M. Cannon, *J. Am. Ceram. Soc.* **63**, 53 (1980).
3. A. H. Chokshi, *J. Mater. Sci.* **25**, 3221 (1990).
4. J. Cho, M. P. Harmer, M. Chan, J. M. Rickman, A. M. Thompson, *J. Am. Ceram. Soc.* **80**, 1013 (1997).
5. H. Yoshida, Y. Ikuhara, T. Sakuma, *J. Mater. Res.* **13**, 2597 (1998).
6. K. Matsunaga, H. Nishimura, H. Muto, T. Yamamoto, Y. Ikuhara, *Appl. Phys. Lett.* **82**, 1179 (2003).
7. According to coincidence site lattice theory, a Σ31 [0001] tilt grain boundary is representative of a high angle random GB.
8. F. R. Chen, C. C. Chu, J. Y. Wang, L. Chang, *Philos. Mag. A* **72**, 529 (1995).
9. T. Höche, P. R. Kenway, H. J. Kleebe, M. Rühle, P. A. Morris, *J. Am. Ceram. Soc.* **77**, 339 (1994).
10. Y. Ikuhara, T. Watanabe, T. Saito, H. Yoshida, T. Sakuma, *Mater. Sci. Forum* **294**, 273 (1999).
11. K. Mastunaga, H. Nishimura, T. Saito, T. Yamamoto, Y. Ikuhara, *Philos. Mag. A* **83**, 4071 (2003).
12. H. Nishimura, K. Matsunaga, T. Saito, T. Yamamoto, Y. Ikuhara, *J. Am. Ceram. Soc.* **86**, 574 (2003).
13. T. Gemming, S. Nufer, W. Kurtz, M. Ruhle, *J. Am. Ceram. Soc.* **86**, 581 (2003).
14. A. G. Marinopoulos, C. Elsässer, *Acta Mater.* **48**, 4375 (2000).
15. D. E. Jesson, S. J. Pennycook, *Proc. R. Soc. London Ser. A* **441**, 261 (1993).
16. P. M. Voyles, D. A. Muller, J. L. Grazul, P. H. Citrin, H. J. L. Gossmann, *Nature* **416**, 826 (2002).
17. G. Duscher, M. F. Chisholm, U. Alber, M. Ruhle, *Nat. Mater.* **3**, 621 (2004).
18. Information on materials and methods can be found on *Science* Online.
19. J. D. Gale, *General Utility Lattice Program* (Royal Institution of Great Britain, London, 1993).
20. C. R. A. Catlow, R. James, *Phys. Rev. B* **25**, 1006 (1982).
21. G. V. Lewis, C. R. A. Catlow, *J. Phys. C* **18**, 1149 (1964).
22. S. Fabris, C. Elsässer, *Acta Mater.* **51**, 71 (2003).
23. J. Chen, Y. N. Xu, P. Rulis, L. Z. Ouyang, W. Y. Ching, *Acta Mater.* **53**, 403 (2005).
24. W. Y. Ching *et al.*, *Phys. Rev. B* **59**, 12815 (1999).
25. M. F. Ashby, *Surf. Sci.* **31**, 498 (1972).
26. A. D. Sheikh-Ali, J. A. Szpunar, *Mater. Sci. Eng. A* **245**, 49 (1998).
27. This work was supported in part by the Japanese Society for the Promotion of Science (JSPS). W.Y.C. is supported by U.S. Department of Energy (DOE) under grant no. DE-FG02-84DR45170. This research used the supercomputing resources supported by Office of Science and DOE.

Supporting Online Material

www.sciencemag.org/cgi/content/full/311/5758/212/DC1
Materials and Methods
Fig. S1
References

6 September 2005; accepted 6 December 2005
10.1126/science.1119839

Ion Distributions near a Liquid-Liquid Interface

Guangming Luo,[1] Sarka Malkova,[1] Jaesung Yoon,[1] David G. Schultz,[1,2] Binhua Lin,[3] Mati Meron,[3] Ilan Benjamin,[4] Petr Vanýsek,[5] Mark L. Schlossman[1,2]*

Mean field theories of ion distributions, such as the Gouy-Chapman theory that describes the distribution near a charged planar surface, ignore the molecular-scale structure in the liquid solution. The predictions of the Gouy-Chapman theory vary substantially from our x-ray reflectivity measurements of the interface between two electrolyte solutions. Molecular dynamics simulations, which include the liquid structure, were used to calculate the potential of mean force on a single ion. We used this potential of mean force in a generalized Poisson-Boltzmann equation to predict the full ion distributions. These distributions agree with our measurements without any adjustable parameters.

Ion distributions in electrolyte solutions near charged interfaces underlie processes as diverse as electron and ion transfer at biomembranes and redox processes at mineral-solution interfaces and also influence many practical applications in analytical chemistry and electrochemistry. Ion distributions near a charged, planar surface can be predicted by Gouy-Chapman theory, which solves the Poisson-Boltzmann equation with simplifying assumptions (*1*, *2*). This theory considers point-like ions interacting via their mean field in a solvent that is treated as a structureless continuum, ignoring its molecular-scale structure.

Extensive development of theory has addressed the limitations of the Gouy-Chapman theory (*3*) and predicted that deviations are largely a result of the difference between the interfacial and the bulk liquid structure. However, few experimental probes are directly sensitive to the structure near the charged interface, and the limits of the validity of the Gouy-Chapman theory have not been properly tested. Our structural measurements, which demonstrate the failure of Gouy-Chapman theory, are in agreement with predictions based upon a molecular dynamics simulation that includes the effects of interfacial liquid structure.

The Poisson-Boltzmann equation is used to describe ion distributions near electrified interfaces:

$$\frac{d}{dz}\varepsilon(z)\frac{d}{dz}\phi(z) = -\sum_i e_i c_i^{o} \exp[-\Delta E_i(z)/k_B T] \quad (1)$$

where $\phi(z)$ is the electric potential at a distance z from the interface, $\varepsilon(z)$ is the permittivity function, e_i and c_i^{o} are the charge and bulk concentration of ion i, respectively, $\Delta E_i(z)$ is the energy of ion i relative to the bulk phase, and $k_B T$ is Boltzmann's constant times the temperature. The Gouy-Chapman or Debye-Hückel theories of ion distributions assume that E_i depends only upon the electrostatic energy, such that $E_i(z) = e_i\phi_i(z)$, and that the permittivity function is given by a constant bulk value, $\varepsilon(z) \equiv \varepsilon$. However, structural properties of the liquid, such as the ion or solvent sizes and interactions between ions and solvent molecules, that are ignored can lead to packing effects and correlations (ion-solvent, solvent-solvent, and ion-ion) that influence the ion free energy. The liquid structure can be included formally by expressing $E_i(z)$ as $E_i(z) = e_i\phi_i(z) + f_i(z)$, where $f_i(z)$ is a free energy profile of ion i that describes the correlations (*4*, *5*). We show that the potential of mean force calculated by molecular dynamics (MD) simulations for a single ion in a solvent near an interface can be a good approximation for $f_i(z)$.

Classical electrochemical measurements have discovered inadequacies in the Gouy-Chapman theory. Capacitance measurements as a function of applied bias potential at the liquid-liquid interface depend upon the ionic species (*6*), in contradiction with the Gouy-Chapman theory, for which only the ionic charge is relevant. In addition, the shape and the magnitude of the capacitance as a function of interfacial potential are often in disagreement with Gouy-Chapman theory (*7*, *8*). A Stern layer of preferentially adsorbed solvent molecules or ions is often used to explain measurements at the solid electrode–electrolyte solution interface (*9*). The Gouy-Chapman-Stern theory includes the adsorbed layer plus the diffuse ion distribution described by the Gouy-Chapman theory. Preferential adsorption of ions can occur at the liquid-liquid interface, although tension measurements demonstrate that this does not occur for the samples studied here (*10*).

Few experimental techniques can probe ion distributions in solutions near interfaces. The surface scattering of x-rays and neutrons is, in principle, sensitive to this distribution. In particular, several x-ray studies have explored the electrical double layer for different geometries. Bedzyk *et al.* used long-period x-ray standing waves to study the double layer adjacent to a charged phospholipid monolayer adsorbed onto a solid surface (*11*). Their data were consistent with an adsorbed Stern layer and a diffuse layer described by the linearized Gouy-Chapman theory, which predicts an exponentially decaying charge distribution.

A number of x-ray studies have probed the structure of the Stern layer due to counterion adsorption to a Langmuir monolayer on the surface of water but did not make conclusions about the diffuse (or Gouy-Chapman) part of the ionic distribution (*12*–*14*). One of these studies (*14*) suggested the presence of additional ions further from the surface than the Stern layer. Fenter *et al.* used Bragg x-ray standing waves and surface x-ray absorption spectroscopy to probe the structure within the adsorbed (Stern) layer of an electrolyte solution on a mineral surface. They determined (*15*) roughly the partitioning of the ions between the adsorbed layer and the diffuse charge layer but could not probe the form of the ion distribution. Recent small-angle x-ray scattering studies of counterion condensation around DNA found agreement with solutions of the nonlinear Poisson-Boltzmann equation for this geometry that included an atomic model of the DNA (*16*). Further studies by this same group (*17*) provided indirect evidence that ion size needs to be considered in the Poisson-Boltzmann treatment.

The liquid-liquid interface has several advantages over other interfaces for the investigation of ion distributions. It does not impose an external structure on the adjacent liquid as might be expected from the atomic-scale corrugations on a solid surface. A solid surface or a Langmuir monolayer on the water surface often has bound charges whose charge density is unknown but must be determined by the experiment in addition to determining the diffuse ion distribution. Also, the use of large organic ions in the organic phase at a liquid-liquid interface is advantageous for structural determination.

We formed liquid-liquid interfaces between an aqueous solution of hydrophilic ions and a polar organic solution of hydrophobic ions. The ions form back-to-back electrical double layers. Solutions were prepared at a concentration of 0.01 M tetrabutylammonium tetraphenylborate (TBATPB) in nitrobenzene and concentrations of 0.01, 0.04, 0.05, 0.057, and 0.08 M tetrabutylammonium bromide (TBABr) in purified water (*18*). Upon equilibration, the ions partition between the two phases until the electrochemical potential for each ion is equal in both phases. Use of a common ion, in this case TBA^+, whose concentration in both bulk phases is comparable, allows the electric potential across the liquid-liquid interface to be varied by adjusting the concentration of TBABr at a fixed concentration of TBATPB (*19*). We calculated the ion partitioning and the interfacial electric potential with the use of the Nernst equation and the standard Gibbs free energy of transfer of an ion from water to nitrobenzene (table S1) (*18*).

[1]Department of Physics, [2]Department of Chemistry, University of Illinois at Chicago, Chicago, IL 60607, USA. [3]Center for Advanced Radiation Sources, University of Chicago, Chicago, IL 60637, USA. [4]Department of Chemistry, University of California, Santa Cruz, CA 95064, USA. [5]Department of Chemistry and Biochemistry, Northern Illinois University, DeKalb, IL 60115, USA.

*To whom correspondence should be addressed. E-mail: schloss@uic.edu

X-ray reflectivity from the liquid-liquid interface was measured at the Chemistry and Materials section of the Consortium for Advanced Radiation Sources (ChemMatCARS) beamline 15-ID at the Advanced Photon Source (APS, at Argonne National Laboratory) with measurement techniques described in detail elsewhere (*18*). The kinematics of specular reflectivity are illustrated in the inset to Fig. 1. The reflectivity data were measured as a function of the wave vector transfer normal to the interface, $Q_z = (4\pi/\lambda)\sin\alpha$ (the in-plane wave vector components $Q_x = Q_y = 0$, where $\lambda = 0.41360 \pm 0.00005$ Å is the x-ray wavelength and α is the angle of reflection). Figure 1 illustrates the reflectivity data for all of the concentrations studied.

The structure of the liquid-liquid interface is determined by the distribution of ions and solvent molecules and includes the effect of capillary wave fluctuations of the interface. X-ray reflectivity probes the electron density profile of this distribution, where the profile $\langle\rho(z)\rangle_{xy}$ is the electron density as a function of depth (along the z axis) that is averaged over the region of the x-ray footprint that lies in x-y plane of the interface. The Gouy-Chapman theory and a computer simulation were both used to predict ion distributions from which electron density profiles were computed. The reflectivity was calculated from the electron density profiles by using the Parratt formalism and then compared with the measurements (*20*).

The analytic solution to Eq. 1, when $E_i(z) = e_i\phi_i(z)$ and $\varepsilon(z) \equiv \varepsilon$, is the nonlinear Gouy-Chapman theory (*21*). The calculated ion distribution is the concentration along the interfacial normal, $c_i(z) = c_i^o \exp[-\Delta E_i(z)/k_BT]$ for ion i, and is illustrated for the 0.08 M TBABr sample (Fig. 2A). The intrinsic electron density profile $\rho_{intrinsic}(z) = \rho_{solvent} + \sum_i c_i(z)(N_i - v_i\rho_{solvent})$ is calculated from the distributions $[c_i(z)]$ for ion i, from the number of electrons (N_i) for ion i, the ion volume (v_i) in the solution, and the electron density of the solvent ($\rho_{solvent}$). The ions were modeled as spheres with diameters of 3.7 Å for Br^-, 8.6 Å for TBA^+, and 9.5 Å for TPB^-, where the charge is taken to be at the center of the sphere (*22*, *23*). The diameters for Br^- and TBA^+ were determined from our MD simulations of the radial distribution functions and are consistent with literature values (*22*). This electron density profile is referred to as an intrinsic profile because it does not include the effect of capillary waves.

The electron density profile $\langle\rho(z)\rangle_{xy}$ that includes the effect of capillary waves can be calculated by convoluting the intrinsic electron density profile with a Gaussian of width σ_{cap},

$$\langle\rho(z)\rangle_{xy} = \frac{1}{\sigma_{cap}\sqrt{2\pi}} \times \int_{-\infty}^{\infty} \rho_{intrinsic}(z')\exp[-(z - z')^2/2\sigma_{cap}^2]dz' \quad (2)$$

The interfacial width σ_{cap} is calculated from capillary wave theory by using the measured interfacial tension as described previously (*18*, *24*). The tension was measured by using a teflon Wilhelmy plate fully submerged in the water phase (Table 1). We assume that the local ion and solvent distributions are not distorted by the presence of capillary waves. This assumption is expected to be reasonable except for very short wavelength capillary waves (on the order of a bulk correlation length) or very concentrated solutions (*25*, *26*).

The electron density $\langle\rho(z)\rangle_{xy}$ calculated from the Gouy-Chapman model for the 0.08 M TBABr sample is shown in Fig. 3. Although the ion distributions in Fig. 2A are discontinuous, the electron density profile is continuous because of the effects of capillary waves.

The reflectivities calculated from the Gouy-Chapman model are shown as dashed lines in Fig. 1. This model matches the reflectivity data at the lowest concentration but progressively differs from the data with increasing concentration until reaching a difference of 25 standard deviations at the highest concentration. A variation of the Gouy-Chapman theory, the modified Verwey-Niessen model (*10*), which describes the liquid-liquid interface as consisting of two back-to-back, ion-free solvent layers that separate the Gouy-Chapman ion distributions, also fails to describe our data (*27*).

To include liquid structure in the calculation of the ion distributions, we take the energy $E_i(z)$ in Eq. 1 to be $E_i(z) = e_i\phi_i(z) + f_i(z)$. A model for $f_i(z)$ is provided by the potential of mean force calculated by MD simulations. The potential of mean force is determined by calculating the mean force on a single ion positioned at different distances from the interface between pure water and pure nitrobenzene (*18*). The exact $E_i(z)$ requires the consideration of ion-ion interactions, but this is not computationally feasible at present. Instead, we approximate $E_i(z)$ by a sum of the electrostatic term $e_i\phi_i(z)$ plus the potential of mean force for a single ion (*28*).

The potentials of mean force for TBA^+ and Br^- at the nitrobenzene-water interface are shown in Fig. 4. Ions can penetrate and transfer through a liquid-liquid interface as illustrated by the continuity of the potential of mean force in Fig. 4. The ion diameter and hydration and solvation effects contribute to the distance required for the potential of mean force

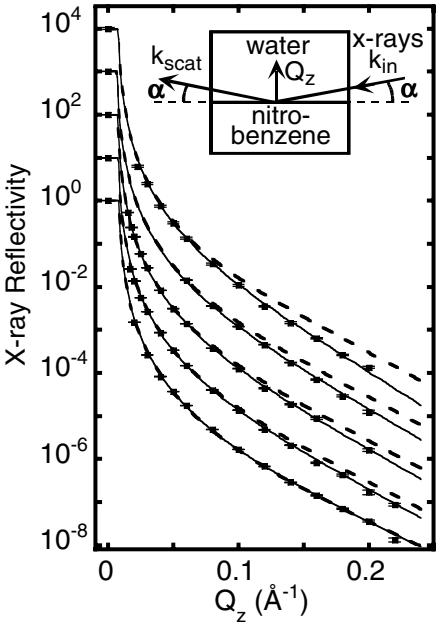

Fig. 1. X-ray reflectivity, $R(Q_z)$, as a function of wave vector transfer Q_z from the interface between a 0.01 M solution of TBATPB in nitrobenzene and a solution of TBABr in water at five concentrations (0.01, 0.04, 0.05, 0.057, and 0.08 M, bottom to top) at a room temperature of 24° ± 0.5°C. Solid lines are predictions using the potential of mean force from MD simulations. Dashed lines are predicted by the Gouy-Chapman model. No parameters have been adjusted in these two models. Data for different concentrations are offset by factors of 10 ($R = 1$ at $Q_z = 0$). Error bars are indicated by horizontal lines through the square data points and are usually much smaller than the size of the squares. The points at $Q_z = 0$ are measured from transmission through the bulk aqueous phase. **(Inset)** The kinematics of x-ray reflectivity: $\mathbf{k}_{in}$, incoming x-ray wave vector; $\mathbf{k}_{scat}$, scattered wave vector; and α, angles of incidence and reflection.

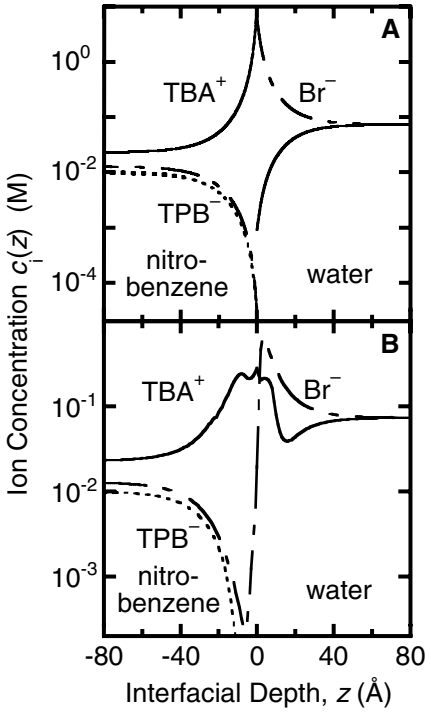

Fig. 2. Ion distributions at the interface between a 0.08 M TBABr solution in water and a 0.01 M TBATPB solution in nitrobenzene. Solid lines, TBA^+; short-long dashed line, Br^-; short dashed line, TPB^-. **(A)** Gouy-Chapman theory. **(B)** Calculation from MD simulation of the potential of mean force.

Table 1. Interfacial tension γ and capillary width of the samples. Samples are labeled by the initial concentration (in M) of TBABr in water. Tension values agree with literature measurements (*19*).

	0.01 M	0.04 M	0.05 M	0.057 M	0.08 M
γ (10^{-3} N/m) ($\pm$0.1)	19.6	15.7	14.8	14.7	13.0
σ_{cap} (Å)	5.8	6.5	6.7	6.8	7.2

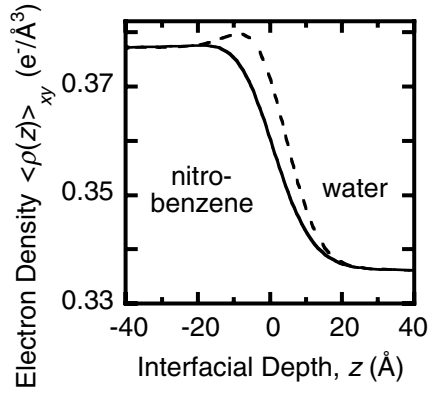

Fig. 3. Electron density, $\langle \rho(z) \rangle_{xy}$, as function of depth through the interface between a 0.08 M TBABr solution in water and a 0.01 M TBATPB solution in nitrobenzene. Dashed line, calculation from Gouy-Chapman model; solid line, calculation from MD simulation of the potential of mean force.

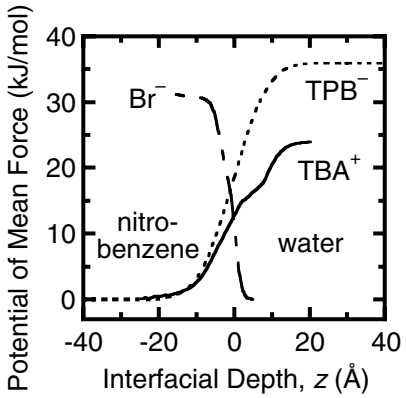

Fig. 4. Potential of mean force for TBA^+ (solid line) and Br^- (short-long dashed line) at the nitrobenzene-water interface calculated from MD simulations. The function for TPB^- (short dashed line) is provided by an analytic model (*18*). The potential of mean force for ion transfer is calculated by using the integral of the average force acting on the ion center of mass: $\Delta A = A_2 - A_1 = -\int_{z_1}^{z_2} \langle F_z(z) \rangle dz$, where F_z is the projection along the z axis of the total force acting on the ion's center of mass (*18*).

to cross from one bulk value to the other. We have not calculated the potential of mean force for TPB^- ions, so we postulated a simple functional form for TPB^- that has these qualitative features (Fig. 4) (*18*). Because the interfacial concentration of TPB^- is small, the electron density calculation is not sensitive to this function.

The electric potential $\phi(z)$ is calculated by solving Eq. 1 numerically (*29*) with the use of the functions $f_i(z)$ for TBA^+, TPB^-, and Br^- displayed in Fig. 4, setting $E_i(z) = e_i\phi_i(z) + f_i(z)$, and approximating $\varepsilon(z) \equiv \varepsilon$. Figure 2B illustrates the ion distributions calculated from $c_i(z) = c_i^o \exp[-\Delta E_i(z)/k_B T]$ for the 0.08 M TBABr sample. Lower concentrations exhibit qualitatively similar distributions but with lower ion adsorption, as expected from the variation in tension (Table 1). The distributions far from the interface are similar to those predicted by the Gouy-Chapman theory (Fig. 2A) but differ substantially in both amplitude and form near the interface. Broadening of the ion distributions at the interface is expected from the finite sizes of the ions and solvent molecules. For TBA^+, the enhanced broadening on the water side of the interface is a result of the reduced slope in the potential of mean force in that region, most likely caused by resistance of the ion to lose its hydration shell. Also, the ion distributions in Fig. 2B vary continuously across the interface because the MD simulation allows for ion penetration through the interface, in contrast to the interfacial discontinuity present in the Gouy-Chapman distributions.

The electron density profile $\langle \rho(z) \rangle_{xy}$ calculated from the ion distributions in Fig. 2B is illustrated in Fig. 3. As anticipated from the underlying ion distributions, the electron density near the interface is smaller than that predicted by the Gouy-Chapman theory. Figure 1 demonstrates that the reflectivities calculated from these electron densities match the measured reflectivities closely. We emphasize that this is not a fit and that there are no adjustable parameters. This analysis allows the data from samples of five different concentrations, which have different ion distributions, to be explained by the potentials of mean force $f_i(z)$ for each ion.

The agreement between the predictions of the MD simulation and the x-ray measurements indicates that the aspects of liquid structure included in the MD simulations, such as ion sizes and ion-solvent interactions, alter the ion distributions. The MD simulations do not include ion-ion correlations that at high concentrations are expected to lead, for example, to the formation of interfacial ion pairs. Our results suggest that these correlations do not substantially affect the ion distributions probed in this experiment, most likely because the correlations are weak at the concentrations of our samples.

This work provides a method for including liquid structure in the analysis of structural measurements of ion distributions near charged or electrified interfaces. This method allows the potentials of mean force produced by MD simulations or analytic theory to be tested by experiment. We anticipate that this method can also be applied to study ion distributions near charged solid surfaces, liquid-vapor interfaces, and the surfaces of charged biomolecules. A number of fundamental phenomena that alter the form of the potential of mean force remain to be tested at the liquid-liquid interface. These include the existence of water fingering, predicted by MD simulations to occur when strongly hydrated ions pass from the aqueous to the organic phase (*30*), and the existence of a barrier for ion transfer across the interface.

References and Notes

1. G. Gouy, *C. R. Acad. Sci.* **149**, 654 (1910).
2. D. L. Chapman, *Philos. Mag. Ser. 6* **25**, 475 (1913).
3. S. Levine, C. W. Outhwaite, L. B. Bhuiyan, *J. Electroanal. Chem.* **123**, 105 (1981).
4. J. G. Kirkwood, *J. Chem. Phys.* **2**, 767 (1934).
5. L. I. Daikhin, A. A. Kornyshev, M. Urbakh, *J. Electroanal. Chem.* **500**, 461 (2001).
6. H. H. Girault, in *Modern Aspects of Electrochemistry*, J. O. M. Bockris, Ed. (Plenum, New York, 1993), vol. 25, p. 1.
7. Z. Samec, V. Marecek, D. Homolka, *J. Electroanal. Chem.* **187**, 31 (1985).
8. C. M. Pereira, A. Martins, M. Rocha, C. J. Silva, F. Silva, *J. Chem. Soc. Faraday Trans.* **90**, 143 (1994).
9. O. Stern, *Z. Elektrochem. Angew. Phys. Chem* **30**, 508 (1924).
10. C. Gavach, P. Seta, B. d'Epenoux, *J. Electroanal. Chem.* **83**, 225 (1977).
11. M. J. Bedzyk, G. M. Bommarito, M. Caffrey, T. L. Penner, *Science* **248**, 52 (1990).
12. J. M. Bloch *et al.*, *Phys. Rev. Lett.* **61**, 2941 (1988).
13. F. Leveiller *et al.*, *Science* **252**, 1532 (1991).
14. D. Vaknin, P. Kruger, M. Losche, *Phys. Rev. Lett.* **90**, 178102 (2003).
15. P. Fenter *et al.*, *J. Colloid Interface Sci.* **225**, 154 (2000).
16. R. Das *et al.*, *Phys. Rev. Lett.* **90**, 188103 (2003).
17. K. Andresen *et al.*, *Phys. Rev. Lett.* **93**, 248103 (2004).
18. Materials and methods are available as supporting material on *Science* Online.
19. J. D. Reid, O. R. Melroy, R. P. Buck, *J. Electroanal. Chem.* **147**, 71 (1983).
20. L. G. Parratt, *Phys. Rev.* **95**, 359 (1954).
21. W. Schmickler, *Interfacial Electrochemistry* (Oxford Univ. Press, Oxford, 1996).
22. H. Ohtaki, T. Radnai, *Chem. Rev.* **93**, 1157 (1993).
23. B. S. Krumgalz, *J. Chem. Soc. Faraday Trans.* **78**, 437 (1982).
24. D. M. Mitrinovic, A. M. Tikhonov, M. Li, Z. Huang, M. L. Schlossman, *Phys. Rev. Lett.* **85**, 582 (2000).
25. K. R. Mecke, S. Dietrich, *Phys. Rev. E* **59**, 6766 (1999).
26. L. I. Daikhin, A. A. Kornyshev, M. Urbakh, *J. Electroanal. Chem.* **483**, 68 (2000).
27. G. Luo *et al.*, data not shown.
28. Both $\phi(z)$ and $f(z)$ include the potential drop due to the neat liquid-liquid interface. We assume that the potential drop across the neat interface is much smaller than that produced by the ions.
29. D. M. Burley, V. C. L. Hutson, C. W. Outhwaite, *Mol. Phys.* **23**, 867 (1972).
30. I. Benjamin, *Science* **261**, 1558 (1993).

31. M.L.S. and P.V. acknowledge support from NSF-CHE0315691, and I.B. acknowledges support from NSF-CHE0345361. M.L.S. thanks J. Gebhardt, T. Graber, and H. Brewer for help with the ChemMatCARS ID beamline and B. Hou for assisting with the x-ray measurements. ChemMatCARS is supported by NSF-CHE, NSF-DMR, and the U.S. Department of Energy (DOE). The APS is supported by the DOE Office of Basic Energy Sciences.

Supporting Online Material

www.sciencemag.org/cgi/content/full/311/5758/216/DC1
Materials and Methods
Fig. S1
Table S1

20 September 2005; accepted 30 November 2005
10.1126/science.1120392

Femtosecond Multidimensional Imaging of a Molecular Dissociation

O. Geßner,[1] A. M. D. Lee,[1,2] J. P. Shaffer,[3] H. Reisler,[4] S. V. Levchenko,[4] A. I. Krylov,[4] Jonathan G. Underwood,[5] H. Shi,[6] A. L. L. East,[6] D. M. Wardlaw,[2] E. t. H. Chrysostom,[7] C. C. Hayden,[7] Albert Stolow[1,2]*

The coupled electronic and vibrational motions governing chemical processes are best viewed from the molecule's point of view—the molecular frame. Measurements made in the laboratory frame often conceal information because of the random orientations the molecule can take. We used a combination of time-resolved photoelectron spectroscopy, multidimensional coincidence imaging spectroscopy, and ab initio computation to trace a complete reactant-to-product pathway—the photodissociation of the nitric oxide dimer—from the molecule's point of view, on the femtosecond time scale. This method revealed an elusive photochemical process involving intermediate electronic configurations.

Chemical transformation involves the coupled motions of electrons and nuclei, leading to the flow of both charge and vibrational energy within a reacting molecule. These extremely fast processes can be studied with the use of ultrashort laser pulses, yielding important insights into the underlying dynamics [Nobel Prize lecture by Zewail (*1*); see also (*2*)]. One approach to disentangling the intrinsically coupled electronic and vibrational dynamics in excited polyatomic molecules is time-resolved photoelectron spectroscopy (TRPES) (*3*–*5*), yielding a picture of both charge and energy flow as a function of time. These measurements, however, are usually made in the laboratory frame, where averaging over the random orientations of the molecule generally leads to a loss of information. Ideally, one would prefer to observe these dynamics from the molecule's point of view rather than the laboratory point of view. One attempt to realize this is to prealign polyatomic molecules before studying their field-free dynamics (*6*–*8*). A more general approach is time-resolved coincidence imaging spectroscopy (TRCIS), which measures fully correlated photofragment and photoelectron recoil distributions as a function of time (*9*, *10*), thereby permitting dynamical observations from the molecule's point of view. Here, we used TRPES to measure lifetimes and energetics, combined with TRCIS to measure evolving charge distributions on the molecular frame, to elucidate the dynamics of a complex reaction—the ultraviolet (UV) photodissociation of the nitric oxide dimer—all the way from initial excitation to final product emission.

The small size and simple cis-planar (C_{2v}) structure of the nitric oxide dimer $(NO)_2$ belies a complex photochemistry (Fig. 1). The broad (190 to 240 nm), featureless UV spectrum (*11*, *12*) arises from a parallel transition to an ill-characterized dissociative continuum (depicted as a gray box). The dissociation yields NO monomer fragments in both the ground [NO(X)] and the first excited [NO(A)] electronic states (*13*). The NO(A) state has dominant Rydberg 3s orbital character. Unfortunately, neither the featureless absorption spectrum (*11*, *14*) nor the apparently statistical product-state distributions (*15*, *16*) offer much insight into the dynamics. More detailed product-state distributions (*17*, *18*) from $(NO)_2$ excitation just above the NO(A 3s) channel threshold confirm that the photofragment recoil direction is strongly peaked parallel to the pump laser polarization and that the excited molecule retains planar geometry during dissociation. The parallel nature of the optical transition and the fragment recoil direction dictate that the states involved are of B_2 symmetry.

Ab initio studies of the electronically excited dimer states revealed extraordinary complexity, including the existence of low-energy (infrared-resonant) states (*19*–*21*). One study established that there exist states in the gray region of Fig. 1 that are of B_2 symmetry; these states consist of a diffuse $3p_y$ Rydberg state (y axis along the N-N bond) and a localized valence state that carries the oscillator strength (*22*, *23*). Photofragment indistinguishability permits both in-phase and out-of-phase combinations of [NO(A 3s) + NO(X)] with [NO(X) + NO(A 3s)] products. As shown in Fig. 2, for C_{2v} geometry the in-phase combination would produce a dimer Rydberg 3s state of A_1 symmetry, whereas the out-of-phase combination would produce a dimer Rydberg $3p_y$ state of B_2 symmetry (where y is along the N-N bond).

Our experimental methods were as described (*9*, *24*). Briefly, a supersonic molecular beam source (15% NO in He) produced cold $(NO)_2$, which was pumped with femtosecond pulses at 209.6 nm and probed, via single-photon ionization, with femtosecond pulses at 279.5 nm. The time resolution (i.e., instrumental response function or "cross-correlation") was 160 ± 10 fs. The pump and probe laser polarizations were parallel to each other. The dynamics were monitored in two independent experiments. High-resolution time- and energy-resolved spectra were recorded with TRPES, whereas three-dimensional (3D) energy- and angle-resolved photoelectron-photoion correlations were measured with TRCIS at five specific time delays.

TRPES tracks the evolving excited state all the way from initial excitation ($\Delta t = 0$) to final

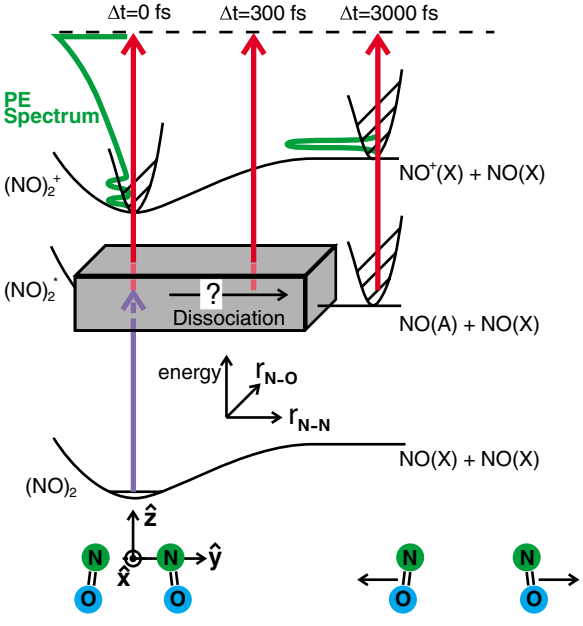

Fig. 1. Schematic representation of the femtosecond pump-probe TRPES study of the NO dimer dissociation dynamics. The gray box represents the complex region the molecule must pass through upon UV photodissociation into NO(A) + NO(X). The TRPES method monitors the complete time evolution of the excited state. Our molecular frame axis convention is shown (bottom), with the y axis along the N-N bond. The purple arrow represents the pump (excitation) laser photon. The red arrows represent the probe (ionization) laser photon that interrogates the evolving excited state, shown here at three selected time delays. The green curves represent the photoelectron kinetic energy (PE) spectrum observed after ionization at these time delays.

[1]Steacie Institute for Molecular Sciences, National Research Council Canada, Ottawa, Ontario K1A 0R6, Canada. [2]Department of Chemistry, Queen's University, Kingston, Ontario K7L 3N6, Canada. [3]Department of Physics and Astronomy, University of Oklahoma, Norman, OK 73019, USA. [4]Department of Chemistry, University of Southern California, Los Angeles, CA 90089, USA. [5]Department of Physics and Astronomy, Open University, Milton Keynes MK7 6AA, UK. [6]Department of Chemistry, University of Regina, Regina, Saskatchewan S4S 0A2, Canada. [7]Combustion Research Facility, Sandia National Laboratories, Livermore, CA 94551, USA.

*To whom correspondence should be addressed. E-mail: albert.stolow@nrc.ca

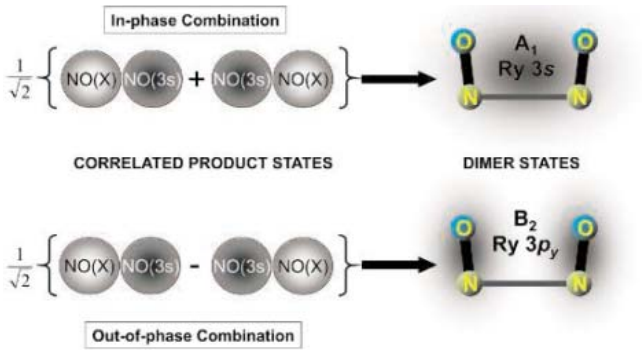

Fig. 2. A depiction of the consequences of photofragment indistinguishability. Quantum mechanically, the product states are linear combinations of [NO(X) + NO(A)] with [NO(A) + NO(X)]. As shown, the in-phase combination would correlate with an A_1 symmetry 3s Rydberg dimer state, whereas the out-of-phase combination would correlate with a B_2 symmetry $3p_y$ Rydberg dimer state (where y is the N-N bond axis). Our results indicate that the participating state is the $(NO)_2$ Rydberg $3p_y$ state.

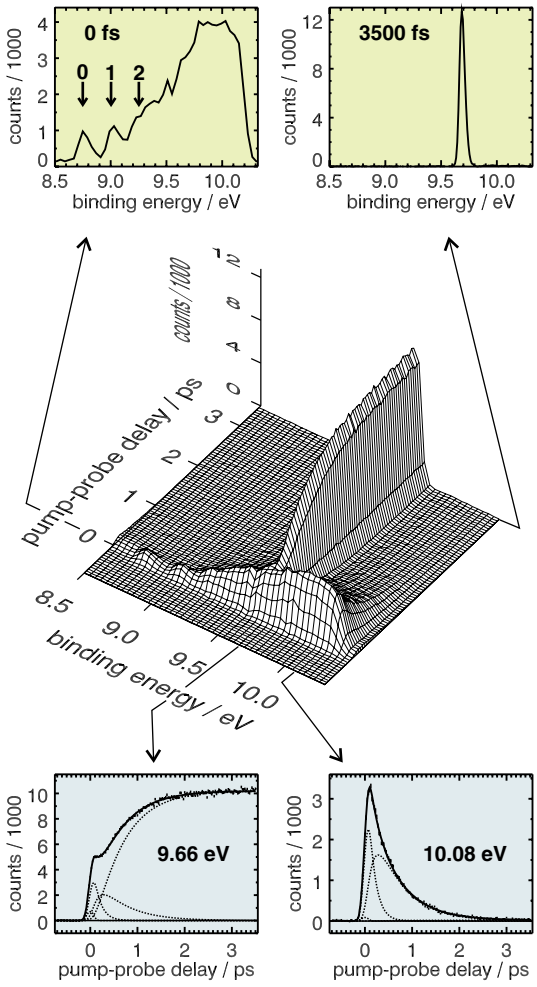

Fig. 3. A TRPES scan showing photoelectron spectra as a function of time delay in a 2D plot. The binding energy is the total photon energy (pump plus probe) minus the electron kinetic energy. The green insets (top) are examples of photoelectron spectra at two time delays. The blue insets (bottom) are examples of the evolution of the photoelectron intensity at two binding energies. Note that the 2D data are globally fit at all energies and time delays simultaneously. The solid lines in the blue graphs are from the 2D fits to a sequential two-step dissociation model. The dotted lines are the respective initial-, intermediate-, and final-state signal components plus a small instrumental response contribution.

products (Δt > 3000 fs), illuminating the obscure gray region in Fig. 1. Previous TRPES studies investigated the NO(A 3s) channel, revealing that the products emerge on the subpicosecond time scale (*25*–*28*). An early study proposed a two-step nonadiabatic mechanism (*25*), whereas later work favored a more direct process via a dimer 3s Rydberg state (*26*–*28*).

The 2D plot in Fig. 3 shows TRPES spectra of $(NO)_2$ from initial excitation to final dissociation. Cuts parallel to the binding energy axis yield the photoelectron spectrum at given time delays (green insets). Cuts parallel to the pump-probe time delay axis reveal the evolution of a given photoelectron band (blue insets). At Δt = 0, a broad spectrum due to photoionization of $(NO)_2$* shows two resolved peaks assigned to 0 and 1 quanta of the cation N=O symmetric stretch mode (v_1). The v_1 = 2 peak merges with a broad, intense Franck-Condon dissociative continuum. (Note that v_1 = 3 would be above the dissociation limit of the dimer cation.) That this broad continuum dominates the spectrum shows that $(NO)_2$* photoionization favors dissociation of the dimer. By contrast, single-photon ionization of the ground state does not (*29*), which suggests that $(NO)_2$* is geometrically distorted with respect to both the neutral and cation ground states.

At long times (Δt = 3500 fs), we see the sharp photoelectron spectrum of the free NO(A 3s) product. The 10.08-eV band shows the decay of the $(NO)_2$* excited state. The 9.66-eV band shows both the decay of $(NO)_2$* and the growth of free NO(A 3s) product. To extract dynamical information, we used nonlinear fitting procedures to globally fit the complete 2D data of Fig. 3 at all photoelectron energies and time delays simultaneously.

These data cannot be fit by single-exponential kinetics. They are fit with high accuracy by a two-step sequential model, meaning that an initial bright state $(NO)_2$* evolves to an intermediate configuration, which itself subsequently decays to yield free NO(A 3s) products. The evidence most strongly supporting the intermediate configuration is seen in the 9.66-eV electron band, showing product growth. The delayed rise of the free NO(A 3s) product cannot be fit by a single-exponential decay followed by single-exponential growth with the same time constant. The 10.08-eV dissociative ionization band, dominant at early times, is revealing of $(NO)_2$* configurations preceding dissociation. As seen in Fig. 3, its time evolution, which cannot be fit by a single-exponential decay, provides another clear view of the intermediate step.

We conclude that only two time constants in a sequential model are required to very accurately fit these 2D data at all photoelectron energies and all time delays simultaneously. The decay time of the initial state is 140 ± 30 fs, which matches the rise time of the intermediate configuration. This intermediate configuration has a subsequent decay time of 590 ± 20 fs. These two time constants result in a maximum for the intermediate configuration signal at ~330 fs delay. The two components can be seen as the dotted lines in the fits to the 10.08-eV data (along with a small instrumental response signal). In the 9.66-eV band, the dotted lines from the fits show that the rise of the NO(A 3s) product channel is first delayed by 140 ± 30 fs but then grows with a time constant of 590 ± 20 fs. We emphasize that although only two cuts are shown, the data are fit at all time delays and photoelectron energies simultaneously (*30*). In sum, we show clear evidence for an intermediate configuration in $(NO)_2$ UV photodissociation.

To identify this intermediate configuration, we applied the TRCIS method, which records the 3D recoil momentum vectors of both photoelectrons and photoions in coincidence (*9*). This 6D fully correlated data set may be cut, projected, or filtered to reveal both scalar and

vector correlations as a function of time. We restrict our discussion here to angular correlations.

The pump transition dipole is along the molecular frame *y* axis, the N-N bond axis (see Fig. 1). The pump transition therefore forms an anisotropic distribution of excited $(NO)_2$* states in the lab frame, with the N-N bond aligned along the laser polarization axis. As we are concerned with intermediate configurations in $(NO)_2$* evolution, we consider the photoionization probing of $(NO)_2$*, which leads predominantly to dissociative ionization (Fig. 3). Dissociative photoionization has long been recognized as a route to recoil or molecular-frame photoelectron angular distributions in non–time-resolved studies (*31*, *32*). The dissociative ionization of $(NO)_2$* produces NO^+ fragments strongly directed along the laser polarization axis. The NO^+ fragment recoil direction therefore indicates the lab frame direction of the N-N bond (molecular frame *y* axis) before ionization. Rotating the electron momentum vector into the fragment recoil frame on an event-by-event basis allows for reconstruction of the $(NO)_2$* photoelectron angular distribution in this recoil frame, rather than the usual lab frame. Here the recoil frame coincides with the molecular frame, differing only by azimuthal averaging about the N-N bond. Out of all fragment recoil events, we selected only those directed ("up" or "down") along the parallel pump and probe laser polarization axis. By choosing events from this selected set, we restrict the data to excited-state ionization events arising from interactions with the *y* component of the ionization transition dipole. This restriction greatly limits the allowed partial waves for the emitted electron, especially in the present case where only a single electronic continuum is accessed (*30*).

In Fig. 4 we present time-resolved lab and recoil frame photoelectron angular distributions arising from photoionization of $(NO)_2$* in the 9.9- to 10.3-eV band of Fig. 3. As can be seen, this dissociative ionization region contains significant contributions from the intermediate configuration. In general, the time dependence of photoelectron angular distributions is related to the evolution of excited-state electronic structure (*5*, *33*–*35*). Here, the lab frame photoelectron angular distributions have a largely isotropic character that shows little time evolution, obscuring information about excited-state dynamics. By contrast, the recoil frame photoelectron angular distributions show a highly anisotropic character and a variation with time delay. The solid lines in the polar plots of Fig. 4 are fits to Legendre polynomials (*36*).

The recoil frame photoelectron angular distributions have dominant intensity perpendicular to the laser polarization axis. An A_1 Rydberg 3s intermediate state would most likely yield maximum intensity parallel to the laser polarization axis, contrary to what is observed. This rules out the A_1 Rydberg 3s state as the intermediate configuration. We used states of B_2 symmetry to model the recoil frame photoelectron angular distributions, a choice corroborated by our ab initio calculations. We also presumed that the molecule largely retains C_{2v} symmetry, an assumption consistent with the observed retention of planarity during dissociation (*17*).

Proceeding further required a detailed analysis of the photoelectron angular distributions (*36*). The outgoing free electrons are described in terms of their angular momenta by the so-called partial waves, using spherical harmonics labeled by the quantum numbers *l* and *m*. For example, in the atomic limit, a Rydberg p-state would produce s and d partial waves upon single-photon ionization ($\Delta l = \pm 1$). In the molecular case, we decompose the free-electron wave function into symmetry-adapted spherical harmonics (*35*). For C_{2v}, these harmonics are described by their C_{2v} symmetry and by $l_{|\lambda|}$, where *l* and $|\lambda|$ are the orbital angular momentum and projection quantum numbers, respectively. Values of $l = 0, 1, 2\ldots$ are labeled s, p, d, …, whereas values of $|\lambda| = 0, 1, 2, \ldots$ are labeled σ, π, δ, … In our case, ionization of a B_2 electronic state to an A_1 cation state via a *y*-polarized transition means that the free

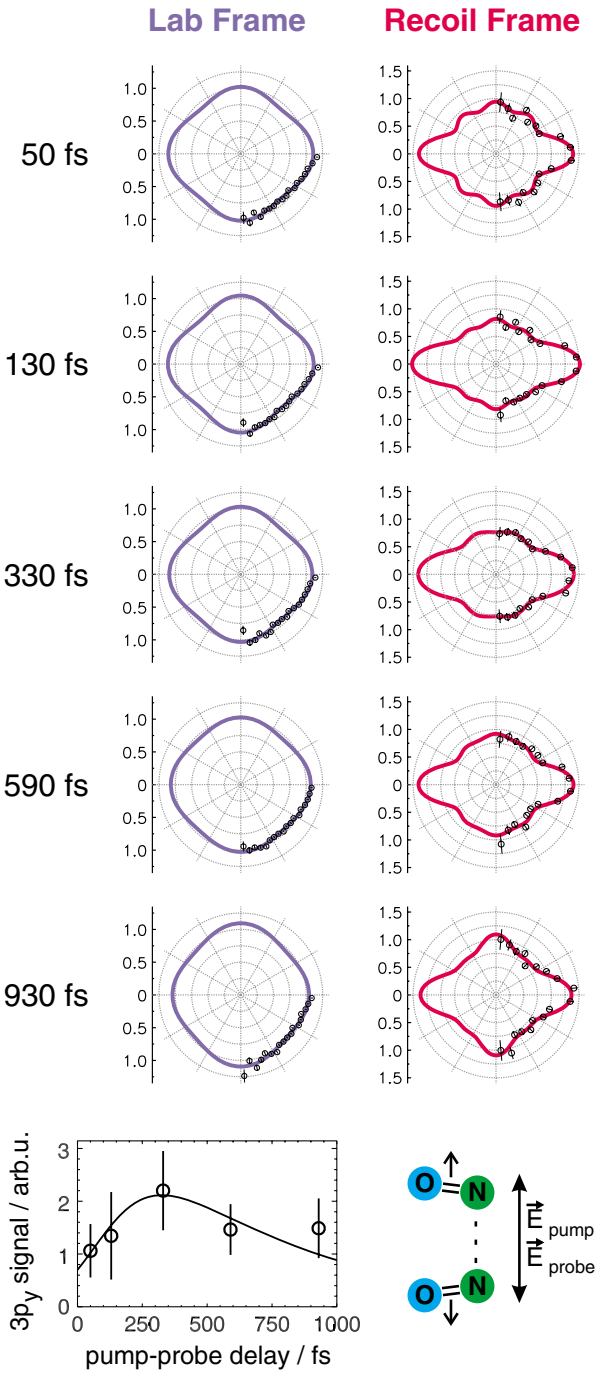

Fig. 4. A TRCIS study showing lab frame (**left**) and recoil frame (**right**) photoelectron angular distributions (PADs) from the 9.9- to 10.3-eV dissociative ionization region of Fig. 3. The laser polarizations and recoil frame axes are along the *y* direction, as shown (**bottom right**). The lab frame PADs show featureless and almost invariant behavior. The recoil frame PADs show strong anisotropies that vary with time. The fit curves (solid lines) include even-order Legendre polynomials P_L up to $L = 4$ for the lab frame and up to $L = 8$ for the recoil frame. The average partial wave contribution expected from Rydberg $3p_y$ ionization is plotted at the lower left as a function of time. The time dependence of the intermediate configuration extracted from Fig. 3 is plotted here as the solid line, agreeing well with the time dependence of the $3p_y$ ionization contribution. This confirms the intermediate configuration as being of Rydberg $3p_y$ character.

electron must have A_1 symmetry, significantly restricting the allowed free-electron states. The A_1 symmetry partial waves are s_σ, p_σ, d_σ, d_δ, f_σ, f_δ, g_σ, g_δ, and g_γ. Our modeling of the data is not unique, and the individual partial wave contributions varied depending on the model input parameters. In general, the s, p, and d partial waves were dominant. To obviate the dependence of our conclusions on any specific partial wave amplitude, we contracted the amplitudes into two sets: those expected from $3p_y$ ionization and those not. Ionization of a dimer $3p_y$ Rydberg state via a *y*-polarized transition would produce only electrons with s_σ, d_σ, and d_δ character. Therefore, the ratio of $(s_\sigma + d_\sigma + d_\delta)$ to the sum of all other contributions Σ_{pfg} is a measure of $3p_y$ Rydberg character in the $(NO)_2$* excited electronic states. At the bottom of Fig. 4 we plot the time dependence of this ratio, labeled "$3p_y$ signal"; this plot shows that dimer $3p_y$ Rydberg character rises from early times, peaks at ~330 fs, and subsequently falls. The solid curve is the time dependence of the intermediate configuration extracted from Fig. 3, showing that the $3p_y$ character follows the time behavior of the intermediate configuration. The agreement substantiates the intermediate configuration as being of $3p_y$ character.

Our ab initio studies fully support this picture (*36*). Briefly, a very bright diabatic charge transfer (valence) state carries the transition oscillator strength. At our pump photon energy, a vibrationally excited (we roughly estimate $v_1 \sim 4$) adiabatic $(NO)_2$* state of mixed charge-transfer/Rydberg character is populated. This quickly evolves, via N=O stretch dynamics, toward increasing $3p_y$ Rydberg character. The 140-fs initial decay constant is the time scale for the initial valence state to develop intermediate $3p_y$ character and explains the emergence of $3p_y$ ionization dynamics seen in Fig. 4 at intermediate time scales. The 590-fs sequential time constant is the time scale for evolution of the dimer $3p_y$ configuration to free products via intramolecular vibrational energy redistribution, coupling the N=O stretch to the low-frequency N-N stretch (*37*). The dimer $3p_y$ state adiabatically correlates to free NO(A 3s) + NO(X) products. Finally, a dimer A_1 Rydberg 3s state was found at lower energy than the bright valence state but does not cross the latter in the Franck-Condon region.

The dynamics of excited polyatomic molecules generally involves the complex mixing of electronic states. Here we studied the case of Rydberg-valence mixing in a molecular dissociation, a situation found in the photochemistry of higher excited states of molecules. By placing ourselves in the frame of the molecule, we are able to observe new details of the evolution of the electronic states that cannot be extracted from lab frame measurements alone. We expect that multidimensional femtochemistry, seen from the molecule's point of view, will shed light on the dynamical evolution of increasingly complex chemical processes.

References and Notes

1. A. H. Zewail, *Angew. Chem. Int. Ed.* **39**, 2586 (2000).
2. A. Stolow, D. M. Jonas, *Science* **305**, 1575 (2004).
3. V. Blanchet, M. Z. Zgierski, T. Seideman, A. Stolow, *Nature* **401**, 52 (1999).
4. A. Stolow, *Annu. Rev. Phys. Chem.* **54**, 89 (2003).
5. A. Stolow, A. E. Bragg, D. M. Neumark, *Chem. Rev.* **104**, 1719 (2004).
6. H. Stapelfeldt, T. Seideman, *Rev. Mod. Phys.* **75**, 543 (2003).
7. J. G. Underwood, B. J. Sussman, A. Stolow, *Phys. Rev. Lett.* **94**, 143002 (2005).
8. T. P. Rakitzis, A. J. van den Brom, M. H. M. Janssen, *Science* **303**, 1852 (2004).
9. J. A. Davies, J. E. LeClaire, R. E. Continetti, C. C. Hayden, *J. Chem. Phys.* **111**, 1 (1999).
10. J. A. Davies, R. E. Continetti, D. W. Chandler, C. C. Hayden, *Phys. Rev. Lett.* **84**, 5983 (2000).
11. J. Billingsley, A. B. Callear, *Trans. Faraday Soc.* **67**, 589 (1971).
12. E. Forte, H. van den Berg, *Chem. Phys.* **30**, 325 (1978).
13. O. Kajimoto, K. Honma, T. Kobayashi, *J. Chem. Phys.* **89**, 2725 (1985).
14. V. Dribinski, A. B. Potter, I. Fedorov, H. Reisler, *Chem. Phys. Lett.* **385**, 233 (2004).
15. Y. Naitoh, Y. Fujimura, K. Honma, O. Kajimoto, *Chem. Phys. Lett.* **205**, 423 (1993).
16. Y. Naitoh, Y. Fujimura, K. Honma, O. Kajimoto, *J. Phys. Chem.* **99**, 13652 (1995).
17. A. V. Demyanenko, A. B. Potter, V. Dribinski, H. Reisler, *J. Chem. Phys.* **117**, 2568 (2002).
18. A. B. Potter, V. Dribinski, A. V. Demyanenko, H. Reisler, *J. Chem. Phys.* **119**, 7197 (2003).
19. A. L. L. East, *J. Chem. Phys.* **109**, 2185 (1998).
20. R. Sayos, R. Valero, J. M. Anglada, M. Gonzalez, *J. Chem. Phys.* **112**, 6608 (2000).
21. M. Tobita *et al.*, *J. Chem. Phys.* **119**, 10713 (2003).
22. S. V. Levchenko, A. I. Krylov, as reported in (*14*).
23. Our C_{2v} *y* axis lies along the N-N bond, following Herzberg's convention. Our earlier paper (*14*) used the alternate convention, and there the N-N bond was called the *x* axis. No conclusions depend on the axis convention used.
24. S. Lochbrunner *et al.*, *J. Electron Spectrosc. Relat. Phenom.* **112**, 183 (2000).
25. V. Blanchet, A. Stolow, *J. Chem. Phys.* **108**, 4371 (1998).
26. M. Tsubouchi, C. A. de Lange, T. Suzuki, *J. Chem. Phys.* **119**, 11728 (2003).
27. M. Tsubouchi, T. Suzuki, *Chem. Phys. Lett.* **382**, 418 (2003).
28. M. Tsubouchi, C. A. de Lange, T. Suzuki, *J. Electron Spectrosc. Relat. Phenom.* **142**, 193 (2005).
29. F. Carnovale, J. B. Peel, R. G. Rothwell, *J. Chem. Phys.* **84**, 6526 (1986).
30. The amplitudes of all fit functions vary smoothly and continuously as a function of electron kinetic energy. This absence of any threshold effects suggests that all ionization is into the electronic continuum of the $^2A_1$ dimer cation ground state. Indeed, our ab initio calculations show that the configurations involved in the UV-excited NO dimer states contain only single electron excitations. The Koopmans' ionization correlations for these UV states would therefore be to the ground electronic state of the cation, consistent with our observations.
31. J. H. D. Eland, *J. Chem. Phys.* **70**, 2926 (1979).
32. K. G. Low, P. D. Hampton, I. Powis, *Chem. Phys.* **100**, 401 (1985).
33. T. Seideman, *Annu. Rev. Phys. Chem.* **53**, 41 (2002).
34. K. L. Reid, *Annu. Rev. Phys. Chem.* **54**, 397 (2003).
35. K. L. Reid, J. G. Underwood, *J. Chem. Phys.* **112**, 3643 (2000).
36. See supporting material on *Science* Online.
37. O. Gessner *et al.*, in preparation.

38. Supported by the Natural Sciences and Engineering Research Council of Canada (A.M.D.L., D.M.W., A.L.L.E., and A.S.), NSF (H.R., A.I.K.), and the U.S. Department of Energy, Office of Basic Energy Science, Division of Chemical Sciences, Geosciences, and Biosciences (C.C.H.).

Supporting Online Material

www.sciencemag.org/cgi/content/full/1120779/DC1
Materials and Methods
References

30 September 2005; accepted 28 November 2005
Published online 15 December 2005;
10.1126/science.1120779
Include this information when citing this paper.

A Bacterial Inhibitor of Host Programmed Cell Death Defenses Is an E3 Ubiquitin Ligase

Radmila Janjusevic,[1]* Robert B. Abramovitch,[2,3]* Gregory B. Martin,[2,3]† C. Erec Stebbins[1]†

The *Pseudomonas syringae* protein AvrPtoB is translocated into plant cells, where it inhibits immunity-associated programmed cell death (PCD). The structure of a C-terminal domain of AvrPtoB that is essential for anti-PCD activity reveals an unexpected homology to the U-box and RING-finger components of eukaryotic E3 ubiquitin ligases, and we show that AvrPtoB has ubiquitin ligase activity. Mutation of conserved residues involved in the binding of E2 ubiquitin–conjugating enzymes abolishes this activity in vitro, as well as anti-PCD activity in tomato leaves, which dramatically decreases virulence. These results show that *Pseudomonas syringae* uses a mimic of host E3 ubiquitin ligases to inactivate plant defenses.

Type III secretion systems (T3SS) translocate bacterial virulence proteins into host cells to modulate diverse eukaryotic biochemical processes (*1*–*5*). *Pseudomonas syringae* pathovar (pv.) *tomato* DC3000 causes disease in tomato and *Arabidopsis* and uses a T3SS to evade the host's programmed cell death (PCD) response, which sacrifices a limited portion of the plant to protect the rest from systemic infection (*6*). The *Pseudomonas syringae* type III effector AvrPtoB is delivered into plant cells, where it elicits a host response that varies for resistant and susceptible tomato lines (*7*). In resistant plants, AvrPtoB is rec-

ognized by the Pto resistance (R) protein and elicits PCD that limits pathogen spread, which results in host immunity. In susceptible plants, however, AvrPtoB suppresses PCD associated with plant immunity, which allows the pathogen to multiply in the host and to cause disease. AvrPtoB targets a conserved PCD pathway, because AvrPtoB inhibits PCD induced by diverse agonists in plants (such as mouse BAX) and also suppresses PCD in yeast (*8*). The primary amino acid sequence of AvrPtoB has provided no clues about its possible function.

An acidic, C-terminal domain (CTD) of AvrPtoB, spanning residues 436 to 553, forms a protease-resistant, soluble, and stable recombinant construct that is amenable to structural determination (Fig. 1A) [figs. S1 to S3; (*9*)]. The structure of this domain reveals a globular fold centered on a four-stranded β sheet that packs against two helices on one face and has three very extended loops connecting the elements of secondary structure (Fig. 1B). A large and partially disordered N-terminal region spanning residues 436 to 475 packs loosely against a more tightly packed "core fold" that consists of a three-stranded β sheet packed against an α helix. The molecular surface of the AvrPtoB CTD is notable for several localized regions of differing electrostatic potential. One face of the molecule in particular shows a large basic patch sandwiched between two large acid patches (Fig. 1C).

Unexpectedly, the AvrPtoB CTD shows remarkable homology to the RING-finger and U-box families of proteins involved in ubiquitin ligase complexes in eukaryotes (Fig. 2A) (*10*–*16*). This similarity begins in AvrPtoB at residue 476, extends to the C terminus of the protein, and encompasses the "core-fold" secondary structural elements of this ββαβ family (a three-stranded β sheet with a single helix and two extended loops). For example, alignments of AvrPtoB with the human Rbx1 RING-finger and the U-box domain of *At*PUB14 from *Arabidopsis* have root-mean-square deviations in Cα positions of 2.4 Å (52 residues) and 1.1 Å (52 residues), respectively (*10*, *16*, *17*). We find the AvrPtoB CTD more similar to eukaryotic U-boxes, however, judging from both structural alignments and the lack of zinc coordination in the fold to support the extended loops (*15*, *16*).

This similarity to eukaryotic RING-finger and U-box proteins extends beyond the conserved fold to crucial functional aspects of this family of proteins. In particular, a highly conserved binding site for recruiting elements of the ubiquitin ligase machinery is present in this bacterial virulence factor. The E3 ubiquitin ligases have a substrate (or adaptor-substrate) binding site, as well as a site to recruit proteins conjugated to ubiquitin so as to mediate transfer to the substrate—the so-called E2 "ubiquitin-conjugating" enzymes (*18*). These E2 enzymes are found to bind to a conserved region in eukaryotic RING-finger proteins (conserved in U-box proteins) that is characterized in part by a spatially clustered, three–amino acid surface patch (*10*, *16*). This patch contains a highly conserved proline from the second large

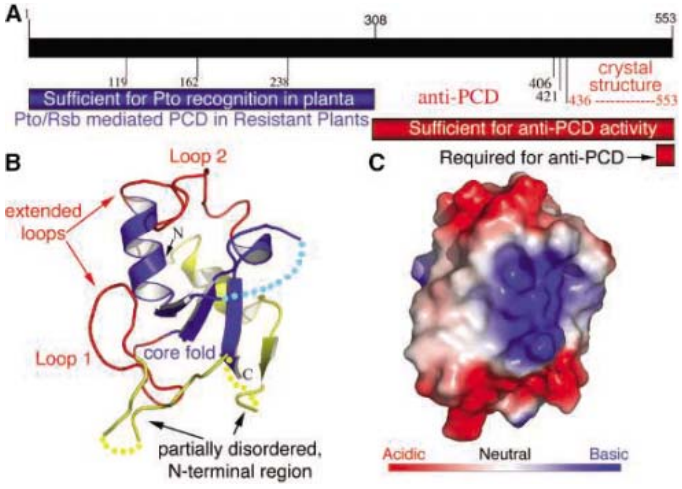

Fig. 1. Overall structure of the AvrPtoB CTD domain. (**A**) Domain structure of AvrPtoB. Numbers below the bar show points of cleavage with the protease subtilisin. The blue bar indicates the region sufficient for recognition by the plant Pto kinase for the mounting of PCD uninhibited by the CTD, whereas red bars indicate regions necessary or sufficient for anti-PCD activity in plants (*7*). (**B**) Overall structure of AvrPtoB(436–553): in blue, a "core fold" contributing most of the hydrophobic core and stabilizing the domain, in red, the long extended loops linking elements of secondary structure and which are critical to function (see text), in yellow, the extended, partially disordered N-terminal region that packs loosely against the core fold. Dotted lines indicate connecting regions of polypeptide not modeled because of disorder. N, N terminus; C, C terminus. (**C**) Molecular surface of the AvrPtoB CTD aligned as in panel (B). The surface is colored by relative electrostatic potential, such that red is acidic (or negatively charged) and blue is basic (or positively charged).

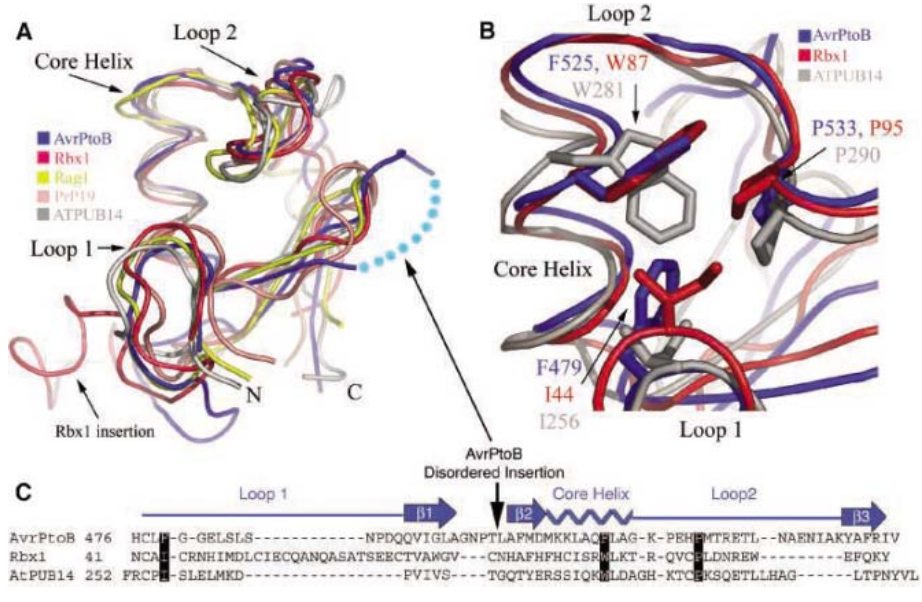

Fig. 2. AvrPtoB mimics host RING-finger and U-box proteins. (**A**) Structural alignment of the AvrPtoB CTD (the core fold) with the RING-finger and U-box structures of Rbx1 [Protein Data Bank (PDB) ID 1LD], Rag1 (PDB ID 1RMD), PrP19 (PDB ID 1N87), and *At*PUB14 (PDB ID 1T1H). (**B**) Visualization of the E2–binding site residues of Rbx1 with homologous regions in AvrPtoB and *At*PUB14 [the polypeptide backbone from the alignment in panel (A)]. The corresponding residue numbers are indicated next to the amino acid. (**C**) Structure-based sequence alignment of AvrPtoB, Rbx1, and *At*PUB14 focusing on the conserved, core fold. Secondary structure of AvrPtoB is indicated in blue above the sequence. Black highlights the three putative E2-binding residues shown in panel (B). The location of the AvrPtoB disordered insertion is indicated.

[1]Laboratory of Structural Microbiology, The Rockefeller University, New York, NY 10021, USA. [2]Boyce Thompson Institute for Plant Research, Ithaca, NY 14853, USA. [3]Department of Plant Pathology, Cornell University, Ithaca, NY 14853, USA.

*These authors contributed equally to this work.
†To whom correspondence should be addressed. E-mail: stebbins@rockefeller.edu (C.E.S.); gbm7@cornell.edu (G.B.M.)

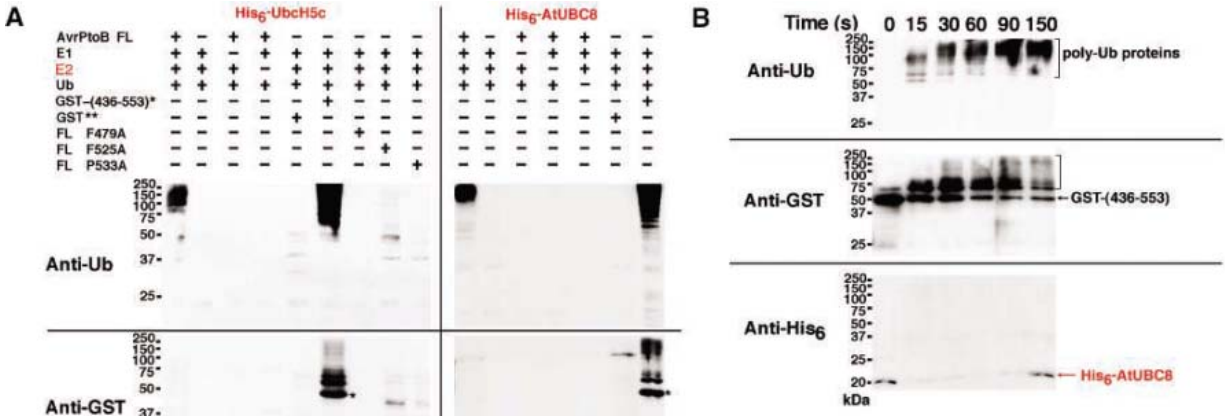

Fig. 3. The AvrPtoB CTD has eukaryotic-like ubiquitin ligase activity. (**A**) Autoubiquitination activity of AvrPtoB full-length protein (FL) and a CTD GST–AvrPtoB(436–553) fusion that was used for crystallization [labeled GST-(436–553]. In vitro ubiquitination assays were performed in the presence of ATP with the indicated combinations of proteins as described in (*9*). Proteins were resolved by SDS–polyacrylamide electrophoresis (SDS-PAGE) and were subjected to immunoblot analysis with indicated antibodies. Polyubiquitinated forms of AvrPtoB FL and AvrPtoB(436–553) were detected with antibodies against Ub or against Ub and GST, respectively. Antibodies against His_6 were used for detection of $2XHis_6$-tagged ubiquitin-conjugating proteins (E2, human UbcH5c or its *Arabidopsis* homolog *At*UBC8; colored in red; position indicated with arrows). FL mutants F479A, F525A, and P533A (*33*) are the E2–binding site mutants of full-length AvrPtoB. E1, ubiquitin-activating enzyme; Ub, ubiquitin. One asterisk indicates position of GST–AvrPtoB(436–553); two asterisks indicate the position of GST. SYPRO FL: gel was stained with SYPRO Ruby protein gel stain, and the position of wt FL AvrPtoB and each E2–binding site mutant is indicated by a black arrow. (**B**) Time-dependent in vitro autoubiquitination of GST–AvrPtoB(436–553). Reaction mix containing E1, E2 (*Arabidopsis* His_6-UbcH8), GST–AvrPtoB(436–553), and ubiquitin was incubated for indicated times at 30°C as described (*9*), visualized by SDS-PAGE. The ubiquitinated proteins, GST–AvrPtoB(436–553), and His_6-UbcH8 were detected in immunoblot analysis with the indicated antibodies as in Fig. 3A.

loop in this fold (following the first helix), a bulky hydrophobic residue in the first helix, and a hydrophobic residue in the first large loop. Mutation of these residues typically impairs E2 binding and ligase activity (*10*). The AvrPtoB CTD has a highly conserved patch very similar to those found in eukaryotic RING-finger and U-box proteins, and both the nature of the residues and their spatial positioning is highly conserved (Fig. 2, B and C). In particular, the proline is conserved (AvrPtoB Pro^{533}), and large, hydrophobic residues (AvrPtoB Phe^{479} and Phe^{525}) superimpose well on known E2 binding residues in eukaryotic RING-finger and U-box proteins (Fig. 2B).

This analysis of the structure raised the possibility that *P. syringae* AvrPtoB is functioning as a mimic of host E3 ubiquitin ligases. To test this hypothesis, we examined full-length and CTD AvrPtoB constructs for ubiquitin ligase activity and, in particular, for the common capacity seen in eukaryotic E3 ligases to autoubiquitinate. We performed ubiquitination assays (*9*) in vitro using exclusively recombinant, purified proteins (ubiquitin, E1 and E2 enzymes) in the presence of adenosine triphosphate (ATP), and full-length AvrPtoB, as well as the crystallized CTD construct fused to glutathione *S*-transferase (GST). Assays were performed with human UbcH5c, an E2 enzyme that showed activity in a screen of eight E2 enzymes (*9*), as well as a homologous *Arabidopsis* E2, *At*UBC8. Similar results were obtained with both E2s: in the presence of full-length or CTD, E1, E2, ubiquitin, and ATP, a characteristic ladder to high molecular weight was observed in immunoblots with a monoclonal antibody to ubiquitin, indicating the addition of multiple ubiquitin molecules (Fig. 3A). A time course confirmed a gradual accumulation of higher molecular weight species of polyubiquitinated proteins (Fig. 3B). Probing the blot with an antibody against GST (to label the GST-AvrPtoB CTD fusion protein) or an antibody against His_6 (to visualize the recombinant E2 enzymes tagged with a hexahistidine sequence) revealed that the banding is mostly due to autoubiquitination of AvrPtoB. The lack of a single component—E1, E2, ubiquitin, or the full-length or CTD AvrPtoB constructs—abolished this activity (Fig. 3A). We examined whether the putative E2 binding site identified in the structure was important for this ubiquitin ligase activity. Alanine substitutions were made in each of the three conserved E2–binding site residues of AvrPtoB (figs. S4 and S5) and examined in the assay described above. Each of the mutants lost ubiquitination activity, which indicated that the putative E2 binding site in AvrPtoB is critical to the ubiquitin ligase activity of the CTD (Fig. 3A). Together, these results strongly suggest that AvrPtoB, and in particular the CTD, is an active E3 ligase and likely mimics eukaryotic enzymes of this family in both structure and function.

We next examined the importance of this E2 binding site in an infection assay *in planta*. There appear to be two distinct mechanisms that lead to AvrPtoB-mediated PCD. The first is dependent on both the Pto and Prf resistance (R) proteins in resistant tomato: AvrPtoB elicits PCD on the RG-PtoR tomato line that contains both R proteins, but does not elicit PCD on *pto* or *prf* mutant plants, RG-pto11 and RG-prf3, respectively (*19*). AvrPtoB is thus not able to suppress PCD triggered by the Pto R protein. The second mechanism by which AvrPtoB triggers PCD is Pto-independent and involves another putative R protein (Rsb), along with Prf. In plants lacking Pto-mediated resistance, AvrPtoB acts as a suppressor for PCD activated by the Rsb. Thus, loss of AvrPtoB anti-PCD activity (for example, through a deletion of the CTD, leaving residues 1 to 387, designated NTD) results in a gain of Rsb-mediated PCD on the RG-pto11 line (Fig. 4A). Rsb-mediated PCD in the RG-pto11 line therefore provides an assay to screen for anti-PCD activity of AvrPtoB by looking for a gain of PCD.

We began by examining the effects of transient expression of AvrPtoB constructs in tomato leaves (*9*). The three E2–binding site mutants that abolished E3 ligase activity elicited PCD on RG-PtoR and did not elicit PCD on RG-prf3,

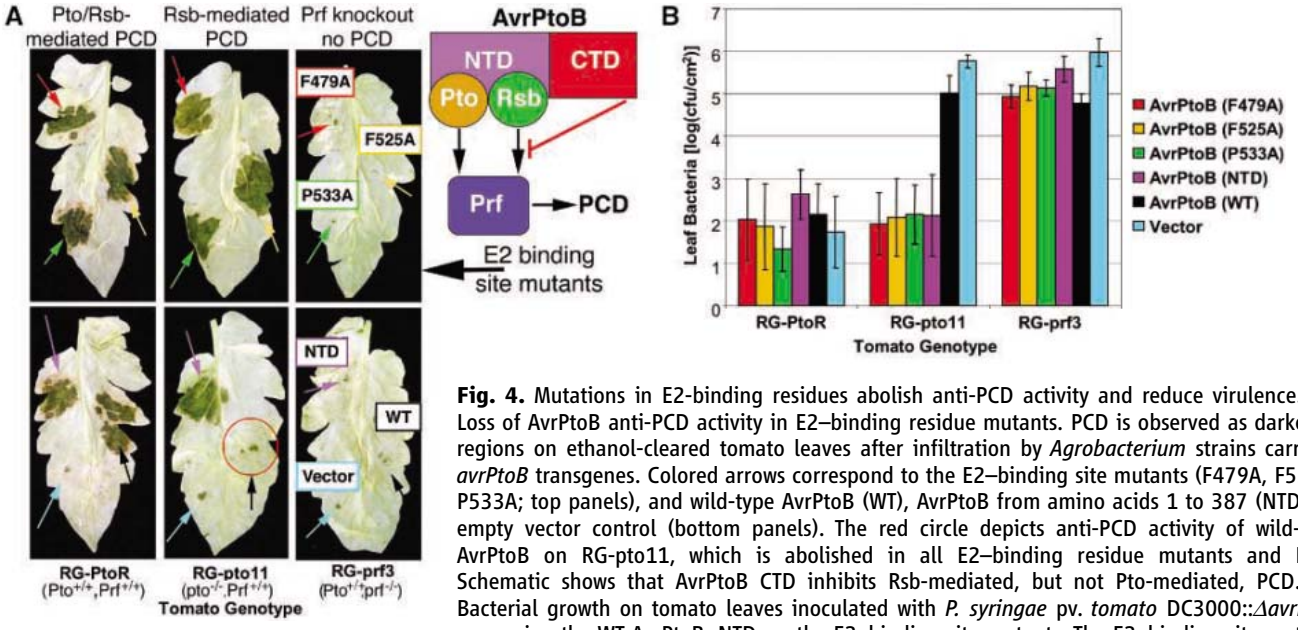

Fig. 4. Mutations in E2-binding residues abolish anti-PCD activity and reduce virulence. (**A**) Loss of AvrPtoB anti-PCD activity in E2–binding residue mutants. PCD is observed as darkened regions on ethanol-cleared tomato leaves after infiltration by *Agrobacterium* strains carrying *avrPtoB* transgenes. Colored arrows correspond to the E2–binding site mutants (F479A, F525A, P533A; top panels), and wild-type AvrPtoB (WT), AvrPtoB from amino acids 1 to 387 (NTD), or empty vector control (bottom panels). The red circle depicts anti-PCD activity of wild-type AvrPtoB on RG-pto11, which is abolished in all E2–binding residue mutants and NTD. Schematic shows that AvrPtoB CTD inhibits Rsb-mediated, but not Pto-mediated, PCD. (**B**) Bacterial growth on tomato leaves inoculated with *P. syringae* pv. *tomato* DC3000::*ΔavrPtoB* expressing the WT AvrPtoB, NTD, or the E2–binding site mutants. The E2–binding site mutants elicit Pto-independent immunity on RG-pto11 leaves and consequently grow less than WT. All strains cause disease on susceptible RG-prf3 and elicit immunity on RG-PtoR. Growth was measured 6 days post inoculation as colony-forming units (CFU) per square centimeter of leaf area, and the experiment was repeated three times.

which revealed that these proteins are expressed and recognized by Pto and are not toxic to tomato (Fig. 4A). However, like the AvrPtoB NTD, and unlike the wild-type protein control, all three E2–binding site mutants elicited PCD on RG-pto11 leaves (Fig. 4A), which indicated that these proteins have lost anti-PCD activity. We then examined the importance of the E2 binding site in the context of a *P. syringae* infection of tomato. The same mutants were first transformed into the *P. syringae* DC3000::Δ*avrPtoB* mutant and expressed from the native *hrp* promoter (*20*). All the mutants caused disease on susceptible RG-prf3 tomato plants (Fig. 4B). However, on RG-pto11, the E2–binding site mutants elicited Pto-independent host immunity, comparable to that of the AvrPtoB NTD and the immunity observed on resistant RG-PtoR tomato plants (Fig. 4B). Wild-type AvrPtoB, however, caused disease on RG-pto11 mutants, because it suppresses Pto-independent PCD mediated by Rsb. Therefore, the disruption of these putative E2–binding site residues abrogates AvrPtoB anti-PCD and virulence activities in tomato. These mutagenesis results directly connect the loss of ubiquitin ligase activity observed in vitro with the loss of anti-PCD and virulence in tomato, which indicates that it is the E3 ligase activity of AvrPtoB that is critical for cell death suppression and for increased virulence of *P. syringae*.

The role of E3 ligases as inhibitors of PCD is well established (*21*–*25*). Interestingly, some viral proteins act in host cells as E3 ligases, although the exact mechanisms of their action remain unclear (*26*–*29*). Our data suggest that AvrPtoB functions as an E3 ligase in the infected cell, recruiting E2 enzymes and substrates (directly or in concert with another protein) and transferring ubiquitin or a ubiquitin-like molecule to cellular proteins involved in the regulation of PCD. An important strategy used by bacterial pathogens to manipulate host tissues is the functional mimicry of eukaryotic biochemical processes, and this mimicry often extends to the structural level (*30*). The use of eukaryotic ubiquitin-mediated systems for protein degradation by bacterial pathogens has been recently documented (*31*, *32*). *Salmonella* temporally regulates bacterial invasion and host cell recovery through two T3SS substrates that have differing half-lives within host cells (*31*). In addition, the VirF protein of *Agrobacterium* contains an F-box motif that targets it to plant homologs of the E3 adaptor protein Skp1, which leads to degradation of the plant nuclear factor VIP1 (*32*). These bacterial factors differ from AvrPtoB, however, in that they rely on exploiting a host E3 ligase system, rather than embodying such enzymatic activity. Because AvrPtoB links E3 ubiquitin ligases and PCD and, furthermore, extends beyond plants to yeast cells as well as PCD activated in plants by the BAX protein, the bacterium has evolved this E3 ligase mimic to target a fundamental aspect of PCD that is highly conserved across several branches of eukaryota.

References and Notes

1. C. J. Hueck, *Microbiol. Mol. Biol. Rev.* **62**, 379 (1998).
2. J. E. Galan, A. Collmer, *Science* **284**, 1322 (1999).
3. G. R. Cornelis, *Philos. Trans. R. Soc. Lond. B Biol. Sci.* **355**, 681 (2000).
4. J. E. Galan, *Annu. Rev. Cell Dev. Biol.* **17**, 53 (2001).
5. M. L. Zaharik, S. Gruenheid, A. J. Perrin, B. B. Finlay, *Int. J. Med. Microbiol.* **291**, 593 (2002).
6. J. R. Alfano, A. Collmer, *Annu. Rev. Phytopathol.* **42**, 385 (2004).
7. R. B. Abramovitch, G. B. Martin, *FEMS Microbiol. Lett.* **245**, 1 (2005).
8. R. B. Abramovitch, Y. J. Kim, S. Chen, M. B. Dickman, G. B. Martin, *EMBO J.* **22**, 60 (2003).
9. Materials and methods are available as supporting materials on *Science* Online.
10. N. Zheng *et al.*, *Nature* **416**, 703 (2002).
11. N. Zheng, P. Wang, P. D. Jeffrey, N. P. Pavletich, *Cell* **102**, 533 (2000).
12. J. Jiang *et al.*, *J. Biol. Chem.* **276**, 42938 (2001).
13. C. Patterson, *Sci. STKE* **2002**, pe4 (2002).
14. D. M. Cyr, J. Hohfeld, C. Patterson, *Trends Biochem. Sci.* **27**, 368 (2002).
15. M. D. Ohi, C. W. Vander Kooi, J. A. Rosenberg, W. J. Chazin, K. L. Gould, *Nat. Struct. Biol.* **10**, 250 (2003).
16. P. Andersen *et al.*, *J. Biol. Chem.* **279**, 40053 (2004).
17. L. Holm, C. Sander, *J. Mol. Biol.* **233**, 123 (1993).
18. A. R. Willems, M. Schwab, M. Tyers, *Biochim. Biophys. Acta* **1695**, 133 (2004).
19. K. F. Pedley, G. B. Martin, *Annu. Rev. Phytopathol.* **41**, 215 (2003).
20. N. C. Lin, G. B. Martin, *Mol. Plant Microbe Interact.* **18**, 43 (2005).
21. A. Hershko, A. Ciechanover, *Annu. Rev. Biochem.* **67**, 425 (1998).
22. M. Estelle, *Curr. Opin. Plant Biol.* **4**, 254 (2001).
23. V. Jesenberger, S. Jentsch, *Nat. Rev. Mol. Cell Biol.* **3**, 112 (2002).
24. S. Hu, X. Yang, *J. Biol. Chem.* **278**, 10055 (2003).
25. L. R. Zeng *et al.*, *Plant Cell* **16**, 2795 (2004).
26. L. Coscoy, D. Ganem, *Trends Cell Biol.* **13**, 7 (2003).
27. N. Imai *et al.*, *J. Virol.* **77**, 923 (2003).
28. J. Huang *et al.*, *J. Biol. Chem.* **279**, 54110 (2004).
29. K. Cadwell, L. Coscoy, *Science* **309**, 127 (2005).
30. C. E. Stebbins, J. E. Galan, *Nature* **412**, 701 (2001).
31. T. Kubori, J. E. Galan, *Cell* **115**, 333 (2003).
32. T. Tzfira, M. Vaidya, V. Citovsky, *Nature* **431**, 87 (2004).
33. Single-letter abbreviations for the amino acid residues are as follows: A, Ala; F, Phe; and P, Pro.

34. We thank H. Mueller at Rockefeller University and T. Radhakannan, R. Ramagopal, and W. Shi of Brookhaven beamline X9A for access to and assistance

with crystallographic equipment and R. Bennett, C. Pepper, A. Gazes, and G. Latter of Rockefeller University for computational facilities support. Protein N-terminal sequencing and mass-spectroscopic analysis were performed at the Rockefeller University under the direction of H. Deng. We thank D. Schneider for bioinformatics support and S. Manon of the Rockefeller Chemical Biology Spectroscopy Resource Center for access to circular dichroism equipment. We thank the *Arabidopsis* Biological Resource Center and donors of stock U09652: J. Ecker, A. Theologis, and R. Davis [SSP Consortium: Salk, Stanford, PGEC (Plant Gene Expression Center)]. This work was supported in part by a Burroughs-Welcome Investigators in Pathogenesis of Infectious Disease award and funds from the Rockefeller University to C.E.S., a fellowship from the Natural Sciences and Engineering Research Council of Canada to R.B.A., and funds from the Triad Foundation and the U.S. Department of Agriculture National Research Initiative to G.B.M. Coordinates have been deposited in the Protein Data Bank under PDB ID 2FD4.

Supporting Online Material
www.sciencemag.org/cgi/content/full/1120131/DC1
Materials and Methods
Figs. S1 to S5
Table S1
References

13 September 2005; accepted 9 December 2005
Published online 22 December 2005;
10.1126/science.1120131
Include this information when citing this paper.

PER-TIM Interactions in Living *Drosophila* Cells: An Interval Timer for the Circadian Clock

Pablo Meyer, Lino Saez, Michael W. Young*

In contrast to current models, fluorescence resonance energy transfer measurements using a single-cell imaging assay with fluorescent forms of PER and TIM showed that these proteins bind rapidly and persist in the cytoplasm while gradually accumulating in discrete foci. After ~6 hours, complexes abruptly dissociated, as PER and TIM independently moved to the nucleus in a narrow time frame. The per^L mutation delayed nuclear accumulation in vivo and in our cultured cell system, but without affecting rates of PER/TIM assembly or dissociation. This finding points to a previously unrecognized form of temporal regulation that underlies the periodicity of the circadian clock.

In *Drosophila melanogaster*, PER and TIM are two essential proteins of the circadian clock that shift from the cytoplasm of clock cells to the nucleus once a day, promoting ~24-hour oscillations of *per* and *tim* transcription. They do this in a regulated manner, and the period length of *Drosophila*'s circadian rhythm is in part determined by how long these proteins are held in the cytoplasm before entering the nucleus (*1–4*).

Formation of PER/TIM heterodimers appears to promote the nuclear accumulation of both proteins. In vivo, a 4- to 6-hour delay in PER nuclear accumulation may be influenced by the slow cytoplasmic assembly of PER/TIM heterodimers, such that once formed, the PER/TIM heterodimer is rapidly transferred from the cytoplasm to the nucleus. It is thought that in the nucleus PER physically interacts with CLOCK and CYCLE, transcriptional activators of *per* and *tim*, inhibiting CLOCK/CYCLE activity and hence closing a delayed feedback loop that contributes to oscillating RNA and protein levels (*1–4*).

Recently, the proposal that PER and TIM translocate to the nucleus as obligate heterodimers, and even the necessity of TIM for PER's nuclear accumulation, have been questioned (*5–8*). To follow PER and TIM during their passage from the cytoplasm to the nucleus and to determine the role of PER/TIM interaction in the regulation of nuclear accumulation, we developed a single-cell, fluorescent, live-imaging assay using a *Drosophila* cell line (Schneider's line 2, S2). Although S2 cells do not express several clock genes and are not rhythmic, this cultured cell system has become an important tool for investigating intracellular mechanisms contributing to *Drosophila*'s circadian clock (*9–14*).

We constructed C-terminal fusions of PER and TIM with cyan fluorescent protein (CFP) and yellow fluorescent protein (YFP), respectively, and monitored these separately or together in S2 cells (fig. S1). Expression of *per-cfp* (without TIM) was followed in two cell lines. In one line, PER-CFP production was controlled by a heat shock promoter. These cells were constantly monitored for 10 hours after induction (~100 cells in 10 independent experiments). In the second line, an actin promoter drove *per-cfp* expression, and 40 cells in two experiments were followed for 10 hours after transfection. PER-CFP was detected only in the cytoplasm of live S2 cells in both studies. In a third study, we followed cells in which *tim-yfp* was driven by a heat shock promoter in the absence of PER (130 cells in 10 experiments). TIM was retained in the cytoplasm in most but not all cells 10 hours after induction (123 cytoplasmic, 7 nuclear). In contrast, when cotransfected, *per-cfp* and *tim-yfp* gave predominantly nuclear fluorescence for both proteins in most cells (209 nuclear out of 265 cells monitored in 39 experiments at 8 hours after induction). The behavior of the proteins in our S2 cell system is therefore concordant with in vivo findings (*1–4*) and indicates that the fluorescent tags do not detectably interfere with either cytoplasmic retention of the individually expressed proteins or with interactions that promote nuclear accumulation.

To evaluate the validity of an existing model in which rates of PER/TIM interaction affect the timing of their nuclear translocation (*1–4*), we compared PER-CFP/TIM-YFP fluorescence resonance energy transfer (FRET) measurements dynamically by continuously imaging CFP and YFP in live single cells. We calculated FRET within subcellular compartments on a pixel by pixel basis (Fig. 1A; fig. S2 and Movie S1A) and by averaging over the whole cell as a function of time after PER and TIM induction (Fig. 1B). Temporal profiles of changing FRET levels were then compared to contemporaneous nuclear accumulation profiles of PER calculated for each image as the ratio of mean pixel value in the nucleus to mean pixel value in the whole cell (Fig. 1B). We found that maximum levels of FRET were reached during the earliest stages of PER-CFP and TIM-YFP accumulation (within 30 min of PER and TIM production), indicating that physical interaction followed PER-CFP/TIM-YFP synthesis without a measurable delay (Fig. 1B left). Moreover, high levels of FRET were maintained for several hours preceding the onset of nuclear accumulation of PER and TIM (Fig. 1, A and B). Unexpectedly, FRET declined rapidly as PER and TIM proteins were transferred from the cytoplasm to the nucleus. As PER and TIM became predominantly nuclear, FRET levels remained low in all subcellular compartments, which were typically monitored for a further 100 min (Fig. 1, A and B; fig. S2).

We further observed that immediately following coinduction, PER and TIM were always diffusely present in the cytoplasm. However, this largely uniform distribution was followed by a gradual accumulation in prominent cytoplasmic foci (Figs. 1 and 2; Movies S1A and S2). These foci remained in the cytoplasm until PER and TIM translocated to the nucleus (Figs. 1 and 2; Movies S1A and S2). Notably, we did not detect the formation of foci when either PER or TIM was expressed alone (*15*). In addition, when PER and TIM were coexpressed, the foci often disappeared

Laboratory of Genetics, The Rockefeller University, 1230 York Avenue, New York, NY 10021, USA.

*To whom correspondence should be addressed. E-mail: young@rockefeller.edu

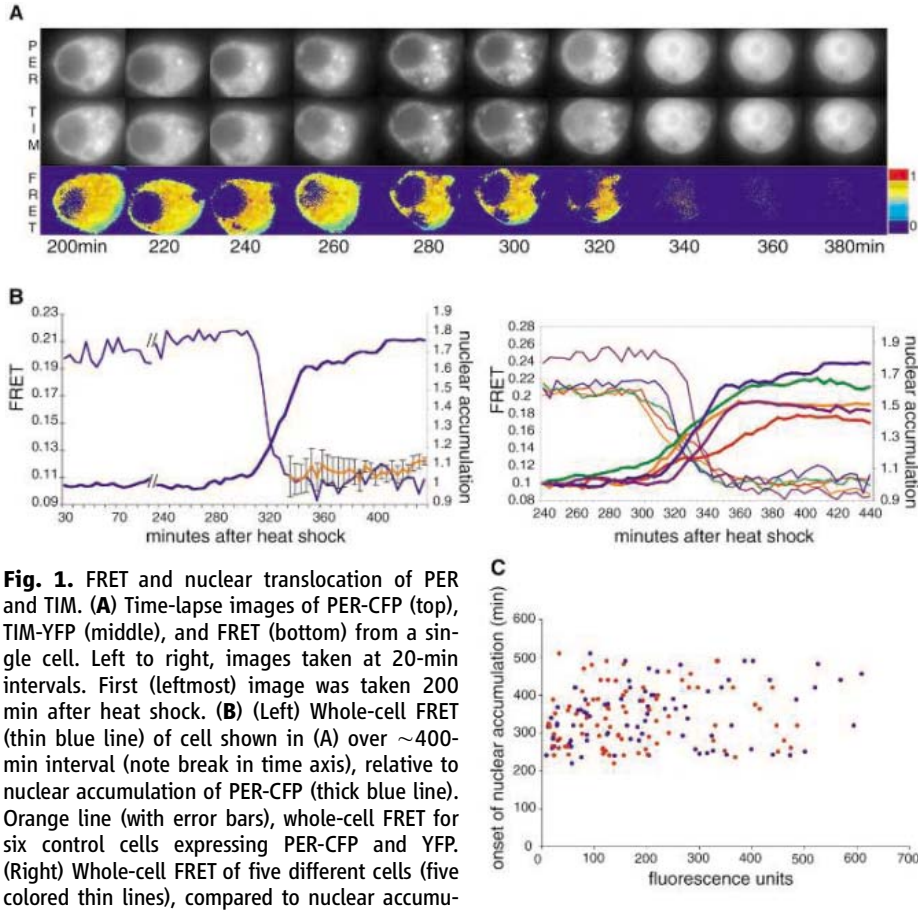

Fig. 1. FRET and nuclear translocation of PER and TIM. (**A**) Time-lapse images of PER-CFP (top), TIM-YFP (middle), and FRET (bottom) from a single cell. Left to right, images taken at 20-min intervals. First (leftmost) image was taken 200 min after heat shock. (**B**) (Left) Whole-cell FRET (thin blue line) of cell shown in (A) over ~400-min interval (note break in time axis), relative to nuclear accumulation of PER-CFP (thick blue line). Orange line (with error bars), whole-cell FRET for six control cells expressing PER-CFP and YFP. (Right) Whole-cell FRET of five different cells (five colored thin lines), compared to nuclear accumulation of PER-CFP (thick lines respective colors). (**C**) Onset of nuclear accumulation in single cells for PER-CFP (blue dots) and TIM-YFP (red dots) as a function of their mean fluorescence levels. The onset is determined as the inflexion point of the nuclear accumulation profile.

earlier in PER-CFP images than in TIM-YFP images (Fig. 2 red arrows). Thus, formation of these foci may be an important step in the temporal control of nuclear entry.

The abrupt decrease in FRET upon nuclear translocation could reflect either dissociation or a change in conformation of the PER-CFP/TIM-YFP complex. To differentiate between these two possibilities, we independently measured the rates of nuclear accumulation for PER and TIM. If PER and TIM undergo a conformational change but remain physically associated as nuclear translocation occurs, individual rates of PER and TIM nuclear accumulation should be equal.

In a survey of 85 cells, we found that the onset of nuclear accumulation, determined as the inflexion point of the nuclear accumulation profile for PER-CFP, occurred in a narrow time frame, 340 ± 70 min after heat shock in our S2 cells (Fig. 1C). Consistent with our observation that PER and TIM associate rapidly and that these association kinetics have no influence on the onset of nuclear translocation in our S2 cell system, we found that the time of onset of nuclear accumulation in these experiments was not correlated with the level of PER-CFP (correlation coefficient $R^2 = 0.0523$) or TIM-YFP ($R^2 = 0.0038$) expressed in the cytoplasm (Fig. 1C). To determine whether the kinetics of the nuclear accumulations of PER-CFP and of TIM-YFP were similar, we next calculated the rate of each protein's nuclear accumulation as the coefficient of a first-order linear regression. The latter was taken from the steepest slope of the profile of nuclear translocation, scaled to the mean fluorescence in each cell. We found that the rates of nuclear accumulation of PER-CFP and TIM-YFP were independent ($R^2 = 0.0476$) (Fig. 3A). Also, although the rate of accumulation of PER-CFP was positively correlated with the level of PER-CFP ($R^2 = 0.5366$), this rate was independent of the level of TIM-YFP produced in the same cell ($R^2 = 0.0004$) (Fig. 3B). Similarly, TIM-YFP accumulation rates were correlated with the TIM-YFP level ($R^2 = 0.4243$), but not with the PER-CFP level in the same cell ($R^2 = 0.0057$) (Fig. 3C). To control for a possible effect of the fluorescent protein tags on these results, we reversed the associations of CFP and YFP and followed the nuclear accumulation of PER-YFP and TIM-CFP. This study confirmed that the kinetics of accumulation were determined by PER and TIM and not by their tags (fig. S3A).

One issue that is not resolved by measuring these accumulation rates is whether the PER/TIM complex dissociates before or after traveling to the nucleus. As shown in Fig. 2, comparisons of PER and TIM nuclear translocations within individual cells reveal that onset of PER nuclear accumulation often precedes that of TIM, as recently reported in vivo (*5*). Earlier work has shown that, in the absence of PER, TIM shuttles between the nucleus and cytoplasm through the action of both nuclear localization and nuclear export signals (*16*). Possibly, TIM transports PER to the nucleus in a complex, after which the proteins separate, allowing TIM to return to the cytoplasm to transport more PER.

To determine whether this property of TIM contributes to the independent rates of PER and TIM nuclear translocation observed in our studies, we used leptomycin B to block TIM-YFP nuclear export (*16*). In the presence of this inhibitor of nuclear export, for cells expressing only TIM-YFP, the protein was constitutively localized to the nucleus in most cells (45 cells out of 50 surveyed). In contrast, in cells expressing only PER-CFP, PER remained in the cytoplasm (50 out of 50 cells) in the presence of the drug (*17*, *18*). Intriguingly, addition of leptomycin B to cells coexpressing PER-CFP and TIM-YFP suppressed the rapid transfer of TIM-YFP to the nucleus. Instead, both proteins were sequestered in the cytoplasm for several hours before nuclear translocation (369 ± 58 min, 29 cells), as previously observed in the absence of drug (fig. S3B). Evidently, even in the presence of leptomycin B, TIM is retained by its interaction with PER. Addition of leptomycin B also failed to modify the divergent profiles of PER and TIM nuclear accumulation; rates of PER and TIM nuclear accumulation remained uncorrelated ($R^2 = 0.0372$) in a study of these cells (Fig. 3A). The latter finding indicates that although we have confirmed TIM shuttling between the nucleus and cytoplasm, this mechanism cannot explain the independent rates of PER-CFP and TIM-YFP nuclear accumulation that we have observed. Our measurements hence favor an alternative mechanism for nuclear translocation wherein most of the cytoplasmically derived complexes dissociate in the cytoplasm as the proteins translocate to the nucleus (*19*).

The per^L mutation produces a delayed nuclear translocation phenotype in pacemaker cells of the *Drosophila* brain (*20*). This results in long-period behavioral rhythms of ~28 hours (*21*). per^L involves a single amino acid substitution (*22*), and it also depresses the physical interaction of PER^L and TIM when the proteins are coexpressed in yeast (*23*). The tim^{UL} mutation is associated with a distinct single–amino acid substitution that delays PER and TIM nuclear turnover, resulting in a 33-hour behavioral rhythm (*24*). In contrast to

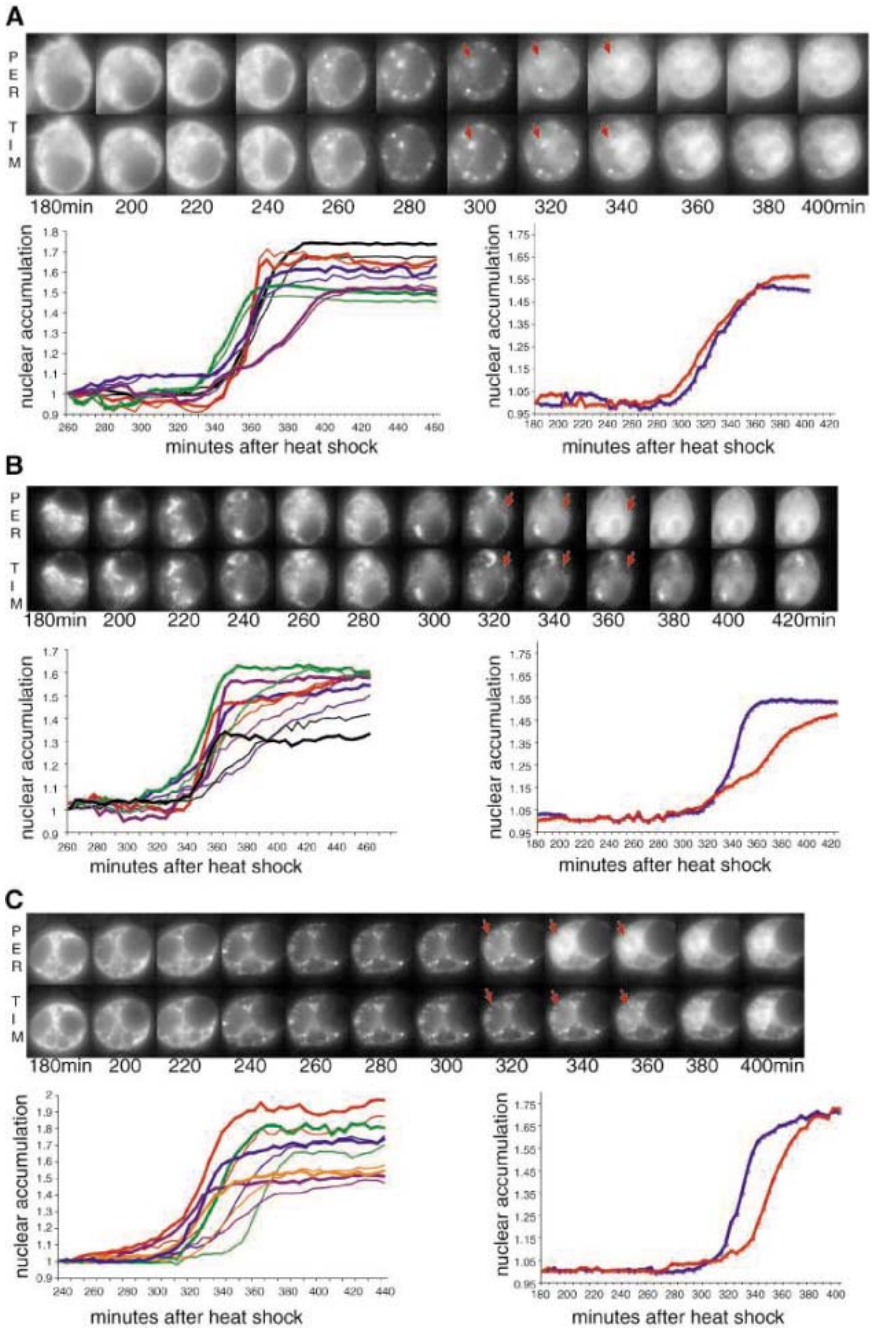

Fig. 2. Temporal profiles of nuclear accumulation of PER-CFP and TIM-YFP in single cells. Time-lapse images of cells expressing PER-CFP (top) and TIM-YFP (bottom). Red arrows indicate cytoplasmic foci appearing after synthesis and disappearing with nuclear entry. Right panel under each imaged cell shows nuclear accumulation profiles of PER-CFP (blue) and TIM-YFP (red). Left panel, five different cells; PER-CFP, thick lines; TIM-YFP, thin lines. In a survey of 85 cells, (**A**) PER-CFP and TIM-YFP profiles and onsets of nuclear accumulation were equal in 27. (**B**) PER-CFP and TIM-YFP nuclear accumulation profiles were different, but onsets of nuclear accumulation were equal in 35 of 85 cells. (**C**) PER-CFP and TIM-YFP nuclear accumulation profiles were equal, but onset of PER-CFP nuclear accumulation was advanced 25 ± 11 min compared with TIM-YFP in 23 of the 85 cells.

per^L, tim^{UL} has no effect on the timing of nuclear translocation in vivo (*24*).

The mean onset of PER-CFP nuclear accumulation in cells coexpressing PER-CFP and TIM^{UL}-YFP is 299 ± 33 min (20 cells), and it is also independent of PER-CFP and TIM^{UL}-YFP levels (Fig. 4, A and B). Furthermore, we found no persistent FRET when PER-CFP and TIM^{UL}-YFP moved to the nucleus: FRET decay was not delayed when compared to the onset of nuclear accumulation (Fig. 4C). We observed a loss of FRET with TIM^{UL} in parallel with nuclear translocation, which suggests that, as for wild-type TIM, TIM^{UL}/PER heterodimers dissociate as nuclear translocation proceeds in this mutant. Previous studies have shown that, in tim^{UL} mutants, PER is found in high molecular weight complexes late at night when it is presumably nuclear (*24*). We cannot rule out the possibility that, following translocation, PER and TIM form new associations that do not support FRET in the nucleus in both wild-type and TIM^{UL}-expressing cells.

S2 cells reproduced the delay in nuclear translocation onset when PER^L was expressed in place of PER. In PER^L-expressing cells, the mean onset of nuclear accumulation was at 492 ± 97 min after induction, as compared with 340 ± 70 min in PER-expressing cells (25 cells, Wilcoxon test $P = 10^{-8}$) (Fig. 4, A and D). The onset of PER and TIM nuclear accumulation remained independent of PER^L-CFP and TIM-YFP levels (Fig. 4A). The profiles of nuclear accumulation of these proteins also indicated significant independence in their rates of translocation (*15*). FRET decayed as PER^L-CFP and TIM-YFP were transferred to the nucleus (Fig. 4E), and as previously seen from PER/TIM combinations, maximum levels of FRET arose without a measurable delay in cells expressing PER^L (Fig. 4E). This result was not predicted by earlier models, which assumed that an altered rate of PER^L and TIM physical association chiefly determines the temporal delay found in nuclear accumulation. Because nuclear translocation instead followed a protracted interval of maximum FRET in PER^L-expressing cells, a step distinct from PER/TIM assembly appears to trigger nuclear translocation in S2 cells and is likely also responsible for delayed nuclear translocation in vivo.

Our studies indicate that cytoplasmically formed PER/TIM complexes are not translocated to the nucleus: FRET disappears in parallel with PER and TIM nuclear accumulation, suggesting a dissociation of the complex, and measurements of PER and TIM nuclear accumulation rates show that, for a given cell, these are different and independent for each protein. Because PER/TIM associations are not sufficient to initiate nuclear accumulation, these results point to a mechanism in which physical interaction precedes an activity that precisely times nuclear translocation of both proteins. In this respect, PER and TIM appear to act as constituents of an intracellular interval timer. A better understanding of this timer might be sought in the discrete cytoplasmic foci we have observed to routinely precede nuclear translocation (Figs. 1 and 2). These foci may reflect condensations of cytoplasmic PER/TIM complexes together with additional factors responsible for their posttranslational modifications. Such factors could include the kinases SGG, DBT, and CK2 or the phosphatase PP2A, each known to affect the phosphorylation of PER

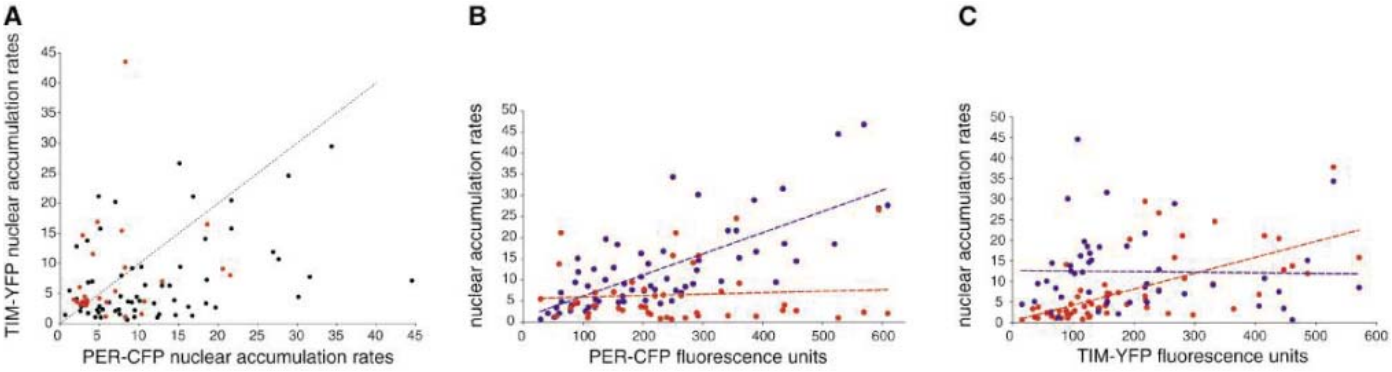

Fig. 3. Nuclear translocation rates. (**A**) Single-cell rates of TIM-YFP nuclear accumulation against rates of PER-CFP nuclear accumulation (black circles) and when leptomycin B was added (red circles). Rates were calculated as the linear regression for the maximum steepness of the nuclear accumulation profile and scaled through multiplying by the mean pixel fluorescence for the cell. Rates were calculated per image frame; one frame corresponds to 4 min. The dotted line represents the diagonal for visual support. (**B**) Single-cell rates of nuclear accumulation for PER-CFP (blue) and TIM-YFP (red) plotted against PER-CFP fluorescence levels for each cell. (**C**) Same rates as in (B) but plotted against TIM-YFP fluorescence levels. Colored dotted lines represent the linear regression for points of the same color.

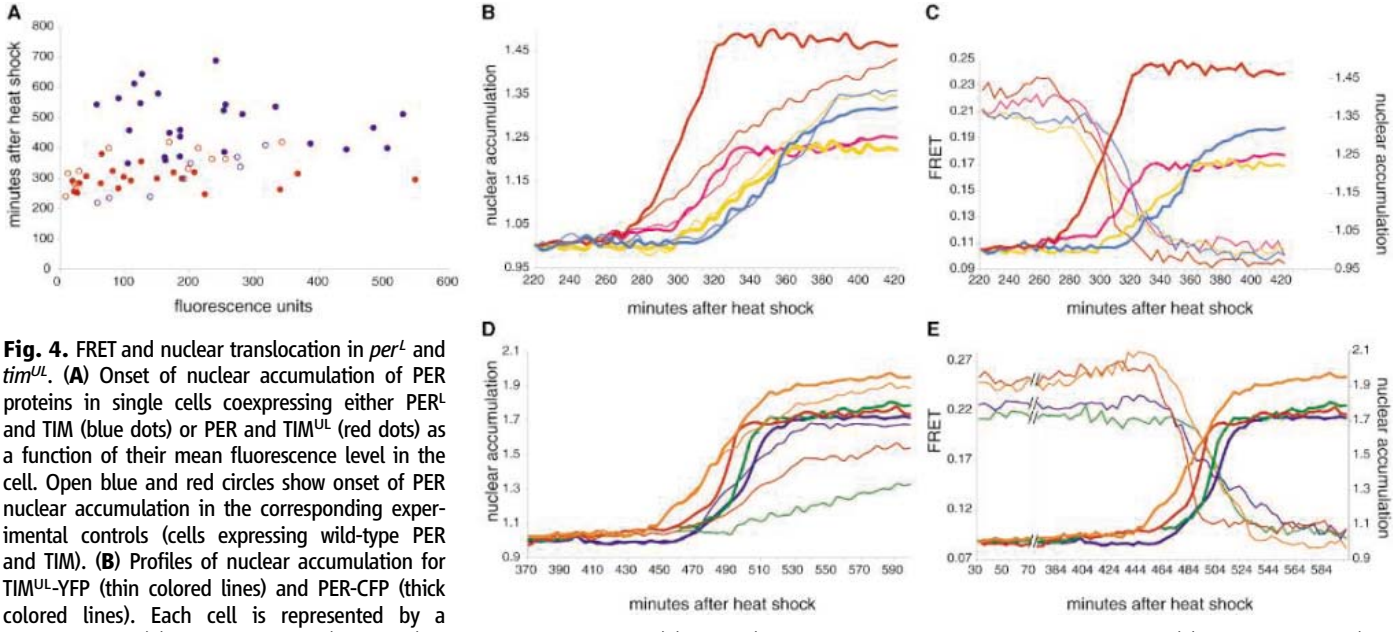

Fig. 4. FRET and nuclear translocation in per^{L} and tim^{UL}. (**A**) Onset of nuclear accumulation of PER proteins in single cells coexpressing either PER^{L} and TIM (blue dots) or PER and TIM^{UL} (red dots) as a function of their mean fluorescence level in the cell. Open blue and red circles show onset of PER nuclear accumulation in the corresponding experimental controls (cells expressing wild-type PER and TIM). (**B**) Profiles of nuclear accumulation for TIM^{UL}-YFP (thin colored lines) and PER-CFP (thick colored lines). Each cell is represented by a different color. (**C**) Whole-cell FRET (thin lines) for the same cells as in (B) relative to PER-CFP nuclear accumulation (thick lines). (**D**) Profiles of nuclear accumulation for PER^{L}-CFP (thick colored lines) and TIM-YFP (thin colored lines). Each cell is represented by a different color. (**E**) Whole-cell FRET (thin lines) for the same cells as in (D) relative to PER^{L}-CFP nuclear accumulation (thick lines). Note the break in the time axis, to show early time points.

and TIM and to influence the timing of nuclear translocation in vivo (*1*–*4*, *25*).

References and Notes

1. M. W. Young, S. A. Kay, *Nat. Rev. Genet.* **2**, 702 (2001).
2. R. Allada, P. Emery, J. S. Takahashi, M. Rosbash, *Annu. Rev. Neurosci.* **24**, 1091 (2001).
3. R. Stanewsky, *J. Neurobiol.* **54**, 111 (2003).
4. J. C. Hall, *Methods Enzymol.* **393**, 61 (2005).
5. O. T. Shafer, M. Rosbash, J. W. Truman, *J. Neurosci.* **22**, 5946 (2002).
6. P. Nawathean, M. Rosbash, *Mol. Cell* **13**, 213 (2004).
7. D. C. Chang, S. M. Reppert, *Curr. Biol.* **13**, 758 (2003).
8. J. C. Dunlap, *Dev. Cell* **6**, 160 (2004).
9. L. Saez, M. W. Young, *Neuron* **17**, 911 (1996).
10. T. K. Darlington *et al.*, *Science* **280**, 1599 (1998).
11. M. F. Ceriani *et al.*, *Science* **285**, 553 (1999).
12. H. W. Ko, J. Jiang, I. Edery, *Nature* **420**, 673 (2002).
13. S. Sathyanarayanan, X. Zheng, R. Xiao, A. Sehgal, *Cell* **116**, 603 (2004).
14. P. Nawathean, J. S. Menet, M. Rosbash, *Methods Enzymol.* **393**, 610 (2005).
15. P. Meyer, L. Saez, M. W. Young, data not shown.
16. L. J. Ashmore *et al.*, *J. Neurosci.* **23**, 7810 (2003).
17. Although our results are consistent with in vivo responses to leptomycin B (*16*), they differ from another study showing PER in nuclei of S2 cells in the presence of this drug (*6*). In the latter study, PER was coexpressed with CLOCK (*6*), which is a transcriptional activator of *tim* in S2 cells (*18*). In the presence of TIM, nuclear rather than cytoplasmic localization of PER would be expected with or without leptomycin B.
18. M. J. McDonald, M. Rosbash, *Cell* **107**, 567 (2001).
19. Because only full-length nuclear PER and TIM fusion proteins are recognized in Western assays using antibodies to green fluorescent protein (GFP), loss of FRET cannot reflect proteolytic separation of CFP and/or YFP during nuclear translocation (*15*).
20. K. D. Curtin, Z. J. Huang, M. Rosbash, *Neuron* **14**, 365 (1995).
21. R. J. Konopka, S. Benzer, *Proc. Natl. Acad. Sci. U.S.A.* **68**, 2112 (1971).
22. M. K. Baylies, T. A. Bargiello, F. R. Jackson, M. W. Young, *Nature* **326**, 390 (1987).
23. N. Gekakis *et al.*, *Science* **270**, 811 (1995).
24. A. Rothenfluh, M. W. Young, L. Saez, *Neuron* **26**, 505 (2000).
25. S. A. Cyran *et al.*, *J. Neurosci.* **25**, 5430 (2005).

26. We thank A. North for her interest and help while using the Delta Vision Microscope at the Rockefeller University Bio-Imaging Resource Center; M. Sigman for help using Matlab; and C. Bargmann, J. Blau, and L. Vosshall for helpful comments on the manuscript. This work was supported by a grant from the NIH (GM54339) to M.W.Y, and a Burroughs Wellcome Fellowship to P.M.

Supporting Online Material

www.sciencemag.org/cgi/content/full/311/5758/226/DC1
Figs. S1 to S3
Movies S1 and S2
References

29 July 2005; accepted 10 November 2005
10.1126/science.1118126

The snoRNA HBII-52 Regulates Alternative Splicing of the Serotonin Receptor 2C

Shivendra Kishore and Stefan Stamm*

The Prader-Willi syndrome is a congenital disease that is caused by the loss of paternal gene expression from a maternally imprinted region on chromosome 15. This region contains a small nucleolar RNA (snoRNA), HBII-52, that exhibits sequence complementarity to the alternatively spliced exon Vb of the serotonin receptor 5-HT_{2C}R. We found that HBII-52 regulates alternative splicing of 5-HT_{2C}R by binding to a silencing element in exon Vb. Prader-Willi syndrome patients do not express HBII-52. They have different 5-HT_{2C}R messenger RNA (mRNA) isoforms than healthy individuals. Our results show that a snoRNA regulates the processing of an mRNA expressed from a gene located on a different chromosome, and the results indicate that a defect in pre-mRNA processing contributes to the Prader-Willi syndrome.

Small nucleolar RNAs (snoRNAs) are non–protein-coding RNAs that are 60 to 300 nucleotides (nt) long and that function in guiding 2′-O-methylation and pseudouridylation in ribosomal RNAs (rRNAs), small nuclear RNAs (snRNAs), and tRNAs (*1*). HBII-52 is a brain-specific C/D box snoRNA. These snoRNAs have the conserved boxes C [(A/G) UGAUGA] and D (CUGA) near their 5′ and 3′ ends, respectively. HBII-52 is located on the IC-SNURF-SNRPN locus on human chromosome 15q11-13. In this region, 47 almost-identical copies of HBII-52 snoRNA genes are localized between unrelated, non–protein-coding exons. The locus is maternally imprinted (*2*). The loss of paternally expressed genes in 15q11-13 results in the Prader-Willi syndrome (PWS), which is characterized by neonatal muscular hypotonia and failure to thrive. In early childhood, patients develop hyperphagia, obesity, and hypogonadism. Further, they develop behavioral problems and are mentally retarded.

HBII-52 lacks any complementarity to an rRNA, snRNA, or tRNA. However, its antisense element exhibits complementarity to the alternatively spliced exon Vb of the serotonin receptor 5-HT_{2C}R, which is a seven-transmembrane receptor located on the X chromosome (Fig. 1, A and B). Exon V of the serotonin receptor contains at least two alternative 5′ splice sites, giving rise to exon Va– and Vb–containing isoforms. Exon Vb encodes the second intracellular loop of the receptor, which is crucial for G protein binding. Skipping of exon Vb causes a frame shift, resulting in a receptor that is truncated after the third transmembrane domain (Fig. 1A) (*3*). The alternative exon Vb is part of a 5-HT_{2C}R pre-mRNA region that is subject to RNA editing (*4*). At least five sites (A to E) in exon Vb can be edited from A to I. Exon Vb editing promotes its inclusion but changes the amino acid sequence of the intracellular loop (*5*). This change decreases serotonin efficacy of receptors generated through RNA editing 10- to 100-fold (*3*). Sequence comparison showed that the antisense element of HBII-52 and its complementary target sequence within the serotonin receptors are almost fully conserved between mammalian species (fig. S1, A to C). In contrast, there are nucleotide exchanges at 19 positions in other regions of the II-52 snoRNAs (fig. S1B), suggesting a functional relevance of the antisense element sequence.

In agreement with earlier studies (*3*), we found that the rat ortholog of HBII-52, RBII-52, and 5-HT_{2C}R exon Vb are expressed in all areas of the brain, except the choroid plexus (fig. S2A). Thus, there is a positive correlation between RBII-52 expression and exon Vb usage. To test this correlation functionally, we performed cotransfection experiments with an exon Vb splicing reporter and an MBII-52 expression clone, derived from the mouse ortholog (*6*). We generated a minigene of the 5-HT_{2C}R (pRSV-5HT) comprising exons IV, Va, Vb, and VI. The snoRNA was expressed from the construct pCMV-MBII-52 (cmv, cytomegalovirus) that contained MBII-52 and two flanking exons (Fig. 2A) (*2*). We transfected an increasing amount of pCMV-MBII-52 in Neuro2A cells and detected the accumulation of an increasing amount of MBII-52 snoRNA of the expected size by Northern blot analysis (Fig. 2C). We then cotransfected the pRSV-5HT reporter minigene together with an increasing concentration of pCMV-MBII-52. By using primers 5aF and 6R located in the exons Va and VI for polymerase chain reaction (PCR) analysis, we amplified only the mRNA isoform lacking exon Vb. We therefore used the isoform-specific primer 5bF, located in exon Vb, which allowed the detection of the alternative exon in this assay. The usage of exon Vb was significantly increased when the concentration of MBII-52 was increased ($P < 0.0002$) (Fig. 2B). Often, neuron-specific exons are not properly used when reporter constructs are expressed in immortalized cell lines (*7*, *8*). We therefore activated the distal splice site by mutating it into the mammalian consensus (pRSV-5HTcons) (fig. S2B). This allowed us to use the primers 5aF/6R located in the flanking exons Va and VI to detect the increase of exon Vb usage (Fig. 2B). Because these primers amplify both isoforms, the products can be directly compared. An increase of MBII-52 snoRNA resulted in a significant increase of exon Vb inclusion from 5 to 20% ($P < 0.0004$). These experiments are consistent with MBII-52 promoting exon Vb inclusion of the 5-HT_{2C} receptor pre-mRNA.

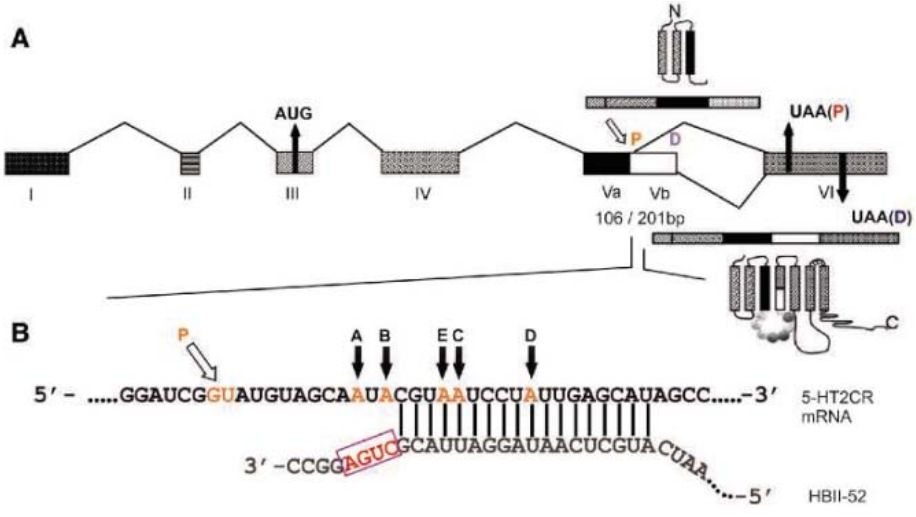

Fig. 1. Complementarity between HBII-52 snoRNA and 5-HT_{2C}R receptor. (**A**) Structure of the human 5-HT_{2C}R receptor. P and D indicate the location of proximal and distal splice sites, respectively. UAA(P) and UAA(D) are the stop codons resulting from their usage. Exons are indicated as boxes with roman numbers. The mRNA isoforms and the resulting proteins are schematically shown (the white box indicates alternative exon Vb). The amino acids encoded by the alternative exon Vb are indicated in the second intracellular loop. (**B**) Base complementarity between the antisense element of the human HBII-52 snoRNA and the human 5-HT_{2C}R receptor. Solid arrows indicate the A → I editing sites (A to E). Open arrow, proximal splice site; box, D box.

Institut für Biochemie, Emil-Fischer-Zentrum, Friedrich-Alexander Universität Erlangen-Nürnberg, Fahrstraße 17, 91054 Erlangen, Germany.

*To whom correspondence should be addressed. E-mail: stefan@stamms-lab.net

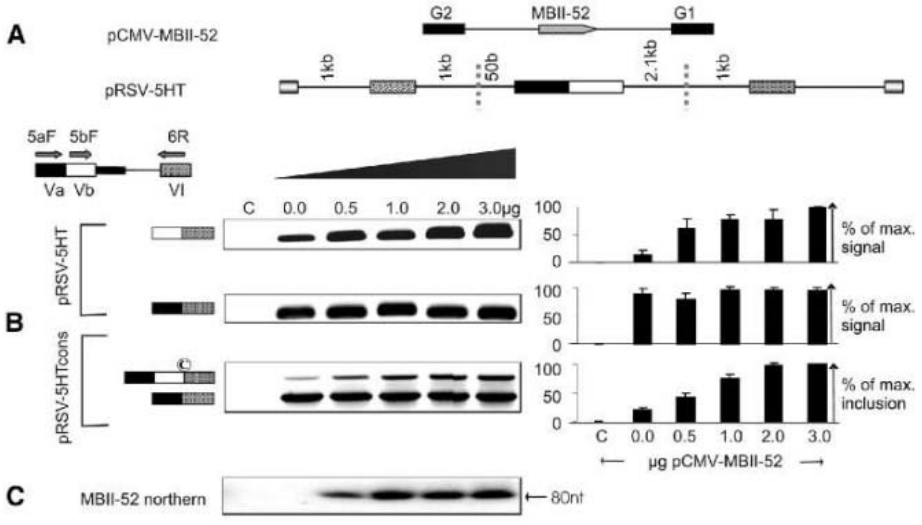

Fig. 2. HBII-52 snoRNA promotes inclusion of exon Vb of the 5-HT_{2C}R. (**A**) Schematic structure of the pCMV-MBII-52 and pRSV-5HT minigenes (fig. S2B). (**B**) Cotransfection of increasing amounts of pCMV-MBII-52 with reporter minigenes in Neuro2A cells. The numbers indicate micrograms of transfected plasmid. The lane labeled C indicates PCR control without reverse transcription. For the wild-type minigene, pRSV-5HT exon-specific primer pairs 5aF/6R and 5bF/6R were used; for the activated minigene, pRSV-5HTcons primers 5aF and 6R that amplify both forms were used. The right panel shows quantification of at least four experiments. At least four independent experiments were quantified by setting the maximum signal (pRSV-5HT) or maximum exon inclusion (pRSV-5HTcons) to 100%. The circled C indicates the consensus 5′ splice site (CAG/GTAAGT). Error bars indicate SD. (**C**) Northern blot showing the increase in MBII-52 expression.

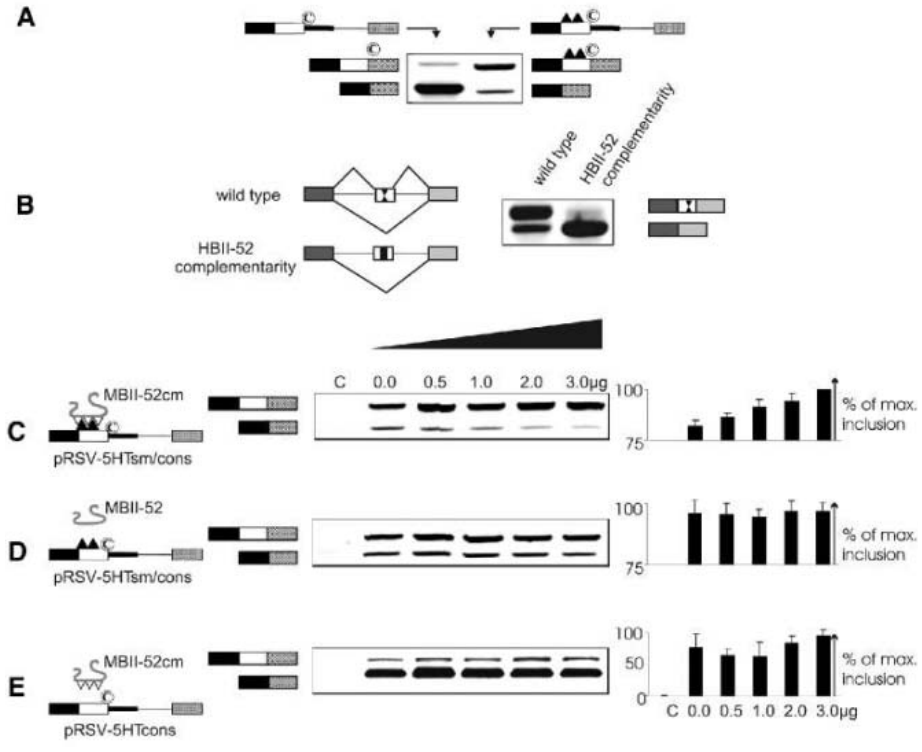

Fig. 3. The snoRNA complementarity region of 5-HT_{2C}R harbors silencing activity that is influenced by snoRNA binding. (**A**) Constructs with the activated distal splice site harboring the wild-type or mutated snoRNA-CR were transfected in Neuro2A cells. The mutation is schematically indicated by triangles on top of exon Vb. The structures of the PCR products are schematically indicated, depending on which minigene was used. The circled C indicates the consensus 5′ splice site. (**B**) The 18-nt snoRNA-CR was introduced into the alternative exon of SXN, a beta-globin based reporter construct, transfected into Neuro2A cells, and analyzed by RT-PCR. (**C** to **E**) Influence of the complementarity between snoRNA and exon Vb on exon Vb usage. The constructs schematically shown on the left were cotransfected in Neuro2A cells. Representative ethidium bromide stained gels are shown (center), and at least four independent experiments are quantified (right). The complementary mutations are indicated by triangles. Error bars indicate SD.

The snoRNA complementarity region (snoRNA-CR) in exon Vb harbors several recently identified putative silencing elements (fig. S3) (*9*). We therefore changed it from CGTAATCCTATTGAGCAT to CGAAAGCCTTTAGACCAT (pRSV-5HTsm/cons, fig. S2B), where the underlined nucleotides indicate those that were mutated. When combined with the consensus 5′ splice site, this mutation now strongly activates exon Vb inclusion (Fig. 3A). The silencing activity was confirmed in a heterologous SXN globin-based reporter system (*10*), where the presence of the snoRNA-CR almost completely silences exon inclusion (Fig. 3B).

We next investigated whether the complementarity between the snoRNA and exon Vb is necessary to influence alternative splicing. We mutated the antisense element of MBII-52 from ATGCTCAATAGGATTACG to ATGGTCTAAAGGCTTTCG (MBII-52cm). This compensatory mutation exhibits sequence complementarity to the mutated snoRNA-CR in pRSV-5HTsm/cons. MBII-52cm further promotes inclusion of exon Vb when cotransfected with the pRSV-5HTsm/cons reporter ($P = 0.004$) (Fig. 3C). In contrast, expressing wild-type MBII-52 snoRNA had no effect (Fig. 3D) on this reporter. Finally, the pRSV-5HTcons reporter containing the original snoRNA-CR was not significantly influenced by the mutated MBII-52cm snoRNA (Fig. 3E), indicating that binding between the snoRNA and exon Vb is necessary for the regulation of alternative splicing.

To test whether HBII-52 exhibits an antisense effect, we mutated the C and D boxes of HBII-52, which prevents formation of a small nucleolar ribonucleoprotein (snoRNP) (*11*), and we used a polymerase II–derived HBII-52 RNA that is not processed into a mature snoRNA. None of these constructs had a significant effect, suggesting that HBII-52 works as an RNP (fig. S4, A to C). We obtained similar results using the minigene constructs with the authentic distal splice site of exon Vb and exon-specific primers (fig. S5), and we did not observe an effect of MBII-52 on the alternative splicing pattern of the unrelated TRA2-beta1 or YT521-B pre-mRNAs (fig. S6).

To test whether HBII-52 binds to exon Vb of the 5-HT_{2C} receptor in vivo, we used an assay that captures the snoRNA:mRNA complex. Binding of HBII-52 to exon Vb was determined by a PCR assay that uses a chimeric primer binding to the 3′ end of the HBII-52 snoRNA and the adjacent part of exon Vb (Fig. 4A and fig. S7). This primer amplifies only RNA from a complex of HBII-52 and 5-HT_{2C}R exon Vb RNAs, but it does not amplify the individual RNAs (Fig. 4A, lanes 1 and 2). We transfected HEK293 with combinations of

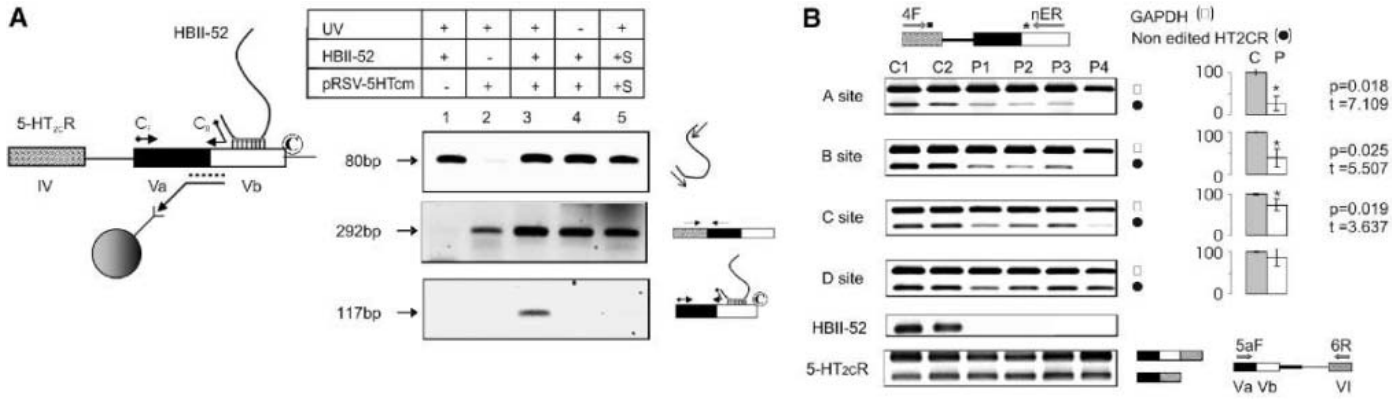

Fig. 4. HBII-52 snoRNA promotes inclusion of nonedited exon Vb by binding to exon Vb RNA. (**A**) HBII-52 binds to 5-HT_{2C}R RNA in vivo. The experimental strategy is shown on the left. 5-HT_{2C}R nuclear RNA complexes were isolated by using a biotinylated oligonucleotide binding to exon Va/b sequences (indicated by dots). The primer pair C_R (GGGCCUCAGUAUUGCUAC) and C_F (TATGTCTGGCCACTACCTAGATATTT) specifically amplifies complexes between HBII-52 snoRNA and 5-HT_{2C}R RNA, because the primer C_R binds only to the complex (fig. S7). The experimental conditions are diagrammed on the right. In lane 5, HBII-52 and 5-HT_{2C}R expression clones were transfected into separate cells (+S), and the resulting lysates were mixed after UV irradiation. The identity of the PCR products is shown on the right (80 nt, HBII-52; 292 nt, 5-HT_{2C}R mRNA; 117 nt, complex-specific amplicon). (**B**) Changes of 5-HT_{2C}R mRNA isoform expression in PWS patients detected by isoform-specific RT-PCR. RNA from similar hippocampal areas from PWS patients (P) and age-matched controls (C) were amplified by RT-PCR. Primers complementary to the nonedited sites, indicated by a star in the scheme on top, were used. GAPDH was amplified in the same reactions. Representative RT-PCR results are shown for each editing site, and their statistical evaluation is shown on the right. The signal was normalized to GAPDH and set to 100% in the control samples (right). The amplification of HBII-52 in controls, but not PWS patients, confirmed the clinical diagnosis (HBII-52). Primers 5aF and 6R amplify similar ratios of isoforms in all samples. Error bars indicate SD.

pCMV-MBII-52 and pRSV-5HTcons constructs and covalently attached base-paired RNA complexes by psoralen crosslinking.

Only when both 5-HT_{2C} pre-mRNA and MBII-52 snoRNA are present in the same cell and subjected to psoralen ultraviolet (UV) crosslinking can a complex between snoRNA and mRNA be detected (Fig. 4A, lane 1 to 3). A complex is not observed without crosslink (lane 4) or when separate cells are transfected, irradiated with UV, and the lysates mixed (lane 5), suggesting that there is an interaction between MBII-52 and 5-HT_{2C} exon Vb in vivo.

This result suggests that in addition to the known editing-dependent pathway of exon Vb inclusion (*5*), HBII-52 snoRNA promotes exon Vb inclusion. HBII-52 snoRNA is absent in patients suffering from PWS, predicting a reduction of the nonedited 5-HT_{2C}R mRNA isoform. We analyzed mRNA from PWS patients and performed reverse transcriptase (RT)–PCR using editing site-specific primers and RNA from the hippocampus, where editing is most prevalent. The last 3′ nucleotide of the primers was complementary to the nonedited nucleotide, amplifying only the nonedited 5-HT_{2C}R mRNA isoform (fig. S8). We coamplified glyceraldehyde phosphate dehydrogenase (GAPDH) in a multiplex primer reaction as a loading control. We found that the amounts of mRNA-containing nonedited exon Vb sequences at the A, B, C, and D sites were reduced to 25, 39, 74, and 89%, respectively, when compared with healthy controls. RT-PCR showed that HBII-52 was absent in PWS patients but present in control individuals. Amplification of all isoforms with primers in exons Va and VI demonstrates that their overall ratio and amount are not significantly changed (Fig. 4B). These findings show a dependency of 5-HT_{2C}R isoform composition on the presence of HBII-52 in a physiological system. They suggest a defect of the 5-HT_{2C}R receptor system in patients with PWS.

Our experiments indicate that HBII-52 influences alternative splicing of the 5-HT_{2C}R pre-mRNA. HBII-52 snoRNA partially blocks a silencer located in the snoRNA-CR in exon Vb. This silencer can also be weakened by editing exon Vb at positions C, D, and E, explaining why editing promotes exon Vb inclusion (*5*). Psoralen crosslink experiments indicate a transient complex between HBII-52 snoRNA and exon Vb. Similar to other C/D-box snoRNAs (*12*), HBII-52 is localized in the nucleolus (*13*), whereas pre-mRNA splicing occurs in the nucleoplasm where snoRNAs are generated during pre-mRNA splicing. It is therefore possible that they can interact transiently with pre-mRNAs, similar to serine/arginine-rich (SR) proteins that are localized predominantly in nuclear speckles but function outside (*14*). Similar to recent reports, we found no evidence that HBII-52 affects editing of nucleoplasmic 5-HT_{2C}R transcripts (fig. S9) (*13*). Our data indicate that HBII-52 promotes the formation of nonedited forms of 5-HT_{2C}R mRNA by an editing-independent mechanism, most likely through the masking of a silencer.

Only mRNAs containing exon Vb encode a functional 5-HT_{2C}R receptor. Because editing of exon Vb changes the amino acid sequence of the receptor and its coupling to G-proteins, it influences the serotonin response. Isoforms of 5-HT_{2C}R mRNA containing nonedited sequences of exon Vb are abnormally low in patients with PWS. Because these 5-HT_{2C}R isoforms show the strongest effect to serotonin, this finding explains why PWS patients respond to selective serotonin reuptake inhibitor treatment (*15*, *16*) and points to defects in the serotonergic system as a contributing cause of PWS.

References and Notes

1. T. Kiss, *Cell* **109**, 145 (2002).
2. J. Cavaille *et al.*, *Proc. Natl. Acad. Sci. U.S.A.* **97**, 14311 (2000).
3. Q. Wang *et al.*, *J. Neurochem.* **74**, 1290 (2000).
4. C. M. Burns *et al.*, *Nature* **387**, 303 (1997).
5. R. Flomen, J. Knight, P. Sham, R. Kerwin, A. Makoff, *Nucleic Acids Res.* **32**, 2113 (2004).
6. O. Stoss, P. Stoilov, A. M. Hartmann, O. Nayler, S. Stamm, *Brain Res. Protocols* **4**, 383 (1999).
7. S. Stamm, D. Casper, V. Hanson, D. M. Helfman, *Brain Res. Mol. Brain Res.* **64**, 108 (1999).
8. L. Zhang, M. Ashiya, T. G. Sherman, P. J. Grabowski, *RNA* **2**, 682 (1996).
9. Z. Wang *et al.*, *Cell* **119**, 831 (2004).
10. L. R. Coulter, M. A. Landree, T. A. Cooper, *Mol. Cell. Biol.* **17**, 2143 (1997).
11. W. Filipowicz, V. Pogacic, *Curr. Opin. Cell Biol.* **14**, 319 (2002).
12. N. J. Watkins, A. Dickmanns, R. Luhrmann, *Mol. Cell. Biol.* **22**, 8342 (2002).
13. P. Vitali *et al.*, *J. Cell Biol.* **169**, 745 (2005).
14. D. L. Spector, *Annu. Rev. Biochem.* **72**, 573 (2003).
15. R. D. Nicholls, S. Saitoh, B. Horsthemke, *Trends Genet.* **14**, 194 (1998).
16. E. Dykens, B. Shah, *CNS Drugs* **17**, 167 (2003).

17. This work was supported by the Deutsche Forschungsgemeinschaft and the Bundesministerium für Bildung und Forschung. We thank K. Collins, H. Soreq, J. Brosius, M. Frilander, T. Cooper, B. Horsthemke, M. Lalande, C. Burge, W. Neuhuber and I. Blümke for critical discussions. The brain and tissue bank was sponsored by NIH grant no. NO1-HD-1-3138.

Supporting Online Material

www.sciencemag.org/cgi/content/full/1118265/DC1
Materials and Methods
Figs. S1 to S9
References

1 August 2005; accepted 30 November 2005
Published online 15 December 2005;
10.1126/science.1118265
Include this information when citing this paper.

Excitatory Effect of GABAergic Axo-Axonic Cells in Cortical Microcircuits

János Szabadics,[1*] Csaba Varga,[1*] Gábor Molnár,[1*] Szabolcs Oláh,[1] Pál Barzó,[2] Gábor Tamás[1]†

Axons in the cerebral cortex receive synaptic input at the axon initial segment almost exclusively from γ-aminobutyric acid–releasing (GABAergic) axo-axonic cells (AACs). The axon has the lowest threshold for action potential generation in neurons; thus, AACs are considered to be strategically placed inhibitory neurons controlling neuronal output. However, we found that AACs can depolarize pyramidal cells and can initiate stereotyped series of synaptic events in rat and human cortical networks because of a depolarized reversal potential for axonal relative to perisomatic GABAergic inputs. Excitation and signal propagation initiated by AACs is supported by the absence of the potassium chloride cotransporter 2 in the axon.

The position of AACs is unique in cortical microcircuits for two reasons: AACs exclusively innervate pyramidal cells and do not form synapses on other cells types; and the input to the axon initial segment of pyramidal cells is provided completely by AACs, apart from a few synapses arriving occasionally from basket cells (*1*–*4*). The input from AACs is surrounded by a high concentration of sodium channels (*5*). These synapses are the closest to the suggested site of the action potential initiation (*5*, *6*). The effect of AACs on the postsynaptic cells is mediated by γ-aminobutyric acid type A ($GABA_A$) receptors. Thus, the polarity of postsynaptic responses is predominantly determined by chloride extrusion mechanisms (*7*–*9*) dominated by the potassium chloride cotransporter 2 (KCC2) in the mature cerebral cortex (*10*). To characterize the function of AACs in cortical microcircuits, we investigated the distribution of KCC2 and the reversal potential of GABAergic inputs in pyramidal cells and revealed that AACs evoke excitatory instead of inhibitory responses. We then confirmed the excitatory action of AACs in cortical networks.

Differential KCC2 expression in distinct types of neurons influences reversal potentials in various brain regions (*10*–*13*). However, quantification of this cotransporter in different regions of neurons is lacking. We used high-resolution immunolocalization to determine the subcellular distribution of KCC2 on layer 2/3 pyramidal cells of rat and human cortex (Fig. 1). In the rat, membranes of somata (n = 38) and membranes of axon initial segments (n = 11) contained higher densities of gold particles compared with background ($P < 0.0001$ for soma, $P < 0.05$ for axon, Fig. 1B). Comparison of immunogold densities after the subtraction of background labeling (0.04 ± 0.01 gold/μm) showed a decrease by a factor of ~44 from somatic to axon initial segment plasma membranes (from 1.34 ± 0.04 to 0.08 ± 0.03 gold/μm, $P < 0.0001$). Density levels dropped at the border between the hillock and the initial segment and remained stationary on individual axon initial segments measured up to 40 μm from the soma. We confirmed our results on the subcellular distribution of KCC2 in the cortex of a human patient, where a ~52-fold difference in labeling was detected between the membranes of somata (n = 20, 1.51 gold/μm) and axon initial segments (n = 4, 0.04 gold/μm) after the subtraction of background (0.01 gold/μm).

Low KCC2 density and decreased chloride efflux support higher $[Cl^-]_{in}$, leading to depolarizing effects of GABA (*7*–*9*, *14*, *15*). Thus, the low concentration of KCC2 detected in the axon initial segment predicts that responses evoked by AACs are depolarizing at resting membrane potential. We directly compared the reversal potential of GABAergic inputs arriving at the perisomatic region of pyramidal cells elicited by AACs and basket cells in layers 2/3 of rat somatosensory cortex in vitro (Fig. 2A). We performed paired recordings of presynaptic interneurons and postsynaptic pyramidal cells using gramicidin perforated patches in order to keep the postsynaptic $[Cl^-]_{in}$ undisturbed. Basket cells (n = 5), targeting somata (23 ± 7%), dendritic shafts (62 ± 12%), and spines (15 ± 8%), as examined in the electron microscope, elicited unitary inhibitory postsynaptic potentials (IPSPs) with reversal potentials of –73.3 ± 3.0 mV (range, –67.1 to –76.6 mV). AACs were identified on the basis of light microscopic reconstructions showing axonal candles or cartridges specific to this cell type (*3*, *4*) (Fig. 2B). The

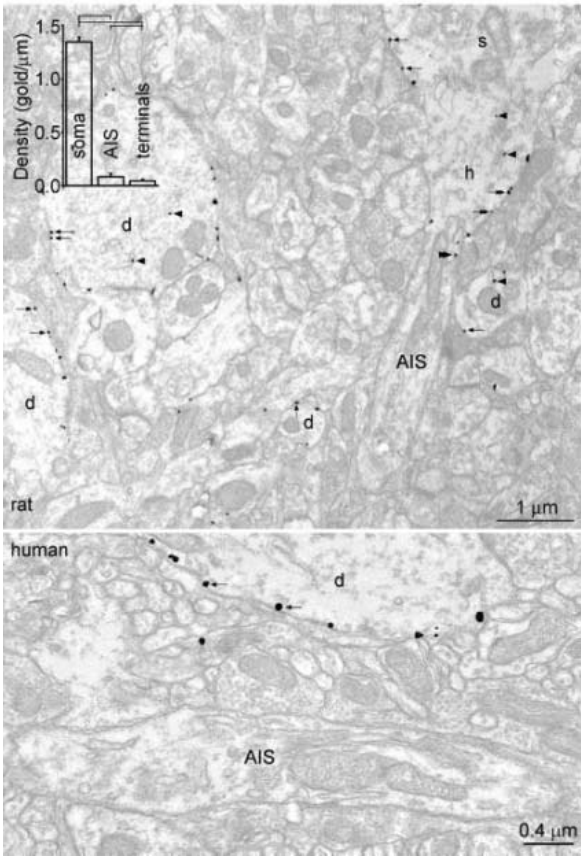

Fig. 1. Localization of KCC2 immunoreactivity in layer 2/3 of rat (**top**) and human (**bottom**) cerebral cortex. Gold particles labeling KCC2 (arrows) are predominantly found along somatic (s) and dendritic (d) membranes and cytoplasm (arrowheads). Gold particles (double arrows) are also attached to the membrane of the axon hillock (h), but the density of gold particles (double arrowheads) drops on the axon initial segment (AIS). (Inset) Quantitative evaluation of immunogold distribution of KCC2 on different subcellular compartments of cortical pyramidal cells. Bars indicate significant differences.

[1]Department of Comparative Physiology, [2]Department of Neurosurgery, University of Szeged, Közép fasor 52, Szeged, H-6726, Hungary.

*These authors contributed equally to this work.

†To whom correspondence should be addressed. E-mail: gtamas@bio.u-szeged.hu

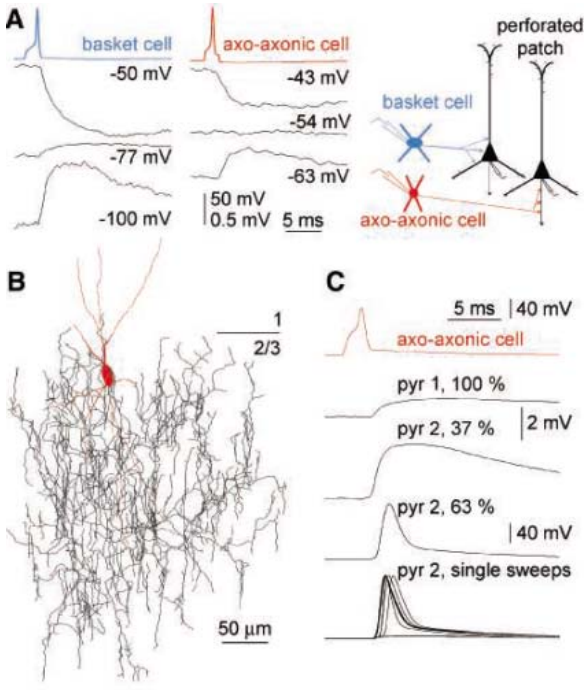

Fig. 2. Depolarizing effect of AACs. (**A**) Unitary interactions from basket and AACs to pyramidal cells reveal different reversal potentials for perisomatic and axonal GABAergic inputs (–72 and –54 mV, respectively). (**B**) Reconstruction of an AAC in the layer 2/3 of somatosensory cortex of the rat (soma and dendrites, red; axons, black). (**C**) Simultaneous triple recording of an AAC (red) and two pyramidal cells (black, pyr 1 and 2) recorded with axonal $[Cl^-]_{in}$ in whole-cell mode. Single action potentials in the AAC elicited subthreshold depolarizing GABAergic postsynaptic potentials (dIPSPs) on pyramid 1 and triggered postsynaptic action potentials in the majority of trials on pyramid 2 from resting membrane potential.

reversal potential of GABAergic responses evoked by AACs was more depolarized (n = 7; –51.1 ± 5.4 mV; range: –42.5 to –58.3 mV, $P < 0.001$). Experiments in which the postsynaptic cells were recorded in whole-cell configuration with an intracellular solution producing a reversal potential of –48.2 ± 4.4 mV (n = 9) for GABAergic responses (Fig. 2B). Applying these conditions, AACs evoked exclusively subthreshold responses from the resting membrane potential (–72 ± 2 mV) in 15 pyramidal cells with amplitudes of 0.75 ± 0.4 mV. However, in two pyramidal cells in which the amplitude of the subthreshold responses was 3.1 and 1.2 mV, single spikes in two presynaptic AACs elicited postsynaptic action potentials with a probability of 62 and 57%, peak latencies of 2.48 and 2.61 ms, and a temporal variance of 0.35 and 0.58 ms, respectively. Inputs from basket cells could not evoke action potentials at similar circumstances in spite of having a larger amplitude 2.53 ± 1.81 (range, 0.33 to 5.43 mV, n = 33).

The experiments described above show that AACs elicit depolarizing, excitatory responses at axon initial segments of postsynaptic pyramidal cells. Although our whole-cell recordings suggest that spike-to-spike coupling might occur between AACs and pyramidal neurons, a clear demonstration of spike transmission requires experiments in which the pyramidal cells are undisturbed. Thus, we looked for the synaptic output of pyramidal neurons left unrecorded in the network to detect their firing (*16*, *17*). In supragranular cortical layers, pyramidal neurons are the exclusive locally triggered sources of glutamatergic excitatory postsynaptic potentials (EPSPs) and the only targets of AACs (*4*). EPSPs triggered by AACs are therefore sufficient for detecting pyramidal cell firing. We applied simultaneous recordings from up to four neighboring AAC and various cortical neurons using an intracellular solution with low $[Cl^-]_{in}$ at membrane potentials of –56 ± 3 mV in order to easily discriminate EPSPs and IPSPs in the rat and human cortex (Fig. 3). Single spikes in rat AACs triggered temporally fixed series of multiple synaptic events with reliabilities characteristic to unitary, single cell–to–single cell transmission (Fig. 3, A to E). 22 out of 48 AACs (46%) elicited short latency (0.81 ± 0.31 ms) unitary IPSPs in pyramidal cells (n = 9), which were followed by longer latency (3.71 ± 0.90 ms, $P < 0.001$), presumably disynaptic EPSPs on the same (n = 3) or different (n = 5) pyramidal cells and on various interneurons (n = 19). Application of the AMPA receptor antagonist 2,3-dihydroxy-6-nitro-7-sulfamoylbenzo[*f*]quinoxaline (NBQX) (10 µM) reversibly blocked these EPSPs (n = 3, Fig. 3, E and F). Disynaptic EPSPs were highly reliable (failure rate: 25.8 ± 20.7%), and their kinetic properties were similar to monosynaptic EPSPs evoked by pyramidal cells on the same types of postsynaptic neurons. Disynaptic, recurrent EPSPs were detected while we recorded the firing pattern of several AACs (n = 18, Fig. 3B) and were similar to depolarizing afterpotentials found in hippocampal AACs (*18*). In these cells, as in the hippocampal AACs, spike doublets were also identified during spontaneous firing. Abandoning and repatching of the recorded AACs (n = 4) with a new pipette did not change the identified synaptic signal sequences, which excluded the possibility that multiple events could be activated by interactions between the recording pipette and parts of different cells (Fig. 3C). Pharmacological experiments showed that AACs are capable of recruiting local glutamatergic cells through GABAergic synapses (n = 7, Fig. 3, E and F). The specific $GABA_A$ receptor antagonist gabazine (20 µM) reversibly blocked monosynaptic IPSPs, as well as disynaptic EPSPs. The dual sensitivity of disynaptic EPSPs to gabazine and NBQX rules out the involvement of gap junctions in the underlying circuit. We also recorded from human layer 2/3 axo-axonic cells (n = 4) and confirmed GABAergic recruitment of local pyramidal cells (Fig. 3D). Moreover, a human example also showed that second-order spikes in pyramidal cells initiated by axo-axonic GABAergic synapses project powerfully to neighboring interneurons and trigger third-order action potentials. Third-order feedback EPSPs similar to depolarizing afterpotentials were also detected in human AACs.

Our results show that instead of exclusively inhibiting the axon initial segment, AACs can act as unique excitatory neurons in the cortex. High sodium channel density and/or sodium channels with a shifted voltage dependence at relatively proximal parts of the axon (*5*, *19*) and the high-density synaptic input in an area with a very high surface-to-volume ratio favor the output-generating effectiveness of depolarizing inputs from AACs. The unique proximity of input from AACs to the first axonal branch point suggested as the site of spike initiation in neurons might also contribute to the generation of AAC-triggered EPSPs in the network (*6*). Although ephaptic or gap-junctional coupling was proposed for functional interaction between axons as a mechanism for signal propagation in neural circuits (*17*), the dual sensitivity to $GABA_A$ and AMPA receptor antagonists of network events triggered by AACs shows the requirement of chemical synapses. The ionic equilibrium for GABAergic inputs is dynamically regulated by cellular and network mechanisms (*7*–*9*, *14*). Intraneuronal chloride gradients are important in neural computation (*12*, *13*) and depolarized GABA reversal potentials in interneurons could lead to GABAergic excitation within networks of GABAergic cells (*10*, *13*, *20*). The membrane potential of pyramidal cells and thus the effectiveness of axo-axonic spike transmission is regulated by local circuits through dynamic

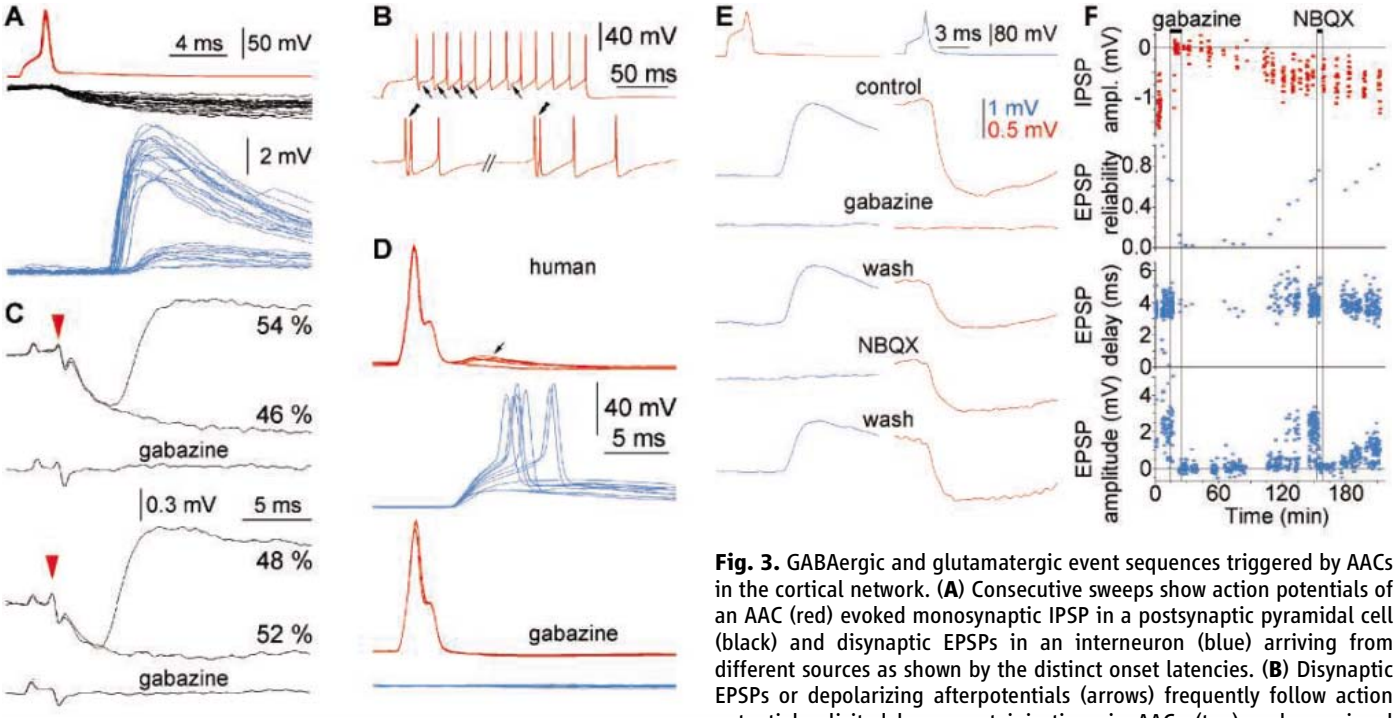

Fig. 3. GABAergic and glutamatergic event sequences triggered by AACs in the cortical network. (**A**) Consecutive sweeps show action potentials of an AAC (red) evoked monosynaptic IPSP in a postsynaptic pyramidal cell (black) and disynaptic EPSPs in an interneuron (blue) arriving from different sources as shown by the distinct onset latencies. (**B**) Disynaptic EPSPs or depolarizing afterpotentials (arrows) frequently follow action potentials elicited by current injections in AACs (top) and occasional spike doublets occur (double arrowheads) during spontaneous firing (bottom). (**C**) Spikes in an AAC (red triangles) elicited monosynaptic IPSPs, which were followed by convergent disynaptic EPSPs in 54% of trials in a pyramidal cell (black). Application of gabazine (20 μM) blocked IPSPs, as well as the EPSP. Repatching the presynaptic cell during washout with a different recording pipette did not alter the IPSP-EPSP sequence and its sensitivity to gabazine. (**D**) A human axo-axonic cell (red) shows recurrent, disynaptic EPSPs (arrow) on single consecutive sweeps following the action potential, which elicited disynaptic EPSPs capable of initiating third-order spikes in a simultaneously recorded interneuron (blue). Disynaptic EPSPs and downstream spikes were blocked by gabazine (20 μM). (**E** and **F**) Both GABAergic and glutamatergic mechanisms are necessary for reliable triggering of disynaptic EPSPs. (E) An interneuron (blue) elicited a unitary IPSP in an AAC (red), and the AAC triggered a disynaptic EPSP in the interneuron. Application of gabazine (20 μM) blocked both responses (averages of 20 traces) with a recovery on washout. NBQX (10 μM) reversibly eliminated the disynaptic EPSP and had no effect on the IPSP. (F) The reliability (averages of ten consecutive sweeps) and single amplitudes of the disynaptic EPSPs showed recovery in parallel with the amplitude of the IPSP, but the onset delay of disynaptic EPSPs remained relatively stationary.

changes in the proportional balance of in excitation and inhibition during diverse cortical tasks (*21*, *22*). Our results paradoxically suggest that postsynaptic hyperpolarization or "down" state and sodium channel deinactivation helps axo-axonic spike triggering, but "up" states, depolarization, and sodium channel inactivation could limit axo-axonic inputs to shunting or hyperpolarizing. AACs, therefore, might have a bistable role in neural circuits. Indeed, firing of AACs stereotypically precedes or follows activation of pyramidal cells depending on the operational state of the network in vivo (*23*, *24*). Simultaneous activation of a fraction of the several hundred postsynaptic pyramids innervated by a single AAC (*3*, *4*) could lead to synchronous recruitment of network activity as observed during the onset of cortical ripples (*24*). AACs do not target GABAergic interneurons (*3*, *4*); therefore, they are well suited for initiating repeatable event sequences in the cortical microcircuit (*25*, *26*) through selective spike triggering in pyramidal cells followed by downstream recruitment of inhibition that enforces spatiotemporal fidelity in signal propagation (*27*, *28*).

References and Notes

1. J. Szentagothai, M. A. Arbib, *Neurosci. Res. Program Bull.* **12**, 305 (1974).
2. P. Somogyi, *Brain Res.* **136**, 345 (1977).
3. T. F. Freund, G. Buzsaki, *Hippocampus* **6**, 347 (1996).
4. P. Somogyi, G. Tamas, R. Lujan, E. H. Buhl, *Brain Res. Brain Res. Rev.* **26**, 113 (1998).
5. C. M. Colbert, D. Johnston, *J. Neurosci.* **16**, 6676 (1996).
6. B. A. Clark, P. Monsivais, T. Branco, M. London, M. Hausser, *Nat. Neurosci.* **8**, 137 (2005).
7. U. Misgeld, R. A. Deisz, H. U. Dodt, H. D. Lux, *Science* **232**, 1413 (1986).
8. K. J. Staley, B. L. Soldo, W. R. Proctor, *Science* **269**, 977 (1995).
9. J. A. Payne, C. Rivera, J. Voipio, K. Kaila, *Trends Neurosci.* **26**, 199 (2003).
10. C. Rivera *et al.*, *Nature* **397**, 251 (1999).
11. M. Martina, S. Royer, D. Pare, *J. Neurophysiol.* **86**, 2887 (2001).
12. A. Gulacsi *et al.*, *J. Neurosci.* **23**, 8237 (2003).
13. K. E. Gavrikov, A. V. Dmitriev, K. T. Keyser, S. C. Mangel, *Proc. Natl. Acad. Sci. U.S.A.* **100**, 16047 (2003).
14. B. E. Alger, R. A. Nicoll, *Nature* **281**, 315 (1979).
15. A. T. Gulledge, G. J. Stuart, *Neuron* **37**, 299 (2003).
16. B. Katz, R. Miledi, *J. Physiol.* **192**, 407 (1967).
17. D. Debanne, *Nat. Rev. Neurosci.* **5**, 304 (2004).
18. E. H. Buhl *et al.*, *J. Neurophysiol.* **71**, 1289 (1994).
19. G. Stuart, N. Spruston, B. Sakmann, M. Hausser, *Trends Neurosci.* **20**, 125 (1997).
20. J. Chavas, A. Marty, *J. Neurosci.* **23**, 2019 (2003).
21. M. Steriade, A. Nunez, F. Amzica, *J. Neurosci.* **13**, 3252 (1993).
22. Y. Shu, A. Hasenstaub, D. A. McCormick, *Nature* **423**, 288 (2003).
23. Y. Zhu, R. L. Stornetta, J. J. Zhu, *J. Neurosci.* **24**, 5101 (2004).
24. T. Klausberger *et al.*, *Nature* **421**, 844 (2003).
25. M. Abeles, *Corticonics* (Cambridge Univ. Press, Cambridge, 1991).
26. Y. Ikegaya *et al.*, *Science* **304**, 559 (2004).
27. F. Pouille, M. Scanziani, *Nature* **429**, 717 (2004).
28. R. D. Traub, M. A. Whittington, I. M. Stanford, J. G. Jefferys, *Nature* **383**, 621 (1996).

29. This work was supported by the Wellcome Trust, NIH N535915, Boehringer Ingelheim Fonds, the Hungarian National Office for Research and Technology (NKTH) RET008/2004, and the Hungarian National Foundation for Scientific Research (OTKA) TO49535. The authors thank Z. Nusser for comments on a previous version of the manuscript and E. Tóth for technical assistance.

Supporting Online Material

www.sciencemag.org/cgi/content/full/311/5758/233/DC1
Materials and Methods
References

13 October 2005; accepted 5 December 2005
10.1126/science.1121325

Long-Term Transmission of Defective RNA Viruses in Humans and *Aedes* Mosquitoes

John Aaskov,[1] Katie Buzacott,[1] Hlaing Myat Thu,[1,2] Kym Lowry,[1,3] Edward C. Holmes[4]*

In 2001, dengue virus type 1 (DENV-1) populations in humans and mosquitoes from Myanmar acquired a stop-codon mutation in the surface envelope (E) protein gene. Within a year, this stop-codon strain had spread to all individuals sampled. The presence of truncated E protein species within individual viral populations, along with a general relaxation in selective constraint, indicated that the stop-codon strain represents a defective lineage of DENV-1. We propose that such long-term transmission of defective RNA viruses in nature was achieved through complementation by coinfection of host cells with functional viruses.

Many RNA virus populations show high levels of genetic diversity because of the error-prone nature of their replication with RNA-dependent RNA polymerase and their large population sizes (*1*). However, most studies of genetic diversity in RNA viruses have considered consensus nucleotide sequences, which represent a population average of the myriad of diverse viral genomes within an infected host. The exceptions tend to be longitudinal studies of viruses generating chronic infections, such as the human immunodeficiency virus (*2*) and the hepatitis C virus (*3*). There have been few equivalent studies of RNA viruses causing acute infections, although they provide an opportunity to determine how population genetic diversity is shaped by rapidly alternating cycles of intra- and interhost evolution. Flaviviruses, such as dengue virus (DENV), constitute an ideal model system because they have distinct human and mosquito hosts and because transmission rates vary dramatically among "wet" and "dry" seasons as a result of the availability of breeding sites for the *Aedes* mosquito vectors. In areas where dengue is hyperendemic and three or four DENV serotypes may cocirculate, outbreaks occur in cycles of 3 to 5 years, often with changes in the relative proportions of each virus serotype sampled (*4*, *5*).

To reveal the evolution of RNA virus populations within and among hosts, we examined DENV-1 recovered from patients at the Yangon Children's Hospital in Myanmar between August 2000 and December 2002, as well as from mosquitoes sampled at the same time (*5*, *6*). This sampling period covered a year (2000) in which relatively few cases of dengue occurred (1229 in Yangon) and two dengue "seasons" (2001, 2002) during which the largest numbers of dengue cases on record were reported in Yangon (7383 and 5185 cases, respectively). In the 2001 season, 95% of the viruses recovered were DENV-1, and most patients had primary infections and mild disease (*5*). In contrast, all four DENV serotypes were recovered from patients in 2002 in the following proportions: DENV-1, 43%; DENV-2, 35%; DENV-3, 4%; and DENV-4, 18%. 2002 also was characterized by a higher incidence of patients with secondary infections and more severe disease.

We sequenced 20 clones corresponding to the viral envelope (E) glycoprotein genes of DENV-1 populations from 14 individuals—11 from sera from dengue patients and 3 from isolates from individual mosquitoes—at a single time point during their infection. Ten clones from an additional mosquito also were sequenced as described previously (*7*). The number of variable nucleotide sites within individual viral populations ranged from 47 to 162, the average pairwise genetic diversity within each sample was approximately 1%, and the average ratio of nonsynonymous to synonymous substitutions (d_N/d_S) was 0.565 (Table 1) (*8*). Despite such extensive diversity, the majority (mean 77%) of the mutations occurred only once within an individual, and overall consensus sequences were more conserved; three pairs of individuals had identical consensus sequences, and the total number of variable sites among consensus sequences was 76. This was reduced to only 23 if the divergent population from patient D1.Myanmar.43826/01 was excluded. Such contrasting patterns of genetic variation within and among individuals suggest that the majority of the mutations in DENV are deleterious and eventually removed by purifying selection, resulting in consensus sequences that are relatively stable in the long term and in lower d_N/d_S ratios than observed at the intrahost level (*9*, *10*). Further evidence that these data represent genetic diversity before the action of widespread natural selection was that stop codons were detected in at least one clone from 13 of the 15 virus populations, mostly the result of frame shifts after single-nucleotide deletions.

However, the most striking feature of these data was the high frequency of a stop codon at amino acid E 248 (nucleotide 742), caused by a C → U transition. This stop-codon mutation was found in 68 of the 290 sequences (23%), representing 9 of the 15 individuals (6 human, 3 mosquito). It was first detected in three of four virus populations from mosquitoes collected in June 2001 as the outbreak in that year began, and then in one of the five virus populations recovered from patients during the 2001 dengue season. However, all five virus populations sampled in 2002 contained viruses with the stop codon at E 248. Moreover, in three samples—D1.Myanmar.Mos206/01, D1.Myanmar.48572/02, and D1.Myanmar.49440/02—the stop codon was the most common form.

To determine whether this stop-codon mutation arose independently in each patient, such that it represents a hot spot for mutation or recombination, or was transmitted among patients, we conducted a phylogenetic analysis on all 290 DENV-1 sequences (Fig. 1) (*11*). This revealed that the stop-codon sequences formed a single phylogenetic group that was strongly associated with seven other amino acid changes at E 242, 269, 316, 363, 373, 417, and 458, and no evidence of recombination. Hence, the stop-codon variant represents a distinct lineage of DENV-1 that has been transmitted among humans and mosquitoes for at least 18 months. To determine the age of each amino acid mutation associated with the stop-codon lineage, we mapped their occurrence onto the phylogenetic tree using parsimony (*12*). The eight amino acid changes that defined the stop-codon lineage fell on the main trunk of the tree, with most synonymous mutations specific to individual viruses. The first amino acid changes to appear (those that fall deepest in the tree) were the stop-codon mutation at E 248 and the only change 5′ to it, at E 242 (Fig. 1).The remaining six amino acid changes were acquired sequentially from the stop codon toward the carboxy terminal of the E protein; that is, in the order E 269, E 316, E 363 and E 373 together, E 417, and finally E 458. Our phylogenetic analysis also revealed the existence of a second distinct viral lineage, defined

[1]School of Life Sciences, Queensland University of Technology, 2 George Street, Brisbane, 4001, Australia. [2]Department of Medical Research, Ziwaka Road, Yangon 11191, Myanmar. [3]Australian Army Malaria Institute, Enoggera, Brisbane, 4051, Australia. [4]Center for Infectious Disease Dynamics, Department of Biology, The Pennsylvania State University, Mueller Laboratory, University Park, PA 16802, USA.

*To whom correspondence should be addressed. E-mail: ech15@psu.edu

Table 1. Characteristics of DENV-1 populations. Virus populations sampled from individual mosquitoes are shown in italics. DF, dengue fever; DHF, dengue hemorrhagic fever; DSS, dengue shock syndrome; S, number of segregating sites; π, mean pairwise genetic diversity; d_N/d_S, mean number of nonsynonymous/synonymous substitutions per site.

Virus population	Date isolated (mm/yyyy)	Day of symptoms	Infection/disease	No. clones	No. clones with stop codon	S	Unique mutations (%)	π	d_N/d_S
D1.Myanmar.Mos059/01	06/2001			20	0	83	58 (70)	0.010	0.523
D1.Myanmar.Mos194/01	06/2001			20	10	162	141 (87)	0.015	0.690
D1.Myanmar.Mos206/01	06/2001			10	6	79	13 (16)	0.023	0.121
D1.Myanmar.Mos305/01	06/2001			20	10	85	69 (81)	0.009	0.855
D1.Myanmar.37045/00	08/2000	4	Primary/DHFII	20	0	54	52 (96)	0.004	0.464
D1.Myanmar.38518/01	05/2001	5	Primary/?	20	0	143	115 (80)	0.013	0.265
D1.Myanmar.40530/01	07/2001	2	Primary/DHFI	20	1	128	106 (83)	0.012	0.233
D1.Myanmar.40906/01	07/2001	5	Primary/DF	20	0	70	44 (63)	0.008	0.558
D1.Myanmar.43549/01	09/2001	2	Primary/DHFII	20	0	51	46 (90)	0.004	0.846
D1.Myanmar.43826/01	10/2001	2	Primary/DHFI	20	0	54	53 (98)	0.004	0.635
D1.Myanmar.47185/02	07/2002	4	Primary/DSS	20	9	87	67 (77)	0.009	0.631
D1.Myanmar.47662/02	07/2002	2	Primary/DF	20	1	78	65 (83)	0.007	0.345
D1.Myanmar.48572/02	08/2002	2	Primary/DF	20	11	47	34 (72)	0.006	1.107
D1.Myanmar.49440/02	09/2002	4	Primary/DF	20	11	89	70 (79)	0.009	0.624
D1.Myanmar.50457/02	12/2002	3	Secondary/DF	20	9	112	86 (77)	0.012	0.582
Mean						88	68 (77)	0.001	0.565

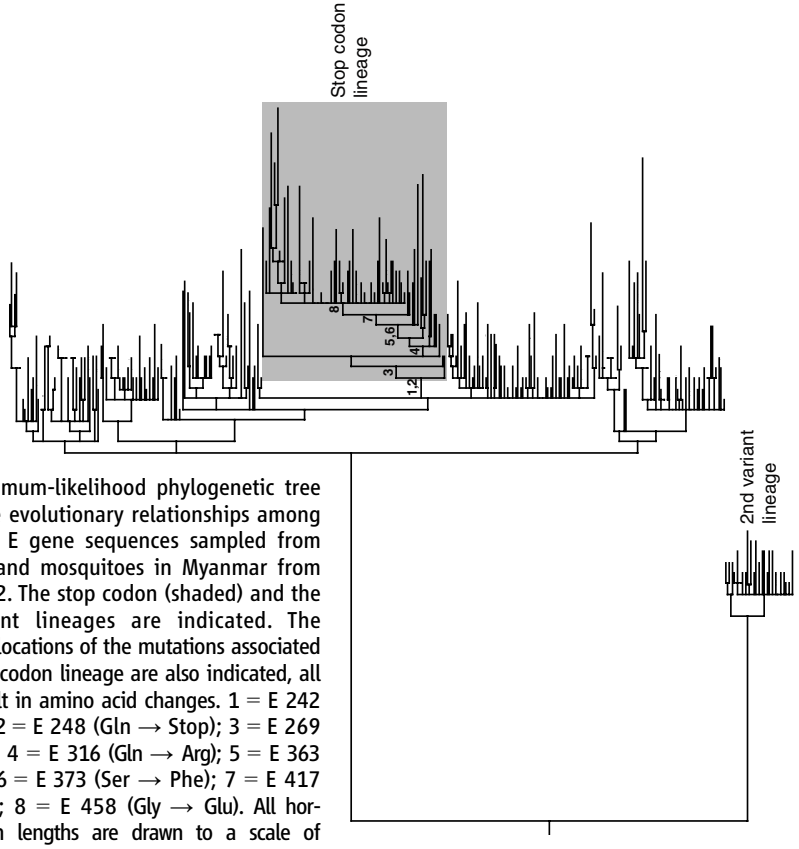

Fig. 1. Maximum-likelihood phylogenetic tree depicting the evolutionary relationships among 290 DENV-1 E gene sequences sampled from 15 patients and mosquitoes in Myanmar from 2000 to 2002. The stop codon (shaded) and the second-variant lineages are indicated. The phylogenetic locations of the mutations associated with the stop-codon lineage are also indicated, all of which result in amino acid changes. 1 = E 242 (Thr → Ser); 2 = E 248 (Gln → Stop); 3 = E 269 (Glu → Gly); 4 = E 316 (Gln → Arg); 5 = E 363 (Lys → Asn); 6 = E 373 (Ser → Phe); 7 = E 417 (Asp → Gly); 8 = E 458 (Gly → Glu). All horizontal branch lengths are drawn to a scale of nucleotide substitutions per site.

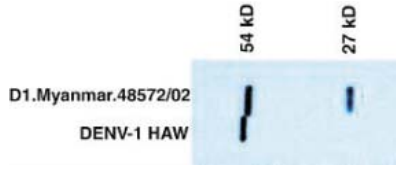

Fig. 2. Indirect ELISA with a monoclonal antibody (M17) to DENV-1 E protein on Western blots of lysates of *Aedes albopictus* cells (C6-36) infected with the prototype strain DENV-1 HAW or a Myanmar population of DENV-1, which contains a stop codon at E248.

by seven amino acid changes. This comprised 25 sequences from four individuals, including all those from patient D1.Myanmar.43826/01, which explains why this individual has such a divergent consensus sequence.

There are two possible explanations for the long-term transmission of the stop-codon lineage of DENV-1: (i) that "read-through" of a stop codon, as occurs in some alphaviruses (*13*), has allowed the production of a full-length and functional E protein, or (ii) that it represents a defective strain of DENV-1 that is transmitted through the population by means of a complementation mechanism. To test these hypotheses, we determined the number of E protein species within viral samples containing the stop-codon variant (Fig. 2) (*14*). Mosquito cells infected with the prototype strain of DENV-1 (HAW), which has a functional codon at E 248, contained a single species of E protein with a molecular weight of 54 kD, which is approximately that predicted from its complete amino acid sequence. In contrast, cells infected with viruses from D1.Myanmar.48572/02, characterized by a mixture of wild-type and stop codons at E 248, contained two forms of E protein. One resembled the full-length E, whereas a smaller band had a molecular weight of 27 kD, that predicted for the amino-terminal region of the E protein up to a stop codon at E 248. The stop-codon

Table 2. Numbers of nonsynonymous and synonymous substitutions per site (d_N/d_S) for different regions and lineages of DENV-1. Because of the large size of the wild-type DENV-1 lineage, this analysis was conducted on a random sample of 66 sequences from 14 individuals.

Lineage (n)	5′ to stop (247 amino acids)	3′ to stop (247 amino acids)
Wild type (66)	0.234	0.494
Stop codon (68)	0.586	1.020

mutation therefore generates a prematurely truncated and hence nonviable E protein.

Additional evidence that the stop-codon lineage comprised defective viruses was supplied by an analysis of selection pressures (*8*) and substitution patterns. Most notably, there was about a twofold increase in d_N/d_S in the region 3′ to the stop codon in the stop-codon lineage, and the d_N/d_S value observed, 1.020, was exactly that expected under strictly neutral evolution (Table 2). A similar increase in d_N/d_S was observed 5′ to the stop codon in the stop-codon lineage. This suggests that selection pressures in this region have also been relaxed, even though protein translation seems to proceed normally. There was no evidence for positive selection in either gene region (*15*). Further, all eight amino acid changes that characterized the stop-codon lineage were nonconservative and occurred at sites that were invariant among all available DENV-1 E gene sequences sampled from localities other than Myanmar (n = 155), which suggests that they have a major effect on fitness. Similarly, these mutations were not predicted to have any effect on RNA secondary structure, either on the positive or the negative strands, and frequent stop codons were observed in alternate reading frames. Hence, the stop-codon lineage is associated with the stepwise accumulation of amino acid changes by mutation-drift that would most likely be deleterious in a fully functional virus. However, the underlying cause of the sequential ordering of substitutions in the stop-codon lineage, chance or otherwise, is unknown.

These results have important implications for the evolutionary dynamics of RNA viruses. First, although the consensus nucleotide sequence from each infected individual is similar, a number of distinct lineages have been stably transmitted among human and mosquito populations. Hence, the consensus sequence paints a misleading picture of population genetic diversity, which may have a complex genealogical history. More striking was the observation that an evolutionary lineage that is associated with defective viruses due to the acquisition of a stop codon has been transmitted for 18 months among humans and mosquitoes and through periods of relatively high and low DENV prevalence. The most likely mechanism for such sustained transmission is complementation, in which defective genomes are rescued through the parasitism of functional proteins from wild-type viruses. Although there is growing evidence for the importance of complementation in RNA viruses (*16*–*19*), that defective viruses can be retained through so many cycles of transmission in nature is unexpected. Indeed, DENV-1 recovered from patients in New Caledonia in February 2003 and in Singapore in August 2004 also contained the stop codon at E248, indicating that this defective strain has entered transmission cycles thousands of kilometers apart. Such long-term complementation not only implies that multiple infections of the same cell are commonplace (*18*) but that long-term population sizes are large enough to prevent severe bottlenecks at transmission. That at least three lineages of DENV-1 have been transmitted among humans and mosquitoes in Myanmar also argues against the occurrence of widespread population bottlenecks.

It seems counterintuitive that mutations that generate intragenic stop codons or that disrupt the structure or function of the E protein (for example, the disruption of a disulfide bridge by a Cys-Arg change at E 121) should reach such high frequency within viral populations. It is theoretically possible that the transmission of defective lineages is selectively advantageous for coinfecting wild-type viruses by ensuring the presence of viruses differentially adapted to human or mosquito cells, decoying host immune responses, or allowing the production of extra capsid and membrane proteins. However, we observed a general relaxation in selective constraint in the stop-codon lineage, and in most evolutionary models complementation has an adverse effect on fitness because deleterious mutations are allowed to persist in the population (*20*). In this context, it is noteworthy that the increased frequency of the stop-codon strain was concomitant with a major reduction in DENV-1 prevalence in Myanmar. Whether this was a cause, a consequence, or coincident with these larger scale epidemiological patterns is unknown, although "hyperparasites," as perhaps represented by the stop-codon strain of DENV-1, are predicted to have important effects on pathogen transmission and virulence (*21*).

References and Notes

1. A. Moya, E. C. Holmes, F. González-Candelas, *Nat. Rev. Microbiol.* **2**, 279 (2004).
2. R. Shankarappa *et al.*, *J. Virol.* **73**, 10489 (1999).
3. P. Farci *et al.*, *Science* **288**, 339 (2000).
4. A. Nisalak *et al.*, *Am. J. Trop. Med. Hyg.* **68**, 191 (2003).
5. H. M. Thu *et al.*, *Emerg. Infect. Dis.* **10**, 593 (2004).
6. Sera were collected from patients admitted to the Yangon Children's Hospital, Myanmar. Nonengorged female *Aedes aegypti* mosquitoes were collected in and around the homes of dengue patients and stored, individually, in sterile microfuge tubes. DENV was recovered from individual mosquitoes in cultures of C6-36 *Aedes albopictus* cells and serotyped as described previously (*5*).
7. S. Craig *et al.*, *J. Virol.* **77**, 4463 (2003). See (*22*).
8. The mean numbers of nonsynonymous and synonymous substitutions per site (ratio d_N/d_S) were estimated using the Nei-Gojobori method as implemented in the MEGA2 package (*23*).
9. E. C. Holmes, *J. Virol.* **77**, 11296 (2003).
10. V. Wittke *et al.*, *Virology* **301**, 148 (2002).
11. Phylogenetic trees were estimated using the maximum-likelihood method available in PAUP* (*24*). The GTR+I+Γ_4 model of nucleotide substitution was employed, with the relevant parameter values estimated from the empirical data (available from the authors on request). Because of the large number of sequences analyzed, branch swapping was restricted to the nearest-neighbor interchange (NNI) method.
12. D. R. Maddison, W. P. Maddison, *MacClade: Analysis of Phylogeny and Character Evolution, Version 4* (Sinauer Associates, Sunderland, MA, 2000).
13. E. G. Strauss, R. Levinson, C. M. Rice, J. Dalrymple, J. H. Strauss, *Virology* **164**, 265 (1988).
14. C6-36 ***Aedes albopictus*** mosquito cells infected with different strains of DENV-1 were lysed 4 days after infection, and the viral and cellular proteins were separated on 10% polyacrylamide gel electrophoresis (PAGE) gels. After transfer of proteins to nitrocellulose by Western blotting, DENV-1 E protein was detected by indirect enzyme-linked immunosorbent assay (ELISA) with DENV-1–specific monoclonal antibody M 17 (*25*). The size of the E protein and its fragment was estimated by comparison with prestained molecular weight markers.
15. Codon-specific analyses of d_N/d_S were undertaken using the single-likelihood ancestor counting (SLAC) method available at the Datamonkey web facility (*26*). This analysis was conducted with both the HKY85 and general reversible (REV) models of nucleotide substitution on phylogenetic trees inferred under the Neighbor-Joining method, and a cut-off P value of 0.1.
16. J. Garcia-Arriaza, S. C. Manrubia, M. Toja, E. Domingo, C. Escarmís, *J. Virol.* **78**, 11678 (2004).
17. B. Kassanis, H. L. Nixon, *Nature* **336**, 435 (1960).
18. I. S. Novella, D. D. Reissig, C. O. Wilke, *J. Virol.* **78**, 5799 (2004).
19. M. Lopez-Ferber, O. Simon, T. Williams, P. Caballero, *Proc. R. Soc. Lond. B. Biol. Sci.* **270**, 2249 (2003).
20. R. Froissart *et al.*, *Genetics* **168**, 9 (2004).
21. D. R. Taylor, A. M. Jarosz, R. E. Lenski, D. W. Fulbright, *Am. Nat.* **151**, 343 (1998).
22. In all cases, DNA sequencing was performed on both strands. Our final data set consisted of 290 sequences, 1485 bp (495 amino acids) in length. All sequence data generated in this paper have been submitted to GenBank (accession numbers DQ264868 to DQ265157).
23. S. Kumar, K. Tamura, I. B. Jakobsen, M. Nei, *Bioinformatics* **17**, 1244 (2001).
24. D. L. Swofford, *PAUP*: Phylogenetic Analysis Using Parsimony (*and Other Methods), Version 4.* (Sinauer Associates, Sunderland, MA, 2003).
25. D. W. Beasley, J. G. Aaskov, *Virology* **279**, 447 (2001).
26. S. L. Kosakovsky Pond, S. D. W. Frost, *Bioinformatics* **21**, 2531 (2005).

27. We thank I. Novella, C. M. Rice, R. Urwin, and three reviewers for helpful suggestions.

19 May 2005; accepted 5 December 2005
10.1126/science.1115030

Herpesviral Protein Networks and Their Interaction with the Human Proteome

Peter Uetz,[1*] Yu-An Dong,[2*] Christine Zeretzke,[3] Christine Atzler,[3] Armin Baiker,[3] Bonnie Berger,[2] Seesandra V. Rajagopala,[1] Maria Roupelieva,[3] Dietlind Rose,[3] Even Fossum,[3] Jürgen Haas[3]†

The comprehensive yeast two-hybrid analysis of intraviral protein interactions in two members of the herpesvirus family, Kaposi sarcoma–associated herpesvirus (KSHV) and varicella-zoster virus (VZV), revealed 123 and 173 interactions, respectively. Viral protein interaction networks resemble single, highly coupled modules, whereas cellular networks are organized in separate functional submodules. Predicted and experimentally verified interactions between KSHV and human proteins were used to connect the viral interactome into a prototypical human interactome and to simulate infection. The analysis of the combined system showed that the viral network adopts cellular network features and that protein networks of herpesviruses and possibly other intracellular pathogens have distinguishing topologies.

Herpesviruses are widely spread throughout vertebrates and have large, double-stranded DNA genomes encoding between about 70 and 170 viral proteins, which is only one order of magnitude less than the number of proteins encoded by bacterial genomes. Although studies have revealed a large number of interactions between herpesviral and host proteins, relatively little is known about interactions among herpesviral proteins, particularly for those herpesviruses that replicate poorly in cell culture, e.g., Kaposi sarcoma–associated herpesvirus (KSHV) (*1*). We thus generated genomewide protein interaction maps for two human pathogens: KSHV, which is a member of the γ-herpesvirus subfamily associated with Kaposi sarcoma and B cell lymphomas (*2*), and varicella-zoster virus (VZV), which is a member of the α-herpesvirus subfamily that causes chickenpox and shingles (*3*).

We cloned the open reading frames (ORFs) of both viruses (currently there are 89 ORFs identified in KSHV and 69 ORFs in VZV) by recombinatorial cloning and generated yeast two-hybrid (Y2H) bait and prey arrays. To circumvent the limitation of the Y2H system for transmembrane proteins, we cloned full-length proteins as well as extra- and intracellular domains separately. In KSHV, we tested more than 12,000 viral protein interactions involving both full-length proteins and protein fragments and identified 123 nonredundant interacting protein pairs (fig. S1 and table S1). To date, only a small number of intraviral protein interactions have been reported for KSHV, of which 71% were captured by our screen (table S2). To further confirm the quality of our Y2H results and generate a set of high-confidence interactions, we tested all positive Y2H interactions in parallel by both β-galactosidase and coimmunoprecipitation (CoIP) assays (fig. S2). About 50% of the protein interactions could be confirmed by CoIP (table S1), and many of the remaining ones have orthologous interactions in other herpesviruses that could be confirmed (table S3). Although our array-based two-hybrid system is internally controlled, some of the interactions not confirmed by CoIP may be nonphysiological and, for example, caused by autoactivation. A comparison between protein interactions and expression profiles of KSHV-infected cells indicated that protein interactions occurred predominantly between proteins expressed at the same time point after infection (fig. S3). In VZV, we detected 173 nonredundant intraviral protein interactions out of ~10,000 tested bait-prey pairs (table S4).

Although cellular protein interaction networks exist for several model organisms, none of the studies on viral protein interactions published so far produced a large enough data set to constitute a protein interaction network. In many cellular protein interaction networks, most nodes have few neighbors, although some have many interaction partners (so-called hubs). The degree distributions of cellular protein networks were reported to follow a power-law decay, and they have been classified as scale-free (*4*). Like their cellular counterparts, KSHV and VZV had relatively many hubs, a key characteristic of scale-free networks (Fig. 1A; fig. S4). However, in contrast to known cellular protein interaction networks, in which nodes with a single interaction partner are most abundant, the viral networks had relatively few such "peripheral" nodes lying on the "edge" of the network. In KSHV, for example, the degree distribution peaks at nodes with three neighbors. This unusual characteristic at low node degrees is one of the reasons that viral networks appear as single, highly coupled modules and presumably reflects their incompleteness as stand-alone networks. Whereas cellular protein networks have been shown or assumed to be scale-free, the degree distribution of viral networks does not present such a clear-cut picture (fig. S5). If viral networks are approximated by a power-law distribution, they have unusually small power coefficients distinctive from those of known cellular networks and defying current dynamic network evolution models (Fig. 1B and Table 1).

Another important characteristic of complex networks is the so-called small-world property (*5*). In a small-world network, the average distance between any two nodes is short (short characteristic path length, or the six degrees of separation phenomenon) and local neighborhoods are more densely connected (high clustering coefficient). Both viruses exhibited a short characteristic path length and a short network diameter (the maximum distance between any two nodes), which also suggests their coupling as single modules (Table 1). To assess the viral levels of local clustering, we generated random networks of the same size and degree distribution. The level of local clustering was low in KSHV and VZV, indeed, comparable to the level in equivalent random networks, and thus these viral networks cannot be classified as small-world. In contrast, most cellular protein interaction networks are unambiguously small-world, even after the effect on local clustering due to degree distribution and network size, which is substantial, is filtered out. For example, the clustering coefficient of the *Saccharomyces cerevisiae* protein interaction network is increased ~30-fold over simulated networks (Table 1). In *S. cerevisiae*, Maslov and Sneppen demonstrated that hubs tend to avoid each other while prefering low-connectivity nodes (*6*). As a result, the yeast network has well-separated modules, and errors in one module do not easily propagate to other modules. In the viral networks, there was no such declining degree correlation, and hubs did not tend to avoid each other, which offers additional evidence that these viral networks could be viewed as single, highly coupled modules (fig. S6). Because of these unusual topological features, viral networks should be more resistant to deliberate attacks than cellular networks, as both network size and characteristic path length remain more stable after the most highly connected nodes are removed (Fig. 1, C and D).

Whereas sequence and phylogenetic analyses identify a core set of genes conserved in all herpesviruses, the KSHV interactome allowed us to determine a core set of interactions conserved in all herpesviruses. Using the recip-

[1]Institut für Genetik, Forschungszentrum Karlsruhe, Postfach 3640, Karlsruhe, D-76021 Germany. [2]Department of Mathematics, Massachusetts Institute of Technology, Cambridge, MA 02139 USA. [3]Max-von-Pettenkofer Institut, Ludwig-Maximilians-Universität München, Pettenkoferstrasse 9a, 80336 München, Germany.

*These authors contributed equally to this work.
†To whom correspondence should be addressed. E-mail: haas@lmb.uni-muenchen.de

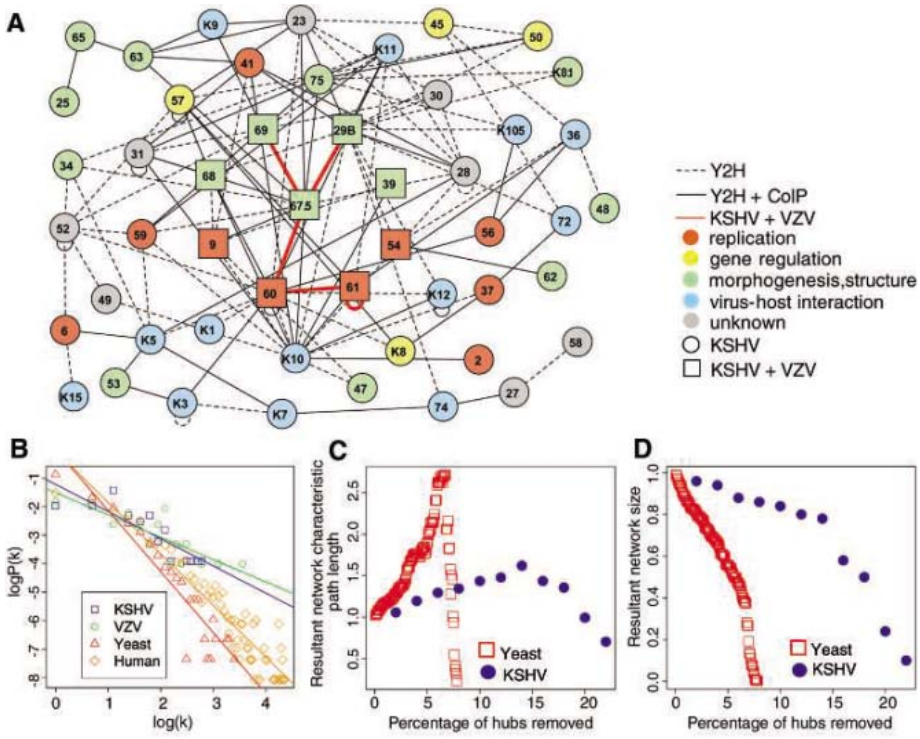

Fig. 1. Topology of the KSHV protein interaction network. (**A**) Protein interaction map of KSHV. KSHV proteins are indicated as nodes, and protein interactions either as hatched (found only by Y2H) or solid (confirmed by CoIP) edges. Orthologous proteins interactors in KSHV and VZV are marked by squares, and orthologous interactions detected in both viruses by red edges. KSHV ORFs were assigned to five functional classes depicted in different colors on the basis of GenBank annotations for the corresponding ORF or its orthologs. (**B**) Comparison of the approximated power-law degree distribution of two herpesviral (KSHV and VZV) networks and two cellular (yeast and human) networks. The yeast data set is derived from Schwikowski *et al*. (*9*), and the *Homo sapiens* (predicted) data set from Lehner and Fraser (*12*). For each network, node degrees k and their relative frequency (i.e., probability) are plotted on a bilogarithmic scale and fitted by linear regression. (**C** and **D**) Simulations of deliberate attack on KSHV and yeast networks by removing their most highly connected nodes (in decreasing order). After each node is removed, the new network characteristic path length (average distance between any two nodes) and size (number of nodes) of the remaining single largest connected component (SLCC) are computed and plotted as a multiple or fraction of the original parameters. KSHV exhibits much higher attack tolerance, because the increase in path length and the decrease in network size are considerably smaller.

Table 1. Comparison of network parameters of cellular and viral protein interaction networks. The table indicates key parameters of eight viral and cellular networks (all analyses were done using the SLCC of the respective network). Among 123 nonredundant KSHV protein interactions, 8 are self-interactions and the SLCC consists of 115 edges; among 173 nonredundant VZV protein interactions, 13 are self-interactions and one edge is isolated, leaving the SLCC with 159 edges. Only 1 of the 123 interactions in KSHV and 10 of the 173 in VZV were detected bidirectionally, and 1 interaction in KSHV and 13 in VZV were redundantly detected by distinct fragments of the same proteins. Interactions detected only in one direction are a common phenomenon in two-hybrid assays and most likely are due to steric hindrance of either bait or prey fusion proteins. The data sets were derived from the following sources: vaccinia virus, from McCraith *et al*. (*13*); *S. cerevisiae I*, from Schwikowski *et al*. (*9*); *S. cerevisiae II*, from the Database of Interacting Proteins (DIP; October 2004 release); *H. sapiens I*, from Rual *et al*. (*8*); *H. sapiens II*, from Stelzl *et al*. (*7*); and *H. sapiens* (predicted), from Lehner and Fraser (*12*). The table includes the number of nodes and edges in the SLCC; the average node degree (i.e., number of neighbors); the power coefficient γ and its P value (the slope and its significance under linear regression) as fitted by a power-law degree distribution ("scale-free" property); the characteristic path length and diameter, as well as the clustering coefficient and its fold enrichment over comparable random networks ("small-world" property). For each real network, a corresponding ER (Erdös-Rényi) randomization has the same number of nodes and edges, and an ES randomization, generated through an edge-swapping algorithm, also has the same degree distribution. The fold enrichments shown are over the theoretical clustering coefficient under the ER model and the median clustering coefficient of 1000 ES randomizations, respectively (see supporting online material). Note that the network parameters of the two yeast networks are surprisingly stable, although a large number of interactions have been included additionally into the DIP database in comparison to the initial data set generated by Schwikowski and colleagues (*9*). The recently reported *H. sapiens* networks have rather low levels of local clustering, which was discussed as being caused by their incompleteness (*8*). NA, not applicable owing to the low number of edges.

Network parameters	KSHV	VZV	Vaccinia virus	*S. cerevisiae* I	*S. cerevisiae* II	*H. sapiens* I	*H. sapiens* II	*H. sapiens* (predicted)
Nodes	50	55	7	1,548	2,397	1,307	1,598	3,169
Edges	115	159	6	2,358	6,101	2,483	3,072	10,636
Average degree	4.60	5.78	1.71	3.05	5.09	3.80	3.84	6.71
Power coefficient	0.95	0.78	NA	2.14	2.01	1.54	1.66	1.81
P value	1.2×10^{-4}	1.1×10^{-4}	NA	3.6×10^{-11}	7.7×10^{-23}	1.2×10^{-20}	5.8×10^{-25}	1.4×10^{-30}
Characteristic path length	2.84	2.34	NA	7.28	5.10	4.36	4.85	6.40
Diameter	7	5	NA	23	13	12	13	20
Clustering coefficient	0.146	0.393	NA	0.213	0.296	0.060	0.012	0.186
Enrichment over ER	1.55	3.67	NA	108.1	139.5	20.6	4.8	87.9
Enrichment over ES	0.76	1.01	NA	29.2	29.5	0.92	0.28	11.7

rocal best BLAST hit approach, we determined the orthology relationships among the viruses and predicted 114 orthologous protein interactions in herpes simplex virus 1 (HSV-1), VZV, murine cytomegalovirus (mCMV), and Epstein-Barr virus (EBV) (table S1). Intriguingly, most of the predicted interactions (72 out of 112 tested, or 64%; table S3) could be confirmed by CoIP despite the rather low level of sequence similarity between KSHV proteins and their orthologs (only in the 20 to 40% range). Although in general KSHV proteins

with viral interaction partners are not more conserved than are those without (fig. S7a), for KSHV proteins with interaction partners there was a significant correlation between the number of protein interactions and homology to the respective EBV ortholog (fig. S7b). When we compared the protein networks of KSHV and VZV, we found that only 9 of the 50 protein interactors in KSHV have orthologous interactors in VZV (Fig. 1A; table S1). Analysis of the KSHV network suggests that 19 interactions should exist between orthologous viral proteins in VZV, of which we could detect 5 in our Y2H screen (26%). This low result is not surprising, because the number of predicted interactions in HSV-1, mCMV, and EBV that were confirmed by Y2H was also considerably lower than the number confirmed by CoIP, indicating an inherent technical limitation of the Y2H system.

The network analyses of the KSHV and VZV interactomes revealed unique features of viral systems that also manifested themselves on the local level (fig. S8). Because we hypothesized that many of these features could be attributed to missing virus-host interactions, we modeled the interplay between viral and human protein networks. To date, only rather small subnets of the human interactome have been reported (*7*, *8*). Unfortunately, only a few published human proteins targeted by KSHV lie within these reported human subnets and only a few virus-host interactions could be predicted on the basis of homology between KSHV and human proteins. However, using a prototypical human protein interaction network [derived from high-confidence interactions in *S. cerevisiae*, *Caenorhabditis elegans*, and *Drosophila melanogaster* (*9*–*11*)] that is considerably larger than the experimental subnets, we were able to efficiently connect the viral and the human networks by predicting interactions between KSHV and human proteins if both proteins have known interacting orthologs in either *S. cerevisiae*, *C. elegans*, or *D. melanogaster* (*12*). By this approach, we found 20 predicted interactions between 8 KSHV and 20 human proteins that are connected within the human network. Nineteen of these 20 virus-host interactions were tested by CoIP and an unexpectedly large percentage (13 out of 19, or 68%) could be confirmed (table S9). Although published viral-host interactions tend to involve genes or interactions specific to human or higher eukaryotes (because most human targets have no orthologs or orthologous interactions in the three lower-eukaryotic model organisms), our predicted viral-host interactions involve genes and interactions conserved from yeast to human and hence might reflect more general host-interacting mechanisms.

Using the predicted KSHV-human interactions, we were able to merge the two interactomes with each other (Fig. 2, A and B). The topology of the KSHV network changed

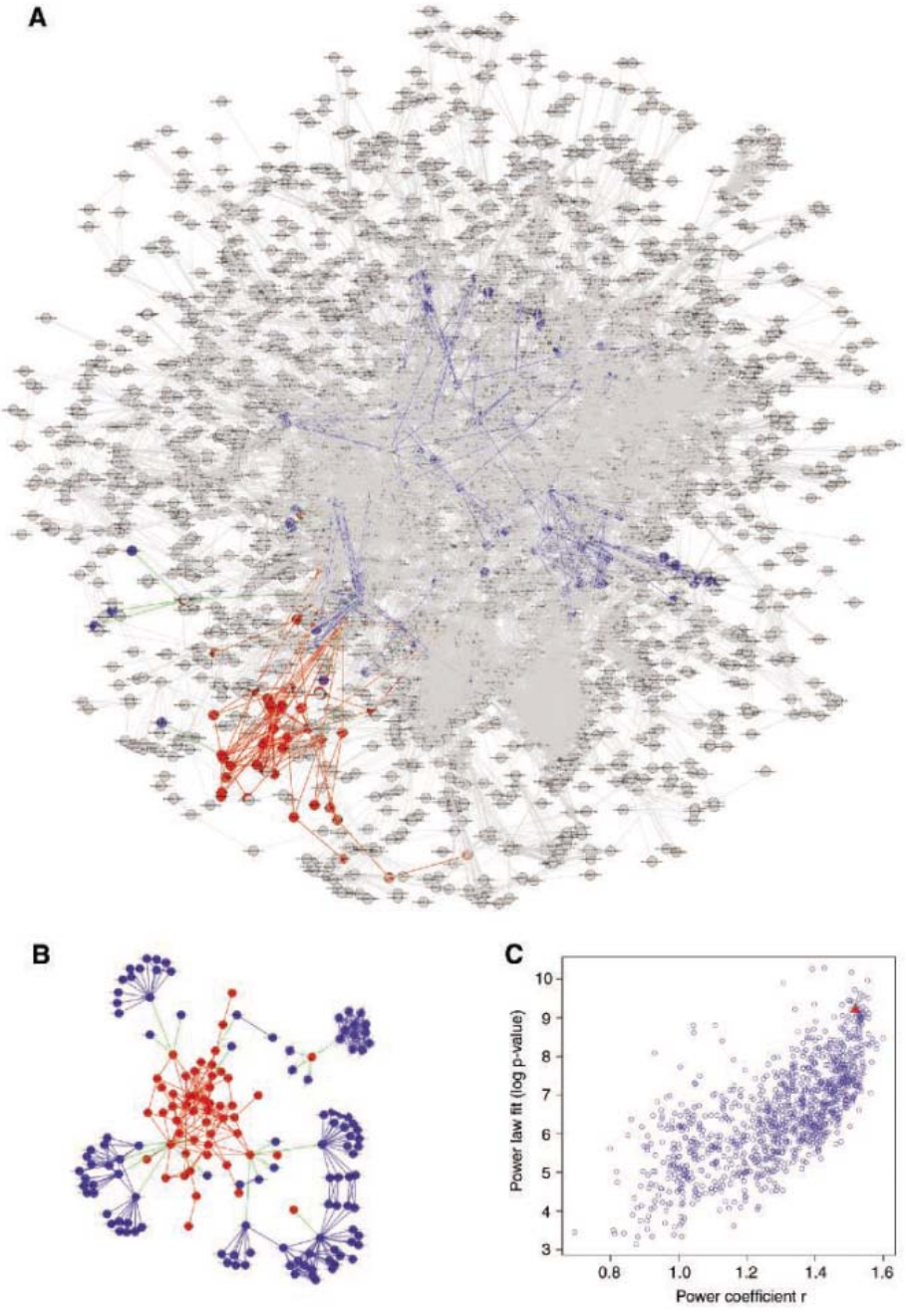

Fig. 2. Interplay between the KSHV and a predicted high-confidence human network. (**A**) Global view of the interplay between the KSHV and a predicted high-confidence human interaction network consisting of 10,636 edges among 3169 nodes. Viral proteins are depicted as red nodes, cellular interacting proteins (level 1 and 2) as blue nodes, and cellular proteins (level >2) as gray nodes. Interactions between viral proteins are depicted as red edges, those between viral and cellular proteins as green edges, and those between cellular level 1 and 2 proteins as blue edges. (**B**) Local view of the combined KSHV and human interaction networks (level $\leq$ 2). (**C**) The combined viral-host network has a bigger and statistically more significant power coefficient and thus adopts scale-free features. The combined virus-host network was compared to 1000 random networks, which were generated by rewiring fixed virus interactors to swapped cellular proteins with the same degree as the actual target. The power coefficient and the power-law fit of the predicted (red triangle) and 1000 random (blue circles) KSHV-human networks are indicated on the *x* axis and the *y* axis, respectively. Among 1000 random networks, 65 have a higher power coefficient, 19 a more significant power-law fit, and only 8 a higher power coefficient that is more significant (empirical *P* value <0.01).

completely from a highly coupled module to a more typical scale-free network of interacting submodules once it was connected to its host. To rigorously assess the impact of the two systems upon each other, we performed a combined viral-host network analysis. Starting with the KSHV network (level 0), we first added in their direct human targets (level 1), then added in those human targets' own cellular interactions partners (level 2), and so on, until the viral network was completely assimilated into the host network. To evaluate the topology of the combined virus-host network, we reasoned that a correctly combined system should be different from randomly combined networks. To generate an ensemble of equivalent random viral-host networks, we adopted the following simulation strategy: the identity and degree of KSHV interactors are fixed, while their human targets are randomly chosen from the host network so that each random target has the same degree as the predicted target that it replaces. Because degree distribution reflects global topology, with the KSHV and human protein networks differing substantially in this respect, it offers an ideal measure to assay the coupled system. Indeed, at level 2, the predicted viral-host network not only exhibited a better power-law fit, but the power coefficient was also bigger, both crucial features of the human network (empirical P value < 0.01 in 1000 simulations) (Fig. 2C). Thus, at the level carrying most biological relevance (KSHV's human targets and their direct interaction partners) and subjected to minimal noise (level 3 already includes a sizable fraction of the human network and many of the interactions are conceivably no longer relevant to the viral-host context), the combined virus-host network assimilated human network properties to a large extent (fig. S9). When we predicted VZV-human interactions and modeled the combined system, we saw very similar results, demonstrating the general utility of our approach (fig. S10; table S10).

Although we have shown that virus and host interactomes possess distinct network topologies, their interplay may lead to emergent new system properties that represent specific features of the viral pathogenesis. Obviously, numerous biological hypotheses resulting from our study remain to be investigated in detail. The availability of protein interaction networks in other herpesviruses and large-scale virus-host interaction data in the near future will boost our knowledge of the function of many still poorly characterized viral proteins and the phylogeny of herpesviruses. It may eventually lead to a considerably improved understanding of viral pathogenesis and evoke new therapeutic strategies.

References and Notes

1. P. Uetz, S. V. Rajagopala, Y. Dong, J. Haas, *Genome Res.* **14**, 2029 (2004).
2. Y. Chang *et al.*, *Science* **266**, 1865 (1994).
3. A. J. Davison, J. E. Scott, *J. Gen. Virol.* **67**, 1759 (1986).
4. A. L. Barabasi, R. Albert, *Science* **286**, 509 (1999).
5. D. J. Watts, S. H. Strogatz, *Nature* **393**, 440 (1998).
6. S. Maslov, K. Sneppen, *Science* **296**, 910 (2002).
7. U. Stelzl *et al.*, *Cell* **122**, 957 (2005).
8. J. F. Rual *et al.*, *Nature* **437**, 1173 (2005).
9. B. Schwikowski *et al.*, *Nat. Biotechnol.* **18**, 1257 (2000).
10. L. Giot *et al.*, *Science* **302**, 1727 (2003).
11. S. Li *et al.*, *Science* **303**, 540 (2004).
12. B. Lehner, A. G. Fraser, *Genome Biol.* **5**, R63 (2004).
13. S. McCraith, T. Holtzmann, B. Moss, S. Fields, *Proc. Natl. Acad. Sci. U.S.A.* **97**, 4879 (2000).

14. This work was supported by grants provided by Bayerisches Staatsministerium für Wissenschaft, Forschung und Kunst (BayGene), Deutsche Forschungsgemeinschaft (SFB 576), Sander-Stiftung (1999.096.1), Helmholtz Gemeinschaft (P.U. and Y.-A.D.), and LMU München (FoeFoLe). We thank A. Arvin, Y. Chang, D. Ganem, S.-J. Gao, W. Hammerschmidt, Y. Kawaguchi, U. Koszinowski, P. Moore, B. Moss, F. Neipel, P. Pitha-Rowe, T. Schulz, B. Sodeik, C. Wood, and Y. Yuan for plasmids, cosmids, bacterial artificial chromosomes, and viruses. This manuscript is dedicated to C.A..

Supporting Online Material

www.sciencemag.org/cgi/content/full/1116804/DC1
Materials and Methods
Figs. S1 to S10
Tables S1 to S10
References and Notes

30 June 2005; accepted 21 November 2005
Published online 8 December 2005;
10.1126/science.1116804
Include this information when citing this paper.

Magnetosomes Are Cell Membrane Invaginations Organized by the Actin-Like Protein MamK

Arash Komeili,[1]*†‡ Zhuo Li,[2]* Dianne K. Newman,[1,3] Grant J. Jensen[2]

Magnetosomes are membranous bacterial organelles sharing many features of eukaryotic organelles. Using electron cryotomography, we found that magnetosomes are invaginations of the cell membrane flanked by a network of cytoskeletal filaments. The filaments appeared to be composed of MamK, a homolog of the bacterial actin-like protein MreB, which formed filaments in vivo. In a *mamK* deletion strain, the magnetosome-associated cytoskeleton was absent and individual magnetosomes were no longer organized into chains. Thus, it seems that prokaryotes can use cytoskeletal filaments to position organelles within the cell.

Prokaryotes are highly organized cells with many ultrastructural similarities to eukaryotic cells (*1*). In addition to a dynamic cytoskeleton composed of homologs of actin, tubulin, and intermediate filaments (*2*), some prokaryotes also possess intracellular membranous organelles (*3*–*6*). The magnetosome chains of magnetotactic bacteria are among the best studied examples of membranous prokaryotic organelles. Magnetosome chains contain 15 to 20 ~50-nm magnetite crystals that together act like the needle of a compass to orient magnetotactic bacteria in geomagnetic fields, thereby simplifying their search for their preferred microaerophilic environments (*3*). The distinct properties of magnetosomal magnetite crystals have drawn attention to their potential use in biotechnology, bioremediation, and geobiology (*3*). Furthermore, the cell biological characteristics of magnetosomes make them an ideal model system for the study of organelle biology in prokaryotes. Each magnetite crystal within a magnetosome is surrounded by a lipid bilayer, and specific soluble and transmembrane proteins are sorted to the magnetosome membrane (*7*, *8*).

Electron cryotomography (ECT) is an emerging technology that can reveal the three-dimensional (3D) ultrastructure of small, intact prokaryotic cells in a near-native, "frozen-hydrated" state (*9*, *10*). Here, we used ECT to define the precise physical characteristics of the magnetosome chain and to identify the molecular factors controlling its subcellular positioning and organization.

To image magnetotactic bacteria by ECT, exponential-phase cultures of *Magnetospirillum magneticum* sp. AMB-1 were plunge-frozen and imaged in a transmission electron cryomicroscope. Dual-axis image tilt series were recorded (*11*), from which 3D reconstructions of individual cells were calculated (Movie S1). A slice through the middle of one typical reconstruction (Fig. 1A and Movie S2) clearly showed the inner and outer membranes and the peptidoglycan layer. The cytoplasm was full of ribosomes, recognized as the numerous, dense, ~25-nm particles. Large, approximately

[1]Division of Geological and Planetary Sciences, [2]Division of Biology, [3]Howard Hughes Medical Institute, California Institute of Technology, Pasadena, CA 91125, USA.

*These authors contributed equally to this work.
†Present address: Department of Plant and Microbial Biology, University of California, Berkeley, Mail Code 3102, Berkeley, CA 94720, USA.
‡To whom correspondence should be addressed. E-mail: komeili@nature.berkeley.edu

spherical poly-β-hydroxybutyrate storage granules, outer membrane blebs, and deep invaginations in the membranes were also apparent in all cells.

Of greatest interest, however, were the long chains of high-contrast magnetite crystals present in every cell and clearly surrounded by the magnetosome membrane. ECT images of cells grown in iron-poor conditions also provided a clear view of chains of empty magnetosomes (Fig. 2B and Movie S3) (*12*). Surprisingly, ~34% (97 out of 283, in 15 different cells) of magnetosomes were clearly invaginations of the inner membrane rather than freestanding vesicles. These included magnetosomes in different locations within the chain containing magnetite crystals ranging in size from undetectable to full (Fig. 1, B to E). All of the remaining 66% of the magnetosomes were positioned close enough to the membrane to be invaginations, but most were located just above or below the inner membrane with respect to the electron beam, where the missing "pyramid" of data in reciprocal space blurred details of their connectivity. Thus, invagination from the cell membrane appears to be a permanent characteristic of the magnetosome and not just a step in the development of a cytoplasmic vesicle. This contrasts with the generally accepted view that magnetosomes are separated from the cell membrane (*3*). This idea stems from freeze-fracture electron microscopic studies in which no obvious connections to the cell membrane can be observed (*7*). The narrow membranous invaginations we observed here, however, would likely be missed by most fracture angles.

Although the observation that magnetosomes are invaginations ensures that they will always be close to the inner membrane, the observed linearity of magnetosome chains implies that some additional structural constraint has to be present. By inspecting the volumes surrounding each magnetosome chain, we discovered networks of long filaments 200 to 250 nm in length running parallel to four to five individual magnetosomes along the chain in all wild-type cells regardless of the growth condition (Fig. 2, A to C). At any one position within the chain, up to seven of these filaments flank the magnetosome with no obvious spatial pattern. Recent genetic, genomic, and proteomic analyses of magnetotactic bacteria have led to the identification of a large genomic island containing many of the genes known or suspected to be involved in magnetosome functioning (*12*–*14*). In ECT reconstructions of a spontaneous nonmagnetic AMB-1 mutant missing this genomic island (*15*), neither magnetosome invaginations nor comparable filaments were detected, which suggests that the two structures were functionally as well as spatially related (*16*).

To identify the molecular components of the magnetosome cytoskeleton, we focused on the *mamAB* gene cluster that lies within the genomic region lost in the spontaneous nonmagnetic mutant (*14*). The products of the *mamAB* cluster are essential for magnetite production and are known to localize to magnetosomes (*8*, *13*). One gene within this cluster, *mamK*, is predicted to code for a homolog of the bacterial actin-like protein MreB, which forms filaments and has been implicated in cell shape determination, establishment of cell polarity, and chromosome segregation (*17*–*19*). Another homolog of MreB, ParM, also forms filaments and is involved in the proper segregation of certain naturally occurring plasmids

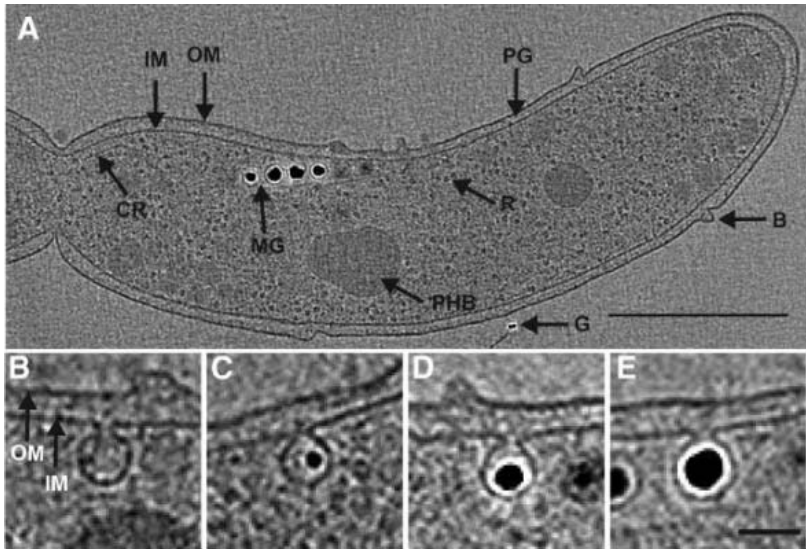

Fig. 1. Electron cryotomography of *Magnetospirillum magneticum* sp. AMB-1 reveals that magnetosomes are invaginations of the inner membrane. (**A**) General features of AMB-1 cells highlighted in a 12-nm-thick section of an ECT reconstruction. Outer membrane, OM; inner membrane, IM; peptidoglycan layer, PG; ribosomes, R; outer membrane bleb, B; chemoreceptor bundle, CR; poly-β-hydroxybutyrate granule, PHB; gold fiduciary marker, G; magnetosome chain, MG. Scale bar, 500 nm. (**B** to **E**) Representative magnetosomes containing no magnetite (B), small (C), medium-sized (D), and fully-grown (E) crystals are invaginations of the inner membrane. Scale bar, 50 nm.

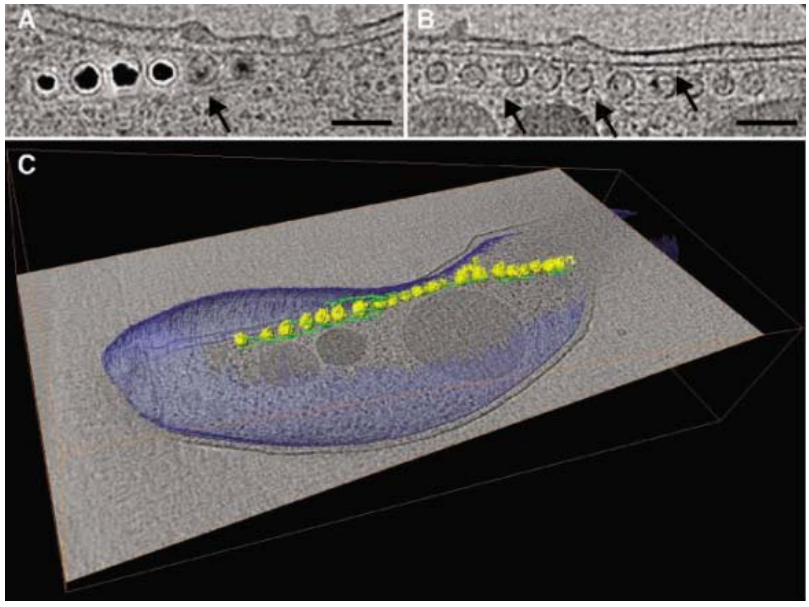

Fig. 2. Magnetosome chains are flanked by long cytoskeletal filaments. (**A**) Larger view of the magnetosome chain in Fig. 1A. (**B**) Similar view of a magnetosome chain grown in the absence of iron, which prevents the formation of magnetite crystals. Arrows point to the long filaments. (**C**) Three-dimensional organization of magnetosomes (yellow) and their associated filaments (green) shown in (B) with respect to the whole cell (blue). Scale bars, 100 nm.

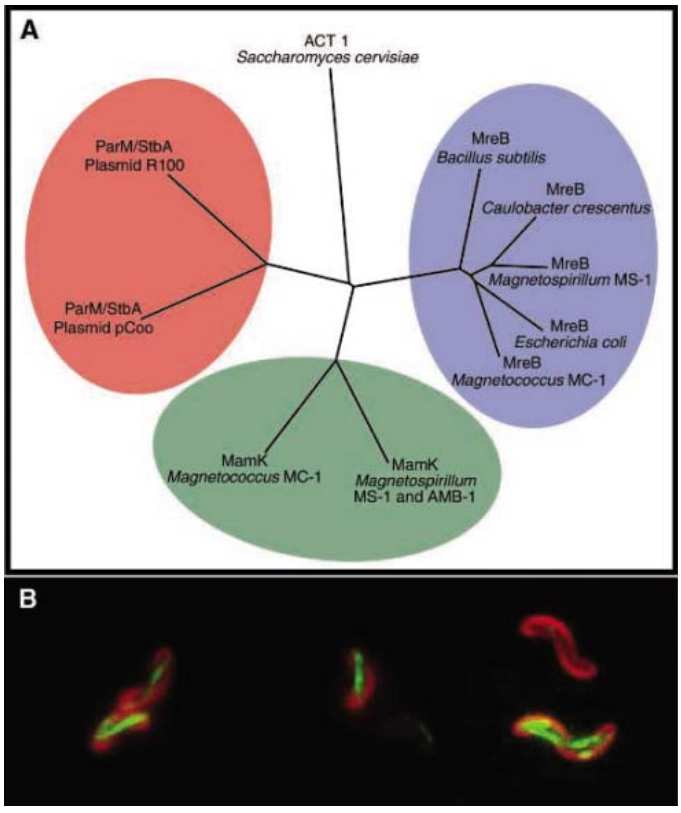

Fig. 3. MamK, a homolog of the bacterial actin-like protein MreB, forms filaments in vivo. (**A**) Phylogenetic relationship between MamK and other bacterial actin-like proteins demonstrated by an unrooted tree. These proteins separate into three distinct groups: MamK (green), ParM/StbA (red) and MreB (blue). (**B**) MamK fused to GFP (green) appears to form filaments in vivo localized to the inner curvature of the cell (cell membrane stained red with FM4-64).

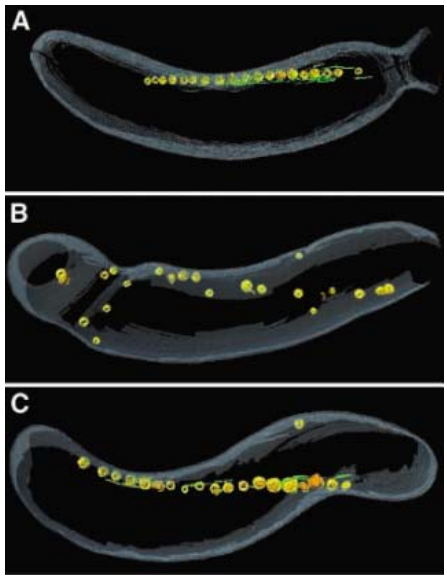

Fig. 4. MamK is required for the proper organization of the magnetosome chain. (**A**) Three-dimensional reconstruction of a wild-type AMB-1 cell. The cell membrane (gray), magnetosome membrane (yellow), magnetite (orange), and magnetosome-associated filaments (green) are rendered. (**B**) Δ*mamK* mutant, where magnetosomes appear disordered and no filaments are found in their vicinity. (**C**) Δ*mamK* cell expressing *mamK-GFP* on a plasmid showing full reversal of the mutant phenotype.

(*20*). Although the genome of AMB-1 has not been fully sequenced, the closely related species *Magnetospirillum magnetotacticum* MS-1 and *Magnetococcus* MC-1 both contain a copy of *mamK* in their *mamAB* operons as well as a predicted *mreB* gene in operons with homologs of other genes involved in cell shape determination (*16*). MamK proteins are more similar to each other (the MS-1 and AMB-1 MamK proteins are identical in sequence) than they are to the MreB homologs found within their respective genomes (Fig. 3A). MreB, ParM, and MamK are also predicted to form three phylogenetically and functionally distinct groups of prokaryotic actin-like proteins.

MreB, ParM, and MamK also display different localization patterns within the cell. In *Escherichia coli*, *Bacillus subtilis*, and *Caulobacter crescentus*, MreB appears to form helical filaments adjacent to the cell membrane. In *E. coli*, ParM appears as an approximately straight line with no consistent relation to the membrane (*2*, *21*). Here, green fluorescent protein (GFP) fusions to the C terminus of MamK were used to explore its subcellular localization. MamK-GFP appeared in straight lines extending across most of the cell approximately along its inner curvature (Fig. 3B), consistent with the magnetosome-associated filaments in both localization and extent. Notably, the magnetosome-associated filaments observed in the ECT reconstructions had a thickness of roughly 6 nm (~2.5 voxels), just as expected for an F-actin-, ParM-, or MreB-like filament (*21*, *22*). Thus, MamK is the most likely candidate for the magnetosome-associated cytoskeleton.

To test this idea, we generated a nonpolar, in-frame deletion of *mamK* in AMB-1. This mutant forms magnetite, turns in magnetic fields, and has no cell shape or growth defects compared with wild type (*16*). Whereas in ECT reconstructions the individual magnetosomes were still seen to be invaginations of the cell membrane, the mutant lacked the long, highly organized chains seen in wild-type AMB-1 (Fig. 4 and Movie S4). Instead, small groups of a few (two to three) neighboring magnetosomes separated by large gaps appeared dispersed throughout the cell, and no filaments comparable to those found in the wild-type cells were associated with the magnetosomes. To ensure that these defects were due to the absence of *mamK* alone, we complemented the Δ*mamK* cells with *mamK-GFP* and observed both the restoration of long, ordered magnetosome chains and the reappearance of magnetosome-associated filaments in approximately 15% of the cells (Fig. 4C). Many of the cells did not exhibit complete complementation, probably because of the expression of MamK-GFP from a heterologous promoter on a low-copy plasmid. Although we cannot eliminate the possibility that MamK is required for the filaments to form without actually being part of their structure, the simplest interpretation of all these results is that MamK is the long filament seen that organizes magnetosome membrane invaginations into a chain roughly parallel to the long axis of the cell.

These results have important implications for the mechanism of magnetite synthesis within magnetosomes. The precursor of magnetite in magnetotactic bacteria is a ferrihydrite mineral that forms in the periplasm (*23*). The opening between magnetosomes and the periplasm might thus enable the direct transport of ferrihydrite between these two compartments. These results also expand our view of the bacterial cytoskeleton, showing that just as in eukaryotes, actin-like proteins are used to position membranous organelles (*24*). MamK could act in establishing the specific localization of the chain through the proper subcellular targeting of magnetosome biogenesis factors, or it could be important in the maintenance of the chain after the production of magnetosomes. Finally, our findings also present a problem in evaluating the evolutionary relationship between magnetosomes and eukaryotic intracellular organelles. Because magnetosomes do not separate from the cell membrane, they might be analogous to photosynthetic membranes in bacteria. They may also represent a step in the development of mechanisms for membrane bud formation before the invention of membrane fission.

References and Notes

1. Z. Gitai, *Cell* **120**, 577 (2005).
2. J. Moller-Jensen, J. Lowe, *Curr. Opin. Cell Biol.* **17**, 75 (2005).

3. D. A. Bazylinski, R. B. Frankel, *Nat. Rev. Microbiol.* **2**, 217 (2004).
4. M. Seufferheld *et al.*, *J. Biol. Chem.* **278**, 29971 (2003).
5. J. S. Sinninghe Damste *et al.*, *Nature* **419**, 708 (2002).
6. J. A. Fuerst, *Annu. Rev. Microbiol.* (2005).
7. Y. A. Gorby, T. J. Beveridge, R. P. Blakemore, *J. Bacteriol.* **170**, 834 (1988).
8. K. Grunberg, C. Wawer, B. M. Tebo, D. Schuler, *Appl. Environ. Microbiol.* **67**, 4573 (2001).
9. J. Kurner, A. S. Frangakis, W. Baumeister, *Science* **307**, 436 (2005).
10. J. Kurner, O. Medalia, A. A. Linaroudis, W. Baumeister, *Exp. Cell Res.* **301**, 38 (2004).
11. C. V. Iancu *et al.*, *J. Struct. Biol.* **151**, 288 (2005).
12. A. Komeili, H. Vali, T. J. Beveridge, D. K. Newman, *Proc. Natl. Acad. Sci. U.S.A.* **101**, 3839 (2004).
13. K. Grunberg *et al.*, *Appl. Environ. Microbiol.* **70**, 1040 (2004).
14. S. Schubbe *et al.*, *J. Bacteriol.* **185**, 5779 (2003).
15. Materials and methods are available as supporting material on *Science* Online.
16. A. Komeili ***et al.***, data not shown.
17. L. J. Jones, R. Carballido-Lopez, J. Errington, *Cell* **104**, 913 (2001).
18. Z. Gitai, N. Dye, L. Shapiro, *Proc. Natl. Acad. Sci. U.S.A.* **101**, 8643 (2004).
19. Z. Gitai, N. A. Dye, A. Reisenauer, M. Wachi, L. Shapiro, *Cell* **120**, 329 (2005).
20. J. Moller-Jensen, R. B. Jensen, J. Lowe, K. Gerdes, *EMBO J.* **21**, 3119 (2002).
21. F. van den Ent, J. Moller-Jensen, L. A. Amos, K. Gerdes, J. Lowe, *EMBO J.* **21**, 6935 (2002).
22. F. van den Ent, L. A. Amos, J. Lowe, *Nature* **413**, 39 (2001).
23. S. Ofer *et al.*, *Biophys. J.* **46**, 57 (1984).
24. D. Pruyne, A. Legesse-Miller, L. Gao, Y. Dong, A. Bretscher, *Annu. Rev. Cell Dev. Biol.* **20**, 559 (2004).

25. We thank W. Tivol and G. Henderson for technical assistance, D. Morris for help with image processing, and K. Ryan for critical reading of the manuscript. This work was supported in part by NIH grant PO1 GM66521 to G.J.J., DOE grant DE-FG02-04ER63785 to G.J.J., a Searle Scholar Award to G.J.J., and gifts to Caltech from the Ralph M. Parsons Foundation, the Agouron Institute, and the Gordon and Betty Moore Foundation. D.K.N. was supported by grants from the Packard and Luce Foundations. A.K. was a Senior Research Fellow of the Beckman Institute and was supported by the Arnold and Mabel Beckman Foundation.

Supporting Online Material

www.sciencemag.org/cgi/content/full/1123231/DC1
Materials and Methods
References
Movies S1 to S4

5 October 2005; accepted 12 December 2005
Published online 22 December 2005;
10.1126/science.1123231
Include this information when citing this paper.

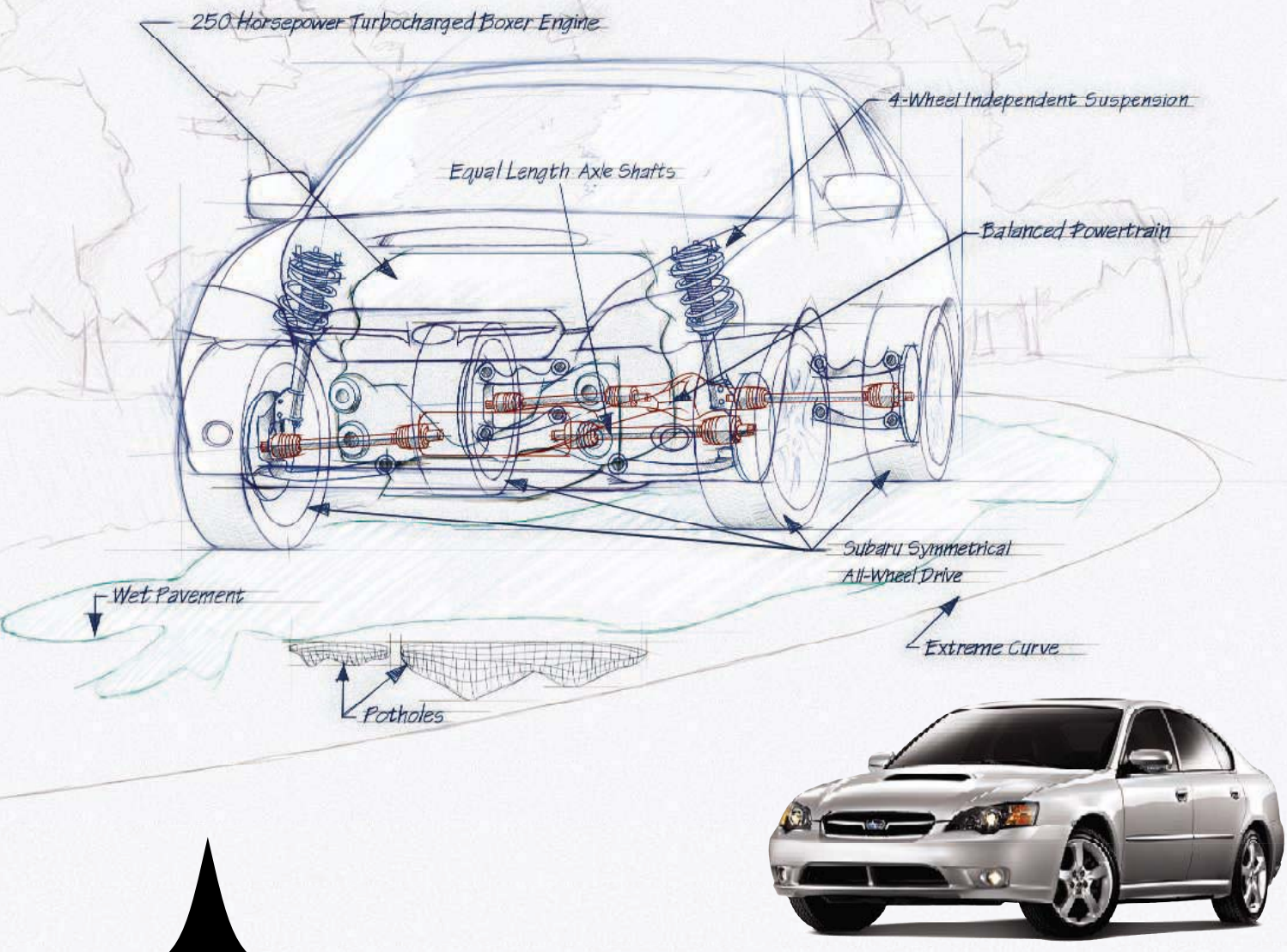

What's outside a Subaru affects what goes into one.
The 2006 Subaru Legacy® 2.5 GT with Symmetrical All-Wheel Drive standard. Inside, a horizontally opposed engine. Equal length axle shafts. A balanced powertrain. Linear power disbursement to all four wheels. What does this all mean? It means stability. It means a car that monitors the road. A car that knows when to transfer power from the wheels that slip to the wheels that grip. It means more traction at all speeds and road conditions. And a car that's fun to drive. It means it's a Subaru.

SAVE UP TO $3000*.
Subaru is proud to continue its sponsorship of the American Association for the Advancement of Science (AAAS). AAAS Members can **save up to $3,000* off** the manufacturer's retail price (depending on model and accessories) on the purchase or lease of a new Subaru from participating dealers. To qualify, you must be a AAAS member in good standing for at least six consecutive months prior to participation in this program. Please contact AAAS at 202.326.6417 **BEFORE** visiting your local Subaru dealer. Access subaru.com to find a nearby dealer or learn more about Subaru vehicles.

Science
AAAS

Think. Feel. Drive.™

SUBARU

*From MSRP to dealer invoice. Limited time offer subject to change without notice. Terms and conditions apply. This offer replaces all other existing offers, cannot be redeemed for cash and is not applicable in Canada and Hawaii.

Magnetic Field Cancellation

The Mag-NetX magnetic field cancellation system is designed to compensate for magnetic interference that diminishes the performance of scanning and transmission electron microscopes, electron beam lithography systems, focused ion beam instruments, and other tools that incorporate a charged beam. Building on its expertise as a manufacturer of active vibration isolation systems that cancel building floor vibrations, the manufacturer developed the Mag-NetX to actively compensate for magnetic field fluctuations caused by nearby machinery, elevators, power lines, and other external sources. Designed for both point-of-use and OEM applications, the open cube-shaped Mag-NetX detects magnetic fields and sends out an equal and opposite field to cancel the interference. The system comprises a dedicated controller with automated calibration and self-test features, AC and DC magnetic sensor, and Helmholtz coils in a structural casing. It can be floor-mounted, wall-mounted, or tool-mounted and sized to user-specific requirements.

Technical Manufacturing Corporation (TMC)
For information 978-532-6330 www.techmfg.com

Conjugation Kits and Linkers

SureFIRE conjugation kits are a new line of pre-activated enzymes and unique linkers. They offer a fast and reliable approach to labeling proteins and antibodies. The enzyme-labeling kits provide all necessary reagents for labeling proteins with either alkaline phosphatase or horseradish peroxidase. Resultant conjugates are suitable for enzyme-linked immunosorbent assays, blotting, immunohistochemistry, and other immunodetection applications requiring high sensitivity and reproducibility. The fast protocols require just 20 minutes of hands-on time with conjugation complete in three hours for alkaline phosphatase and 90 minutes for horseradish peroxidase.

KPL For information 301-948-7755 www.kpl.com

Microarray Data Generation and Analysis Services

Gene Logic offers Microarray Data Generation and Analysis Services, including: gene expression data generation from tissue, cells, blood, or RNA; optimized gene expression profiling of whole blood using a proprietary protocol to reduce globin interference; RNA isolation from low-yield tissues or samples that are difficult to process; custom bioinformatics analysis for biomarker or drug target identification and mechanisms of toxicity; custom platform development; and single nucleotide polymorphism genotyping from DNA, blood, or tissue.

Gene Logic
For information 888-436-3564 www.genelogic.com

Liquid Handling

The Bravo high-speed, precision liquid handling platform has a space-saving nine plate-position footprint that can fit inside a standard laminar flow hood to enable automated liquid handling for cell-based assays or hazardous reagents. With seven different easy-to-change head types and numerous plate pad options, it can be fully customized to meet the needs of a wide range of assays. The unique, open design permits access from all sides for integration with other devices and unencumbered stand-alone use. It features the high-accuracy pipette heads of the company's Vprep pipettor for dispensing from 100 nl to 200 ml in 96-well, 384-well, and 1536-well formats or to a single column or row of any of these plates types.

Velocity11 www.velocity11.com

Kinase Assay

The Transcreener Kinase Assay is designed to streamline assay development and reduce drug candidate screening costs by combining all of the user's kinase assays into one. It is a homogenous fluorescence polarization high-throughput screening assay that directly detects ADP, the common product of all kinase reactions. This assay can be used to profile kinase proteins, substrates, and inhibitors.

BellBrook Labs
For information 866-313-7881 www.bellbrooklabs.com

Protein Blocking Agent

A non-animal protein blocking agent, Nap-Blocker, offers improved assay sensitivity, minimal nonspecific binding, and a high signal-to-background ratio. Nap-Blocker ensures no cross-reaction with animal source antigens and antibodies because it is free of animal proteins. Applications include protein immunoblotting and enzyme-linked immunosorbent assays.

G-Biosciences/Genotec
For information 314-991-6034 www.Gbiosciences.com

X-Ray Diffraction Measurements

The LynxEye detector is designed for higher-speed and higher-resolution x-ray diffraction measurements than is possible with traditional so-called "point" detectors. LynxEye is a cost-effective, one-dimensional detector for measuring a wide angular range simultaneously, thereby significantly reducing measurement times compared with point detectors, while achieving high resolution and excellent peak shape. The LynxEye detector features a large 14.4 mm by 16 mm active area. Because there is no need for counting gas, cooling water, or liquid nitrogen, the LynxEye is a virtually maintenance-free, compact, and robust detector for everyday use. It will be beneficial in many materials research applications, such as fast qualitative and quantitative phase analysis, crystal structure refinement, micro-stain and crystallite size determination, and stress measurements.

Bruker AXS
For information 978-663-3660 www.bruker-axs.com

Newly offered instrumentation, apparatus, and laboratory materials of interest to researchers in all disciplines in academic, industrial, and government organizations are featured in this space. Emphasis is given to purpose, chief characteristics, and availability of products and materials. Endorsement by *Science* or AAAS of any products or materials mentioned is not implied. Additional information may be obtained from the manufacturer or supplier by visiting www.science.labvelocity.com on the Web, where you can request that the information be sent to you by e-mail, fax, mail, or telephone.

Over 23 million downloads of articles last year. Now that's big.

In 2004 over 23 million HTML and PDF articles were downloaded from *Science* Online. More people than ever are accessing the seminal original research, breaking news, and in-depth special sections published each week in *Science*. So if you want to make a really big impression with your research article or advertising, choose *Science*. Become a member of AAAS at **aaas.org/join**. To advertise, go to **scienceadvertising.org**.

Science
AAAS

GET THE BIG PICTURE IN *SCIENCE*

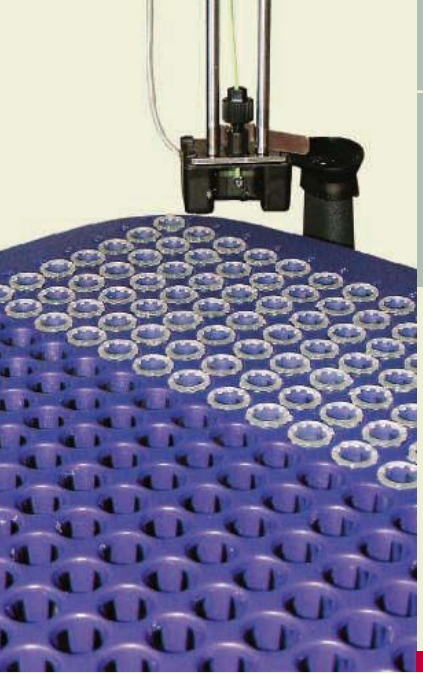

Life Science Technologies

Laboratory Automation:
SMALLER, FASTER, CHEAPER

Genomics, proteomics, and systems biology have one key factor in common: They generate huge amounts of data. To handle that information reliably, life scientists turn to laboratory automation. In response to that demand, vendors now offer tools and technologies that appeal to both individual researchers new to the field and sophisticated users. **by Peter Gwynne and Gary Heebner**

During the past half decade, the emergence of such disciplines as genomics, proteomics, and systems biology has changed the nature of life science, by allowing researchers to study many molecules simultaneously rather than just a few. That ability has led to the creation of huge numbers of new potential drug targets and volumes of data describing them.

Liberation from Routine Tasks

Those developments have forced scientists to turn to automated procedures that liberate them from routine tasks and lower the cost of research and development. "Automation is becoming critical in all forms of life science research as we go from a one-gene/one-protein/one-phenotype model to a number of genes working in concert with a wide array of proteins responsible for disease phenotypes," says Mark Roskey, vice president of North American sales at **Caliper Life Sciences**. "Lab automation is becoming more and more prevalent," agrees Craig Weiss, director of marketing at **Matrix Technologies**. "Companies are seeing the cost-benefit advantage of buying a piece of equipment and freeing Ph.D.s to do research."

Lab automation offers benefits beyond allowing scientists to carry out more tasks faster. "People need to know that the results of research can be trusted," says Simon May, business development manager for **ABgene**. "Lab automation enables that." Ralf Bartl, business development manager for **Xiril**, takes a similar view. "Major points in modern life science are validation and data quality; legal validation, patents, and clinical testing have become crucial issues," he explains. "Automation allows a much higher reproducibility of data and better documentation of the data, and allows you to produce more data points more easily."

The technology also has a role in potentially dangerous experimentation. "In the presence of infectious or potentially infectious material, it ensures the safety of personnel," explains Andreas Schaefer, director of R&D for **Qiagen**.

Inclusion of companies in this article does not indicate endorsement by either AAAS or *Science*, nor is it meant to imply that their products or services are superior to those of other companies.

Lab automation works at two levels, according to Jason Goncalves, general manager of the software solutions business at **Stratagene**. "One involves robots and allows a group to process more samples," he explains. "The other increases throughput by permitting scientists to look at, for example, more genes per assay." Indeed, the availability of automation has helped to stimulate improvements in data density throughout the world of life science. "**Affymetrix** has moved from an 11-micron to a 5-micron platform," Goncalves points out. "That permits scientists to understand biology at a level that wasn't understandable before."

Beyond Discovery

John Blume, vice president of RNA products at Affymetrix, amplifies that point. "The improvement in data quality makes it possible to do types of analysis that weren't easy to do before," he explains. "Automation in this era of the genome has also moved beyond discovery, into areas such as high throughput toxicology and clinical trials. We're pushing automation upstream in order to push our technology downstream."

Vendors are also pushing automation technology into laboratories that could not afford it in the past. "During the last couple of years, automation has come into academic labs that take systems biology–like approaches and for which standardization is key to assuring compatibility of data between labs," says Schaefer. "I see a trend for automation to become more of a commodity, available for smaller labs as well as larger ones," Bartl adds. "Each lab doing liquid handling or some robotics can now use automation to get their jobs done."

At the same time, lab automation tools have become easier and cheaper to use. "The instruments are becoming smaller; they fit on a benchtop rather than filling half the room," Weiss

IN THIS ISSUE:

- High throughput screening
- Liquid handling
- Automated workstations
- Robotics
- Microarrays
- Microfluidics
- Scientific software

Institutional Site License Available

Q What can *Science* STKE give me?

A The definitive resource on cellular regulation

STKE – Signal Transduction Knowledge Environment offers:

- A weekly electronic journal
- Information management tools
- A lab manual to help you organize your research
- An interactive database of signaling pathways

STKE gives you essential tools to power your understanding of cell signaling. It is also a vibrant virtual community, where researchers from around the world come together to exchange information and ideas. For more information go to www.stke.org

To sign up today, visit promo.aaas.org/stkeas

Sitewide access is available for institutions.
To find out more e-mail stkelicense@aaas.org

Science stke AAAS

says. "And when they permit you to go from 300-microliter to 10-microliter samples, you cut reagent costs 30-fold."

Because many scientists without backgrounds in the field now rely on lab automation, vendors of equipment focus strongly on user-friendliness. But while they aim to craft tools that naïve users can apply in plug-and-play fashion, they also ensure that their equipment contains enough bells and whistles to satisfy the most sophisticated experts in core facilities and other large laboratories. "Whether you're a graduate student or head of high throughput screening at a large pharma, we have a tool for you," Matrix's Weiss says. "We aim to be versatile with various components."

Blume adds one caution: Lab managers should not regard automation as essential at all times. "Automation used to mean soup to nuts," he says. "But people have realized that they need to push it only into those areas that benefit from it – not into areas that are best served by manual work."

High Throughput Screening

Because the ability to test a large number of compounds quickly and efficiently can provide a competitive advantage, high throughput screening (HTS) has become a key element in drug discovery. Several techniques developed in recent years help researchers to achieve the high productivity essential for this type of screening.

The concept of homogeneous assays, for example, makes screening robust, simple, and easier to automate by eliminating error-prone washing and transferring steps. Those assays permit a complete series of reactions to occur in a multiwell plate without the need to wash the sample and change reagents between steps. This format, which can apply to radioactive, fluorescent, and luminescent assays, provides a great deal of convenience for researchers and eliminates steps that could introduce additional error into an experimental design.

Applied Biosystems and **PerkinElmer**, among other companies, offer instruments and systems for HTS and incorporate homogeneous assay formats. Applied Biosystems offers instruments that automate many routine laboratory procedures, including chromatography, mass spectrometry, and DNA and peptide synthesis.

Several companies have developed homogeneous assay kits that are compatible with HTS instruments. **BD Biosciences**, **Promega**, and **Upstate**, for example, have a wide range of HTS-compatible assay kits for drug discovery. Promega offers several homogeneous assays to study membrane integrity and other cellular characteristics critical to drug discovery. These assays incorporate a homogeneous format that provides researchers with several benefits: Scientists can run the assay in the cell culture plate in which cells are grown, eliminating the sample transfer step common in many assays; the plates are incubated for 10 minutes before reading data, instead of the 30 minutes or more with classic LDH assays; and the assays can be performed in a single multiwell plate without separating cells from the supernatant liquid.

To increase throughput while reducing tedious and expensive human intervention, suppliers have developed several laboratory automation tools. These range from simple semiautomated liquid handling systems to fully integrated automated systems that consist of multiple robot arms, pipetting stations, incubators, plate washers, and detectors.

Conserving Compounds

To reduce the costs of screening and conserve precious compounds and reagents, scientific groups increasingly rely on miniaturized assays. High density formats such as 96-, 384-, 1,536-well, and even denser arrangements reduce assay volumes to low- or even submicroliter ranges. "In addition to cutting costs, high density plates and lower dispense volumes allow you to skip some dilution steps," says Matrix's Weiss. "You spend less time doing the screens and setting up the plates, and you use less labware."

Scientists can buy microwell plates from BD Biosciences, **Corning**, **Greiner Bio-One**, and Matrix Technologies in formats that include different materials, well shapes, and well depths, in addition to transparent and nontransparent bottoms and coated or treated plates to provide molecule-friendly surfaces. Suppliers often design their microwell plates and other plasticware products for use with the automated systems typically found in large corporate pharmaceutical laboratories.

Handling small volumes of reagents can be difficult because the physics of moving and measuring small volumes differs significantly from that of larger, more conventional volumes. "The process of delivering 0.1 or 0.2 microliters is fairly straightforward, but dealing with various concerns and doing it over and over in a walkaway fashion is very challenging," Weiss points out. "There's really no system on the market for below 0.1 microliters that you can simply plug in and allow to go."

Nevertheless, vendors are moving toward that goal. Companies that provide tools for handling microvolumes, in addition to Matrix Technologies, include **Eppendorf** and **Hamilton**. "We're working on the challenge of getting below 0.1 microliters and lower in noncontact fashion," Weiss says. Matrix aims to make its tools work on existing automation platforms and to make them versatile enough to work with a range of sample sizes from less than 0.1 microliters to 300 microliters all on the same platform. "And all our liquid handlers from the $20,000 unit to the $90,000 unit use the same software," Weiss continues. "Once you've learned how to use one, you can use them all."

Automation: Full and Semi

Many of the procedures involved in drug discovery are routine and repetitive – and hence ideal candidates for laboratory automation via semiautomated or automated workstations. These instruments can deliver small volumes of reagent or wash the samples in microwell plates or other vessels for virtually 24 hours a day, seven days a week. Instruments produced by Applied Biosystems, **Tecan**, and Xiril, among other suppliers, can free researchers from the need to perform or even oversee those boring and mundane tasks, thereby permitting them to work on more value-added tasks such as designing experiments.

How much automation do scientists need? "In high throughput applications you have to have full automation of the whole process; otherwise you have to stay with the machine the whole time," says Xiril's Bartl. "In low throughput situations you may have two or three manual steps per day – such as some pipetting, some readout, and some PCR."

Xiril has created space-saving, flexible systems that combine liquid handling and robotic manipulation. "We came up with a liquid handling concept that allows functionality at lower cost," Bartl explains. "Smaller and medium-sized labs have been pleased to have our technology available at less than the typical $100,000 cost of a fully automated workstation." The company offers three instruments (numbered 75, 100, and 150) whose optional arm and tip configurations and simple integration of modular hardware components enable them to handle a wide range of workloads. "The system is plug-and-play in terms of handling the hardware," Bartl says. "And for the software it's one-stop functionality. That makes it really simple for the routine user. And it's easy to transfer understanding to new users."

New Platforms

A traditional approach to automation replaces lab technicians' eyes and hands with automated workstations. Another approach is to change the platform for experimentation, and thus allow for expanded sample processing. Several approaches developed over the past few years have proved useful in genomics and proteomics research.

Microarrays are small slides of glass or other inert material whose surfaces hold hundreds or thousands of samples in the form of spots organized in regular patterns. Scientists can use robotic systems called microarrayers to perform the placements or buy ready prepared microarrays from vendors who synthesize specific molecules such as DNA in situ on the surfaces. Industrial chips, made by such companies as Affymetrix, **NimbleGen Systems**, and **SuperArray Bioscience**, can hold thousands of features on a single slide. In the case of DNA microarrays, this makes screening a complete genome on a single slide quite feasible.

Where does lab automation fit into microarraying? "The demand for lab automation is driven more by the application than the robot," says Affymetrix's Blume. "The applications that drive hundreds or thousands of processes, including drug discovery and clinical monitoring, clearly benefit from automation. If, say, I need to analyze 3,000 samples over the course of 90 days, lab automation is clearly necessary. The applications that drive hundreds or thousands of processes, including drug discovery and clinical monitoring, clearly benefit from automation. There's no application we currently have that we regard as physically being able to run only on the robot. But we envision creating new paths for people doing three or six assays at a time."

Caliper Life Sciences has collaborated with Affymetrix on automating target preparation for microarray experiments. "The high throughput arrays that Affymetrix is bringing to market are especially well suited to automation, due to the target preparation requirements of these high-density chips," Roskey says. The collaboration resulted in the launch of Affymetrix's GCAS system last September.

In another venture, announced last spring, Affymetrix linked up with Chinese company **CapitalBio Corporation** on joint R&D and commercialization programs and a collaboration on promoting and advancing standards on microarray technologies, products, and industrial processes. In October, the collaborative announced an initiative to support and promote functional genome research on rice. "The Affymetrix GeneChip technology complements CapitalBio's products and services nicely and completes our total offering to the research community," said CapitalBio's senior vice president David Sun.

Lure of the LabChip

Several companies, including **Agilent** and **MetriGenix**, have developed microfluidic lab-on-a-chip devices for genomic and proteomic research. Lab-on-a-chip technology and automation offer an intriguing combination, according to Kevin Hrusovsky, president and CEO of Caliper Life Sciences. "There's sample preparation, when you're bringing together all the reactants from different locations. And after sample preparation you have to analyze," he says. "Automating the analysis and the sample preparation are two different things historically. But on our LabChip they are done together."

Agilent's automated 2100 Bioanalyzer System, designed to analyze proteins, nucleic acids, and even whole cells, relies on Caliper's LabChips. "The chip itself replaces a lot of automation," Hrusovsky says, "but you have to put it in an instrument. We design instruments to go with these chips that allow you to completely walk away from the experiment and come back later to pick up your data."

Caliper continues to develop its chip technology in the context of automation. "We now have sippers on our chips that can reach into microwells to access sample. This allows us to bring the benefits of microfluidics technology to applications such as high throughput screening," Hrusovsky says. "Our next frontier is diagnostics, where we hope to improve clinical testing through microfluidics. Agilent, among others, has licensed our chip technology for diagnostics applications. We believe that someday soon microfluidics will make clinical testing not only easier to automate but also cheaper and more accurate."

Purification and PCR

Several companies have developed automated systems for purifying nucleic acids. "It's a growing market that covers the most laborious

step in the whole procedure," says Qiagen's Schaefer. His company has recently introduced the BioRobot Universal System, a setup that integrates all the instrumentation, software, purification technologies, and enzyme technologies required for applications relevant to medium- and high-throughput systems biology. By automating nucleic acid and protein purification and reaction setup, the system saves hands-on time and ensures an efficient, streamlined workflow. "You don't have to change the layout or the tools the robot uses to carry out RNA, DNA, and protein extraction," Schaefer explains. "The system has a tremendous amount of applications," says Schaefer, "and we've added features from our other systems, such as clot detection and CFR21 Part II compatibility."

Research that involves PCR also benefits from lab automation, via thermal cyclers from such companies as ABgene, Applied Biosystems and **Roche**. ABgene offers a high throughput thermal cycler and molecular biology reagents for performing PCR in large numbers. The company's H2OBIT is a high throughput water bath thermal cycler that can simultaneously process up to 24 microwell plates – equivalent to 9,216 reactions per run when using 384-well plates.

A robotic arm rapidly transfers a basket of plates between three water baths, resulting in temperature ramping times that are considerably faster than those of the traditional Peltier block cyclers. "It allows people to do ultrahigh throughput PCR," May explains. "Standard thermal cyclers are pretty low throughput machines and pretty expensive. Our H2OBIT allows you to use any plate format and greatly increases throughput." A computer management system allows full data tracking of all PCR runs and enables integration into a Laboratory Information Management System. "There's full data tracking," May says. "If you have the relevant information technology resources, it's easy to use."

Demand for Data Management

The huge volumes of data generated in automation-enabled research on genomics, proteomics, and systems biology, as well as drug discovery and development, have one key demand. "A data management system is a critical infrastructure component of any laboratory doing true high throughput biology," says Stratagene's Goncalves. The system must handle capturing, loading, sorting, querying, and viewing the information from both biological and chemical perspectives, and have the flexibility to grow with the need for processing increasing numbers of samples. "It should also be user-friendly for the typical user but scriptable for the sophisticated user," Goncalves adds.

Accelrys and **MDL Information Systems** offer products and services to companies that need a high level of integration and multiple user access to screening data. Other firms, among them **DNASTAR**, **Invitrogen**, and **MiraiBio**, focus on molecular biology applications such as DNA sequencing and gene data mining. Stratagene, through its recent acquisition of Iobion Informatics, offers three related products for archiving data. "ArrayAssist is our data analysis package. It supports any type of array data, but is specifically focused on the next generation Affymetrix arrays such as GeneChip Exon arrays," Goncalves says. "GeneTraffic is our data management solution. And a next generation pathway product, PathwayArchitect software, allows you to identify pathways that are biologically relevant." Stratagene bases its technology on the concept of a scriptable workflow. "Advanced users can make their algorithms available to everyone," Goncalves explains. "It's perfect for a core facility because of its disparate needs."

Recent advances in laboratory automation systems have provided significant benefit for researchers who deal with large numbers of samples. Biotechnology firms and pharmaceutical companies continue to adopt newer and better techniques to shorten their generation of leads while improving the quality of those leads. Advances in laboratory automation will inevitably help to produce more drugs in less time and at lower cost.

Peter Gwynne (pgwynne767@aol.com) is a freelance science writer based on Cape Cod, Massachusetts, U.S.A. Gary Heebner (gheebner@cell-associates.com) is a marketing consultant with Cell Associates in St. Louis, Missouri, U.S.A.

Featured Companies

ABgene, molecular biology instruments and supplies, http://www.abgene.com

Accelrys – a subsidiary of **Pharmacopeia,** scientific software, http://www.accelrys.com

Affymetrix, DNA microarrays, http://www.affymetrix.com

Agilent Technologies, lab-on-a-chip systems, http://www.agilent.com

Applied Biosystems, high throughput screening systems, http://www.appliedbiosystems.com

BD Biosciences, products for lab automation, http://www.bd.com

Caliper Life Sciences, microfluidic devices, automated laboratory instruments, http://www.caliperls.com

CapitalBio Corporation, DNA microarrays, http://www.capitalbio.com

Corning Inc. – Life Sciences Division, products for lab automation, http://www.corning.com

DNAStar, scientific software, http://www.dnastar.com

Eppendorf AG, automated liquid handling systems, http://www.eppendorf.com

Greiner Bio-One International [Germany], products for lab automation, http://www.gbo.com/bioscience

Hamilton Company, automated liquid handling systems, http://www.hamiltoncomp.com

Hitachi Genetic Systems/MiraiBio, scientific software, http://www.miraibio.com

Invitrogen Corporation, scientific software, http://www.invitrogen.com

Matrix Technologies Corporation, automated liquid handling systems, http://www.matrixtechcorp.com

MDL Information Systems, Inc., scientific software, http://www.mdl.com

MetriGenix Corporation, lab-on-a-chip devices, http://www.metrigenix.com

NimbleGen Systems, Inc., DNA microarrays, http://www.nimblegen.com

PerkinElmer Life and Analytical Sciences, high throughput screening systems, http://las.perkinelmer.com

Promega Corporation, high throughput screening assay kits, http://www.promega.com

Qiagen GmbH [Germany], separation and purification products, http://www.qiagen.com

Roche Applied Science, automated thermal cyclers, http://www.biochem.roche.com

Stratagene, scientific software, http://www.stratagene.com

SuperArray Bioscience Corporation, DNA microarrays, http://www.superarray.com

Tecan, microfluidic devices, automated laboratory instruments, http://www.tecan.com

Upstate, high throughput screening assay kits, http://www.upstate.com

Xiril AG, automated liquid handling systems, http://www.xiril.com

More Red Hot research papers than anyone else. Now that's big.

Research published in *Science* tops Thompson Scientific's list of The Red Hot Research Papers of 2004. Fifteen papers out of the total 46, in fact. The only journal to come close had just six on the list.

Year after year, *Science* publishes the leading-edge research papers that matter most. Is it any wonder that researchers consistently rank *Science* as the most useful journal? Join us at **aaas.org/join** and get the big picture in *Science* every week. To advertise, go to **scienceadvertising.org**.

Science
AAAS

GET THE BIG PICTURE IN *SCIENCE*

ScienceCcareers.org

Classified Advertising

Marie Curie
1867–1934

For full advertising details, go to **www.sciencecareers.org** and click on **How to Advertise,** or call one of our representatives.

United States & Canada

E-mail: advertise@sciencecareers.org
Fax: 202-289-6742

JILL DOWNING
(CT, DE, DC, FL, GA, MD, ME, MA, NH, NJ, NY, NC, PA, RI, SC, VT, VA)
Phone: 631-580-2445

KRISTINE VON ZEDLITZ
(AK, AZ, CA, CO, HI, ID, IA, KS, MT, NE, NV, NM, ND, OR, SD, TX, UT, WA, WY)
Phone: 415-956-2531

KATHLEEN CLARK
Employment: AR, IL, LA, MN, MO, OK, WI, Canada; Graduate Programs; Meetings & Announcements (U.S., Canada, Caribbean, Central and South America)
Phone: 510-271-8349

EMNET TESFAYE
(Display Ads: AL, IN, KY, MI, MS, OH, TN, WV; Line Ads)
Phone: 202-326-6740

GABRIELLE BOGUSLAWSKI
(U.S. Recruitment Advertising Sales Director)
Phone: 718-491-1607

Europe & International

E-mail: ads@science-int.co.uk
Fax: +44 (0) 1223-326-532

TRACY HOLMES
Phone: +44 (0) 1223-326-525

HELEN MORONEY
Phone: +44 (0) 1223-326-528

CHRISTINA HARRISON
Phone: +44 (0) 1223-326-510

SVITLANA BARNES
Phone: +44 (0) 1223-326-527

JASON HANNAFORD
Phone: +81 (0) 52-789-1860

To subscribe to *Science*:
In U.S./Canada call 202-326-6417 or 1-800-731-4939
In the rest of the world call +44 (0) 1223-326-515

Science makes every effort to screen its ads for offensive and/or discriminatory language in accordance with U.S. and non-U.S. law. Since we are an international journal, you may see ads from non-U.S. countries that request applications from specific demographic groups. Since U.S. law does not apply to other countries we try to accommodate recruiting practices of other countries. However, we encourage our readers to alert us to any ads that they feel are discriminatory or offensive.

ScienceCareers.org
We know science AAAS

POSITIONS OPEN

CASE
CASE WESTERN RESERVE UNIVERSITY

FACULTY POSITION
Proteomics, Department of Pharmacology
Case School of Medicine, Cleveland, Ohio

The Department of Pharmacology, in collaboration with the Case Center for Proteomics and Mass Spectrometry, is recruiting for a faculty member in the area of Proteomics and Mass Spectrometry. Appointment in all ranks will be considered, and outstanding startup package is available. The successful candidate will have access to state-of-the-art mass spectrometry equipment (LCQ-Deca XP, LTQ, LTQ-FT, QStar XL, 4000 QTrap, MALDI-TOF instruments) within the Center and a network of renowned scientists. Responsibilities will include, in addition to developing an independent research program, collaborative support of the proteomics research in the Department of Pharmacology. The candidate should have a Ph.D. in biochemistry, analytical chemistry, or a related field, and must have experience in proteomics including, but not limited to, liquid chromatography, biological mass spectrometry, and protein analysis/characterization. Experience in proteomics of membrane biology research is preferred and excellent oral communication skills are required. Please send cover letter, curriculum vitae, and three reference contacts to: **Cami Thompson, e-mail: cami@case.edu.**

In employment, as in education, Case Western Reserve University is committed to Equal Opportunity and World Class Diversity.

ASSISTANT PROFESSOR
Freshwater Fisheries Science

The Department of Wildlife Ecology is seeking applicants for an Assistant Professor position with a focus on freshwater fisheries science. This is a tenure-track, academic-year appointment at the University of Maine. The successful candidate will be responsible for developing an externally funded research program that addresses freshwater fish ecology and management. A Ph.D. degree in fisheries or wildlife science or a related discipline is required. A full position description can be seen at **website: http://www.umaine.edu/eo/faculty.**

Submit curriculum vitae, statement of teaching and research interests, official university transcripts, and contact information for three references who have been asked to send letters. Applications review will begin on February 1, 2006. Starting date is September 1, 2006. Send applications to: **Dr. James Gilbert, Chair, Department of Wildlife Ecology, 5755 Nutting Hall, University of Maine, Orono, ME 04469-5755.**

The University of Maine is an Equal Opportunity/Affirmative Action Employer.

State University of New York (SUNY) Upstate Medical University is seeking a **PROJECT DIRECTOR** to work with a team studying the genetics of renal disease. Rank and competitive salary dependent on qualifications. Will manage genetic studies of renal disease in rodents by supervising two technicians, completing data analyses, and working with the Principal Investigator on manuscript and grant submissions. Expertise in rodent genetics and QTL mapping required. Will be expected to develop an independent research program in rodent genetics. Minimum qualifications are Ph.D. in genetics or related field, postdoctoral fellowship, and experience in quantitative genetics. Knowledge of renal disease and faculty-level experience preferred. Apply to: **Dr. Steven J. Scheinman, Dean, College of Medicine, SUNY Upstate Medical University, 750 East Adams Street, Syracuse, NY 13210** or **e-mail: scheinms@upstate.edu.** *SUNY Upstate Medical University is an Affirmative Action/Americans with Disabilities Act/Equal Employment Opportunity employer committed to excellence through diversity. Women and minorities are encouraged to apply.*

POSITIONS OPEN

The **University of Nevada, Las Vegas (UNLV), Department of Chemistry** is seeking candidates for a full-time, nine-month tenure-track, appointment at the **ASSISTANT** or **ASSOCIATE PROFESSOR** level in biochemistry, commencing fall 2006. Applications are encouraged from individuals with interests in enzymatic biosensing or related fields. The Department **(website: http://sciences.unlv.edu/Chemistry)** has experienced significant growth resulting in a doctoral program initiated in 2005. The successful candidate will be expected to excel in teaching biochemistry at both undergraduate and graduate levels; develop rigorous extramurally funded research programs; and provide service to the Department, College, University and the profession. A Ph.D. in chemistry or biochemistry from an accredited college or university is required and postdoctoral experience is preferred. Salary competitive; contingent on labor market. Position contingent upon funding. Application materials must include a cover letter, curriculum vitae, proposed research plans (five-page limit), statement of teaching philosophy and interests, and three letters of recommendation. Materials should be addressed to: **Dr. David Hatchett, Search Committee Chair,** and are to be submitted via online application at **website: https://hrsearch.unlv.edu.** Review of applications will begin immediately. To assure consideration completed applications are due by February 10, 2006. *UNLV is an Affirmative Action/Equal Opportunity educator and employer committed to excellence through diversity.*

BIOLOGIST, NEUROBIOLOGY
Whitman College

Biology (Neurobiology). The Department of Biology at Whitman College invites applications for a one-year sabbatical replacement position as Visiting Assistant Professor of Biology beginning August 2006. Teaching duties include the upper-level elective neurobiology, one semester of the introductory course biological principles with lab, supervision of student research and theses; and either an additional upper-level elective or a course for nonmajors. Preference will be given to candidates who have completed their Ph.D. Whitman College is a selective, liberal arts college of 1,400 students committed to excellence in undergraduate teaching and research. Please send (as hard copy): application letter, curriculum vitae, three letters of recommendation, transcripts, and statements of teaching and research interests to: **Dr. Ginger S. Withers, Neurobiology Search, Department of Biology, Whitman College, 345 Boyer Avenue, Walla Walla, WA 99362. Telephone: 509-527-5326; fax: 509-527-5904.** Deadline: February 17, 2006. For additional information about Whitman College, see **website: http://www.whitman.edu.** *Applicants who would enrich the diversity of the campus community are strongly encouraged to apply and to address how they can contribute to that diversity.*

FACULTY POSITION
in Comparative Oncology

The University of Minnesota College of Veterinary Medicine and Cancer Center announce the establishment of the Perlman **ENDOWED CHAIR** in Comparative Oncology. Applications are invited for this high priority and unique faculty position in the Veterinary Clinical Sciences Department and Cancer Center. The successful candidate will be expected to lead a major comparative oncology program with a high level of commitment from multiple organizations within the University.

Candidates should have a D.V.M./V.M.D. and/or Ph.D., or equivalent postdoctoral research experience. Residency training, board certification in oncology, and the D.V.M./V.M.D. degree, though not required, would further strengthen the application.

Please go to **website: http://www1.umn.edu/ohr/employment/openings/job134107.html** for a full position description and application instructions. *The University of Minnesota is an Equal Opportunity Educator and Employer.*

DIRECTOR, DIVISION OF CELL BIOLOGY AND BIOPHYSICS

National Institute of General Medical Sciences (NIGMS)
National Institutes of Health (NIH)
Department of Health and Human Services (DHHS)

The Challenge: The NIGMS Division of Cell Biology and Biophysics supports a significant research grant program seeking greater understanding of the structure and function of cells, cellular components, and the biological macromolecules that make up these components. The research ranges from traditional cell biology and biophysics to studies of single molecules and work in structural genomics and proteomics. The long-term goal of the Division is to find ways to prevent, treat, and cure diseases that result from disturbed or abnormal cellular activity. The division has three components: the Biophysics Branch, the Cell Biology Branch, and the Structural Genomics and Proteomics Technology Branch. The Institute is seeking a leader in this field to direct the Division of Cell Biology and Biophysics, to coordinate the division's efforts with other federal agencies and the broader scientific community, and to supervise a staff of 11. Information about the division is available at: http://www.nigms.nih.gov/About/Overview/CBB.htm

Position Requirements: Candidates must have an M.D., Ph.D., or equivalent degree and post-doctoral training in the fields relevant to the position. The ideal candidate will have:

- Broad knowledge of both cell biology and biophysics;
- A demonstrated record of leadership and accomplishment in activities beyond the candidate's own research program; and
- Experience in the management of programs and people.

The position will be filled under Title 42, offering a competitive salary commensurate with qualifications and experience, within the range of $125,304 to $175,700. A recruitment or relocation bonus may be available. Relocation expenses will be paid.

How to Apply: The official vacancy announcement is available at: http://www.nigms.nih.gov/about/job_vacancies.html. To be considered for this position, send to the address below a CV, bibliography, the names and contact information of four references, and a "vision statement," not to exceed three pages, that describes your vision for the fields of cell biology and biophysics, where you see the fields going over the next ten years, and the role that NIGMS should play in enabling necessary developments.

nigmsjobs@mail.nih.gov or FAX to 301-451-5686
Applications must be received by midnight on the closing date: February 15, 2006

You may contact Erin Bandak, Human Resources Specialist, with questions about this vacancy on 301-594-2324.

WWW.NIH.GOV

Health Research in a Changing World

Fighting Diseases and Improving Lives

DEPARTMENT OF HEALTH AND HUMAN SERVICES
NATIONAL INSTITUTES OF HEALTH
NATIONAL INSTITUTE OF ALLERGY AND INFECTIOUS DISEASES

Are you ready for an exciting career that could help improve millions of lives around the world? Then consider joining the scientific and medical forces at NIAID. As part of the Division of Microbiology and Infectious Diseases (DMID) at NIAID, the Parasitology and International Programs Branch (PIPB) is responsible for planning and conducting programs of extramural research aimed at understanding the biology of protozoan and helminth parasites and their interaction with the human host as well as their vectors and intermediate hosts. PIPB/DMID has the following scientific opportunities available:

Program Officer/Medical Officer

As a Program/Medical Officer, the selected candidate will provide leadership and scientific/medical expertise and guidance in the planning, development, implementation and evaluation of basic and clinical research concepts, projects and initiatives to appropriate advisory groups; identify opportunities and problem areas, research gaps and relevant program needs and make recommendations for and facilitate new research efforts, clinical studies, clinical trials or other initiatives; and communicate with grantees/contractors, cooperative group members/representatives and others on policy interpretation, merit review and evaluation processes and procedures, and on decisions, concerns or other issues/matters of a medical/scientific nature. The selected candidate will also oversee and advise on preclinical development of candidate vaccines for parasitic diseases. In order to be considered for this position, applicants should have experience in basic and/or clinical research to examine the causes, diagnosis, treatment and prevention of infectious diseases; research on bacteriology, mycology, virology, or research on parasitic and other tropical diseases or vector biology is required. Experience in vaccine development and/or project management is highly desirable. For the Program Officer position, a Ph.D. and relevant experience are highly desirable. The selected candidate must posses an M.D. to be considered for the Medical Officer position.
To apply for the Program Officer vacancy, please visit
http://usajobs.opm.gov.
Vacancy number: NIAID-05-102836
GS-403/601-13/14 Salary: $74,782-$114,882
Open: 12/5/05-3/3/06

To apply for the Medical Officer vacancy, please visit
http://usajobs.opm.gov.
Vacancy number: NIAID-05-102836A
GS-602-13/14 Salary: $79,521-$114,882
Open: 12/5/05-3/3/06
In addition to the base salary, a Physician Comparability Allowance up to $30,000 per annum may be paid.

Applications must be submitted to Nolan Jones, Human Resource Specialist, 301-402-0957

Program Officer

As a Program Officer, the selected candidate will provide leadership and scientific expertise and guidance in the planning, development, implementation and evaluation of basic and clinical research concepts, projects and initiatives to appropriate advisory groups; identify opportunities and problem areas, research gaps and relevant program needs and make recommendations for and facilitate new research efforts; and communicate with grantees/contractors, cooperative group members/representatives and others on policy interpretation, merit review and evaluation processes and procedures, and on decisions, concerns or other issues/matters of a medical/scientific nature. The selected candidate will provide scientific and programmatic oversight and advice for research involving basic aspects of parasite biology, including genomics, functional genomics, molecular biology and biochemistry, and cell biology of protozoan and helminthic parasites. In order to be considered as Program Officer, applicants should have experience in basic and/or clinical research to examine the causes, diagnosis, treatment and prevention of infectious diseases; research on bacteriology, mycology, virology, or other viral diseases or research on parasitic and other tropical diseases and vector biology is required. Research experience at the Ph.D. and postdoctoral level is highly desirable, including but not limited to molecular biology and/or biochemistry.
To apply for the Program Officer vacancy, please visit
http://usajobs.opm.gov.
Vacancy number: NIAID-05-102837
GS-403/601-13/14 Salary: $74,782-$114,882
Open: 12/5/05-3/3/06
Applications must be submitted to Nolan Jones, Human Resource Specialist, 301-402-0957

To have your resume reviewed and for other opportunities, please visit: http://healthresearch.niaid.nih.gov/science and click "submit your resume"

DHHS and NIH are Proud to be Equal Opportunity Employers

Positions @ NIH
THE NATIONAL INSTITUTES OF HEALTH

Postdoctoral Positions

National Institute of Child Health and Human Development

Gene Regulation in Yeast
Alan G. Hinnebusch, Ph.D., ahinnebusch@nih.gov
http://eclipse.nichd.nih.gov/nichd/lgrd/bio_hinnebusch.htm

SUMO Proteins
Mary Dasso, Ph.D., mdasso@helix.nih.gov
http://eclipse.nichd.nih.gov/nichd/test/lgrd/sccr/index.htm

Synthetic Oligosaccharide-based Glycoconjugate Vaccines
Vince Pozsgay, Ph.D., pozsgayv@mail.nih.gov
http://eclipse.nichd.nih.gov/nichd/annualreport/2004/ldmi/bdpi.htm

Mitochondrial Function in Mouse Models That Misregulate Iron Metabolism
Tracey Rouault, M.D., rouault@mail.nih.gov
http://eclipse.nichd.nih.gov/nichd/cbmb/shim/shim.html

Molecular Analysis of Pineal Function
David C. Klein, Ph.D., Dr. med. H.c., kleind@mail.nih.gov
http://eclipse.nichd.nih.gov/nichd/ldn/SNE/index.htm

Development & Function of Drosophila Color-Vision Circuitry
Chi-Hon Lee, MD. PhD., leechih@mail.nih.gov
http://eclipse.nichd.nih.gov/nichd/lgrd/unc/index.htm

Molecular Studies on the Replication of HIV
Judith G. Levin, Ph.D., levinju@mail.nih.gov
http://jlevinlab.nichd.nih.gov

Molecular Genetics of Mouse Development
Heiner Westphal, M.D., hw12m@nih.gov
http://www.westphal.nichd.nih.gov

Middle Childhood and Early Adolescence & Infant Perception, Cognition, and Cognitive Neuroscience
Marc H. Bornstein, Ph.D., Marc H Bornstein@nih.gov
http://www.cfr.nichd.nih.gov

Electrophysiology
Bai Lu, Ph.D., lub@mail.nih.gov
http://neuroscience.nih.gov/Lab.asp?Org_ID=275

Applicants must have less than five years of postdoctoral experience.

NIDDK

POSTDOCTORAL FELLOWSHIPS IN DNA REPAIR AND RECOMBINATION AT THE NIH

We are a group of molecular and structural biologists whose main interests are in the areas of DNA repair and recombination. We are all located in a single building on the main intramural campus of the NIH in Bethesda, Maryland, a 20-minute ride from Washington, D.C. The intramural program of the NIH offers an outstanding research environment and many opportunities for collaborations. Applications are invited from individuals of the highest caliber with Ph.D., M.D., or M.D., Ph.D. degrees. Salary and benefits will be commensurate with experience of the candidate. The current research interests of the group include:

-Biochemistry and molecular biology of double-strand break repair and homologous recombination. Current interests include mouse meiosis (Dev Cell (2003) **4**: 497; NSMB (2005) **12**: 449; JCS (2005) **118**: 3233) and evolutionary genomics (Nature Genetics (2004) **36**: 642) (**Dan Camerini-Otero**).

-Molecular mechanism of retroviral DNA integration. Biochemical, structural and functional analysis of HIV integrase and other proteins and nucleoprotein complexes involved in retroviral integration (http://orac.niddk.nih.gov/www/craigie/crahome.html). (**Bob Craigie**: bobc@helix.nih.gov)

- Structural Biology of Site-Specific DNA Recombination. Current interests include the Adeno-Associated Virus (Mol. Cell (2002) **10**:327; (2004) **13**:403), and other eukaryotic and prokaryotic recombination systems. (Nature (2004) **432**:995; Mol. Cell (2005) **20**:143; NSMB (2005) **12**:715). (**Fred Dyda**: Fred.Dyda@nih.gov)

- Molecular Mechanisms of DNA Mismatch Repair. Biochemistry and molecular biology of mismatch repair and the cellular response to DNA damage. (Nature (2000) **407**:703; J. Mol. Biol. (2003) **334**:949; Proc. Natl. Acad. Sci. (2003) **100**:14822). (**Peggy Hsieh**: ph52x@nih.gov)

- Single-molecule biochemical study of macromolecular complex assembly/disassembly dynamics involved in DNA transposition, site-specific recombination and related reactions. (Mol. Cell (2002) **10**: 1367). (**Kiyoshi Mizuuchi**: kmizu@helix.nih.gov)

Interested candidates should send a letter stating their interests, their curriculum vitae and list of publications, and arrange to have letters from three references emailed to one of the investigators above or if you would like to be considered for more than one lab to **Dan Camerini-Otero (camerini@ncifcrf.gov) at: Bldg. 5, Rm 201, 5 Memorial Dr MSC 0538, National Institutes of Health, Bethesda, MD 20892-0538.**

WWW.NIH.GOV

NIDDK

Bioorganic Chemist

The National Institute of Diabetes and Digestive and Kidney Diseases (NIDDK), a major research component of the NIH and DHHS, is recruiting for a tenure track investigator to join the Laboratory of Bioorganic Chemistry.

The successful candidate will be a Ph.D. or M.D. scientist with at least five years research experience beyond receipt of degree. Research experience should be in synthetic organic or medicinal chemistry, especially as applied to specific projects in biomedical research. The applicant must have a proven record of accomplishments in synthetic, bioorganic and/or medicinal chemistry and will be expected to propose an independent research program that applies the principles of organic chemistry to biomedical challenges. Innovative approaches to achieving integration of chemistry and biology, such as devising new approaches to target discovery, use of molecular modeling, and other technologies, will be important factors. The position offers unparalleled opportunities for interdisciplinary collaboration within NIDDK and throughout NIH.

The successful candidate will be offered a competitive salary commensurate with research experience and accomplishments, and a full Civil Service package of benefits (including retirement, health, life and long term care insurance, Thrift Savings Plan participation, etc.) is available. Appointees must be U.S. citizens, resident aliens, or non-resident aliens with a valid employment authorized visa.

Applicants must submit a C.V. and bibliography, a brief statement of research interests, a plan for future research, and the names of three references to: **Dr. John Hanover, Chair, Search Committee, Laboratory of Bioorganic Chemistry, c/o MaryBeth Grothe, Building 8A, Room B1A-02, MSC 0810, National Institutes of Health, Bethesda, MD 20892-0810**. Applications must be received by **February 15, 2006.**

***Position Description*:** The successful candidate will carry out independent research consistent with the scientific goals of the Laboratory of Bioorganic Chemistry (LBC) of NIDDK. He/she must demonstrate a record of publication in chemistry and the ability to communicate to professional audiences effectively. A major research area of NIDDK and an important part of the research program of LBC are investigations of the functional properties of macromolecular systems, such as enzymes, biological receptors, and transport mechanisms, at the molecular level. This research employs the theory and laboratory techniques of modern organic chemistry, including synthesis of low molecular weight compounds to be used as enzyme inhibitors, receptor ligands, biological tracers, and mechanistic probes. Extensive use of newly developed reactions and chemical processes, including parallel and/or combinatorial syntheses, are used to develop selected synthetic targets and compound libraries. Modern procedures for isolation, purification, and identification of chemical species, including use of modern spectroscopy, such as NMR and mass spectrometry, are required. Computer databases, computer modeling and computer analyses are also extensively used. In addition, theory and techniques of modern molecular biology, biochemistry, and pharmacology are used to interface organic chemistry and biology.

Health Research in a Changing World

Fighting Diseases and Improving Lives

Tenure Track Position in Bacterial Pathogenesis
Laboratory of Clinical Infectious Diseases
National Institute of Allergy and Infectious Diseases
National Institutes of Health
Department of Health & Human Services

The National Institute of Allergy & Infectious Diseases (NIAID), Division of Intramural Research (DIR), Laboratory of Clinical Infectious Diseases (LCID) is seeking an outstanding investigator to develop a clinical and basic program in bacterial pathogenesis.

The LCID studies the pathogenesis, pathophysiology, treatment and prevention of infectious diseases, including emerging infections and pathogens that are of concern in biodefense, as well as microorganisms that cause persistent, recurrent, or fatal disease. Current areas of clinical and basic expertise in the LCID include viral, fungal, and mycobacterial pathogenesis and pathophysiology and the pathophysiology of defects in cellular apoptosis.

The successful candidate will establish an independent research program in bacterial pathogenesis with both laboratory and clinical components. The incumbent will develop clinical protocols, which may include natural history, pathophysiology, mechanism of action, treatment, or all of the above. Board eligibility/board certification or the equivalent in Internal Medicine or Pediatrics and Infectious Diseases or Allergy and Immunology are desirable, but Ph.D.'s with active clinical programs are also encouraged to apply. Sufficient independent resources including space, support personnel and an annual budget for services, supplies and salaries have been committed to the position to ensure success.

The appointment is a Tenure Track appointment and will be at the appropriate level under Title 42, which is equivalent to a University Assistant Professor rank. Salary is dependent on experience and qualifications.

Interested candidates may contact Dr. Steven Holland, Chief, LCID, DIR, and NIAID at 301/402-7684 or email (smh@nih.gov) for additional information about the position.

To apply for the position, candidates must submit a curriculum vitae, bibliography, three letters of reference, a detailed statement of research interests, and reprints of up to three selected publications by January 31, 2006 to Patrick Murray, Ph.D., Chair, NIAID Search Committee, c/o Mrs. Lynn Novelli, Committee Manager, 10 Center Drive, MSC 1356, Building 10, Room 4A26, Bethesda, Maryland 20892-1356. Further information on this position and guidance on submitting your application is available on our website at: http://healthresearch.niaid.nih.gov/science

Please reference "Science" on your resume.

UNIVERSITY OF SOUTHERN DENMARK

www.jobs.sdu.dk

Associate Professor in Research on Modern Artificial Intelligence and Robotics

Applications are invited for a position as associate professor in Modern Artificial Intelligence and Robotics at The Maersk Mc-Kinney Moller Institute for Production Technology, the University of Southern Denmark, in Odense, starting on 1 April 2006. The Institute performs internationally-oriented research in robotics, software engineering and modern artificial intelligence, and the successful applicant will mainly be involved in research and development activities in the field of modern artificial intelligence and robotics.

For further information please contact Professor Henrik Hautop Lund, tel. +45 6550 3575, e-mail: hhl@mip.sdu.dk and/or by visiting the web site of the University: www.sdu.dk

Applicants should be aware that it is necessary to read the full text for this position before applying.

Please find the full notice with further information and address on the University`s homepage: www.jobs.sdu.dk/index.php?vis=eng

Deadline for applications: February 2, 2006 at 12:00 hrs.

SYDDANSKUNIVERSITET.DK

University at Buffalo
The State University of New York

Assistant Professor

Faculty Positions in Pharmaceutical Sciences – Department of Pharmaceutical Sciences, School of Pharmacy and Pharmaceutical Sciences, Faculty of Health Sciences (http://pharmacy.buffalo.edu).

Applications are invited for two tenure track positions, which will be filled at the level of Assistant Professor. We seek applicants with a demonstrated record of research excellence in the areas of pharmacokinetics, pharmacodynamics, and/or pharmacometrics relevant to important therapeutic and disease areas. A Ph.D. in a relevant field and post-doctoral experience are highly desirable. The successful candidate is expected to develop an independent and extramurally funded research program and to participate in undergraduate and graduate instruction. Applicants should submit a letter of application, curriculum vitae, the names and addresses of three references, and a statement of research interests.

Submit application materials by email to:
jb@buffalo.edu
Joseph Balthasar, Ph.D.,
Search Committee Chair
School of Pharmacy and
Pharmaceutical Sciences
457B Cooke Hall
University at Buffalo
Buffalo, New York 14260-1200
Telephone 716-645-2842 ext. 270
FAX 716-645-3693

An Affirmative Action / Equal Opportunity Employer

ENGINEERING FACULTY

The Pratt School of Engineering at Duke University is seeking outstanding faculty at the assistant, associate or full professor level in the broadly defined area of biomaterials as it relates to topics such as biomanufacturing, bio-interface science, Bio-MEMS, biosensing, and drug and gene delivery. Qualified candidates must have a PhD degree or equivalent in Engineering or a related science discipline. Candidates for appointment at the associate and full professor level must possess a distinguished record of research accomplishments and publications and a demonstrated ability to mentor graduate students and develop an innovative research and educational program. Candidates at the assistant professor level must demonstrate the potential to become leaders in their discipline. Successful candidates will be expected to attract significant external funding, perform research at the cutting edge of their field, and teach undergraduate and graduate courses in materials science and engineering within the Pratt School of Engineering. Appointments will be considered in one or more departments within the Pratt School of Engineering consistent with the research and teaching interests of the candidate.

Qualified candidates should send a letter of application including statement of research interest, teaching philosophy, curriculum vitae and names and addresses/email/phone numbers of at least three references to: **Chair, Biomaterials Faculty Search Committee, c/o Glenda Hester, Pratt School of Engineering, Box 90271, Durham, NC 27708**.

Duke University

Duke University is an Equal Opportunity/Affirmative Action Employer.

Colby

Biology Department
Animal Ecologist

COLBY COLLEGE is seeking an Animal Ecologist to fill a one-year position as Faculty Fellow in Biology to begin **September 1, 2006**. Candidates should have a Ph.D. in the biological sciences with broad training in Ecology. Assignments will include the team-teaching of three courses: Introductory Ecology, Advanced Ecology, and Environmental Science. The candidate will also participate in the instruction of one section of Introductory Biology laboratory. Familiarity with liberal arts colleges, teaching experience, and post-doctoral experience are desirable. Please submit a letter of application, statement of teaching interests, curriculum vitae, undergraduate and graduate transcripts, and three letters of recommendation to: **Frank A. Fekete, Chair, Animal Ecologist Search, Department of Biology, 5729 Mayflower Hill, Colby College, Waterville, Maine 04901, Tel: (207) 859-5729, Email: fafekete@colby.edu.** Application review will begin on January 20th, 2006 and continue until the position is filled.

Colby is an Equal Opportunity/Affirmative Action employer, committed to excellence through diversity, and strongly encourages applications and nominations of persons of color, women, and members of other under-represented groups. For more information about the College, please visit the Colby web site:

www.colby.edu

Ajinomoto Co., Inc. is pleased to announce the recipients of the 3ARP grant 2005.

Ajinomoto Co., Inc. appreciate the interest and participation of a large number of scientists. We received over 130 high-quality proposals from around the world for this program in 2005. After extensive review and deliberation, the following 9 proposals were selected for funding.

Focused Category

Prof. Leticia Castillo (Baylor College of Medicine, USA)
Nutrition and functional requirement of methionine in septic children

Prof. Yoshinori Moriyama (Okayama University, Japan)
Vesicular glutamate transporter: Molecular architecture and physiological roles in metabolic regulation

Prof. Johannes Van Goudoever (Erasmus MC-Sophia M, Belgium)
Optimizing nutrition for infants with an impaired gut function

Exploratory Category

Prof. Douglas Burrin (USDA-ARS, Children's Nutrition Research Center, USA)
Vasoactive and tropic actions of enteral arginine in the neonatal porcine intestine

Prof. Pierre Fafournoux (Institut National de la Recherche Agronomique(INRA), France)
Role of the GCN2 kinase in the feeding behavior response to variations in dietary amino acid supply

Prof. John Fernstrom (University of Pittsburgh, USA)
An exploratory biochemical study to assess if serotonin & catecholamine neurons in brain respond to chronic, diet-related changes in plasma amino acids

Prof. Jonathan Powell (The Johns Hopkins University, USA)
Regulation of T-cell activation and tolerance by branch chain amino acids

Prof. Christopher Proud (University of British Columbia, Canada)
Identification and characterization of cellular components involved in the control of mTOR signaling by amino acids

Prof. Gozoh Tsujimoto (Kyoto University, Japan)
Identification and characterization on physiological roles of receptor(s) to nutrients in gastro-intestinal tract

Monterey Bay Aquarium Research Institute

2006 POSTDOCTORAL FELLOWSHIPS

Founded in 1987 and supported by the David and Lucile Packard Foundation, The Monterey Bay Aquarium Research Institute (MBARI) is a non-profit oceanographic research institute, dedicated to the development of state-of-the-art instrumentation, systems, and methods for scientific research in the oceans. MBARI's research center includes science and engineering laboratories, as well as an operations facility to support our research vessels and oceanographic equipment, including remotely operated and autonomous underwater vehicles. Located in Moss Landing, California, the heart of the nation's largest marine sanctuary, MBARI places a balanced emphasis on science and engineering, with established programs in marine robotics, ocean physics, chemistry, geology, and biology, as well as information management and ocean instrumentation research and development.

MBARI invites applications each year for several postdoctoral fellowships in the fields of biological, chemical, and physical oceanography, marine geology, and ocean engineering. Fellowships may require occasional trips to sea. Awards are typically for two years.

Candidates must complete their Ph.D. degree prior to commencing the two-year appointment between October 2006 and March 2007. **Application deadline: Friday, March 3, 2006**. Selected candidates will be contacted in April. **Note**: It is helpful for applicants to communicate with potential research sponsors at MBARI (http://www.mbari.org/about/researchers.html) for guidance on project feasibility, relevance to ongoing MBARI research, and resource availability.

Application requirements:
- Curriculum vitae
- At least three professional letters of recommendation
- Succinct statement of the applicant's doctoral research
- Potential research goals at MBARI
- Supplemental Information online form **(http://www.mbari.org/oed/jobs/forms/postdoc_form.htm)**

Competitive compensation and benefits package.
MBARI considers all applicants for employment without regard to race, color, religion, sex, national origin, disability, or veteran status.

Address your application materials to:
MBARI, Human Resources
Job code: Postdocs-2006
7700 Sandholdt Road, Moss Landing, CA 95039-9644

Submit by e-mail to jobs@mbari.org (preferred), or by snail mail, or by fax to (831) 775-1620.

M B A R I

EOE • MBARI Welcomes Diversity

ASSISTANT PROFESSOR
Plant and Environmental Microbiology
University of California, Riverside

The Department of Plant Pathology invites applications for a tenure-track faculty position emphasizing the functional genomics or fundamental biology of prokaryotes in agronomic or natural systems. Genetic, genomic, biochemical, chemical, proteomic, and/or systems biology approaches may be used to investigate ecological, physiological, or molecular interactions of prokaryotes with hosts, microbes, or environment. Research involving plant pathogens, symbionts, or epiphytes are especially welcome. The position will join a vibrant community of researchers studying microbe-host and microbe-environment interactions, and will have access to modern campus facilities in genomics, proteomics, and microscopy. Consult **www.plantpathology.ucr.edu** for details about the department. Applicants will be expected to pursue vigorous, extramurally funded research and contribute to undergraduate and graduate teaching in microbiology or plant pathology. A Ph.D. and demonstrated excellence in research are required.

Send curriculum vitae, statements of research and teaching interests, selected reprints, and three letters of reference to: **Dr. Howard Judelson, c/o C. Brusuelas, Department of Plant Pathology, University of California, Riverside, California 92521-0415**. **Email: cherylfb@ucr.edu**. Deadline: **February 14, 2006**, or until position is filled.

The University of California is an Affirmative Action/Equal Opportunity Employer.

Faculty Positions in Molecular Cardiology

MSSM
MOUNT SINAI SCHOOL OF MEDICINE

The Center for Molecular Cardiology at the Mount Sinai School of Medicine invites applications for independent, tenure-track faculty positions at the Assistant or Associate Professor level in the areas of cardiovascular developmental biology and genetics. Exceptionally well-qualified candidates at a more senior level may also be considered.

We are searching for two faculty positions, one in genetics, focusing on gene discovery for human or animal cardiovascular traits, and the other in development biology, preferably one who studies cardiogenesis using contemporary genetic approaches in the mouse. Individuals should be highly interactive and receptive to multidisciplinary collaborations. Mount Sinai offers numerous shared research facilities including mouse transgenic and imaging cores and state-of-the-art animal facilities.

Applications should include a CV, a brief description of current research and future research plans, copies of no more than four primary publications, and names of and contact information for three references. Please send applications to: **Bruce D. Gelb, M.D., Director, Center for Molecular Cardiology, Box 1498, Mount Sinai School of Medicine, One Gustave L. Levy Place, New York, NY 10029. Email: bruce.gelb@mssm.edu.** Equal opportunity employer. We particularly welcome applications from women and under-represented minorities in science.

Center for the Study of BIOLOGICAL COMPLEXITY

VCU

Computational Bioinformatics - Faculty

The Center for the Study of Biological Complexity and the School of Engineering at VCU invite applications for a tenure eligible Assistant Professor to Professor level position in computational bioinformatics. The successful candidate will hold a Ph.D. in Computer Science or related field and is expected to develop a program of externally funded research. Interests should include algorithm development, interpretation, and scientific visualization of multi-scale/multi-dimensional biological datasets, database architecture and algorithm design, simulation of complex biological systems, or other relevant areas of computational biology and bioinformatics. The successful candidate will participate in teaching within the VCU's comprehensive new Bioinformatics Program.

The successful applicant will join the Center for the Study of Biological Complexity (**www.vcu.edu/csbc/**) in VCU Life Sciences, and the School of Engineering as part of our effort to integrate Life Sciences and Engineering. The School of Engineering, launched in 1996 and now enrolling over 1000 students, is home to the new department of Chemical and Life Science Engineering, Computer Science and Biomedical Engineering. The Center for the Study of Biological Complexity is an academic think tank that promotes integrative and interdisciplinary approaches to biological and biomedical research. The Center houses VCU's high performance computing facilities, including hardware, software, databases and support for bioinformatics, modeling and scientific visualization. The Center also maintains state of the art resources for genomic, proteomic and pharmacogenomic research, and houses students in VCU's programs in bioinformatics and systems biology.

Send a statement of research and teaching interests, curriculum vitae, three references and supporting documents by **March 1, 2006**, to: **Gregory A. Buck, Center for the Study of Biological Complexity, Virginia Commonwealth University, P.O. Box 842030, Richmond, Virginia 23284-2030, by e-mail at buck@mail2.vcu.edu**.

VCU is an Equal Opportunity/Affirmative Action Employer.
Women, minorities and persons with disabilities are encouraged to apply.

Virginia Commonwealth University

UCSF

ASSISTANT PROFESSOR

Division of Infectious Disease and Program in Microbial Pathogenesis and Host Defense

University of California, San Francisco

The Division of Infectious Disease in the Department of Medicine, the Microbial Pathogenesis and Host Defense Program, the Biomedical Sciences graduate training program, and the graduate Program in Biological Sciences at the University of California, San Francisco, invite applications for an in-residence position at the Assistant Professor level in the field of Microbial Pathogenesis. Candidates should have an M.D. or M.D./Ph.D., be board-certified or board-eligible in Infectious Disease, have at least three years of relevant postdoctoral experience with a strong record of recent research accomplishments, and evidence of ability to successfully compete for extramural funding. Exceptional candidates of higher rank will be considered. The successful candidate will be expected to establish a vigorous, independent, well-funded research program. The successful candidate will join the Microbial Pathogenesis and Host Defense Program and will be eligible to become a member of the Biomedical Sciences graduate program and the graduate Program in Biological Sciences. The successful candidate will also participate in appropriate clinical activities of the Infectious Disease Division.

Please send by email a CV, a statement of research accomplishments and future research plans, PDFs of relevant reprints, and arrange to have three letters of reference sent to: **Kate O'Brien, obrienk@itsa.ucsf.edu, Box 0414, MedSci S469, University of California, San Francisco, 513 Parnassus Ave, San Francisco, CA 94143-0414.**

The University is an Equal Opportunity/Affirmative Action Employer. All qualified applicants are encouraged to apply, including minorities and women.

MGH 1811

Massachusetts General Hospital Harvard Medical School

Faculty Position in Brain Tumor Research

The Massachusetts General Hospital and Harvard Medical School are seeking applications at the level of Assistant or Associate Professor to establish a dynamic, integrative research program in the biology of gliomas. Potential areas of interest include mouse models, tumor stem cell biology, pharmacology, growth factors and immunology although other themes will be considered. The appropriate candidate should hold either a Ph.D. or M.D. degree or both. Departmental assignment within Harvard Medical School will depend on research focus. The candidate should be an accomplished investigator with demonstrated research excellence, publications in the biomedical literature, and peer-reviewed grant support. The appropriate candidate should be able to develop concepts that lead to a better understanding of the biology of gliomas and their therapy.

This opportunity includes generous start-up funds and new laboratory space in the Simches Research Center at MGH that opened in 2005. The position features many opportunities to collaborate with other scientists involved in glioma research at Massachusetts General Hospital. This position will also include collaboration with a large clinical brain tumor program at Harvard Medical School supported by multiple NIH grants and the opportunity to supervise research fellows supported by an NCI-sponsored training grant in neuro-oncology. Applications from women and representatives of minority groups are encouraged. Interested candidates should forward a curriculum vitae, a brief statement of research interests and 3 letters of recommendation to: **Valerie J. Smith; Stephen E. and Catherine Pappas Center for Neuro-Oncology; Yawkey 9E; Massachusetts General Hospital; 55 Fruit Street; Boston, MA 02114-2696; vjsmith@partners.org**.

The Massachusetts General Hospital is an Equal Opportunity Employer.

The DHHS, U.S. Food and Drug Administration's Center for Biologics Evaluation and Research, Division of Viral Products, in the Office of Vaccines Research and Review offers exciting employment opportunities in the area of influenza virus research and review. Excellent space, including newly renovated P3 facility, is available to support state of the art research that enhances CBER's regulatory mission to assure the safety, efficacy, and availability of influenza virus vaccines. This is an outstanding opportunity to have a direct impact on public health. Positions are located at CBER's facility on the NIH campus, in Bethesda, Maryland.

There are several positions, which may be filled at different levels, including **Staff Fellow -** This position requires an advanced degree in a related discipline e.g., Ph.D., or MD) and at least two years of post-doctoral experience. The salary range for this position is from $43,365 to $81,747 for scientists or $54,287 – $81,747 for physicians; **Senior Staff Fellow -** This position requires an advanced degree in a related discipline, completion of post-doctoral training, and ability to establish an independent research program - salary range from $52,468 to $97,213 for scientist or $54,287 - $97,213 for physicians; **Interdisciplinary Scientist -** This senior investigator position may be subject to peer review. An advanced degree and established research program is highly desirable. Salary range for this position is from $74,782 to $114,882 (scientists and physicians), physicians may be eligible for a Physicians Comparability Allowance of up to $16,000; and **Supervisory Interdisciplinary Scientist -** This Lab Chief position may be subject to peer review. An advanced degree and an established research program are highly desirable. The ability to manage the Division's influenza program is essential. Salary range from $88,369 to $114,882 (scientists and physicians); physicians will be eligible for Physician Comparability Allowance up to $16,000 or Physicians' Special Pay.

Please send CV plus names of 3 references to: **Arnetta Courtney, Recruitment Specialist, 1401 Rockville Pike, HFM-123, Rockville, Maryland 20850**; email: **Recruitment@cber.fda.gov**.

The FDA is an Equal Opportunity Employer and has a smoke free environment.

UTB TSC

TWO TENURE TRACK FACULTY POSITIONS - DIABETES

As an effort to expand Biomedical Research the department of Biological Sciences is searching for new faculty at any academic level (tenure–eligible). Key criteria include: a record of excellence in research (grant funding and peer-reviewed publications); an innovative research plan that will apply skill and knowledge in biochemistry, nutrition, pharmacology, molecular biology, molecular genetics and/or cell biology to solve community-based problems in Diabetes; and a commitment to training and teaching a students at both undergraduate and graduate levels. Qualifications: MD and/or PhD. Experience working with minority health disparities are desirable.

The University of Texas at Brownsville/Texas Southmost College is a minority oriented university located at desirable location, friendly weather "by the border near the sea" in a rapidly growing community with plenty of attractions.

Submit a letter of interest outlining research and educational interests, curriculum vitae, list of three references, and a recent representative peer-reviewed publication to: **Dr. Emilio R. Garrido-Sanabria or Dr. Luis V. Colom, Department of Biological Sciences, Center of Biomedical Studies, University of Texas Brownsville, 80 Fort Brown, LHSB 2.810, Brownsville, Texas 78520; Tel: (956) 882-5048; Fax: (956) 882-5043.**

Review of qualified applications will begin Friday, January 20, 2006 and will continue until position is filled. Appointment begins September 16, 2006. For full position descriptions see: **www.utbtsc.edu/human_resources** (to be confirmed after posting)

The University of Texas at Brownsville/Texas Southmost College is committed to Affirmative Action and Equal Opportunity in Employment and Education.

Vice Provost for Research

Oakland University

Oakland University (**www.oakland.edu**), located in southeastern Michigan, the home of Automation Alley, a Michigan SmartZone, and the Michigan Life Sciences Corridor, seeks applications and nominations for the position of Vice Provost for Research. Classified as "Doctoral/Research University-Intensive" by the Carnegie Foundation, Oakland University is strongly committed to graduate education through its doctoral programs as well as its extensive undergraduate programs that are offered to nearly 17,000 students.

The Vice Provost for Research reports to the Provost and directs the Office of Grants, Contracts and Sponsored Research, which oversees pre- and post-award processes, as well as regulatory compliance activities to ensure the ethical and responsible conduct of research. As the University's chief advocate for research, the selected individual will lead the development of a clear vision for research at Oakland, inclusive of all disciplines, including incentive programs to facilitate activities to enhance the research infrastructure of the institution, resulting in a significant increase in the level of external funding. The successful candidate will be expected to work closely with the Provost and Deans to develop financial strategies that promote the research mission of the University. He or she will also be responsible for the further development and management of policies related to the stewardship of intellectual property and technology transfer. This individual will be expected to cultivate relationships both within and outside the University in order to expand collaborations with industry and government, as well as educational and research institutions.

Required Qualifications: A strong record in the application for and management of externally funded grants and/or contracts; university teaching experience and a record of scholarly activity suitable for a tenured senior faculty appointment; demonstrated leadership abilities; broad knowledge of research funding sources; administrative experience with the ability to interact effectively in a culturally and ethnically diverse community; knowledge of matters related to research compliance such as protection of human participants, conflict of interest, and the care and use of experimental animals.

Preferred Qualifications: Demonstrated success in developing and managing multidisciplinary research; knowledge of trends in mission-related research; familiarity with intellectual property and technology transfer issues.

Application and Nomination: This appointment will be effective on or about August 15, 2006. Review of applications will begin **February 15, 2006** and continue until the position is filled. Interested applicants must submit a letter of application addressing the above qualifications, curriculum vitae, and the names, addresses, phone numbers, and email addresses of five references. References will not be contacted until advanced stages in the screening process. Applications and nominations should be sent electronically as pdf files to **Provost@Oakland.edu**.

Located 25 miles north of Detroit in Rochester, Michigan, Oakland University offers extensive cultural and social programs.

The University is an Equal Opportunity Employer, and encourages applications from women and minorities.

Institut de Science et d'Ingénierie Supramoléculaires (ISIS)

PROFESSORSHIP IN BIOPHYSICS

Applications are invited for candidates to set up and lead a biophysics laboratory in the Institut de Science et d'Ingénierie Supramoléculaires (ISIS), **http://www.isis-ulp.org**

The successful candidate will be tenured and will have up to 450 m^2 (5000 ft^2) of usable lab and office space in a purpose built institute, opened in 2002, in the heart of the central campus of the Université Louis Pasteur, Strasbourg, France. The establishment of the biophysics laboratory will be supported by a generous start-up package.

ISIS was founded by Prof. Jean-Marie Lehn (Nobel Prize in Chemistry, 1987). At ISIS multidisciplinary research is carried out at the interface between physics, chemistry and biology. ISIS has excellent equipment and facilities including: fluorescent activated cell-sorter, class 10000 clean room equipped with mask-aligner and other equipment for photolithography, microfluidics fabrication and testing facilities, nanofabrication platform (dual focused ion beam and e-beam), robots for synthesis, facilities for hydrogenation and ozonolysis, scanning tunneling and atomic force microscopy, spectroscopy, chromatography, mass spectroscopy and NMR, as well as microplate readers, PCR machines and other equipment for molecular biology.

The new biophysics laboratory in ISIS will be expected to have a strong experimental, and not purely theoretical, base. However, applications are welcome from candidates working in any field which applies theories and methods of the physical sciences to questions of biology, including neurosciences, molecular and supramolecular structural studies, development and application of biophysical techniques, and development of detailed physical mechanisms to explain specific biological processes.

To apply, please send a statement of future intentions and a full CV, including the names, addresses and email of three scientific referees by February 28th 2006 to:

Prof. Thomas Ebbesen, Director
Institut de Science et d'Ingénierie Supramoléculaires (ISIS)
8 allée Gaspard Monge, BP 70028, F-67083 Strasbourg Cedex FRANCE
Phone: +33 (0)3 90 24 51 17 **Fax:** +33 (0)3 90 24 51 18
e-mail: nano@isis-ulp.org **website:** http://www.isis-ulp.org

Science Careers Forum

- How long should it take to get my Ph.D.?
- Academia or industry?
- What will make my resume/cv stand out?
- How do I negotiate a raise?

Connect with Experts

Moderator Dave Jensen
Industry Recruiter

Mr. Jensen has over 20 years of experience in human resource consulting and staffing for the biotechnology and pharmaceuticals industry.

Adviser Bill Lindstaedt
Director,
UCSF Career Center

Mr. Lindstaedt has been providing career related advice to scientists and engineers for nearly 15 years, with a particular emphasis on working with graduate-level trainees in the life sciences.

Adviser Naledi Saul
Assistant Director,
UCSF Career Center

Ms. Saul has 7 years of career counseling with 4 years focused on counseling graduate students and postdocs in the biomedical and health sciences. Her forte is working with scientists pursuing careers in the public health arena.

Adviser Jim Austin
Editor, Science's
Next Wave

Dr. Austin has a Ph.D. in physics and worked in academia before coming on board to write about traditional and nontraditional career paths for scientists.

Visit www.sciencecareers.org and click on Career Forum

ScienceCareers.org
We know science AAAS

HUMAN MICROBIAL PATHOGENESIS
FACULTY POSITIONS — OPEN RANK
CENTER FOR MOLECULAR & TRANSLATIONAL HUMAN MICROBIAL PATHOGENESIS RESEARCH

THE METHODIST HOSPITAL RESEARCH INSTITUTE

The Methodist Hospital Research Institute at The Methodist Hospital in Houston, Texas, seeks several exceptional scientists studying the molecular basis of human microbial pathogenesis. Individuals who currently lead multiple-PI teams and collaborating PIs who desire to co-locate also will be considered.

The Methodist Hospital System consists of 1,450 beds, including 950 located in the Texas Medical Center in Houston. With our partners at Weill Cornell Medical College and New York-Presbyterian Hospital in New York City, there are 3,500 beds and many outpatients available for human microbial pathogenesis research. Collaborative opportunities also are available with the University of Houston and other local institutions.

The hospital has entered an unprecedented expansion phase that includes building a 300,000 SF state-of-the-art research building with bio-containment and non-human primate facilities, and a 560,000 SF ambulatory care building, both designed to foster interdisciplinary collaboration.

We are interested in candidates using new technologies to study molecular events occurring at the host-pathogen interface.

Successful applicants will be responsible for establishing or expanding nationally recognized, externally funded research programs.

Applicants must have an advanced degree (PhD, DVM, MD, or MD/PhD). Successful applicants will receive an outstanding recruitment package. Interested individuals should send via e-mail a curriculum vitae; description of research interests, future directions, and grant funding information; and the names of at least three references to:

James M. Musser, M.D., Ph.D. c/o Ms. Irene Harrison
Co-Director and Executive Vice President
The Methodist Hospital Research Institute
6565 Fannin, Mail Stop B154, Houston, TX 77030
E-mail: iaharrison@tmh.tmc.edu

Methodist The Methodist Hospital Research Institute

LEADING MEDICINE℠

USDA Agricultural Research Service
www.ars.usda.gov

National Program Leaders
Soil and Water Resource Management and Air Quality and Global Climate Change

(Interdisciplinary: Ecologist, Soil Scientist, Environmental Engineer, Agricultural Engineer, Physical Scientist, Hydrologist or Chemist; GS-0408/0470/0819/0890/1301/1315/1320-14/15)

The USDA, Agricultural Research Service, National Program Staff, Natural Resources and Sustainable Agricultural Systems in Beltsville, MD, is seeking two National Program Leaders for: (1) Soil and Water Resource Management and (2) Air Quality and Global Climate Change. These senior level positions direct research policies and programs for USDA's chief in-house science agency. The National Program Leaders plan, lead, coordinate and implement comprehensive research programs conducted at sites nationwide. For program information on the Soil and Water Resource Management position contact **Mark Weltz** on **301-504-6246**, email: **mark.weltz@nps.ars.usda.gov**. Contact **Robert Wright** on **301-504-4638**, email: **robert.wright@nps.ars.usda.gov** for program information on the Air Quality and Global Climate Change position.

Candidates need an extensive scientific background and must have advanced research experience in one or more of the specialty areas. Recruitment is at the GS-14/15 levels. Salary commensurate with experience (GS-14, $88K-$114K; GS-15, $103K-$135K per year plus benefits). Pre-employment check and a full background investigation may be required. This is a permanent, full-time position.

Candidates must be U.S. Citizens. Application must address specific education and experience requirements. To request copy of vacancy announcement, call **(301) 504-1482** or go to **http://www.usajobs.opm.gov** for **#ARS-X6E-0064 (Soil and Water Resource Management)** and **#ARS-X6E-0063 (Air Quality and Global Climate Change)**. Announcements open on December 12, 2005. Applications must be postmarked by **February 27, 2006**.

USDA/ARS is an Equal Opportunity Employer and Provider.

Director: Romberg Tiburon Center for Environmental Studies
San Francisco State University

The Romberg Tiburon Center for Environmental Studies (**http://rtc.sfsu.edu**), the marine and estuarine science campus of San Francisco State University (SFSU), seeks candidates for the Director of this unique research and instructional facility.

The Center is located on 34 acres fronting San Francisco Bay on the Tiburon Peninsula in Marin County. The Center is staffed by 19 scientists and 14 support personnel, in addition to research technicians, post doctoral fellows, and SFSU graduate and undergraduate students. The Center has multiple research facilities including a 38' research vessel and a fleet of small boats, aquaria and greenhouse space, and a genetics laboratory. RTC scientists currently bring about $13 million in external grant funds to the Center. RTC has experienced 10 years of exceptional growth and seeks a visionary leader from the marine science community to accelerate this momentum.

The position responsibilities include:

- providing leadership, vision and strategic planning to promote Center expansion,
- obtaining external funds for continued facilities development, including marine operations,
- recruiting and mentoring of faculty to ensure exemplary research and instruction,
- planning and implementing of instructional programs at the Center,
- promoting student scholarship through developing financial support,
- promoting the Center at community, state and federal levels,
- maintaining scholarly activity in the Director's area of interest,
- overall administration and supervision of the staff and facility.

Applicants should possess a doctorate with a strong research record in estuarine, coastal, and/or oceanographic systems; solid experience in administration and management of a field station or a large, preferably multi-disciplinary, research program; and excellent leadership and communication skills. Salary will be commensurate with qualifications; a complete benefits package is available. Submit letter of interest, curriculum vitae, and contact information of at least three references to: **Dean Sheldon Axler, College of Science & Engineering, San Francisco State University, 1600 Holloway Ave, San Francisco, CA 94132 by 3 March 2006.**

San Francisco State University is an Equal Opportunity/Affirmative Action Employer and strongly encourages applications from underrepresented groups.

ASSISTANT DIRECTOR
North Carolina Central University (NCCU)
Biomedical/Biotechnology Research Institute (BBRI)

Applications are invited for the position of **Assistant Director** in the BBRI at NCCU. The BBRI is a 40,000 sq. ft. state-of-the-art research facility that houses NCCU's Cardiovascular Disease, Neuroscience of Drug Abuse, and Cancer Programs. The Institute also offers core facilities that include genomics, bioinformatics, zebrafish transgenic modeling, and a modern animal resources complex.

The candidate will have responsibility for assisting the BBRI Director with providing administrative and scientific leadership for all programs and activities. The candidate will work with project teams, support staff, and NCCU administrators to establish research and training priorities that support the mission of the institute. Specific duties include: assisting with recruitment; developing and implementing research, education, and training programs; procuring extramural funding; ensuring that program activities are compliant with institute, university, and agency policies and procedures; and promoting interdisciplinary and inter-institutional collaborations. The proximity of the BBRI to the Research Triangle Park will afford the candidate unique opportunities to develop research partnerships with a high probability for success.

The candidate will be an NCCU faculty member responsible for conducting independent research related to the program themes of the BBRI. Qualified candidates must hold a Ph.D and/or MD., have a record of effective research program management, and meet requirements for an NCCU tenure-track faculty appointment in a basic science department. Additional requirements include: a strong record of peer-reviewed research publications and research funding; teaching experience at the undergraduate and/or graduate level; and excellent oral and written communication skills.

Review of applicant will begin immediately and will continue until the position is filled. Applicants should submit curriculum vitae, a description of research interests, and contact information for three references to: **Dr. Ken R. Harewood, Director, BBRI, NCCU, 1801 Fayetteville Street, Durham, NC 27707**. For more information, visit **http://www.nccu.edu/BBRI**

NCCU is an Equal Opportunity, Affirmative Action Employer.

ASSISTANT/ASSOCIATE PROFESSOR DEVELOPMENTAL/REPRODUCTIVE TOXICOLOGY

The College of Veterinary Medicine at North Carolina State University in Raleigh, North Carolina announces a tenure track faculty position in Developmental/Reproductive Toxicology with an initial appointment at 70% research 30% teaching. Applicants should have a DVM and/or PhD or equivalent degree. The search will remain open until February 15, 2006, or until filled. The successful candidate is expected to advance the field of developmental/reproductive biology through an active, extramurally funded program in this area.

The responsibilities of the new faculty member will include: (1) Developing, and/or maintaining, an extramurally funded research program in developmental/reproductive toxicology in areas such as environmental effects on fetal/placental function, long term effects of prenatal exposure, and/or epigenetic toxicology of the fetus and placenta. There will be extensive opportunities for interaction with related programs in epigenetic effects of assisted reproductive technologies, environmental toxicology at the organismal, cellular and molecular level, and understanding the effect of fetal exposures on late onset disease; (2) Acting as Course Leader and lecturer in a 2-credit course in veterinary embryology taught to students in the professional veterinary curriculum; (3) Participating in graduate education. In addition, the applicant will have broad collaborative opportunities with nearby institutes such as the Environmental Protection Agency (EPA), the National Institute of Environmental Health Sciences (NIEHS), as well as neighboring Universities (University of North Carolina and Duke).

The application should be submitted using an electronic on-line procedure. Please use the web site: **http://jobs.ncsu.edu** and search by Identification Number B-96-0512, to complete the Applicant Profile. Applications should include (1) a curriculum vitae, (2) a statement of research interests and projected research programs, (3) a statement describing the applicant's teaching philosophy and (4) the names and addresses of three references the committee may contact. Questions about the position can be directed to: **Dr. Jorge A. Piedrahita, Search Committee Chair, College of Veterinary Medicine, North Carolina State University, 4700 Hillsborough St., Raleigh, NC 27606; Jorge_piedrahita@ncsu.edu**.

North Carolina State University is an Equal Opportunity and Affirmative Action employer. In addition, NC State University welcomes all persons without regard to sexual orientation.

Center for the Study of BIOLOGICAL COMPLEXITY **VCU**

Mathematical Biologist – Faculty

Mathematics and Applied Mathematics, Biology, and the Center for the Study of Biological Complexity invite applications for a tenure eligible Assistant, Associate or Professor level faculty position. The successful candidate will have a Ph.D. in Mathematics or related field, and is expected to develop an independent, externally funded research program, and to collaborate with other faculty in these programs. He or she will teach applied mathematical biology and other relevant courses. Research interests should be in mathematical modeling of biological systems, genome/cellular-level metabolic network and pathway analysis, new strategies for modeling complex multi-scale biological processes, complex dynamical systems, or other relevant areas. Experience generating and testing hypotheses at the systems level and a track record of independent funding are essential.

The successful applicant will join an expanding inter-disciplinary mathematical biology group focused around the Center for the Study of Biological Complexity and the Departments of Mathematics and Biology. The Center (**www.vcu.edu/csbc/**) is an academic think tank that promotes integrative and interdisciplinary approaches to biological and biomedical research. It houses state of the art facilities for high performance computing, bioinformatics, genomic, proteomic and pharmacogenomic research, as well as VCU's programs in bioinformatics and systems biology. Mathematics and Biology are established and dynamic programs in the College of Humanities and Sciences and support an interdisciplinary emphasis on mathematical biology and systems biology.

Send a statement of research and teaching interests, curriculum vitae, three references and supporting documents by **March 1, 2006**, to: **Gregory A. Buck, Center for the Study of Biological Complexity, Virginia Commonwealth University, P.O. Box 842030. Richmond, Virginia 23284-2030**. Applications preferred by e-mail: **buck@mail2.vcu.edu**.

VCU is an Equal Opportunity/Affirmative Action Employer.
Women, minorities and persons with disabilities are encouraged to apply.

Virginia Commonwealth University

Faculty Positions

JOHNS HOPKINS
SINGAPORE
DIVISION OF BIOMEDICAL SCIENCES

The Johns Hopkins University School of Medicine (JHUSOM), Baltimore, MD, is undertaking a search for faculty members to join the Division of Johns Hopkins in Singapore (DJHS), an academic division of JHUSOM located in Singapore. The general focus of research is cellular and molecular medicine and areas of interest include adult and embryonic stem cell biology, T cell and dendritic cell biology, cardio-vascular biology, virology, cancer, and general cell biology. We welcome applications for the following positions:

Assistant, Associate and Full Professor Faculty

Applications are requested for tenure-track positions at the Assistant Professor, Associate Professor and Professor level. All faculty appointments will be to departments of JHUSOM with joint appointments to DJHS. The plans are for the Division to grow to a faculty of about 14 biomedical scientists. Employment of all faculty will be based in the DJHS facilities in Singapore.

Candidates should have PhD and/or MD degrees and a strong track record of research appropriate for appointment in the JHUSOM, and indicative of a high potential for creative scholarship. Generous salaries, benefits, and start up packages are available with funding for research programs for up to 3 years.

Based in Singapore, DJHS represents an outstanding and unique opportunity for scientists who wish to achieve their career goals in a rapidly growing and dynamic region of the world that places great emphasis and importance in the life sciences. DJHS offers an exceptional environment for research, teaching and training with state-of-the-art facilities and equipment. The Division occupies space in Biopolis, a life sciences hub built by the Singapore government that houses a critical mass of scientists and research programs of both research institutes and biotechnology companies, all within close proximity and situated adjacent to campus of the National University of Singapore. Communication and interaction with colleagues at JHUSOM is facilitated by excellent multi media technology.

Applicants should post, fax or e-mail their letter of inquiry and curriculum vitae to:

Ian McNiece, PhD
Director, Division of Johns Hopkins in Singapore
Professor of Oncology
Johns Hopkins University School of Medicine

31 Biopolis Way, #02-01, The Nanos
Singapore 138669
Tel: (65) 6874 0197
Fax: (65) 6874 0177
Email: imcniec1@jhmi.edu

The Johns Hopkins University is an affirmative action and equal opportunity employer.

ETH

Eidgenössische Technische Hochschule Zürich
Swiss Federal Institute of Technology Zurich

Professor / Assistant Professor (Tenure Track) in Climate Physics and Diagnostics

The Department of Environmental Sciences of ETH Zurich is seeking to fill a faculty position in climate physics and diagnostics. Candidates should have an excellent international track record in research, be interested in both disciplinary as well as system-oriented multidisciplinary research, and be able to effectively lead a research team. The position will be within the Institute for Atmospheric and Climate Science (**http://www.iac.ethz.ch**). While the position will preferably be filled at the assistant professor level, well-established candidates with an outstanding record and high international visibility will be considered for a tenured position at the level of an associate or full professor. The base funding of the position will be commensurate with the level of the appointment.

Assistant professorships at ETH Zurich have been established to promote the careers of younger scientists. The initial appointment is for four years with the possibility of renewal for an additional two-year period and promotion to a permanent position.

The successful candidate is expected to develop an innovative research program that makes an important contribution to the physical understanding of the global climate system. Particularly welcome are candidates who intend to pursue research on the quantitative aspects of the atmospheric component of the climate system by exploiting new data sets such as satellite data, reanalysis data, and/or data from global climate models. The core research activities of the new professor could be in one or more fields related to for instance the global energy balance (including radiative studies) or interannual to centennial climate variability. Teaching duties will include both undergraduate and graduate level courses in climate physics, atmospheric sciences, and earth system sciences. Courses at Master level may be taught in English.

Applications with a curriculum vitae and a list of publications should be sent **to the President of ETH Zurich, Prof. Dr. E. Hafen, ETH Zentrum, CH-8092 Zurich, Switzerland, no later than February 28, 2006**. ETH Zurich specifically encourages female candidates to apply with a view towards increasing the proportion of female professors.

Albany Medical College

Faculty Positions
Center for Cardiovascular Sciences

Albany Medical College invites applications for tenure-track faculty positions in the Center for Cardiovascular Sciences. We seek highly motivated individuals with a record of research productivity, grant funding, and a desire to participate in Graduate and Medical Education. The applicant's research should complement existing programs in the Center that include vascular smooth muscle and endothelial cell function and regulation, nitric oxide and reactive oxygen species biology, cardiovascular development, and heart failure. A Ph.D. or M.D./Ph.D. degree and three years of productive post-doctoral experience are minimal requirements for appointment at the Assistant Professor level. Applicants for Associate Professor should have 3-5 years experience at the Assistant Professor level and a nationally recognized and funded research program.

Investigators in the Center for Cardiovascular Sciences have exciting opportunities for collaboration with scientists at neighboring institutions including the Ordway Research Institute, Rensselaer Polytechnic Institute, and the New York State Wadsworth Laboratories. The Capital Region offers diverse cultural and recreational attractions with easy access to Boston, New York City, and the Adirondack, Catskill, and Berkshire Mountains. For further information about the Center and Albany Medical College, please visit **www.amc.edu**.

Applicants should submit a current curriculum vitae, brief description of research interests and plans, and three letters of recommendation by **March 1, 2006** to:

Dr. Harold A. Singer
Director, Center for Cardiovascular Sciences
Albany Medical College (MC-8)
47 New Scotland Avenue
Albany, New York 12208

An Equal Opportunity/Affirmative Action Employer.
Women and Minorities are encouraged to apply.

THE UNIVERSITY OF TEXAS
HOUSTON
HEALTH SCIENCE CENTER

Chair
Department of Integrative Biology and Pharmacology
The University of Texas Medical School at Houston

The University of Texas Health Science Center at Houston Medical School is seeking an established, dynamic scientist with a creative vision to fill the position of Chair of the Department of Integrative Biology and Pharmacology. The Department is ranked third in NIH funding out of 27 in departments of integrative biology in U.S. medical schools with an outstanding history of research, training and service. Major strengths include signal transduction, membrane transport and live-cell imaging research (see **http://ibp.med.uth.tmc.edu/**).

The successful candidate will be a leader with a superb record of scholarly activity, history of a vigorous extramurally funded research program, and evidence of effective administrative leadership and service within the academic community. The candidate will also be an exemplary teacher, dedicated to medical and graduate education, and committed to the mentoring of junior faculty.

Excellent resources are available, including 20,000 sq ft of additional new research space that will become available in 2007 and the opportunity to recruit a significant number of new faculty. Nominations and applications should be sent electronically to **John.H.Byrne@uth.tmc.edu** or paper copies by surface mail to: **Dr. John H. Byrne, Department of Neurobiology and Anatomy, P.O. Box 20708, Houston, TX 77225.** All inquiries, nominations and applications will be treated confidentially.

The University of Texas Health Science Center at Houston is an EO/AA Employer. M/F/D/V. This is a security sensitive position and thereby subject to Texas Education Code 51.215. A background check will be required for the final candidate.

SCOTT & WHITE

College of Medicine
The Texas A&M University System
Health Science Center

Pediatric Hematology-Oncologist

The Section of Pediatric Hematology/Oncology at **Scott and White Clinic** and the **Texas A&M University System Health Science Center College of Medicine** (TAMUS HSC-COM) are seeking a clinician scientist with current research grants for a faculty position in a rapidly growing program. The candidate should be BE/BC in pediatric oncology and committed to an academic career. The successful candidates will join and enhance ongoing efforts in basic and translational research, with an institutional commitment to building a world-class experimental therapeutics program. An outstanding start-up package includes high quality laboratory space, excellent benefits and competitive salaries commensurate with academic qualifications. The position guarantees 75% protected time for research activities.

Scott & White Clinic is a 500+ physician directed multi-specialty group practice that is the leading provider of cancer care in Central Texas. Scott and White Clinic and the 486 bed tertiary Scott & White Memorial Hospital is the main clinical teaching facility for TAMUS HSC-COM. Outstanding clinical practice and laboratory facilities on campus that perform state of the art molecular and cellular biology research, flow cytometry, genomics and biostatistics are in place to support the research effort.

Please contact: **Don Wilson, M.D. Professor and Chairman, Department of Pediatrics, Scott & White, 2401 S. 31st, Temple, TX 76508. (800)725-3627 dwilson@swmail.sw.org Fax (254) 724-4974.**

For more information about Scott & White, please visit www.sw.org For Texas A&M www.tamhsc.edu. Scott & White is an equal opportunity employer.

POSTDOCTORAL POSITION IN CANCER BIOLOGY

The Center for Cancer and Immunology Research at Children's National Medical Center in Washington, DC invites applications for a postdoctoral position (MD or PhD) in glycolipid biochemistry, tumor biology and cell signaling. The laboratory focuses on the development and metastasis of pediatric neural tumors including medulloblastoma and neuroblastoma. The successful applicant will possess demonstrated expertise in either glycolipid isolation and biochemistry (including experience with HPLC), tumor cell biology with emphasis on genetic approaches (transfection, knockouts, siRNA), or tumor or immune cell signaling. Applicants MUST be U.S. citizens or be in possession of CURRENT resident alien status, and must possess superior communication skills in English, and a demonstrated record of accomplishment. Academic appointment is at the George Washington University.

Qualified candidates for this NIH funded position, available immediately, should send curriculum vitae and names and addresses of two references to: **Stephan Ladisch, MD, Director, Center for Cancer and Immunology Research, Children's Research Institute, Children's National Medical Center, 111 Michigan Avenue, NW, Washington, DC 20010. FAX (202) 884-3929; email: sladisch@cnmc.org**.

Max Planck Institute for Demographic Research
Directors:
Prof. James W. Vaupel, Prof. Jan M. Hoem

National Centre for Statistical Ecology
Director:
Prof. Byron J. T. Morgan

The Max Planck Institute for Demographic Research (MPIDR) and The National Centre for Statistical Ecology (NCSE) aim to further their collaboration through appointment to a

PhD position
involving the

Development of Statistical Methods for the Analysis of Biodemographic Age-Trajectories

This will involve collaboration between the MPIDR Biodemography research program and the NCSE at the University of Kent. Time will be spent both in Germany (Rostock) and in the United Kingdom (Canterbury). In Rostock, the successful candidate will complement an existing research team of just over 20 biodemographers, including a number of evolutionary ecologists. The team aims to gain a fundamental understanding of how lifespan is shaped by the evolution of integrated age-specific life-histories. The National Centre for Statistical Ecology (NCSE) is a joint venture linking the Universities of Cambridge, Kent and St Andrews, funded under the EPSRC multidisciplinary critical mass in Mathematics initiative. In Canterbury, the student will form part of a thriving group, working on many different aspects of statistical ecology, biometry in general, and other areas of applied and theoretical statistics.

The project will involve developing new statistical methods for modeling the age-trajectories of demographic rates, particularly survival. We anticipate that mark-recapture data, mostly from bird and mammal populations, will be the main material used in the development of these methods. As well as their main research project, the successful candidate will work towards their doctorate through structured coursework, focused workshops and seminar programs.

We are seeking able graduate scientists with strong academic track records in quantitative disciplines. Applications should be addressed to the Director of the MPIDR, Prof. James W. Vaupel and the Director of the NCSE, Prof. Byron J.T. Morgan, and should include a CV with a statement of academic interests and relevant experience, qualifications (details of all grades for exams, projects, and coursework), and the contact details of 3 referees. Details of any publications should be listed. Material should be e-mailed to: **MPIDR-NCSE-Age-Models@demogr.mpg.de** by latest 15th March 2006. See **www.demogr.mpg.de, http://www.ncse.org.uk/** and **http://www.kent.ac.uk/ims/groups/statistics/index.htm** for more information.

The Max Planck Society and the University of Kent wish to increase the share of women in areas where they are underrepresented, and strongly encourage women to apply.

The Max Planck Society and the University of Kent are committed to employing more handicapped individuals and encourage especially them to apply.

MAX PLANCK SOCIETY

The Medical College of Georgia
Assistant Professor
Department of Pathology

The Department of Pathology at the Medical College of Georgia continues the expansion of its program in investigative pathology. We invite applications for two tenure-track faculty positions at the level of Assistant Professor engaged in basic and/or translational research related to cancer. Candidates must have completed productive postdoctoral training and developed original and externally fundable research programs related to the genesis, progression and prevention of cancer. Areas of special interest include, but are not limited to, animal models of cancer, tumor-host microenvironment, molecular control of cell proliferation and metastasis, and cancer-specific translational research. The positions are supported by generous start-up package, and laboratories will be available in the new Cancer Research Center. The new appointees will become part of a growing group investigating the role of G proteins in tumor cell proliferation and metastasis.

Applicants should send curriculum vitae including a statement of research interests and future plans, and the names of three references to:

Dr. Yehia Daaka, Professor and Endowed Chair
C/O Ms. Carol Hardy
Medical College of Georgia
Department of Pathology, BF-104
1120 15th Street
Augusta, Georgia 30912

The Medical College of Georgia is a Minority/Female/Veterans: Equal Employment Opportunity, Affirmative Action, and Americans with Disabilities Act Employer.

Position in Psychiatric Drug Discovery
University of California San Francisco
Department of Psychiatry

THE DEPARTMENT OF PSYCHIATRY AT THE UNIVERSITY OF CALIFORNIA SAN FRANCISCO invites applications for a Psychiatrist who will conduct laboratory-based research on drugs and receptors that can be applied to the evaluation and discovery of psychiatric medications. This position will require directing an independent research group, and will also include teaching medical students and residents. It is at the Assistant to Full Professor level in a state-funded series and can begin on July 1, 2006 or thereafter. Applicants must have an M.D., clinical training in psychiatry, be Board certified in Psychiatry and hold a California medical license at time of appointment. A joint appointment in relevant UCSF graduate programs will be offered if appropriate.

Applicants should submit their CV, brief statement of research interest, three letters of reference and three representative journal articles by **March 1, 2006** to: **Samuel H. Barondes, M.D., Search Committee Chair, c/o Astrid Prackatzsch, Department of Psychiatry, 401 Parnassus Avenue, San Francisco, CA 94143-0984**.

UCSF is an Affirmative Action/Equal Opportunity Employer. The University undertakes affirmative action to assure equal employment opportunity for underrepresented minorities and women, for persons with disabilities, and for Vietnam era veterans and special disabled veterans.

Basic Scientist/Psychiatrist
University of California San Francisco
Department of Psychiatry

THE DEPARTMENT OF PSYCHIATRY AT THE UNIVERSITY OF CALIFORNIA SAN FRANCISCO invites applications for a Psychiatrist with established skills in laboratory research in areas of basic science generally relevant to psychiatric problems. This position is at the Assistant Professor level and can begin on July 1, 2006 or thereafter. Applicants must be board eligible or certified in Psychiatry and have a California medical license at time of appointment and have a Ph.D. and/or postdoctoral training in a laboratory science. A joint appointment in the UCSF Neuroscience Program will be offered if appropriate.

Applicants should submit their CV, brief statement of research interest, three letters of reference and three representative journal articles by **March 1, 2006** to: **John Rubenstein, M.D., Ph.D., Search Committee Chair, c/o Astrid Prackatzsch, Department of Psychiatry, 401 Parnassus Ave., San Francisco, CA 94143-0984.**

UCSF is an Affirmative Action/Equal Opportunity Employer. The University undertakes affirmative action to assure equal employment opportunity for underrepresented minorities and women, for persons with disabilities, and for Vietnam era veterans and special disabled veterans.

Max-Planck-Gesellschaft
Max Planck Society

The Max Planck Society for the Advancement of Science (MPG) is seeking an exceptionally qualified and experienced

Head of the Max Planck Digital Library

The Max Planck Digital Library (MPDL) will be the central scientific service unit responsible for the development and operation of the digital infrastructures necessary for providing the Max Planck Institutes with scientific information and for supporting web-based scholarly communication.

The head of the MPDL will be responsible for all system-wide information services and the strategic positioning of the MPG in the arena of information and scholarly communication management.

For further information, please refer to http://mpdl.mpg.de. The MPG will begin reviewing applications by March 1, 2006.

The Max Planck Society seeks to increase the number of women in those areas where they are underrepresented and therefore explicitly encourages women to apply. The Max Planck Society is committed to employing more handicapped individuals and especially encourages them to apply.

Max-Planck-Gesellschaft
zur Förderung der Wissenschaften e. V.
Vice-President Prof. Dr. Kurt Mehlhorn
Postfach 10 10 62, 80084 München, Germany
E-Mail: HR@gv.mpg.de
www.mpg.de

ASSISTANT OR ASSOCIATE PROFESSOR
DIVISION OF STEM CELL TRANSPLANTATION
DEPARTMENT OF PEDIATRICS
STANFORD UNIVERSITY SCHOOL OF MEDICINE

The Division of Stem Cell Transplantation of the Department of Pediatrics at the Stanford University School of Medicine is seeking a full time research scientist with considerable potential and expertise in hematopoietic stem cell transplantation (HSCT) research. The position is at the Assistant or Associate Professor level in the University Tenure Line (UTL) Professoriate. The candidates must have M.D. or M.D.-Ph.D. degrees, be board eligible/certified in pediatrics or medicine, and have post-doctoral fellowship training in a relevant specialty, e.g., hematology-oncology, bone marrow transplantation, or immunology. Successful candidates will lead our multidisciplinary basic and translational projects in research on hematopoietic stem cell transplantation. Research program areas to develop may include studies of stem cell biology; cancer biology, including cancer stem cells; immune development, regulation, function, and immune deficiency; and gene therapy.

The laboratory-based investigators' research will be supported by generous funding by the Lucile Packard Children's Hospital as part of a major Stem Cell Research program. The candidates are expected to make important contributions to relevant scientific disciplines, e.g., stem cell biology, cancer biology, immunology, and gene therapy. Clinical investigators will be expected to perform research that will address important aspects of HSCT, such as the development of novel HSCT protocols or the assessment of outcome.

Interested candidates should send a copy of their *curriculum vitae*, a brief letter outlining their interests, and the names of three references to: **Kenneth I. Weinberg, M.D., Professor and Division Chief, Pediatric Stem Cell Transplantation, Stanford University, 1000 Welch Road, Suite 300, Mail Code 5798, Palo Alto, CA 94304-1812; E-mail:lkm@stanford.edu.**

Stanford University is an Equal Opportunity Employer and is committed to increasing the diversity of its faculty. It welcomes nominations of and applications from women and members of minority groups, as well as others who would bring additional dimensions to the university's research, teaching and clinical missions.

The Ohio State University
Sr. Bioinformatics Engineer

The Ohio Supercomputer Center at OSU is accepting applications for a Sr. Bioinformatics Engineer. The successful applicant will be responsible for **facilitating statewide efforts in applied biology, structural computational biology, and complex systems.** He/She will conduct research in applied biology and complex systems and develop algorithms that support mathematical modeling for purposes that include bridging sequence to structure, functional analysis, macromolecular dynamics, kinetics, intra or inter-cellular reactions, stochastic modeling, and systems biology and develop theories that support on-going research. **This position is located in Springfield, OH.**

Minimum requirements for this position include a **Master's degree, Ph.D. desired, preferably in the areas of computational biology, bioinformatics or other life science degrees or an equivalent,** experience in developing algorithms that support mathematical modeling and experience in functional analysis, stochastic modeling and systems biology. Candidates should have a sound background in theory, simulation, and experimentation and show enthusiasm for a collaborative, interdisciplinary environment. Candidates should also have a strong track record in building research teams and in project management.

For a complete position description, or to apply online, please go to www.jobsatosu.com, Click Search Postings, and enter Requisition# 318850.

OSC Innovations in computing, networking, and education

To build a diverse workforce Ohio State encourages applications from individuals with disabilities, minorities, veterans, and women. EEO/AA employer.

FACULTY POSITIONS
DEPARTMENT OF PHYSICS
THE UNIVERSITY OF TEXAS AT AUSTIN

The Department of Physics at The University of Texas at Austin is seeking candidates for tenure track assistant professorship positions in physics starting in September 2006. In special cases, appointments at more senior levels will be considered. Successful candidates will assume full teaching responsibilities for undergraduate and graduate courses in the Department of Physics and are also expected to conduct vigorous research programs. Research areas of current highest priority for the Department are Biophysics/Soft-Condensed Matter Experiment, Cosmology/Relativity/Theoretical Physics, AMO/Quantum Information Science, Condensed Matter/Nanoscience Experiment, and Particle/Astrophysics Experiment. Outstanding candidates in other areas of departmental focus will also be considered. Excellent English language communication skills are required. Applicants must have a Ph.D. (or equivalent) and a demonstrated potential for excellence in teaching and research.

Interested applicants should send a curriculum vitae, a list of publications, a statement of research interests, a research plan, and should arrange for at least five letters of recommendation to be sent to: **Prof. John T. Markert, Chair, Department of Physics, The University of Texas at Austin, 1 University Station C1600, Austin, TX 78712-0264**. Review of completed applications has already begun and is ongoing.

The University of Texas at Austin is an Equal Opportunity/Affirmative Action Employer.

Executive Director
US Arctic Research Commission
www.arctic.gov

The US Arctic Research Commission, an independent government agency, invites applications from qualified individuals with terrestrial, marine or atmospheric research experience in the Arctic, including research management and participation in the field or at sea. A Ph.D. is desired. Applications are encouraged from individuals whose research expertise is complemented by knowledge and experience in:

1. Federal planning and budgetary process
2. international Arctic research activities
3. ongoing research interests of Alaska, local jurisdictions and NGOs.

This is a **SENIOR EXECUTIVE SERVICE** position.
SALARY: $109,808 to $152,000
LOCATION: Arlington, VA
DEADLINE: Open until filled. First application review on January 31, 2006
APPLY: www.usajobs.opm.gov
Vacancy announcement: ARC-SES-06-001
QUESTIONS: Ms. Ellen Bliss, DOI, National Business Center, **703-390-6613**

This opening may be filled through the Intergovernmental Personnel Act authority. US citizenship is required. The USARC is an Equal Opportunity Employer.

POSITIONS OPEN

ASSISTANT OR ASSOCIATE PROFESSOR
Department of Pharmacology Kansas City University of Medicine and Biosciences

Please see our ad at **website: www.kcumb.edu**; click on Employment. *Equal Opportunity Employer.*

PEDIATRIC INFECTIOUS DISEASE/VIROLOGY

RESEARCH ASSISTANT/ASSOCIATE PROFESSOR, non-tenure earning. The Division of Pediatric Infectious Diseases at the University of Alabama at Birmingham (UAB) is seeking a faculty candidate to oversee operations of a laboratory that will function as a molecular biology laboratory for a group of NIH supported investigators. This individual will also be expected to pursue independent research that will lead to extramural support. Candidates with a Ph.D. or M.D. with at least four years of postgraduate laboratory training and experience in molecular biology techniques including vector construction, protein expression, and characterization of recombinant molecules. Interested candidates should direct inquiries and curriculum vitae to:

William Britt, M.D.
Professor, Pediatric Infectious Diseases
1530 3rd Avenue South
CHB 107
Birmingham, Alabama, 35294
or **e-mail: bbritt@peds.uab.edu.**

UAB is an Affirmative Action/Equal Opportunity Employer.

ASSISTANT PROFESSOR
Nephropathology

Columbia University Medical Center seeks M.D. for Assistant Professor level position in Department of Pathology. Applicants must have completed residency in anatomic pathology and at least one year of formal fellowship training in nephropathology, with established expertise in clinical (light microscopy, immunofluorescence, electron microscopy) and research aspects of renal pathology. A record of scholarly publications in the area of nephropathology is highly desirable. Candidates must have New York State license and be prepared to handle clinical responsibilities of a busy nephropathology practice. Send curriculum vitae, two-page summary of research interests and plans, and two letters of recommendation to: **Michael Shelanski, M.D., Ph.D., Chairman, Department of Pathology, Columbia University Medical Center, 630 West 168th Street, Mailbox 23, New York, NY 10032.** *Columbia University takes Affirmative Action toward Equal Employment Opportunity.*

The National Oceanic and Atmospheric Administration (NOAA), National Centers for Coastal Ocean Science (NCCOS) seeks a GS-0401-15, **ENVIRONMENTAL SCIENTIST,** to serve as the **DEPUTY DIRECTOR** of NCCOS. The position opened December 14, 2005, and closes January 18, 2006. The salary range is $103,947 to $135,136. To view a copy of the vacancy announcement and develop and submit a resume, please visit **website: https://jobs1.quickhire.com/scripts/doc.exe.** The vacancy number is NOS-CCOS-2006-0007.

MOLECULAR BIOCHEMIST to study transcription-induced hypermutation in human cell lines. Expertise in genetic engineering and cell culture techniques required. This position is available in March 2006. Send curriculum vitae to **e-mail: barbara.wright@mso.umt.edu.** *Affirmative Action/Equal Opportunity Employer.*

DISTURBANCE ECOLOGIST

The Department of Biology at the University of Central Florida (UCF) invites applications for an open rank tenure-track Faculty Position in disturbance ecology. The candidate's research should focus on population, community, and/or ecosystem responses to disturbance, where disturbance is widely defined and includes processes such as land-use change, hydrologic change, fires, storms, invasive species, or pollution. Candidates should have a demonstrated ability to establish and maintain a vigorous, extramurally funded research program. The successful candidate must have a Ph.D. and appropriate postdoctoral training and will contribute to our Ph.D. program in conservation biology and M.S. program in biology as well as teach graduate and undergraduate courses. UCF has a strong research emphasis and provides competitive startup funds and teaching loads for new hires. See **website: http://www.cas.ucf.edu/biology/** for Department details. Applicants should send a letter of intent, curriculum vitae, one-page statements of research plans and teaching philosophy, and arrange for three letters of recommendation to be sent directly to: **Dr. Graham A.J. Worthy, Chair, Disturbance Ecologist Search Committee, Department of Biology, University of Central Florida, Orlando, FL 32816-2368.** Review of applications will begin March 1, 2006, with an anticipated start date of August 2006. Search documents may be viewed by the public upon request in accordance with Florida statute. *The University of Central Florida is an Affirmative Action/Equal Opportunity Employer.*

A POSTDOCTORAL POSITION IN MICROBIAL PATHOGENESIS is available to investigate virulence mechanisms of *Haemophilus ducreyi*, the etiologic agent of chancroid. Emphasis will be placed on the elucidation of the mechanism(s) by which the *H. ducreyi* LspA1 and LspA2 proteins target macrophage Src protein tyrosine kinases to inhibit phagocytosis. Position requires Ph.D. in microbiology, biochemistry, cell biology, or a related biological science and experience with recombinant DNA techniques. This project will use DNA microarray and mutant analyses in conjunction with phagocytosis models to elucidate the relevant signaling pathway. Position includes salary, fringe benefits, and the opportunity to work in a dynamic research environment. Position available immediately. Send curriculum vitae and the names and telephone numbers of three references to:

Dr. Eric J. Hansen
Department of Microbiology
The University of Texas Southwestern Medical Center at Dallas
5323 Harry Hines Boulevard
Dallas, TX 75390-9048
Fax: 214-648-5905
E-mail: eric.hansen@utsouthwestern.edu

University of Texas Southwestern is an Equal Opportunity/Affirmative Action Employer.

POSTDOCTORAL FELLOW

Two Postdoctoral Positions available at Blood Systems Research Institute (BSRI), in San Francisco. One position to study viral entry by emerging viral agents, in which host cell factors required to facilitate viral membrane fusions will be examined (see **Simmons et al.,** *Proceedings of the National Academy of Sciences,* **102:**11876-11881, 2005). Second position is to study the development of liver stem cells (see **D.L. Suskind, and M.O. Muench,** *J Hepatol,* **40:**26, 2004). BSRI is a research institute dedicated to the science of transfusion medicine **(website: http://www.bsrisf.org).** Candidates must possess a Ph.D. or equivalent, and a strong background in virology or molecular biology. Send curriculum vitae by January 30, 2006, to: **e-mail: bsricareers@bloodsystems.org** or to: **Human Resources, BSRI, 270 Masonic Avenue, San Francisco, CA 94118. Fax: 415-775-3859.** Pre-employment drug screen required. *Equal Opportunity Employer, Minorities/Females/Persons with Disabilities/Veterans.*

DIRECTOR, DIVISION OF HUMAN RESOURCE DEVELOPMENT
National Science Foundation, Arlington, Virginia

NSF's Directorate for Education and Human Resources seeks candidates for the position of Director, Division of Human Resource Development (HRD). The Division serves as a focal point for NSF's agency-wide commitment to enhancing the quality and excellence of science, technology, engineering, and mathematics (STEM) education and research through broadening participation by underrepresented groups and institutions. Information about the Division's activities may be found at **website: http://www.nsf.gov/ehr/hrd/about.jsp.**

Appointment to this Senior Executive Service position may be on a career basis, on a one- to three-year limited term basis, or by assignment under the Intergovernmental Personnel Act (IPA) provisions.

Announcement S20060038, with position requirements and application procedures is posted on NSF's home page at **website: http://www.nsf.gov/about/career_opps/.**

Applicants may also obtain the announcements by contacting Executive Personnel Staff at **telephone: 703-292-8755** (hearing impaired individuals may call **TDD 703-292-8044**). Applications must be received by February 7, 2006. *NSF is an Equal Opportunity Employer.*

POSTDOCTORAL FELLOWS

Postdoctoral Positions are available immediately in the laboratory of **Dr. Lawrence Rothblum** to study the molecular mechanism underlying ribosomal DNA transcription and its regulation. Current projects include: (1) The identification of phosphorylated residues in mammalian Rrn3 and the characterization of the role(s) of those residues in transcription initiation. This project combines mass spectroscopy, in vitro mutagenesis and in vitro transcription. (2) The assessment of the role of UBF in regulating rDNA transcription during cardiac hypertrophy using both cultured cardiomyocytes and in vivo models of cardiac hypertrophy. Applicants should have a strong background in biochemistry or cell biology. Experience in protein purification, signal transduction or mass spectrometry would be advantageous. We offer a competitive salary and benefits package. The Weis Center is located on the campus of Geisinger Medical Center, a tertiary care hospital providing care to patients in northeastern and central Pennsylvania. Geisinger Medical Center is located in an attractive semirural community that affords an outstanding quality of life plus convenient access to major metropolitan areas. Please submit curriculum vitae and names of three references by mail only to: **Kristin Gaul (LIR), The Weis Center for Research, 100 North Academy Avenue, Danville, PA 17822-2600.** *Equal Opportunity Employer/Minorities/Females/Persons with Disabilities/Veterans.*

SCIENTIST. Performs scientific research incorporating new technologies related to recombinant protein expression in eukaryotic cells. Requirements: Ph.D in biomedical sciences, biochemistry, or foreign degree equivalent. Four years of research experience in recombinant protein expression, purification, and the in vitro characterization of mammalian genes, including gene cloning, tissue culture, transfections, PCR, sodium dodecyl sulfate-polyacrylamide gel (SDS-PAGE), immunoprecipitations, flow cytometry, Western blotting, reagent preparation, and data analysis; and 18 months of research experience isolating primary mammalian tissues, including immune and skin cells, the in vivo characterization of novel mammalian genes, and the maintenance of multiple cell lines. Experience may be gained concurrently. Send resume to: **Viral Logic Systems Technology Corporation, Attn: J. Strain, 1616 Eastlake Avenue East, Suite 200, Seattle, WA 98102.**

University of Pittsburgh
Pittsburgh Center for Pain Research
Tenure Track Faculty Positions

The University of Pittsburgh announces the establishment of the **Pittsburgh Center for Pain Research** (PCPR) under the direction of **Dr. Gerald F. Gebhart**. The PCPR is a multidepartmental center whose major goals are to integrate basic and clinical studies on pain, understand fundamental mechanisms of pain and discover and develop new effective treatments for pain. The Center is seeking to recruit up to four tenure track positions in basic or translational research and invites applications at all levels. Applicants should have research interests in fields relevant to the understanding of pain biology including, but not limited to, neuroimmunology, receptor-cell signaling, neuronal development and plasticity, neuroimaging and genetics of pain. Applicants at the Assistant Professor level must have a Ph.D. or M.D. degree plus 3 years of postdoctoral experience. Candidates at more senior levels should have an established and productive extramurally funded independent research program. Appointments will be in appropriate participating departments, including Anesthesiology, Medicine (Gastroenterology) and Neurobiology.

Positions available until filled. Applicants should submit a current CV and list of publications, a brief statement of research plans (three pages or less) and names of three references. Address correspondence to: **PCPR Search Committee, 3550 Terrace Street, Scaife Hall, Room S-843, The University of Pittsburgh, Pittsburgh, PA 15261**. Electronic submission of applications is preferred (email: **carpenterh@dom.pitt.edu**). Applications should be received by **March 1, 2006** to ensure full consideration.

The University of Pittsburgh is an Affirmative Action, Equal Opportunity Employer.

Postdoctoral Intramural Research Fellowship Positions
National Institute of Allergy and Infectious Diseases (NIAID)

The Molecular Genetics Section, Laboratory of Zoonotic Pathogens, NIAID, NIH, Rocky Mountain Laboratories (RML), Hamilton, Montana, is seeking Post-doctoral /Visiting Fellow candidates to pursue studies of *Borrelia burgdorferi*, the agent of Lyme disease. Current projects utilize molecular genetics in conjunction with an animal and tick model to investigate the pathogenesis of *B. burgdorferi* infection. Emphasis is placed on understanding the structure and function of the more than 20 different plasmids of the segmented genome of *B. burgdorferi*, and the contributions of specific genes at different stages of the mouse-tick infectious cycle. A developing interest is directed at visualizing individual DNA molecules within the cell, and tracking their replication and segregation during bacterial growth.

The NIH Rocky Mountain Laboratories supports research on a number of significant bacterial and viral human pathogens. State-of-the-art genomic, proteomic, microarray, sequencing and biological imaging core services are available to help identify and characterize factors important to the host-pathogen-vector interactions. The Rocky Mountain Laboratories have newly renovated laboratory, animal and insectary facilities located in the scenic Bitterroot Valley of western Montana, with easy access to some of the finest outdoor recreational opportunities in North America.

Candidates with experience in microbiology, molecular biology or vector-borne animal models of infection are encouraged to apply. Applicants must hold a Ph.D, D.V.M, or M.D. degree. Salary will be commensurate with experience and health benefits are provided.

Please send a curriculum vitae, bibliography and three letters of reference to: **Patricia Rosa, Ph.D., Laboratory of Zoonotic Pathogens, Rocky Mountain Laboratories, NIAID, 903 South 4th Street, Hamilton, MT 59840; email: prosa@niaid.nih.gov.**

Department of Health and Human Services and National Institutes of Health are Equal Opportunity Employers.

WESTERN UNIVERSITY OF HEALTH SCIENCES
COLLEGE OF OSTEOPATHIC MEDICINE OF THE PACIFIC

BIOCHEMISTRY RESEARCH AND TEACHING FACULTY POSITIONS

The College of Osteopathic Medicine of the Pacific/ Western University of Health Sciences has implemented a strategic 10 year plan to significantly increase faculty numbers and expand in the areas of research and medical education. The department of Basic Medical Sciences is seeking PhD biochemists for tenure track faculty positions at the level of Assistant, Associate or Full Professor to **EITHER:**

(1) **participate in both research and limited teaching.** Competitive salary, significant start-up support and abundant laboratory space will be offered. The successful applicants are expected to already have obtained extramural funding (such as NIH/NSF/other grants) or successfully completed a postdoctoral program with strong confidence in their ability to obtain grants. The individuals will have ample protected time to fulfill their research goals.

(2) **teach** basic and clinical medical biochemistry to osteopathic medical students. The successful applicants must have several years of experience in teaching medical biochemistry. Innovative curriculum development in the candidate's area of expertise and publications that will lead to attainment of educational grants will be required.

Applicants should submit a cover letter expressing their interest, statements of research activity and teaching philosophy along with curriculum vitae, current support, and contact information of three potential references to:

Nissar A. Darmani, Ph.D. Chair,
Department of Basic Medical Sciences
Western University of Health Sciences
College of Osteopathic Medicine of the Pacific
309 E. Second Street
Pomona, CA 91766-1854

POSITIONS OPEN

TENURE-TRACK POSITION, DIVISION OF BIOLOGICAL SCIENCES, the University of Montana. The Division of Biological Sciences and the Graduate Program in Biomolecular Structure and Dynamics invite applications to fill a tenure-track position in biochemistry or related field. Preference will be given to applicants whose field of expertise is investigating the structure and function of biomolecules related to infectious disease, mechanisms of development, signal transduction, and cell surface interactions or other areas of structural/mechanistic biology and structural bioinformatics. The successful candidate will be expected to develop a vigorous, externally-funded research program, and will contribute to undergraduate and graduate teaching. The new faculty member will participate in the Graduate Program in Biomolecular Structure and Dynamics **(website: http://www.umt.edu/grad/programs/biomolecular/)** and its associated Center, which promote collaboration between researchers in biology, chemistry, and pharmaceutical sciences. A Ph.D. in biochemistry or a related field and postdoctoral experience is required. We seek to fill this position at the **ASSISTANT PROFESSOR** level; applications at the **ASSOCIATE** level will be considered.

To apply, send a complete curriculum vitae, description of future research plans, summary of research accomplishments, statement of teaching philosophy, documented evidence of teaching excellence, and three reference letters to: **Stephen Lodmell, Chair, Search Committee, Division of Biological Sciences, The University of Montana, Missoula, MT 59812.** Information about the Division of Biological Sciences can be accessed from our webpage, at **website: http://biology.dbs.umt.edu/dbs/default.htm.** The review of applications will begin on February 13, 2006.

The University of Montana is an Equal Opportunity/Affirmative Action Employer, and encourages applications from women, minorities, veterans and persons with disabilities. The position is eligible for veterans' preference in accordance with State law.

TENURE-TRACK FACULTY POSITION
Faculty Excellence Initiative
on AIDS/Drugs of Abuse
University of South Carolina

Applications are invited for a faculty position at the Assistant, Associate, or Full Professor level in the Department of Pathology, Microbiology and Immunology, University of South Carolina School of Medicine, to pursue research on HIV/AIDS and drugs of abuse. A Ph.D., M.D., or equivalent is required. It is expected that the individual will establish a strong, independent, NIH-funded research program. The Department seeks outstanding candidates who will develop translational research in collaboration with clinicians who are treating a large number of HIV/AIDS patients. Applicants for Associate/Full Professor should have extramural funding. The review will begin immediately and will continue until the position is filled. Applicants should submit curriculum vitae, future research plans, and three letters of reference to: **Dr. Mitzi Nagarkatti, Chair, Department of Pathology and Microbiology, University of South Carolina, School of Medicine, Columbia, SC 29208. E-mail: pathmicroimads@gw.med.sc.edu.** *The University of South Carolina is an Affirmative Action, Equal Opportunity Institution.*

NIH-funded **POSTDOCTORAL POSITION** is available immediately to study the effect of deep brain stimulation on Parkinson's disease (PD) and epilepsy. Multiple channel, single unit recording technique will be used in rodent model of PD and epilepsy to examine behaviorally effective deep brain stimulation on basal ganglia neural responses. Experiences in electrophysiology and data analysis are desirable. Contact: **Jingyu Chang, Ph.D. Associate Professor, Department Department of Physiology and Pharmacology Wake Forest University School of Medicine, Winston-Salem NC 27157. Telephone: 336-716-8547. E-mail: jchang@wfubmc.edu.**

POSITIONS OPEN

ASSISTANT/ASSOCIATE PROFESSOR
Medicinal Chemistry of CNS-Targeted Molecules
The University Of Montana

Applications are invited for a tenure-track Faculty Position in the Department of Biomedical and Pharmaceutical Sciences to strengthen research and graduate education in the medicinal chemistry of small molecules active in the central nervous system (CNS) as part of an NIH funded Center of Biomedical Research Excellence (COBRE) in Structural and Functional Neuroscience. Research in the Center focuses on CNS protein structure/function as related to transport, membrane protein dynamics, and neuropathology. Much of the progress and growth of the Center has been linked to the successful integration of medicinal chemistry, biochemistry, and physiology with the aim of developing small molecules to advance our understanding of neuronal function and CNS disease. We wish to continue this effort by recruiting a new Assistant or Associate Professor. Successful candidates will be expected to establish vigorous externally funded research programs that complement Departmental and Center strengths, supervise graduate students, and be committed to teaching excellence at the graduate and undergraduate levels. Applicants must have a doctoral degree, postdoctoral research experience, and demonstrated ability or potential to secure NIH funding. A competitive startup package is available. The University of Montana is also the recipient of a NSF ADVANCE award focused on increasing the presence of women in science. Applications received by February 15, 2006, will receive full consideration; review will continue until the position is filled. More detailed information may be obtained from the **Center Director R. Bridges, (e-mail: richard.bridges@umontana.edu)** or from **website: http://www.umt.edu/csfn.**

The Skaggs School of Pharmacy, which is nationally ranked fifth in NIH-funded research among United States schools of pharmacy, is part of the University of Montana campus in Missoula. This cosmopolitan Rocky Mountain community of 70,000 has been singled out in national publications for its high quality of life. Abundant recreational opportunities in surrounding state and national forests and nearby Glacier National Park complement a thriving intellectual atmosphere.

Send letter of application, including curriculum vitae, statement of research plans, teaching interests, and three letters of reference to: **CSFN Search, R.J. Bridges, Department of Biomedical and Pharmaceutical Sciences, Skaggs School of Pharmacy, The University of Montana, Missoula MT 59812-1075.**

Equal Opportunity/Affirmative Action Employer.

RESEARCH ASSISTANT PROFESSOR
OR RESEARCH ASSOCIATE

Four immediate openings at Dartmouth Medical School in the Electron Paramagnetic Resonance (EPR) Center for the Study of Viable Systems for Research Assistant Professor (two openings) and Research Associate (two openings). For the Research Assistant Professor positions, a Ph.D. is required with expertise and experience in EPR instrumental development and/or microwave engineering. The selected individuals should be capable of independently carrying out research developments that are consistent with the research directions of the EPR Center and eventually should be able to secure external funding for related research.

For the Research Associate positions (requires M.S. or the equivalent in experience) the skills needed include expertise in at least one of the following: Tumor or Cell Biologist; EPR Instrumentalist; and microwave engineering skills. Submit complete curriculum vitae and statement of pertinent experience, and request three references be sent to: **Harold M. Swartz, M.D., Ph.D., Dartmouth Medical School, 702 Vail, Hanover, NH 03755. Fax: 603-650-1717. E-mail: harold.swartz@dartmouth.edu.** *Dartmouth Medical School is an Equal Opportunity/Affirmative Employer and encourages applications from women and members of minority groups.*

POSITIONS OPEN

ASSISTANT OR ASSOCIATE PROFESSOR
Marine Ecology
University of Washington, Tacoma

Interdisciplinary Arts and Sciences at the University of Washington, Tacoma (UWT) seeks a **MARINE ECOLOGIST** to contribute to the development of an expanding undergraduate environmental science/studies curriculum within an interdisciplinary framework. The successful candidate will be engaged in innovative teaching and research in the ecology, evolution, and conservation of coastal marine organisms and ecosystems, and teach selected courses in such areas as marine ecology, ecology, evolution, conservation biology, biological invasions, marine invertebrates, biological oceanography, introduction to environmental science, and introductory biology, as well as other upper and lower-division courses in the specialty area of the successful candidate. Preference will be given to candidates experienced with Pacific Coast intertidal habitats, especially invertebrates and algae. Field experience and interest in developing student-faculty undergraduate research is highly desirable. This tenure track/tenured faculty position begins 16 September 2006, and requires a Ph.D. by the time of appointment. For a more complete description of this position and UWT visit our **website: http://www.tacoma.washington.edu/ias.** Screening of applications will begin 1 February 2006, and will continue until the position is filled. To apply, send electronically: a letter describing your interests in and qualifications for this position, including a description of your teaching philosophy and research interests, a curriculum vitae, three letters of reference, syllabi or a description of courses you would like to teach in our program and evidence of teaching effectiveness to: **e-mail: tfaculty@u.washington.edu.** For additional information contact: **Dr. Cheryl Greengrove** at **e-mail: cgreen@u.washington.edu.** *The University of Washington is an affirmative action, equal opportunity employer.*

ASSISTANT/ASSOCIATE PROFESSOR
PHYSIOLOGIST, TENURE-TRACK

The Department of Comparative Biomedical Sciences is seeking a Physiologist at the rank of tenure-track Assistant/Associate Professor. Applicants must be capable of teaching at least two organ systems in comparative vertebrate physiology. Required qualifications: Ph.D. or equivalent degree in physiology and/or biological/biomedical sciences. Additional qualifications desired: D.V.M. degree; postdoctoral experience. Primary responsibilities include: teaches in a two-semester, team-taught, physiology course in the veterinary professional curriculum; establishes a competitive, extramurally funded research program. The Department has numerous well-funded investigators in cell and molecular biology. Salary and rank will be commensurate with qualifications. Application deadline is February 15, 2006, or until candidate is selected. An offer of employment is contingent on a satisfactory pre-employment background check. Submit letter of application and resume (including e-mail address) to: **Dr. William G. Henk, Professor, Comparative Biomedical Sciences, School of Veterinary Medicine, Louisiana State University, Reference 000097, Baton Rouge, LA 70803. Telephone: 225-578-9898; e-mail: henk@vetmed.lsu.edu.**

LSU is an Equal Opportunity/Equal Access Employer.

POSTDOCTORAL POSITIONS
in Hematology/Stem Cells/Gene Therapy

NIH-funded Fellowships are available immediately to work with faculty in the Division of Hematology at the University of Washington in Seattle. Research areas include hematopoietic and embryonic stem cell biology, gene and cell therapy, hematopoiesis, and coagulation. Fellows work in an outstanding research environment and enjoy the Pacific Northwest lifestyle. Apply online at **website: http://depts.washington.edu/hemeweb/,** link to the Research Training Program.

ZFIN, the zebrafish model organism database, seeks **SCIENTIFIC CURATORS** to join our dynamic, interactive team of biologists and computer scientists at the **University of Oregon** in Eugene, OR.

ZFIN curators acquire, analyze and index information about zebrafish gene structures, expression patterns and mutant phenotypes. Successful candidates will be primarily responsible for the curation of zebrafish phenotype data. Particular attention will be given to phenotypes that serve as models of human disease. Zebrafish phenotypes and their human orthologs will be annotated using common terms and methods when possible. Curators also participate in database, web interface and ontology design by providing biological perspectives for new content and display.

A Ph.D. in Life Sciences or M.S. with appropriate experience is required. Applicants should have backgrounds in developmental genetics, comparative genomics or phenotype evaluation, preferably in zebrafish.

Applications received by **January 30, 2006**, receive first consideration. More information is available on **ZFIN.org** about the staff and the database. Send curriculum vitae and references to: **E. McCumsey, Institute of Neuroscience, 1254 University of Oregon, Eugene, OR 97403-1254 USA or fax (541)346-4548.**

The UO is an AA/EO/ADA institution committed to cultural diversity. We invite applications from candidates who share our commitment to diversity.

Postdoctoral Positions
Drug Discovery Research
Medical University of South Carolina

Multiple **Postdoctoral Positions** are immediately available in the newly established Drug Discovery Program at MUSC in Charleston. A central component of this Program is a compound screening and computational chemistry core facility managed by **Dr. Charles D. Smith**. These positions offer the opportunity to work in an interactive and collegial environment, with the support of strong research facilities and professional development initiatives. Additionally, candidates may have opportunities to participate in the growing biotechnology commercialization activities in the Charleston area. Candidates with experience in the following areas are encouraged to apply.

Target identification and validation – molecular and biochemical characterization of signaling pathways in cancer.
Assay development – design and implementation of screening assays using purified proteins and cell-based methods.
Computational chemistry – virtual screening and QSAR analyses.
Pharmacology – *in vivo* testing of new drugs, especially in cancer models, and/or PK/ADMET analyses.

Please send cover letter, indicating research interests, curriculum vitae, and the names and addresses of 3 references to: **Dr. Charles D. Smith, c/o Sandy Spence, Department of Pharmaceutical Sciences, MUSC, 280 Calhoun St., POB 250140, Charleston, SC 29425; (843) 792-3117; spencesj@musc.edu.**

MUSC is an Equal Opportunity Employer.

WESTERN UNIVERSITY OF HEALTH SCIENCES COLLEGE OF OSTEOPATHIC MEDICINE OF THE PACIFIC

IMMUNOLOGY FACULTY POSITIONS

The College of Osteopathic Medicine of the Pacific/ Western University of Health Sciences has implemented a strategic 10 year plan to significantly increase faculty numbers and expand in the areas of research and medical education. The department of Basic Medical Sciences is seeking PhD immunologists for tenure track positions at the level of Assistant, Associate or Full Professor. Competitive salary, significant start-up support, and abundant laboratory space will be offered. The successful applicants are expected to already have obtained extramural funding (such as NIH/NSF/other grants) or have successfully completed a postdoctoral program with strong confidence in their ability to obtain grants. Limited teaching in the medical program will be required. The individuals will have ample protected time to fulfill their research goals. Innovative curriculum development in the candidate's area of expertise will be encouraged.

Applicants should submit a cover letter expressing their interest, statements of research activity and teaching philosophy along with curriculum vitae, current support, and contact information of three potential references to: **Nissar A. Darmani, Ph.D. Chair, Department of Basic Medical Sciences, Western University of Health Sciences, College of Osteopathic Medicine of the Pacific, 309 E. Second Street, Pomona, CA 91766-1854.**

UNIVERSITY OF MISSOURI-COLUMBIA

RESEARCH ASSOCIATE

A non-tenure-track position to maintain and operate sequential ICP-AES instrumentation and to assist the Director in nutritional, environmental, research, and service analyses is currently available. M.S. minimum in analytical science, or related field, with 1 or more years of postgraduate research and/or service experience in ICP-AES and absorption spectrometric instrumentation and related sample preparations for analysis. Familiarity with GLP guidelines and strong oral and written communication skills are considered a plus. Annual salary range is $34-40K, commensurate with experience. Please submit a letter of application, current curriculum vitae/resume with two letters of reference to **Dr. Thomas Mawhinney, Search Committee, University of Missouri – Columbia, Analytical Services, Room 4 Agriculture Building, Columbia, MO 65211. Telephone 573-882-2608, E-mail mawhinneyt@missouri.edu**. Applications will be accepted until the position is filled. Female and minority applications are strongly encouraged.

The University of Missouri-Columbia does not discriminate on the basis of race, color, religion, national origin, ancestry, sex, sexual orientation, age, disability, or status as a disabled veteran or veteran of the Vietnam era. MU is an EO/AA/ADA Employer. To request ADA accommodations, please contact our ADA Coordinator at (573) 884-7278 (V/TTY).

Visit the University of Missouri-Columbia's Web site at http://mujobs.missouri.edu

POSITIONS OPEN

THE GENOMICS RESEARCH CENTER
Academia Sinica, Taipei, Taiwan

Nominations and applications are invited for all levels of **RESEARCH** and **TECHNICAL POSITIONS** in the following areas: chemical biology (synthetic organic chemistry and drug discovery), cell-based research (cell biology related to cancer and infectious diseases), key technology development (nanobiotechnology, new methods for detection, analysis, and profiling), biotech incubation center (technology transfer, evaluation, and business development).

For consideration, please send a copy of curriculum vitae, including a list of publications, two to three references, and a cover letter describing your area of interest, and for a **PRINCIPAL INVESTIGATOR** position, a brief statement of research plan to:

Dr. Chi-Huey Wong, Director
Genomics Research Center
Academia Sinica
128 Academia Road, Section 2
Nankang District, Taipei 115
Taiwan
Telephone: +886-2-2789-9922
Fax: +886-2-2789-9923
E-mail: chwong@gate.sinica.edu.tw
Website: http://www.genomics.sinica.edu.tw/

POSTDOCTORAL RESEARCH ASSOCIATE, ELECTROPHYSIOLOGY. Position available for M.D., Ph.D. or MD.-Ph.D. electrophysiologist to join multidisciplinary research team studying role of sodium channels in neurological disorders (see **S.G. Waxman and S.D. Dib-Hajj,** *Trends in Molecular Medicine* **11(12):** 555–562, 2005). Expertise in patch-clamp is essential, and experience studying voltage-gated sodium channels or related channels using voltage-clamp and current-clamp is highly desirable. Send statement of interest, curriculum vitae, and three letters of reference to: **Stephen G. Waxman, M.D., Ph.D., Chair, Department of Neurology, LCI-708, Yale University School of Medicine, P.O. Box 208018, New Haven, CT 06520-8018.** *Yale University is an Affirmative Action and Equal Opportunity Employer. Women and members of underrepresented minority groups are encouraged to apply.*

POSTDOCTORAL POSITION available to study mechanisms by which Sprouty proteins regulate receptor tyrosine kinase signaling. See *Arterioscler. Thromb. Vasc. Biol.* **25(3):** 533-538, 2005; *J. Biol. Chem.* **278:** 284-288, 2003, and ibid. **Edwin et al.** (e-publication, *J. Biol. Chem.,* Dec 2005, doi:10.1074/jbc.M508300200). Applicants must have a recent Ph.D. in one of the basic science disciplines, experience in molecular and cell biology techniques and in studying protein-protein interactions. Please send curriculum vitae and names of three references to: **Tarun B. Patel, Chair, Department of Pharmacology, Loyola University, Chicago, Stritch School of Medicine, 2160 South First Avenue, Chicago, IL 60153.** *Equal Employment Opportunity/Affirmative Action.*

ECRI, a health services research and publishing organization designated as an evidence-based practice center (EPC) by the U.S. Agency for Healthcare Research and Quality, is seeking a **CHIEF METHODOLOGIST** to oversee technical work conducted by the Health Technology Assessment Group on assessments of medical drugs, devices, and procedures, including project design and methods of analysis. Act as ECRI's primary statistical resource (including project/study design and data analysis) when requested by other ECRI groups. For details on this position, please go to Careers at ECRI on the homepage of **website: http://www.ecri.org.**

POSITIONS OPEN

ASSISTANT/ASSOCIATE/FULL PROFESSORS –
Tenure-Track
Clinical and Translational Research
Texas Tech University Health Sciences Center
School of Pharmacy
Microbial and/or Immunological Aspects of Infectious Diseases with Emphasis in Aging

The Pharmacy Practice Department has openings for 12-month tenure-track faculty positions in clinical and translational research in the microbial and/or immunological aspects of infectious disease emphasizing aging populations. Although only 10 years old, the School of Pharmacy is ranked among the top 38 colleges of pharmacy with respect to federal research funding. Positions are state-funded and offer remarkable opportunities for creative scientists with co-appointment to the Garrison Institute on Aging. Qualifications include a Ph.D., Pharm.D., or M.D. and postdoctoral training. History of external competitive funding is strongly preferred. Preference will be given to investigators in infectious disease (either microbial or immunological) with demonstrated interest in aging and ability to work in an interdisciplinary environment with basic and clinical scientists. Aggressive startup packages will be provided. Additionally, the school's multicampus structure (Dallas/Ft. Worth, Amarillo, and Lubbock) provides the infrastructure for multi-site research. Positions available at the main Lubbock campus. Interested investigators should send their curriculum vitae, statement of research interest, funding history, teaching interests within a Pharm.D. and Ph.D. (biomedical sciences) program, and contact information for at least three references. Review of applications will commence immediately and continue until positions are filled. Address all correspondence to:

Dr. C.A. Bond
Professor and Search Committee Chair
Department of Pharmacy Practice
Texas Tech University Health Sciences Center
School of Pharmacy
1300 Coulter
Amarillo, TX 79106
E-mail: cab.bond@ttuhsc.edu
Telephone: 806-356-4000, extension 244
Fax: 806-356-4018

Interested applicants must complete the online application process at **website: https://jobs.texastech.edu.**

Equal Employment Opportunity/Affirmative Action Employer. Women and minorities are strongly encouraged to apply.

POSTDOCTORAL FELLOW POSITION
Opening in Hickey Laboratory

The University of North Carolina at Chapel Hill School of Pharmacy has an opening for a Postdoctoral Fellow position in **Anthony J. Hickey's** laboratory. Dr. Hickey's laboratory is involved in studying the delivery to, and disposition of drugs and vaccines from the lungs. A position is available to work in conjunction with other personnel in the laboratory on the delivery of antitubercular agents, and certain protein and peptide molecules to the lungs of rodents. Subsequently, the disposition of these molecules will be studied in terms of pharmacokinetics (PK) and pharmacodyamics (PD). Conventional sampling and analytical techniques will be employed to perform PK studies. PD studies will be performed in a guinea pig model of tuberculosis. Two NIH grants and a large collaborative award to Dr. Hickey will support this work.

For more information call: **Dr. Hickey** at: **telephone: 919-962-0223** or **e-mail: ahickey@e-mail.unc.edu.**

To apply, please send resume or curriculum vitae, and a letter indicating interest to:

Anthony J. Hickey, Ph.D.
University of North Carolina
School of Pharmacy
Kerr Hall, CB# 7360
Chapel Hill, NC 27599-7360

University North Chapel is an Equal Opportunity Employer. Women and minorities are encouraged to apply.

POSITIONS OPEN

DIRECTOR, MAMMALIAN GENETICS ENGINEERING CORE FACILITY
The University of Arizona

The University of Arizona, Tucson, invites applicants for a Research Faculty Position. The Director of the Mammalian Genetics Engineering Core Facility will establish and direct the following services: vector design for transgenic and gene targeting constructs, vector construction, gene targeting in ES cells, DNA microinjection and blastocyst injection. Experience in these areas and experience directing a similar core facility is preferred. Applicants must have a minimum of Ph.D., M.D., D.V.M. or equivalent degree, and postdoctoral training. Please submit a letter of application, a summary of research and/or technology accomplishments and objectives, curriculum vitae, and the names and contact information for three appropriate references.

To apply, please visit **website: http:// www.uacareertrack.com** and search for job 34159.

The University of Arizona is an Equal Employment Opportunity/Affirmative Action Employer, Minorities/ Women/ Persons with Disabilities/Veterans.

ASSISTANT PROFESSOR
Molecular Plant-Fungal Interactions

Division of Plant Sciences **(website: http://plantsci.missouri.edu),** University of Missouri, Columbia (UMC) invites applications for a tenure-track position in molecular plant-fungal interactions. Ph.D. in plant pathology, microbiology, plant molecular biology or related field and postdoctoral experience is required. This position is expected to establish an active, extramurally funded research program in the area of plant-fungal interactions using modern molecular approaches, and to participate in the teaching (undergraduate and graduate) and service missions of the Division. UMC has a history of excellence in plant science and provides a rich environment for research collaboration. Electronically submit, by April 15, 2006, a letter describing qualifications and career goals and curriculum vitae to: **e-mail: plantsci@missouri.edu.** Arrange to have selected reprints and three letters of reference sent to: **Division of Plant Sciences, Attn: Margie, 1-41 Agriculture Building, University of Missouri, Columbia, MO 65211.** Direct questions to: **Dr. Gary Stacey, Chair, Search Committee, telephone: 573-884-4752** or **e-mail: staceyg@missouri.edu.** JD 1506188; File 050700. *Affirmative Action/Equal Opportunity Employer.*

POSTDOCTORAL POSITIONS in stress gene signaling at **Harvard School of Public Health.** Projects include: (1) radiation-genomics and toxicogenomics to study signal transduction after ionizing radiation and molecular markers for exposure to genotoxic agents, (2) oncogenic and genotoxic stress signaling with emphasis on mouse models, kinase and phosphatase signaling. Applicants must have a doctoral degree and experience is preferable in mouse modeling, molecular biology, and/or protein biochemistry. See **website: http://www.hsph.harvard.edu/fornacelab.** Submit curriculum vitae and contact information for three references to: **Dr. A.J. Fornace Jr., 1-121, HSPH, 665 Huntington Avenue, Boston, MA 02115** or by **e-mail: afornace@hsph.harvard.edu.**

POSTDOCTORAL POSITION available to study role tumor neurosis factor (TNF) receptor signaling in cancer and immunity. Send curriculum vitae and names and e-mail addresses of three references to: **Dr. David Donner, Department of Surgery and UCSF Cancer Center, 1600 Divisadero Street, Box 1932, University of California, San Francisco, CA 94143; e-mail: donnerd@surgery.ucsf.edu.**

POSITIONS OPEN

DARWIN FELLOW

The Graduate Program in Organismic and Evolutionary Biology (OEB) at University of Massachusetts Amherst announces a two-year Postdoctoral Fellowship/Lectureship. OEB draws together more than 80 faculty from the Five Colleges (University of Massachusetts Amherst and Smith, Hampshire, Mount Holyoke and Amherst Colleges), offering unique training and research opportunities in the fields of ecology, organismic and evolutionary biology. Our research/lecture position provides recent Ph.D.s with an opportunity for independent research with an OEB faculty sponsor as well as experience developing and teaching a one-semester undergraduate biology course. Position subject to availability of funds. First year salary: $30,000. Second year salary: $32,000. Applicants in the area of collections-based research are particularly encouraged to apply.

To apply, send curriculum vitae, three letters of reference, statements of research and teaching interests, and letter of support from your proposed OEB faculty sponsor. A list of faculty and additional information is available at **website: http://www.bio.umass.edu/oeb.**

OEB Darwin Fellowship
319 Morrill Science Center
611 N. Pleasant Street
University of Massachusetts Amherst
Amherst, MA 01003
Telephone: 413-545-0928
E-mail: darwin@bio.umass.edu

Application review begins January 30, 2006. Start date is August 13, 2006.

The University of Massachusetts Amherst is an Affirmative Action/Equal Opportunity Employer. Women and members of minority groups are encouraged to apply.

NIH-funded **POSTDOCTORAL POSITION** is available in the Cancer Biology Department of **Wake Forest Medical School** to study effects of antitumor peptides and short interfering RNA vectors targeted to breast cancer cells. Qualified candidate must be a U.S. citizen or permanent resident and have a Ph.D. in biochemistry (or a related field) or an M.D. with a strong commitment to basic science research. Submit application electronically, including curriculum vitae, and three reference names with contact information to: **Dr. James P. Vaughn, Assistant Professor of Cancer Biology** at **e-mail: jvaughn@wfubmc.edu.** *Equal Opportunity/Affirmative Action Employer.*

POSTDOCTORAL FELLOW
Imaging Apoptosis
Center For Molecular Imaging Research

The Center for Molecular Research at Massachusetts General Hospital/Harvard Medical Medical School is seeking a Postdoctoral Fellow for a research program in imaging pharmacotherapy induced apoptosis. The candidate should have a Ph.D. and experience in cell based and molecular/biochemical assays. Send resume and statement of research interests to: **Dr. Lee Josephson** at **e-mail: ljosephson@partners.org. Website: http://www.mgh-cmir.org.**

Additional job postings not featured in this issue can be viewed online at **website: http://www.sciencecareers.org.** New jobs are added daily!

Manage your job search more effectively by creating an account at **website: http://www.sciencecareers.org.** You can post your resume (open or confidentially) in our database and use it to apply to multiple jobs simultaneously. Track the jobs you have applied to in special tracking folders. Plus, you can create Job Alerts that will e-mail you notification of jobs that match your search criteria.

POSITIONS OPEN

POSTDOCTORAL POSITIONS
Integrative Neurophysiology of Cortical/Basal Ganglia Interactions

(1) Candidates should have experience with patch clamp recordings in brain slices or anatomical methods to map the connectivity of neuronal circuitry that involves multiple brain loci, such as the neocortex and basal ganglia, in the rodent brain. Experience with analysis of rodent behavior is also relevant.

(2) The project is part of a larger effort to use a combination of molecular, genetic, cellular, and systems approaches to analyze the neural circuitry underlying a well-defined behavior. This multidisciplinary effort involves the laboratories of **Doug Nitz, Niraj Desai, Weimin Zheng,** and **Fred Jones** at the Neurosciences Institute. The immediate objective is to relate the electrophysiological properties of neurons with their patterns of connectivity with other brain regions. In addition to more traditional techniques, the project will make extensive use of dynamic clamp methodology and molecular perturbation techniques.

Submit curriculum vitae, statement of research interests, and names of three references to: **Dr. W. Einar Gall, Research Director, The Neurosciences Institute, 10640 John Jay Hopkins Drive, San Diego, CA 92121. E-mail: jobs@nsi.edu.**

POSTDOCTORAL POSITION

A Postdoctoral Position is available in the Department of Microbiology and Immunology at Dalhousie University to study molecular mechanisms of gram-positive streptococci in biofilm infections. Experience in molecular biology, microbiology, and bioinformatics is required. Applicants should send their curriculum vitae, including three references, to: **Dr. Yung-Hua Li, Room 5215, 5981 University Avenue, Halifax, NS, Canada, B3H 3J5, fax: 1-902-494-6621, e-mail: yung-hua.li@dal.ca.**

POSTDOCTORAL RESEARCH ASSOCIATE, Boston, Massachusetts. Job entails and requires experience in performing biochemical research on parathyroid hormone-receptor interactions, making conference presentations, and publishing results. Send resumes to: **Angela Wittelsberger, Department of Physiology, Tufts University, School of Medicine, 136 Harrison Avenue, Boston, MA 02111.**

COURSES AND TRAINING

COURSES AND TRAINING
Third Annual
EXPERIMENTAL NEUROGENETICS OF THE MOUSE
May 8-16, 2006
University of Tennessee Health Science Center
Memphis, Tennessee U.S.A.

This lecture and hands-on workshop is to train students and researchers in the use of mice in the analysis of nervous system structure and function. Topics covered include mouse informatics, genetics of Mendelian and complex disorders of the nervous system, and various approaches to examining gene function (e.g., knockouts, ethyl nitro sourea, mutagenesis, RNA interference, inbred lines).

A significant part of the course will be devoted to phenotypic analysis of mice for neurological traits using behavioral, anatomical, physiological, and molecular screens. Invited speakers include **Ellen Hess, Ilan Golani,** and **Doug Walhsten,** plus faculty affiliated with the Tennessee Mouse Genome Consortium. See **website: http://mouseneurogenetics.utmem.edu,** or contact: **Pat Goss, e-mail: pgoss@utmem.edu.**

MARKETPLACE

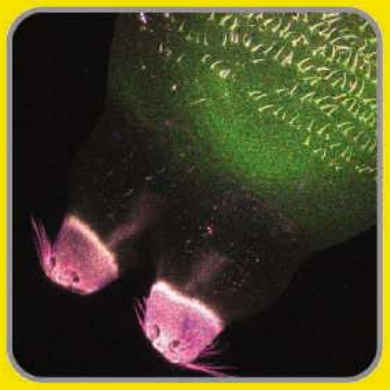

Nikon C1 Plus: Award winning confocal imagery*

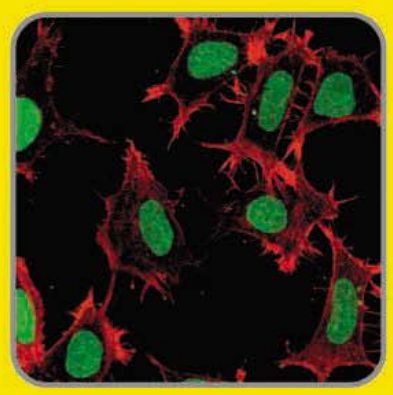

New! Nikon C1si: True spectral imaging through fast one-shot 32 channel capture at the highest resolution

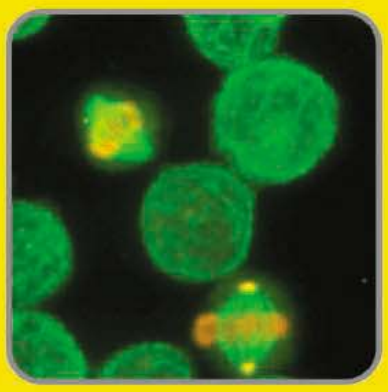

New! Nikon LiveScan Swept Field Confocal: 3 to 1200 frames per second

The next breakthrough **is yours.**

NIKON'S NEW FAMILY OF CONFOCAL MICROSCOPES IS READY TO SUPPORT THE EXTREMES OF YOUR RESEARCH.

Your research is our inspiration for developing Nikon's series of confocal microscopes. Whether you're conducting fixed stain research, or complex live cell confocal studies, Nikon now offers three modular instruments - all with cutting edge innovations.

Choose the C1si to capture the widest spectral range at user selectable resolution and conduct spectral unmixing for true color. All in a single scan representation with no overlap. Or use the flexible slit and pinhole combination of the LiveScan Swept Field Confocal for high-speed live cell image capture with minimal photobleaching effects. Whatever your need, Nikon has engineered the next generation in confocal imaging technology with your future breakthrough in mind.

C1 Plus
Laser point-scanning modular confocal system. 3-channel fluorescence and 1-channel transmission.

C1si
True spectral detection for fluorescence probe applications where differentiation is vital.

LiveScan SFC
Field scanning system that enables fast confocal image capture with low photobleaching – using multiple pinholes and slits.

For more information call 1-800-52-NIKON or visit www.nikonconfocal.com

*Winner of 3 out of 4 best of confocal image workshop competitions

The Eyes of Science

Nikon

2006 Catalog | from R&D Systems

Quality | Selection | Performance | Results

R&D Systems New Catalog

Cancer | Development | Endocrinology | Immunology | Neuroscience | Proteases | Stem Cells

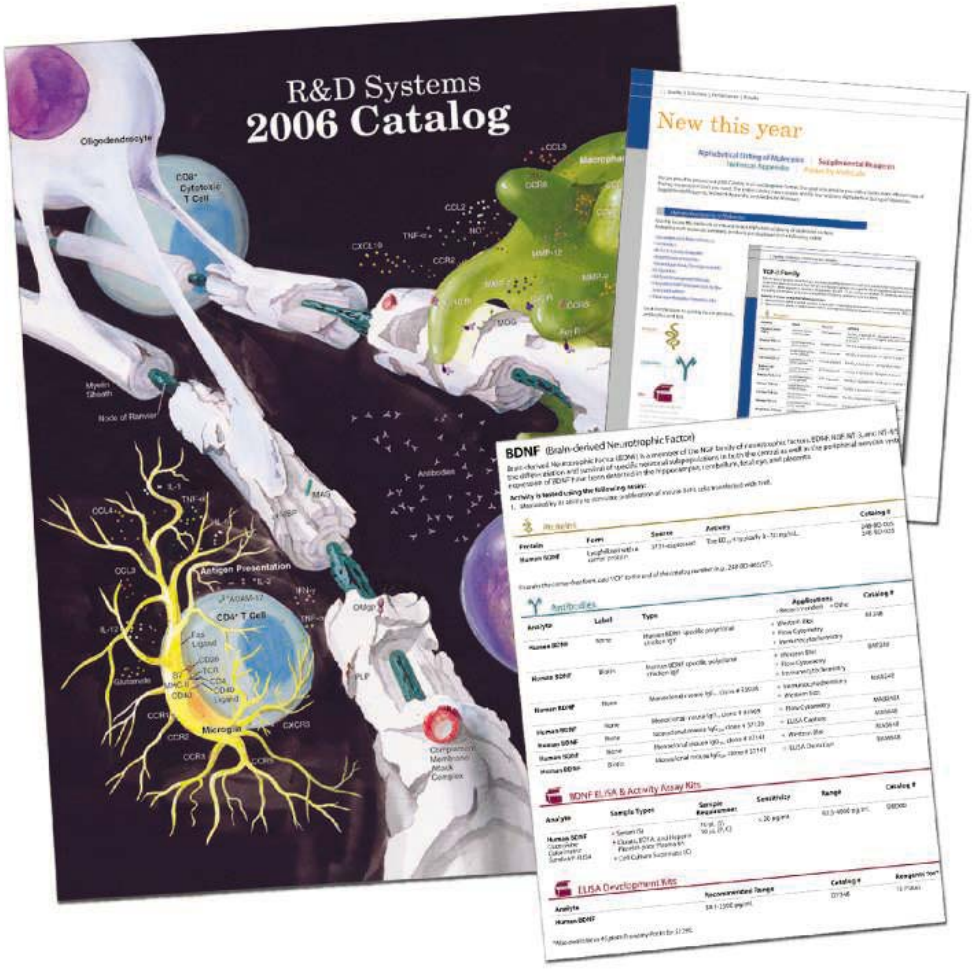

Now Organized by Molecule

Locate your molecule alphabetically and follow the icons to your product of interest.

= proteins

= antibodies

= kits

More than 8,000 products:

- Antibodies
- Proteins
- ELISA Kits & Reagents
- Apoptosis Kits & Reagents
- Cell Selection Kits & Reagents
- Multiplex Assays
- Antibody Arrays
- Signal Transduction Kits & Reagents
- Stem Cell & Cell Culture Reagents
- & More

REQUEST A CATALOG ONLINE @ www.rndsystems.com/go/catalog

www.RnDSystems.com | (800) 343-7475

U.S. & Canada
R&D Systems, Inc.
Tel: (800) 343-7475
info@RnDSystems.com

Europe
R&D Systems Europe Ltd.
Tel: +44 (0)1235 529449
info@RnDSystems.co.uk

Germany
R&D Systems GmbH
Tel: 0800 909 4455
infogmbh@RnDSystems.co.uk

France
R&D Systems Europe
Tel: 0800 90 72 49
info@RnDSystems.co.uk

R&D SYSTEMS